

به نام خدا



مرکز دانلود رایگان مهندسی متالورژی و مواد

www.Iran-mavad.com



***ADVANCES IN
CORROSION SCIENCE
AND TECHNOLOGY
VOLUME 5***

ADVANCES IN CORROSION SCIENCE AND TECHNOLOGY

Editors:

M. G. Fontana and R. W. Staehle

*Fontana Corrosion Center, Department of Metallurgical Engineering
The Ohio State University, Columbus, Ohio*

Editorial Board:

VITTORIO CARASSITI

*Universita di Ferrara
Ferrara, Italy*

MORRIS COHEN

*National Research Council
Ottawa, Ontario, Canada*

JOSEPH E. DRALEY

*Argonne National Laboratory
Argonne, Illinois*

T.P. HOAR

*University of Cambridge
Cambridge, England*

JEROME KRUGER

*National Bureau of Standards
Washington, D.C.*

PAUL LACOMBE

*Université Paris-Sud Centre D'Orsay
Orsay, France*

MARCEL POURBAIX

*CEBELCOR
Brussels, Belgium*

SAKAE TAJIMA

*Tokyo City University
Tokyo, Japan*

A Continuation Order Plan is available for this series. A continuation order will bring delivery of each new volume immediately upon publication. Volumes are billed only upon actual shipment. For further information please contact the publisher.

***ADVANCES IN
CORROSION SCIENCE
AND TECHNOLOGY
VOLUME 5***

***Edited by
Mars G. Fontana and Roger W. Staehle***

PLENUM PRESS • NEW YORK AND LONDON

The Library of Congress cataloged the first volume of this title as follows:

Advances in corrosion science and technology. v. 1-
New York, Plenum Press, 1970-

v. illus. 24 cm.

Editors: v. 1- M. G. Fontana and R. W. Staehle.

1. Corrosion and anti-corrosives—Collected works. i. Fontana,
Marsilio Guido, 1910- ed. ii. Staehle, R. W., 1934- ed.

TA418.74.A3

620.1'1223

76-107531

Library of Congress

71 (7)

Library of Congress Catalog Card Number 76-107531

ISBN-13 : 978-1-4615-9064-4

e-ISBN-13 : 978-1-4615-9062-0

DOI : 10.1007/978-1-4615-9062-0

©1976 Plenum Press, New York

Softcover reprint of the hardcover 1st edition 1976

A Division of Plenum Publishing Corporation

227 West 17th Street, New York, N.Y. 10011

All rights reserved

No part of this book may be reproduced, stored in a retrieval system, or transmitted, in any form or by any means, electronic, mechanical, photocopying, microfilming, recording, or otherwise, without written permission from the Publisher

PREFACE

This series was organized to provide a forum for review papers in the area of corrosion. The aim of these reviews is to bring certain areas of corrosion science and technology into a sharp focus. The volumes of this series are published approximately on a yearly basis and each contains three to five reviews. The articles in each volume are selected in such a way as to be of interest both to the corrosion scientists and the corrosion technologists. There is, in fact, a particular aim in juxtaposing these interests because of the importance of mutual interaction and interdisciplinarity so important in corrosion studies. It is hoped that the corrosion scientists in this way may stay abreast of the activities in corrosion technology and *vice versa*.

In this series the term “corrosion” is used in its very broadest sense. It includes, therefore, not only the degradation of metals in aqueous environment but also what is commonly referred to as “high-temperature oxidation.” Further, the plan is to be even more general than these topics; the series will include all solids and all environments. Today, engineering solids include not only metals but glasses, ionic solids, polymeric solids, and composites of these. Environments of interest must be extended to liquid metals, a wide variety of gases, nonaqueous electrolytes, and other nonaqueous liquids. Furthermore, there are certain complex situations such as wear, cavitation, fretting, and other forms of degradation which it is appropriate to include. At suitable intervals certain of the review articles will be updated as the demands of technology and the fund of new information dictate.

Another important aim of this series is to attract those in areas peripheral to the field of corrosion. Thus, physicists, physical metallurgists, physical chemists, and electronic scientists all can make very substantial contributions to the resolution of corrosion problems. It is hoped that these reviews will make the field more accessible to potential contributors from these other areas. Many of the phenomena in corrosion are so complex that

it is impossible for reasonable progress to be made without more serious and enthusiastic interdisciplinary interest.

This series, to some extent, serves as a “dynamic” handbook. It is well known that preparing a handbook is a long, tedious process and parts become out of date by the time the final volume is published. Furthermore, certain subjects become out of date more quickly than others. Finally, in a handbook it is never possible to prepare the individual discussions with sufficient detail and visual material to be properly useful to the reader. It is hoped that the format of this series serves to overcome some of these difficulties.

In addition to the discussion of scientific and technological phenomena the articles in this series will also include discussions of important techniques which should be of interest to corrosion scientists.

M. G. FONTANA

R. W. STAEBLE

CONTENTS

Chapter 1

Surface Chemistry and Corrosion of Glass

Augustus M. Filbert and Michael L. Hair

Introduction	1
The Nature of Glass	2
Structure	2
Glass Composition	4
Chemical Attack on Glass: Tests for Durability	7
Powder Tests	7
Weight Loss Tests	8
Solubility of Silica	10
Glass Structure and Ion Selectivity	11
Chemical Attack on Glass	15
General Considerations	15
Water and Steam	17
Acid Solutions	18
Alkaline Solutions	23
Chelating Agents	28
Sulfur Dioxide and Sulfur Trioxide	33
Ion Exchange in Molten Salts	34
Phase Separation	34
Surface Chemistry	40
Miscellanea	49
Weathering of Glass Surfaces	49
Corrosion Resistance of Ceramics	49
High-Temperature Attack on Glasses and Glass Ceramics	49
Utilization of Corrosion Effects	50
Summary	51
References	51

*Chapter 2***Halogen Corrosion of Metals***Phillip L. Daniel and Robert A. Rapp*

Introduction	55
Pertinent Properties of Binary Metal Halides	57
Thermodynamic Properties	57
Melting Temperatures	59
Diffusion Properties	59
Vapor Pressures	68
Experimental Methods Used to Study Metal–Halogen Reactions . . .	70
Manometric Method	70
Gravimetric Method	71
Photometric Method	72
Electrical Resistance Method	72
Quartz Crystal Microbalance	73
Reaction Morphologies, Mechanisms, and Kinetics	73
Reaction of Pure Metals	74
Reaction of Alloys	86
Laboratory Studies of Halogen Attack on Metals and Alloys	89
Nickel and Nickel Alloys	92
Copper and Copper Alloys	114
Iron and Iron Alloys	124
Aluminum and Aluminum Alloys	135
Other Metals	140
Conclusions	158
References	160

*Chapter 3***Oxidation of Zirconium and Its Alloys***B. Cox*

Introduction	173
Historical Development	173
Influence of the Nuclear Reactor Industry on Development . . .	174
Comparison of General Features of Gaseous Oxidation and Aqueous Corrosion	177

Oxidation in Dry Gases	180
Oxygen and Air	180
Carbon Dioxide	216
Molten Sodium	222
Fused Salts	225
Oxidation in High-Temperature Aqueous Environments	227
Historical Background	227
Corrosion in Water and Steam	240
Corrosion in Organic Coolants	291
Oxidation Mechanisms	295
Zircaloy-Type Alloys	297
Zr–Nb Alloys	331
Other Alloys	334
Hydrogen Absorption	337
Hydrogen Absorption from Gaseous Hydrogen	338
Hydrogen Absorption via the Decomposition of H_2O	343
References	362
Index	393

SURFACE CHEMISTRY AND CORROSION OF GLASS

Augustus M. Filbert

*Corning Glass Works
Research and Development Laboratories
Corning, New York*

and

Michael L. Hair

*Xerox Research Center of Canada
2480 Dunwin Drive
Mississauga, Ontario*

INTRODUCTION

Because most silicate glasses have a high resistance to corrosion in normal environments, glass *per se* is frequently considered to be an inert substance. Such is not the case, as can be attested to by certain optical glasses that are readily stained in the atmosphere (e.g., dense flints and barium crowns) or etched by mild acid action, the effects being readily observed with the naked eye. Most glasses, including the “chemically resistant” glasses, will experience localized chemical attack and form a surface composition that may be substantially different from that of the bulk glass. Surface phenomena, such as the adsorption of gases, reaction with biological species, and reflection of light, may be critically influenced by such corrosion of glass surfaces, even though it is on a minute scale. Any discussion of the corrosion of glass thus has to reach two audiences of widely different interests, the engineer, who is usually most interested in the gross effect and its influence on mechanical properties, and the chemist, who is concerned at the molecular level with the chemical or catalytic changes that occur or are induced as a result of such corrosion.

THE NATURE OF GLASS

Before attempting to discuss the corrosion of glass surfaces, we must first ask ourselves what we mean by a glass. Glass is such a common material, universally observed and utilized daily, that its definition may appear superfluous. However, we must first emphasize that there is no single, chemically definable "glass." Although the literature is full of such references as "the solution was placed in a glass container," it must be realized that there are many different glasses, which vary widely in composition. They may look alike, mechanically they may act alike, but the chemical properties of their "corroded" surfaces are not alike. Why, for instance, does the biologist, trained to use borosilicate glasses for all his chemical work, never use it for culture growth but switches to a glass of soda-lime composition? The answer is very simple, of course. The culture grows much better on the soda-lime surface, and sometimes not at all on the borosilicate.

As a start, however, let us describe glass as a noncrystalline solid, differing from solid crystalline substances by a number of characteristic properties. Glasses are plastic at high temperatures, rigid at low temperatures, and, under normal manufacturing conditions, do not crystallize; they are isotropic. As defined by the American Society for Testing and Materials¹: "Glass is an inorganic product of fusion, which has cooled to a rigid condition without crystallizing." Fanderlik² has amplified this definition as follows: "Its properties are, to a considerable extent, dependent on its thermal history, i.e., on the manner by which the glass has passed from the plastic into the rigid state." This addition is particularly relevant to borosilicate glasses with regard to their annealing processes (heat treatments) and resulting chemical stability. Note, however, that the definitions cover a state of matter and not a chemical composition.

Structure

In the evolution of theories to describe the structure of glass, two types of models have arisen: the atomistic-type theory of a continuous lattice (Zachariasen³ and Warren⁴) and the more recent polymeric-type theory (Smekal⁵ and Stevels⁶). Both theories are interrelated, instructive, and able to satisfactorily interpret the influence of various oxides as building materials of the glassy network.

Zachariasen³ suggested that the atoms in a glass form an extended three-dimensional network which, although lacking symmetry, has an energy

content comparable to that of the crystal network. He postulated that the following four rules should be satisfied before an oxide can be classified as a glass former :

1. Each oxygen atom must be linked to no more than two cations.
2. The number of oxygen atoms around any one cation must be small, i.e., three or four.
3. The oxygen polyhedra must share corners (not faces or edges) to form a three-dimensional network.
4. At least three corners must be shared.

The work of Warren⁴ and others, who used x-ray diffraction to study the structure of glass, supported Zachariasen's concept, and the combinations of these efforts have resulted in the random network theory for the structure of glass. This is shown schematically in Fig. 1.

Stevens,⁶ on the other hand, considered glass as a polymer and suggested that certain properties of silicate glasses are independent of the nature of the network-modifying ions. He suggested that the glassy state which develops during cooling of the liquid melt arises from increasing bond formation. This, in turn, raises the melt viscosity and restricts the mobility of individual polymeric molecules. Crystallization requires a total regrouping of the

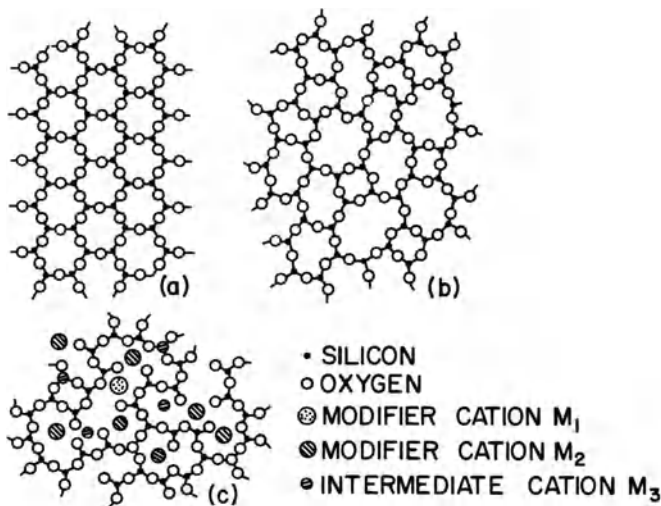


Fig. 1. Two-dimensional schematic representation of (a) a crystalline structure; (b) a simple glass; and (c) a multicomponent glass.

molecules, with destruction and reformation of bonds. However, the mobility of the particles is too low, and with further cooling the vitreous state is reached. Only by very slow cooling can the regrouping of atoms give rise to crystallization.

Many questions must be answered before a better understanding of the structure of any glass is obtained. X-ray diffraction studies apparently allow spatial assignment of nearest neighbors only, and more detailed structure is implied through the study of other properties, such as density, viscosity, thermal expansion, elastic constants, Raman and infrared spectra, dielectric constants, and color. It is important to note that a unified picture of the glassy state is not available and that this makes detailed discussion of the chemistry of corrosion and surface properties almost impossible. In particular, in our opinion, phase separation within the glasses is a very important, little understood, and mostly ignored parameter in explaining corrosion. This will be discussed briefly later, but it should be understood that the treatment in this chapter is based primarily upon traditional knowledge and is subject to further research.

Glass Composition

The terms *glass formers*, *intermediates*, and *modifiers* are usually used to define the role of various oxides in glasses. The glass formers (e.g., B_2O_3 , SiO_2 , GeO_2 , P_2O_5) can, by themselves, form a three-dimensional random network. Modifiers (e.g., Na_2O , CaO) tend to bond ionically to the anions in the glassy network and are used to alter such glass properties as viscosity, conductivity, thermal expansion, and chemical durability. Intermediates (Al_2O_3) do not generally form glasses but can enter a glass in either a forming or a modifying position.

Oxides may also be considered as *formers*, *stabilizers*, or *fluxes*. In this case glass formers are considered as defined above, and the other two groups are functionally considered. Fluxes are added to lower melting and working temperatures by decreasing viscosities (e.g., Na_2O , K_2O , B_2O_3), whereas stabilizers are added to improve chemical durability and/or to prevent crystallization (e.g., CaO , MgO , Al_2O_3).

Silica Glass

Fused silica, the “ideal” glass, is the most important of the single oxide glasses. Because it possesses a highly cross-linked, three-dimensional bonding (see Fig. 2a), silica glass is useful at high temperatures, has a low

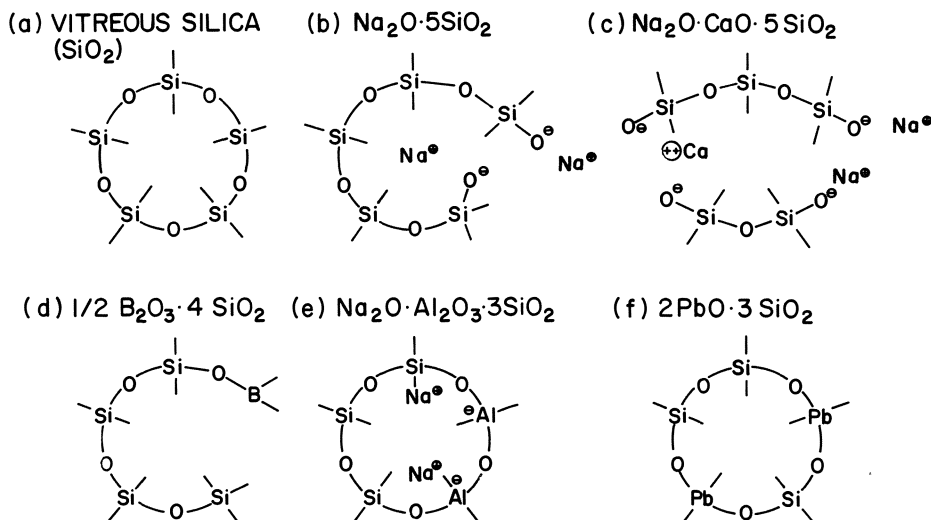


Fig. 2. Schematic representations of glass structures. Si—O—Si indicates bonding through bridging oxygens common to two SiO_4 tetrahedra.

coefficient of thermal expansion, and has a *high resistance to chemical attack*. The molecular bonding that gives silica glass these properties also contributes to its difficulty of preparation by the usual melting and drawing techniques.

Alkali Silicates

Fluxes are added to silica glass to increase the workability of the glass at standard glass manufacturing temperatures ($\sim 1500^\circ\text{C}$). The most common additive, soda (Na_2O), “softens” the glass by disrupting Si—O—Si bonds, as shown in Fig. 2b. The addition of fluxes to a glass decreases its viscosity, increases its thermal expansion, and *worsens its chemical durability*. (The addition of alkali also increases solubility of the glasses, and therefore alkali silicates form the foundation of the soluble silicate industry.)

Soda-Lime Glasses

Stabilizing oxides, such as calcium oxide, are added to glasses to decrease the solubility of sodium silicates and to make them *more chemically durable*. An optimum soda-lime glass is composed of 72% silica, 15% soda,

10% lime and magnesia, 2% alumina, and 1% miscellaneous oxides—a somewhat complicated chemical composition. The alumina content is optimized to ensure *high chemical durability* and to decrease crystallization problems. Figure 2c schematically shows the structure of a soda-lime-silica glass.

Borosilicate Glasses

Boric oxide is a glass former, and it enters a silica network as shown in Fig. 2d. The B^{3+} , however, is surrounded by only three oxygen ions in triangular coordination. The local planar structure, when inserted into the tetrahedral environment, exhibits weak forces in one direction and “softens” the glass. B_2O_3 is thus a flux when added to silica, but does not raise the expansion of the glass as much as the alkali or alkaline earth oxides. If the boric oxide concentration of a glass is very high, *chemical durability* becomes a problem. Alkali additions permit lower B_2O_3 levels to be used and give glasses with *better durability*. The low thermal expansion coefficient of low-alkali borosilicates makes them ideal for use in the manufacture of laboratory apparatus, baking ware, etc., and is the basis of the well-known Corning Code 7740 line of glasses.

Aluminosilicate Glasses

The addition of alumina to an alkali silicate glass causes an increase in viscosity and also *enhances the chemical durability*. This is explained in Fig. 2e. The alumina assumes a tetrahedral coordination, re-forming Si—O bonds severed by alkali additions (see Fig. 2b). The glass also shows increased resistance to devitrification. The Na/Al ratio in the glass is an important parameter which can be linked to both phase separation and the ion selectivity of the glass when used as an electrode, where the electrical conductivity is a minimum at $Al/Na = 1$.

Lead Glasses

Lead oxide is generally considered to be a modifying oxide, although in some cases the lead is known to go into the network-forming position (see Fig. 2f). The addition of PbO yields soft glasses with high refractive index and density but does not reduce electrical resistivity. The chemical durability of lead glasses is generally more a function of other oxides in the glass than of the lead content itself.

For further information on the composition, manufacture, and properties of glass, the reader is referred to an excellent review by Hutchins and Harrington⁷ and references therein.

CHEMICAL ATTACK ON GLASS: TESTS FOR DURABILITY

Much of the work on the chemical attack on glass has been directed toward the practical purpose of determining the durability of different compositions when exposed to corrosive conditions. Indeed, numerous tests are described in the literature for determining the resistance of different glass types to attack by various media.⁸ These encompass procedures for examining the attack of high-silica, soda-lime-silica, and borosilicate glasses by acid, neutral, and alkaline solutions.⁹ Because the reactions of these chemicals with the glass surface are complex and strongly influenced by slight changes in the concentration and temperature of the corrosive agent, durability measurements made from accelerated laboratory tests are frequently shown to be as critically dependent on the test conditions as on the glass under examination. Other important considerations include the glass configuration (i.e., powder or bulk), the effect of reaction products on the glass surface, and the role of decomposed glass fragments that may be formed as a function of the corrosive attack on the glass surface.

Since glass articles in normal use may be exposed to corrosive attack by water, acid, alkali, salt, organic, or biological solutions at extremes of temperature, or be in contact with gases and vapors in the atmosphere, corrosion may occur by one or a combination of different means. Thus, glass may (a) have part of its structure preferentially dissolved, leaving a leached surface layer or a totally porous entity; (b) be dissolved in such a way as to continuously expose fresh glass surface; and/or (c) react with the corrosive material to form new surface compounds, which can inhibit further reaction. The following ASTM standard tests do not differentiate among these mechanisms.

Powder Tests

Powder tests have been employed by both the American Pharmaceutical Society¹⁰ and the American Society for Testing and Materials.¹¹ An outline of one sample U.S.P. test is as follows. The test glass is crushed, and a test sample of powder of specified mesh size is selected. The powder is placed in contact with a given volume of distilled water and is then autoclaved for

30 min at 121°C. The alkali extracted from the glass is then titrated with sulfuric acid using methyl red as an indicator. Results are generally expressed as equivalents of dilute acid required to neutralize the alkali extracted from the glass. The ratio of extracted alkali to original glass weight may also be calculated.

The test is a simple one and, by giving an indication of extractable alkali, allows judgment of test glasses for application as bottles, window-panes, laboratory ware, etc. Some representative powder test data on selected glass compositions are given in Table 1.¹²

Weight Loss Tests

In a weight loss test, a glass sample with known (geometric) surface area is selected. The sample is weighed and placed in a container with a given quantity of the selected reagent. The container and contents are held at temperature for a given period of time, after which the sample is carefully dried and reweighed. Results are expressed as the loss of weight per unit of surface area (mg/cm^2) for the total test period. The exact experimental

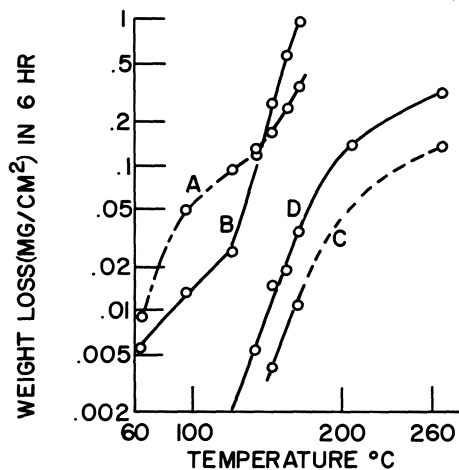


Fig. 3. Rates of attack by distilled water versus temperature on several glass compositions: (A) soda-lime bulb glass; (B) medium-lead electrical glass; (C) high-lead silica glass (58% PbO); (D) low-expansion borosilicate glass. (Data taken from Taylor and Smith.¹³)

No.	Type of glass	Powder tests		Weight loss tests ^b			
		Am. Pharm. Soc.: distilled H ₂ O ^c	ASTM—A: N/50 H ₂ SO ₄ ^e	H ₂ O at 20 psi, pH ^{+d}	5% HCl, 24 hr, 100°C	5% NaOH, 6 hr, 99°C	N/50 Na ₂ CO ₃ , 6 hr, 100°C
1	Silica glass	—	—	—	—	—	—
2	96% Silica glass	0.0003	0.002	7.7	0.0004	0.9	0.07
3	Soda-lime—window sheet	—	—	—	—	—	—
4	Soda-lime—plate	0.03	—	10.5	—	0.8	0.18
5	Soda-lime—containers	0.05	0.03	—	0.05	0.8	1.5
6	Soda-lime—lamp bulb	0.09	0.04	11.2	0.01	1.1	1.1
7	Lead glass—electrical	0.07	0.15	11.5	0.02	1.6	0.25
8	Lead glass—high lead	0.0006	—	8.0	Disinte- grated	3.6	0.81
9	Aluminoborosilicate (apparatus)	—	0.005	—	—	1.0	0.13
10	Borosilicate—low expansion	0.0025	0.005	8.5	0.0045	1.4	0.12
11	Borosilicate—low electrical loss	—	—	—	0.02	3.45	0.77
12	Borosilicate—tungsten sealing	0.13	—	—	Completely leached	3.87	1.4
13	Aluminosilicate	0.003	0.06	9.1	0.35	0.35	0.17
14	Special—alkali resistant	—	0.05	—	0.008	0.09	0.03

^aFrom Shand.^{1,2}^bWeight loss in mg/cm² of exposed surface.^cExpressed as % Na₂O extracted.^dAlkalinity of water, pH⁺ after 2 hr at 121°C.

procedure will vary as a function of type of glass, its rate of attack, and the reagent employed.

Table 1 gives weight loss data for several glasses under attack by 5% hydrochloric acid, 5% sodium hydroxide, and 0.02 *N* sodium carbonate.¹² Figure 3 shows plots for water attack on a number of glasses at elevated temperatures.¹³ Increasing temperatures from 120 to 170°C reverses the rate of attack on glasses A and B, a phenomenon also observed when changes are made in the alkali concentrations of a given reagent.

The advantages of the weight loss test are that total loss of material (not just alkali) is measured, and that the measured loss is determined as a function of the (geometric) glass surface area available for attack.

SOLUBILITY OF SILICA

As silica is the major component of most important glasses, the solubility of silica would appear to be a primary parameter in any discussion of glass corrosion. In general, however, silica is only slightly soluble in aqueous solutions below pH 8. A complete discussion of silica solubility can be found in the work of Stöber¹⁴ and the review by Eitel.¹⁵ The major problem in determining the thermodynamic constants lies in the formation of polymeric silicic acids after dissolution and the effect of these soluble polymers on further equilibrium. As far as this chapter is concerned, the general considerations necessary for further discussion are summarized in Fig. 4. In

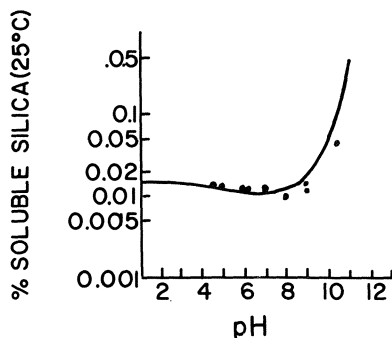


Fig. 4. Equilibrium concentration of molybdate-reactive silicic acid as a function of pH. (Data taken from Eitel.¹⁶)

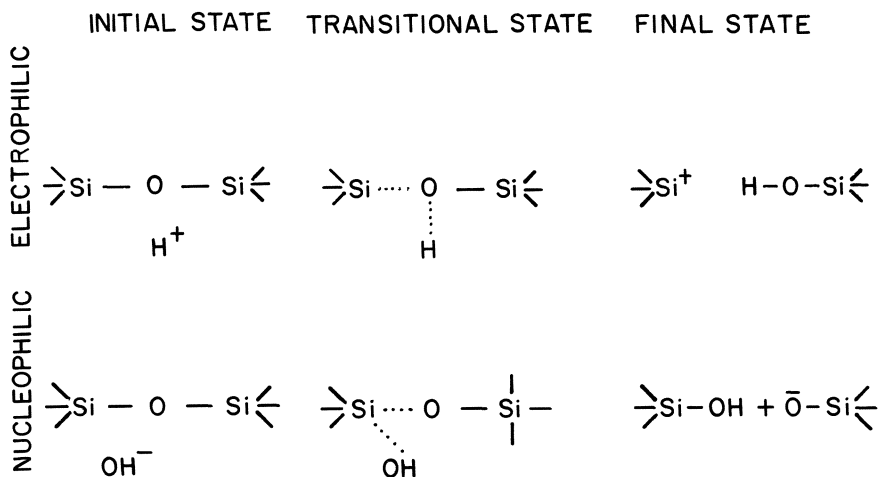


Fig. 5. Diagrammatic representation of electrophilic and nucleophilic attack on Si—O—Si bond.

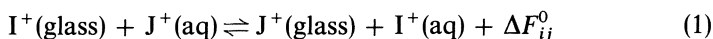
the diagram the percentage of soluble silica is plotted as a function of pH (the soluble silica being defined as that which is reactive with molybdate in the usual quantitative test). It can be seen that in acid solutions the silica shows essentially a small constant solubility, whereas in alkaline solutions the solubility rises rapidly with pH as soluble sodium silicates are formed. The general reaction can be understood in terms of electrophilic or nucleophilic attack on the siloxane bridges (Fig. 5). It is readily apparent that electrophilic attack on the acidic siloxane bridge is unlikely and that dissolution in acid solutions will be a slow process. Nucleophilic attack, however, can occur very readily and accounts for the increased solubility in alkaline solutions.

More recent work on the dissolution of silica, in particular the kinetics of the solution of silica in aqueous solutions, can be found in Alexander *et al.*¹⁷ and O'Connor and Greenberg.¹⁸

GLASS STRUCTURE AND ION SELECTIVITY

In any discussion of a system involving aqueous solution and a glass containing alkali metal ions, it is obvious that the ion-exchange reaction which occurs at the surface of the glass, and in which the alkali metal ion is exchanged for a proton, is of the utmost importance. For instance, should we

be able to explain why sodium-containing glasses of one composition are more soluble than potassium-containing glasses of the same molecular composition? The problem of relating glass composition to ion exchange has been tackled extensively by Eisenman and coworkers. Following the arguments of Eisenman,^{19,20} the competing interactions of cations with the glass versus water can be represented by an ion exchange reaction,



where I^+ and J^+ represent two cationic species in the glass and in dilute aqueous solution. The standard free energy change of the reaction ΔF_{ij}^0 is given by the equations

$$\Delta F_{ij}^0 = -RT \ln K_n = -RT \ln \left(\frac{[I^+]}{[J^+]} \right) \left[\frac{J_{(\text{glass})}^+}{I_{(\text{glass})}^+} \right]^n \quad (2)$$

$$\Delta F_{ij}^0 = \bar{F}_{I^+(\text{hyd})} - \bar{F}_{J^+(\text{glass})} - \bar{F}_{I^+(\text{glass})} \quad (3)$$

where \bar{F} represents the partial molal free energy of either hydration or interaction with the glass and n is defined after Rothmund and Kornfield. The first two terms on the right-hand side of equation (3) are known from

Table 2. Electrostatic-Free Energy Data

	Electrostatic energies with site, kcal/mole	Differences of electrostatic energies referred to Cs^+ , kcal/mole	$\bar{F}_{I^+(\text{hyd})} - \bar{F}_{\text{Cs}^+(\text{hyd})}$ experimental, kcal/mole	ΔF_{ij}^0 , kcal/mole	r^- , Å
SiO^- site					
H^+	-493.2	-359.1	-192.673	+166.427	1.07
Li^+	-220.4	-86.3	-54.299	+32.001	0.91
Na^+	-183.2	-49.1	-30.393	+18.707	0.86
K^+	-153.8	-19.7	-12.745	+6.955	0.83
Rb^+	-145.3	-11.2	-7.679	+3.521	0.81
Cs^+	-134.1	0	9	9	0.79
$(\text{ALOSi})^-$ site					
H^+	-200	-105.3	-192.673	-87.373	2.0
Li^+	-123.1	-28.4	-54.299	-25.899	2.1
Na^+	-115.3	-20.6	-30.393	-9.793	1.93
K^+	-104.3	-9.6	-12.745	-3.145	1.85
Rb^+	-100.2	-5.5	-7.679	-2.179	1.83
Cs^+	-94.7	0	0	0	1.82

the literature and are recorded in the third column of Table 2. The second two terms on the right-hand side of equation (3), however, must depend upon the glass composition.

Eisenman points out that the partial molal free energy can be estimated if it is assumed that the sites in the glass can be approximated by a simple monopolar site, as shown in Fig. 6. The actual atomic structure of the site of cation exchange in an alkali silicate glass is diagramed in Fig. 6a and is referred to as an SiO^- -type site. In Fig. 6c the exchange site is one in which a triply charged ion has replaced some of the Si^{4+} in fourfold coordination and is referred to as an $(\text{AlOSi})^-$ -type site. In the simplest electrostatic picture (i.e., as considered by Pauling²¹) the complex ions can be considered in terms of equivalent monopolar sites, as shown in Fig. 6b and Fig. 6d. Such calculations by Pauling for the silicate anion H_3SiO_4^- show that the proton can be represented by a single positive charge with a radius of 0.4 \AA .

Table 2 shows the values of free energies calculated for the ion exchange interaction using this type of model and the equivalent radius of the SiO^- and $(\text{AlOSi})^-$ sites when "screened" by the various cations. Note that the $(\text{AlOSi})^-$ site has a much larger equivalent radius than the SiO^- site, owing to its higher acidity and lower effective field strength. The interesting feature is the prediction regarding the order of ion selectivity as we go from the SiO^- site to the $(\text{AlOSi})^-$ site, the former being selective to H^+ over Cs^+ , the latter

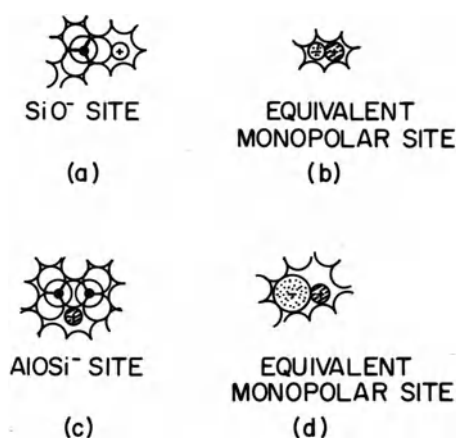


Fig. 6. Ion exchange sites in sodium aluminosilicate glasses and the equivalent monopolar sites. (After Eisenman.¹⁷)

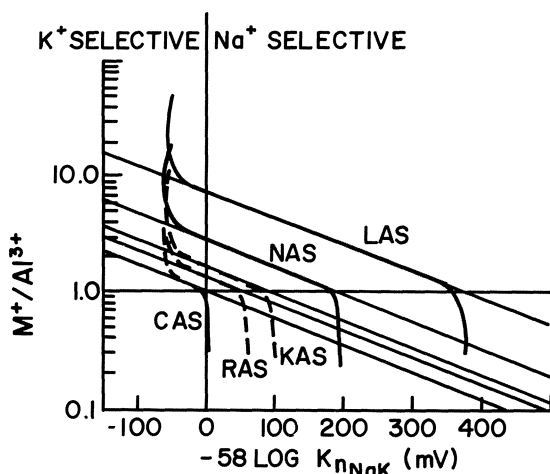


Fig. 7. Electrochemical selectivity as a function of glass composition for a series of alkali aluminosilicate glasses.

being preferentially selective to Cs^+ over H^+ . These simple calculations are the basis of Eisenman's selectivity rules. Following an approach originally due to Fajans²² and Weyl and Marboe,²³ Eisenman argues that the addition of cations to the glass "screens" the site, and thus there is a dependence of field strength on the $\text{M}^+/\text{Al}^{3+}$ ratio. As Na^+ is added to the glass, it will decrease the field strength (increase r^-) and become more responsive to K^+/Na^+ ions. This thesis finds approval in Fig. 7, where the electrochemical selectivity of a series of alkali metal aluminosilicate glasses is plotted as a function of the $\text{M}^+/\text{Al}^{3+}$ ratio in the glass. Note the abrupt change in properties when $\text{M}^+/\text{Al}^{3+} = 1$.

Application of this reasoning to the effect of glass structure on solubility predicts that for a constant $\text{M}^+/\text{Al}^{3+}$ ratio, a sodium-containing glass would have sites of lower field strength (i.e., show a preference for K^+ rather than Na^+) and presumably would be less susceptible to attack by protons. Similarly, it can be argued that B^{3+} in a borosilicate glass, because it is smaller than Al^{3+} and has a more intense field, would produce a lower field strength site than the corresponding aluminosilicate. Thus, the introduction of boron into a glass in place of aluminum should make it less susceptible to attack by protons and presumably more stable in acid solutions.

Although these ideas as expounded by Eisenman are of great help in considering a molecular approach to ion exchange, they are subject to some

criticism, as they ignore the possibility of phase separation and hydration. Also, the “proof” of the hypothesis (namely, the electrochemical selectivities that have been obtained) has been determined on glass samples many of which had been exposed to aqueous solution for several weeks before their electrochemical properties were stabilized!

CHEMICAL ATTACK ON GLASS

General Considerations

To understand the chemical durability of glasses, it is important to become familiar with the mechanism of glass hydrolysis by such agents as water, steam, acids, alkalis, and salts.

We have seen that silica is readily attacked by alkali, but rarely, if at all, by acids. When water acts on a glass, the glass is not “dissolved” but is hydrolytically decomposed. In this case we are concerned with hydrolysis of $\text{Si}-\text{O}-\text{R}$ bonds rather than $\text{Si}-\text{O}-\text{Si}$ bonds. R, the alkali or alkaline earth ion (Na^+ , Ca^{2+} , etc.), can now form a water soluble salt which passes into the hydrolytic residue and is replaced by an H^+ or H_3O^+ ion. The original $\text{Si}-\text{O}-\text{R}$ bond is therefore converted to $\text{Si}-\text{O}-\text{H}$, and a surface gel forms which contains both the original $\text{Si}-\text{O}-\text{Si}$ bonds and the newly formed $\text{Si}-\text{OH}$ bonds. Penetration of H^+ farther into the glass structure is thus a diffusion process and, *in principle*, the hydrolysis might be expected to increase with time according to the diffusion law. As the alkali content in the glass is increased, more $\text{Si}-\text{OH}$ bonds are formed and the rate of dissolution should increase. (But it should be noted that if the increased quantity of alkaline hydrolysis products is not removed from the glass surface, a process resembling the attack of alkalis will then occur that will nullify the simple kinetic argument.)

Below pH 7, alkali or alkaline earth ions are replaced by H^+ , but the original glass backbone structure, the $\text{Si}-\text{O}-\text{Si}$ bonds, is unaffected. Alkali solutions, on the other hand, will be expected to break $\text{Si}-\text{O}-\text{Si}$ chains to form both $-\text{Si}-\text{O}-\text{Na}$ and $\text{Si}-\text{OH}$ groups. Alkali attack will thus be more intensive than either water or acid attack, and simple diffusion kinetics are not usually observed. In this case the dependence of the amount of leached matter with time is often linear. Leaching of the glass with acid can *increase* the chemical durability of the surface, whereas leaching with alkali cannot. (Note, however, that both hydrofluoric and phosphorous acid will

attack glass in the same manner as alkali since both acids affect the —Si—O—Si— chains.)

Perhaps the best experimental data on the decomposition of glasses by aqueous solution have come from Douglas and coworkers.^{24–31} In unbuffered solutions, for instance, Douglas and El-Shamy²⁸ have shown that the rate of removal of alkali can generally be expressed by the equation $Q = kt^\alpha$, where Q is the quantity of alkali extracted in time t and K is a constant. In unbuffered solutions, at very short times and low temperatures, α was equal to $\frac{1}{2}$ but approached 1 at long times and higher temperatures.^{25–27} For durable binary alkali oxide–silica glasses, α remained near $\frac{1}{2}$ even at high temperatures and for long times, whereas it rapidly attained its value of unity with less-durable glasses.

El-Shamy *et al.*³¹ have recently published data on the kinetics of the reaction of water with glass, emphasizing the dependence on pH, in this case in buffered pH solutions. The rates of removal of alkali, lime, and silica for a series of simple alkali oxide–silica and soda-lime-silica glasses were investigated as a function of both pH and glass composition. The pH range covered was from 1 to 13. At low pH values⁹ the rate of alkali extraction was essentially constant and independent of the pH of the solution. Above pH 9, however, the rate decreased with increasing pH, except for glasses containing more than 10% calcium oxide. In that case the rate increased rapidly with decreasing pH, below about pH 3. This increase was accompanied by an extraction of lime from the glass, an effect that was negligible in the other experiments.

In the above experiments, the extraction of silica varied with pH of the solution in a manner opposite to that of alkali, being very low and constant at pH values below 9 and increasing thereafter with increasing pH. These results were interpreted by El-Shamy *et al.* in terms of an equilibrium assumed to exist at the interface between hydrogen ions in the solution and various hydroxylated surface silicon atoms.

Corrosive attack on glass surfaces by salt solutions is more complicated than similar attack by acids or bases, as the rate of surface attack can also depend on the catalyzing effect of specific ions present. Certain salts, especially those of zinc, aluminum, and beryllium, if present even in trace amounts in a leaching solution, can act as poisons and retard the leaching process. The mechanism for this is not known, but it is probably due to adsorption of hydrated ions, which can reverse the normal negative charge on the glass surface.

Budd⁹ has discussed chemical attack on silicate glasses in terms of electrophilic reagents (those which seek to attack positions of excess electrons)

or nucleophilic reagents (those which seek areas of electron deficiency), i.e.,

O^{2-}	strongly nucleophilic
OH^{-}	strongly nucleophilic
F^{-}	moderately nucleophilic
H^{+}	strongly electrophilic

Because of the electronegativity difference between Si and O, the electrons are more tightly bonded to the oxygen, leaving the Si with an effective positive charge, which is then a center of nucleophilic attack. Although the network modifiers are not a part of the chemical reaction, they do, because of their screening effect, affect the rate of the reaction. The general considerations are summarized in Fig. 5.

Water and Steam

As we have seen, silica is almost insoluble in an aqueous environment except at temperatures in excess of 250°C. The attack of glass by water is thus primarily due to the existence in the glass structure of the soluble (and ion exchangeable?) components, such as alkali. Commercial glasses of the sodium silicate type are far less durable than silica glass under most conditions. The alkali oxide “fluxes,” such as Na_2O and K_2O , are not considered part of the silica network but remain in “holes” in the glass structure (Figs. 1 and 2), where they retain some degree of mobility and therefore can be extracted. The addition of modifying oxides, such as CaO , MgO , Al_2O_3 , and B_2O_3 , cause the formation of low field strength sites which reduce the diffusion coefficient of alkali ions and increase the durability of the glass. Dissolution of the alkali in glass, however, does raise the alkalinity of an aqueous solvent so that other glass components will then be subject to nucleophilic attack. When acid oxides such as B_2O_3 are present in the glass, they are also extracted, neutralize the alkali, and reduce the nucleophilic attack. Nordberg³² has presented examples of this occurrence using powdered glass specimens (250–400 μm) heated in water at 120°C for 1 hr. With 10 g of glass in 100 ml of water, soda-lime glass raised the pH of the water to above 11, whereas low-expansion borosilicate glass (Corning code 7740) increased it only to 8.5.

Table 3 presents a classification of various glass compositions according to their water resistance. Glasses marked “excellent” will normally be chemically resistant to water at temperatures under 100°C, whereas glasses classified “fair to poor” have limited application. Figures 8 and 9 are electron micrographs of the surface of a soda-lime glass before and after washing with water³³ and illustrate the corrosive effect.

Table 3. Water Resistance of Glasses^a

Grading	Glass type	Corning code No.
Excellent	Silica	7940
	96 % Silica	7900
	Durable borosilicate	7740, 7331, 7800
	Aluminosilicate	1710, 1720, 1723
	High lead	8870
Good	Soda-lime	0080
	Alkali lead	0010, 0120
	Lead borosilicate	7720
	Borosilicate sealing	7052, 7055
	High alkali	—
Fair to poor	Borosilicate sealing	7040, 7050
	Calcium aluminate	—
	Phosphate	—
	Borate	—

^aAfter Nordberg.³²

Taylor and Smith,¹³ using the glass compositions shown in Fig. 10, measured the weight of material extracted from the glass when distilled water was heated to 260°C in sealed tubes for 6 hr. The material extracted was measured by evaporating the water and weighing the residue. The results are shown in Fig. 10. The high-lead glass (E) showed the least attack at high temperatures, and this was attributed to the formation of a protective film on the surface of the glass. No silica was found in the extracted material. When the glasses were tested under erosive conditions, however (such as tubular condensers exposed to escaping steam for 100 hr), the lead glass (E) lost 13 times as much glass as the borosilicate glass (A). Although borosilicate glasses are, therefore, used for boiler gages because of their durability and clarity after attack, even this glass finally becomes deeply etched under erosive conditions, and there is at present no totally satisfactory glass for this application.

References 34–49 are a series of papers related to the effect of water on glasses of various types.

Acid Solutions

With most silicate glasses the acidity of the solution has little effect on the corrosion. Alkali and basic oxide components are dissolved to yield a highly siliceous surface layer, which then resists further chemical attack,



Fig. 8. Surface of fractured soda-lime glass.

and the dissolved base components are neutralized by the acid solution. Soda-lime compositions (used as plate glass) and borosilicate compositions (laboratory ware) both readily form such protective films on their surface, and acid attack is minimal.⁵⁰ The increased porosity and the new surface composition can, however, have gross effects on adsorption properties (Hair⁵¹).

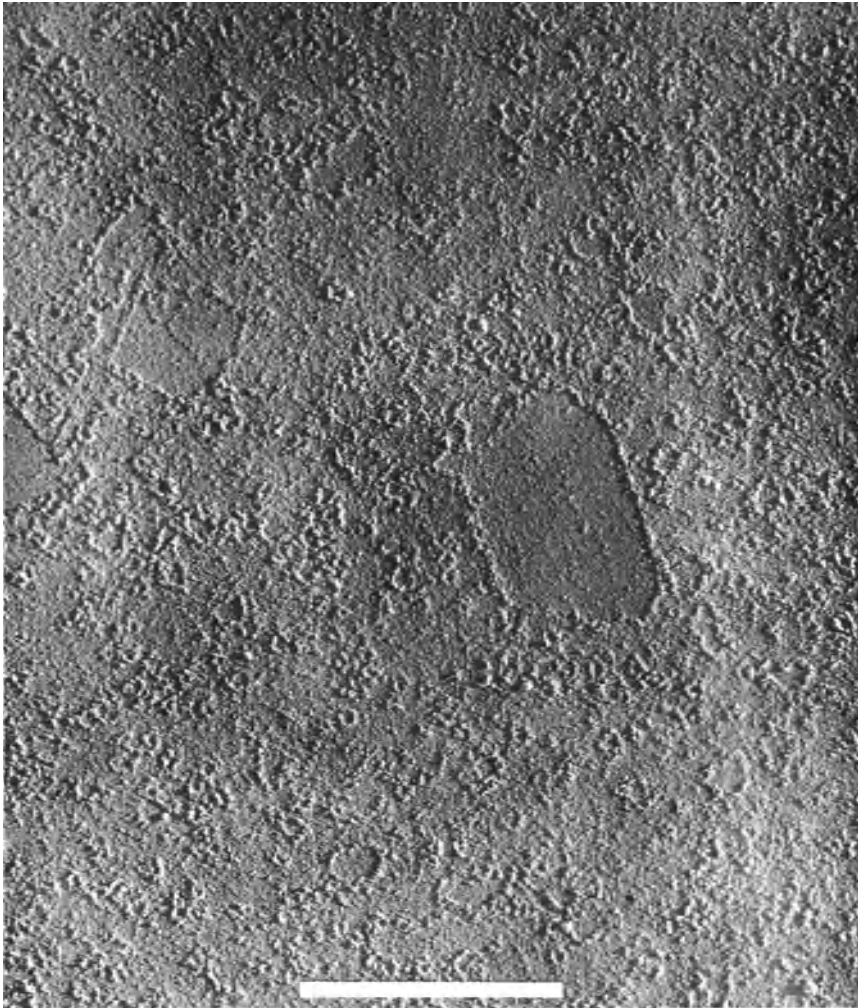


Fig. 9. Surface of soda-lime glass washed with water.

On the other hand, some optical glasses, such as the dense barium crowns, are readily attacked by weak acids (acetic, boric, and phosphoric acids), but this is primarily due to their lower silicate content. Large quantities of barium, lead, and other heavy metal oxides are added to such glasses to obtain specified optical properties, and it is the ready solubility of these

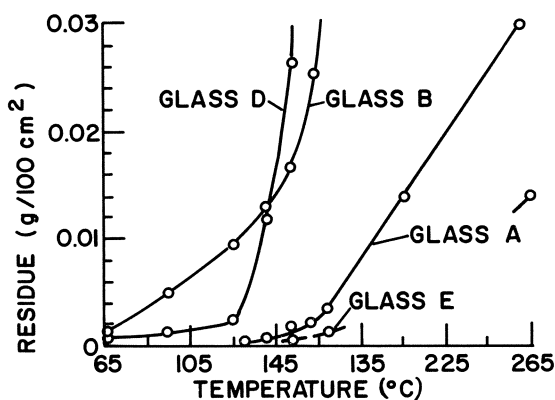


Fig. 10. Material removed at high temperatures from sealed glass tubes exposed to distilled water. (A) borosilicate; (B) soda-lime silicate; (C) high-soda-lime silicate (similar to but more residue than B at temperature); (D) lead-silicate; (E) high-lead silicate. (After Taylor and Smith.¹³)

oxides that greatly reduces durability with regard to both weak and strong acids.

The mineral acids generally do not react with silicate glasses of reasonable SiO_2 content and are normally contained in such bottles. Lower- SiO_2 -containing glasses are attacked, however. This is shown in Fig. 11 for HCl attack at two temperatures.⁵² Hydrofluoric acid is the outstanding exception

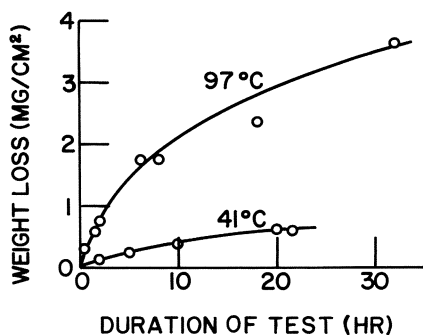


Fig. 11. Solubility of a glass of low durability (sodium silicate) in 5% HCl versus time.

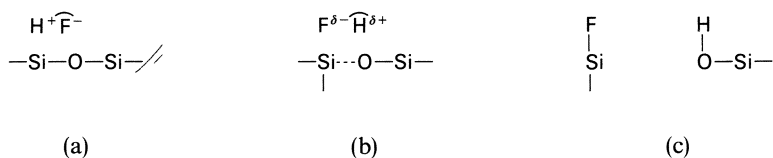


Fig. 12. Hydrofluoric acid attack on Si—O—Si bond.

to this general rule, and it attacks silicate glasses very readily. As with other acids, the nonbridging oxygens are presumably attacked by protons to form silanol groups, but the reaction rate is increased as a result of the simultaneous attack of the F^- ion on the silicate structure, as shown in Fig. 12.⁵³ The highly electronegative fluorine atom is also known to readily replace hydroxyl groups on a silica surface.⁵⁴

Phosphoric acid reacts with silicate glasses at elevated temperatures, but chemical reaction is only slight below 250°C . Nordberg's summary of the acid durability of a series of selected glasses is shown in Table 4. Figures 13–15 are electron micrographs of the surface of soda-lime glasses that have been washed with nitric, hydrofluoric, or phosphoric acid.³³ Figure 13 shows the surface of a piece of soda-lime glass which had been washed by boiling in dilute nitric acid for 10 min. The large masses of soluble material are gone, and there is some smoothing action, but craters remain in the glass surface. The same result is seen after treating the same glass in boiling solutions of dilute sulfuric, hydrochloric, or perchloric acid.

Figure 14 shows the surface of a piece of soda-lime glass that has been washed by boiling in 1% hydrofluoric acid for 1 min. The craters are gone as well as the large masses of soluble material. The hydrofluoric acid has removed the surface layer uniformly, leaving a flat stratum in place of the rough-textured one, and producing a surface nearly identical to that of a freshly fractured sample (see Fig. 8).

Figure 15 shows the surface appearance of soda-lime glass that has been washed by boiling in 1% phosphoric acid for 10 min. The result is similar to that seen in Fig. 14, but the slight roughness on the surface suggests that the surface corrosion has not proceeded as far as it has in Fig. 14.

A combination of acid attacks can be used to produce glass surfaces with a desired texture. Thus, a mixture of HF and H_2SO_4 has been used on $\text{Na}_2\text{O--SiO}_2$ glass chromatography beads⁵⁵ to produce the "raspberry" effect shown in Fig. 16.

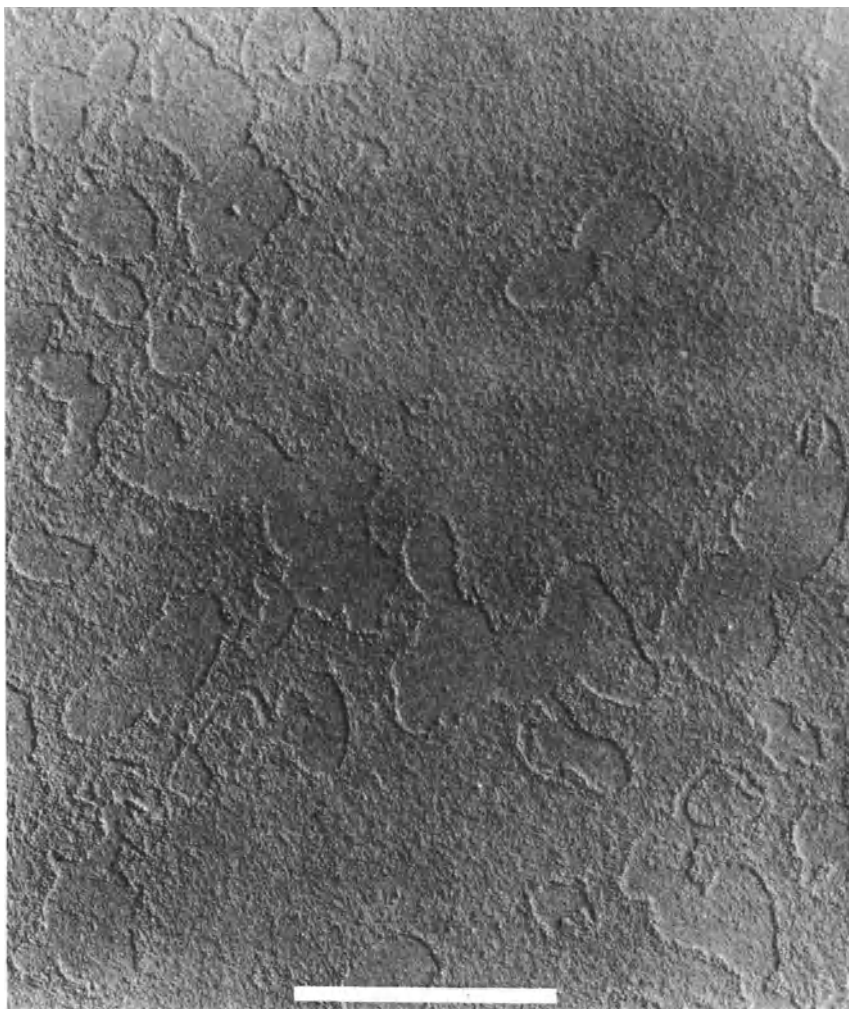


Fig. 13. Surface of soda-lime glass washed with nitric acid.

Further information regarding acid attack on glass can be found in references 56–66 (see also references 47–49).

Alkaline Solutions

As might be expected from data on the solubility of silica, it is found that basic solutions corrode silicate glasses more extensively than either neutral

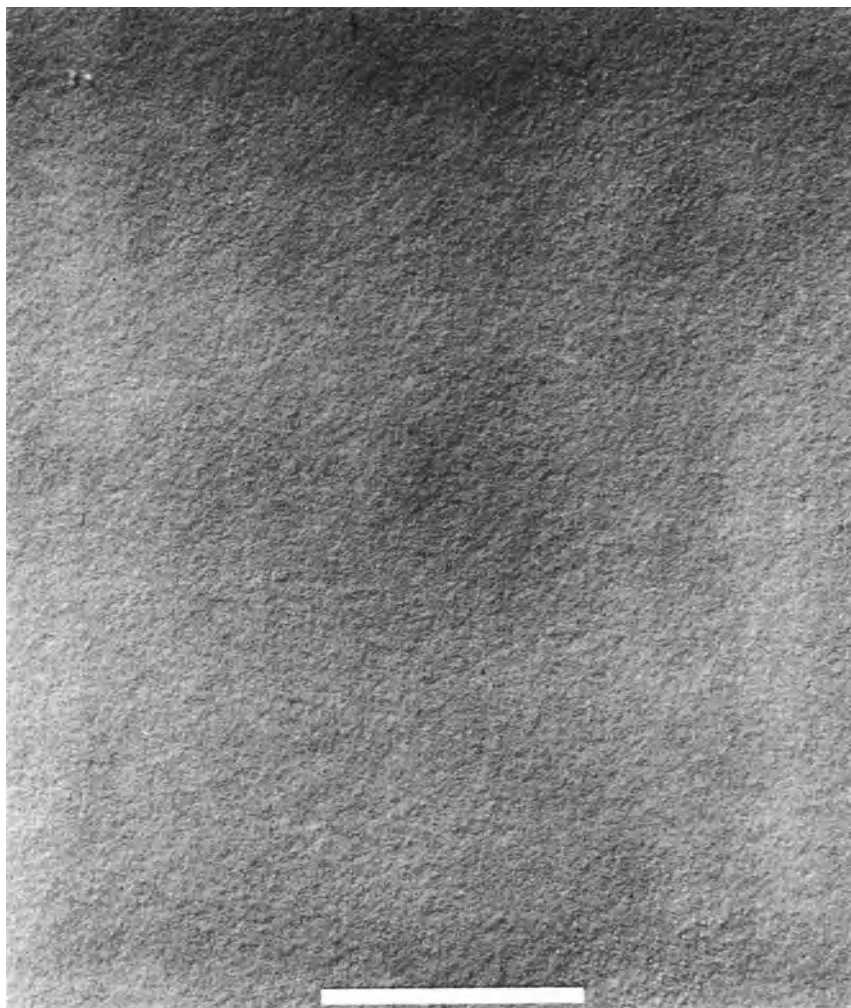


Fig. 14. Surface of soda-lime glass washed with hydrofluoric acid.

or acid solutions, the alkali providing hydroxyl ions for nucleophilic attack of the silica network.^{52–55} A protective high-silica layer is not formed in this case, and dissolution of the glass proceeds at a fairly constant rate. For instance, the rate of attack of a soda-lime glass by a 5% solution of sodium hydroxide at 95°C is linear with time, as shown in Fig. 17.¹²

Neutral corroding solutions will often increase in basicity as a result of

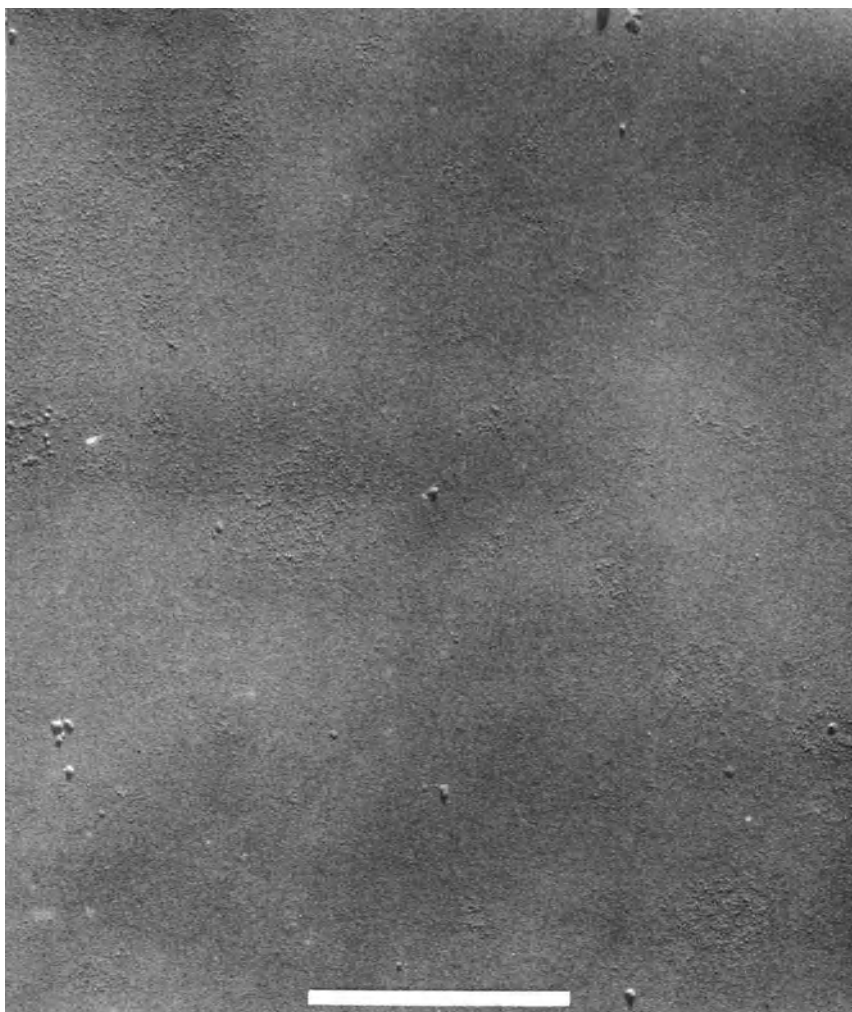


Fig. 15. Surface of soda-lime glass washed with phosphoric acid.

the dissolution of alkalis from the particular glass under consideration, and thus their corrosion of the glass surface will be greater than might be expected from simple pH considerations and the kinetics will also change with time. The increase in solution pH will depend not only on its original value but also on the total chemical constitution of the glass. The effect of solution pH on relative attack rate on a low-expansion borosilicate glass is

Table 4. Acid Durability of a Range of Glasses^a

Corning No.	Glass type	Plate test: 24 hr, 5 % HCl, 100°C; weight loss, mg/cm ²	Powder test: . 4 hr, N/50 H ₂ SO ₄ , 90°C (% Na ₂ O)
7900	96 % Silica	0.0004	—
7740	Borosilicate—chemical	0.005	0.005
7280	Alkali resistant	0.01	0.05
0080	Soda-lime—bulb	0.01	0.08
0010	Lead glass—electrical	0.02	0.15
1720	Aluminosilicate	0.35	0.06
7050	Borosilicate—tungsten sealing	Leached	—
8870	High lead	Disintegrated	—

^aAfter Nordberg.^{3,2}

shown in Fig. 18. It should be noted, however, that as basic solutions dissolve silica, and the concentration of silica in solution increases, a decrease in general attack rate is noted.^{12,13}

Table 5 presents data on the alkali durability of a series of glasses exposed to 5% sodium hydroxide solution for 6 hr at 100°C. Included in the

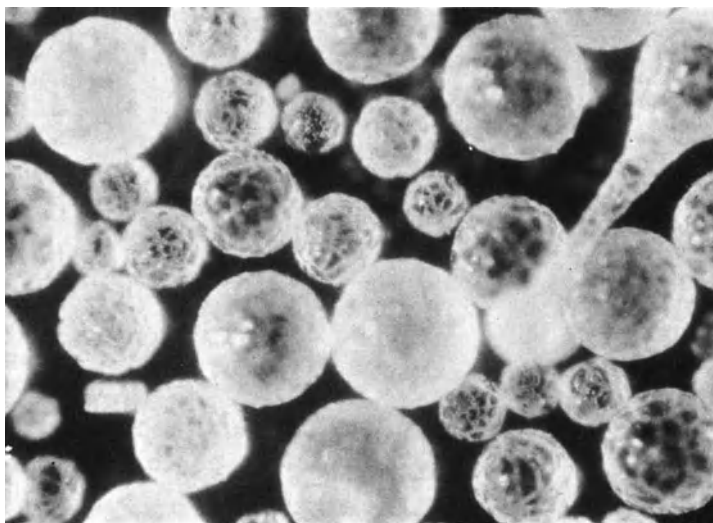


Fig. 16. "Raspberry" effect produced by combined HF/H₂SO₄ attack on Na₂O/SiO₂ glass chromatography beads. (From Eaton and MacDonell.⁵⁵)

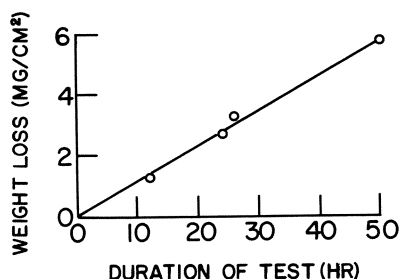


Fig. 17. Solubility of a soda-lime glass in 5% NaOH at 95°C versus time. (From Shand.¹²)

series is a glass specifically designed to make it alkali resistant by the addition of zirconia.

Figure 19 is an electron micrograph of a piece of soda-lime glass that has been washed by boiling in 1% sodium hydroxide solution for 10 min.¹⁴ The large attacked masses are readily observed as evidence of corrosion on

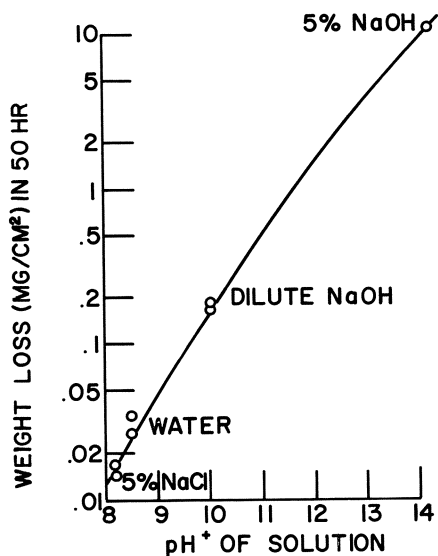


Fig. 18. Durability of low-expansion borosilicate glass versus pH of the reagent at a temperature of 95°C. (From Shand.¹²)

Table 5. Alkali Durability of a Range of Glasses^a

Corning code No.	Glass type	6 hr, 5 % NaOH, 100°C; weight loss, mg/cm ²
7900	96 % Silica	0.9
7740	Borosilicate	1.4
0080	Soda-lime—bulb	1.1
0010	Lead glass—electrical	1.6
7050	Borosilicate—tungsten sealing	3.9
8870	High lead	3.6
1710	Aluminosilicate	0.35
7280	Alkali resistant	0.09

^aAfter Nordberg.^{3,2}

the glass structure itself. Such alkaline attack is graphically displayed in Fig. 20, where the rate of attack by such reagents increases rapidly with increasing temperature at a rate of approximately $2\frac{1}{2}$ times for every 10°C. For the alkaline solutions of low concentration, the attack rate increases with concentration, but at high alkaline concentrations, a maximum attack rate is attained.¹² Figure 21 shows the rates of attack by NaOH of a sodium borosilicate glass at various temperatures.

For further information on the alkali attack of glasses, the reader is referred to references 66–69.

Chelating Agents

Although there are many data available dealing with the attack of glass by different kinds of chemical reagents (see reference 8 and Table 6), relatively little study has been directed toward investigating attack by chelating agents. One exception is a classic paper by Ernsberger.⁷⁰ He suggested that chelating agents, which might be expected to influence the rate of attack of plate glass by aqueous solution, would include those which can complex with cations of the glass, i.e., with Si^{4+} , Al^{3+} , or Mg^{2+} . If the resultant complex is water soluble, one would expect the rate of attack to be faster than that observed with the same solution in the absence of the chelating agent. If insoluble, a decrease in rate should be observed.

Since weight loss methods could not be employed in these studies, interferometric techniques were used. The effect of pH on the rate at 100°C is shown in Fig. 22. The addition of the chelating agents ethylenediamine-

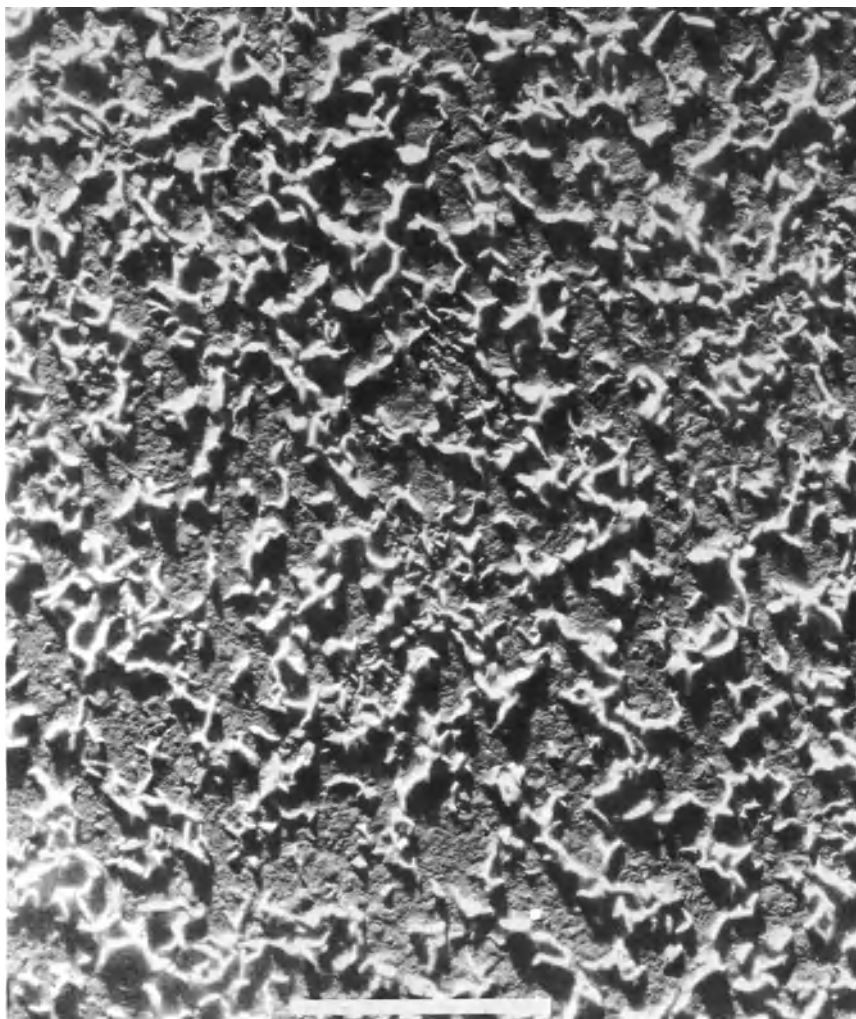


Fig. 19. Surface of soda-lime glass washed with sodium hydroxide.

tetracetic acid (EDTA) and catechol sodium acetate increases the rate and shows a maximum attack to take place at pH 12.5. It can be seen from Fig. 23 that carbonates and phosphates shift the pH of maximum attack rate.

The effect of the chelating agent EDTA is to remove aluminum, magnesium, and calcium ions in the form of soluble complexes, and in so doing to

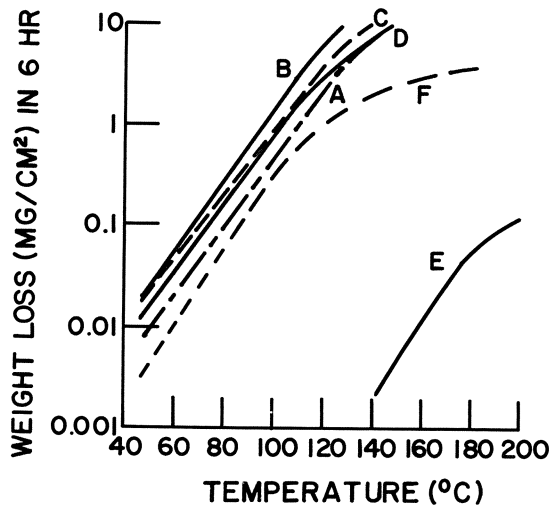


Fig. 20. Solubility of glasses in various alkali solutions and in distilled water. Low-expansion borosilicate glass: (A) in 1% NaOH; (B) in 5% NaOH; (C) in 6.9% KOH; (D) in 5% Na₂CO₃; (E) in distilled water. Alkali-resisting glass: (F) in 5% NaOH. (From Shand.¹²)

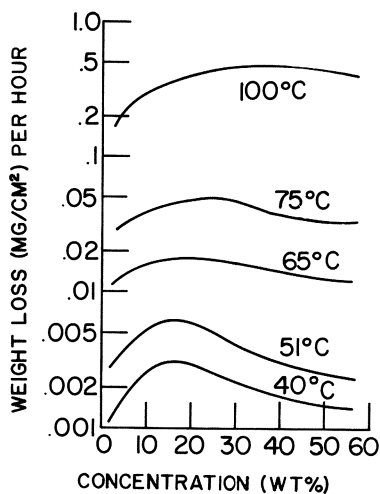


Fig. 21. Rates of attack by NaOH at different temperatures as a function of concentration on a low-expansion borosilicate glass. (From Shand.¹²)

Table 6. Chemical Corrosion of Glass, Applies Only to Highly Durable Compositions^a

Type of reagent	Temp., °C	Degree of attack ^b	Remarks
Water	To boil	Negligible	Will not absorb or swell
	Elevated	See Fig. 3-6	
Sea water—5% sea salt	Boil	Loss 0.03–0.08 mg/cm ² , 24 hr	1 yr in ocean, no visible effect
Acids			
HF	All	Severe attack	Not recommended
H ₃ PO ₄	100	21% H ₃ PO ₄ , loss 0.005 mg/cm ² , 24 hr	Glass satisfactory except at high conception; exception: raw acid with fluorides
	100	85% H ₃ PO ₄ , loss 0.014 mg/cm ² , 24 hr	
Other inorganic	Boil	Negligible, 5% HCl; Table 3-2	
Organic		Negligible	
Bases			
Strong		NaOH; Figs. 3-4, 3-5, Table 3-2	
		KOH; Fig. 3-4	
Weak	80	NH ₄ OH, max. attack, 3% solution, 0.33 mg/cm ² , 100 hr	
Halogens	To 150	Negligible	Dry fluorine questionable
Metal salts			
Acid	To 150	Negligible	
Neutral	To 150	Negligible	
Basic	100	N/50 Na ₂ CO ₃ ; Table 3-2	
	150	5% Na ₂ CO ₃ ; Fig. 3-4	
Inorganic nonmetallic halides	To 150	Negligible	Fluorides excepted
Sulfur dioxide	To 150	Negligible	Slight bloom may appear on surface
Ammonia (dry)	To 150	Negligible	Ammonium hydroxide
Oxidizing chemicals	To 150	Negligible	(see Bases)
Reducing chemicals	To 150	Negligible	
Hydrocarbons	To 150	Negligible	Includes chlorinated hydrocarbons
Amines	To 150	Negligible	Amines with pro- nounced basic reaction questionable
Polyhydroxy aliphatics	To 150	Negligible	
Mercaptans	To 150	Negligible	
Oils and fats	To 150	Negligible	

^aFrom Shand,^{1,2} p. 92. Figures and tables are those in Shand.^bA weight loss of 1 mg/cm² is equivalent to a depth loss of 0.01 mm/(glass density) or 0.0004 inch/(glass density) for those cases where the attack is not selective.

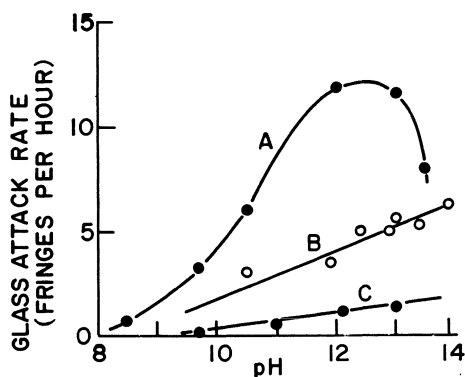


Fig. 22. Attack rate as a function of pH for plate glass in (A) 0.2% EDTA 0.4% catechol; (B) 0.2% EDTA; (C) 0.5 *M* sodium acetate. In each case, the pH was adjusted by addition of saturated aqueous NaOH. Temperature 100°C. (From Wichers.⁶⁰)

negate any protective action normally observed with these ions. Since catechol is sterically adapted to react with the silicon, there is also an increase in the rate at which silicon atoms are removed from the glass network. Consequently, the rate of dissolution for the catechol/EDTA solution is greater than that for the EDTA alone.

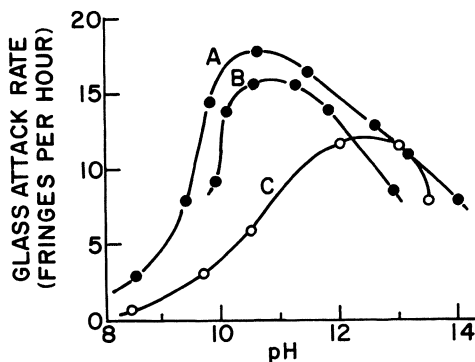


Fig. 23. Attack rate as a function of pH for plate glass in (A) 0.5 *M* sodium phosphate, 0.2% EDTA, and 0.4% catechol; (B) 0.5 *M* sodium carbonate, 0.2% EDTA, and 0.4% catechol; (C) curve for comparison. Temperature 100°C. (From Wichers.⁶⁰)

Sulfur Dioxide and Sulfur Trioxide

Just as alkali can be removed from glass by reaction with water, other reagents which can interact with Na^+ will tend to bring about a surface reaction or proton exchange. Thus, SO_2 will interact with alkali in glasses to form sulfates and give an alkali-depleted surface layer. This reaction has been carefully studied by Douglas and Isard,⁷¹ who determined the kinetics at several temperatures. Between 20 and 100°C, in SO_2 saturated with water vapor, the reaction is limited by the rate of diffusion of sodium ions to the surface. The reaction is an ion exchange, involving the same process, and proceeds at the same velocity as the reaction with water. Between 100 and 600°C, and in atmospheres not saturated with water vapor, the SO_2 reaction is limited by the rate of diffusion of sodium through a compacted surface layer which arises from a secondary dehydration process. With completely anhydrous agents the SO_2 reaction involves the simultaneous diffusion of sodium and oxygen ions to the glass surface, and the speed is limited by the rate of diffusion of the oxygen ions. Above about 700°C this process predominates over ion exchange. As a result of this reaction, sodium sulfate is formed on the surface of the glass; this is the “bloom” which is often found on the surface of sodium-lime glasses.

It is interesting to note that the water solubility of bottles and other glass articles which are annealed in open-fired and muffle furnaces, where the glass is exposed to furnace fumes, is greatly reduced. The strength is also increased. It is known that removal of soda from a glass surface at an elevated temperature can, on cooling, give appreciable strengthening due to a lowering of the expansion coefficient of the surface layer. Mochel and Nordberg⁷² have reported that rate of soda depletion of glasses, previously accomplished by treating with SO_2 in the presence of oxygen and water, can be doubled if a platinum catalyst is used to catalyze the oxidation of SO_2 to SO_3 before the gas reacts with the glass. In this case the soda depletion follows Fickian diffusion laws both with and without the catalyst, and the energy of activation is the same for both reactions. Again, alumina plays an important role in the process. The presence of alumina in the glass causes a marked increase in the strength that can be obtained by the SO_2/SO_3 treatment. Although the percentage of soda retained in the leached layer increases as the alumina is increased, the total amount of soda removed from the glass also increases, indicating that the depiction depth was greater.

Ion Exchange in Molten Salts

As mentioned above, ion exchange reactions at the surface of a glass can be used to give increased mechanical strength to the material. A larger alkali metal ion is substituted for a similar ion of smaller radius, usually by immersing the glass article in a molten salt bath somewhat below the annealing temperature; i.e., Na^+ is inserted into the surface layer of a Li^+ -containing glass by immersion in a molten NaNO_3 bath. Because of its commercial implications, many scientific data have been generated on this process over the last two decades, and several reports are available.^{73–75} For the purpose of this chapter, we merely want to acquaint readers with the possibility that the process has been applied to the glass they are interested in, and point out again that the solubility of the glass in this case will depend upon the character of the stressed surface layer and bear little resemblance to that of the published composition.

PHASE SEPARATION

In the preceding discussions concerning the chemical interactions which occur when glasses are corroded, it is implied that the glass is a uniform, single phase structure that can be represented by the chemical composition. It is becoming very obvious that this is not true and that many, if not most, glasses are, in fact, two-phase systems. This is particularly exemplified by the sodium borosilicate glass system. Although the well-known Corning Code 7740 borosilicate glasses are found in this system, certain sodium borosilicate glass compositions exist (see Fig. 24) which, after heat treatment, can be leached with acid to form a porous glass framework.^{76–78} During the heat treatment the base glass separates into two intermingled and continuous glassy phases and, depending upon the conditions of thermal treatment, the phase separation is revealed as a turbidity that can vary from clear, through weak opalescence, to complete milkiness. Figures 25–27 show this phase separation phenomenon, as evidenced by electron micrographs of fractured samples of borosilicate glass which had been heat treated under different conditions. High-temperature heat treatments may lead not only to a change in the size of the microregions but can also produce chemical inversion in which the borate phase is enriched with silica at the expense of the surrounding silica framework. On cooling, separate isolated borate regions are formed—enclosed in the mass of SiO_2 .^{79,80} This type of distribu-

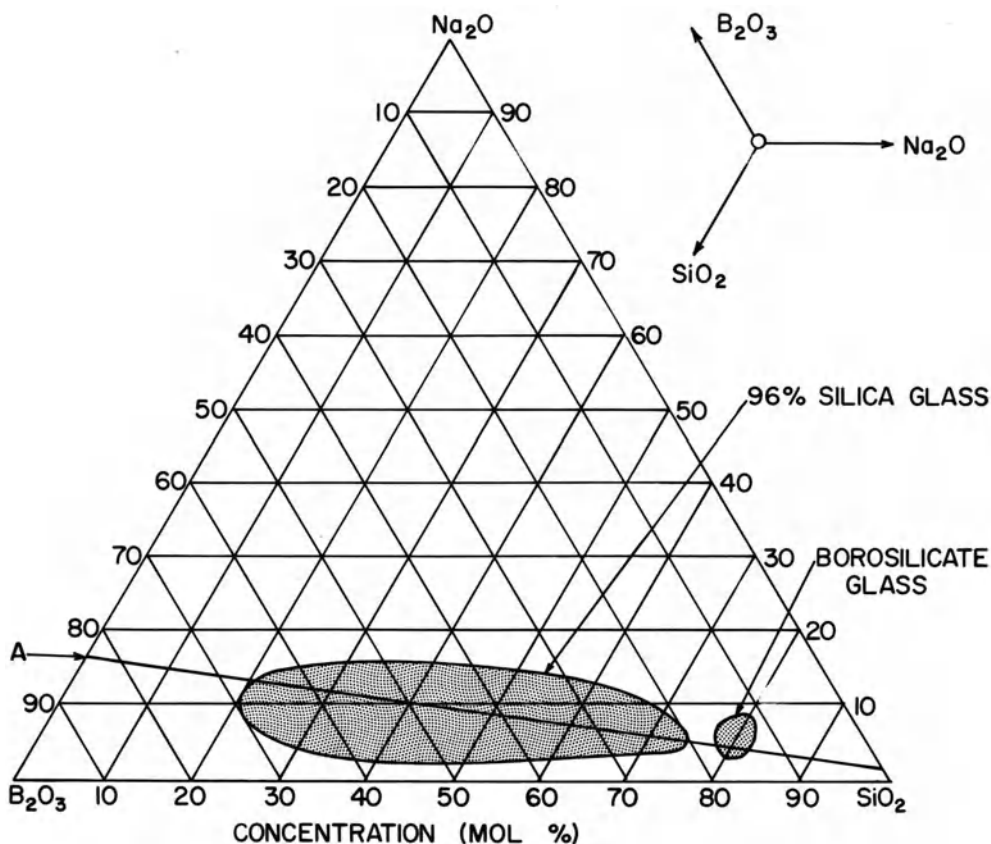


Fig. 24. Areas of borosilicate composition that can be leached to give porous glasses.

tion of the borate regions in the glass makes them less soluble in a leaching medium, and during leaching a high percentage of B_2O_3 may remain in the porous glass. The borate phase, however, is generally soluble in acids, whereas the high-silica phase is not. Thus, the B_2O_3 rich phase may be preferentially leached out of the structure, leaving a porous body of very high silica content. (Note, however, that the surface layer may still contain an appreciable amount of B_2O_3 .⁸¹) Pore diameters for these glasses are in the range 30–60 Å, and the pore volume is approximately 28% of the total sample volume.⁸² An electron micrograph of one such porous glass is shown in Fig. 28.

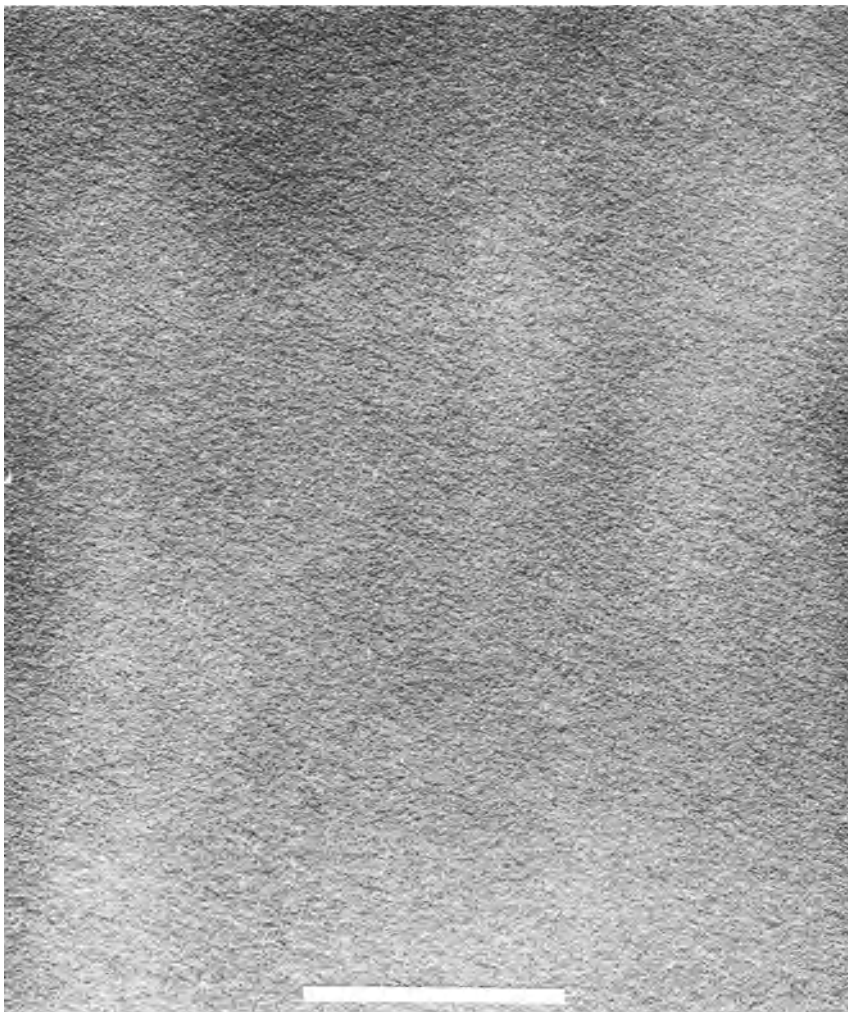


Fig. 25. Phase-separable borosilicate glass. No heat treatment. Fractured, preetched $1\frac{1}{2}$ min in water at room temperature.

Larger-pored glass can be prepared from the same borosilicate glass compositions.⁸³ After the heat treatment and acid leaching steps, a mild caustic treatment enlarges pore diameters by removing silicous residue from pore interiors. Careful control of the various physical and chemical treatments enables glasses to be produced which exhibit extremely narrow pore size distribution, as shown in Fig. 29.

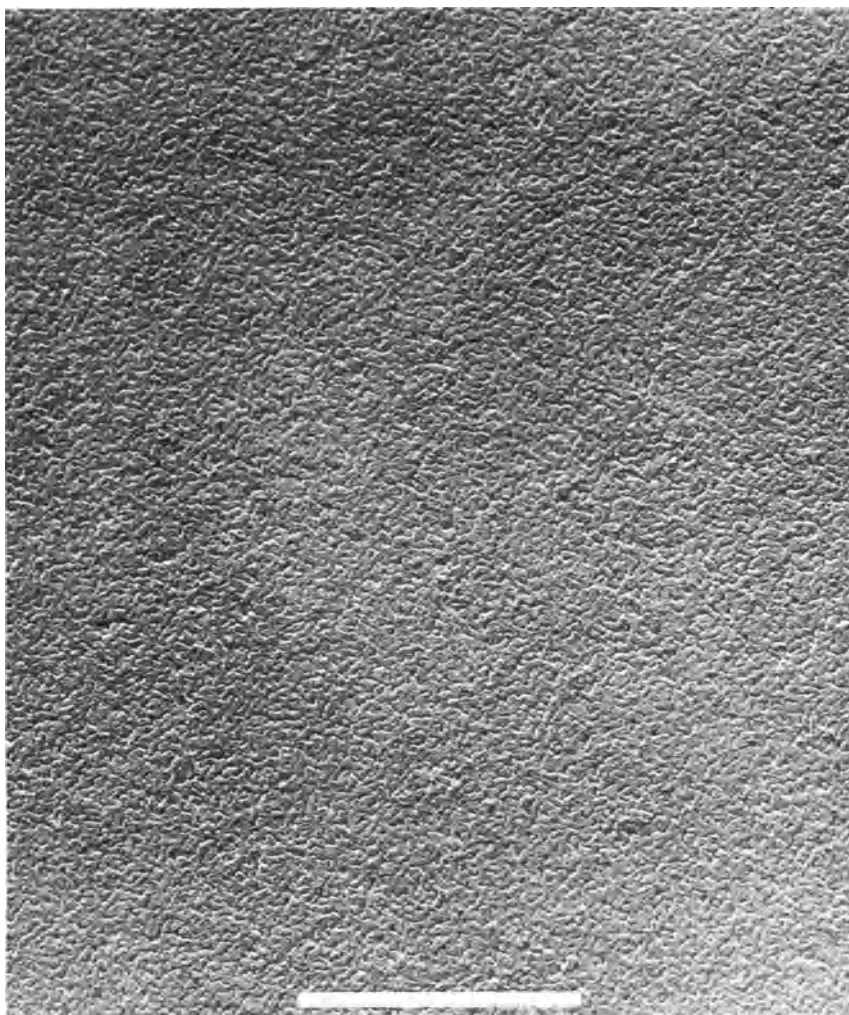


Fig. 26. Phase-separable borosilicate glass. Heat treatment : 3 hr at 580°C. Fractured, etched 1 min in water at room temperature.

It is quite clear that if such gross phase separation occurs in any glass, there is no utility whatsoever in trying to correlate the corrosion of the glass with any chemical composition. Many glasses have now been shown to consist of two intermingled glassy phases—even the simple sodium silicate glasses have been shown to give porous materials that have very small pore size (about 7 Å) and exhibit molecular sieve-like properties.⁸⁴ It has been

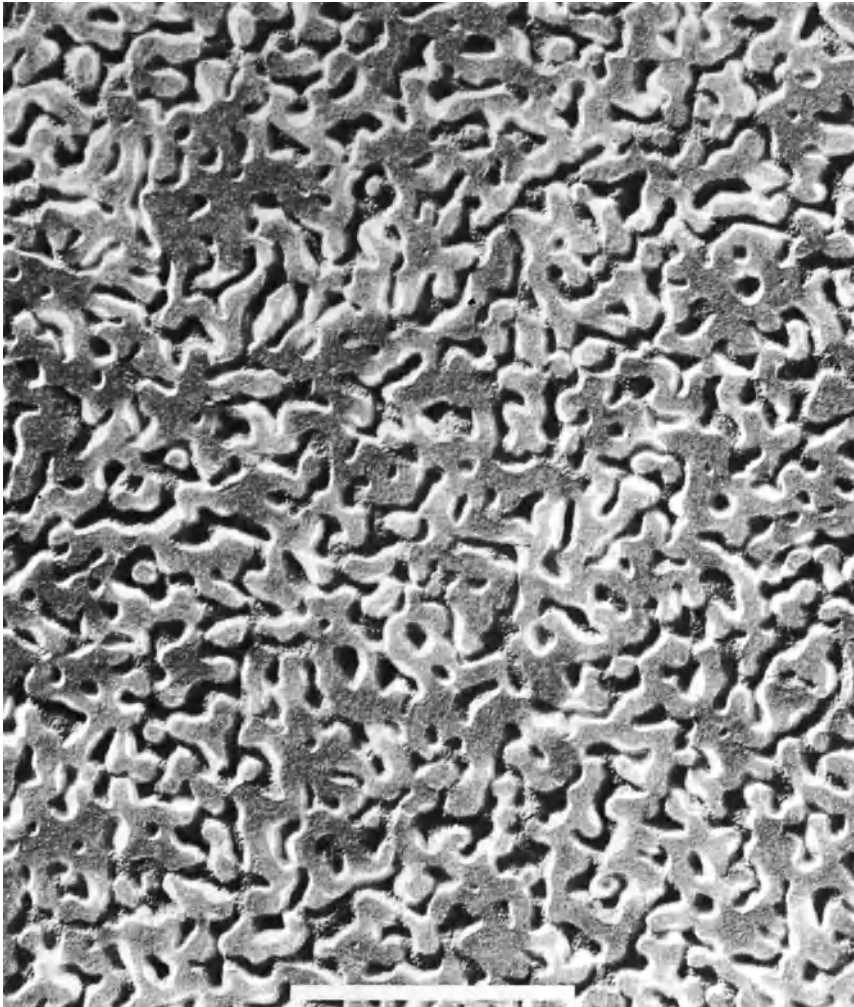


Fig. 27. Phase-separable borosilicate glass. Heat treatment : 168 hr at 580°C. Fractured, preetched 90 sec in H₂O at room temperature.

suggested⁸⁵ that the hydroxyl bands which are readily observed in the infrared region of the spectrum of these glasses might be attributed to hydroxyl groups in different phases, and a semiquantitative estimate of various compositions has been made. Although partial data are available for many glasses, the only complete series is that for the sodium alumin-

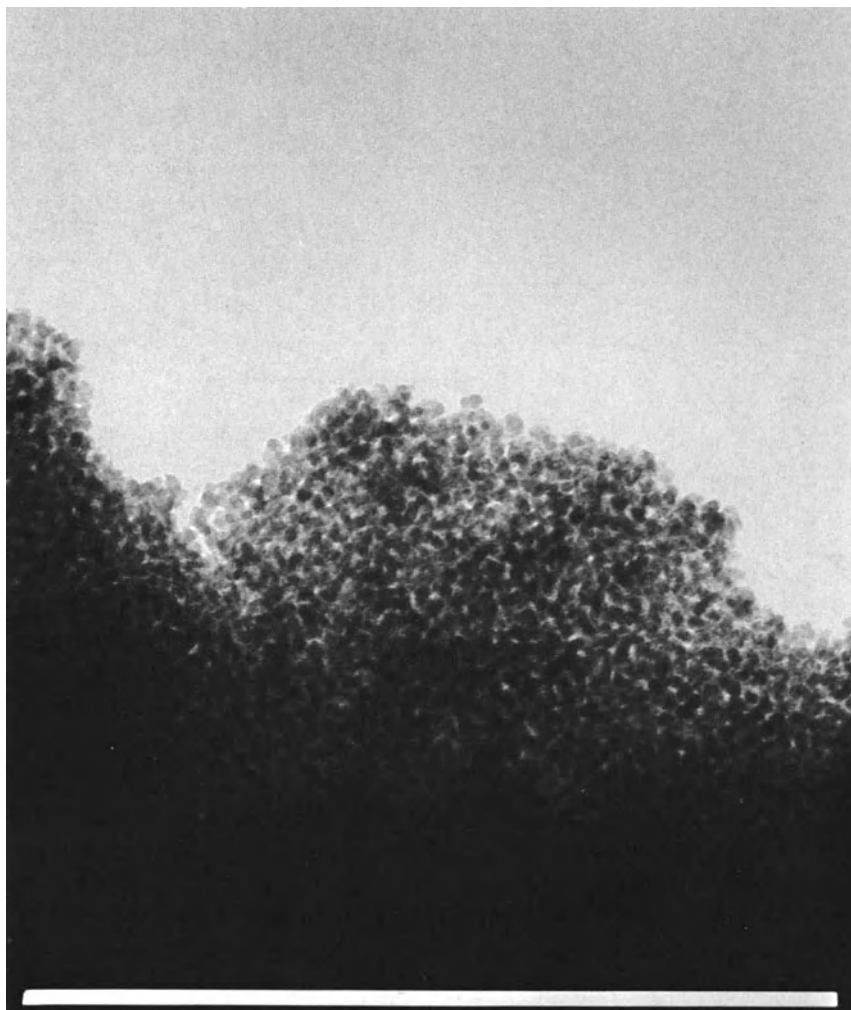


Fig. 28. Transmission electron micrograph of a porous glass.

silicate glasses. These are interesting, as the hydroxyl ratios can be compared directly with the structural ideas and electrochemical data supplied by Eisenman.¹⁹ Hair proposed that “phase separation” might occur in a sodium aluminosilicate glass, a sodium silicate “phase” and a sodium aluminosilicate “phase” being formed. A specific hydroxyl band was assigned to each phase

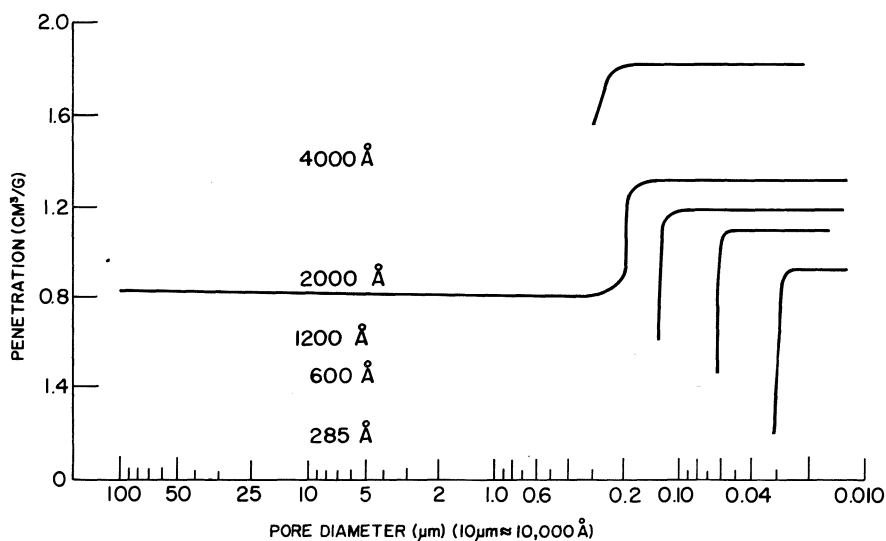


Fig. 29. Mercury intrusion data showing pore size distribution of some controlled pore glasses.

and it was assumed that the electrochemical ion selectivity of these glasses was due to a pore size effect caused by leaching rather than an ion exchange effect as proposed by Eisenman. The results are of interest in that a plot of $\log K_{\text{NaK}}^{\text{Pot}}$ against $\text{OH}_1/\text{OH}_{11}$ gave a good linear plot, even in the high-alkaline regions, where the Eisenman relationship shows deviations. These data are only suggestive of structural discontinuities but are worth bearing in mind in any discussion dealing with corrosion and the molecular structure of the glass.

SURFACE CHEMISTRY

As far as the molecular nature of glass surfaces is concerned, very little can be said about the details either of the surface structure or of the way gases will subsequently absorb physically or chemically on such surfaces. This is an obvious corollary of our lack of knowledge of the structure of the solid state. However, work within the past 15 years using infrared techniques on porous materials has enabled scientists to obtain a reasonably good model

of amorphous silica surfaces and porous glass. By extrapolation it is possible to guess at the most likely molecular structures and interactions.

The molecular interactions that occur on a glass surface are obviously very dependent upon the corrosion which that glass surface has experienced. It is common practice to assume that glass surfaces are inert and, in normal applications, molecular surface effects are usually ignored. However, in high-vacuum applications, the glass surface can exhibit considerable catalytic effects. Thus, unsaturated hydrocarbons may be polymerized, alcohols may be dehydrated, and extraordinary high physical adsorption may be noted.⁸⁶ An explanation (but no proof) for these effects can be found by assuming that glass surfaces as observed can be treated by an extrapolation of our knowledge of silica surfaces. The effects of small amounts of impurity on high-surface-area silicas have been well studied because of the implications in catalysis. By assuming that the various glass surfaces can be treated as impure silicas, some rationale for their chemical behavior in the gas/solid state can be found.

Before considering these reactions it is important to emphasize that the molecular surface which is exposed in a vacuum system is very dependent upon the pretreatment that the glass itself has received. In its manufacture the glass has been exposed to a very high temperature, and there is considerable volatilization of oxides such as Na_2O and B_2O_3 from the surface of the glasses. Thus commercial glass, even in its pristine form, will have a surface that contains an excess of silica compared to the bulk constitution. The exact composition will be dependent upon the atmosphere that exists at the time of manufacture and will be altered by variations in humidity, exposure to oils and greases, etc.

Perhaps more important to our considerations, however, are the treatments that the individual scientists always give their glass surfaces in order to "clean" them prior to use. Typically, the glass is cleaned with anything from acidified dichromate to alkaline detergent, depending upon the user's concept of "cleanliness." From our discussion thus far it is obvious that exposure to such aqueous cleaning agents must cause some dissolution of the glass surface, giving an increased surface area and ion exchange of H^+ for Na^+ . It is this process more than any other which makes it difficult to speculate on the molecular interactions that have occurred on a particular glass surface. The scientist usually "flames" his vacuum equipment before use to remove hydrocarbon residues and in the process dehydrates the surface layer, which is already deficient in Na^+ because of the washing step.

The glass surfaces which have been most closely studied from a molecular

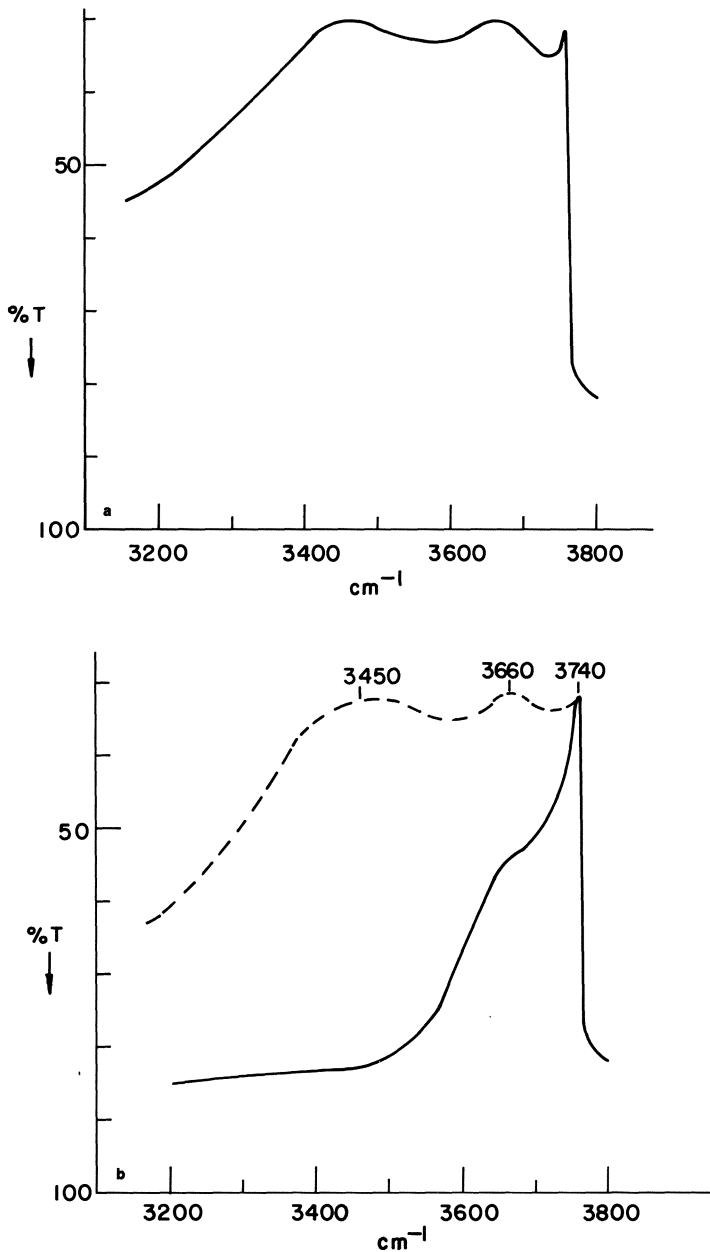
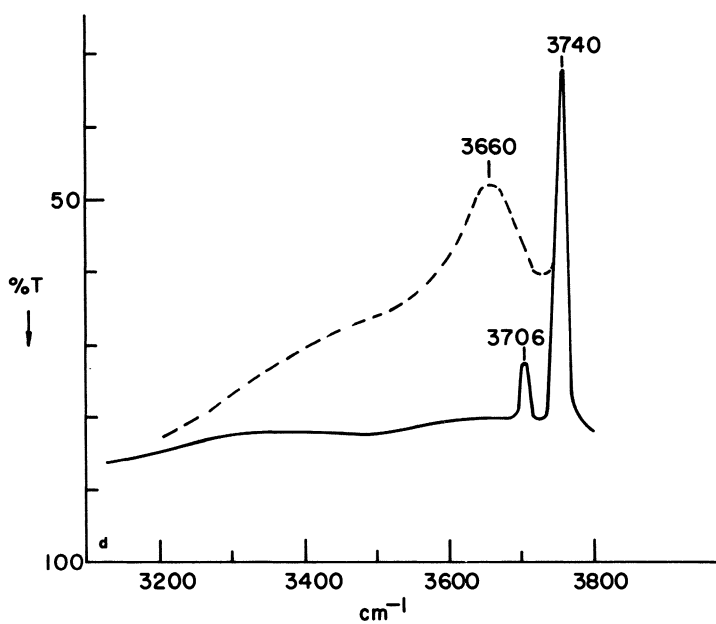
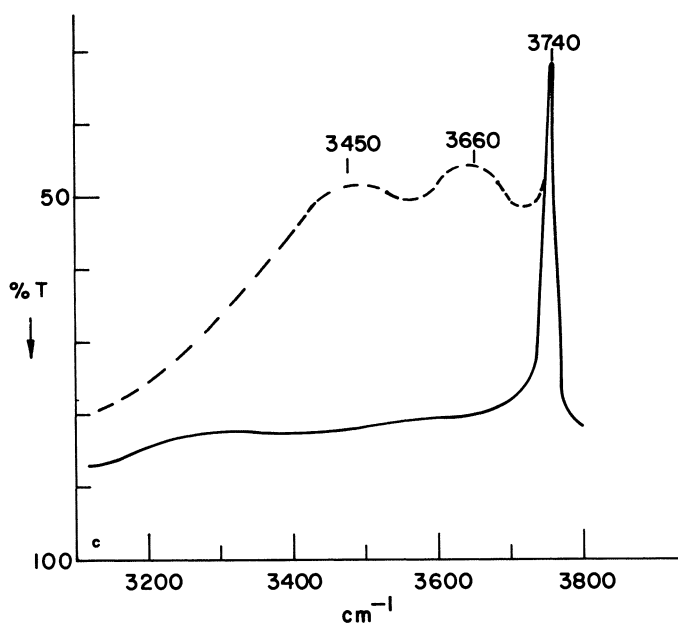


Fig. 30. Dehydration-hydration of porous glass. The solid lines are obtained after evacuation at (a) 100°C; (b) 300°C; (c) 500°C; (d) 700°C. The dashed lines are after reexposure to water. (From Wang and Tooley.⁴¹)



point of view are undoubtedly those of the porous glass type. These materials have a high surface area ($150 \text{ m}^2/\text{g}$) and, because they can be prepared as very thin plates ($1/10 \text{ mm}$), are ideal for the study of adsorbed molecules using infrared techniques. Details of such studies can be found in two textbooks.^{54,87} Initially it was felt that because these glasses have a composition which approximates $97\% \text{ SiO}_2$ – $3\% \text{ B}_2\text{O}_3$, they could be used as a substitute for pure silica in surface studies. However, it will be seen that this assumption is invalid and that the impurities themselves give us an idea of the complex nature of glass surfaces.

The similarities of porous glass and silica surfaces can be demonstrated by consideration of Fig. 30. A freshly prepared porous glass gives the infrared spectrum shown in Fig. 30a. If the glass is then dehydrated at temperatures ranging from 100 to 700°C , the series of spectra shown by the solid lines is obtained. These spectra can be compared with those obtained by McDonald during the dehydration of a silica gel.⁸⁸ The single well-defined band at 3740 cm^{-1} , which is observed after heating to 500°C , is attributed to a freely vibrating surface silanol group.^{88,89} The band at 3660 cm^{-1} is assigned to adjacent hydroxyl groups which are hydrogen bonded to each other; and the broad band which peaks at 3450 cm^{-1} is assigned to molecular water.

Rehydration of the porous glass gives the spectra shown by the dashed lines in Fig. 30. The concurrent growth of the bands at 3665 and 3450 cm^{-1} , together with the observation that the freely vibrating hydroxyl frequency is barely perturbed during the water adsorption process, indicates that water adsorption occurs preferentially on the adjacent hydroxyl groups.

In contradistinction to this, it is known that lone-pair molecules such as ammonia adsorb preferentially on freely vibrating hydroxyl groups. Thus, when ammonia is adsorbed on a porous glass surface, we expect to find perturbation of the freely vibrating hydroxyl group and the appearance in the spectrum of two new bands at about 3400 and 3320 cm^{-1} which are due to the symmetric and asymmetric N—H vibrations of the adsorbed ammonia. The results with porous glass are shown in Fig. 31. Initially the glass was dehydrated so that only the freely vibrating hydroxyl group was present on the surface (a). On addition of ammonia the hydroxyl group is indeed perturbed (b), but four bands are produced in the 3300 - to 3400-cm^{-1} region instead of the two bands observed when ammonia is added to pure silica. After evacuation at room temperature the physically adsorbed ammonia is removed (c). The freely vibrating hydroxyl reverts to its original intensity, and the bands at 3400 and 3320 cm^{-1} disappear from the spectrum, as expected. Two bands remain (3365 and 3280 cm^{-1}), however, and are not

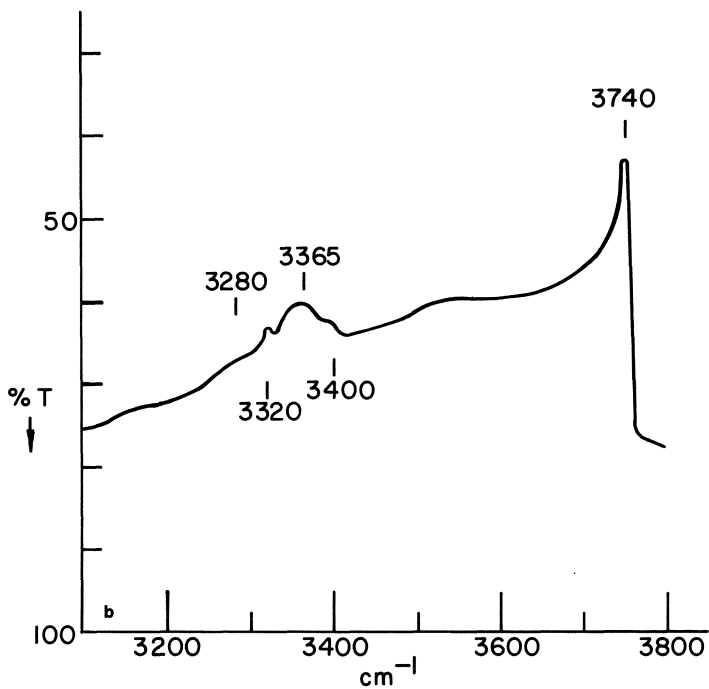
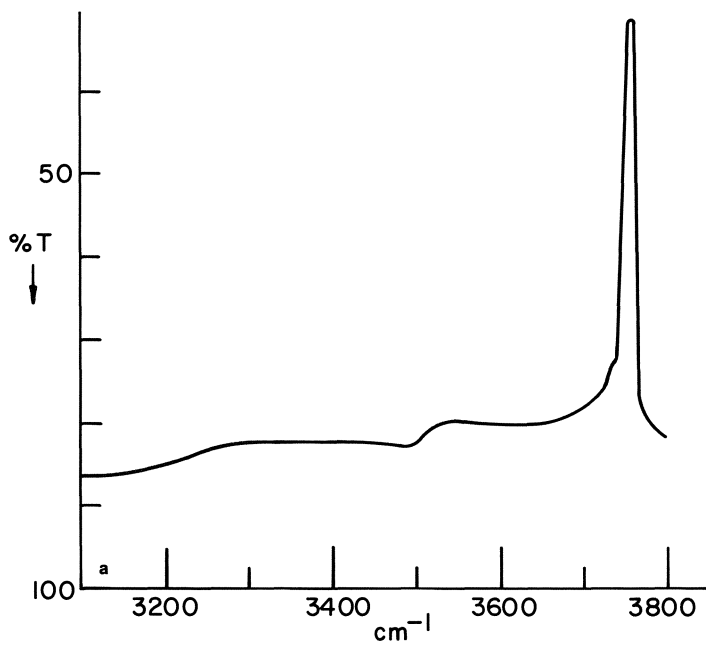
removed until the temperature of the sample has been raised to about 200°C. This chemisorbed ammonia is attributed to ammonia coordinately bonded to a Lewis-acid-type site on the glass surface (Fig. 32).

Gravimetric determination of the amount of this chemisorbed ammonia enabled Hair and Chapman⁸¹ to estimate the amount of boron present on the surface of this glass. By assuming a 1:1 correlation between the number of molecules of ammonia adsorbed and the number of boron atoms on the surface, and from a knowledge of the total surface area of the glass, a B:Si ratio of 1:3 was obtained. This is surprisingly high considering that chemical analysis of the material indicates a ratio of about 1:20. The conclusion is, therefore, that there is a concentration of boron at the surface of this porous glass, and it might be expected that this leached glass surface correlates more closely with the acidic silica aluminas than that of a pure silica material. Thus, we have an explanation of the reason butenes are polymerized on porous glass but not on silica.⁹⁰

Additional confirmation for this increased acidity comes from pH titrations of the porous glass. Such data show that the porous glass surface contains two types of acid sites.⁹¹ One of these is analogous to that found on the silica surface and has a pK_a value of 7, but the second is a stronger acid and has a pK_a value of about 5.1. Thus, the effect of this gross leaching of a borosilicate glass has been to increase both the surface area of the material and the chemical activity of the surface.

One additional point which can be noted from Fig. 30 is that when the porous glass is heated to temperatures in excess of 500°C, the boron tends to leave the surface of the glass and form whiskers of boric acid. Figure 30d shows a small, sharp band appearing at about 3700 cm^{-1} . This band is attributed to a freely vibrating surface B—OH group, a site that is apparently of major importance in the initial stages of water adsorption.⁹²

Lewis acid sites have been identified spectroscopically on sodium aluminosilicate glasses which have undergone a hydration–dehydration cycle,⁵¹ and they have been implied in chromatographic studies of corroded soda-lime glasses. In the latter case, preferential leaching of the Na^+ ions would lead to a surface rich in both Ca^{2+} and SiO_2 . Although the surface hydroxyl groups associated with the silica can be removed by reaction with chlorosilanes, the Ca^{2+} ions will not be affected by this process. If an exposed Ca^{2+} ion functions as a Lewis acid site it will cause adsorption in the chromatographic process, particularly in the case of lone-pair adsorbates. This can be seen from Fig. 33, where a nonpolar material, phenanthrene, and two polar materials, benzophenone and diphenylamine, were injected



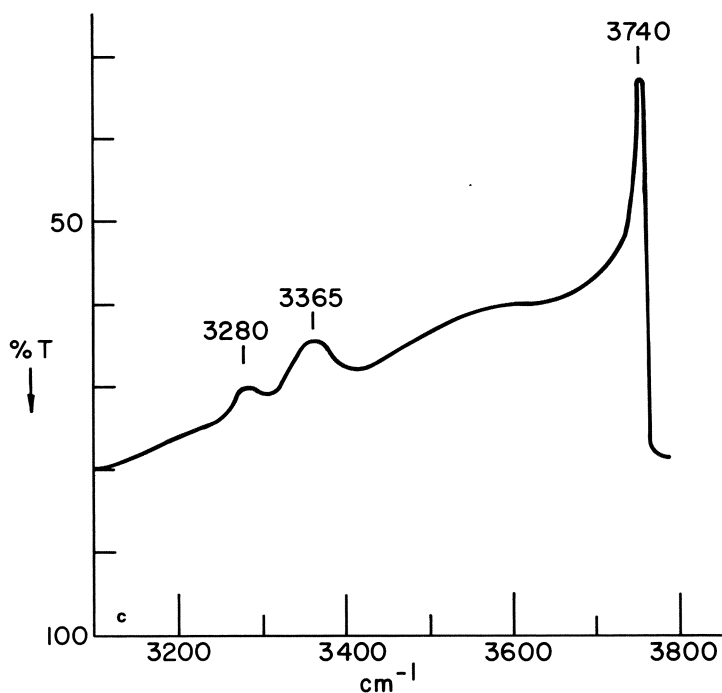


Fig. 31. Adsorption of NH_3 on porous glass: (a) initial sample; (b) after addition of ammonia at room temperature; (c) after evacuation and removal of physically adsorbed NH_3 .

through a column containing soda-lime beads coated with silicone oil as the separating medium.⁹³ Any adsorption on the glass surface can be detected as a tailing of the elution peak. This is clearly seen in the case of the polar materials, both of which exhibit considerable tailing on elution from the chromatographic column.

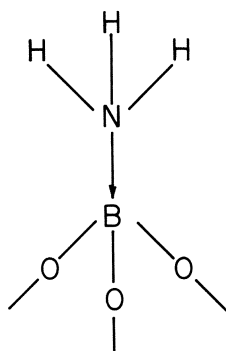


Fig. 32. Ammonia adsorption on Lewis acid site.

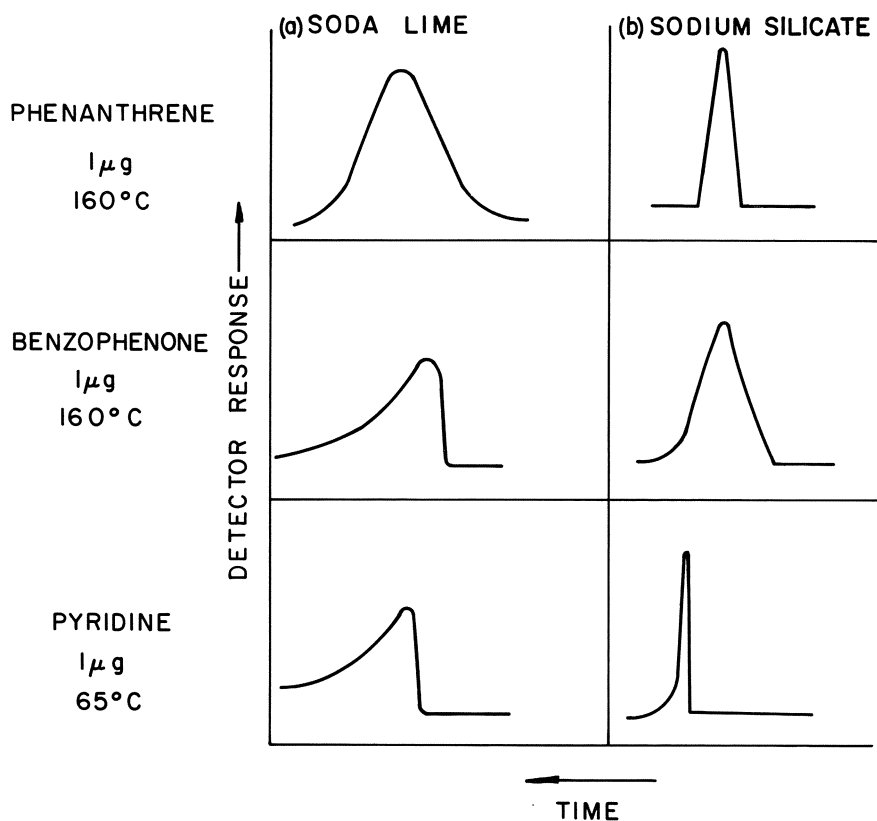


Fig. 33. Elution peaks for phenanthrene, benzophenone, and pyridine on coated beads made from (a) soda-lime glass; (b) sodium-silicate glass.

To prepare a glass bead with an inactive surface suitable for chromatography, a glass composition was needed which, on leaching, did not give rise to active Lewis acid sites. Exposed Ca^{2+} ions were projected as the culprit for the huge adsorption in the case of the soda-lime glass. Filbert and Hair argued that a sodium silicate glass should give all the desired properties: sodium ions, even exposed on the external surface, would not function as an adsorption site for most molecules. Chromatographic results obtained with such glasses are shown in Fig. 33. The symmetry of the elution peaks shows that the strong adsorption has been eliminated.

MISCELLANEA

Weathering of Glass Surfaces

“Weathering” is a term commonly given to the attack of glass surfaces by atmospheric gases and moisture.^{94–102} The surface of the glass becomes dimmed, fogged, and, in extreme cases, pitted. Glasses of poor chemical durability may be affected by moisture alone, but with most common compositions (i.e., soda-lime glasses), increased surface alkalinity and enhancement of the attack are needed to cause problems.¹⁰³ Since weathering effects increase with increasing alkali content in the glass, high silica, boro-silicate, and aluminoborosilicate glasses show resistance to the weathering phenomenon.

Corrosion Resistance of Ceramics

The corrosion resistance of polycrystalline ceramics is so variable that generalizations are almost impossible. Many such ceramics are specifically designed for corrosion resistance against a particular agent, usually at elevated temperature. Thus, certain refractories can withstand molten slags and steel, while others are more resistant to molten glass.

High-Temperature Attack on Glasses and Glass Ceramics

The chemical corrosion of glass and glass ceramics at high temperatures has not been studied in as much detail as the attack by acids, water, and bases. Molten salts, for example, have been shown to be containable in vessels made of high-silica glass or pure fused silica. Molten alkalis or carbonates, however, will attack all glasses fairly rapidly.

Most glasses soften at temperatures of metal and alloy melts, but they can tolerate molten solders. Although high-silica glasses can withstand molten gold, more electropositive metals, such as molten aluminum and magnesium, will react with silica and high-silica glasses at elevated temperatures, reducing the SiO_2 to silicon and silicides. Alkali oxide and lead oxide vapors react with high-silica-glass surfaces at elevated temperatures to initiate devitrification of the glass, with the formation of cristobalite. This results in the frosting of the glass surface, and subsequent breakage of the

item on cooling below 300°C. The breakage results from a large volume change accompanying the inversion of cristobalite from the α to the β form.

UTILIZATION OF CORROSION EFFECTS

Although corrosion is usually avoided whenever possible, surface attack can be used beneficially for some applications. First, it should be clear from the series of electron micrographs in Figs. 13–15 that various acids may be used to polish glass surfaces. When certain glasses are immersed in hydrofluoric acid for short periods of time, with intermittent washing to remove the products of chemical action, surface flaws and imperfections are removed, with the result that the modulus of rupture may be increased several hundred percent. The glasses are sometimes said to be “acid polished.” Similarly, a glass surface can be etched to create a very thin surface film, which may be either reflective or dispersive. A particularly well known example of the formation of a light-scattering film is the use of a mixture of HF and sulfuric acid on the inside of electric light bulbs. A similar type of acid attack has been used to prepare the surfaces of silicate beads to make highly efficient chromatographic columns. By control of the etching solution, surfaces reminiscent of either orange peel or raspberries can be produced which help the spreading of the partitioning liquid on the surface of the glass beads^{55,104} and prevent “puddling” of the liquid at the points of contact. A very interesting and potentially important use of special films has been discussed by Rappaport,¹⁰⁵ who, by special leaching of zirconia-containing glasses, has been able to prepare surfaces that stimulate the growth of mammalian brain and liver cells *in vitro*. Correlation was obtained between crystal violet adsorption and efficiency of attachment.

The most extreme form of etching is that of the phase-separated glasses. As discussed previously, provided the glass compositions are chosen with care, a rigid structure results which is 96% silica and has high surface area and porosity. Such a material finds use in the electronic industry as a desiccant. On sintering, it is known as Corning Code 7900-type glass and can be used as a substitute for fused silica. Control of the temperature, length of time of heat treatment, and leaching conditions control the pore size of the resultant porous glass. Pore sizes from 20 to 4000 Å in diameter have been prepared and the resulting bodies used as supports for superconducting filaments at one extreme of pore size,¹⁰⁶ and also for the separation and purification of viruses, etc., at the other.¹⁰⁷ Quite clearly, partial leaching can also occur, giving surface films with similar adsorption properties.

SUMMARY

In summary it can be said that the effect of corroding liquids on a glass body is a very complex chemical system which is made even more complicated by our lack of knowledge of the structure of the glass. The simplest approach for users of glass is simply to measure the amount of glass removed by a particular treatment to which the glass article is likely to be subjected. However, in defining the chemistry of the process, the following considerations should be made:

1. The initial pH of the corroding solution.
2. The changes in pH that occur as the constituents of the glass are removed.
3. The possibility of film formation on the surface of the glass either during manufacture or by deposition from solutions during the actual corrosion process.
4. The effect of glass composition on the ion exchange which must occur between the glass and the surrounding solution.
5. The possibility (probability) of phase separation within the glass itself, which leads to pitting and nonuniform surface removal. In such cases all extrapolations based on bulk composition are invalid. Only when the true structure of glasses is known can we hope to obtain a full and complete knowledge of the corrosion of the particular glass surface.

REFERENCES

1. American Society for Testing and Materials, ASTM C162-56, Standard Definitions of Terms Relating to Glass Products, ASTM Standard 1965, Pt. 13, 145-159 (1965).
2. M. Fanderlik, *Sklar Keram.* **4**, 14 (1954).
3. W. H. Zachariasen, *J. Am. Ceram. Soc.* **54**, 3841 (1932).
4. B. E. Warren, *J. Appl. Phys.* **13**, 602 (1942).
5. A. G. Smekal, *J. Soc. Glass Technol.* **33**, 411 (1951).
6. J. M. Stevels, *Glass Ind.* **35**, 69 (1954).
7. J. R. Hutchins, III and R. V. Harrington, in Kirk-Othmer, *Encyclopedia of Chemical Technology*, 2nd ed., John Wiley, **10**, 533 (1966).
8. R. M. Beattie, *J. Soc. Glass Technol.* **36**, 37 (1952).
9. S. M. Budd, *Phys. Chem. Glasses* **2**, 111 (1961).
10. American Pharmaceutical Society, *U.S. Pharmacopeia*, 15th ed., p. 923, Mack Publishing Co., Easton, Pa. (1955).
11. American Society for Testing and Materials, Standard Methods of Test for Resistance of Glass Containers to Chemical Attack, ASTM Designation C225-54.

12. E. B. Shand, *Glass Engineering Handbook*, McGraw-Hill, New York (1958).
13. W. C. Taylor and R. D. Smith, *J. Am. Ceram. Soc.* **19**, 331 (1936).
14. W. Stöber, *Kolloid-Z.* **147**, 131 (1956).
15. W. Eitel, in *Silicate Science*, Vol. 4, Academic Press, New York (1966).
16. W. Eitel, in *Silicate Science*, Vol. 1, p. 320, Academic Press, New York (1964).
17. G. B. Alexander, W. M. Heston, and R. K. Iler, *J. Phys. Chem.* **58**, 453 (1954); **61**, 1539 (1957).
18. T. L. O'Connor and S. A. Greenberg, *J. Phys. Chem.* **62**, 1195 (1958).
19. G. Eisenman, *Biophys. J.* **2**(2), 259 (1962).
20. G. Eisenman, *The Glass Electrode*, Interscience, New York (1962).
21. L. Pauling, *The Nature of the Chemical Bond*, Cornell University Press, Ithaca, N.Y. (1940).
22. K. Fajans, *Chimia* **13**, 349 (1959).
23. W. A. Weyl and E. C. Marboe, *The Constitution of Glasses*, Vols. I and II, John Wiley, New York (1964–1967).
24. T. M. El-Shamy and R. W. Douglas, *Phys. Chem. Glasses* **13**(3), 77 (1972).
25. M. A. Rana and R. W. Douglas, *Phys. Chem. Glasses* **2**(6), 179 (1961).
26. M. A. Rana and R. W. Douglas, *Phys. Chem. Glasses* **2**(6), 196 (1961).
27. C. R. Das and R. W. Douglas, *Phys. Chem. Glasses* **8**(5), 178 (1967).
28. R. W. Douglas and T. M. El-Shamy, *J. Am. Ceram. Soc.* **50**(1), 1 (1967).
29. R. W. Douglas and J. O. Isard, *J. Soc. Glass Technol.* **33**, 289 (1949).
30. T. El-Shamy and R. W. Douglas, *Glass Technol.* **13**, 77 (1972).
31. T. El-Shamy, J. Lewins, and R. W. Douglas, *Glass Technol.* **13**, 81 (1972).
32. M. E. Nordberg, *Chemical Durability of Glass*, Corning Glass Works, Corning, N.Y.
33. R. M. Tichane and G. B. Carrier, *J. Am. Ceram. Soc.* **44**, 606 (1961).
34. A. K. Lyle, "Chemical Durability of Containers," *Glass Ind.* **1**, 147 (1934).
35. L. Holland, "Surface Chemistry and Corrosion of Glass, Part I," *Glass Ind.* **11**(1), 191 (1963).
36. S. Nagaeda, "Solubility of Glass in Alkaline, Acidic, and Neutral Solution," *J. Ceram. Assoc. Japan* **49**, 140 (1941).
37. W. C. Taylor, "Method of Testing Chemical Durability," *J. Soc. Glass Technol.* **20**, 405T (1936).
38. I. R. Beattie, "The Reaction Between Glass and Water," *J. Soc. Glass Technol.* **37**, 178, 240T (1953).
39. R. Kiyoura, S. Kawakulo, and Y. Ito, "Decomposition of Glass by Water at High Temperature," *J. Ceram. Assoc. Japan* **57**, 51 (1949).
40. M. A. Rana and R. W. Douglas, "The Reaction Between Glass and Water: Part I. Experimental Methods and Observations," *Phys. Chem. Glasses* **6**, 179 (1961).
41. F. F. Wang and F. V. Tooley, "Detection of Reaction Products Between Water and Soda-Lime-Silica Glass," *J. Am. Ceram. Soc.* **11**, 467 (1958).
42. F. F. Wang and F. V. Tooley, "Influence of Reaction Products on Reaction Between Water and Soda-Lime-Silica Glass," *J. Am. Ceram. Soc.* **12**, 521 (1958).
43. J. D. Cauwood, C. M. M. Muirhead, and W. E. S. Turner, "The Durability of Lime-Soda Glasses," *J. Soc. Glass Technol.* **3**, 228T (1919).
44. R. W. Douglas and J. O. Isard, "The Action of Water and Sulphur Dioxide on Glass," *J. Soc. Glass Technol.* **33**, 289T (1949).
45. S. Sen and F. V. Tooley, "Determination of Calcium, Sodium and Silicate Ions in Extracts from Chemical Durability Tests on Glass," *J. Am. Ceram. Soc.* **33**, 178 (1950).
46. H. R. Persson, "Chemical Surface Resistance of Glass Containers," *Glastek. Tidskr.* **17**, 91 (1962).
47. G. W. Morey, *Properties of Glass*, 2nd ed. (ACS Monograph 77), Reinhold Publishing Corporation, New York (1954).

48. R. H. Doremus, *Glass Science*, John Wiley, New York (1973).
49. F. R. Bacon and O. G. Burch, *J. Am. Ceram. Soc.* **23**, 1, 147 (1940).
50. E. F. Dick, G. E. Lorey, R. D. Skumer, and H. E. Simpson, *J. Am. Ceram. Soc.* **34**, 31 (1951).
51. M. L. Hair, in *Clean Surfaces* (G. Goldfinger, ed.), Dekker, New York (1970).
52. E. B. Shand, *Glass Engineering Handbook*, McGraw-Hill, New York (1958), p. 94.
53. S. Levine *et al.*, Defense Documents Center Document AD 641-500 (1966).
54. M. L. Hair, *Infrared Spectroscopy in Surface Chemistry*, Marcel Dekker, New York (1967).
55. H. L. MacDonell and D. L. Eaton, *Anal. Chem.* **40**, 1453 (1968).
56. S. Nagaeda, "Method of Testing the Chemical Durability of Glass for Acidic Solution," *J. Ceram. Assoc. Japan* **51**, 338 (1943).
57. J. F. Greene and A. L. Hinson, "Autoclave Test of Glass Containers with Acid Test Liquid," *Bull. Natl. Formul. Comm. Am. Pharm. Assoc.* **17**, 48 (1949).
58. D. K. Hoganson, J. H. Healy, F. Y. Wang, and D. B. Johnson, "Acid Corrosion Testing of Glass to 400°F," *Bull. Am. Ceram. Soc.* **41**, 156 (1962).
59. "Determination of Resistance to Acids of Glass," Czechoslovak Standard CSN.
60. E. Wichers, A. N. Finn, and W. S. Clabaugh, *J. Res. Natl. Bur. Std.* **26**, 537 (1941).
61. N. H. Ray, "The Action of Phosphoric Acid on Glass," *J. Non-Crystal Solids* **5**, 71 (1970).
62. J. Suire, "Reactions Between Glass and Hydrofluoric Acid," *Silicates Ind.* **36**, 73 (1971).
63. M. S. Tarnopol and A. E. Junge, *J. Am. Ceram. Soc.* **29**, 36 (1946).
64. H. Wessel, *Silikattechnik* **2**, 17 (1951).
65. S. K. Dubrovo and Y. A. Schmidt, *Izv. Akad. Nauk SSSR Otd. Khim. Nauk* **3** 403 (1955).
66. D. Hubbard and E. H. Hamilton, *J. Res. Natl. Bur. Std.* **27**, 143 (1941).
67. G. A. Hudson and F. R. Bacon, *Bull. Am. Ceram. Soc.* **37**, 185 (1958).
68. S. K. Dubrovo, *Zh. Prikl. Khim.* **33**, 27 (1960).
69. F. Trenz, *Sklar Keram.* **12**, 51 (1962).
70. F. M. Ernsberger, *J. Am. Ceram. Soc.* **42**, 373 (1959).
71. R. W. Douglas and J. O. Isard, *J. Soc. Glass Technol.* **42**, 2271 (1949).
72. E. L. Mochel and M. E. Nordberg, Belgian Patent 618,737 (1962).
73. S. D. Stookey, J. S. Olcott, H. M. Garfinkel, and D. L. Rothermel, *Tech. Papers Intern. Congr. Glass*, 6th, Washington, D.C. (1962), p. 411.
74. H. M. Garfinkel, D. L. Rothermel, and S. D. Stookey, *Tech. Papers Intern. Congr. Glass*, 6th, Washington, D.C. (1962), p. 404.
75. M. E. Nordberg, E. L. Mochel, H. M. Garfinkel, and J. S. Olcott, *J. Am. Ceram. Soc.* **47**(5), 215 (1964).
76. M. E. Nordberg, *J. Am. Ceram. Soc.* **27**, 299 (1944).
77. O. S. Molchanova, *Ion Exchange in Molten Salts*, Acad. Sci. USSR Press, Moscow-Leningrad (1955).
78. N. I. Ananich, O. K. Botvinkin, and M. L. Mironova, *Steklo i Keram.* **22**, 1, 15 (1965).
79. N. A. Voishvillo, *Opt. i Spektroskopiya* **3**, 371 (1957).
80. N. A. Voishvillo, *Opt. i Spektroskopiya* **2**, 281 (1957).
81. M. L. Hair and I. D. Chapman, *J. Am. Ceram. Soc.* **49**, 651 (1966).
82. H. P. Hood and M. E. Nordberg, U.S. Patent 2,221,709, "Borosilicate Glass" (1940).
83. W. Haller, *Nature*, **4985**, May 15 (1965).
84. L. S. Yastrebova *et al.*, *Chem. Abstr.* **61**, 19149c (1966).
85. M. L. Hair, *J. Phys. Chem.* **74**, 1145 (1970).
86. J. R. H. Ross and M. W. Roberts, *J. Catalysis* **4**, 620 (1965).
87. L. H. Little, *Infrared Spectra of Adsorbed Molecules*, Academic Press, New York (1966).
88. R. S. McDonald, *J. Phys. Chem.* **62**, 1168 (1958).
89. A. N. Siderev, *Opt. Spectry. (USSR) (English Transl.)* **8**, 424 (1960).
90. L. H. Little, H. E. Klauser, and C. H. Amberg, *Can. J. Chem.* **39**, 42 (1961).

91. I. Altug and M. L. Hair, *J. Phys. Chem.* **71**, 4260 (1967).
92. M. J. D. Low and Ramasubramanian, *J. Phys. Chem.* **71**, 3077 (1967).
93. A. M. Filbert and M. L. Hair, *J. Gas. Chromatog.* **6**, 150 (1968).
94. H. E. Simpson, *Glass Ind.* **36**, 515 (1955).
95. F. L. Bishop and F. W. Mowrey, *Bull. Am. Ceram. Soc.* **31**, 1, 13 (1952).
96. W. C. Levensgood, *J. Am. Ceram. Soc.* **38**, 178 (1955).
97. F. Moser, *Glass Ind.* **42**, 5, 244 (1961).
98. I. S. Owens and E. C. Emanuel, *J. Am. Ceram. Soc.* **25**, 359 (1942).
99. H. E. Simpson, *J. Am. Ceram. Soc.* **42**, 7, 337 (1959).
100. G. F. Stockdale and F. V. Tooley, *J. Am. Ceram. Soc.* **33**, 1, 11 (1950).
101. H. E. Simpson, *Glass Ind.* **36**, 515 (1955).
102. H. E. Simpson, *J. Am. Ceram. Soc.* **38**, 2, 81 (1955).
103. S. Tsuchihashi, *J. Ceram. Assoc. Japan* **64**, 103 (1956).
104. A. M. Filbert and M. L. Hair, *J. Gas. Chromatog.* **6**, 218 (1968).
105. K. Rappaport, in *The Chemistry of Biosurfaces*, Vol. 2 (M. L. Hair, ed.), Marcel Dekker, New York (1972).
106. J. H. P. Watson, *Phys. Rev.* **148**, 223 (1966).
107. W. Haller, *Nature* **206**, 693 (1965).

HALOGEN CORROSION OF METALS

Phillip L. Daniel

*Materials Technology Department
Goodyear Atomic Corporation
Piketon, Ohio*

and

Robert A. Rapp

*Department of Metallurgical Engineering
The Ohio State University
Columbus, Ohio*

INTRODUCTION

Halogens and many halogen compounds are very corrosive. In fact, iodine was discovered when, as an impurity in soda ash, it caused corrosion of copper vessels.¹ Hence, materials for containing and handling halogens and corrosive halogen compounds must be selected with particular care.

The search for halogen-resistant materials has been directed mainly toward evaluation of existing materials, i.e., materials developed for other purposes, and little research has been directed toward the development of new materials designed specifically for halogen resistance. Materials evaluation procedures have generally taken the form of scoping studies, wherein many materials are tried in halogen atmospheres for short periods. A few careful laboratory studies of pure metals have also been made. Results of both types of studies on metals and alloys are reviewed in this chapter.

The chapter consolidates and interprets experimental metal-halogenation data that have been published in the open literature through 1973. Available halogen-attack data are reviewed for the more common metals of the periodic table of elements. Halogen corrosion data are not reviewed for the lanthanide or actinide metals; these metals are of little interest as materials of construction, and it is not felt that their corrosion

behavior relates sufficiently to that of more commonly used metals to justify their inclusion in this review. Halogenation of these very reactive metals as a means of separating them from one another is a common practice; hence, considerable information about the properties of their halides is available.⁴ In this chapter, oxidation and corrosion theories are applied to the problems of destructive metal and alloy halogenation. The resistance of various metals to halogenation is related, through a discussion of reaction mechanisms, to physical and thermodynamic properties of metal halide reaction products.

Consideration of halogenation mechanisms is necessary because of the large number of variables involved, including temperature, flow rate, laminar or turbulent nature of flow, halogen partial pressure, diluent gases, active impurity gases such as oxygen, water and halide vapors, abrasion, thermal and mechanical stresses, metal impurities and microstructures, vibration, and radiation. In fact, the practical variations of alloy compositions and environmental conditions are virtually infinite, so that one cannot possibly evaluate all of them in laboratory or pilot-plant studies. But from some basic laboratory data on reaction kinetics and observations of product morphologies and phases, coupled with an understanding of the scaling and vaporization processes involved, one can anticipate unforeseen problems, determine the cause of existing problems, and design better laboratory tests to evaluate materials for commercial service. Moreover, because of the large number of variables involved, numerical rate data are of little value unless one understands the dependence of these data on laboratory conditions and the changes that are likely to occur when the laboratory-tested material is put into a particular industrial environment.

Although the corrosion of metals and alloys by pure halogens receives predominant attention in this chapter, many of the mechanisms and principles involved are common to the related problems of corrosion by interhalogens, gas mixtures, hydrogen halides, metal halides, and other halogenating agents. The basic reaction mechanisms and principles still apply, but additional reactants and reaction products must be considered. Other gases can act as diluents through which halogen gases and volatile reaction products must diffuse to and from the reaction zones. Metals may be passivated not only by binary metal halides, but by oxides, oxyhalides, hydrates, and the like. Metals may also be passivated against halogen attack by deposition of solid reduction products on the metal surfaces, for example,



where $MeX_4(s)$ blocks further rapid $M - MeX_6(v)$ reaction. On the other

hand, such product compounds could accelerate reaction rates. For example, if liquid or volatile oxyhalides or hydrates are formed, they may prevent passivation.

PERTINENT PROPERTIES OF BINARY METAL HALIDES

In this section, a few properties of binary metal halides are summarized and their influences on halogen-metal reaction kinetics are briefly discussed. A subsequent section of this chapter discusses in more detail the theory of halogen-metal reaction and the interplay of the halide properties presented here with reaction morphology, mechanism, and kinetics. Important properties include: relative coefficients of thermal expansion for halide and parent metal; thermodynamic stabilities of condensed and volatile halide species; and halide melting points, vapor pressures, plasticities, electrical conductivities, and ionic diffusion coefficients. The most frequently used reference for compiling this and subsequent sections was the review series *Halides of the Transition Elements* by Canterford, Colton, and Brown.²⁻⁴

Thermodynamic Properties

The thermodynamic stability of any condensed phase relative to a tentative chemical reaction can be determined by calculation from a knowledge of the standard free energies of formation for each reactant and product compound, plus consideration of any deviation from standard conditions for the phase involved. Thus, for the formation of a condensed lowest halide product M_xX on the metal M , the pertinent reaction can be written



with

$$\Delta G_1 = \Delta G_1^0 + RT \ln \frac{a_{M_xX}}{a_M^\chi \cdot P_{X_2}^{1/2}} \quad (2)$$

where $\Delta G_1^0 = \Delta G_{M_xX}^0$ is the standard Gibbs energy of formation for M_xX based on unit fugacity standard state for X_2 gas and coexistence standard states for the condensed phases, i.e., M saturated with respect to M_xX , and M_xX saturated with respect to M .

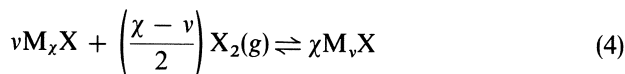
If the metal and product phases are present or would form in their standard states (at unit activity), then the critical halogen partial pressure

$P_{X_2}^*$ for the existence or formation of the bulk halide M_xX is given by

$$P_{X_2}^* = \exp \left(\frac{2 \Delta G_{M_xX}^0}{RT} \right) \quad (3)$$

For $P_{X_2} < P_{X_2}^*$, $\Delta G_1 > 0$, and the bulk halide is thermodynamically unstable ; for $P_{X_2} > P_{X_2}^*$, $\Delta G_1 < 0$, and spontaneous formation of M_xX is expected unless M_xX should be unstable relative to the formation of some other phase by another chemical reaction.

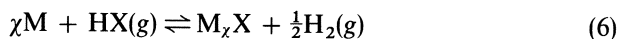
For the further formation of a higher halide product M_vX on M_xX ,



Here, the critical halogen activity for the formation of M_vX on M_xX is given by

$$P_{X_2}^* = \exp \left[\frac{2(\chi \Delta G_{M_vX}^0 - v \Delta G_{M_xX}^0)}{(\chi - v)RT} \right] \quad (5)$$

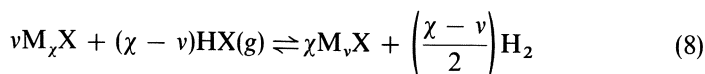
If the tentative reaction should involve a two-component gas mixture, such as hydrogen and hydrogen halide, the equivalent reactions would convert to



with

$$\left(\frac{P_{H_2}^{1/2}}{P_{HX}} \right)^* = \exp \left(\frac{\Delta G_{HX}^0 - \Delta G_{M_xX}^0}{RT} \right) \quad (7)$$

For the formation of M_vX on M_xX ,



with

$$\left(\frac{P_{H_2}^{1/2}}{P_{HX}} \right)^* = \exp \left[\frac{v \Delta G_{M_xX}^0 + (\chi - v) \Delta G_{HX}^0 - \chi \Delta G_{M_vX}^0}{(\chi - v)RT} \right] \quad (9)$$

In gas mixtures such as H_2 - HX , the critical conditions for equilibrium coexistence between two condensed phases are expressed as critical ratios of the partial pressures, in this case, $P_{H_2}^{1/2}/P_{HX}$.

Tabular data and parametric functions for the Gibbs energies of formation for halide compounds have been compiled in the JANAF tables⁵ among many other sources.^{2-4,6-14} Reed¹⁵ has recently presented these data

in plots of ΔG_f^0 per mole of F_2 versus temperature; Reed's plots are reproduced here as Figs. 1–6. However, recent, precise measurements of ΔG^0 formation for the fluorides were published by Skelton and Patterson.¹⁶ These data, which are added to Figs. 1 and 2, are preferred by the authors to the values compiled by Reed. These plots provide a quantitative means (with some understandable uncertainty because of the small scale) for the evaluation of Eqs. (3), (5), (7), and (9). The reader is cautioned that in these plots the ΔG_f^0 data have been normalized relative to 1 mole of F_2 , while the equations presented here require values of ΔG_f^0 per mole of the condensed phase or per molecular formula for the gaseous species.

Melting Temperatures

The melting temperatures for the metal halides are compiled in Table 1. The reader is reminded to use a binary phase diagram for ascertaining minimum liquidus temperatures when the reaction products comprise multiple scales, e.g., FeX_2 and FeX_3 upon the reaction of pure Fe in X_2 . Likewise, upon the reaction of a binary alloy in an X_2 environment, the mixture of product compounds for each component can establish a liquidus temperature far below those of the constituent compounds. Then, one must consult the pertinent ternary or quasi-binary phase diagrams^{17,18} to establish liquidus temperatures.

When the reaction product is a liquid, for example $AgF \cdot AgF_2$ at 300°C, it may remain on the metal surface and offer some tenuous resistance to further halogenation of the metal. But even when a liquid halide remains on the metal surface, it usually dissolves a significant quantity of one or both reactants and hence permits the reaction to continue at a significant rate. Obviously, the formation of liquid reaction products must be avoided.

Diffusion Properties

Information about relative diffusion rates in halides may be inferred from halide melting points. Such information, though tenuous, may be valuable since more substantive diffusion data for metal halides are not generally available. At temperatures below one-half the melting point, bulk diffusion of halogen and metal ions through the halide scale will be very slow, but above one-half the melting point, volume diffusion may be significant. For example, at $0.5T_m$, the diffusion coefficient for cations in sodium chloride is less than 10^{-13} cm²/sec, but at $0.75T_m$, $D_{Na}^*(NaCl)$ is about 3×10^{-10} cm²/sec.¹⁹ At

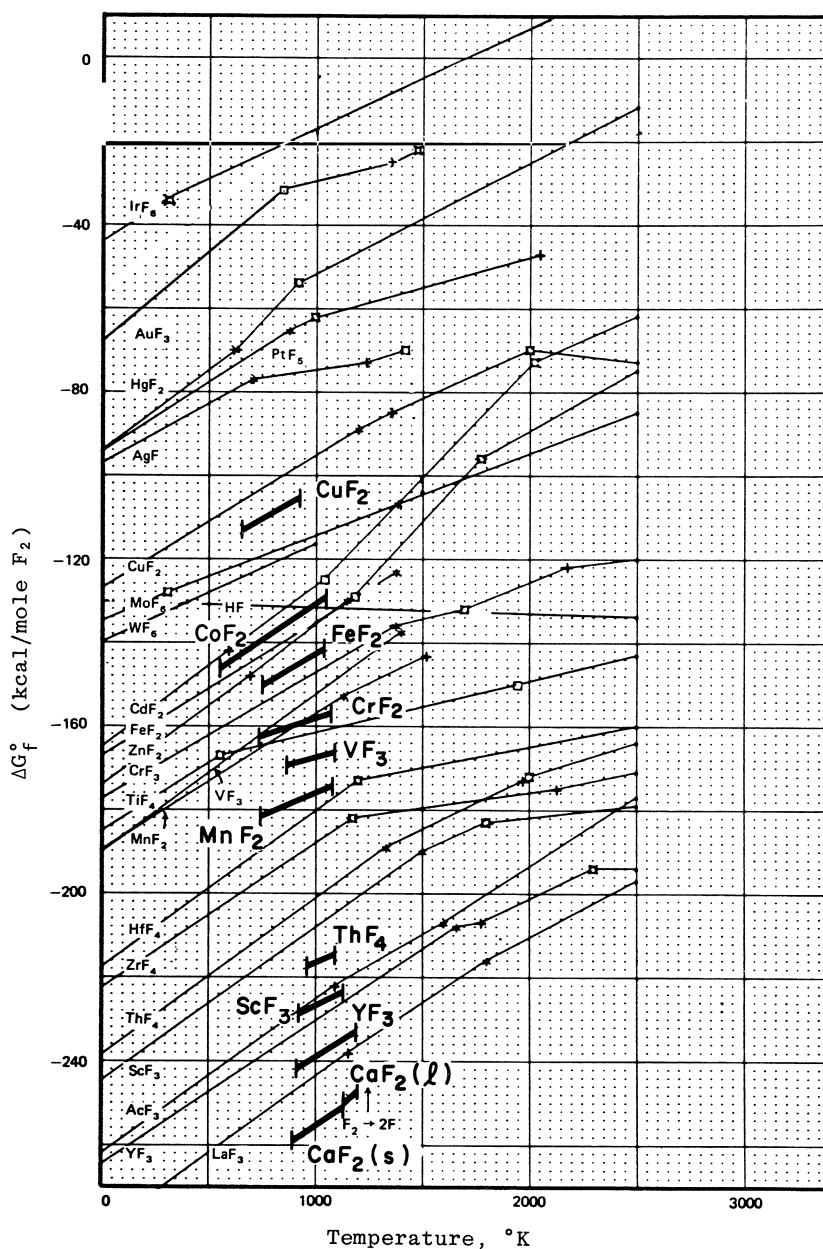


Fig. 1. Standard free energies of formation of condensed transition and group IIB metal fluorides from JANAF tables⁵ via Reed.¹⁵ (Reprinted from *Free Energy of Formation of Binary Compounds* by T. B. Reed by permission of the MIT Press, Cambridge, Mass.)

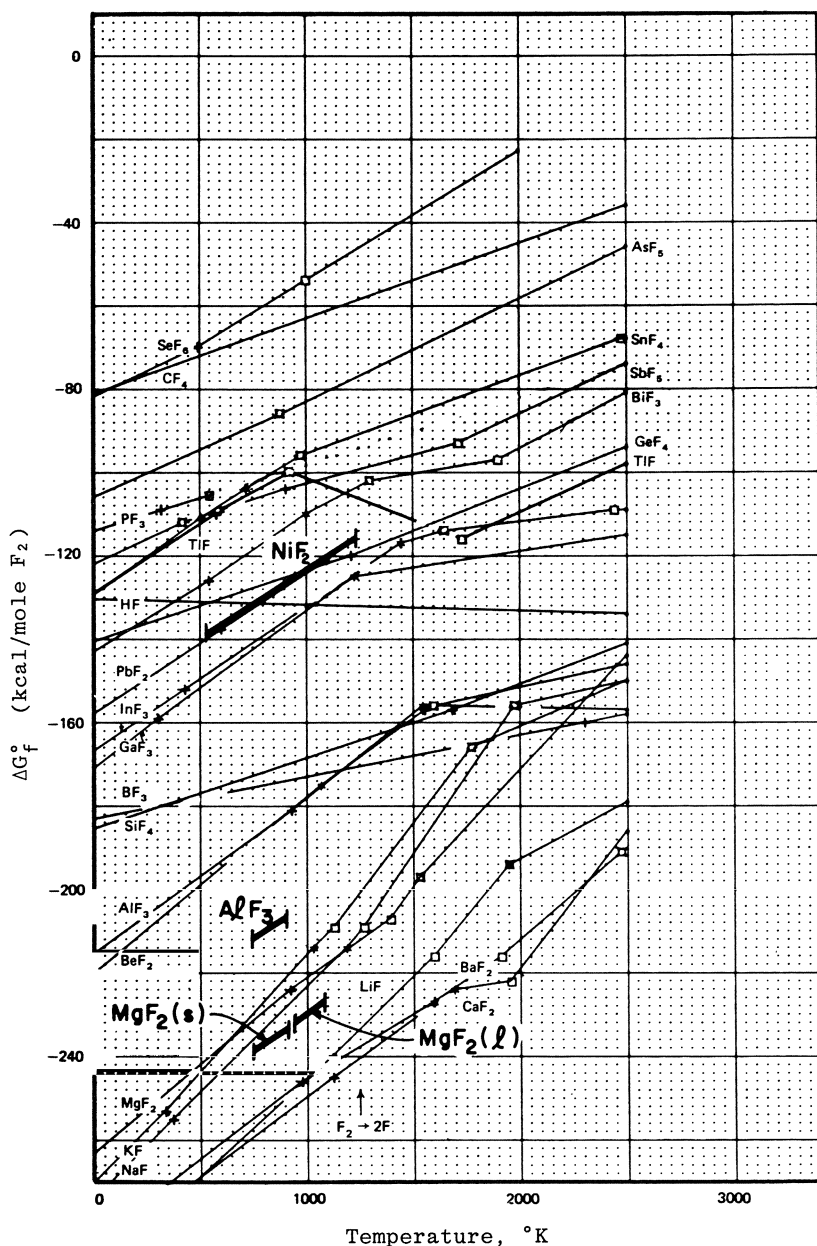


Fig. 2. Standard free energies of formation of condensed group I-VIA fluorides from JANAF tables⁵ via Reed.¹⁵ (Reprinted from *Free Energy of Formation of Binary Compounds* by T. B. Reed by permission of the MIT Press, Cambridge, Mass.) Heavy lines represent data from recent electrochemical measurements of Skelton and Patterson.¹⁶

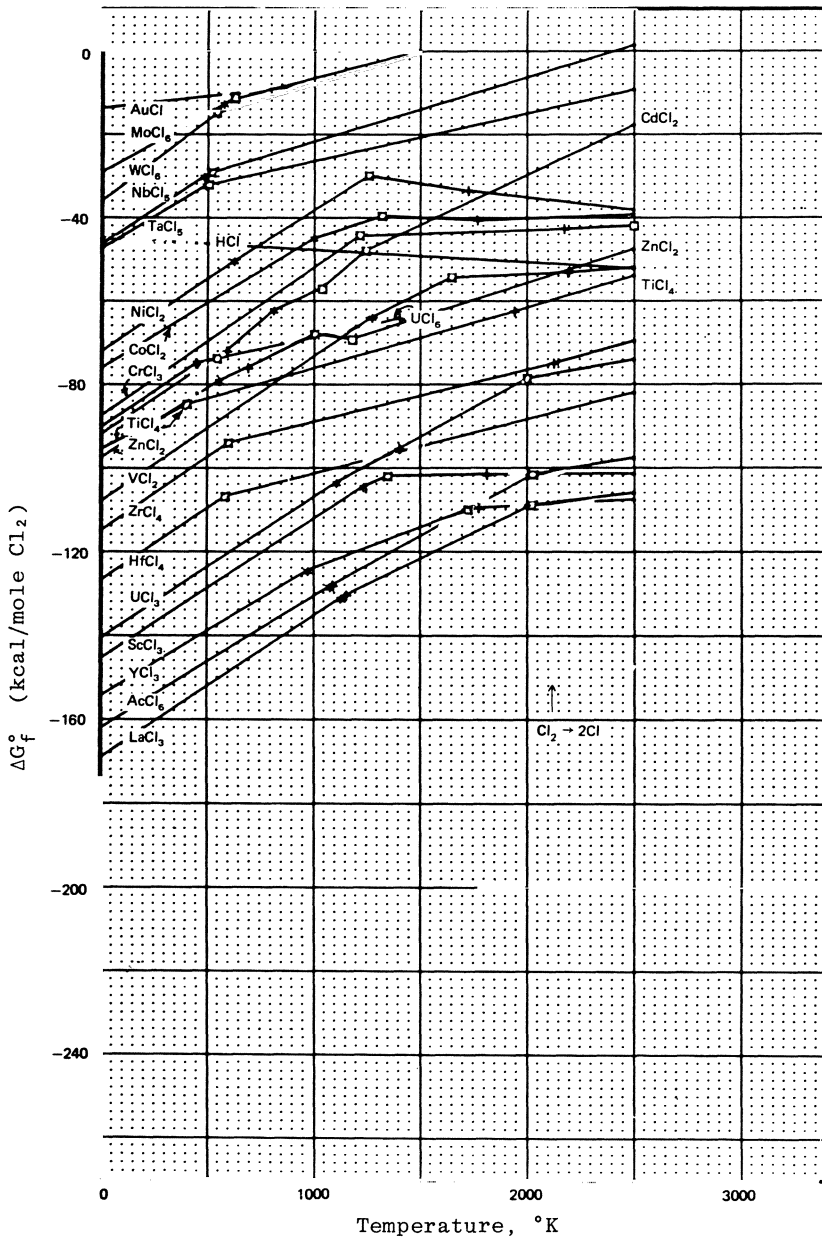


Fig. 3. Standard free energies of formation of condensed transition and group IIB metal chlorides from JANAF tables⁵ via Reed.¹⁵ (Reprinted from *Free Energy of Formation of Binary Compounds* by T. B. Reed by permission of the MIT Press, Cambridge, Mass.)

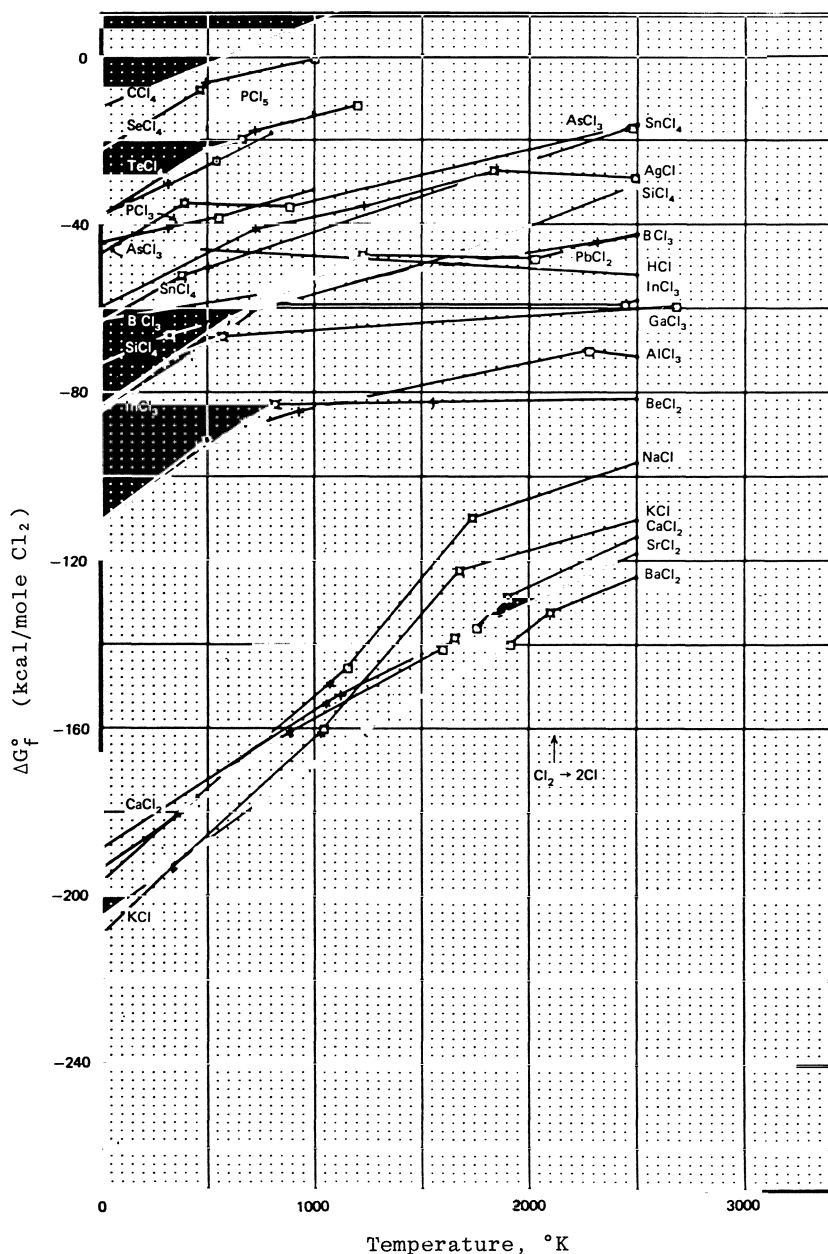


Fig. 4. Standard free energies of formation of condensed group I-VIA chlorides from JANAF tables⁵ via Reed.¹⁵ (Reprinted from *Free Energy of Formation of Binary Compounds* by T. B. Reed by permission of the MIT Press, Cambridge, Mass.)

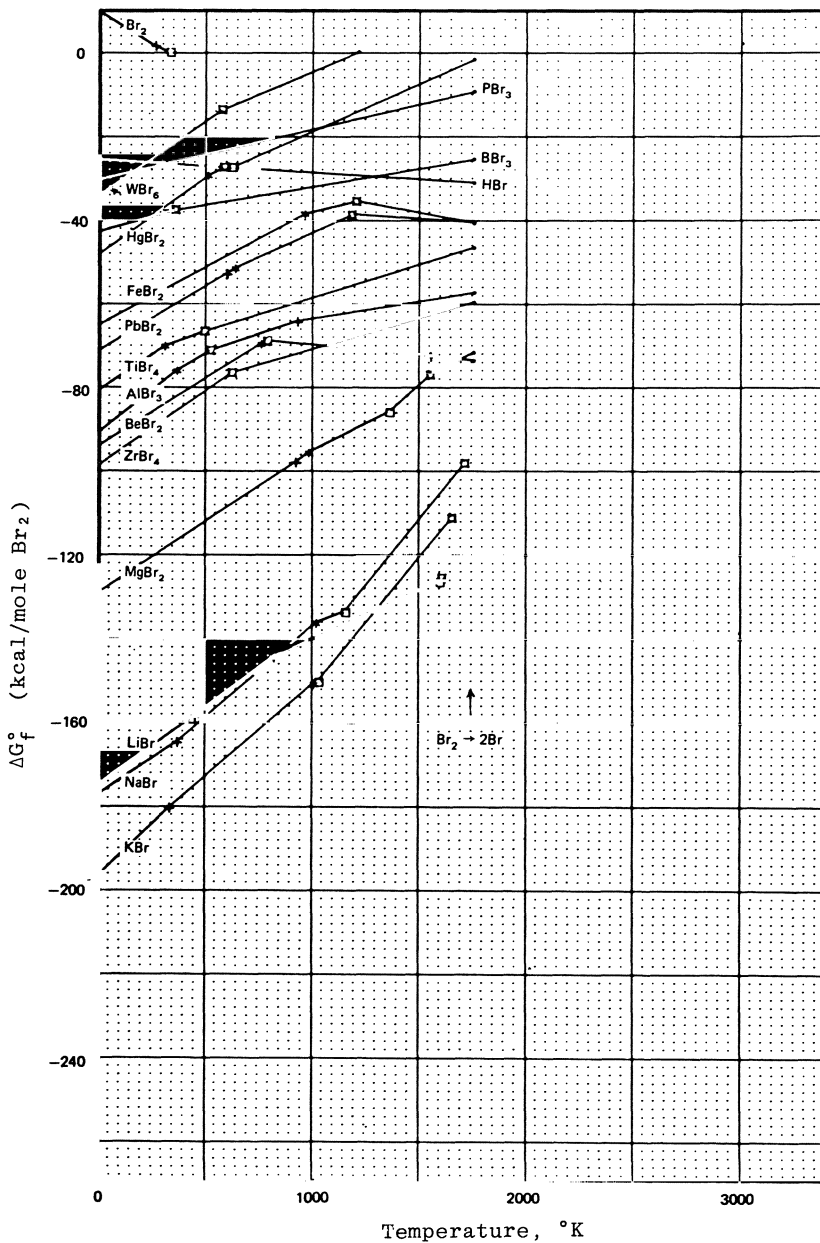


Fig. 5. Standard free energies of formation of some condensed metal bromides from JANAF tables⁵ via Reed.¹⁵ (Reprinted from *Free Energy of Formation of Binary Compounds* by T. B. Reed by permission of the MIT Press, Cambridge, Mass.)

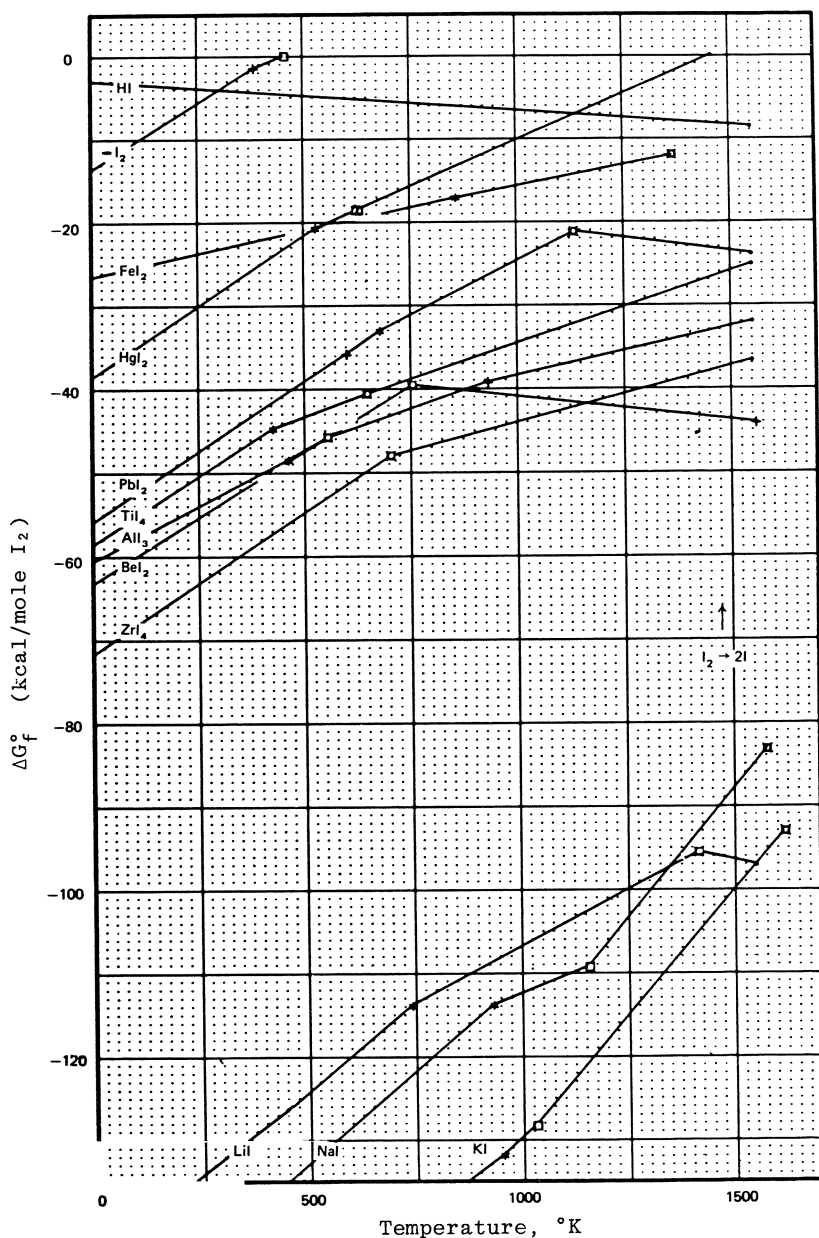


Fig. 6. Standard free energies of formation of some condensed metal iodides from JANAF tables⁵ via Reed.¹⁵ (Reprinted from *Free Energy of Formation of Binary Compounds* by T. B. Reed by permission of the MIT Press, Cambridge, Mass.)

Table 1. Binary Metal Halide Melting Points^a (T_m) and Temperatures^a (T_4) at Which the Halide Vapor Pressure is 10^{-4} atm^{2-5,7,14}

	Fluorides		Chlorides		Bromides		Iodides	
	T_m	T_4	T_m	T_4	T_m	T_4	T_m	T_4
<i>Alkali metal halides</i>								
LiX	848	908	610	665	550	630	469	621
NaX	992	928	801	742	750	690	660	(651) ^b
KX	857	788	772	706	740	671	685	629
RbX	775	716	715	672	680	657	640	(608)
CsX	703	609	645	611	635	623	621	600
RbX ₃							190	
CsX ₃					180		208	
CsX ₅							73	
<i>Alkaline earth metal halides</i>								
BeX ₂	803	533	410	269	488	251	480	225
MgX ₂	1263	1257	714	(663)	710	(626)	650	(425)
CaX ₂	1418	1429	772	(1039)	742		740	
SrX ₂	1400	1400	872		653		515	
BaX ₂	1290	(1581)	962		854		712	
RaX ₂					728			
<i>Transition metal halides</i>								
CuX	908		430	387	488	435	588	529
AgX	435	(340)	455	780	432	811	558	683
TiX ₂			1025	921			600	650
VX ₂			1350	726		527	> 1000	581
CrX ₂	894	(928)	820	741	842	716	869	702
MnX ₂	920	(992)	652	607	695		613	
FeX ₂	1020	906	676	536	689	509	594	476
CoX ₂	1250	962	740	587	678		515	
NiX ₂	1450	939	1030	607	965	580	780	
CuX ₂	950	760	622		498			
PdX ₂			678	474	717		> 740	
AgX ₂	690							
TiX ₃	1200			454				
VX ₃	1400	885		521		337		
CrX ₃	1404	855	1150	611	> 800	615	> 600	
MnX ₃		947						
FeX ₃	1027	673	303	167		156		
PtX ₃			435					
AuX ₃				182				
TiX ₄		108	- 23	(- 38)	39	20	150	(92)
VX ₄			- 20	(- 36)				
CrX ₄	> 100					516		
ZrX ₄	932	583	483	146	450	169	499	227
NbX ₄				239			503	
HfX ₄		615	434	132	424	137	449	244

Table 1 (contd.)

	Fluorides		Chlorides		Bromides		Iodides	
	T_m	T_4	T_m	T_4	T_m	T_4	T_m	T_4
<i>Transition metal halides (contd.)</i>								
TaX ₄				241	392		> 398	
ReX ₄	125							
PtX ₄	> 600							
VX ₅	19	-59						
CrX ₅	30							
NbX ₅	79	43	205	81	267	151		
MoX ₅	64	(24)	194	58				
TcX ₅	50							
RuX ₅	86	(49)						
RhX ₅	95							
TaX ₅	97	(37)	216	80	267	145	496	208
WX ₅			240	72	276			
ReX ₅	48	(31)	220					
OsX ₅	70	(43)						
IrX ₅	104							
PtX ₅	80							
MoX ₆	17	-82						
TcX ₆	37	-66	25					
RuX ₆	54							
RhX ₆	70							
WX ₆	2	-91	280	11	309			
ReX ₆	19	-81	25					
OsX ₆	32	-73						
IrX ₆	44	-71						
PtX ₆	61	-58						
ReX ₇	48	-68						
<i>Zinc group</i>								
Hg ₂ X ₂	570		400		407		290	
ZnX ₂	875	(806)	318	(349)	398	(320)	446	316
CdX ₂	1110	(976)	568	467	567	403	390	347
HgX ₂	645		278	97	238	97	250	116
<i>Boron group</i>								
InX			225	234	290	269	365	317
TiX	327	334	429	357	460	361	440	369
GaX ₂			164					
InX ₂			235		235		212	
BX ₃	-128	-171	-107	-112	-47	-67	50	2.3
AlX ₃	> 1273	825	193	76	97	53	191	144
GaX ₃	> 800		78	79	122	(83)		
InX ₃	1170		586	288	436	170	210	
TiX ₃			25					

Table 1 (contd.)

	Fluorides		Chlorides		Bromides		Iodides	
	T_m	T_4	T_m	T_4	T_m	T_4	T_m	T_4
<i>Carbon group</i>								
GeX ₂					122			
SnX ₂	212		247	(245)	215		320	
PbX ₂	822	(664)	498	484	373	432	412	397
Si ₂ X ₆	-19	-97			95			
CX ₄	-184		-24	(-80)	90	-3		
SiX ₄	-90	-160	-70	(-87)	5		122	(55)
GeX ₄			-49	(-66)	26	(-8)	146	88
SnX ₄			-33	-50	31	(-19)	145	83
PbX ₄	600		-15					

^aTemperatures are expressed in degrees centigrade.

^bValues in parentheses are of low reliability.

$0.5T_m$, the diffusion coefficient for silver ions in silver bromide is less than 10^{-11} cm²/sec, but at $0.75T_m$, D_{Ag}^* (AgBr) is about 10^{-7} cm²/sec.¹⁹ One-half the melting point of CuF₂ is 327°C. While fluorination of copper follows logarithmic kinetics below 300–350°C, above 300–350°C it follows parabolic kinetics characteristic of diffusion-controlled scale formation. Using this relationship between halide melting points and diffusion coefficients, at 150°C one would expect much more rapid SnF₂ ($T_m = 212^\circ\text{C}$) scale formation on tin than MgF₂ ($T_m = 1263^\circ\text{C}$) scale formation on magnesium, providing that scale growth rates are diffusion limited in both cases. Of course, other factors, such as crystal structure, also strongly influence the diffusion coefficients. Therefore, the $0.5T_m$ -diffusion coefficient relationship described here is tenuous indeed.

Vapor Pressures

Table 1 shows the temperatures (T_4) at which the halide vapor pressure attains a value of 10^{-4} atm. Some entries were extrapolated from experimental data obtained at a higher or lower temperature; when this extrapolation was carried across the melting temperature, a change in the enthalpy of vaporization equal to ΔH_{fusion} was assumed. Thermodynamically, this procedure is fully justified.

In a succeeding section, "Reaction Morphologies, Mechanisms, and Kinetics," a quantitative evaluation of scale evaporation in terms of the

pertinent halide vapor pressure is discussed. The problem is complex and the volatilization rate depends on sample geometry, flow rate, laminar or turbulent nature of flow, and gas interdiffusivities, as well as on halide vapor pressure. The problem is analogous to solving a similar heat transfer problem and use is frequently made of this analogy to analyze the kinetics; see, for example, reference 20. When reaction rates are high, the exothermic heat of scaling may increase the halide surface temperature significantly above that of the surrounding halogen gas. Homogeneous condensation of the vapor in the gas stream near the halide surface may reduce saturation in the boundary layer adjacent to the halide and, hence, increase the evaporation rate.²⁰ Evaporation may also be enhanced by condensation of vapor onto cooler adjacent surfaces. For low halogen flow rates or for static systems, transport to such condensation sites may be the rate-limiting step in halide volatilization.

In this and the succeeding section, vaporization of the type $MX_n(c) \rightarrow MX_n(v)$ is tacitly assumed. Complications arise when other types of vaporization also occur.²¹ Other types of dissociative, associative, and reactive vaporization include, for example, $MX_n(c) \rightarrow M(v) + (n/2)X_2(v)$, $mMX_n(c) \rightarrow (MX_n)_m(v)$, $MX_n(c) + (m/2)X_2(v) \rightarrow MX_{n+m}(v)$, $MX_n(c) + H_2O(v) \rightarrow MX_n \cdot H_2O(v)$, $MX_n(c) + mHX(v) \rightarrow MX_n \cdot mHX(v)$, $MX_n(c) + \frac{1}{2}O_2(v) \rightarrow MOX_n(v)$, and $MX_n(c) + MeX_m(v) \rightarrow MMeX_{n+m}(v)$. The authors recommend Kellog's method²¹ for the analysis of equilibrium vapor pressures for vapor species that differ in composition from the condensed phase. However, these considerations are much more pertinent to oxidation and sulfidation than to halogenation.

In a pure 1.0-atm halogen gas stream, vaporization involving H_2O , O_2 , HX , and MeX_m cannot occur, and the disproportionation $MX_n(c) \rightarrow M(v) + (n/2)X_2(v)$ may be suppressed by the high halogen gas pressure. This leaves $MX_n(c) \rightarrow MX_n(v)$, $mMX_n(c) \rightarrow (MX_n)_m(v)$, and $MX_n(c) + (m/2)X_2(v) \rightarrow MX_{n+m}(v)$ as the more important types of volatilization. The data given in Table 1 generally include all species of the type $(MX_n)_m$, but no account was taken of higher-valence-state vapor species, MX_{n+m} , which are not stable as the condensed phase. The formation of such species, however, would only serve to increase further the volatilization rate, which, at the indicated temperatures, is already significant.

At the 10^{-4} -atm vapor-pressure temperatures indicated in Table 1, significant vaporization occurs unless the equilibrium halide vapor pressure is attained in a static or recirculating halogen atmosphere. Metals to be used in flowing halogen atmospheres should always be tested under flowing rather than static conditions.

EXPERIMENTAL METHODS USED TO STUDY METAL-HALOGEN REACTIONS

This section briefly describes some experimental techniques for the determination of reaction kinetics. In general, the methods used to study metal-halogenation kinetics are the same as those used to study metal-oxidation kinetics. These methods and the associated literature are surveyed by Kofstad²² and by Wood.²³ However, because of the highly toxic and reactive nature of the halogen gases, several specific problems are encountered in halogenation studies. Halogen-resistant materials of construction must be chosen for the experimental systems, outleakage of halogen gases into the laboratory must be avoided, and halogen gases used in the experimental systems must be assimilated for disposal.

The use of a glass apparatus for fluorine can introduce several problems—the attack of the walls in the presence of moisture and the adsorption on the specimens by vapors emitted from grease (even totally fluorinated grease). Manometric apparatus constructed from metallic materials can partially escape these difficulties.

Manometric Method

A manometric or pressure-drop method is described by Brown *et al.*²⁴ Samples to be halogenated are placed into a reaction system of known volume, a quantity of halogen gas is added to the system, and the system is sealed. The pressure of halogen gas in the system is then monitored as halogenation occurs. This method is generally used only where nonvolatile halides are formed. The quantity of halogen consumed by the halogenation reaction can be calculated from the pressure drop. Subsequently, the amount of scale formed per unit area of metal sample and the corresponding reaction rate can be calculated.

Brown *et al.* used a glass system, taking care to assure that the system and fluorine gas were free of moisture since glass is attacked by moist fluorine. A fully fluorinated grease was used to lubricate stopcocks. The fluorine pressure of the system was monitored with a membrane-type manometer; the fluorine-containing system was separated from a second gas volume by an impervious membrane. The air pressure in the second system was adjusted to balance the pressure in the fluorine system, i.e., adjusted to give zero distension of the separating membrane. This balancing air pressure was then measured with an oil manometer. Brown *et al.* state that pressure changes of 0.01 torr can easily be detected by their technique.

O'Donnell²⁵ and Spakowski used a similar technique and also a glass system. However, instead of using a membrane-type manometer, O'Donnell used conventional mercury manometers with fluorinated oil floating on top of the mercury to prevent contact between the mercury and fluorine gas.

Gravimetric Method

Several gravimetric methods are used to measure the extent of metal-fluorine reactions. The simplest gravimetric method is that described by Myers and DeLong.²⁶ Metal samples are weighed with a conventional laboratory balance before and after halogenation and linear rate constants, for example, as inches of scale growth per month, are calculated. This procedure gives no information about the time dependence of the scale growth kinetics and should not be considered adequate for the comparison of the halogen resistance of different metals. When test durations are short, the validity of the comparison is questionable because metals may follow different reaction kinetics. For example, the reaction kinetics may be linear for one metal and parabolic or logarithmic for another, so that the kinetic curves would cross at some time, which would account for an opposite ranking of materials for short-time and long-time performance.

A gravimetric procedure can, however, be used to determine reaction kinetics: many duplicate metal samples would be introduced simultaneously into the halogen environment, and then these would be individually withdrawn for weighing after many different time intervals. The method is valid to the extent that the results are reproducible. A less satisfactory alternative procedure is to halogenate in steps, weighing samples between exposures. In this case, halide scales are exposed to atmospheric moisture during weighing and are subjected to thermal cycling if the halogenation temperature is different from room temperature. Hence, the scale may be altered by the weighing process. Of course, weighings might also be done in a dry box.

In their studies of metal halogenation, Vincent *et al.* have preferred to use visual and microscopic examination of alloy surfaces as a definitive method for the initial classification of the metals as halogen-resistant or halogen-incompatible. Gravimetric methods are then only used to study further the halogenation kinetics for those resistant alloys which promise the possibility of engineering application.

Using a quartz helical balance, Kuriakose and Margrave²⁷ followed continuously the weight change of silicon and boron samples during fluorination. Their apparatus consisted of a glass system with a vertical tube in which the metal sample being fluorinated was suspended by a fine nickel wire from

one end of a quartz helix. After the extension of the helix is calibrated in terms of sample weight, changes of less than 1 mg can be measured accurately.

Torsion and other types of balances can also be used for studying halogenation kinetics. If the balances are exposed to fluorine gas, they must be constructed of quartz and other materials that do not react with fluorine, at least not after an initial passivating exposure. Gulbransen²⁸ describes a torsion balance constructed mainly of fused quartz. If materials that react with the halogen gas are used in construction of the balance, the halogen must be excluded from the balance chamber by, for example, a counterflow of nitrogen.

Moist fluorine and hydrogen fluoride react with glass and quartz. Hence, where glass systems and quartz balances are used in contact with fluorine gas, moisture and hydrogen fluoride must be excluded from the gas. This may be accomplished by passing the gas through a cold trap containing methyl cyclohexane slush (liquid nitrogen will condense fluorine as well as hydrogen fluoride) and then through a sodium fluoride trap.²⁴ Otherwise, a microbalance constructed entirely from resistant metals could be used.

Photometric Method

The photometric method was used by Shiu *et al.*²⁹ to study the chlorination of sodium and by Hung *et al.*³⁰ to study the fluorination of nickel. Dignam and Huggins³¹ describe the technique well. The metal specimen is a thin film through which light is transmitted. Light passes into and out of the test system through halogen-resistant windows, for example, quartz or sapphire. The light used may be visible, ultraviolet, or infrared; the wavelength used is one absorbed or reflected by the metal film but not absorbed by the windows, the halide corrosion product, or the halogen gas. Attenuation of the light beam caused by reflection and absorption by the metal film is calibrated in terms of the metal film thickness. A beam splitter and reference cell are used to avoid data noise arising from variations in the light source intensity. By this method, metal recession can be continuously measured to an accuracy of about $\pm 10 \text{ \AA}$.

Electrical Resistance Method

Rosner *et al.*^{32,33} describe some applications of the electrical resistance method for studying the kinetics of halogen attack on metals by atomic and molecular fluorine and chlorine. The electrical resistance of a wire specimen

is continuously measured and the magnitude and variation in the wire cross-section are calculated from the resistance values.

Quartz Crystal Microbalance

Hasegawa *et al.*³⁴ and Shiojiri *et al.*³⁵ use a quartz crystal microbalance to measure the weight gain of silver films in iodine vapor. As AgI forms on a silver-coated quartz crystal, the resonant frequency of the crystal is changed and this change is related to weight gain. The device has a sensitivity of less than 2×10^{-5} mg/cm² and is commonly used to measure the thickness of vapor-deposited films.

All the above methods have been used to study halogen-metal reaction kinetics and illustrate a few approaches to the materials and halogen containment problems. Later sections of this chapter review information about halogen attack on specific metals and, in so doing, suggest possible materials for use in halogen systems. One of the most commonly used is nickel. Further discussions of halogen handling procedures, safety precautions, and disposal methods are beyond the scope of this treatise, and the reader is referred to the literature of vendors supplying halogen gases and to references 36–43. Sterner and Singleton⁴³ give an extensive bibliography of additional references on the topic. The American Chemical Society provides a good monograph,⁴⁴ which also contains an extensive bibliography on chlorine handling procedures and precautions.

REACTION MORPHOLOGIES, MECHANISMS, AND KINETICS

When a metal or alloy reacts with halogen gas to form a solid product, the product may physically separate the two reactants. This circumstance acts to slow the reaction rate if the product phase is compact and free of macroscopic cracks and voids. On the other hand, cracked or porous scales allow ingress of halogen molecules and reduce the degree of protection. One must also account for dissolution of the nonmetal into the metal and the evaporation of the scale. Thus, the rate of scale growth or metal recession depends greatly upon chemical, physical, and mechanical properties of the intervening product scale.

Detailed information is available on scale growth in metal-oxygen (and air) systems and can be used to interpret scale growth in metal-halogen systems, where experimentation is much more difficult. We shall summarize

the scaling behavior of pure metals and that of alloys; we hope that an understanding of features common to both oxidation and halogenation will lead to progress in the understanding and control of metal-halogen reactions. In the interest of brevity, some generalizations and simplifications are presented quite blandly without perhaps sufficient reference to exceptions, qualifications, or substantiating literature.

Reaction of Pure Metals

Diffusion-Controlled Scale Growth at High Temperatures

When the predominant ionic defects in a compact scale are cation vacancies, the growth of a protective layer occurs by the outward diffusion of cations with a counterflow of vacancies and positive holes. Likewise, scale also forms at the scale/gas interface when the diffusion of interstitial cations and electrons predominate. If the predominant defects were anion interstitials (plus positive holes) or anion vacancies (plus electrons), a compact scale would grow at the metal/scale interface. A variety of marker movement observations is available to establish the site of scale growth.

Wagner^{45,46} has described the diffusion-controlled, parabolic growth of a compact, one-phase, layered scale on a pure metal to obtain the result:

$$\frac{dn}{dt} = \frac{1}{\xi} \frac{RT}{2FF'z_X^2} \int_{P_{X_2}^i}^{P_{X_2}^0} t_e(t_M + t_X) \sigma d \ln P_{X_2} \quad (10)$$

where dn/dt is the rate of growth of an MX scale in moles/cm² sec; ξ is the instantaneous scale thickness; z_X is the valence of the anion; t_e , t_M , and t_X are the electrical transference numbers of electrons, cations, and anions; σ is the total electrical conductivity of the scale formed; $P_{X_2}^i$ and $P_{X_2}^0$ are the nonmetal activities at the metal/scale and scale/gas interfaces, respectively; and F and F' are differing values for the Faraday constant having their appropriate units. Equation (10) shows that the growth of a compact scale can essentially be limited by the transport of electrons when $(t_M + t_X) \gg t_e$ (when the scale is a solid electrolyte), or by the transport of ions when $(t_M + t_X) \ll t_e$ (when the scale exhibits predominant electronic conduction). For many halides, the partial electrical transference numbers have been established as a function of P_{X_2} .

To explain the growth of a compact, one-phase, layered scale which

exhibits predominant electronic conduction, $t_e \gg (t_M + t_X)$, Wagner⁴⁷ has converted Eq. (10) as follows:

$$\frac{dn}{dt} = \frac{1}{\xi} \frac{1}{2V_{MX}} \int_{P_{X_2}^0}^{P_{X_2}^0} \frac{z_M}{z_X} (D_M^* + D_X^*) d \ln P_{X_2} \quad (11)$$

where V_{MX} is the molar volume of the product compound, and D_M^* and D_X^* are the self-diffusion coefficients for the cation and anion, respectively. These expressions for instantaneous scaling rate can be used for comparison with k_p , the gross parabolic scaling rate constant, defined by

$$\xi^2 = 2k_p t \quad (12)$$

through the relation

$$k_p = k_m V_{MX} \quad (13)$$

where k_m represents the quantities in parentheses in either Eq. (10) or Eq. (11).

While the validity of Wagner's theory for the growth of oxide scales has been frequently checked²² by comparison of experimental values of k_p with calculated values of k_m through Eqs. (11) and (13), comparable use of this possibility has not been made for the analysis of halogenation reactions. Obviously, these equations provide the basis to predict the dependence of k_p on both temperature and $P_{X_2}^0$.⁴⁶ For the formation of compact oxide scales on copper, nickel, cobalt, iron, and manganese, good agreement between k_p and the calculated k_m has been found at sufficiently high temperatures, i.e., at about 1000°C or $T/T_{\text{melt}}(\text{scale}) > 0.75$. Experimental activation energies and P_{O_2} dependencies for parabolic oxidation also agree with the predicted values. Such comparisons are, however, dependent upon the purity of the metal when the scale exhibits a low concentration of native ionic defects.²²

Local Cell Action in Halogenation

Because a number of halides exhibit predominant ionic conduction,⁴⁸ the phenomenon of local cell action can contribute to the consumption of a metal by halide scale formation. Ilschner-Gench and Wagner⁴⁹ reacted a silver specimen attached to a metallic (tantalum) substrate with iodine vapor at 174°C. As shown in Fig. 7, a thin compact AgI product of thickness δ formed directly on the silver at locations distant from the substrate. But, in addition, an overgrowth of AgI of large additional thickness ψ' extended across the tantalum substrate. Because AgI exhibits predominant ionic conduction, the growth of the AgI scale to a thickness ψ on the top of the

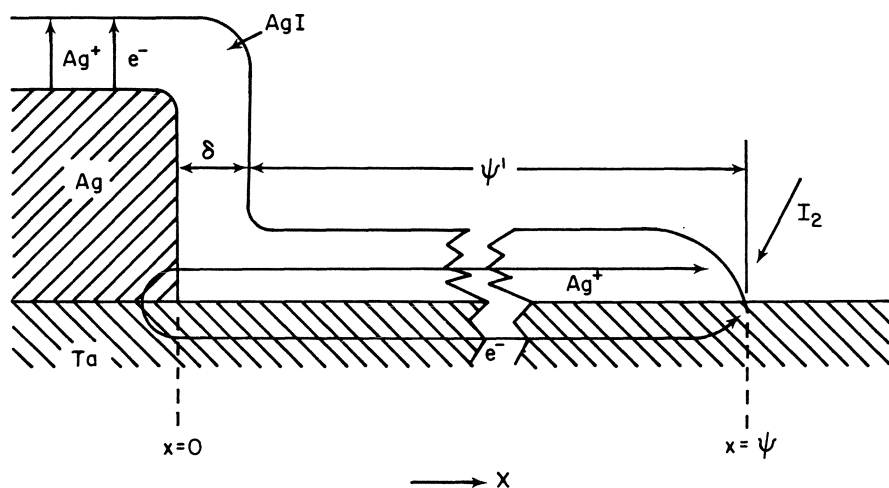


Fig. 7. Ilschner-Gench and Wagner⁴⁹ model for local cell action during the scaling of metals.

silver was controlled by the transport of electrons through AgI in accordance with Eq. (10). However, the rate of formation of the AgI overgrowth to a thickness ψ was controlled by the diffusion of Ag^+ cations through the overgrowth because electrons were short-circuited through the tantalum to the reaction site. The observed values of δ and ψ were exactly calculated from known conductivity values. Obviously, overgrowth formation should be anticipated whenever the corrosion product is a predominant ionic conductor.

Simultaneous Diffusional Growth and Evaporation of Scales

The relatively high vapor pressures of the halide compounds which form as surface products cause the loss of molecules from the scale to the vapor at the same time that the scale is growing by diffusional transport. In the oxidation of metals, this mixed reaction mode is also known but less important (less frequent) in comparison, because the oxides generally exhibit lower vapor pressures. Furthermore, for the oxides, the vapor species frequently differ in stoichiometry (composition) from the condensed phase; this circumstance introduces thermodynamic consequences (the vapor pressure of each species depends upon the activity of the nonmetal in the environment), as well as kinetic consequences (countertransport of reactant and product molecules are required in the gas phase).

In the analysis of gravimetric kinetics or measurements of either scale thickness or metal recession, this mixed mechanism must be considered in order to infer the identity and rates of the elementary reaction steps. Tedmon⁵⁰ described the oxidation rates of pure chromium and Cr₂O₃-forming Fe–Cr alloys at temperatures greater than 1100°C as the sum of a parabolic, diffusion-controlled scale thickening and a time-independent vaporization loss. The rate equation for the thickening of the scale is

$$\frac{d\xi}{dt} = \frac{k_p}{\xi} - k_v \quad (14)$$

where ξ is the scale thickness, k_p is the parabolic rate constant for the diffusion step, and k_v is the linear rate constant for the vaporization step.

For short times or thin films, Eq. (14) predicts parabolic behavior; however, with continued growth, the two terms on the right-hand side of Eq. (14) approach each other so that a steady-state scale thickness, $\xi_{s.s.}$, equal to k_p/k_v , is approached. The integration of Eq. (14) for $\xi = 0$ at $t = 0$ yields the result:

$$t = \frac{k_p}{k_v^2} \left[-\frac{k_v \xi}{k_p} - \ln \left(1 - \frac{k_v \xi}{k_p} \right) \right] \quad (15)$$

This functional dependence of ξ on t is schematically illustrated in Fig. 8.

In the consideration of metal recession, y , the metal is consumed both by an increase in ξ and by scale vaporization:

$$\frac{dy}{dt} = \frac{V_M}{V_{MX_v}} \left(\frac{d\xi}{dt} \right) + \frac{V_M}{V_{MX_v}} k_v = \frac{V_M}{V_{MX_v}} \left(\frac{k_p}{\xi} \right) \quad (16)$$

where V_M and V_{MX_v} are the molar volumes of the metal and the MX_v scale, respectively.

To interpret gravimetric kinetics for the growth of an MX_v compound scale, the rate equation must account for the weight gain for the net scale present minus the weight loss resulting from metal recession:

$$\frac{d(\Delta m/A)}{dt} = \rho_{MX} \frac{d\xi}{dt} - \rho_M \frac{dy}{dt} \quad (17)$$

where ρ_M and ρ_{MX_v} are the bulk densities of the metal and the scale, respectively. The combination of Eqs. (14), (16), and (17) gives

$$\frac{d(\Delta m/A)}{dt} = \frac{v N_X}{V_{MX_v}} \left(\frac{k_p}{\xi} \right) - \rho_{MX_v} k_v \quad (18)$$

where N_X is the atomic weight of the nonmetal.

Simple analytic integrations of Eqs. (16) and (18) are not obvious, so a quantitative evaluation of recession or gravimetric kinetics to obtain the fundamental rate constants k_p and k_v must proceed via numerical methods through integration of Eq. (16) or (18) after substitution of ξ from Eq. (15) [Eqs. (16), (17), and (18) differ from those found in the literature].⁵⁰ In any case, as $\xi_{s,s.}$ is attained, the rates of both metal recession and weight gain correspond solely to the linear rates of evaporation. This behavior is schematically illustrated in Fig. 8.

The Evaporation of Scales and the Reactive Evaporation of Metal

The maximum possible rate of vaporization, J_i , of any species i is related to its vapor pressure P_i by the Hertz–Langmuir equation:

$$J_i \left(\frac{\text{molecules}}{\text{cm}^2\text{-sec}} \right) = \frac{P_i}{\sqrt{2\pi m_i k T}} \quad (19)$$

where m_i is the mass of the molecule and k is Boltzmann's constant. This maximum possible rate is only experienced when the substance loses vapor at its equilibrium gross flux, J_i , with no backflux being returned and condensed at the surface. In gravimetric units, the actual net rate of vaporization may be expressed

$$G_i \left(\frac{\text{g}}{\text{cm}^2\text{-sec}} \right) = \frac{\alpha_i P_i (\text{atm})}{2.256 \times 10^{-2}} \left(\frac{M_i}{T} \right)^{1/2} \quad (20)$$

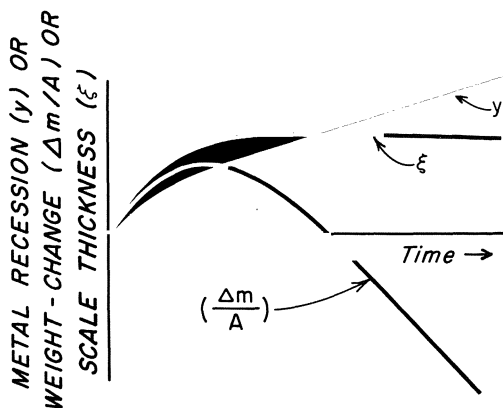


Fig. 8 Parabolic scale growth with linear evaporation of halide scales.

where P_i is the vapor pressure expressed in atmospheres, M_i is the molecular weight of the vapor species, and G_i is the weight of species i lost in vaporization per unit area per unit time. The parameter α_i is defined here to equal the fraction of the maximum possible evaporation rate resulting for a given set of environmental pressure, composition, temperature, and flow conditions. By this definition, α_i can describe net evaporation in the presence of vapor condensation caused by back-diffusion from a stagnant boundary layer or direct impingement from another vapor source. In this sense, our α_i differs from the usual evaporation coefficient.⁵¹ The actual rate of metal recession per side as described by Eq. (16) for the evaporation of MX_v molecules is given as

$$\frac{dy}{dt}(\text{cm/sec}) = \frac{\alpha_i V_{\text{MX}_v} P_i(\text{atm})}{2.256 \times 10^{-2}} \left(\frac{M_i}{T} \right)^{1/2} \quad (21)$$

The magnitude of the parameter α_i for scale evaporation could vary greatly depending upon the evaporation mechanism and the total pressure and flow rate of the reactive gaseous ambient. In our context, only a few generalizing remarks are possible. If a scale evaporates into a low-pressure ambient in the Knudsen (free or molecular) pressure regime, α_i might approach unity, especially if relatively cool surrounding surfaces would prevent the return of vapor molecules to the surface. Of course, to prevent the total loss of the scale and the exposure of bare metal, the rate of arrival of reactive halogen molecules in the low-pressure ambient must be equal to or greater than the rate of halogen loss by scale vaporization. Otherwise, the bare metal surface will react with a certain fraction of the impinging reactive molecules and the rate of attack (recession rate) will be limited by the arrival of the reactive molecules. Gelain *et al.*⁵² have conducted such a study of vaporization of SiO from Si and SiO_2 at low pressures.

For scale vaporization in the viscous pressure range, a number of mechanisms must be considered. If the rate of impingement of reactive molecules greatly exceeds the rate of loss by vaporization, the scale should attain partial chemical equilibrium with the P_{X_2} of the ambient. This aspect is important to reactive vaporization where the vapor species differ in composition from the condensed phase. As shown schematically in Fig. 9, the rate of vaporization of MX_v should be determined by the mass transfer of the volatile molecules MX_v through a stagnant boundary layer of effective thickness Δ . Depending upon the compositions of $\text{MX}_v(s)$ and $\text{MX}_v(v)$, a net flux of halogen X_2 to or from the surface is required.

Under steady-state conditions; the rate of vaporization J_{MX_y} can be expressed from Ficks' law as

$$J_{MX_y} = \frac{D[P_{MX_y}(\text{surface}) - P'_{MX_y}(\text{gas})]}{\Delta RT} \quad (22)$$

where D is the interdiffusion coefficient for the gas mixture, and $P_{MX_y}(\text{gas})$ is usually zero. For the streaming of the gases over a flat plate, the effective thickness of the boundary layer is given by

$$\Delta = 1.5LN_{Sc}^{-1/3}N_{Re}^{-1/2} \quad (23)$$

where L is the sample length and N_{Sc} and N_{Re} are the commonly used Schmidt and Reynolds numbers.

For the reactive vaporization of Cr_2O_3 to form $CrO_3(v)$, Graham and Davis⁵³ substantiated the theoretical expectation that

$$\Delta \propto v^{-1/2}P_t^{1/2} \quad (24)$$

where v is the uniform gas flow velocity and P_t is the total pressure. Although $P_{CrO_3}(\text{surface})$ was inferred to reach its equilibrium value in Ar- O_2 mixtures, the maximum observed value for α_{CrO_3} at $v = 120$ cm/sec and $P_t = 0.1$ atm equaled only 0.0046.

An active-passive transition, as introduced by Wagner⁵⁴ for the reactive vaporization of SiO_2 and $Si(l)$ to form SiO vapor, can occur in the viscous pressure range when a major inert component of the gaseous ambient limits the rate of arrival of a reactive gaseous component involved in the vaporization. Further, the mechanism requires that the vapor pressure of the metal be

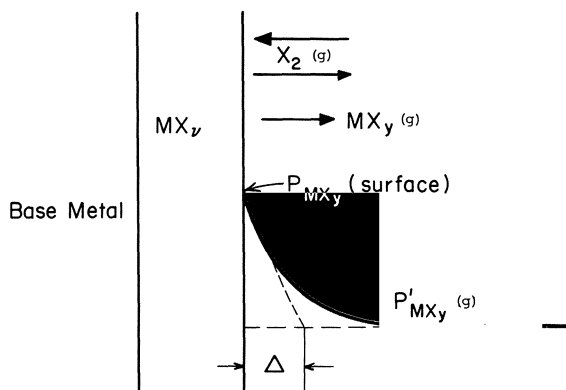


Fig. 9. Transport-limited vaporization of a MX_v scale as MX_y molecules.

low. In this case, the nonmetal activity at the surface and therefore the vapor pressure for the MX_y species at the surface (see Fig. 9) can differ significantly from the nonmetal activity and MX_y vapor pressure in the bulk gas phase. If the diffusion of X_2 to the metal through the boundary layer cannot attain the rate required for the diffusion-limited vaporization of MX_v , then the scale would be completely consumed, leaving the bare metal (active) surface. The rate of vaporization would correspond to the rate of arrival of X_2 .

If P_{X_2} of the bulk gas is increased sufficiently and P_{MX_y} at the surface reaches that value corresponding to the presence of MX_v , then MX_v forms, producing a scale-covered (passive) surface. The critical $P_{\text{X}_2}^*$ required according to this kinetic model to effect the transition can be calculated but, in general, does not even approximate the value expected from the thermodynamic calculation using $\Delta G_{\text{MX}_v}^0$. Further, there is a hysteresis effect on the critical value for $P_{\text{X}_2}^*$.⁵⁴

Another vaporization process that occurs in the viscous pressure range for metals exposed to mixtures of inert and reactive gases is very important to the oxidation of metals but of less interest in halogenation. If both the metal and the product compound exhibit relatively high vapor pressures and the gaseous reactant is again restricted in reaching the surface because of the requirement for diffusion through a stagnant boundary layer, then the metal surface can remain clean (active) and experience a vaporization rate equal to the diffusional flux of the metal atoms through the boundary layer. If the metal and reactant gas can form a stable condensed product at the reaction temperature, then the counterdiffusion and reaction of metal and nonmetal vapors can precipitate a “fog” or “smoke” of the condensed product in the vapor phase.⁵⁵

For the reaction of many liquid metals in Ar-O_2 and He-O_2 mixtures, the vaporization rates are proportional to P_{O_2} of the gas mixture and depended on the flow velocity of the gas mixture as well.⁵⁵ The maximum possible reaction rate corresponds to the Hertz–Langmuir flux of Eq. (19). Quantitative predictions of the reactive vaporization rates are possible for systems with well-defined gas flow conditions. Because metal halides are generally much more volatile than the metals, we would expect that a metal might be maintained clean and active in halogen reactions by the formation of halide molecules at the surface⁵⁴ but not as fog in the vapor phase.⁵⁵

Low-Temperature Scaling (Thin Films)

The separation of scaling behavior into temperature or scale thickness regimes is arbitrary, but such considerations are useful in localizing certain

important aspects of scaling kinetics. Complete agreement among authors on the most important features of the low-temperature scaling model is lacking, but clearly both the physics and the morphology of the scale contribute to the mechanism.⁵⁶ Only a brief discussion is possible here.

As a bare metal surface is exposed to an oxidant, an adsorbed film of a specific structure, as can be revealed by LEED studies, is set up. With a highly efficient capture of incident molecules, the adsorbed state progresses rapidly to a stable film (several Å thick), at which time the growth rate slows because either (a) cations, anions, or electrons are effectively immobile in the film, or (b) cations or anions are hindered at the metal/film or at the film/gas interface, respectively, from entering the scale.

At the film/gas interface, dissociated oxidant molecules (i.e., atoms) are reduced when tunneling electrons are trapped to provide an excess of negative surface charge. The resulting electric field across the growing film provides (a) a reduction in the potential energy barriers required for the diffusion of ions or for the tunneling of electrons across the film, and/or (b) a reduction in potential energy barriers for the insertion of ions into the oxide. Various authors differ on the selection of the rate-limiting step.

The morphological features of the thin film, as influenced by moisture and other impurities, may also provide “windows” for easy electronic tunneling or rapid ionic diffusion (short-circuit paths) in the film. Such paths seem to close by structural rearrangement as the film thickens, and thus the energy barrier to ion transport or ion insertion may increase (linearly?) with increasing film thickness.

If the rate of ionic or electronic diffusion or ionic insertion depends upon the electric field ($d\phi/dx$) provided by adsorbed oxygen ions, then for a constant, equilibrium adsorbed state, the driving force (reduction in barriers) of the electric field decreases in importance as the film thickens to become a thin scale (from tens to hundreds of angstroms). But at the same time, the morphological restructuring of the scale is contributing in a similar manner. Theories based on these considerations lead either to a logarithmic rate equation [$y = k_e \ln(t_c + at)$] or to an inverse logarithmic kinetic expression [$(1/y) = b - k_{i.l.} \ln t$]. In the plotting of kinetic data, one cannot usually distinguish between these rate “laws.”

Data for halogenation of metals at low temperatures can frequently be fit to logarithmic expressions. Obviously such an empirical description does not establish the rate-controlling mechanism, because many kinetic models lead to similar rate laws.

Wagner⁵⁷ has treated the more difficult cases of scale growth in the thin-film range whereby an electrical charge localized to one interface is compensated by a diffuse charge distributed throughout the scale (as opposed to compensation by an opposing charge at the opposite interface). This treatment provides complicated expressions for the expected kinetics. To perform an experiment of fundamental significance in this area is extremely difficult, requiring ultrapure specimens and gas, with a surface fully characterized with regard to structure and completely free of adsorbants.

Scaling at Intermediate Temperatures

The structural and microscopic characterization of thin oxide scales formed on copper, iron, and nickel establish that the high density and the epitaxial nature of initial oxide islands formed on metals set up a high density of incoherent crystalline boundaries and line defects during the early stages of scale formation.²² If the reaction temperature is relatively low, generally $T/T_{\text{melt}} \leq 0.6$, then the influence of these numerous paths for the short-circuit diffusion of ions through the thin scale can account for scaling rates which are higher by several orders of magnitude than those expected from the extrapolation of kinetic data from higher temperatures. As a result of these short-circuit paths the scaling rates at intermediate temperatures are relatively high and are quite dependent upon crystallographic orientations of the surface grains.⁵⁸ The activation energies for the “effective” parabolic rate constants in this temperature range are much lower than that for lattice diffusion.⁵⁹

Support for the importance of short-circuit diffusion in the intermediate temperature range is gained from the response of scaling kinetics to vacuum “aging” of the scale, i.e., the interruption of the steady-state, rapid, scale growth by the removal of the oxidant to allow annealing and grain growth in the scale.⁶⁰ Such an aging treatment yields reduced postanneal scaling rates, presumably because the population of short-circuit diffusion paths has been reduced.

An alternative explanation, or at least a cooperative effect, for intermediate temperature scaling kinetics is offered by the “doping effect,”⁶¹ which is described in more detail shortly. As the scaling temperature is lowered, the sensitivity of the point defect concentrations to impurities in growing scales is extremely high, such that there is usually a negligible chance that one might observe “intrinsic” scaling behavior. Impurities in the scale

can generally change the activation energy, the P_{X_2} dependence, the aging behavior, and the like. The influence of impurities at low concentrations can usually be evaluated only by a conscious variation of the impurity type and concentration in the range of interest—a difficult study which is seldom undertaken.

Finally, for transition metals like iron, which form several compounds in the layered scale, many factors complicate the morphological and kinetic behavior of scale formation.^{62–64} The composite effect is too complex for review here. However, it is obvious that the halogenation of metals in the intermediate temperature range, which is the usual service condition because of excessive scale vaporization at higher temperatures, has in no way been studied in as much detail as the oxidation of metals. However, guidelines and interpretations of metal oxidation are available for comparison in future halogenation studies.

Morphological Aspects of High-Temperature Scaling

When the predominant ionic defects in a scale are vacant cation sites, then a compact protective layer grows by outward diffusion of cations with a counterflow of vacancies and positive holes. As the scale thickens, its resistance to plastic deformation increases, particularly at points of constraint such as the edges and corners of a specimen. With the continual arrival of vacancies through the scale to the metal/scale interface, the reduced plasticity of the scale can lead to the condensation of vacancies to form voids and ultimately a porous zone at the metal/scale interface.

The formation of this duplex scale morphology, with compact columnar grains at the external surface and a porous zone at the metal/scale interface, is favored: (a) at lower temperatures where scale plasticity is lower; (b) for impure metals (or dilute alloys) containing more reactive solutes, because the formation of a product compound as an internal precipitate within the metal matrix could occur; (c) for metals containing impurities which form volatile compounds with the reactant gas (e.g., hydrogen or carbon in halogenation reactions); and (d) at specimen corners and edges where geometrical constraints oppose plastic deformation of the scales. The principal detriment of duplex scale formation is the resulting poor scale/metal adhesion, which leads to scale cracking and exfoliation particularly upon thermal cycling.

The investigation of morphological details in the scale is possible when a suitable radioactive tracer of the reactant is available. In the sulfidation of silver, copper, iron, nickel, and several binary alloys, Brückman⁶⁵ and

Mrowec⁶⁶ used sulfur radiotracers to study the formation of the inner porous scale and the phenomena resulting from its formation. For slab specimens of the pure metals, the inner porous scale was initiated at corners and edges while metal/scale adherence was maintained along the flat faces of the specimen. Upon further reaction, the initially compact outer scale was perforated. Thereafter, tracer molecules were not only consumed for scale growth at the scale/gas interface but also reached the inner porous zone by diffusion through the perforations in the outer scale. Brückman and Mrowec suggested that an anisotropic dissociative mechanism occurs in the porous inner scale with preferential formation of molecules along grain boundaries which ultimately results in the perforation of the outer scale. In the sulfidation of alloys for which an insoluble internal precipitate is formed, the porous inner scale layer was initiated essentially at the start of the sulfidation at all areas on the specimen (not just corners and edges). For these alloys, the perforation of the outer scale also occurred early and generally over the specimens, and the sulfide formed at the metal/scale interface contributed quite significantly to the scaling rate.

The existence of a porous zone at the metal/scale interface beneath a compact outer scale is not likely to accelerate parabolic scaling kinetics unless the vapor transport of metal or nonmetal species across the void is very rapid. Of course, if the void should lead to an actual perforation of the outer layer, the scaling kinetics could be greatly increased. A particular problem caused by a porous inner scale region is the reduced adherence of the protective outer layer to the metal. Particularly upon thermal cycling or impact by foreign objects, the scale is subject to spallation with resultant renewed rapid kinetics.

When the predominant ionic defects in a scale are vacant anion sites or anion interstitials (as in the case for FeF_2 , for example), then the diffusional growth of a product scale occurs by the inward diffusion of anions with an equivalent transport of positive holes or electrons. The new scale forms at the metal/scale interface beneath the previously formed scale. Because the products of reaction generally comprise more volume than the consumed metal, the scale must deform plastically to accommodate the volume increase, or else tensile stresses are introduced into the external surface of the outer scale and cause it to fracture. Particularly at corners and edges, plastic deformation is restricted as the scale thickens, such that fractures occur and lead to a porous scale through which the molecular reactants can diffuse. Gravimetric measurements for this type of oxidation are not very meaningful since the corners and edges of samples can produce excessive amounts of

product scale. Metal recession as deduced from microscopic measurements of sample thickness at a location distant from corners and edges can provide the best accounting for the intrinsic rate of scale growth.

Inherent morphological problems and rapid scaling kinetics associated with the growth of scales by inward anion diffusion have been experienced in the oxidation of the metals niobium, tantalum, vanadium, zirconium, hafnium, titanium, and uranium. Generally for the oxidation of these metals, the steady-state scaling kinetics are linear. In the case of niobium oxidation, the initial oxidation kinetics show a sequence of parabolic segments (resulting from periodic scale fractures) which ultimately leads to linear behavior (a time-dependent rate). Both microscopic correlation of kinetics and morphology as well as marker observations lead to the conclusion that the steady-state linear rate corresponds to the rate of diffusion of oxygen ions through a thin, compact Nb_2O_5 layer maintained at some approximately constant thickness at the metal/scale interface.^{67,68} The repeated fracture of this thin compact scale by induced stresses prevents the realization of parabolic (protective) behavior.

Reaction of Alloys

Selective Oxidation

The scaling behavior of binary alloys, as revealed mostly through previous studies of the reactions of alloys with air or oxygen, is best interpreted in terms of the differing thermodynamic reaction tendencies of the alloy components in combination with their relative content and diffusivity in the bulk alloy. Let us consider a binary solid solution alloy A–B for which the lowest compound B_vX of component B is more stable (has a more negative $\Delta G_{\text{B}_v\text{X}}$) than the lowest compound A_xX of component A. Generally, the selective oxidation of the less noble component, B, is manifested in one of two limiting product morphologies^{69–71}: (1) for sufficiently dilute concentrations of B in A–B (often less than about 10 at. % B), tiny precipitates of B_vX are formed at an internal reaction front in the alloy beneath a scale of A_xX if the permeability (solubility times diffusivity) of X dissolved in A is much greater than the product of the diffusivity times the bulk content of the reactive solute, or else (2) for greater solute B contents (often greater than about 20 at. % B) or for alloys in which the nonmetal atoms are essentially insoluble, the compound B_vX will form the predominant external scale layer on the A–B alloy. Intermediate behavior is sometimes observed and can be important to the science and technology but will not be detailed here. These

intermediate morphologies include: (1) formation of a solid solution $(A, B)_vX$ scale, (2) the simultaneous internal precipitation and scale growth of B_vX , (3) preferential formation of B_vX in grain boundaries of the alloy, and (4) reaction between scale components to form a ternary compound.

Frequently, the more stable compound B_vX also exhibits a lower diffusivity for its more mobile ionic species than does the compound A_xX . In this case, the internal precipitation of B_vX in the alloy eliminates the possibility that the B component can reach the external surface and establish a compact layer of the slow growing B_vX compound. The resultant formation and faster growth of the A_xX scale then follows kinetics similar to those for the scaling of pure metal A; this situation represents an inadequacy of the alloy composition to protect the alloy. Once initiated, both the internal precipitation of B_vX and the scale growth of A_xX should obey nearly parabolic kinetics and the mechanism does not change with time.

Alternatively, when the B content of the alloy is sufficient to establish an external scale of B_vX , B atoms diffuse to the surface through the alloy to supply the diffusional growth of B_vX . Immediately beneath the scale, B is depleted and A is enriched. The scaling kinetics should resemble those for the scaling of pure metal B. For inadequate interdiffusion in the alloy compared to the transport in the scale, solute depletion beneath the scale can result in the formation of A_xX and the rupture of the protective B_vX scale. However, mechanisms for the healing of ruptured protective scales are also known. Generally, a reaction-resistant alloy is designed to form a protective, slow-growing B_vX scale at steady state.⁷²

Little (if any) data are available for the solubilities and diffusivities of halogens in metals, so that one cannot use the analytic expressions available from alloy oxidation to predict the behavior of alloys with regard to internal precipitation and scale formation in alloy halogenations. But most certainly, the halogens are less soluble and mobile in metals than are the chalcogens oxygen and sulfur. Therefore, the occurrence of internal precipitation during the halogenation of alloys should not be expected in the same degree. To the extent that internal precipitation competes with protective scale formation, this circumstance is favorable.

Transient Reaction (Initial Stages of Scaling)

As a clean surface of an A–B alloy is first exposed to the reacting X_2 gas at elevated temperatures, there is too little time for selecting product formation, and the alloy simply forms the product compounds of each of the alloy components in a molar proportion equal to that in the bulk alloy.⁷³ Then

the reaction kinetics at short times are likely to be higher than those subsequently experienced during the steady-state growth of the protective B_vX scale. At short times, the tiny grains of the thin initial duplex scale each grow according to their individual transport rates such that the faster growing product (often the less stable A_xX compound) overgrows the slower growing product (usually the more stable B_vX compound). As a result of the depletion of A, the underlying B_vX grains grow laterally to ultimate impingement at the metal/scale interface. In this way, the steady-state protective scale of B_vX may be found beneath an external A_xX scale whose supply and growth are stopped after the underlying scale is established.

When scale vaporization is important, as in the halogenation of alloys, the transient reaction stage might be used to place a less volatile, more noble compound on top of a more volatile, but slower growing, less noble compound. After sufficient time, of course, the outer scale could be lost completely by vaporization.

The Doping Effect

Data on alloy oxidation⁷⁴ show that the steady-state parabolic growth of a protective scale can be quite dependent upon the presence of aliovalent solutes (dopants) *dissolved* in the scale. Such solute ions differ in ionic charge (or lattice position) from the cations or anions of the host compound and are therefore “electrically active.” Because gross electrical neutrality is required for a growing scale, the summation of the relative charges for negative ionic defects (cation vacancies or anion interstitials) and electrons and negative dopants equals the summation of the relative charges for positive ionic defects (interstitial cations and anion vacancies) and positive holes and positive dopants. Obviously in this electrical neutrality condition, the concentration of the ionic defect whose transport accounts for scale growth is a prominent term which is balanced by the defects of opposite charge. By the introduction into the host compound (scale) of a *soluble* aliovalent dopant of the same sign of charge as the most mobile ionic defect, the concentration of this defect will be reduced drastically according to well-established defect equilibria conditions.⁷⁵ Reduction of the concentration of the fastest ionic defect species obviously reduces the diffusive flux of this species and the scaling rate of the alloy as well.*

* This discussion presumes that the scale is a predominant electronic compound. When the scale is a “solid electrolyte,” the scaling rate should be lowered as the concentration of the predominant *electronic* species is lowered through doping.

In fact, the early success of this theory may have resulted in excessive belief in the occurrence of the doping effect. Potential dopants are added either as alloying elements into the alloy or else as molecular species in the gas phase. Through both thermodynamic and morphological circumstances, the dopant might not be dissolved into the scale: for example, (1) a reactive alloyed dopant might be internally oxidized and experience difficulty in dissolving into the scale, (2) for components with greatly differing ionic size, electrical charge, or thermodynamic reaction tendency, the solubility for the dopant can be vanishingly small, or (3) the dopant might not be available to the scale at an interface where growth is occurring. In short, while the doping effect has been solidly demonstrated for several alloy systems, each alloy–environment combination must be considered thoroughly before one concludes that the “doping effect” caused or will cause some important change in scaling kinetics.

To design alloys intended for service in halogens on the basis of the doping effect, one must know at least the identities (and hopefully the concentrations) of the predominant ionic and electronic defects in the compound (scale) of the pure metal. One must know that the intended dopant ion is sufficiently soluble and has a certain electrical charge in the host lattice. Finally, for the reaction scheme under consideration, the dopant must reach the scale in a manner such that dissolution should occur.

Fortunately, much is known about the point defects in many halide compounds, particularly in the alkali halides. But further studies of point defects in the most protective scales (compounds), such as NiF_2 , would be justified.

LABORATORY STUDIES OF HALOGEN ATTACK ON METALS AND ALLOYS

Results of many laboratory studies of halogen–metal reactions are reported in the literature. Many of these results are summarized in this section. Because nickel, copper, iron, aluminum, and their alloys are commonly used structural materials, studies of halogen attack on these metals are reviewed in detail. Studies of halogen attack on other metals are summarized in less detail, but references are given to the original literature. These summaries include (1) observed reaction kinetics, (2) postulated reaction mechanisms, and (3) important experimental parameters such as temperature, halogen–gas pressure and flow rate, and metal and gas purities.

These summaries are intended not only to illustrate the factors involved in halogen attack on metals but also to provide a guide for materials selection. For this reason, experimental results are expressed in a form which permits easy comparison of halogen resistance between metals for which the kinetic rate laws are different. Rate constants for linear, logarithmic, parabolic, and other reactions are not easily comparable, nor do they convey clearly the engineering implications, especially if the units are, for example, (mg of halogen gas consumed)²/cm⁴ sec. Hence, many of the rate equations presented in this section have been extrapolated to determine the amount of metal that would be consumed after one year of halogen attack. Such extrapolation from laboratory studies of short duration (a few minutes or hours) may of course be inaccurate. Short-duration tests can only identify with certainty rapid initial attack or ignition. However, when only short-duration results are available, they do permit visualization and comparison of experimental data. Often, short-duration results provide an order-of-magnitude idea of the expected metal recession rates for extended durations.

To present these data so that they can be easily compared and extrapolated to longer times, we have approximated many of the reaction-rate versus time curves (presented graphically in the original references) with analytical logarithmic and power-law equations. In some cases, the kinetics may be equally well approximated by other equations. However, the analytical expressions do allow valid, though rough, comparison of corrosion rates for different materials, and the procedure is superior to the common practice of reporting only average corrosion rates for experiments of unspecified length.

The conversion of corrosion data to commensurate form may also occasionally introduce errors. For example, many of the conversions involve densities of the corrosion products. The densities of thin halide films may not be exactly the same as those of bulk halides, and in some cases the exact identity of the halide films is not known. However, the conversions are made because corrosion measurements of different workers are of much greater value when they can be cross-compared and when they can be related to metal recession rates. In many cases, especially for pure metals, the conversions are quite accurate.

The analytical expressions used throughout this section are the power-law equation, $y^n = k_n t$, and the logarithmic equation, $y = k_e \ln(t_0 + at)$, where (1) y is halide film thickness, thickness of the metal layer consumed, weight gain, gas consumption, or metal consumption per unit area; (2) k_n , k_e , and t_0 are constants; and (3) t is lapsed time of the reaction. For linear

kinetics $n = 1$ and $y = k_1 t$. For parabolic kinetics $n = 2$ and $y^2 = k_2 t$. The parabolic rate constant k_2 used here should not be confused with the practical rate constant, k_p , which is defined by the equation $y^2 = 2k_p t$, where y is halide film thickness. With the convention used throughout this section the reaction rates are

$$\left(\frac{dy}{dt}\right) = \frac{ak_e}{t_0 + at}$$

for power-law kinetics and

$$\left(\frac{dy}{dt}\right) = \frac{ak_e}{t_0 + at}$$

for logarithmic kinetics.

The activation energy for power-law kinetics is defined as

$$Q = -R \frac{d \ln k_n}{d(1/T)}$$

Also, in this section, pressure dependence of reaction rates is expressed as $k_n \propto P^{1/m}$; when values of m are given, this relationship is implied.

The halogenation of many pure metals (nickel, copper, iron, aluminum) has been studied carefully. The studies cover wide temperature ranges and are frequently duplicated by several workers. However, halogenation of other pure metals and halogenation of most alloys have not been so carefully investigated. The information that is available is frequently conflicting. Many of the conflicts probably arise from gaseous impurities such as oxygen and moisture, differences in gas pressures and flow conditions, poor temperature control, poor measuring procedures, interference effects between different metals and alloys halogenated in the same reactor, and differences in metal impurity contents. For alloys, further complications arise because some authors have not provided adequate information about alloy composition; for example, an alloy may be identified only as "Monel." There are many different Monels; some Monels are quite resistant to fluorine at 400°C, while others ignite and burn at this temperature.

Attempts to correlate the results of short, scoping halogenation experiments are frustrating. For example, much of the fluorination data in the literature for Inconel are given in terms of linear kinetics. The linear rate constants given by different investigators for 500–600°C fluorination of Inconel vary from 0.0015 mg/cm² min at 600°C and 0.01 mg/cm² min at 500°C to 0.15 mg/cm² min at 550°C and 9 mg/cm² min at 536°C. Attempts

to fit the original data to power-law or logarithmic kinetics produce even greater spread in the results. In general, rate constants reported for similar halogenation conditions frequently differ by three to five orders of magnitude.

Nonetheless, much useful information can be obtained from these short-duration scoping studies. Many of the studies include nickel and other “pure” metals among the materials tested. Halogenation rates for the alloys can be normalized relative to the halogenation rates for these pure metals with which the alloys were tested and for which the halogenation kinetics are well known. This procedure eliminates some of the systematic errors involved in the various investigations and, hence, allows correlation of results obtained from different studies. This correlation, which can rarely be achieved for the absolute magnitudes of the rate constants, is evidence for the validity of the procedure. The procedure of interpreting experimental results in terms of halogenation rates for “pure” metals is used throughout this review.

In using the data summarized in this chapter, the reader should be mindful of possibilities of experimental inaccuracies, localized attack such as pitting, gross changes in reaction kinetics resulting from the presence of metal and halogen-gas impurities, and other factors which may affect the utility of the data for a particular application. This survey may provide a useful guide for the selection of potential metals for a given application, but omnipresent extraneous variables necessitate more detailed laboratory and pilot-plant evaluations of materials for specific applications.

Nickel, copper, iron, and aluminum are all used under various restricted conditions in fluorine environments, and all but aluminum are used in chlorine, bromine, and iodine environments. Because of this usage, and because these are the more common base metals for structural alloys, studies of their behavior in halogen environments are described in detail. The reactions of several of these metals with different halogens have been extensively studied. They serve to illustrate important halogen-metal reaction mechanisms and important factors that influence these mechanisms and reaction rates.

Nickel and Nickel Alloys

Nickel is one of the metals most resistant to attack by dry fluorine, chlorine, and bromine. Nickel is used in these halogen environments at temperatures as high as 600, 400, and 300°C, respectively. The resistance of nickel and nickel alloys is well documented for fluorine, chlorine, and bromine, but not for iodine.

Fluorine

Fluorine reacts with nickel to produce a compact NiF_2 scale which adheres tenaciously to the metal substrate. Nickel difluoride exhibits a tetragonal TiO_2 -type lattice, melts at 1450°C ,⁷⁶ and has a relatively low vapor pressure, 2.8×10^{-6} atm at 800°C .⁷⁷ Hence, a NiF_2 scale quickly passivates the surface of nickel, but fluorination continues as reactants diffuse through the NiF_2 scale. The reaction rate decreases as the scale thickens.

Nickel—A Summary. Observed nickel-fluorination kinetics are given in Table 2, as are estimates for the amount of nickel lost to fluorination during the first year of exposure. Nickel fluorination has been studied at temperatures from -200°C to the nickel-fluorine ignition temperature, about 1080 – 1220°C . From 300 to 700°C , the fluorination kinetics are generally parabolic initially but later are more nearly cubic or quadratic. Consequently, predictions of metal loss based on parabolic kinetics may be somewhat high.

Above 700°C , voids form along nickel grain boundaries beneath the NiF_2 scale.⁷⁸ This grain boundary degradation may penetrate five to eight times deeper than the metal recession resulting from layered NiF_2 scale formation. Above 700 – 800°C , the NiF_2 scale begins to evaporate as $\text{NiF}_2(v)$. Consequently, fluorination rate measurements, based on gravimetric methods or on pressure changes, require special interpretation. In the presence of water vapor, NiF_2 hydrolyzes and decomposes at 410°C .⁷⁹

Below 700°C , the growth of NiF_2 scale apparently occurs by the diffusion of fluorine anions to the scale/metal interface where scale formation occurs.^{80,81} That this diffusion process is also rate-limiting is suggested by the parabolic form of the initial fluorination kinetics, and the knowledge that NiF_2 is not a predominant ionic conductor. (Above 700°C , nickel cation diffusion may also be significant.) The activation energy for parabolic scaling is about 17 – 18 kcal/mole over the entire range from 300 to 800°C . At 600°C the fluorination rate exhibits a power dependence on the fluorine pressure, $k_p \propto P_{\text{F}_2}^{1/m}$, where $m = 1.8$ for nickel containing 0.08 wt. % impurities, but $m = 1.1$ for nickel containing 0.6 wt. % impurities of which about 0.3 wt. % is manganese.⁸⁰ This variation in the dependence of fluorination rate on fluorine pressure indicates that impurities, probably manganese, dope the scale and thereby affect the rate of diffusion through the NiF_2 scale.

The resistance of nickel to fluorine extends to many other fluorinating agents, such as UF_6 , GeF_4 , SF_6 , SeF_6 , and MoF_6 . Nickel is also one of the metals most resistant to HF attack. Thus, nickel is widely used for storing and

Table 2. Kinetic Data for Nickel-Fluorine Reactions

$T(^{\circ}\text{C})$	P_{F_2} (atm)	m	n	k_n ($\text{mg F}_2/\text{cm}^2/\text{min}$, a (min^{-1}))	Q (kcal/mole)	Test duration (min)	Ref.	Δy (μm) ^a for $t = 1$ yr
-196	Liquid							
-80	0.26-0.92		1	1.8×10^{-7}		5.26×10^5 (1 yr)	82	0.25
27	1.0	3	^b	3.18×10^{-5} ; 2847		240	84	0.17
30	0.26-0.92		^b	1.4×10^{-5} ; 9000		250	85	0.0012
84	0.26-0.92		1	7.3×10^{-8}		210	84	0.00055
300	0.92		1.9	1.43×10^{-5}	17	210	84	0.21
300	0.92		3.4	1.00×10^{-7}	21.5	480	80	5.0
400	0.92		1.9	1.20×10^{-4}	17	1900	80	0.73
400	0.92		3.7	4.68×10^{-7}	21.5	34	80	15
500	0.92	≥ 10	2.2	3.22×10^{-4}	17	1700	80	1.2
500	0.92		3.5	1.22×10^{-5}	21.5	14	80	18
540	1.0		2	3.8×10^{-4}	59	1800	80	3.0
550	1.0		2	8.0×10^{-4}	59	120	79	25
600	0.92		1.9	2.36×10^{-3}	17	120	79	36
600	0.92	1.82	2.6	6.85×10^{-4}	21.5	14	80	74
600	1.0		2	4.0×10^{-3}	59	1900	80	17
640	1.0		2	1.25×10^{-2}		120	79	80
660	1.0		2	1.45×10^{-2}		150	79	140
710	1.0		2	2.35×10^{-2}		90	79	150
720	1.0		2	2.7×10^{-2}	18.5	150	79	190
770	1.0		2	3.8×10^{-2}	18.5	120	79	210
810	1.0		2	6.0×10^{-2}	18.5	100	79	240
816	0.2-0.9					100	79	310
1200		2.7					78	
							91	
							38	

Ignites and burns

^aEstimated loss of metallic nickel after a 1-yr-long exposure. Above 700°C, grain-boundary attack may penetrate 5-8 times deeper than uniform surface NiF_2 scale formation.

^bKinetics are logarithmic.

handling fluorine and fluorinating agents. The following paragraphs describe in greater detail the more thorough studies of nickel fluorination.

Nickel-Fluorine—A More Detailed Discussion. Nickel is little corroded by liquid fluorine at -196°C (77°K). According to Singleton *et al.*⁸² the fluorination rate of nickel in liquid fluorine is less than $0.25\text{ }\mu\text{m}$ metal recession per year, a metallic nickel loss of less than 0.23 mg/cm^2 per year. Earlier workers reported higher nickel fluorination rates in liquid fluorine: $5\text{ }\mu\text{m/yr}$ ⁴³ to $1450\text{ }\mu\text{m/yr}$.⁸³ These higher rates probably resulted from short exposure times and from high concentrations of HF and other impurities.

Kleinberg and Tompkins^{38,84} observed the fluorination of nickel by gaseous fluorine at -80 , 30 , and 84°C at pressures of $200\text{--}700$ torr. The nickel used had an impurity content of approximately 0.6 wt. \% and the exposure times were $200\text{--}240$ min. After about 10 min at -80°C , the nickel-fluorination kinetics were nearly linear, with a film growth rate of approximately $0.5\text{ }\mu\text{m/yr}$. The nickel-fluorination kinetics at 30°C were roughly logarithmic. According to this study, the fluoride film formed on nickel would be only $1.8 \times 10^{-3}\text{ }\mu\text{m}$ thick after a year-long fluorine exposure. The nickel-fluorination kinetics at 84°C after 20 min of fluorine exposure were again nearly linear with a film growth rate of approximately $0.2\text{ }\mu\text{m/yr}$. These data, including that for the first 20 min, could also be approximated by a logarithmic equation. All the rate constants given here were estimated from graphs in reference 38.

Using manometric and electron diffraction techniques, Cannon *et al.*⁸⁵ studied the room temperature (27°C) fluorination of 0.995 pure nickel. The fluoride film thickness followed a logarithmic equation of the form $y = k_e \ln(at)$, whereby k_e was proportional to the cube root of fluorine pressure from 0.1 to 1.4 atm. This equation predicts a fluoride film thickness of only $3.7 \times 3\text{ }\mu\text{m}$ after a year-long fluorine exposure. These two studies of nickel fluorination near and below room temperature were made without first removing surface oxide present on the specimens. The primary reaction involved was probably fluorination of superficial nickel oxide and not fluorination of metallic nickel. In fact, by electron diffraction techniques, Cannon *et al.*⁸⁵ identified predominant NiO and $\text{NiF}_2 \cdot 4\text{H}_2\text{O}$ on the surface of nickel specimens after room-temperature fluorine exposures.

Cannon *et al.*⁸⁵ hypothesized that the rate-controlling mechanism in room-temperature fluorination of nickel is electron transport by quantum-mechanical tunneling as described by Mott⁸⁶ and by Hauffe and Ilschner.⁸⁷ The electron tunneling mechanism is consistent with the observed logarithmic kinetics, a film thickness of less than $50\text{ }\text{\AA}$, and the low fluorine pressure dependence of the rate constant.

Nickel fluorination at 300–600°C was studied by Jarry *et al.*,⁸⁰ who used a manometric technique. The fluorine in this study contained only 0.07 vol. % impurities, these being oxygen, water vapor, nitrogen, carbon dioxide, silicon tetrafluoride, and argon. The nickel contained 0.08 wt. % impurities of cobalt, iron, carbon, oxygen, and nitrogen. The nickel specimens were heated in vacuum, then exposed to fluorine at 700-torr pressure. Initial (0.04–0.2 mg/cm² weight gain) reaction kinetics were nearly parabolic. Thereafter, the kinetics were more nearly cubic or quadratic with $2.6 < n < 3.7$.

Parabolic rate constants for the initial periods of fluorination gave an activation energy of 17 kcal/mole. The rate constants for nickel fluorination are presented graphically in Fig. 10. The parabolic rate constant at 500°C was almost independent of fluorine pressure, but at 600°C, with a fluoride film thickness of 25 μm or greater, $k_p \propto P_{\text{F}_2}^{1/m}$ with $m = 1.8$.

Jarry *et al.*⁸⁰ also studied the fluorination of less pure A-nickel (0.994 pure) which had approximately the same impurity content as the nickel used for the room-temperature fluorination studies.^{84,85} Fluorination of A-nickel underwent a transition from logarithmic kinetics at 400–500°C to parabolic kinetics at 600°C. The rates for A-nickel exhibited a fluorine pressure power dependence at 600°C of $m = 1.15$, compared to $m = 1.8$ for nickel of higher purity. Hale *et al.*⁷⁸ also observed nearly linear A-nickel fluorination rates at 600 and 700°C but a lower pressure dependence, $m = 2.7$, at 816°C. Unquestionably, the fluorination rate of nickel in the intermediate temperature range is quite sensitive to doping by impurities in the alloy.

Jarry *et al.*^{80,81,88} postulate that the rate of fluorination of nickel is controlled by diffusion, the rate-limiting step being either the outward diffusion of nickel cations or the inward diffusion of fluorine anions. To determine which was occurring, two experiments were made at 600–700°C in fluorine of 1.8 vol. % impurity content, for nickel with an impurity content of 0.6 wt. %. In the first experiment they placed two pieces of nickel face to face but not quite parallel to one another. When samples in this configuration are fluorinated or otherwise tarnished until their scales impinge, either (1) the scales fuse and leave no interface if scale growth occurs by predominant metal cation diffusion, or (2) the scales remain separate with a distinct interface if scale growth occurs by predominant anion diffusion. For the Ni–F₂ reaction, the scales were separated by a distinct interface, indicating predominant fluorine anion diffusion.

In the second experiment, nickel sheet was coated with a thin film of radioactive nickel-63 isotope, then fluorinated, and finally examined in cross-section by autoradiography. Autoradiography showed that the nickel-63

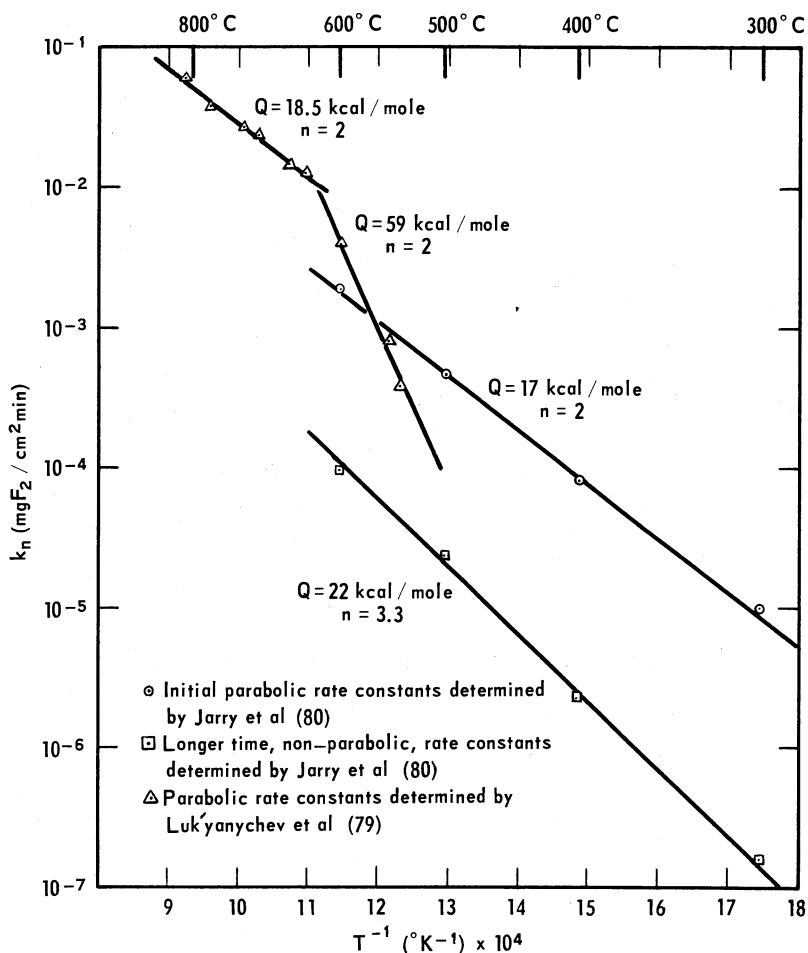


Fig. 10. Experimentally determined rate constants for the nickel-fluorine reaction.

surface layer remained in a narrow band at the scale/gas interface, further indicating that the fluoride scale grows by inward diffusion of fluorine anions.

By a gravimetric method, Luk'yanychev *et al.*⁷⁹ studied the nickel-fluorine reaction from 540 to 810°C for P_{F_2} of 1 atm. The nickel had an impurity content of only 0.06 wt. % of cobalt, iron, silicon, and zinc. The Luk'yanychev gravimetric data very nearly followed parabolic kinetics over the entire ranges of temperature and for times up to 150 min. However, as

illustrated in Fig. 10, these data fitted two different activation energies: 59.0 kcal/mole at 540–600°C, and 18.5 kcal/mole at 720–810°C.

This change in activation energy corresponded to a change in scale morphology. Below about 660°C, the NiF_2 scale consisted of very small grains of about 0.3 μm . Above about 660°C, the NiF_2 scale consisted of larger, well-formed columnar crystals which were 5–8 μm wide. Further, at 800 and 900°C, Hale *et al.*⁷⁸ observed that voids form along grain boundaries just beneath the NiF_2 scale. Such voids do not form at 700°C or below. Luk'yanychev *et al.* hypothesize that the break in activation energy at 660°C accompanies a transition from predominant anion diffusion through the NiF_2 scale at lower temperatures to predominant cation diffusion at higher temperatures. As already described, Jarry *et al.* demonstrated that anion diffusion does predominate in NiF_2 scale growth at 600–700°C. Luk'yanychev *et al.* give no experimental evidence for the predominance of cation diffusion above 700°C. But the observation of voids in nickel grain boundaries at higher temperatures would seem to lend qualitative support to the cationic vacancy mechanism: vacancies coalesce to form voids at the Ni– NiF_2 interface or at grain boundaries in the nickel. Furthermore, this transition from predominant anion diffusion at low temperatures to predominant cation diffusion at high temperatures is consistent with the behavior of TiO_2 , which has the same crystallographic structure as NiF_2 ; in TiO_2 anion diffusion predominates below 900°C, while cation diffusion predominates at higher temperatures.

On the other hand, the decrease in activation energy with increasing temperature observed by Luk'yanychev *et al.* is not consistent with either a switch in diffusion species or the occurrence of short-circuiting diffusion at low temperatures. The doping of the scale at low temperatures (extrinsic behavior) with intrinsic behavior at higher temperatures can, in principle, change the temperature dependence in either direction, depending upon many factors: for example, the nature and concentrations of compensating native defects in pure NiF_2 , or the valence and solubilities of aliovalent impurities introduced into the scale from the impure alloy. Of course, both the concentrations of native defects and the solubilities of the impurities depend upon temperature, while the valencies of species involved might be presumed to be independent of temperature. The potential cationic impurities manganese, silicon, iron, and even cobalt may assume valencies greater than +2 and could represent dopants of positive relative charge, changing the predominant terms in the condition of electroneutrality for NiF_2 . Alternatively, oxygen anions might enter the scale as impurities from the gas phase to create a condition such as $[V_F] = [O_F]$ which would boost the concentration of

fluorine vacancies. With progressive increases in either of these doping agents, the scaling rate might increase markedly (if the species providing predominant diffusion is increased), or else the scaling rate might decrease to a minimum prior to an increase (if the concentration of the predominant native defect is reduced by the introduction of the first trace of an impurity) but then increase with larger impurity contents.

With regard to the temperature dependence for the growth of scales sensitive to impurity doping, nearly any magnitudes and transitions in activation energy would seem possible. On the contrary, the switch in predominant diffusing species with changes in temperature would seem more unlikely. In light of the obvious evidence for impurity effects, correlation of the activation energies with a temperature-dependent doping mechanism seems reasonable. More controlled fluorination experiments supported by studies of point defects in NiF_2 are required to specify the details of the doping effect.

Above about 800°C , evaporation of NiF_2 scale as NiF_2 and NiF vapor species is significant. Over the temperature range $781\text{--}833^\circ\text{C}$, the vapor pressure of NiF_2 (from a study of evaporation from a Knudsen cell into vacuum) is given by the equation⁷⁷

$$\log P_{\text{NiF}_2}(\text{atm}) = 10.17 - \frac{16,900}{T}$$

The NiF_2 vapor pressure at 800°C is then 2.8×10^{-6} atm.

The maximum evaporation rate for NiF_2 can be calculated by using the Hertz–Langmuir equation,

$$G(\text{g}/\text{cm}^2 \text{ sec}) = \sum_i \frac{P_i(\text{atm})}{2.255 \times 10^{-2}} \sqrt{\frac{M_i}{T}}$$

where P_i is the vapor pressure of species i , M_i is the molecular weight of species i , and G is the net rate of evaporation.⁸⁹ For 800°C , the calculated maximum evaporation rate is $2.2 \text{ mg}/\text{cm}^2 \text{ min}$. The actual evaporation rate in static fluorine is much lower but still significant.

Using mass-spectrometric techniques McKinley⁹⁰ studied the nickel–fluorine reaction with fluorine at pressures of $10^{-7}\text{--}10^{-4}$ torr. At 800°C and a fluorine pressure of 10^{-5} torr, McKinley observed the rate of NiF_2 evaporation as $\text{NiF}_2(v)$ of approximately $7.4 \times 10^{-4} \text{ mg}/\text{cm}^2 \text{ min}$. The amount of the NiF species was negligible. At 1100°C the evaporation rate by $\text{NiF}_2(v)$ was $1.86 \times 10^{-3} \text{ mg}/\text{cm}^2 \text{ min}$, while the NiF evaporation rate was $4.76 \times 10^{-3} \text{ mg}/\text{cm}^2 \text{ min}$. Beyond 1100°C , the NiF evaporation rate increased rapidly and predominated.

Above 1000–1100°C, the gaseous reaction products NiF_2 and NiF consume the NiF_2 scale which protects nickel from rapid fluorination at lower temperatures. In the absence of this scale, the exothermic nickel-fluorination reaction proceeds rapidly, heat evolves more rapidly than it is dissipated, the nickel surface temperature rises, and the nickel ignites. This ignition of nickel in fluorine occurs at about 1080–1220°C.^{38,91}

Nickel–Base Alloys. Fluorination of nickel-base alloys has not been studied so extensively as fluorination of pure nickel. Results of fluorination studies on nickel-base alloys are summarized in Table 3. These results are normalized relative to the fluorination rate for “pure” nickel.

Monels are nickel–copper alloys, mostly of 60–70 wt. % nickel, 27–32 wt. % copper, 0.1–0.2 wt. % carbon, and 1.5–7 wt. % other elements such as iron, aluminum, manganese, and titanium. Like nickel, Monel is little attacked by liquid fluorine at -196°C . Kleinberg and Tompkins^{38,84} exposed Monel specimens to liquid fluorine for a full year; weight losses were all less than 0.14 mg/cm^2 . Sterner and Singleton⁴³ indicate that Monel corrodes in liquid fluorine at a rate of about $13 \text{ }\mu\text{m/yr}$, a metal loss rate of about $11 \text{ mg/cm}^2 \text{ yr}$. This estimate is based on 6- to 336-hr test exposures.

Kleinberg and Tompkins^{38,84} also studied the fluorination of Monel by gaseous fluorine at -80 , 30 , and 84°C . At -80°C and 690 torr fluorine pressure, Monel fluorination roughly followed power-law kinetics, $y = k_n t^{1/n}$, with $n \simeq 4.16$ and $k_n = 9.7 \times 10^{-16} (\mu/\text{min})^n$ (estimated from Figs. 3–5 in reference 38). This equation predicts a fluoride film thickness of $0.005 \text{ }\mu\text{m}$ after a year-long fluorine exposure. At 30°C in 312-torr fluorine, the fluorination kinetics were more nearly logarithmic. At 84°C in 498-torr fluorine, the Monel fluorination kinetics level out quickly to nearly linear behavior corresponding to a film thickness growth rate of approximately $0.189 \text{ }\mu\text{m/yr}$.

Cannon *et al.*⁸⁵ observed the fluorination of Monel at 27°C by a manometric technique. The fluorination followed logarithmic kinetics such that at the end of one year the film thickness would be $2.8 \times 10^{-3} \text{ }\mu\text{m}$. The surface film produced by fluorination was studied using electron diffraction techniques. The film included the compounds NiF_2 , CuF_2 , CuOHF , $\text{CuOHF} \cdot \text{CuF}_2$, and $\text{Cu}(\text{OH})_2$. Since surface oxide was not removed from the Monel prior to fluorination, these compounds probably formed by fluorination of surface oxides. Fluorination at 93°C produced a surface film of NiF_2 , $\text{Cu}(\text{OH})\text{F} \cdot \text{CuF}_2$, $\text{NiF}_2 \cdot 4\text{H}_2\text{O}$, $\text{Cu}(\text{OH})_2$, and $\text{CuF}_2 \cdot 2\text{H}_2\text{O}$.

Table 3. Estimated Reaction Rates for Nickel-Base Alloys in Fluorine^a

Alloy (nom., wt. %)	T(°C)											Ref.
	-200	-100	0	100	200	300	400	500	600	700		
Monel (Ni-30 Cu)	≤1	≤1	1	1	1	1	1	1	2	5		26, 38, 43, 83, 85, 92, 93, 131, 142
Monel ^b (Ni-30 Cu)								Ignites				91
Inconel (Ni-16 Cr-8 Fe)	1	1	1	1	1			10-140				26, 83, 92, 93, 131
Illium (Ni-22 Cr-5 Mo)	2-6		1-4						150			83, 131
Duranickel (Ni-5 Al)								3	3			92, 95
Ni-211 (Ni-5 Mn)									6			95
Ni-61 (Ni-3 Ti)								1000				92, 96
Ni-thoria (Ni-2 ThO ₂)									10			233

^aRates are normalized relative to the reaction rates for pure nickel; i.e., the numbers given are the ratios of alloy-fluorination rates to those for pure nickel.

^bMonel alloy probably contained titanium or similar constituent which lowered the alloy resistance to fluorine attack.

Cannon *et al.*⁸⁵ hypothesized that the rate-controlling mechanism in room-temperature fluorination of Monel is, as for nickel, electron transport by quantum-mechanical tunneling. Again, the electron tunneling mechanism is consistent with the observed logarithmic kinetics and the film thickness, including oxide of less than $0.005\text{ }\mu\text{m}$.

Most fluorination rates given in the literature for Monel fluorination are based on a few short experiments. For lack of sufficient kinetic data, the experimenters assume linear kinetics and report only linear rate constants. However, Jackson's data⁸³ indicate that Monel fluorination kinetics at 545°C are not linear but more nearly parabolic. In the $100\text{--}350^{\circ}\text{C}$ temperature range, both copper and nickel form protective fluoride films, so that the fluorination rates decrease with time as these films thicken.

Jackson⁸³ measured the weight change of Monel-400 samples fluorinated for 5, 24, and 120 hr. Major impurities in Monel-400 are 1.35 wt. % iron and 0.9 wt. % manganese. Fluorine was flowed over the samples at 100 ml/min at temperatures of 26, 190, 370, and 540°C . Jackson's results, especially for low temperatures and short exposure times, were erratic. However, several useful conclusions can be drawn. Jackson's measurements indicated that at 540°C the fluorination rate decreased with exposure time.

If Jackson's fluorination kinetics are assumed to be parabolic, the two rate constants from measurements at 362 and 549°C establish an activation energy of about 35 kcal/mole. Weight gains after a year of fluorination at the above rates would be about 2.0 mg/cm^2 at 362°C and 12 mg/cm^2 at 549°C . These figures are of low reliability but do indicate that Monel fluorination rates are of the same order of magnitude as nickel fluorination rates in the $350\text{--}550^{\circ}\text{C}$ range. However, the activation energy for nickel fluorination at $300\text{--}800^{\circ}\text{C}$ is about 17 kcal/mole, which indicates that above about 600°C , Monel fluorination rates exceed nickel fluorination rates. This conclusion is substantiated by Myers and DeLong²⁶ who observed similar fluorination rates for nickel and Monel below 500°C but 2–5 times more rapid fluorination of Monel than for nickel at $600\text{--}700^{\circ}\text{C}$.

The above information on the fluorination of Monel-400 is sketchy and further complicated by the wide variation in Monel alloy compositions. For example, Godwin and Lorenzo⁹¹ observed that Monel ignites at $348\text{--}437^{\circ}\text{C}$. The discrepancy probably lies in the minor alloying constituents; the Monel studies by Godwin and Lorenzo may have contained a constituent such as titanium, which increases the fluorination rate dramatically at higher temperatures.

Inconels are nickel–chromium alloys. As additions to the nickel base, these alloys contain 15–20 wt. % chromium, 1–7% iron, 0.5–2.5% titanium, 0–3% aluminum, and about 0.04% carbon. Several Inconels contain 1–5% niobium and a few contain manganese or molybdenum.

In liquid fluorine and at 25 and 200°C, Inconel (77.3 wt. % nickel, 15.2% chromium, and 7% iron) fluorinates at about the same rate as nickel.⁸³ However, at 350°C and higher temperatures, Inconel fluorinates significantly faster than does nickel. Most estimates of the 350–750°C Inconel fluorination rates range between 10 and 140 times the rates of nickel fluorination at the same temperature.^{26,83,92,93}

Illiums are also nickel–chromium alloys. Illium alloys differ primarily from Inconels in that they have higher molybdenum contents. In liquid fluorine, Illium-R (64.6 wt. % nickel, 21.7% chromium, 5.7% molybdenum, 4.2% iron, 2.5% copper, 0.7% manganese, and 0.5% silicon) fluorinates 2–6 times more rapidly than nickel.⁸³ According to Jackson,⁸³ at 25–350°C Illium-R fluorinates 1–4 times more rapidly than nickel, but at 530°C Illium-R fluorinates over 150 times more rapidly than nickel. The alloying elements chromium, copper, and molybdenum possess higher fluoride vapor pressures than nickel.

Gunther and Steindler⁹² observed the fluorination of several nickel-base alloys at 500°C. Fluorinated alloys included HyMu-80 (79 wt. % nickel, 16% iron, 0.5% manganese, and 0.115% silicon) and INOR-8 (70 wt. % nickel, 16% molybdenum, 7% chromium, 5% iron, 0.8% manganese, 0.35% copper, 0.3% silicon, and 0.2% cobalt) as well as Inconel. Weisert⁹⁴ reports some data on the fluorination of Hastelloy Alloy C (approximately 53 wt. % nickel, 17% molybdenum, 17% chromium, 6% iron, 4% tungsten, 1% manganese, and 1% silicon). Apparently nickel-base alloys containing 50 wt. % or more nickel and containing copper, molybdenum, chromium, and/or iron as secondary constituents fluorinate more rapidly (1–5 times) than pure nickel at temperatures below 300–400°C. Above 400–500°C, these alloys fluorinate significantly faster (10–100 times) than pure nickel.

Duranickel is a nickel-base alloy which contains 4.5 wt. % aluminum, 0.5% titanium, and as much as 0.15% carbon. According to Gunther and Steindler,⁹² at 500°C Duranickel fluorinates about 3 times faster than nickel. According to Miles *et al.*⁹⁵ Duranickel also fluorinates about 3 times faster than nickel at 600°C.

D-Nickel or Nickel-211 is a nickel-base alloy containing 4.5 wt. % manganese and 0.1% carbon. According to Miles *et al.*⁹⁵ at 600°C this alloy fluorinates about 6 times faster than nickel at the same temperature.

Nickel-61 is a filler alloy used for welding nickel. Its composition is approximately 93 wt. % nickel, 3% titanium, 1.5% aluminum, 1% manganese, 1% iron, 0.75% silicon, 0.25% copper, and 0.15% carbon. According to Chilenskas and Gunderson,⁹⁶ at about 475°C, Nickel-61 fluorinates 800–1500 times faster than pure nickel. Gunther and Steindler,⁹² however, report that at 500°C Nickel-61 fluorinates at the same rate as pure nickel. This difference cannot be reconciled. The higher rate is more consistent with the effect of titanium on the fluorination of other alloys in this temperature range.

Trevorrow and Gunther⁹⁷ studied the fluorination of nickel–2 vol. % thorium material. The ThO_2 is present in the nickel as a fine dispersion. Disks of this material were fluorinated with static fluorine at about 700 torr at 600°C. Under these conditions the nickel–thorium material fluorinated 8–12 times faster than did pure nickel. While NiF_2 scale adheres tenaciously to pure nickel, it spalls from the nickel–thorium material. This adherence behavior is exactly the opposite of that observed in the oxidation of nickel or T.D.–nickel in air or oxygen. However, in the oxidation of nickel, outward cation diffusion predominates. Also, in oxidation, ThO_2 is inert, whereas in fluorination it may react.

Chlorine

Dry chlorine reacts with nickel to form a NiCl_2 product film. Nickel dichloride has a high melting point, about 1000–1030°C,^{98–100} but also a high vapor pressure, about 2.25×10^{-3} atm at 700°C.¹⁰¹ Consequently, at low temperatures, a dense, adherent, protective NiCl_2 scale forms. Below 400°C, parabolic chlorination kinetics are obeyed. However, because of its high vapor pressure, the NiCl_2 scale begins to evaporate at 400–450°C. After a time at higher temperatures, the scaling rate becomes equal to the evaporation rate of NiCl_2 . At still higher temperatures or for very low chlorine pressures, the NiCl_2 scale no longer forms, and the rate of reaction on the active surface is limited by the rate of transport in the gas phase by Cl_2 , NiCl , and NiCl_2 molecules. Nickel-chlorination data are summarized in Table 4.

The presence of water vapor in chlorine increases the rate of reaction with nickel.^{102,103} Below about 550°C the presence of 1.5% water vapor in chlorine can increase the rate of reaction (metal consumption) between the chlorine and nickel to double that for the reaction between dry (less than 0.06% water vapor) chlorine and nickel. Thirty percent water vapor in the chlorine can increase the rate of reaction 2–20 times. Above about 550°C the addition of moisture to chlorine seems to have little effect on the rate of reaction between the chlorine and nickel.

Table 4. Kinetic Data for Nickel–Chlorine Reactions

$T(^{\circ}\text{C})$	P_{Cl_2} (atm)	n	k_n (mg X/cm ² hr/min)	X	kcal/mole	Test duration (min)	Ref.	Δy (μm) ^a for $t = 1$ yr
-15	0.13	1 ^b	3.1×10^{-6}	Cl ₂				1.5
350	0.13	2	3.1×10^{-6}	Cl ₂	32.6	3,000–5,000	105	1.2
375	0.13	2	4.3×10^{-6}	Cl ₂	32.6		105	1.4
400	0.13	2	2.8×10^{-5}	Cl ₂	32.6		105	3.6
407	0.13	2	5.6×10^{-5}	Cl ₂	32.6		105	5.0
433	0.13	2	7.27×10^{-5}	Cl ₂	32.6		105	5.8
465	0.13	2 ^d	1.64×10^{-4}	Cl ₂	32.5		105	
465	0.13	1 ^e	-1.80×10^{-4}	Ni	65.0		105	107
485	0.13	2 ^d	3.98×10^{-4}	Cl ₂	32.5		105	
485	0.13	1 ^e	-2.40×10^{-4}	Ni	65.0		105	142
500	0.13	2 ^d	4.46×10^{-4}	Cl ₂	32.5		105	
500	0.13	1 ^e	-5.41×10^{-4}	Ni	65.0		105	319
500	0.13	2 ^d	6.67×10^{-4}	Cl ₂	32.5		105	
500	~ 1 at $16 \text{ cm}^3/\text{min}$	1	-8.33×10^{-4}	Ni	37.1	3,600	107	492
525	0.13	2 ^d	9.0×10^{-4}	Cl ₂	32.5		105	
525	0.13	1 ^e	-4.08×10^{-3}	Ni	65.0		105	2,410
540	~ 1 at $16 \text{ cm}^3/\text{min}$	1	-3.5×10^{-3}	Ni	37.1	3,600	107	2,070
550	0.13	1	-1.02×10^{-2}	Ni	65.0		105	6,020
550	0.13	1	-9.9×10^{-3}	Ni	65.0		105	5,850
660	~ 1 at $16 \text{ cm}^3/\text{min}$	1	-6.82×10^{-2}	Ni	37.1	3,600	107	40,300
740	~ 1 at $16 \text{ cm}^3/\text{min}$	1	-0.203	Ni	37.1	60	107	120,000
770	~ 1 at $16 \text{ cm}^3/\text{min}$	1	-3.65	Ni	37.1	60	107	2.15×10^6
1,127	5.3×10^{-4}	1	-140	Ni			111	82.7×10^6

^aEstimated loss of metallic nickel after a 1-yr-long exposure to chlorine.^bAssumed without demonstrating.^cThese estimates are probably low since some NiCl₂ evaporation probably occurs.^{d,e}Initially (d) $n \approx 2$, but eventually the rate of weight gain decreases and the kinetics are dominated by (e) linear, $n = 1$, NiCl₂ evaporation.

Nickel. Murashkina¹⁰⁴ reports that at -10 to -20°C chlorine containing 0.06% water vapor reacts with nickel to consume about $1.5\ \mu\text{m}$ of nickel per year.

Downey *et al.*¹⁰⁵ studied the reaction of dry chlorine with nickel at 350 – 600°C using a quartz vacuum microbalance. Polycrystalline 99.95% nickel was used and the chlorine contained 0.5% impurities. Samples were first reduced with hydrogen at 900°C , then cooled to the test temperature. At test temperature the reaction chamber was evacuated to 10^{-6} torr and then filled with chlorine to 100 torr.¹⁰⁶ The experimental results are presented in Figs. 11 and 12.

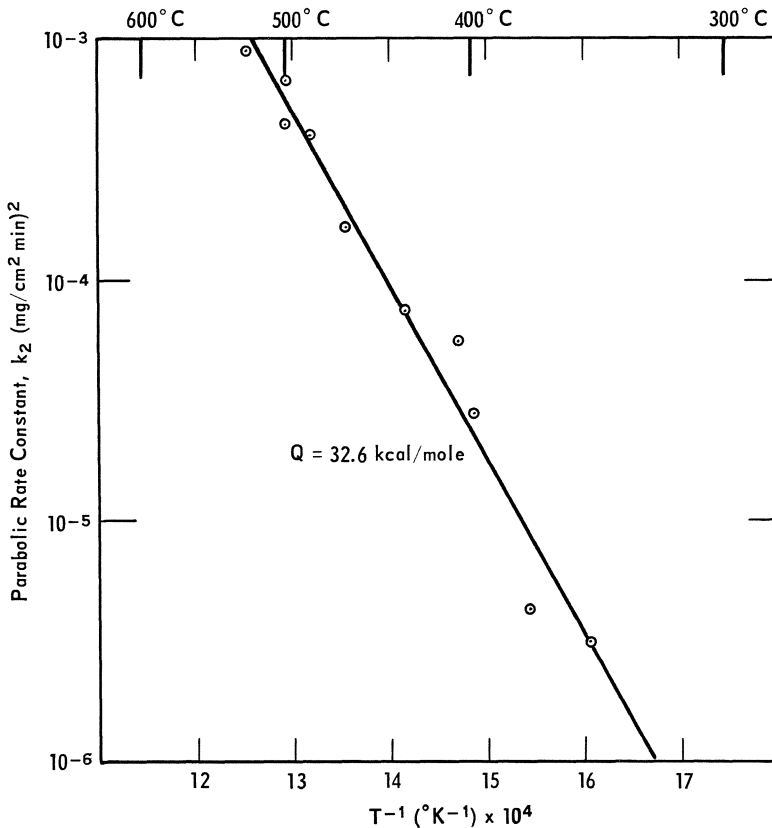


Fig. 11. Parabolic rate constants for the nickel–chlorine reactions from Downey *et al.*¹⁰⁵ Reactions were in static chlorine with $P_{\text{Cl}_2} = 100$ torr.

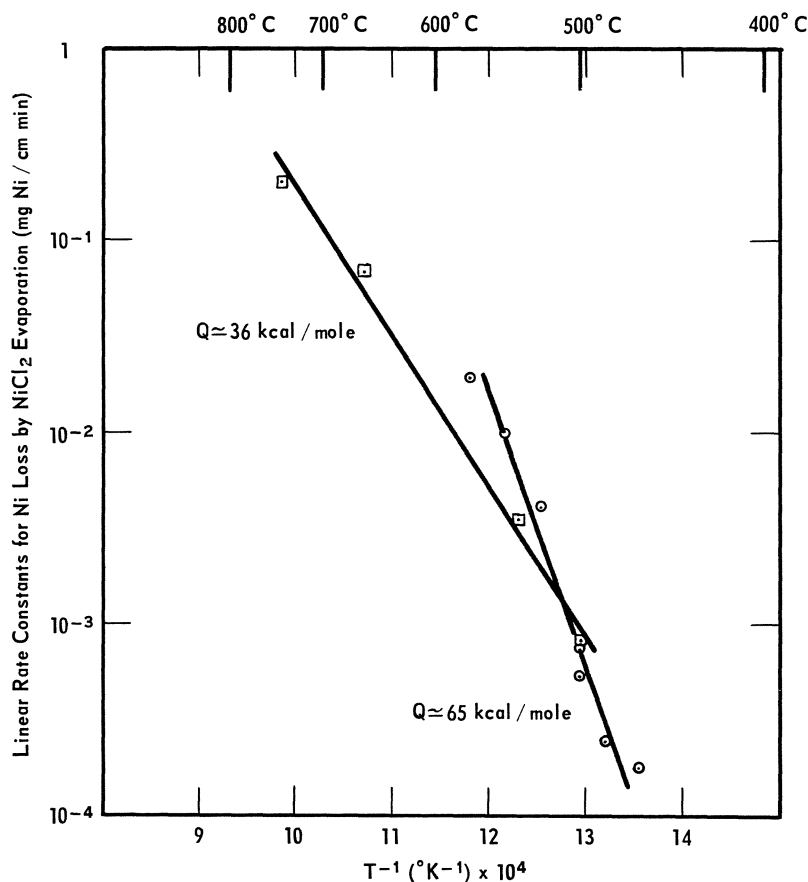


Fig. 12. Rates of nickel loss by NiCl_2 evaporation.

Downey *et al.* observed three different types of nickel-chlorination kinetics over the 350–600°C temperature interval. Below 433°C nickel gained weight according to parabolic kinetics. Between 433 and 525°C nickel initially gained weight according to parabolic kinetics, but later gained weight more slowly than in parabolic kinetics, and finally lost weight according to linear kinetics. This gravimetric behavior is exactly that expected for significant NiCl_2 evaporation in combination with parabolic scale growth. Above 525°C NiCl_2 evaporation is so rapid that the initial period of parabolic weight gain is essentially absent.

The parabolic weight constants of Downey *et al.*, plotted in Fig. 11, indicate an activation energy of about 33 kcal/mole. The rates of nickel loss by NiCl_2 evaporation (as presented in Fig. 12) indicate that the evaporation process has an activation energy of about 65 kcal/mol. Schafer *et al.*¹⁰¹ independently measured an activation energy for NiCl_2 evaporation of about 53 kcal/mole.

Tseitlin and Strunkin^{107,108} observed the 500–740°C reaction of chlorine with nickel containing about 1 wt. % impurities, including 0.86 wt. % cobalt. The linear rates at which nickel lost weight are presented in Fig. 12. For the temperatures at which these data overlap with those of Downey *et al.*, the respective linear rate constants are in good agreement. However, the activation energy calculated from the Tseitlin data for 500–740°C is 36 kcal/mole while that from the Downey data for 465–575°C is 65 kcal/mole.

Below 750°C NiCl_2 scale formed during chlorination of nickel adheres well to the nickel substrate; however, above about 750°C the scale tends to spall,^{107,109} which may account for the apparent increase in activation energy for the nickel–chlorine reaction between 740 and 770°C.

According to Downey *et al.*¹⁰⁵ above 433°C the NiCl_2 scale thickens until the rate of scale formation equals the rate of scale evaporation. At 465–500°C the steady-state amount of scale for 100-torr chlorine is 0.41–0.83 mg/cm², 1.2–2.3 μm . At 525°C the steady-state amount of scale is 0.11 mg/cm², 0.3 μm . At higher temperatures and lower total pressures, the limiting fluoride film thickness is still less.

McKinley and Shuler^{110,111} studied the chlorine reaction on active nickel surfaces at temperatures and pressures such that NiCl_2 scale did not form. The temperature range of their studies was 727–1427°C and the chlorine pressure range was 10^{-7} –0.4 torr. Below 827°C the primary reaction product from the bare nickel surface was $\text{NiCl}_2(v)$ molecules. Above 827°C $\text{NiCl}(v)$ molecules formed, and above 1177°C they were the primary product of the reaction (at 10^{-7} – 10^{-5} torr chlorine pressure).

For chlorine pressures between 0.08 and 0.4 torr the rate of nickel loss is essentially independent of temperature over the 927–1432°C temperature interval. McKinley and Shuler estimate that the activation energy for the reaction is less than 2 kcal/mole. For these pressure and temperature intervals the reaction rate is directly proportional to the chlorine pressure, $m = 1$. The probability of reaction between the nickel and impinging diatomic chlorine molecules is 0.2–0.5. At a chlorine pressure of 0.1 torr, the reaction rate is approximately 35 mg of Ni/cm² min.

Nickel-Base Alloys. Little information is available on the corrosion rates for nickel-base alloys in chlorine. However, estimates from the literature of the ratio of alloy corrosion rates to pure nickel corrosion rates in dry chlorine are presented in Table 5.

According to Murashkina,¹⁰⁴ at -10 to -20°C dry chlorine reacts with Monel at a rate of $2.2\text{--}4.0\text{ }\mu\text{m/yr}$. This is about twice the rate of reaction that Murashkina reports for the reaction of dry chlorine with nickel at the same temperatures.

According to Sheppard *et al.*^{112,113} at -18 to $+60^{\circ}\text{C}$ dry chlorine reacts with nickel at a rate of $0.25\text{--}7.6\text{ }\mu\text{m/yr}$. These rates are based on 36- to 251-hr exposures and assumed linear kinetics. The kinetics are more likely logarithmic. Consequently, metal loss after a 1-yr exposure of Monel to dry chlorine would be correspondingly less. The addition of moisture to the chlorine can increase the rate of reaction with Monel at room temperature by more than 100-fold.

Brown *et al.*¹¹⁴ report that dry chlorine reacts with Monel at $500\text{--}550^{\circ}\text{C}$ about 10 times faster than it reacts with nickel at $500\text{--}550^{\circ}\text{C}$.

According to Brown *et al.*,¹¹⁴ the nickel-chromium alloys Inconel and Chromel-A react with dry chlorine about 1–2 times faster than pure nickel reacts with dry chlorine. However, Halfdanarson and Hauffe¹¹⁵ state that chromium additions up to 16 wt. % have little or no effect on the rate of the nickel-chlorine reaction.

Brown *et al.*¹¹⁴ indicate that at $500\text{--}700^{\circ}\text{C}$ the nickel-molybdenum alloys Hastelloy A, B, and C react with dry chlorine at about the same rate as does pure nickel, a condition which probably also obtains at lower temperatures. At $0\text{--}60^{\circ}\text{C}$ Hastelloy C reacts with dry chlorine about one-fifth to one-thirtieth as fast as Monel reacts with dry chlorine.^{112,113} But Monel reacts with dry chlorine 2–10 times faster than does nickel.^{104,114} The experimental error in these comparisons is large, but the comparisons do indicate that nickel and Hastelloy C react with dry chlorine within an order of magnitude of the same rate.

Chlorimet 3 is a nickel-molybdenum alloy similar to Hastelloy C but containing 1 % silicon and no tungsten. At $0\text{--}60^{\circ}\text{C}$, Chlorimet 3 reacts with dry chlorine at about the same rate as Hastelloy C.^{112,113}

Addition of moisture to chlorine increases the rates of reaction between chlorine and the above alloys at $0\text{--}60^{\circ}\text{C}$. Hastelloy C reacts 2–1000 times faster in wet chlorine than in dry chlorine.^{112,113} Chlorimet 3 reacts 100–1000 times faster in wet chlorine than in dry chlorine.

Table 5. Estimated Reaction Rates for Nickel-Base Alloys in Chlorine^a

Alloy (nom., wt. %)	T(°C)							Ref.
	-100	0	100	200	300	400	500	600
Monel (Ni-30 Cu)		2						104, 112, 113, 114
Chromel A (Ni-20 Cr)		1-2						114
Hastelloy A, B, C (Ni-20 Mo-Fe)		1						112, 113, 114, 192
Chlorimet 3 (Ni-18 Mo-18 Cr)		1						112, 113, 192
Hastelloy D (Ni-10 Si-4 Cu)				5				114

^aRates are normalized relative to the reaction rates for pure nickel.

Hastelloy D is a nickel–silicon alloy containing 10 wt. % silicon, 4% copper, and 1% iron. This alloy reacts rapidly with chlorine. According to Brown *et al.*,¹¹⁴ at 200°C Hastelloy D reacts with chlorine at a rate of about 735 $\mu\text{m}/\text{yr}$. Nickel does not react this rapidly until it reaches a temperature of 500°C. The poor resistance of Hastelloy D to chlorine probably results from its high silicon content (SiCl_4 boils at 57.6°C).

Bromine

Bromine reacts with nickel to form a scale of NiBr_2 . Nickel dibromide melts at about 965°C.⁹⁹ At 700°C, the vapor pressure of NiBr_2 is 5.65×10^{-3} atm.¹¹⁶ At lower temperatures, NiBr_2 scale may protect nickel from rapid reaction with bromine. However, because of its high vapor pressure, NiBr_2 scale begins to evaporate well below its melting point.

Nickel. Haines¹¹⁷ and Lake and Gunkler¹¹⁸ studied bromine attack on nickel at room temperature. Their results are shown along with those of other workers in Table 6. The results shown are average corrosion rates based on total weight loss after exposure and scale removal. The minimum average corrosion rate for nickel exposed to bromine vapor containing only 0.0007% water vapor was 1.0 $\mu\text{m}/\text{yr}$. In liquid bromine containing 0.0007% water, nickel corroded at a rate of 1.8 $\mu\text{m}/\text{yr}$. Addition of moisture to the bromine increased the nickel corrosion rate. In liquid bromine containing 0.029% water, nickel corroded at a rate of 36 $\mu\text{m}/\text{yr}$, 20 times faster than in liquid bromine containing 0.0007% water. In this wet liquid bromine, galvanic corrosion pits the surface of the nickel specimens.¹¹⁹

Miller *et al.*¹²⁰ studied the bromine–nickel reaction at 300 and 500°C. Their results are reported in Table 6 as average corrosion rates for the first 10–11 days. At 300°C, the average reaction rates range from 0.67×10^{-5} to 2.0×10^{-5} mg of Ni/cm² min.

Schafer and Jacob¹¹⁶ give the vapor pressure of solid NiBr_2 as $\log P_{\text{NiBr}_2}(\text{atm}) = 16.681 - (13,112/T) - (0.3497 \times 10^{-3})T - 1.711 \log T$. According to this formula, the vapor pressure of NiBr_2 is 5.65×10^{-3} atm at 700°C and 5.61×10^{-7} atm at 465°C. At each temperature the vapor pressure is roughly double that for NiCl_2 . In the absence of experimental data on NiBr_2 evaporation, a corresponding increment in NiBr_2 evaporation rates compared to those of Fig. 12 for NiCl_2 may be postulated. In the nickel–chlorine reaction, NiCl_2 evaporation measurably influences the reaction kinetics above about 450°C and dominates the reaction kinetics above 550°C.

Table 6. Kinetic Data for Nickel–Bromine Reactions

T(°C)	Bromine state	Br ₂ moisture content (mole %)	k ₁ (mg of Ni/cm ² min)	Test duration (days)	Ref.	Δy (μm) ^a for t = 1 yr
~25	Gas	0.0007	1.7 × 10 ⁻⁶	23	118	1.0
~25	Liquid	0.0007	3.0 × 10 ⁻⁶	23	118	1.8
~25	Liquid	0.003	8.6 × 10 ⁻⁶	69	117	5
~25	Liquid	0.0057	8.6 × 10 ⁻⁶	23	118	5
~25	Liquid	0.0057	3.6 × 10 ⁻⁵	23	118	21
~25	Liquid	0.029	6.0 × 10 ⁻⁵	69	117	36
300	Gas ^b		1.77 × 10 ⁻⁵	11	120	10
300	Gas ^b		9.85 × 10 ⁻⁶	11	120	6
300	Gas ^b		8.60 × 10 ⁻⁶	11	120	5
300	Gas ^b		1.99 × 10 ⁻⁵	10	120	12
300	Gas ^b		1.79 × 10 ⁻⁵	10	120	11
300	Gas ^b		8.83 × 10 ⁻⁶	10	120	5
500	Gas ^b		2.66 × 10 ⁻⁴	10	120	157
500	Gas ^b		9.74 × 10 ⁻⁵	10	120	58

^aEstimated metallic nickel loss after 1-yr-long exposure to bromine, assuming linear kinetics.^bGas flowing over samples at a rate of 150 cm/min.

McKinley¹²¹ studied the nickel–bromine reaction using mass-spectrometric techniques at a bromine pressure of 10^{-7} – 10^{-4} torr at 327–927°C. The evaporation of NiBr molecules was observed above 927°C.

The data for nickel–bromine reactions are summarized in Table 6. Based on these data, estimates of the total amount of nickel consumed after a 1-yr exposure to bromine were made. Linear reaction kinetics were assumed simply because no information on the actual kinetics is available.

Nickel–Base Alloys. Haines¹¹⁷ and Lake and Gunkler¹¹⁸ provide information on the reaction of bromine with Monel at room temperature. According to these workers, dry bromine (0.001–0.003 % water) reacts with Monel at about the same rate as it reacts with nickel. This applies for both liquid and gaseous bromine. Bromine containing 0.005–0.03 % water reacts with Monel 1.5–2.5 times faster than it reacts with nickel.

According to Miller *et al.*¹²⁰ at 300°C bromine reacts with Monel at an average rate of about 2×10^{-3} mg/cm² min. This reaction rate is approximately 100 times faster than that for the bromine–nickel rates at 300°C. Nickel specimens downstream from Monel specimens react with bromine roughly 20 times faster than nickel reacts with bromine in the absence of Monel. The nickel used for these experiments contained 0.4 wt. % impurities and the Monel was 70 wt. % nickel, 25 % copper, 2.5 % iron, 2 % manganese, and 0.5 % silicon. Hence, the presence of copper bromide vapors in bromine appears to accelerate bromine attack on nickel.

At 300°C Duranickel, a nickel–aluminium alloy, reacts with bromine at about the same rate as does pure nickel.¹²⁰ Up to 65°C the nickel–molybdenum–chromium alloy Hastelloy C reacts with bromine at rates less than 50 µm/yr; up to 370°C Hastelloy C reacts with dry bromine at rates less than 500 µm/yr.⁹⁴ In wet liquid bromine Hastelloy C is pitted by galvanic corrosion, which dissolves spheroidal inclusions in the alloy.¹¹⁹

Iodine

Iodine reacts with nickel to form NiI₂ with a melting point of approximately 780°C.⁹⁹ According to Rolsten,¹²² NiI₂ sublimes in a high vacuum at 500–600°C. If nickel forms a protective scale at lower temperatures, the protectiveness of this scale is probably reduced at 500–600°C by NiI₂ evaporation.

Little information is given in the literature on the resistance of nickel and nickel alloys to iodine. Ginzberg and Kabakova¹²³ suggest that up to 250°C, except for some pitting, nickel–chromium alloys are fairly resistant

to iodine attack. Mot²⁴ indicates that the nickel–molybdenum–chromium alloy Hastelloy C is suitable for handling both wet and dry iodine at room temperature. Arbellot¹²⁵ suggests that the nickel–molybdenum alloy Hastelloy B is also suitable for handling moist and dry iodine at room temperature.

Copper and Copper Alloys

Copper and some copper alloys can be used in fluorine up to about 400°C and in dry chlorine up to 150–200°C. Copper may be used to handle moisture-free liquid or gaseous bromine at least at room temperature. The resistance of copper to halogen attack is generally reduced by the presence of moisture in the halogen.

Fluorine

Dry fluorine reacts with copper to form CuF_2 . The melting point of CuF_2 under 1 atm of HF is reported to be $950 \pm 5^\circ\text{C}$,¹³⁶ while the melting point under an atmosphere of nitrogen or helium is reported to be $785 \pm 10^\circ\text{C}$.¹²⁷ Copper difluoride exhibits a distorted nonorthogonal rutile lattice. The vapor pressure at 700°C is 1.66×10^{-5} atm.¹²⁸ Solid copper monofluoride, CuF , is not thermodynamically stable¹⁰ and is not formed during direct fluorination of copper.

Copper—A Summary. Below about $350 \pm 50^\circ\text{C}$, kinetics for the copper–fluorine reaction are logarithmic, $y = k_e \ln(t_0 + at)$. At 400–500°C the copper fluorination kinetics are nearly parabolic, $y^n = k_n t$ with $1.5 \leq n \leq 3$. The activation energy is about 18 kcal/mole, and the kinetics are probably controlled by the diffusion of copper in CuF_2 to the scale/gas interface. While the CuF_2 scale is tough and adherent below about 400°C, above this temperature it is more brittle and more easily detached from the copper substrate. Above 400–450°C, copper fluorination kinetics are altered by sublimation of CuF_2 from the scale. Above about 650°C the rate of CuF_2 sublimation is sufficiently high to result in a net decrease in sample weight after the first 2 hr of fluorination. Kinetic data for copper fluorination are summarized in Table 7.

Copper is highly resistant to HF attack. According to Myers and DeLong,²⁶ at 500–600°C the resistance of copper to HF is equivalent to that of nickel. According to Gillardeau *et al.*,¹²⁹ copper is scarcely attacked

Table 7. Kinetic Data for Copper–Fluorine Reactions

(°C)	P_{F_2} (atm)	m	n	k_n^a ; a (min^{-1}); t_0	Test duration (min)	Ref.	Δy (μm) ^b for $t = 1$ yr
-196	Liquid				5.26×10^5	84	0.3–0.75
-81			ϵ	3.4×10^{-6} ; 9000; 0	180	84	0.000085
-81			ϵ	5.8×10^{-6} ; 18000; 0	180	84	0.00015
22	0.008–0.08	∞	ϵ	5.0×10^{-5} ; 1.6; 32	300	24	0.00076
27	1.0		ϵ	3.9×10^{-5} ; 67; 0	200	85	0.0007
30			ϵ	1.5×10^{-5} ; 88; 0	106	84	0.00029
30			ϵ	4.0×10^{-5} ; 3.3; 0	210	84	0.00064
30			2.8	1.6×10^{-13}	5700	84	0.0029
100	0.008–0.08	∞	ϵ	2.8×10^{-4} ; 0.12; 2.4	300	24	0.0034
150	0.008–0.08	∞	ϵ	5.3×10^{-4} ; 0.56; 11.2	300	24	0.0074
175	0.008–0.08	∞	ϵ	8.6×10^{-4} ; 0.41; 8.2	300	24	0.012
200	0.008–0.08	∞	ϵ	1.86×10^{-3} ; 0.15; 3.0	300	24	0.023
200	0.263		ϵ	0.093; 0.89; 0	210	25	1.4
300	1.0		ϵ	4.5×10^{-2} ; 1.0; 0	240	133	0.6
400	1.0		2	2.1×10^{-3}	240	133	37
427	0.263		1.15	5.1×10^{-3}	< 200	138	1,100
427	0.263		ϵ	0.8234; -0.00441; 0	315	138	0.91 ^d
450	1.0		2	4.5×10^{-3}	240	133	54
450	0.013	1.28	ϵ	0.015; 4.1; 0	50	25	0.24 ^d
450		1.28	ϵ	0.028; 0.48; 0	100	25	0.39 ^d
450		1.28	ϵ	0.042; 0.73; 0	100	25	0.60 ^d
450		1.28	ϵ	0.071; 0.31; 0	200	25	0.95 ^d
450		1.28	ϵ	0.100; 1.2; 0	240	25	1.5 ^d
450		1.28	ϵ	0.104; 1.3; 0	230	25	1.6 ^d
450		1.28	1.4	5.77×10^{-3}	240	25	310
470	1.0		2	6.1×10^{-3}	240	133	63
482	0.263		1.62	7.4×10^{-2}	< 200	138	760
482	0.263		ϵ	1.4207; -0.00613; 0	315	138	1.6 ^d
510	1.0		3	2.8×10^{-2}	240	133	27 ^f
530	1.0		3	3.7×10^{-2}	240	133	30 ^f
538	0.263		ϵ	1.0551; -0.0353; 0	295	138	1.2 ^d
593	0.263		ϵ	1.0801; -0.064; 0	130	138	1.2 ^d
649	0.263		ϵ	1.2482; -0.052; 0	180	138	1.4 ^d
740	1.0		1	-0.07	120	136	41,000
650–750				Ignites and burns		38	

Units for k_s are mg Cu/cm² and units for k_n , power-law kinetics, are (mg Cu/cm²)ⁿ/min.

Estimated metallic copper loss after 1-yr-long exposure to fluorine.

Kinetics are logarithmic.

Static test in closed systems. Estimates seem low when compared to results of other studies.

Kinetics are of the form $y = k[1 - \exp(t_0 + at)]$.

Estimates are probably low because CuF₂ evaporation is not taken into account.

at all by pure HF. In fact, the stoichiometric dissociation of pure HF provides a lower equilibrium fluorine pressure than that for CuF_2 in contact with Cu.

The presence of oxygen in fluorine seems generally to increase the rate of corrosion at low temperatures but reduces weight loss by CuF_2 evaporation at high temperatures. Further, oxygen may prevent ignition of copper in fluorine at 650–750°C, where such ignition normally occurs.

CuF_2 is hygroscopic. It reacts with water to form compounds such as $\text{Cu}(\text{OH})\text{F} \cdot \text{CuF}_2$, $\text{CuF}_2 \cdot 2\text{H}_2\text{O}$, and $\text{Cu}(\text{OH})_2$. Such reactions destroy the protective CuF_2 scale. Hence, the presence of moisture in fluorine greatly speeds the rate of fluorine attack on copper.

Copper-Fluorine—A More Detailed Discussion. Copper is highly resistant to corrosion by high-purity liquid fluorine at -196°C . Kleinberg and Tompkins⁸⁴ left copper specimens submerged in liquid fluorine for a full year. During this exposure, the specimens gained 0.17–0.40 mg/cm², which, assuming only CuF_2 formation, represents a recession of only 0.3–0.75 μm . Toy *et al.*¹³⁰ report that copper corrodes in liquid fluorine at a rate of only 0.15 $\mu\text{m}/\text{yr}$.

Impurities in liquid fluorine and galvanic couples can lead to much higher corrosion rates. In particular, moisture and HF accelerate the corrosion rates of copper in liquid fluorine. Short-duration corrosion tests can indicate erroneously high corrosion rates because passive films are formed during the initial minutes of fluorine exposure. These factors account for the much higher corrosion rates, ranging from 10 μm to 0.5 mm/yr, reported by earlier workers.^{43,83,131}

Kleinberg and Tompkins⁸⁴ studied the reaction of copper powder with gaseous fluorine at -81 , 30 , and 84°C for 100–200 min. The Kleinberg and Tompkins data were presented graphically by Schmidt.³⁸ From these graphs the following conclusions were drawn.

Short-term (100- to 200-min exposures), copper fluorination reactions at -81 and 30°C can be approximated by a logarithmic equation, $y = k_e \ln(at)$, the parameters for which are presented in Table 7. According to these equations, the fluoride film (adsorbed layer) thickness after a 1-yr exposure of copper to fluorine would be only 3–5 Å. At 30°C , the values of k_e and a in Table 7 correspond to a 10- to 22-Å fluoride film thickness after a 1-yr exposure.

Copper-powder fluorination data for a longer term, 95-hr experiment at 30°C did not follow a logarithmic equation but could be more closely approximated by a power-law equation with the parameters given in Table 7.

This power-law equation ($n = 2.8$) predicts a fluoride film thickness of about 100 \AA after a 1-yr exposure at 30°C .

At 27°C and 1 atm fluorine pressure, according to Cannon *et al.*⁸⁵ the copper–fluorine reaction follows the logarithmic equation (see Table 7). The fluorination kinetics were observed for about 200 min by a manometric technique with copper powder containing only 0.1 wt. % impurities.

Like Kleinberg and Tompkins, Cannon *et al.* did not remove surface oxide from the copper prior to the fluorine exposures. Consequently, the study was of surface oxide fluorination rather than of metallic copper fluorination. The reaction products at 27°C were identified as $\text{Cu}(\text{OH})\text{F} \cdot \text{CuF}_2$ and $\text{CuF}_2 \cdot 2\text{H}_2\text{O}$ with some CuF_2 . At 93°C , the major product was $\text{Cu}(\text{OH})\text{F} \cdot \text{CuF}_2$, but CuF_2 and $\text{Cu}(\text{OH})_2$ were also produced.

Cannon suggests that the rate-controlling step in this fluorination process is quantum-mechanical tunneling of electrons through the film of corrosion products. The justifications for this hypothesis are the logarithmic kinetics and the thin film thickness, less than 50 \AA , including the original surface oxide.

The low-temperature studies discussed above and others given in Table 7 involve fluorination of oxide films rather than fluorination of metallic copper. In some cases, the extremely thin film thicknesses reported imply adsorption rather than formation of fluoride films as such. For these reasons, conversion of fluoride film thickness into units of metallic copper consumed by the reactions might not really be valid. However, the conversions are used in order to present the data in a form commensurate with those of other studies and with those most useful to the engineering selection of materials. At least, some order-of-magnitude comparisons can be made.

Brown *et al.*²⁴ fluorinated copper powder between 25 and 250°C and determined fluorine consumption by a pressure-drop method. Initial fluorine pressures were between 6 and 60 torr. Below 300°C , the fluorination rates were independent of fluorine pressure within this pressure range.

For 200°C and lower temperatures, the data of Brown *et al.* fit a logarithmic relationship of the form $y = k_e \ln(t_0 + at)$, where the values of k_e , t_0 , and a are given in Table 7. The data did not obey the usual “activated” temperature dependence, but Q was reported as nearly proportional to the scale thickness, $Q \simeq 0.225(\text{kcal/mole} \cdot \text{\AA})_y$.

At 250°C the copper fluorination kinetics were logarithmic until the scale built up to a thickness of about 670 \AA . Thereafter, the rate of scale formation was lower than that predicted by the logarithmic equation valid for the initial scaling. In a companion paper, Crabtree *et al.*¹³² identified,

by x-ray and electron diffraction, the fluoride scale formed on copper as cupric fluoride, CuF_2 .

By thermogravimetry, Luk'yanychev *et al.*¹³³ observed logarithmic scale growth on copper fluorinated at 300°C. The scale formed at 300–600°C was CuF_2 . These authors suggest that the kinetics may be accounted for by Evan's theory of logarithmic scale growth, whereby continuous mechanical changes in the scale result in scale compaction, which in turn decreases the gas permeability of the scale.¹³⁴

Both Brown and Luk'yanychev *et al.* observe that logarithmic kinetics apply only below some critical temperature. However, they do not report the same value for this critical temperature. Brown *et al.* observed deviation from logarithmic kinetics at and above 300°C. Luk'yanychev *et al.* observed deviation from logarithmic kinetics at 400°C but not at 300°C.

Brown *et al.* also subscribe to Evan's logarithmic growth model and give several reasons for discarding other proposed fluorination mechanisms that assume rate control by either diffusion or quantum-mechanical tunneling as described by Mott and Cabrera.¹³⁵ The main reasons are, respectively, (1) nonparabolic kinetics and variation of apparent activation energy with scale thickness, and (2) persistence of the same logarithmic rate law into the thick scale range, where tunneling theory is no longer applicable.

Luk'yanychev *et al.* also reported thermogravimetric experiments for fluorination of copper (99.9% Cu) at 400–600°C. At these higher temperatures, power-law kinetics were obeyed. The value of n increased with increasing temperature from about 2 at 400–450°C to about 3 at 500–530°C. This deviation from parabolic kinetics at higher temperatures probably results from CuF_2 evaporation. Consequently, the metallic recession rate is probably significantly higher than that indicated by the Luk'yanychev cubic rate constants given in Table 7. Luk'yanychev calculated an activation energy of 17.9 kcal/mole for copper fluorination at temperatures between 400 and 530°C. In this temperature range the rate-controlling step is probably diffusion of ions (or electrons if CuF_2 should exhibit predominant ionic conduction) through the CuF_2 scale as described by Wagner.⁴⁵ Quite simply, thermally activated parabolic scaling kinetics usually implies that the process is diffusion-controlled. Gillardeau *et al.*^{136,137} indicate that copper ions diffuse outward through the CuF_2 scale to the gas/scale interface.

O'Donnell and Spakowski¹³⁸ reported power-law kinetics for short-time copper fluorination with $n = 1.15$ at 427°C and $n = 1.62$ at 482°C. At higher temperatures (538–649°C) the calculated scale thickness was

given more accurately by the logarithmic equation. O'Donnell and Spakowski, like Brown *et al.*, measured system gas pressure drop and calculated fluorine consumption and scale thickness. That these calculated scale thicknesses truly reflect CuF_2 scale growth is questionable since, according to Gillardeau *et al.*,¹³⁶ CuF_2 has a significant vapor pressure at these temperatures.

In long tests, O'Donnell and Spakowski reported that power-law kinetics give way to kinetics of the form $y = k[1 - \exp(at)]$, where a is negative: the fluorine consumption rate after a period of time approaches zero. The higher the fluorination temperature, the shorter the initial period of rapid fluorine consumption. This behavior contradicts Gillardeau's observations of weight loss at high temperatures and long times because of CuF_2 evaporation. CuF_2 scale evaporation would be expected to result in a leveling out of the fluorine consumption rate to a constant significant value, not to zero as O'Donnell and Spakowski observed.

O'Donnell and Spakowski also studied the dependence on P_{F_2} of copper fluorination at 450°C .²⁵ For fluorine pressures between 10 and 130 torr, their 450°C fluorine consumption data fit a logarithmic relationship, $k_e = 7.68 \times 10^{-7} P_{\text{F}_2}^{1/m}$, where $m = 1.28$. Though high-purity fluorine (99.8%) was used, corrosion product formed on the copper included red crystallites along with clear ones, indicating the presence of Cu_2O as well as CuF_2 .

Gillardeau¹³⁶ has shown that small amounts of oxygen in fluorine can form cuprous oxide. Initially, at least, the oxidation rate actually exceeds the fluorination rate in spite of the fact that oxygen is a minor constituent of the gas. In fact, the red crystallites observed by O'Donnell and Spakowski were probably Cu_2O , as observed by Gillardeau. Perhaps the oxide film passivates the surface against rapid fluorine attack. Gillardeau states that reproducible kinetic studies of copper fluorination are impossible above 400°C because CuF_2 evaporates, forming blisters and pores in the remaining CuF_2 scale.

The experimental procedure of O'Donnell and Spakowski may be another reason for their failure to observe continued fluorine consumption resulting from CuF_2 evaporation. O'Donnell and Spakowski used a static system. The rate of scale evaporation in the viscous pressure range is limited by mass transport (diffusion of molecules) through the stagnant boundary film; this rate is minimized in a static system. Lacking evaporation, an accumulation of sufficient thickness of CuF_2 scale would passivate the copper against further attack, as O'Donnell and Spakowski observed.

Myers and DeLong²⁶ studied the $400\text{--}700^\circ\text{C}$ reaction of copper in

fluorine with a high oxygen content; Steindler and Vogel¹³⁹ also studied the 550–750°C fluorination of copper in fluorine, which probably contained 0.1–0.5% oxygen. In both cases thick scales formed at 700–750°C. The scale observed by Myers and DeLong was black, probably cupric oxide. The scale observed by Steindler and Vogel was red, probably cuprous oxide. CuF_2 is white or clear. Because these two studies involved oxidation more than fluorination, the results are not reported in Table 7.

Using thermogravimetric, x-ray, and microscopic techniques, Gillardeau *et al.*^{136,140,141} studied the fluorination of 99.999% purity copper in the temperature range 200–750°C at fluorine pressures of 0.02–760 Torr. Like Luk'yanychev *et al.*¹³³ over their entire range of investigation, Gillardeau *et al.* observed only the formation of cupric fluoride, CuF_2 . No cuprous fluoride, CuF , was detected. Above about 400°C, the protective CuF_2 scale

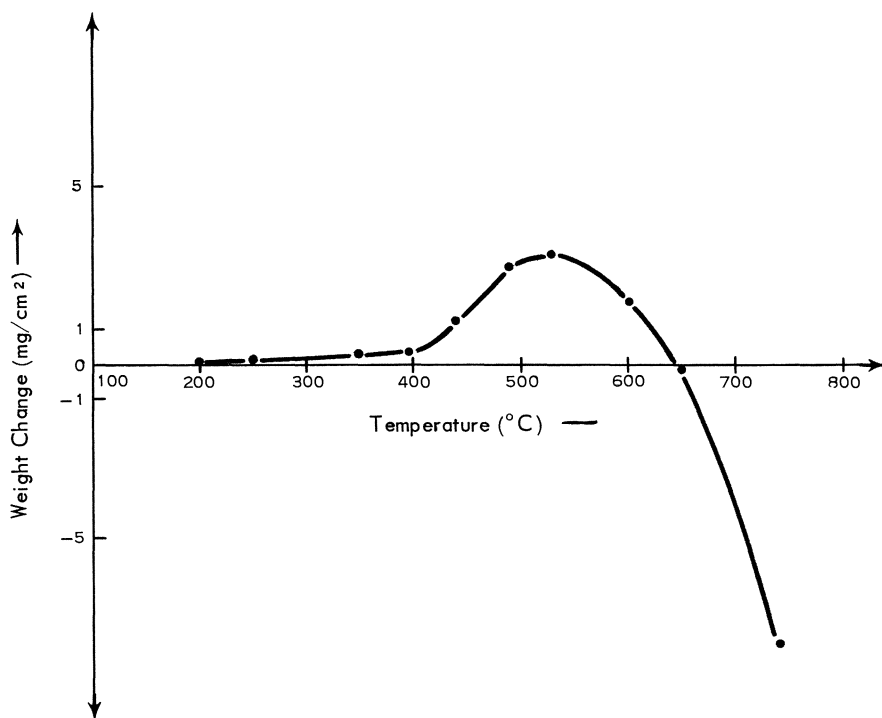


Fig. 13. Copper weight gain after 2-hr exposure to fluorine at 1.0 atm pressure. Copied from Gillardeau *et al.* by permission of Plenum Press.¹³⁶

begins to deteriorate by sublimation of CuF_2 . According to Gillardeau *et al.*, this CuF_2 sublimation is responsible for the deviation of copper-fluorination kinetics from parabolic behavior above 400°C . At higher temperatures, after an initial period of rapid scale formation, copper samples lose weight by CuF_2 evaporation. In Fig. 13, sample weight change after 2 hr of fluorination is plotted against fluorination temperatures. The average weight loss at 740°C corresponds to about $0.07 \text{ mg of Cu/cm}^2 \text{ min}$. As indicated in Table 7, this rate of CuF_2 evaporation would remove 41 mm of copper per year.

Evaporation of NiCl_2 has been extensively studied, as described in the preceding section. At 465°C NiCl_2 has a vapor pressure of $4 \times 10^{-7} \text{ atm}$ and evaporates in 100-torr Cl_2 at a rate of $2 \times 10^{-4} \text{ mg of Ni/cm}^2 \text{ min}$. At 550°C NiCl_2 has a vapor pressure of $1.6 \times 10^{-5} \text{ atm}$ and evaporates at a rate of $1 \times 10^{-2} \text{ mg of Ni/cm}^2 \text{ min}$. At 600 and 700°C , CuF_2 has vapor pressures of about 5×10^{-7} and $1.7 \times 10^{-5} \text{ atm}$, respectively. The evaporation rates of CuF_2 at 600 and 700°C in 100-torr F_2 are then probably about 10^{-4} and $10^{-2} \text{ mg Cu/cm}^2 \text{ min}$, respectively. Metallic copper loss at a rate of $10^{-4} \text{ mg of Cu/cm}^2 \text{ min}$ is within the limits of detection of the above copper fluorination kinetics studies. A rate of about $10^{-3} \text{ mg/cm}^2 \text{ min}$ should dominate the kinetics at 650°C after the first 60–120 min.

The evaporation of protective CuF_2 scale results in rapid fluorination and ignition of copper in fluorine at $650\text{--}750^\circ\text{C}$. This range of ignition temperatures was determined by Godwin and Lorenzo.⁹¹ Two different techniques were employed. In one series of experiments a bomb was filled to 1 atm with fluorine gas. A copper wire was then slowly heated in this environment and the temperature at which the wire ignited was determined. In a second series of experiments, the copper wire was heated to predetermined temperatures and then fluorine was introduced into the bomb.

Copper-Base Alloys. The following paragraph summarizes the information available on the corrosion behavior of a few copper-base alloys in fluorine. Only a qualitative overview is provided; the fluorination rates are expressed in terms of the fluorination rates for pure copper. A quantitative approach to this subject is not justified, as only scant information is available in the literature. Much of this information presents only average corrosion rates determined from experiments for which experimental conditions are not well specified.

In liquid fluorine at -196°C , most of the copper–zinc and copper–nickel alloys corrode at about the same rate as does pure copper.^{43,131}

The copper-silicon alloy Everdur corrodes about twice as fast as does pure copper.⁴³ At room temperature, bronzes and brasses with low zinc contents corrode at about the same rate as does copper, but brass containing 35–40% zinc corrodes 5 times faster.^{38,131} Cu–10 to 30 wt. % Ni in fluorine at room temperature corrodes 2–3 times faster than does pure copper.¹⁴² At 200°C, Cu–15% Zn fluorinates at about the same rate as copper and Cu–40% Zn fluorinates twice as fast. At higher temperatures, copper-zinc alloys fluorinate still more rapidly; the higher the zinc contents, the faster the rates of fluorination.¹³¹

Chlorine

Dry chlorine reacts with copper to form two chlorides: CuCl (cuprous chloride) and CuCl₂ (cupric chloride). Their melting points are about 422–432°C and 622–630°C, respectively.^{143,144} The vapor pressure of CuCl₂ is 1.3×10^{-6} atm at 300°C.¹⁴⁵

The American Brass Company¹⁴⁶ reports that copper and copper alloys at room temperatures are highly resistant to dry chlorine but are corroded by moist chlorine. Brown *et al.*¹¹⁴ recommend that copper be used in dry chlorine environments only below 200°C and in dry HCl environments only below 100°C. Tseitlin¹⁰⁸ recommends the use of copper in dry chlorine only below 150°C.

Tseitlin and Strunkin^{102,103,107,108,147,148} have studied the corrosion of copper by chlorine. The results of their thermogravimetric experiments are summarized in Table 8 and are discussed in the following paragraphs. The results are expressed in terms of average corrosion rates for 6-hr exposures of copper to dry chlorine.

Below 150°C, dry chlorine reacts with copper to form a film of copper chloride, which protects the metal against further rapid attack. Between 150 and 300°C the rate of scale formation increases. Tseitlin's data for this temperature interval indicate an activation energy of about 18 kcal/mole. As the temperature approaches 300°C, CuCl₂ becomes somewhat volatile. At 300°C, the CuCl₂ vapor pressure is 1.3×10^{-6} atm; at this vapor pressure NiCl₂ volatilizes at a rate of about 10^{-3} mg/cm² min. Between 150 and 300°C this rate of CuCl₂ evaporation is not significant compared to the rate of copper chloride scale formation, and most of the corrosion product formed remains on the surface of the copper. However, the product is brittle and can easily flake off the metal.

At 290–310°C copper ignites in dry chlorine flowing at a rate of 250 ml/

Table 8. Average Corrosion Rates for Copper in Chlorine^{147,108}

$T(^{\circ}\text{C})$	Gas flow ^a rate (cm^3/min)	Test duration (min)	k_1 (mg Cu/ cm^2 min)	Δy (cm) ^b for $t = 1$ yr
150	250	360	0.0017	0.088
170	250	360	0.0095	0.50
220	250	360	0.027	1.4
250	250	360	0.16	8.4
285	250	360	0.35	18
300	250	60	44	2300
300	40	360	0.44	23
300	3.5	360	0.11	5.7

^aChlorine pressure was near atmospheric pressure.

^bEstimated loss of metallic copper after a 1-yr exposure to chlorine gas. Because the estimates were made assuming linear kinetics, the estimates are probably too large at lower temperatures, where some passivation does occur.

min; it does not ignite in chlorine flowing at 40 ml/min. When copper samples are exposed to dry chlorine at 290–310°C for only 3–5 min, the surface is covered with fused copper chloride, predominantly CuCl.

Below 200–250°C, oxygen and water vapor in chlorine accelerate the rate of chlorine attack on copper. However, at higher temperatures oxygen and water vapor in chlorine reduce the rate of chlorine attack on copper.^{103,148} Apparently oxygen and moisture in chlorine form an oxide layer over copper, which is more stable and protective than the copper chlorides, which form in pure dry chlorine. Consequently, the presence of these impurities in chlorine reduces the corrosion rate above 200–250°C and moves the ignition temperature up from about 300°C to near 350°C.

According to Brown *et al.*,¹¹⁴ below 200–250°C anhydrous HCl also attacks copper more rapidly than pure dry chlorine, but above 250°C HCl is less aggressive than pure chlorine.

Harrison and Ng¹⁴⁹ studied the reaction of $\text{Cl}_2 + 2\text{CuCl} \rightarrow 2\text{CuCl}_2$ at 75–130°C. After some initial period of CuCl₂ scale formation over the CuCl, the reaction kinetics were parabolic with an activation energy of 11.3 kcal/mole. In this temperature range (below 150°C) the protective scale on the copper probably consists of two layers: (1) an outer layer of CuCl₂, the growth rate of which is controlled by cation or anion diffusion, and (2) an inner layer of CuCl, which supports cation diffusion.

Bromine

Dry bromine reacts with metallic copper to form CuBr and CuBr_2 . CuBr melts at 488–498°C and has a vapor pressure of 2.6×10^{-7} atm at 300°C.^{143,145,150,151} CuBr_2 also melts at about 498°C,¹⁴ but its vapor pressure is not given in the literature. However, the CuBr_2 vapor pressure at 300°C must be substantial, since its rapid vapor phase transport has been observed at this temperature.¹²⁰ CuBr_2 also has a high Br_2 dissociation pressure, about 1×10^{-3} atm at 300°C.

Copper and most copper alloys are resistant to corrosion by moisture-free liquid and gaseous bromine at room temperature.¹⁴⁶ Copper at room temperature is less resistant to moist bromine, and copper alloys containing more than about 15% zinc are particularly subject to rapid corrosion by moist bromine.

Miller *et al.*¹²⁰ exposed copper to analyzed reagent grade bromine vapors at 300°C. Rapid, catastrophic attack ensued. Alloys such as Monel are also rapidly attacked by bromine at 300°C, and samples of nickel downstream from copper or copper-containing alloys also corroded at accelerated rates. The latter observation indicates that some species of copper bromide is evaporating from the copper and copper-containing alloys.

Iodine

Copper reacts with iodine to form the monoiodide, CuI , which melts at about 600°C. The CuI vapor pressure is about 4.3×10^{-5} atm at 600°C and 1.3×10^{-6} atm at 400°C.

The reaction of copper with iodine vapor at 6×10^{-7} to 0.23 torr has been studied.^{152,153} Below 375°C a crystalline film, probably CuI , forms over the surface during the first few minutes of the reaction. Then larger hexagonal crystals form over the surface and the rate of reaction decreases with increasing time. Above 375°C, CuI evaporation is significant.

Iron and Iron Alloys

Iron and iron-base alloys are frequently used in halogen environments. Iron and stainless steels are relatively resistant to fluorine attack at low temperatures. Stainless steels can be used in fluorine up to about 150°C and may also be used for handling dry chlorine. High-silicon irons are commonly used for both dry and wet chlorine. Carbon steel is readily attacked by liquid bromine, but stainless steel can be used to handle very dry, HBr -free, liquid bromine and can also be used in contact with dry iodine.

Fluorine

Iron forms two stable fluorides, FeF_2 and FeF_3 . These fluorides melt at 1020 and 1027°C, and exhibit tetragonal rutile¹⁵⁴ and rhombohedral¹⁵⁵ crystal lattices, respectively. The iron fluorides have appreciable vapor pressures only above 500°C. At 500°C, the vapor pressure of FeF_3 is about 2×10^{-7} atm¹⁵⁶ and that of FeF_2 is still lower.¹⁵⁷ The vapor pressures of FeF_3 and FeF_2 attain values of 10^{-4} atm only at temperatures of about 675 and 900°C, respectively.^{156,157}

Iron—A Summary. Upon exposure to fluorine, iron forms a solid fluoride scale which affords considerable protection against further fluorination. But, unfortunately, the scale is brittle and lacks the adherence that NiF_2 has on nickel. Consequently, the scale spalls easily; above about 300°C scale exfoliation dominates iron-fluorination kinetics.¹⁵⁸

At 300°C, as little as 0.2 vol % oxygen in fluorine greatly accelerates fluorine attack on iron. However, at 200°C oxygen apparently has little effect on the iron-fluorination kinetics.¹⁵⁸

Iron—Fluorine—A More Detailed Discussion. Using the pressure-drop method for determining fluorine consumption, O'Donnell studied the fluorination of spectroscopically pure iron sheet over the temperature range 225–525°C and the pressure range 15–200 torr.^{159,160} A protective surface scale of ferric fluoride, FeF_3 , formed over the sample surface. O'Donnell's iron-fluorination data fit logarithmic equations of the form $y = k \ln(at)$, where y is the amount of fluorine consumed by the reaction. Empirical values of k are given in Table 9 and those of O'Donnell for $P_{\text{F}_2} = 60$ torr are plotted in Fig. 14. The activation energy is only 2 kcal/mole. The fluorination rate is a function of pressure, $k = P_{\text{F}_2}^{1/m}$, where $m = 1.15$ at 525°C and 2.1 at 225°C. The iron-fluorination kinetics were logarithmic, but the fluoride scales were too thick for control by the Mott–Cabrera tunneling effect. Consequently, O'Donnell suggests that the fluorination rate is controlled by diffusion of fluorine gas to the metal/scale interface through the defective scale. This mechanism was first proposed by Evans to account for logarithmic oxidation kinetics.¹⁶¹

Gillardeau *et al.* studied the fluorination of 99.99% iron at 200, 300, and 400°C for a fluorine pressure of 60 torr.^{136,158} The observed rate constants are given in Table 9 and plotted in Fig. 14. The fluoride scale formed at 200°C was predominantly FeF_3 with only traces of FeF_2 . But at 300°C and higher temperatures, an FeF_2 layer always formed beneath an outer

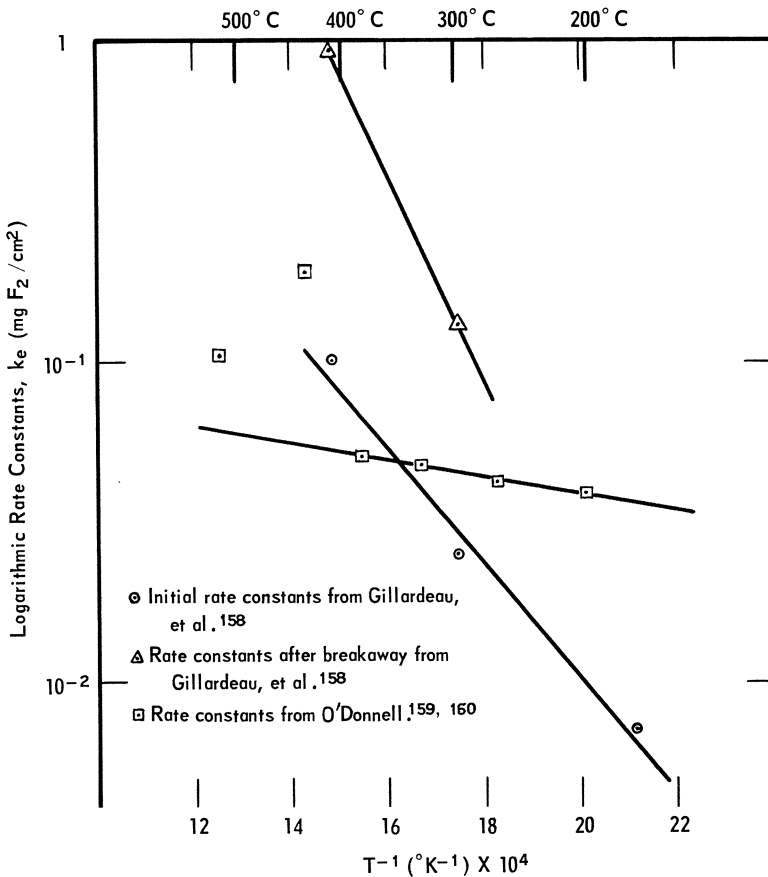


Fig. 14. Observed logarithmic rate constants for the fluorination of iron at $P_{F_2} = 60$ torr.

layer of FeF_3 . In agreement with O'Donnell, Gillardeau *et al.* report logarithmic kinetics and suggest that the fluorination rate is controlled by inward diffusion of fluorine through the defective fluoride scale to the metal/scale interface. This hypothesis is supported by marker experiments. According to Gillardeau *et al.*, the activation energy for the reaction is 8.4 kcal/mole, 4 times that reported by O'Donnell. Gillardeau *et al.* attribute such differences between their results and O'Donnell's to higher concentrations of oxygen and other impurities in O'Donnell's fluorination system.

According to Gillardeau, when some critical scale thickness is reached, the fluoride scale separates from the underlying iron and fluorination of

Table 9. Kinetic Data for Iron–Fluorine Reactions

T (°C)	P_{F_2} (atm)	m	k_e (mg F_2 /cm ²);	a (min ⁻¹); $t_0 = 0$	Test duration (min)	Ref.	Δy (μm) ^a for $t = 1$ yr
200	0.079		0.0071	2.3	300	158	0.13
225	0.026	2.1	0.026	0.81	180	160	0.19
225	0.079	2.1	0.039	0.40	300	160	0.27
225	0.26	2.1	0.075	0.20	275	160	0.49
275	0.079		0.042	1.2	190	160	0.32
300	0.079		0.025	0.73	210	158	0.41 ^b
300	0.079		0.13	0.013	360	158	1.5 ^c
325	0.079		0.047	1.17	220	160	0.36
375	0.079		0.051	1.2	230	160	0.38
400	0.079		0.1	0.86	36	158	1.7 ^d
400	0.079		0.93	0.026	60	158	12 ^e
425	0.079		0.093	0.19	240	160	0.60
525	0.020		0.036	0.55	130	160	0.25
525	0.079		0.105	1.28	220	160	0.79
525	0.13		0.145	0.38	295	160	1.0
620–730	1.0		Ignites and burns			91	

^aEstimates of metallic iron losses after a 1-yr exposure to fluorine. These estimates are generally much too low; over a long period of time exfoliation of scale frequently dominates the kinetics and may result in more nearly linear than logarithmic kinetics.

^bBefore breakaway at 210 min.

^cAfter breakaway at 210 min.

^dBefore breakaway at 36 min.

^eAfter breakaway at 36 min.

iron proceeds more rapidly. This separation probably results from an accumulation of stresses as the fluoride forming at the scale/metal interface occupies 3–4.5 times the volume of the metal consumed.

Such disruption of the protective scale leads to average corrosion rates much higher than implied by the short-term logarithmic rate kinetics. Consider, for example, the hypothetical fluorination kinetics shown in Fig. 15. The short-term kinetics are logarithmic. However, successive losses of the protective scale give rise to cyclical kinetics, which are on the average more nearly linear to the extent that a linear rate constant would be more useful for calculating long-term metal thickness loss than the associated logarithmic rate constants. On a large sample, losses of scale integrity over the sample surface are not in phase, so the measured kinetics appear linear after the first few cycles (Fig. 16). In reality, the average kinetics are not necessarily linear; they may, for example, be logarithmic or parabolic.

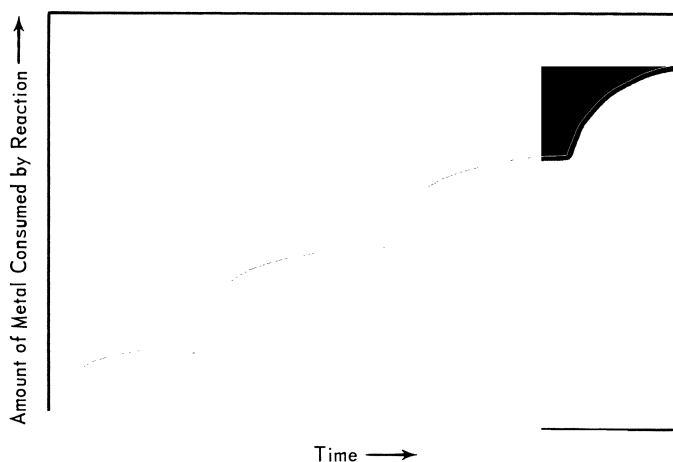


Fig. 15. Hypothetical fluorination kinetics resulting from periodic exfoliation of scale.

There is not sufficient long-term experimental data on the fluorination of iron to establish the long-term average kinetics. But, if the first logarithmic cycle obtained by Macheteau *et al.*¹⁵⁸ were repeated over and over again, the average linear rate constants would be about 0.4 mm of Fe/yr at 300°C

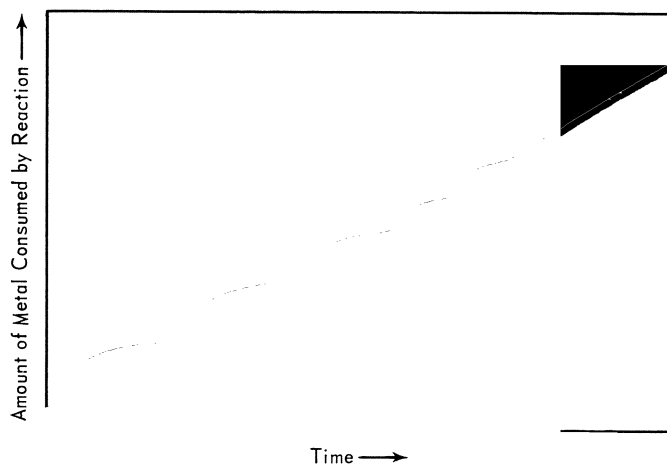


Fig. 16. Hypothetical fluorination kinetics resulting from out-of-phase exfoliation of scale from different areas of the sample surface.

and 7 mm of Fe/yr at 400°C. However, if fluorination continued to follow the initial logarithmic kinetics, after 1 yr the metal loss would be only 0.4 μm at 300°C and 2 μm at 400°C.

According to Godwin and Lorenzo,⁹¹ iron wires ignite in fluorine at 620–730°C. Ignition temperatures were determined both by heating wires in fluorine of atmospheric pressure and also by exposing preheated wires to fluorine.

Iron-Base Alloys. Little information is available on fluorination kinetics for iron-base alloys. Carbon, silicon, and titanium additions significantly reduce fluorination resistance. Chromium additions, as in stainless steels, seem to have little effect below about 200°C but greatly reduce the resistance of iron to fluorine at temperatures above about 250°C. This detrimental effect above 250°C results from the formation of volatile chromium fluorides. In Table 10, fluorination rates for iron-base alloys are compared to those for pure iron.

Chlorine

Iron forms two chlorides, FeCl_2 and FeCl_3 . Their melting points are about 675 and 305°C, and they exhibit rhombohedral CdCl_2 ¹⁵⁵ and hexagonal BiI_3 ¹⁵⁵ crystal lattices, respectively. Their vapor pressures attain values of 10^{-4} atm at about 500 and 165°C and values of 1.0 atm at about 800 and 315°C, respectively. FeCl_2 is thermodynamically quite stable; however, under a chlorine pressure of 1.0 atm, FeCl_3 decomposes at 405°C. Hence, iron may be expected to form a solid chloride, which will tend to sublime at a measurable rate even below 300°C. Typical iron-chlorination rates are indicated in Table 11. There is an abrupt increase in the chlorination rate at some temperature between 250 and 300°C.

Below 250–300°C, oxygen and moisture have little effect on the iron-chlorination rate, but above this temperature range, oxygen and especially moisture present in chlorine decrease the iron-chlorination rate to as little as one thousandth of the rate in pure chlorine.^{103,107,148} This decrease is due to the formation of iron oxides, which prevent volatilization of the iron as $(\text{FeCl}_3)_2(v)$. Since iron is attacked less rapidly by HCl than by Cl_2 , HCl present in chlorine should have little or no effect on iron-chlorination rates.

Heinemann *et al.*¹⁶² studied the reaction of dry chlorine with steel containing 0.08–0.15% C, 0.35–0.65% Mn, and less than 0.05% each of P and S. After exposure to chlorine, specimens were rinsed in water to remove the corrosion products. Below 148°C, the amount of iron consumed was

Table 10. Estimated Reaction Rates for Iron-Base Alloys in Fluorine^a

Alloy (nom., wt. %)	T(°C)										Ref.
	-200	-100	0	100	200	300	400	500			
SAE 1030 (0.5 Mn, 0.3 C, 0.0 Si)					←	← 0.5-2 →	→				26
SAE 1030 (0.6 Mn, 0.3 C, 0.2 Si)						80					26
SAE 1020 (1.0 Mn, 0.2 C, 0.2 Si)					40	70	20				26
SAE 1015 (0.6 Mn, 0.15 C, 0.07 Si)						80					26
"Music wire" (0.5 Mn, 0.9 C, 0.1 Si)						40					26
Stainless steel 304 (18 Cr, 8 Ni, 0.1 C)	5		1		1		3				83
Stainless steel 310 (25 Cr, 20 Ni, 0.2 C)					1	3	20				26
Stainless steel 309 (23 Cr, 14 Ni, Nb, C)					1	8	30				26
Stainless steel 347 (18 Cr, 10 Ni, Nb, C)	3		1		1	25	10-30				26, 83
Stainless steel 430 (16 Cr, 0.1 C)					1	30	3				26

^aRates are normalized relative to the reaction rates for pure iron.

Table 11. Kinetic Data for Iron-Chlorine Reactions

T(°C)	Flow rate (liters/min)	P _{Cl₂} (atm ²)	Diluent gas	m	Test duration (min)	Linear rate constant ^b k ₁ (μm/atm min)	Ref.	Δy (cm) ^c for t = 1 yr
77	100	1.0	None		480	3 × 10 ⁻⁴	162	0.016
166	100	1.0	None		0-15, 15-480	3.3 × 10 ⁻³ , 3.8 × 10 ⁻⁴	162	0.020
198	100	1.0	None		0-15, 15-480	5.2 × 10 ⁻³ , 3.7 × 10 ⁻⁴	162	0.019
200	15	1.0	None		360	2 × 10 ⁻⁴	108	0.011
230	100	1.0	None		0-15, 15-480	8.5 × 10 ⁻³ , 2.2 × 10 ⁻⁴	162	0.012
240	100	1.0	None		0-15, 15-480	9.5 × 10 ⁻³ , 2.4 × 10 ⁻⁴	162	0.013
240	15	1.0	None		360	2 × 10 ⁻⁴	108	0.011
247	100	1.0	None		0-15, 15-480	1.0 × 10 ⁻² , 1.9 × 10 ⁻⁴	162	0.010
251	100	1.0	None		480	1.55	162	82
255	120	^d	Ar	1		0.94	165	49
260	15	1.0	None		360	2 × 10 ⁻⁴	108	0.011
268	120	^d	He	1		1.78	165	94
279	120	^d	Ar	1		2.45	165	130
285	15	1.0	None		360	4 × 10 ⁻⁴	108	0.021
285	15	1.0	None		60	20.4	108	1100
302	120	^d	He	1		4.04	165	210
304	120	^d	Ar	1		4.17	165	220
310	15	1.0	None		60	3.9	108	170
323	120	^d	Ar	1		8.94	165	470
327	120	^d	He	1		11.4	165	600
381	120	^d	Ar	1		40.4	165	2100
381	120	^d	He	1		65.3	165	3400
540	15	^d	N ₂			6.6	107	350
540	15	^d	N ₂			1.5	107	83
595	120	^d	Ar	1		187	165	9800
599	120	^d	He	1		624	165	32800

^aImpurity content of iron ranged from 0.002 to 1.0 wt. %.^bRate constants are given as metal recession rates, microns of metal loss per minute.^cEstimated loss of metallic iron after 1-yr-long exposure to chlorine gas at 1.0 atm pressure.^dTests were made with chlorine partial pressures up to 0.3 atm and total pressures of 1.0 atm. However, the metal recession rates reported

determined by chemical analysis of the iron content of the rinse water. At 148°C and above, the amount of iron consumed was determined by measuring specimen weight before the exposure to chlorine and again after the exposure and subsequent wash. Metal recession rates calculated from the above measurements are given in Table 11. At 77°C the rate of metal recession was nearly constant at $3 \times 10^{-4} \mu\text{m}/\text{min}$. At 77–148°C, FeCl_3 evaporation was not detectable; essentially all the metallic iron consumed by the reaction remained on the specimen surface, probably as FeCl_2 , FeCl_3 , and FeOCl . Above 148°C, the iron content of the scale was less than the amount of metallic phase consumed, indicating iron loss by FeCl_3 evaporation, as expected. From 166 to 247°C, the iron-chlorination rate decreased with time. The average metal recession rate for the first 15 min was 3 to $10 \times 10^{-3} \mu\text{m}/\text{min}$; for the next 465 min the average rate was 2 to $4 \times 10^{-4} \mu\text{m}/\text{min}$. At 251°C the iron-chlorination reaction was much more rapid than at 247°C, 1.55 $\mu\text{m}/\text{min}$ for the first 30 min.

Tseitlin and Strunkin^{107,108} measured the rate of iron consumption in flowing (15 liters/hr) chlorine. Their results, summarized in Table 11, are basically consistent with those of Heinemann *et al.*, who observed a discontinuous increase in the reaction rates for mild steel between 247 and 251°C. Tseitlin's data for a similar mild steel indicate that this discontinuous increase occurs between 260 and 285°C. However, for a steel with a lower alloy content, only 0.18 wt. % as opposed to 0.6–1.0 wt. %, the discontinuity occurs between 285 and 310°C. For iron with 0.3 wt. % carbon and a higher alloy content, 6 wt. %, the discontinuity occurs between 220 and 240°C. Hence, the discontinuous increase in the iron-chlorination rate occurs at lower temperatures for irons with higher alloy, particularly carbon, contents. Earlier experiments by Tseitlin indicate that around 300°C, higher Cl_2 flow rates can also result in much higher reaction rates.¹⁴⁷

The reason for the abrupt increase in reaction rate at some critical temperature is not clearly established. Bohlken^{163,164} suggests that the increase occurs when the surface temperature increases to above the sublimation point of FeCl_3 , and he suggests that carbon or FeC_3 catalyzes the highly exothermic FeCl_3 formation reaction.^{163,164}

Fruehan¹⁶⁵ studied the reaction of pure (99.998 wt. %) iron with Cl_2 -Ar and Cl_2 -He mixtures containing 0–30 vol. % Cl_2 . In the 300–550°C temperature range with flowing (2 liters/min) gas mixtures, the reaction kinetics were linear and the rate constants were directly proportional to the chlorine partial pressure. Below 330°C, the activation energy for the iron-chlorination reaction was 23 kcal/mole. Above 330°C, the iron-chlorination rate was not

proportional to $e^{-1/T}$; hence, an activation energy could not be calculated. Fruehan postulates that the rate-limiting step in the iron-chlorination reaction below 300°C is formation of a $(\text{FeCl}_3)_2$ activated complex, $2\text{FeCl}_2(\text{s}) + \text{Cl}_2(\text{g}) \rightarrow (\text{FeCl}_3)_2$, which then escapes from the surface to form the $(\text{FeCl}_3)_2$ vapor species. Above 330°C, the chlorination rate depends on the flow rate and on the particular diluent gas, and the “activation energy” (if defined) is a function of temperature. Hence, at these higher temperatures, Fruehan postulates that the rate-limiting step is Cl_2 transport through boundary layer gas adjacent to the specimen surface. Part of Fruehan’s iron-chlorination data is presented in Table 11.

Iron-base alloys with high silicon contents, 10–15 wt. %, are considerably more resistant to chlorine attack than pure iron or mild steels.^{166,167} Hence, high-silicon alloys, such as Duriron and Durichlor, are widely used in chlorinating environments. However, no data are available, indicating the exact extent of the chlorination resistance of these alloys.

Tseitlin and Strunkin¹⁰⁷ and Brown *et al.*¹¹⁴ indicate that chromium and stainless steels are also much more resistant to dry chlorine attack than pure iron or mild steel. Tseitlin’s and Brown’s data are summarized in Table 12. Since no detailed kinetic data are available, only average corrosion rates are shown in Table 12, and estimates of metal loss are based on linear kinetics. These estimates are probably high since some passivation probably occurs. Notice that the metal loss rates for the chromium and stainless steels listed in Table 12 exceed 1.0 $\mu\text{m}/\text{min}$ only above 500°C, while pure iron and mild steel corrosion rates listed in Table 11 exceed 1.0 $\mu\text{m}/\text{min}$ at 250–300°C.

Chromium and stainless steels are also more resistant than pure iron to dry HCl .¹¹⁴ However, they are attacked rapidly by moist chlorine below about 300°C. At 200°C the metal recession rate for 18Cr–8Ni stainless steel in dry chlorine is approximately $6 \times 10^{-4} \mu\text{m}/\text{min}$, but the rate in wet, 0.4% water vapor, chlorine is approximately $2 \times 10^{-2} \mu\text{m}/\text{min}$.¹¹⁴ Above 300°C, moisture in chlorine may decrease the chlorination rate of stainless steel because of the formation of oxide, which decreases the rate of chloride evaporation.¹⁰² Above the dew point, moisture has little or no effect on the stainless steel chlorination rate in HCl .¹¹⁴

Bromine

Iron forms two binary bromides, FeBr_2 and FeBr_3 . FeBr_2 melts at 698°C, has the hexagonal CdI_2 - or $\text{Cd}(\text{OH})_2$ -type crystal structure, a vapor pressure of 10^{-4} atm at about 510°C, and is stable to above 900°C under a

Table 12. Metal Recession Rates for Steels in Dry Chlorine^a

Alloy (composition) ^b	T(°C)	Chlorine gas flow rate (liters/hr)	Average metal recession rate ^c k_1 (μm/min)	Ref.	Δy (cm) ^d for $t = 1.0$ yr
Chromium steel (Fe-17 Cr)	300	15	4×10^{-4}	107	0.02
	360	15	3.8×10^{-3}	107	0.2
	440	15	6.7×10^{-2}	107	4
	540	15	1.35	107	70
Stainless steel (Fe-18 Cr-9 Ni-Ti)	418	15	1.1×10^{-3}	107	0.06
	450	15	4.3×10^{-2}	107	2
	480	15	0.13	107	7
	535	15	0.47	107	20
	640	15	46	107	2000
Stainless steel (Fe-18 Cr-8 Ni-Mo)	315	28	1.5×10^{-3}	114	0.08
	340	28	2.9×10^{-3}	114	0.15
	400	28	5.9×10^{-3}	114	0.3
	450	28	2.9×10^{-2}	114	1.5
	480	28	5.9×10^{-2}	114	3
Stainless steel (Fe-18 Cr-8 Ni)	290	28	1.5×10^{-3}	114	0.08
	315	28	2.9×10^{-3}	114	0.15
	340	28	5.9×10^{-3}	114	0.3
	400	28	2.9×10^{-2}	114	1.5
	450	28	5.9×10^{-2}	114	3

^aChlorine pressure was approximately 1.0 atm.^bMajor constituents of alloy. Amounts of constituents present are given in weight percent when the amount exceeds 5.0 wt. %.^cDuration of these corrosion tests was 60–360 min for the first two alloys and 120–1200 min for the last two alloys.^dEstimated metal loss after 1-yr-long exposure.

1-atm bromine pressure. FeBr_3 , with the hexagonal BiI_3 -type crystal structure has a vapor pressure of 10^{-4} atm at about 155°C but decomposes at 140°C under a 1-atm atmosphere bromine pressure. Hence, iron may be expected to form a solid bromide scale with a significant evaporation rate at relatively low temperatures. There are no experimental data available to describe the actual kinetics for corrosion of iron by gaseous bromine.

“Carbon steel” is readily attacked by liquid bromine at room temperature.¹⁶⁸ Stainless steels containing 18 wt. % Cr and 8 wt. % Ni are resistant to dry HBr-free liquid bromine at room temperature but are readily attacked by bromine containing moisture or HBr.¹⁶⁸ For this reason, bromine to be shipped in stainless steel containers is treated with HNO_3 to remove moisture

and HBr. The corrosion of iron and stainless steel by liquid bromine seems to be of galvanic nature and the primary corrosion product is FeBr_2 .¹⁶⁹

Iodine

Iron normally reacts with iodine to form a single iodide, FeI_2 , of the hexagonal CdI_2 - or Cd(OH)_2 -type crystal lattice, which is stable to above 1000°C under 1.0-atm iodine pressure, melts at 590°C , and has a vapor pressure of 10^{-4} atm at about 475°C .³ The vapor phase includes FeI_3 and some Fe_2I_6 as well as FeI_2 .¹²² Hence, in dry iodine vapor, iron may be expected to form a solid scale which may evaporate at higher temperatures.

However, experience with carbon steels indicates that iron is probably not resistant to iodine vapors even at room temperatures.^{123,124} Stainless steels, especially those containing titanium, are recommended for handling dry iodine vapors at temperatures up to $250\text{--}300^\circ\text{C}$ but may be subject to pitting.^{123,170} The recession rate of stainless steel containing 18 wt. % Cr and 8 wt. % Ni in dry iodine at room temperature is reportedly $100\text{ }\mu\text{m/yr}$.¹²⁵ However, stainless steel is rapidly attacked by moist iodine vapor even at room temperature.

Aluminum and Aluminum Alloys

Aluminum alloys, especially those containing magnesium, are highly resistant to fluorine attack at low temperatures and are frequently used in fluorine-handling systems. Aluminum alloys are also used to some extent in room-temperature dry-chlorine environments.

Fluorine

Metallic aluminum reacts with gaseous fluorine to form AlF_3 , a highly stable, polymorphous compound which has a melting point above 1200°C and a vapor pressure of 10^{-4} atm at approximately 1145°C .

Hence, in dry fluorine, aluminum forms a solid scale which protects it from further rapid fluorine attack. The extent of this protection is indicated in Table 13, which gives estimates for the amount of aluminum converted to fluoride after a 1-yr exposure to fluorine at different temperatures.

According to Myers and DeLong,²⁶ the metal recession rate for aluminum in gaseous HF is only about 3 times that for aluminum in dry fluorine. However, moist fluorine is considerably more aggressive.

Table 13. Kinetic Data for Aluminum–Fluorine Reactions

$T(^{\circ}\text{C})$	Parabolic ^a rate constant $k_2 (\mu\text{m}/(\text{cm}^2)^2/\text{min})$	Test duration (min)	Ref.	$\Delta y (\mu\text{m})^b$ for $t = 1.0 \text{ yr}$
26	1.44×10^{-6}	7200	83	0.87
30	2.45×10^{-11}	5400	84	0.0036
201	1.68×10^{-7}	7200	83	0.30
356	0.616	7200	83	570
543	9.06		83	2200

^aParabolic rate constant given for the reaction at 30°C was determined from a plot of scale thickness versus time which approximated a parabolic curve. However, the other parabolic rate constants were determined from only one or two (weight gain, time) data points. Parabolic kinetics were assumed.

^bEstimated metal loss after 1-yr-long exposure to fluorine.

Tests indicate that aluminum (99.0 wt. % purity) reacts with liquid fluorine 3–5 times faster than does pure nickel.^{43,130,131,171} Reported rates of metal consumption range from 1.0 $\mu\text{m}/\text{yr}$ in high-purity liquid fluorine to 2.3 mm/yr in less pure liquid fluorine. Aluminum, if coupled with a more noble metal such as nickel or copper, is particularly subject to galvanic corrosion. Toy *et al.*¹³⁰ reports that aluminum (99.0 wt. %) coupled with copper reacts with liquid fluorine 5 times faster than does uncoupled aluminum.

According to Sterner and Singleton,⁴³ aluminum alloys 6061 (1.0 wt. % magnesium, 0.6 % silicon, 0.25 % copper, 0.2 % chromium) and 7079 (4.3 wt. % zinc, 3.3 % magnesium, 0.6 % copper, 0.2 % manganese, 0.2 % chromium) react with liquid fluorine at about the same rate as aluminum (99.0 wt. %) while alloys 2017 (4 wt. % copper, 0.5 % manganese, 0.5 % magnesium) and 5052 (2.5 wt. % magnesium, 0.25 % chromium) react 2–3 times faster than aluminum (99.0 wt. %).

Kleinberg and Tompkins⁸⁴ studied the fluorination of aluminum powder at -80 , 30 , and 84°C for fluorine pressures between 200 and 700 torr. The reaction rate decreased with increasing time, but the reaction kinetics did not follow simple logarithmic or power-law formulas. Between -80 and $+84^{\circ}\text{C}$ the aluminum fluorination rate decreased with increasing temperature. According to Kleinberg and Tompkins, after 100 min of aluminum fluorination, the respective film thicknesses and film growth rates were $8 \times 10^{-4} \mu\text{m}$ and $1.7 \times 10^{-6} \mu\text{m}/\text{min}$ at -81°C , $4.4 \times 10^{-4} \mu\text{m}$ and $1.1 \times 10^{-6} \mu\text{m}/\text{min}$ at 30°C , and $1.5 \times 10^{-4} \mu\text{m}$ and $-1 \times 10^{-7} \mu\text{m}/\text{min}$ at 84°C .

Davis and Rosen¹⁷² also observed a period of anomalous behavior during the fluorination of aluminum turnings in a 60°C static fluorine environment. The turnings initially consumed fluorine rapidly but evolved more gas than they consumed through the second 24-hr period. Only after about 70 hr of exposure did the consumption rate begin to approach parabolic behavior.

An hypothesis for these anomalous aluminum-fluorination kinetics could be that an aluminum oxide hydrate, not metallic aluminum, is being fluorinated. For example, the dominant initial reaction at -80°C might be $\frac{1}{2}\text{Al}_2\text{O}_3 \cdot 3\text{H}_2\text{O} + 1.28\text{F}_2 \rightarrow \text{AlF}_{1.65}(\text{OH})_{1.35} \cdot (0.375)\text{H}_2\text{O} + 0.9\text{HF} + 0.64\text{O}_2$ and the dominant initial reaction at 80°C might be $\frac{1}{2}\text{Al}_2\text{O}_3 \cdot 3\text{H}_2\text{O} + 2\text{F}_2 \rightarrow \text{AlF}_2(\text{OH}) + 2\text{HF} + \text{O}_2$. The first reaction produces a weight gain of about 20 g/mole of $\text{Al}_2\text{O}_3 \cdot 3\text{H}_2\text{O}$ consumed and produces approximately 1.2 moles of gas for every mole of fluorine consumed. The second reaction produces a weight gain of only about 3.9 g/mole of $\text{Al}_2\text{O}_3 \cdot 3\text{H}_2\text{O}$ consumed but also evolves 3 moles of gas for every 2 moles consumed. Transition from the first to the second reaction would explain the apparent decrease of reaction rate with increasing temperature observed by Kleinberg and Tompkins. It would also explain the evolution of gas observed by Davis and Rosen during an initial period of aluminum fluorination at 60°C. The subsequent parabolic fluorine consumption kinetics could result from simple formation of AlF_3 scale after the surface layer of oxide was consumed.

Because of these gross complications Kleinberg and Tompkins' short-term, 0- to 100-min, aluminum-fluorination data cannot justifiably be used to project long-term, aluminum-fluorination rates. However, their data for aluminum fluorination at 30°C extend to two measurements after approximately 3.75 days and can be approximated by a parabolic curve for the aluminum fluoride film thickness, $y = 3.0 \text{ \AA} + 0.144(\text{\AA}/\text{min})t^{1/2}$ or aluminum metal recession rate of $y = 1.03 \text{ \AA} + 0.0495(\text{\AA}/\text{min})t^{1/2}$. Accordingly, only 37 Å (0.0037 μm) of aluminum would be consumed during the first year of exposure to dry fluorine at 30°C.

Jackson⁸³ studied the reaction of 1100 aluminum (99.0 wt. %) from 20 to 550°C with gaseous fluorine of 1 atm flowing over the metal samples at 100 cm³/min. Jackson determined weight changes after fluorine exposures of 5, 24, and 120 hr. Like Kleinberg and Tompkins, Jackson observed anomalous fluorination behavior at low temperatures for short exposure times; many of the observed weight changes were negative, and in some cases the rate of weight gain appeared to decrease with increasing temperature. The 120-hr aluminum-fluorination data were used to calculate the parabolic rate constants presented in Table 13. Parabolic kinetics are assumed because

the long-term Kleinberg and Tompkins 84°C data and the long-term Davis and Rosen 60°C data could be fitted by parabolic equations. Aluminum-fluorination kinetics for $T \geq 100^\circ\text{C}$ are not reported.

Under the same experimental conditions, Jackson also observed the reaction of gaseous fluorine with aluminum alloys 2024 (4.5 wt. % copper, 1.5 % magnesium, 0.6 % manganese) and 5154 (3.5 wt. % magnesium, 0.25 % chromium). Neither alloy reacted with fluorine as rapidly as 1100 aluminum. According to Jackson, at 550°C 1100 aluminum (99.0 wt. %) reacts with fluorine about 200 times faster than either alloy 2024 or 5154. The superior resistance of these two alloys to fluorine attack probably results from their magnesium contents; selective fluorination of magnesium in the alloys forms a dense scale of MgF_2 which restricts the alloy fluorination rate to well below that for pure aluminum.

The ignition temperature for aluminum in fluorine lies above the melting temperature for metallic aluminum.^{38,91} Evidently, a continuous surface film of AlF_3 adequately separates the molten aluminum from surrounding fluorine to prevent fluorination at a rate sufficient to cause a catastrophic temperature increase. The situation is analogous to that of liquid mercury in an air or oxygen atmosphere.

Chlorine

Dry chlorine reacts with metallic aluminum to form a highly stable chloride, AlCl_3 , which melts at about 192°C,⁶ and has a vapor pressure of 10^{-4} atm at about 75°C.¹⁴ Because of its high vapor pressure, AlCl_3 volatilizes at relatively low temperatures. Consequently, at 150°C aluminum can be consumed by chlorine attack at rates of 1 μm or more per minute. Results of aluminum-chlorination rate studies are given in Table 14.

Apparent incongruities in Table 14 result because of an aluminum oxide film which overlays the metallic aluminum and shields it against chlorine attack. This oxide may afford the aluminum virtually complete protection against chlorine attack for a period ranging from a few minutes to several hours or days. Consequently, in one study or experimental run aluminum may not react detectably with chlorine, but in another virtually identical study or experimental run at the same temperature aluminum may react rapidly. When the reaction is initiated, it is localized along flaws in the oxide film. For example, Tseitlin and Strunkin¹⁰⁷ observed a 5-hr delay in the initiation of an aluminum-chlorine reaction at 500°C. When the reaction did initiate, it was a rapid, highly localized attack.

Table 14. Kinetic Data for Aluminum–Dry Chlorine^a Reactions

T(°C)	Flow rate (cm ³ /min)	Linear rate constant ^b k ₁ (μm/min)	Test duration (min)	Ref.	Δy (cm) ^c for t = 1 yr
120	460	0.0015		114	0.08
150	460	0.003–0.006		114	0.15–0.3 ^d
160	250	3.2	360	107	170
170	250	6.9	360	107	360
175	460	0.03–0.06		114	1.5–3 ^d
200–230	460	Ignites and burns		114	
280	3.5	6 × 10 ⁻⁵	360	147	0.0032 ^d
280	250	8.9	15	147	470

^aChlorine pressure was approximately 1.0 atm.

^bRate constant is given as the metal recession rate, microns of metal loss per minute.

^cEstimated loss of metallic aluminum.

^dThese estimates are probably low because the metal surface is covered with a protective oxide. Such an oxide would probably fail in the course of a more prolonged exposure.

Evans¹⁷³ indicates that the aluminum–chlorine reaction kinetics at 134–254°C and 100–600 torr chlorine pressure are linear and that the linear rate constant is independent of the chlorine pressure. According to Evans, the activation energy over this temperature range is about 2 kcal/mole.

At least at temperatures above 100°C, aluminum reacts much less rapidly with moist chlorine than with dry chlorine.¹⁰³ This is illustrated by

Table 15. Average Rate of Moist-Chlorine Attack on Aluminum^{a,102}

T(°C)	Average metal recession rate (μm/min)		
	Cl ₂ + 0.06 wt. % H ₂ O	Cl ₂ + 1.5 wt. % H ₂ O	Cl ₂ + 30 wt. % H ₂ O
130	0.000	0.000	—
140	—	—	0.000
170	6.9	—	0.001
200	—	0.000	—
290	—	0.002	0.000
320	—	0.002	—
350	—	10	—
400	—	40	—
545	—	—	0.000
616	—	—	0.01
630	—	—	15

^aThe chlorine gas flow rate was 250 cm³/min and the test duration was 360 min.

Tseitlin and Strunkin's^{102,103} aluminum-chlorination data, which are presented in Table 15. In moist chlorine, aluminum must form a protective nonvolatile scale; although this scale has not been identified, $\text{Al}_2\text{O}_3 \cdot x\text{H}_2\text{O}$ would seem reasonable.¹⁷⁴ At 616°C, Tseitlin observed that the scale formed in moist chlorine did not contain chlorine; hence, at this temperature the new scale is probably a simple aluminum oxide.

According to Rabald,¹⁷⁵ at room temperature aluminum reacts more rapidly with moist chlorine than with dry. This would be particularly true if moisture were to condense on the aluminum surface.

Bromine

Aluminum and dry bromine react to form AlBr_3 , which exhibits a monoclinic crystal lattice and melts at 97.5°C. According to Hodges,¹⁷⁶ aluminum reacts vigorously with liquid and gaseous bromine at room temperature and ignites slightly above room temperature. As observed for the chlorination of aluminum, an aluminum oxide surface film may delay initiation of the aluminum-bromine reaction. According to Rabald,¹⁷⁵ aluminum reacts more readily with moist liquid bromine than with dry.

Iodine

Aluminum reacts with iodine to form predominantly AlI_3 , but at high temperatures (1000°C) and low-iodine partial pressures, the aluminum-iodine reaction may produce AlI . Little information is available on the aluminum-iodine reaction kinetics. However, aluminum is definitely not a practical material for handling iodine above 190°C, the melting point of AlI_3 , and is probably corroded rapidly by iodine at much lower temperatures as well. According to Horst,¹⁷⁷ at room temperature the aluminum recession rate in iodine vapor is greater than 1.3 mm/yr ($2.4 \times 10^{-3} \mu\text{m}/\text{min}$). According to Rabald,¹⁷⁵ at room temperature, aluminum is resistant to dry HI but is attacked by moist HI .

Other Metals

The behavior of some primary structural metals in halogen environments was described in detail in the preceding paragraphs. Many other metals are also used in halogen environments as pure metals or as alloy constituents. Even the more expensive metals are of interest since they may find limited application in instrumentation where a special combination of properties is required, or they may illustrate halogen attack mechanisms

which can be applied to the more common metal systems. Experimental data on the behavior of these other metals in halogen environments are summarized briefly in the following subsections.

For many of the less common metals few or no kinetic data are available for the halogen-metal reactions. For these metals, the “pertinent properties of the binary metal halides” presented earlier in this chapter may suggest some possible reaction features, such as halide volatilization or formation of a high-melting nonvolatile scale. However, for the following reasons, these tabulated physical properties cannot be used by themselves to deduce the actual kinetics: (1) although thermodynamically stable, the halide scale may be consumed by vaporization; (2) formation of a solid nonvolatile halide does not ensure “protective” scale formation; and (3) even when a “protective” scale is formed, the reaction may still proceed rapidly. Solid reaction products may be porous or may spall from the metal surface, or volume diffusion through the solid may be rapid.

Beryllium, Magnesium, and the Alkali and Alkaline Earth Metals

Beryllium. Fluorination of beryllium sheet was studied by O'Donnell,^{178,179} who used the pressure-drop method to follow fluorine consumption at 125–775°C and 20–700 torr fluorine pressure. Fluorine reacted with the beryllium sheet to form a continuous scale of BeF_2 . Below 525°C the scale was hexagonal (α -quartz) BeF_2 , while above 525°C the scale was rhombic (tridymite) BeF_2 . The scale thickness increased according to parabolic growth kinetics, $y^2 = k_2t$. The parabolic rate constant increased linearly with increasing fluorine pressure. Parabolic rate constants and estimated metal losses for year-long fluorine exposures are given in Table 16. The activation energy was -0.8 kcal/mole below 525°C and 8 kcal/mole above 525°C. Using the scale impingement technique as described previously for fluorination of nickel,⁸⁰ O'Donnell found that impinging BeF_2 scales fuse together, leaving no interface, thus indicating that BeF_2 scale grows by outward diffusion of beryllium cations to the gas/scale interface.

Few kinetic data are available on the reaction of beryllium with the other halogens. According to Lukesh,¹⁸⁰ there is evidence that beryllium reacts rapidly with chlorine above room temperature. The halides formed on beryllium in chlorine, bromine, and iodine vapors are BeCl_2 , BeBr_2 , and BeI_2 , which have melting points of 405, 490, and 480°C, respectively, and attain vapor pressures of 10^{-4} atm at 230–240°C. The specific volumes for these halides are extraordinarily high, 8–12 times greater than the specific volume for metallic beryllium.

Table 16. Kinetic Data for Beryllium–Fluorine Reactions¹⁷⁹

T (°C)	P_{F_2} ^a (atm)	Parabolic rate constants k_2 (ml F_2 /cm ²) ² /min	Δy (μm) ^b for $t = 1.0$ yr
125	0.263	1.05×10^{-5}	4.9
225	0.263	9.4×10^{-6}	4.7
525	0.079	2.0×10^{-6}	2.2
	0.263	6.9×10^{-6}	4.0
	0.829	3.77×10^{-5}	9.3
	0.921	5.70×10^{-5}	11.5
575	0.263	3.30×10^{-5}	8.7
625	0.263	1.70×10^{-4}	20
	0.829	4.10×10^{-4}	31
675	0.026	4.03×10^{-5}	9.7
	0.053	9.70×10^{-5}	15
	0.079	1.63×10^{-4}	19
	0.263	6.92×10^{-4}	40
775	0.079	1.30×10^{-3}	55
	0.263	2.80×10^{-3}	80

^aTests were in static rather than flowing fluorine.^bEstimated metal loss after 1-yr-long exposure to fluorine attack.

Magnesium. Like beryllium, magnesium is quite resistant to fluorine attack, forming MgF_2 , which melts at 1265°C and probably has a vapor pressure of less than 10^{-6} atm at all temperatures below its melting point.⁷ Magnesium corrodes in liquid fluorine at about the same rate as does aluminum.^{43,131} Jackson observed the fluorination of magnesium (98.5 wt. % magnesium, 1.5% manganese) in flowing, 100 cm³/min, fluorine gas. The reaction kinetics at 345 and 540°C were parabolic with rate constants of 4.0×10^{-5} and $5.6 \times 10^{-3}(\text{mg } F_2)^2/\text{cm}^4 \text{ min}$, respectively; reaction at these rates would consume 0.017 mm of magnesium metal in a year at 345°C and 0.2 mm of metal at 540°C. Because Jackson's magnesium-fluorination data below 250°C are erratic, the reaction kinetics cannot be deduced. However, the observed weight gain after 120 hr corresponds to parabolic rate constants of about $10^{-6}(\text{mg } F_2)^2/\text{cm}^4 \text{ min}$ at 25–200°C. If these kinetics were parabolic, the magnesium fluorination reaction would in 1 yr consume about 0.003 mm of magnesium metal. A similar test of magnesium in static fluorine at 60°C indicates a magnesium-fluorination rate of about $8 \times 10^{-4}(\text{mg } F_2)^2/\text{cm}^4 \text{ min}$ at 60°C¹⁴²; reaction at this rate would in a year consume 0.08 mm of magnesium metal.

Magnesium may also passivate to some extent in chlorine, bromine, and iodine. The respective halide melting points are about 715, 710, and 650°C. Only near its melting point does the vapor pressure of MgCl_2 attain a value of 10^{-4} atm. According to Brown *et al.*,²⁴ the average magnesium metal recession rate in dry chlorine for the first 2–20 hr is 1.5×10^{-3} $\mu\text{m}/\text{min}$ (0.8 mm/yr) at 450°C and 0.06 $\mu\text{m}/\text{min}$ (30 mm/yr) at 565°C. However, Lemarchands and Jacob¹⁸¹ indicate that the magnesium–chlorine reaction is vigorous above about 340°C. Fedoseev¹⁸² observed that magnesium does not ignite in chlorine even at 1000°C, and McCulloch¹⁸³ observed no appreciable reaction between magnesium and iodine vapors even at 600°C.

Alkali and Alkaline Earth Metals. The alkali and alkaline earth metals form predominantly monovalent and divalent halides, respectively. These halides have melting points ranging from 445°C for LiI to 1450°C for SrF_2 . The halides attain vapor pressures of 10^{-4} atm only at temperatures of 600°C or higher.

The fluorides have specific volumes that are less than those of the parent metals; in fluorine atmospheres these metals do not form dense protective fluoride scales even at room temperature.¹⁸⁴ However, in chlorine, bromine, and iodine at low temperatures, some of the metals may form protective films. For example, sodium passivates in both chlorine and bromine at temperatures up to at least 50°C.^{31,185} Shiu *et al.*²⁹ have shown that the sodium–chlorine reaction kinetics are logarithmic at and below room temperature and are independent of the chlorine pressure until the NaCl film attains a thickness of 200 Å, after which the reaction rate is nearly proportional to the square root of the chlorine pressure. Shiu *et al.* postulate that the Mott–Cabrera mechanism is operative. According to Lemarchands, Jacob, and Tamisier,^{181,186} chlorine attack becomes vigorous on sodium, potassium, and calcium only when the heat of reaction is sufficient to evaporate the metal chlorides; this condition occurs for sodium, potassium, and calcium at 260, 230, and 460°C, respectively.

First Row Transition Metals

Titanium. Titanium reacts with fluorine to produce TiF_4 and TiF_3 . The melting point of TiF_4 is about 400°C and the vapor pressure is 10^{-4} atm at about 108°C and 1.0 atm at 284°C. The melting point of TiF_3 is about 1200°C, and its vapor pressure exceeds 1.0 atm only above 1400°C. Titanium reacts with liquid fluorine at about the same rate as do nickel and Monel, about 0.3 mm of metal loss per year.^{131,171} At -80°C , the surface fluoride

on titanium powder grew to a thickness of about 6 \AA within the first 90 min of fluorine exposure and remained at this thickness for the following 150 min.⁸⁴ In static fluorine at atmospheric pressure and $20\text{--}104^\circ\text{C}$ temperature, titanium gained weight initially, but the rate of weight gain decreased with time upon the formation of a protective surface scale.¹⁸⁷ At 88 and 104°C this scale eventually reached a limiting thickness where the rate of scale formation equaled the rate of TiF_4 evaporation, $7.5 \times 10^{-6} \text{ mg of Ti/cm}^2 \text{ min}$ ($5.5 \text{ \mu m of Ti/yr}$) at 88°C and $1.1 \times 10^{-5} \text{ mg of Ti/cm}^2 \text{ min}$ ($8.2 \text{ \mu m of Ti/yr}$) at 104°C . One set of experiments in $100 \text{ cm}^3/\text{min}$ flowing fluorine at 1.0 atm pressure indicates metal recession rates of $1.6 \times 10^{-3} \text{ mg/cm}^2 \text{ min}$ (1.2 mm of Ti/yr) at 150°C and $4 \times 10^{-2} \text{ mg of Ti/cm}^2 \text{ min}$ (300 mm of Ti/yr) at 196°C .⁸³ Another set of experiments in flowing fluorine at 1.0 atm pressure indicates metal recession rates of $8 \times 10^{-4} \text{ mg of Ti/cm}^2 \text{ min}$ (0.6 mm of Ti/yr) at 200°C and a $32 \text{ cm}^3/\text{min}$ flow rate, $8 \times 10^{-2} \text{ mg of Ti/cm}^2 \text{ min}$ (60 mm of Ti/yr) at 300°C and a $72 \text{ cm}^3/\text{min}$ flow rate, and $0.15 \text{ mg of Ti/cm}^2 \text{ min}$ (110 mm of Ti/yr) at 300°C and a $105 \text{ cm}^3/\text{min}$ flow rate.¹⁸⁸

TiCl_4 , TiCl_3 , and TiCl_2 melt at -25 , greater than 440 , and 1025°C , respectively, and their vapor pressures attain values of 10^{-4} atm at about -50 , 590 , and 540°C , respectively.³ The low melting point and high volatility of TiCl_4 prevent effective passivation of titanium in dry chlorine gas even at room temperature. Ignition of titanium in dry chlorine has been observed at temperatures as low as -18°C .^{112,113,189–191} However, oxide film on the titanium surface may delay ignition for some time after the initial exposure to chlorine; any mechanical disturbance, such as scratching of the oxide film, may then initiate the reaction.¹⁸⁹

Moisture in chlorine gas inhibits the titanium–chlorine reaction to such an extent that titanium is commonly used in industrial systems that handle moist chlorine and chlorinating agents.^{112,113,190–194} Evidently, moisture present in chlorine forms a protective oxide film which blocks formation of volatile TiCl_4 . The amount of moisture required to prevent a rapid titanium–chlorine reaction depends on the chlorine pressure, flow rate, and purity, and on the temperature and extent of surface abrasion.¹⁸⁹ To prevent the reaction in pure (99.5 vol. %) chlorine at room temperature, the chlorine must be saturated with water, about 0.93 vol. %. At 200°C the pure chlorine must contain about 1.5 vol. % water vapor. Static chlorine containing 3 vol. % total of CO_2 , H_2 , N_2 , and O_2 must contain 0.4 vol. % water vapor at 25°C and 1.2 vol. % at 175°C to prevent rapid titanium chlorination. The impure gas requires a lower water content, probably because of its higher oxygen content. Also, a lower water content is sufficient to prevent rapid titanium–chlorine reaction in flowing chlorine; for the

chlorine containing 3 vol. % impurities and having a 0.5 ft/sec flow rate, only 0.2 vol. % water vapor was required at 25°C and only 0.5 vol. % at 175°C. Exact kinetics are not reported for the titanium-moist chlorine reaction. However, in moist chlorine, titanium does passivate; at 88°C an average metal recession rate of 5.48×10^{-5} mil/day was observed for the first 18 days of reaction, while an average rate of 1.87×10^{-5} mil/day was observed for the next 184 days of reaction.¹¹² The following average metal recession rates are reported for long duration exposures of titanium to moist chlorine: 0.009 mil/yr for 166 days at about 160,¹¹³ 0.07 mil/yr for 7.2 days at 25°C,¹⁹⁵ 0.0006 mil/yr for 192 days at 93°C,¹¹³ 0.02 mil/yr for 18 days at 88°C,¹¹² 0.008 mil/yr for 202 days at 88°C,¹¹² and less than 0.1 mil/yr for 74 days at 77°C.¹⁹² Hence, titanium is quite resistant to general surface attack by moist chlorine. However, it should be noted that titanium in moist chlorine is highly susceptible to rapid crevice corrosion.

Titanium forms di-, tri-, and tetravalent bromides and iodides. The resistance of titanium to attack by bromine and iodine vapors is probably limited by the low melting points and high vapor pressures of the stable tetravalent corrosion products, TiBr_4 and TiI_4 . The melting points of TiBr_4 and TiI_4 are 39 and 150°C, respectively, and their vapor pressures attain values of 10^{-4} atm at 19°C and probably about 80°C, respectively.³ Titanium has been observed to ignite after 10 min in room-temperature liquid bromine and after 15 min in 100°C dry iodine.¹⁹⁶ The following linear metal recession rates have been observed for the initial reaction of titanium granules with dry iodine vapors: 5.64 $\mu\text{m}/\text{min}$ at 25 torr and 400°C, 5.22 $\mu\text{m}/\text{min}$ at 100 torr and 200°C, 5.22 $\mu\text{m}/\text{min}$ at 25 torr and 200°C, 1.93 $\mu\text{m}/\text{min}$ at 5 torr and 200°C, 0.806 $\mu\text{m}/\text{min}$ at 2 torr and 200°C, 0.121 $\mu\text{m}/\text{min}$ at 1.0 torr and 200°C, and 3.1 $\mu\text{m}/\text{min}$ at 25 torr and 175°C.^{122,197}

Vanadium. Vanadium forms two binary fluorides: VF_2 and VF_5 . VF_5 melts at 19°C and has a vapor pressure of 10^{-2} atm at -17°C . Consequently, vanadium reacts readily with fluorine, volatilizing as VF_5 even at room temperature.

The chlorides of vanadium include VCl_2 , VCl_3 , and VCl_4 which attain vapor pressures of 10^{-4} atm at about -43 , 521, and 725°C, respectively.³ The respective melting points of VCl_2 and VCl_4 are 1350 and -28°C . The low melting point and high vapor pressure of VCl_4 indicate that vanadium would react readily with chlorine at room temperature to form this vapor. A standard method for preparation of VCl_4 is reaction of metallic vanadium with a flowing stream of chlorine gas at 200–500°C.

The bromides of vanadium are VBr_2 , VBr_3 , and VBr_4 , but VBr_4 is said to be thermodynamically unstable at room temperature, dissociating to VBr_3 and Br_2 (equilibrium Br_2 pressure is not given).³ Equilibrium vapor pressures of VBr_3 and VBr_4 attain values of 10^{-4} atm at 337 and 423°C, respectively. Hence, vanadium could form a protective scale in bromine vapor at room temperature, but there are no kinetic data available to indicate the actual behavior of vanadium metal in bromine vapors.

The stable iodides of vanadium include only VI_2 and VI_3 . Under a 1.0-atm iodine pressure, VI_3 dissociates to $VI_2(s)$ and $I_2(v)$ only at a temperature of about 690°C or higher. VI_3 is prepared by reacting vanadium metal with iodine vapor at 400–550°C. No information is available on vanadium–iodine reaction kinetics at lower temperatures.

Chromium. Although higher fluorides of chromium such as CrF_5 and CrF_6 occur under high fluorine pressures, CrF_4 appears to be the highest stable fluoride of chromium above room temperature at atmospheric pressure.^{3,198,199} Chromium reacts readily with flowing fluorine at 350°C³ but is not visibly attacked during a 24-hr exposure to static fluorine at atmospheric pressure and 150°C.¹⁴² A chromium-steel reacts with fluorine at about the same rate as pure iron at 200°C but many times faster than pure iron at 300°C.²⁶

The highest stable chloride of chromium at atmospheric pressure and at or above room temperature is $CrCl_3$, which melts at about 1150°C and sublimes readily in a stream of chlorine at 850°C.³ $CrCl_4$ is prepared by flowing chlorine over chromium at 960–1000°C.³ As indicated in the previous discussion of chlorine attack on iron at temperatures up to 350–400°C and in contrast to the fluorination behavior, chromium (17 wt. %) steel reacts with chlorine much less rapidly than does pure iron.

At atmospheric pressure chromium forms two solid bromides, $CrBr_2$ and $CrBr_3$. The melting point of $CrBr_3$ is above 800°C³ and its vapor pressure is 10^{-4} atm at 615°C.²⁰⁰ The equilibrium $CrBr_4$ vapor pressure over solid $CrBr_3$ is 10^{-4} atm at 516°C and 1.0 atm Br_2 pressure.²⁰⁰ Chromium reacts readily with flowing bromine vapor at 750°C.³

Chromium metal reacts readily with iodine vapor at 2000°C, forming CrI_2 and CrI_3 .¹²²

Manganese. Fluorides of manganese include MnF_2 , MnF_3 , and MnF_4 . MnF_2 melts at 920°C. The melting point of MnF_3 is greater than 950°C; that of MnF_4 is not determined but is above 25°C.³ The vapor pressures of

MnF_2 and MnF_3 are 10^{-4} atm at about 950 and 980°C, respectively.³ Fluorination of manganese proceeds rapidly at 600–700°C, producing MnF_4 , which dissociates slowly to MnF_3 after cooling to room temperature.³ Manganese may hence passivate in fluorine at room temperature and above; there are no experimental data indicating the reaction behavior.

Chlorination of manganese produces only MnCl_2 , which melts at about 650°C and has a vapor pressure of 10^{-4} atm at about 600°C.³ Hence, manganese may also passivate in chlorine up to 400–600°C; however, no experimental information is available on manganese-chlorination kinetics in this temperature interval. The same is true for manganese in bromine and iodine, where the halides formed are MnBr_2 and MnI_2 , which melt at about 695 and 613°C, respectively.²

Cobalt. Cobalt reacts with fluorine and chlorine to form the corresponding divalent and trivalent fluorides and chlorides. Only formation of the cobalt dihalides is reported for cobalt reactions with bromine and iodine.³

Second and Third Row Transition Elements

Zirconium and Hafnium. The zirconium fluorides (ZrF_2 , ZrF_3 , and ZrF_4) have high melting points and low vapor pressures. The melting point of ZrF_4 is about 920°C and its vapor pressure attains a value of 10^{-4} atm at about 470–570°C.³ According to Jackson,⁸³ zirconium (98 wt. % zirconium, 2% hafnium) corrodes in liquid fluorine at a rate of 140 mil/yr. Jackson⁸³ reports the following average metal recession rates for zirconium in flowing (100 cm³/min) gaseous fluorine for a period of 5.0 hr: 1.5 mil/yr at 25°C, 27 mil/yr at 177°C, and 8300 mil/yr at 350°C. Jarry *et al.*²⁰¹ report that at 350–400°C (1) the rate of zirconium fluorination is linear after the first 30–60 min, (2) initially a dense $\alpha\text{-ZrF}_4$ film is formed, but this is soon replaced by formation of loosely packed $\beta\text{-ZrF}_4$, and scale forms by migration of fluorine gas to the scale/metal interface. Under a fluorine pressure of 3.5 atm, zirconium ignites at 340°C.²⁰²

Zirconium forms the chlorides ZrCl_2 , ZrCl_3 , and ZrCl_4 . ZrCl_4 melts at 437°C and has a vapor pressure of 10^{-4} atm at about 150°C. The nature of the zirconium–dry chlorine reaction kinetics has not been determined, but the following average metal recession rates are reported: 0.04 mil/yr for 99 days at 32°C¹¹³ and 0.02 mil/yr for 139 days at –18°C.¹¹² Rates reported for zirconium in moist chlorine gas are considerably higher: 192 mil/yr for 7.2 days at 25°C¹⁹⁵ and greater than 80 mil/yr (160-mil-thick specimen completely consumed) for 73 days at 16°C.¹¹²

Bromides and iodides of zirconium include ZrBr_2 , ZrI_2 , ZrBr_3 , ZrI_3 , ZrBr_4 , and ZrI_4 . ZrBr_4 and ZrI_4 melt at 450 and 500°C and have vapor pressures of 10^{-4} atm at 150 and 170°C.³ Because of similarities in the halide properties, zirconium may be expected to react with bromine and iodine vapors in a manner similar to that in which zirconium reacts with chlorine. There is indication that zirconium is susceptible to stress corrosion cracking in iodine vapors.^{203–205}

HfF_4 has a vapor pressure of 10^{-4} atm at about 615°C and probably melts at near the melting point of ZrF_4 . HfCl_4 , HfBr_4 , HfI_4 melt at about 435, 425, and 450°C, and have vapor pressures of 10^{-4} atm at about 130, 140, and 245°C, respectively. Again, because substantive data are lacking, the resistance of hafnium to halogen attack can only be related to that of zirconium, which forms halides with similar chemical and physical properties.

Niobium and Tantalum. Little information is available on halogenation of niobium or pertinent niobium halide properties. The highest stable halides of niobium are NbF_5 , NbCl_5 , NbBr_5 , and NbI_5 , which melt at about 80, 205, 260, and 400°C, respectively.² NbCl_5 has a vapor pressure of 10^{-4} atm at about 85°C.² The pentahalides can be prepared by reaction of niobium with the halogen vapors at 200–300°C. Niobium is said to be fairly resistant to iodine attack up to about 250°C¹²³ but susceptible to chlorine attack at 180°C.

The highest stable halides of tantalum are also the pentahalides— TaF_5 , TaCl_5 , TaBr_5 , and TaI_5 which melt at about 97, 216, 260, and 496°C, and have vapor pressures of 10^{-4} atm at about 50, 80, 140, and 195°C, respectively.² The pentahalides can be prepared by direct halogenation of tantalum at 200–400°C.²

The resistance of tantalum to liquid fluorine is about the same as that of mild steel; the metal recession rate is about 25 mil/yr.¹⁷¹ The average metal recession rate for tantalum (99.95 wt. %) in 100 cm³/min flowing fluorine at atmospheric pressure and 25°C for 5.0 hr was 13 mil/yr.⁸³ Ignition of tantalum in 100 cm³/min flowing fluorine was observed at 68°C⁸³; moreover, there is some indication that rapid fluorine attack may initiate even at 25°C.²⁰⁶

Tantalum resists attack by dry chlorine, wet chlorine, and hydrogen chloride up to 150°C and is commonly used where such resistance is required.^{167,207} Tseitlin and Strunkin¹⁰² report the following average metal recession rates for tantalum (99.5 wt. %) in flowing (250 cm³/min) dry (less than 0.06 vol. % H_2O) chlorine: less than 0.1 $\mu\text{m}/\text{min}$ at 150°C, 0.1 $\mu\text{m}/\text{min}$ at

200°C, 3.3 $\mu\text{m}/\text{min}$ at 300°C, 595.6 $\mu\text{m}/\text{min}$ at 350°C, and 2358.0 $\mu\text{m}/\text{min}$ at 400°C. For chlorine containing 1.5 vol % water vapor, the observed rates were 0.1 $\mu\text{m}/\text{min}$ at 110°C, 0.3 $\mu\text{m}/\text{min}$ at 300°C, 0.3 $\mu\text{m}/\text{min}$ at 400°C, 4455 $\mu\text{m}/\text{min}$ at 450°C, and 33,840 $\mu\text{m}/\text{min}$ at 500°C. For chlorine containing 30 vol. % water vapor the rates were less than 0.1 $\mu\text{m}/\text{min}$ at 110 and 150°C, 0.1 $\mu\text{m}/\text{min}$ at 300 and 400°C, and 3.9 $\mu\text{m}/\text{min}$ at 500°C. In an 0.1-atm chlorine and 0.9-atm nitrogen mixture the observed metal recession rates were less than 0.1 $\mu\text{m}/\text{min}$ at 250°C, 4.1 $\mu\text{m}/\text{min}$ at 300°C, 27.6 $\mu\text{m}/\text{min}$ at 350°C, and 67.6 $\mu\text{m}/\text{min}$ at 400°C.

Like niobium, tantalum is also said to be resistant to iodine attack up to 250°C.^{1,2,3}

Molybdenum and Tungsten. Molybdenum reacts with fluorine gas to form several fluorides, including stable MoF_6 , which melts at 17°C and has a vapor pressure of 10^{-2} atm at about -40°C .² Hence, molybdenum is highly subject to fluorine attack even at room temperature. The molybdenum–fluorine reaction proceeds rapidly at 150°C² and molybdenum ignites in fluorine gas at 188–220°C.^{38,91} MoCl_5 is stable under 1.0-atm chlorine pressure up to 240°C, melts at 194°C, and has a vapor pressure of 10^{-4} atm at about 60°C.² Molybdenum reacts readily with flowing chlorine at 400°C.² At 650–700°C molybdenum reacts with bromine to form $\text{MoBr}_2(\text{s})$ and $\text{MoBr}_3(\text{v})$, but the reaction is slow.² At 300°C molybdenum reacts with iodine vapor to form $\text{MoI}_2(\text{s})$, $\text{MoI}_3(\text{s})$, and $\text{MoI}_4(\text{v})$.²

Fluorine attack on tungsten at atmospheric pressure and temperatures up to at least 500°C produces predominantly WF_6 , which melts at 2.5°C and boils at 17.5°C.^{2,208} Hence, tungsten does not passivate in fluorine, even at room temperature. The fluorine–tungsten reaction proceeds rapidly at 150–300°C² and ignition occurs at 260–332°C.^{38,91,209} High-temperature (400–2700°C), low-fluorine-pressure (10^{-7} – 10^{-4} atm), tungsten–fluorine reactions are discussed in references 33, 210, and 211. Fluorination of a tungsten–10 wt. % rhenium alloy is discussed in reference 212.

Tungsten forms several lower chlorides and WCl_6 , which melts at 280°C and has a vapor pressure of 10^{-4} atm at about 95°C.² At 600°C chlorination of tungsten in chlorine gas proceeds rapidly and is used to prepare WCl_6 .²

Bromination of tungsten at 450–500°C produces WBr_5 but at lower temperatures produces WBr_6 . These reactions are used to prepare WBr_5 and WBr_6 but are said to proceed slowly.²

Iodine reacts with tungsten to form WI_2 and WI_4 . WI_2 can be prepared by passing iodine vapor over tungsten at 727°C , but the iodides are said to be nonvolatile at lower temperatures and the WI_4 and WI_2 solids are stable only up to 137 and 227°C , respectively, under 1.0-atm iodine pressure.¹²² In a tungsten–iodine system at 1125°C the stable $WI_2(v)$ pressure is 10^{-3} atm.¹²² The tungsten metal recession rate in iodine at a pressure of 400 torr is less than $10^{-3} \mu\text{m/day}$ at 300°C and is only $0.022 \mu\text{m/day}$ at 450°C .¹²² Consequently, tungsten is commonly used to make deposition filaments in iodide deposition bulbs for preparation of iodide chromium, titanium, and zirconium. Iodine is placed in some incandescent lamps. The iodine reacts with tungsten on the lamp walls to form WI_2 , which transports to the hotter filament, where it decomposes and deposits tungsten back onto the filament.

Technetium and Rhenium. Fluorination of technetium proceeds rapidly at 400°C , forming TcF_5 , which melts at 50°C , and a vapor of TcF_6 , which melts at 37°C and has a vapor pressure of 10^{-2} atm at -26°C .² Chlorination of technetium has been observed to proceed slowly at 200°C and rapidly at 400°C , producing $TcCl_4$ and $TcCl_6$.²¹³ $TcCl_4$ readily sublimates in chlorine gas at 300°C .² $TcCl_6$ melts at 25°C , is quite volatile at this temperature, and even under an atmosphere of chlorine at 25°C it tends to decompose to $TcCl_4$.² No information is available on technetium reactions with bromine or iodine vapors.

Fluorination of rhenium at $300\text{--}400^\circ\text{C}$ and 250 torr fluorine pressure proceeds rapidly, producing gaseous ReF_7 and ReF_6 . At 400°C and 3.0 atm fluorine pressure the reaction product is almost exclusively ReF_7 . ReF_7 , ReF_6 , ReF_5 , and ReF_4 melt at 48 , 19 , 48 , and 125°C , respectively, and have vapor pressures of 10^{-2} atm at -17 , -40 , 100 , and probably $>200^\circ\text{C}$, respectively.² Formation of ReF_5 from fluorination of rhenium metal has not been observed.

Chlorination of rhenium proceeds readily at 500°C , producing $ReCl_5$ and some $ReCl_6$. Both products are stable at room temperature. Their melting points are 220 and 25°C , respectively. Bromine vapor reacts with rhenium at $450\text{--}600^\circ\text{C}$ to form $ReBr_5$ and possibly some $ReBr_3$. The melting point of $ReBr_5$ is “a little above room temperature,” while that of $ReBr_3$ is above 500°C .² No information is available on rhenium–iodine reaction kinetics, although several low-valence rhenium iodides are thermodynamically stable at and above room temperature.

Ruthenium and Osmium. Ruthenium is said to react with flowing fluorine at 300°C to form $RuF_5(v)$ and unstable $RuF_6(v)$.² The ruthenium–

chlorine reaction produces only RuCl_3 and possibly vapor phase RuCl_4 .² Similarly, only the trivalent bromide and iodide of ruthenium have been observed.² RuI_3 under 1.0 atm iodine pressure is not stable above 130°C.¹²²

In flowing fluorine, osmium reacts at 200–300°C to form $\text{OsF}_6(v)$.² Reaction of osmium in flowing chlorine at 600°C slowly produces OsCl_4 and OsCl_3 .² No information is available on osmium reactions with bromine or of iodine vapors or on pertinent properties of the corresponding halides.

Rhodium and Iridium. Rhodium is said to resist fluorine attack at room temperature but to react at slightly higher temperatures to form low-melting-point, volatile fluorides.¹⁸⁴ Rhodium reacts readily with chlorine at 300–800°C, forming RhCl_3 .²

Fluorine gas reacts readily with iridium at 300–400°C to form IrF_6 , which melts at 44°C and has a vapor pressure of 10^{-2} atm at -27°C .² In chlorine gas iridium reacts slowly at all temperatures. Above 600°C the reaction produces solid IrCl_3 , which tends to passivate the metal against further rapid reaction.² There is evidence that above 775°C iridium chlorides are not stable and the metal can coexist with chlorine gas.² However, Chow observed volatilization of iridium in a chlorine atmosphere at 840°C.²¹⁴ Iridium exposed to bromine vapors at 100–410°C was not volatilized.

Palladium and Platinum. Palladium resists fluorine attack at 25°C but not at higher temperatures.¹⁸⁴ Reaction of palladium with chlorine gas to form PdCl_2 is imperceptible below 260°C, slow between 260 and 400°C, and vigorous at 525°C.²¹⁵ Palladium does not react with pure HCl at any temperature.²¹⁵ Palladium reacts with bromine to form PdBr_2 , but the reaction is said to be slow at all temperatures.² Palladium reacts with iodine vapors to form PdI_2 , which neither melts nor readily volatilizes up to 740°C.²

Platinum resists fluorine attack at room temperature, but slightly above room temperature it readily forms low-melting, volatile fluorides.¹⁸⁴ Platinum is considerably more resistant to chlorine attack,¹¹⁴ because it forms a “protective” platinum chloride scale. The outer layer of this scale is PtCl_4 up to 370°C. Under 1.0-atm chlorine pressure this layer subsequently decomposes to PtCl_3 , PtCl_2 , PtCl , and Pt at 370, 428, 578, and 583°C, respectively.²¹⁶ Average platinum–chlorine reaction rates for 2- to 20-hr exposures at 480, 510, 540, and 565°C are 30, 60, 120, and 600–1200 mils/yr.¹¹⁴ Platinum does not react at all with dry HCl ¹¹⁴ but is readily attacked by moist chlorine or HCl above 100°C.²¹⁷ Platinum reacts slowly with bromine vapor at 150°C to form PtBr_4 and PtBr_2 .² It reacts with iodine vapors to form PtI_4 and lower iodides. Under 1.0-atm iodine vapor pressure, solid

PtI_4 and PtI_3 decompose to PtI_2 at about 275°C and PtI_2 decomposes to Pt at about 325°C .¹²² However, small amounts of the vapors may exist considerably above these decomposition pressures and, hence, permit vapor phase transport of platinum: in 1.0 atm iodine vapor, $\text{PtI}_3(v)$ over $\text{Pt}(s)$ has an equilibrium vapor pressure of 3×10^{-4} at 727°C .¹²²

Silver. Using the pressure-drop method, O'Donnell²¹⁸ studied the kinetics of reaction between fluorine and silver. O'Donnell's fluorination experiments were done at $25\text{--}300^\circ\text{C}$ and $50\text{--}600$ torr fluorine pressure with 99.999 % pure silver sheet. Below 300°C fluorination of silver produces a solid surface scale consisting of AgF_2 , AgF , and Ag_2F . The scale is predominantly Ag_2F at 25°C , predominantly AgF at 200°C and 50-torr fluorine pressure, and nearly an equal mixture of AgF and AgF_2 at 200°C and 200-torr fluorine pressure. Fluorination of silver at about 300°C produces a liquid surface "scale," possibly a low-melting eutectic, $\text{AgF} \cdot \text{AgF}_2$. Initially the silver fluoride scale growth kinetics are nearly linear, but after 20–80 min the kinetics become approximately parabolic. A few of the observed parabolic rates are given in Table 17. During the initial period of linear kinetics the reaction activation energy is 6.5 kcal/mole for fluorination with 50-torr fluorine pressure and 5.2 kcal/mole with 200-torr fluorine pressure. During later periods of parabolic scale growth the reaction activation energy is 10.2 kcal/mole, nearly independent of fluorine pressure. During both linear and parabolic periods of scale growth, the fluorination rate is maximum for a particular fluorine pressure between 50 and 600 torr. For example, at 100°C the fluorination rate is maximum when the fluorine pressure is about 300 torr; if the fluorine pressure is increased or decreased from 300 torr, the

Table 17. Kinetic Data for Silver–Fluorine Reactions²¹⁸

	P_{F_2} ^a (atm)	Parabolic rate constant k_2 (ml F_2/cm^2) ² /min	Δy (μm) ^c for $t = 1.0$ yr
25	0.066	8×10^{-6}	4.4
	0.263	1.1×10^{-5}	5.2
100	0.066	2×10^{-4}	19
	0.263	3×10^{-4}	21
200	0.066	3.7×10^{-3}	72
	0.263	7.7×10^{-3}	89

^aTests were conducted in static rather than flowing fluorine gas.

^bRate constants are for reaction after initial linear kinetics give way to parabolic kinetics. The total test duration with each set of conditions was about 260 min.

^cEstimated metal loss after 1-yr-long exposure to fluorine attack.

fluorination rate decreases. At 200°C the maximum fluorination rate occurs at about 200 torr. With a fluorine pressure below 200 torr, fluorination produces a scale of Ag_2F and AgF and the fluorination rate increases with increasing fluorine pressure. As the fluorine pressure moves above 200–300 torr, fluorination produces significant amounts of AgF_2 scale. Perhaps this AgF_2 scale is more protective than the Ag_2F – AgF scale, hence reducing the fluorination rate at fluorine pressures above 200–300 torr.

Silver also passivates in chlorine,^{180,219–221} forming a surface scale of AgCl , which melts at 455°C and has a vapor pressure of 10^{-4} atm at about 800°C.² The silver-chlorination kinetics are parabolic^{219,220,222} with the rate-limiting step being electronic transport through the AgCl scale.²²³ Parabolic rate constants, $k_2 = y^2/t$, for silver consumption by the chlorination reaction are $2.3 \mu\text{m}^2/\text{min}$ at 300°C, $10 \mu\text{m}^2/\text{min}$ at 350°C, and $25 \mu\text{m}^2/\text{min}$ at 400°C.²²² Silver chlorination for 1 yr at these parabolic rates would, respectively, convert about 1.1, 2.3, and 3.6 mm of silver to silver chloride. Reference 222 provides further discussion of the chlorination of silver and the variation of rate constants with chlorine pressure. Silver is more resistant to HCl than to pure chlorine¹¹⁴ but is less resistant to moist chlorine than to pure dry chlorine.^{217,224} However, even in water-saturated chlorine, silver still tends to passivate at 10–90°C.²²⁴

In bromine vapor, silver forms a protective scale of AgBr which melts at 432°C and has a vapor pressure of 10^{-4} atm at 781°C.² The reaction kinetics are nearly parabolic at temperatures up almost to the AgBr melting point. For silver bromination at 0.23-atm bromine vapor pressure, Wagner reports recession parabolic rate constants, $k_2 = y^2/t$, of approximately $1.7 \mu\text{m}^2/\text{min}$ at 200°C, $4.0 \mu\text{m}^2/\text{min}$ at 250°C, $7.8 \mu\text{m}^2/\text{min}$ at 300°C, $10.2 \mu\text{m}^2/\text{min}$ at 350°C, and $10.0 \mu\text{m}^2/\text{min}$ at 400°C.²²² These rates of reaction would in 1 yr consume 0.95, 1.4, 2.0, 2.3, and 2.3 mm of silver, respectively. For silver bromination at 25°C and 0.27-atm bromine pressure, Weininger²²⁵ reports a parabolic rate constant, $k_2 = y^2/t$, of $0.0061 \mu\text{m}^2/\text{min}$. At this rate chlorination would in 1 yr convert about $57 \mu\text{m}$ of silver to AgCl . The postulated rate-limiting step in both room-temperature and high-temperature silver chlorination is electron transport from the scale/metal to the scale/vapor interface.^{222,225} At 25°C the parabolic rate constant for silver bromination in 90% water-saturated bromine vapor is about one-half that for silver bromination in dry bromine vapor.²²⁵ For discussions of the bromination of silver–lead, –zinc, and –cadmium alloys, refer to references 226 and 227.

Silver reacts with iodine to form AgI , which melts at 558°C and has a vapor pressure of 10^{-4} atm at about 675°C.² The reaction kinetics are parabolic from 25 to at least 150°C.^{225,228} At room temperature the parabolic

rate constant, $k_2 = y^2/t$, is $0.00356 \mu\text{m}^2/\text{min}$; at this rate, in 1 yr $43 \mu\text{m}$ of silver would be converted to AgI. At higher temperatures silver iodination kinetics are highly subject to doping effects.²²⁸ It is postulated that as the temperature increases, polyvalent impurity cations go into solution in the AgI scale and in so doing increase the concentration of electronic defects and consequently increase the rate of electron transport and in turn the reaction rate, which is limited by the electron transport rate.²²⁸ This doping effect leads to the large spread in experimental data given in references 228–231. Reported parabolic rate constants in some instances increase with increasing temperature, in others are constant, and in others decrease. Smyth and Cutler²²⁸ give rate constants, $k_2 = y^2/t$, for iodination of silver (99.9 + wt. %) of $0.13 \mu\text{m}^2/\text{min}$ at 60°C and $0.030 \mu\text{m}^2/\text{min}$ at 140°C . Silver chlorination recession rate constants for silver (99.99 + wt. %) at 140°C may be as much as $0.3 \mu\text{m}^2/\text{min}$.²²⁸ At 145°C AgI undergoes a phase transition from a hexagonal (wurtzite) crystal structure to a body-centered-cubic structure with an accompanying abrupt increase in the reaction rate.²²⁸ For a detailed discussion of silver iodination, bromination, and chlorination in the moist halogens refer to reference 228. Local cell action in the iodination of silver has already been discussed.⁴⁹

Gold. Gold forms a trifluoride, AuF_3 , which has a melting point greater than 300°C at which temperature it sublimates in a vacuum.² Gold is said to have little tendency to passivate in fluorine,¹⁸⁴ but there are no experimental data available from which the actual gold-fluorination kinetics can be determined.

In chlorine, gold forms Au_2Cl_6 and Au_2Cl_2 .²³² Au_2Cl_2 has a vapor pressure of 10^{-4} atm at about 180°C . In chlorine at 1.0-atm pressure, Au_2Cl_6 decomposes to $\text{Au}_2\text{Cl}_2(\text{s})$ at about 255°C . In flowing chlorine at a pressure of 1.0 atm, as the reaction temperature increases the linear rate of loss by AuCl_3 evaporation increases up to about 255°C . From 255 to about 450°C , gas phase Au_2Cl_6 becomes increasingly unstable and the rate of Au loss by Au_2Cl_6 evaporation decreases. At 450°C , loss of Au by Au_2Cl_2 evaporation begins to dominate and the rate of Au loss increases with increasing temperature to above 800°C . The maximum gold loss rate is approximately $0.3 \mu\text{m}/\text{min}$ ($160 \text{ mm}/\text{yr}$) occurring at about 250°C . At about 150 and 450°C , the gold loss rates in 1.0-atm chlorine are reportedly about $1.7 \times 10^{-3} \mu\text{m}/\text{min}$ ($0.89 \text{ mm}/\text{yr}$). Gold is much more resistant to HCl attack.¹¹⁴

At 150°C gold reacts with bromine vapors to form AuBr. No kinetic information is available.

At 50–100°C gold reacts with iodine vapor to form AuI. At 300°C the rate of gold loss in 0.53-atm iodine vapor is less than 10^{-3} $\mu\text{m/day}$ (0.36 $\mu\text{m/yr}$) and at 450°C it is only 0.065 $\mu\text{m/day}$ (24 $\mu\text{m/yr}$).¹²²

Zinc, Cadmium, and Mercury

Zinc. Zinc tends to passivate in fluorine,^{233,234} forming a scale of ZnF_2 which melts at 875°C²³⁴ and has a vapor pressure of only 10^{-6} atm at 895°C.¹⁴ No information on either the extent of this passivation or the exact zinc-fluorination kinetics is available. Nor are kinetic data available for the other zinc-halogen reactions.

Cadmium. Zirin^{235,236} studied the fluorination of cadmium with fluorine gas as a commercial means for CdF_2 production. Fluorination experiments were conducted at 300–600°C (the melting point of cadmium is 312°C) with a fluorine pressure of 200–300 torr. The purity of the cadmium was 99.0 wt. %. The extent and rate of fluorination were recorded using manometric techniques. The rate of CdF_2 scale growth was in all cases parabolic. Copper and gold markers, initially at the gas/metal interface remained there during fluorination, indicating that the scale grows by inward diffusion of fluorine anions through the fluorite-type CdF_2 lattice.

No information is available on cadmium chlorination or bromination.

In iodine vapor, cadmium forms CdI_2 , which melts at 387°C and has a vapor pressure of 10^{-4} atm at about 335°C.¹⁴ According to Sugier,²³⁷ at 127–220°C and 0.13–0.29-atm iodine vapor pressure, iodination of cadmium proceeds at a decreasing rate for about the first 100 min of exposure but after 100 min proceeds at linear rates. Occasionally, breakaway reactions occur, but they are followed by rapid repassivation to the original linear rate. The observed rates vary from $1.4\text{--}2.8 \times 10^{-8}$ g/cm² sec but are independent of iodine vapor pressure and temperature in the aforementioned ranges. During the period of linear kinetics, the rate-determining step is said to be a surface process occurring at the $\text{CdI}_2(\text{s})/\text{I}_2(\text{v})$ interface.

Mercury. Mercury reacts with halogen vapors to form both monovalent and divalent halides.^{122,238–240}

Silicon, Boron, Gallium, Indium, and Thallium

Silicon and Boron. Fluorides of silicon and boron, SiF_4 and BF_3 , respectively, are gaseous at room temperature. Hence, these elements do not form protective scales when they are exposed to fluorine. Consequently,

both silicon and boron ignite spontaneously in pure fluorine gas at room temperature and 760-torr fluorine pressure.^{241–243} Kuriakose and Margrave²⁴³ studied the fluorination of silicon and boron in fluorine–helium gas mixtures. The fluorine partial pressures were kept sufficiently low, below about 200 torr, to avoid breakaway reactions. Reaction temperatures were varied from 75 to 1000°C and fluorine partial pressures were varied from 2.8 to 52.5 torr. Sample weight loss was followed directly as the extension of a quartz spring from which the sample was suspended. Weight loss, x , followed linear kinetics, $x = kt$, for both silicon and boron samples.

For silicon, the fluorination activation energy is 12 kcal/mole below 150°C and 1.3 kcal/mole above 150°C. Similarly, the activation energy for boron fluorination is 37.9 kcal/mole below 352°C and 2.5 kcal/mole above 352°C. These abrupt changes in reaction activation energies are indicative of changes in fluorination mechanism rate-controlling processes. Kuriakose and Margrave hypothesize that the rate-controlling processes at the lower temperatures are “(1) adsorption of F_2 gas on the metal surfaces and (2) formation of activated complexes which may involve (a) the dissociation of the gas molecules and (b) breaking of bonds in the solid.” This hypothesis is substantiated by their observation that the reaction rate is dependent on pressure: for silicon fluorination, $k \propto P^m$, where m is 0.6–1.0 and for boron fluorination, $k \propto P$. Kuriakose and Margrave hypothesize that the rate-controlling process at the higher temperatures is “the diffusion of fluorine through the product gas layer for which the energy of activation must be very low,” as observed. Further discussion of the fluorination of silicon is included in references 244 and 245.

Chlorination of silicon at 500°C or higher temperature is used to prepare $SiCl_4$ and to etch silicon wafers.^{246–248} Bromination of silicon at 350–600°C is used to prepare $SiBr_4$; it is said that the bromination reaction at 350–600°C does not proceed at an appreciable rate in the absence of silicon impurities.²⁴⁹ SiI_4 is prepared by the iodination of silicon at 600–850°C and BI_3 is prepared by the iodination of boron at 700–800°C.

Gallium, Indium, and Thallium. Little or no information is available on the halogenation of gallium, indium, or thallium.

Germanium, Tin, and Lead

Germanium. With chlorine, germanium forms a low-melting volatile chloride, $GeCl_4$, and at least above 175°C the reaction is rapid with no tendency toward passivation.²⁵⁰ No information on bromination kinetics

for germanium is available, but bromination may also form a low-melting volatile product, as may iodination of germanium. Above 280°C the evaporation rate of GeI_4 is significant and the germanium-iodine reaction proceeds rapidly.^{122,251-257}

Tin. Tin forms two stable fluorides, SnF_2 and SnF_4 , which are somewhat protective at and slightly above room temperature, but the scale formed is brittle,¹⁸⁴ and as the temperature approaches 100°C, volatilization of $\text{SnF}_4(v)$ becomes significant.¹² In fact, SnF_4 is prepared in the laboratory by reaction of the elements at 100–190°C.^{12,258}

Tin reacts readily with chlorine gas, even at room temperature,^{181,246} producing predominantly SnCl_4 , which melts at -33°C and has a vapor pressure of 10^{-4} atm at -50°C .¹⁴ Hence, tin does not passivate at all in chlorine gas. References 165, 246, 259, 260, and 261 discuss the 65–400°C tin-chlorination reaction which is used to prepare SnCl_4 . With bromine and iodine, tin also forms somewhat volatile tetravalent halides, SnBr_4 and SnI_4 , having vapor pressures of 10^{-4} atm at -9 and 78°C , respectively, but no experimental information is available on the reaction kinetics.

Lead. Lead passivates to some extent in fluorine at and a little above room temperature, forming a brittle white mixture of PbF_2 and PbF_4 .^{184,262} Roll reports a 5–50 mil/yr metal recession rate for lead in pure fluorine²⁶³ and cites several examples of industrial use of lead in fluorine-containing atmospheres.²⁶⁴ Lead is much less resistant to HF attack.^{184,262}

In chlorine, lead forms a protective scale of PbCl_2 , which melts at 500°C and has a vapor pressure of 10^{-4} atm at 450°C . Tseitlin and Strunkin^{102,108} report the following average metal recession rates for lead exposed for 6.0 hr to dry (0.06 vol. % H_2O) chlorine with a 250 ml/min flow rate: 61 $\mu\text{m}/\text{yr}$ at 200°C , 130 $\mu\text{m}/\text{yr}$ at 250°C , 140 $\mu\text{m}/\text{yr}$ at 275°C , 1500 $\mu\text{m}/\text{yr}$ at 296°C , and 2500 $\mu\text{m}/\text{yr}$ at 309°C . Average rates for chlorine containing 30 vol. % water vapor were only 1–3 times higher.¹⁰²

PbBr_2 melts at 373°C and has a vapor pressure of 10^{-4} atm at about 420°C .¹⁴ Lead passivates in HBr-free bromine liquid and vapor at room temperature but reacts readily with HBr.^{263,265}

Reacting with iodine vapor, lead forms PbI and PbI_2 . PbI_2 melts at 412°C and has a vapor pressure of 10^{-4} atm at about 370°C .¹²² At room temperature and 167°C the kinetics are parabolic,^{219,266} the rate-determining step being diffusion of iodine along internal scale grain boundaries and pores.²⁶⁶ Roll²⁶³ reports that the average metal recession rate for lead in iodine vapor is greater than 1.3 mm/yr.

Conclusions

In summary, boron, carbon, silicon, germanium, titanium, vanadium, and many of the second and third row transition metals form low-melting volatile halides; hence, these metals are particularly subject to halogen attack, even at low temperatures. It should be noted that, although readily attacked by dry chlorine, titanium is extensively used in contact with wet chlorine and may be fairly resistant to dry fluorine at room temperature.

Silver, zirconium, and probably hafnium are fairly resistant to halogen attack at 25°C but not at temperatures above 100–150°C. Substantive data on halogenation of many other second and third row transition metals are lacking. A few of the more noble of these metals, for example, iridium, platinum, and gold, may resist fluorine attack at temperatures up to 100°C or higher.

The halides of the alkali and alkaline earth metals exhibit melting points ranging from 445°C for LiI to 1450°C for SrF₂ and their vapor pressures attain 10⁻⁴ atm only at temperatures of 600°C or higher. Consequently, in chlorine, bromine, and iodine at low temperatures these metals may form protective films. However, in fluorine, the alkali and alkaline earth metals, excluding beryllium and magnesium, form only porous (nonprotective) fluoride scales.

Beryllium, magnesium, and aluminum form protective fluoride films which keep the first-year metal loss to less than 5 μm at temperatures as high as 200°C. Magnesium may also be resistant to other halogens, since its halides have high melting points and low vapor pressures. However, beryllium is likely to be less resistant to other halogens, since the vapor pressures of its halides attain values of 10⁻⁴ atm at only 225–270°C. Aluminum reacts readily with both chlorine and bromine.

At least at room temperature and a little above, zinc, cadmium, indium, thallium, tin, and lead are also potentially resistant to fluorine attack, since their fluorides have relatively high melting points and low vapor pressures. However, other halides of these metals have significantly lower melting points and higher vapor pressures; consequently, these metals are likely to be less resistant to attack by other halogens (chlorine, bromine, and iodine).

The first row transition metals, except titanium and vanadium, are generally resistant to halogen attack. Of these metals, iron and chromium are the least resistant while nickel and copper are the most resistant. In fluorine, potentially protective iron fluoride scale tends to spall from the metal; in other halogens, the iron halide scales have relatively high vapor pressures. Although there are some indications that manganese, chromium,

and cobalt, at least at low temperatures, are also fairly resistant to halogen attack, there is no substantive evidence to this effect. Nickel and iron fluorination is said to occur by inward diffusion of fluorine anions. Such diffusion may also control the fluorination of cobalt, magnesium, manganese, and zinc, which form fluorides with the same tetragonal $\text{SnO}_2\text{-TiI}_2$ structure as that of NiF_2 .

Little reliable information is available on the halogen resistance of alloys. The alloys most commonly used for handling halogens are those of the above-mentioned halogen-resistant metals, such as nickel, copper, iron, chromium, magnesium, aluminum, and silver. For example, Monel (Ni-Cu) is used for handling all the halogens, aluminum-magnesium alloys are commonly used for fluorine, and stainless steel (Fe-Ni-Cr) for chlorine.

Although a few thorough metal-halogenation studies have been conducted, most of the information about halogen resistance of metals comes from cursory comparisons of commercial metals and alloys. Scale morphologies, defect structures, impurity doping effects, self-diffusion coefficients, solubilities and diffusivities of the halogens in metals, and even kinetics (extensively studied in metals oxidation research) have been much neglected in studies of metal halogenation. Some studies have, in part, been discouraged by the highly toxic and corrosive nature of halogens.

A knowledge of the above-discussed metal and metal-halide scale properties and an understanding of corrosion mechanisms provide the basis for the designing and engineering of corrosion-resistant alloys. This idea of alloy design (used, for example, to develop alloys resistant to high-temperature oxidation and hot corrosion) rather than simple alloy evaluation has not generally been applied to develop halogen-resistant alloys. Such alloy design could be very productive.

Support information needed for this alloy development includes kinetic, morphological, and mechanistic data for halogenation of pure metals. Such data are also needed to give the materials engineer (1) a broader selection of pure metals for use in halogen environments, (2) the ability to forecast the long-term effect of changes in the halogen environment (for example, industrial process gas composition) on industrial processes and process equipment. Metals of particular interest for which data are particularly scarce include chromium, manganese, cobalt, aluminum, zinc, tin, and lead.

To facilitate the forecasting of long-term halogen resistance, some kinetic data should be gathered for at least several hundred hours. Changes in reaction kinetics after several hundred hours, resulting from the buildup

of mechanical stresses, for example, are not uncommon. Experimental studies of halogen-metal reaction kinetics are often complicated by the high volatility of the metal halides and by oxide and oxygen contamination. Where volatilization is involved, gas flow rate is particularly important. Most metals are covered initially by an oxide film when they are placed into the test system. Such surface oxides can grossly alter the metal halogenation kinetics for many hundreds or thousands of hours. Oxygen impurities in the halogen environment can also alter halogenation kinetics. Because oxygen is frequently present in industrial halogen environments, studies of the behavior of metals in halogen-oxygen mixtures are perhaps as important as those in pure halogens.

Long-term forecasting of the behavior of halogen-metal systems and the development of halogen-resistant alloys are facilitated by a knowledge of metal halide defect structures, self-diffusion coefficients, thermodynamic properties, electrical conductivities, and physical properties and a knowledge of alloy self-diffusion coefficient and fluorine solubilities. Considerable thermodynamic data are already available, but the other data are particularly sparse. It is hoped that future studies of metal halogenation will provide this information along with more detailed observations of scale morphology than have been provided in the past.

ACKNOWLEDGMENTS

The authors extend their sincere thanks to Virginia Daniel for typing and otherwise assisting with the preparation of this chapter; to L. Vincent, P. M. O'Donnell, E. J. Barber, H. H. Thomas, and S. W. Wohlfort, who reviewed the manuscript; and to the Goodyear Atomic Corporation for partial support of this project.

REFERENCES

1. A. Standen, H. F. Mark, J. J. McKetta, Jr., and D. F. Othmer (eds.), *Kirk-Othmer Encyclopedia of Chemical Technology*, 2nd ed., John Wiley, New York (1963).
2. J. H. Canterford and R. Colton, *Halides of the Transition Elements: Halides of the Second and Third Row Transition Metals*, John Wiley, London (1968).
3. J. H. Canterford and R. Colton, *Halides of the Transition Elements: Halides of the First Row Transition Metals*, John Wiley, London (1969).
4. D. Brown, *Halides of the Transition Elements: Halides of the Lanthanides and Actinides*, John Wiley, London (1968).

5. *JANAF Thermochemical Tables*, U.S. Department of Commerce PB 168 370, Dow Chemical Co., Clearinghouse for Scientific and Technical Information, Midland, Mich. (1965).
6. C. E. Wicks and F. E. Block, *Thermodynamic Properties of 65 Elements—Their Oxides, Halides, Carbides, and Nitrides*, Bulletin 605, Bureau of Mines, Government Printing Office, Washington, D.C. (1963).
7. L. L. Quill (ed.), *The Chemistry and Metallurgy of Miscellaneous Materials: Thermodynamics*, McGraw-Hill, New York (1950).
8. J. W. Hamer, M. S. Malmberg, and B. J. Rubin, Theoretical Electromotive Force for Cells Containing a Single Solid or Molten Fluoride, Bromide, or Iodide, *J. Electrochem. Soc.* **112**, 750–756 (1965).
9. O. Kubaschewski, E. L. Evans, and C. B. Alcock, *Metallurgical Thermochemistry*, Pergamon Press, Oxford (1967).
10. E. Steinmetz and H. Roth, Freie Standard-Bildungsenthalpien der Fluoride nach der Temperaturfunktion, *J. Less-Common Metals* **16**, 295–342 (1968).
11. W. H. Skelton and J. W. Patterson, *Free Energy Changes for Displacement Reactions Involving Metals and Their Fluorides*, *J. Less-Common Metals* **31**, 47 (1973).
12. J. H. Simons, *Fluorine Chemistry*, Vol. I, Academic Press, New York (1950).
13. J. H. Simons, *Fluorine Chemistry*, Vol. V, Academic Press, New York (1964).
14. R. C. Weast (editor-in-chief), *Handbook of Chemistry and Physics*, Chemical Rubber Co., Cleveland (1970).
15. T. B. Reed, *Free Energy of Formation of Binary Compounds*, MIT Press, Cambridge, Mass. (1971).
16. W. H. Skelton and J. W. Patterson, Free Energy Determinations by Solid Galvanic Cell Measurements for Selected Metal, Metal Fluoride Reactions, *J. Less-Common Metals* **31**, 47–60 (1973).
17. K. Schafer and E. Lax, *Landolt-Börnstein Zahlenwerte und Funktionen aus Physik, Chemie, Astronomie, Geophysik, und Technik*, Vol. II, Pt. 3, Springer-Verlag, Berlin (1956).
18. E. M. Levin, C. R. Robbins, and H. F. McMurdie, *Phase Diagrams for Ceramists* (and supplement), American Ceramic Society, Columbus, Ohio (1969).
19. P. G. Shewmon, *Diffusion in Solids*, McGraw-Hill, New York (1963).
20. E. T. Turkdogan, The Theory of Enhancement of Diffusion-Limited Vaporization Rates by Convection–Condensation Process, *Trans. Met. Soc. AIME (Amer. Inst. Mining, Met., Petrol. Eng.)* **230**, 740–750 (1964).
21. H. H. Kellog, Vaporization Chemistry in Extractive Metallurgy, *Trans. Met. Soc. AIME (Amer. Inst. Mining, Met., Petrol. Eng.)* **236**, 602–615 (1966).
22. P. Kofstad, *High Temperature Oxidation of Metals*, John Wiley, New York (1966).
23. G. C. Wood, Oxidation of Metals, in *Techniques of Metals Research*, Vol. IV, part 2, International Publishers, New York (1970).
24. P. E. Brown, J. M. Crabtree, and J. F. Duncan, The Kinetics of the Reaction of Elementary Fluorine with Copper Metal, *J. Inorg. Nucl. Chem.* **1**, 202–212 (1955).
25. P. M. O'Donnell and A. E. Spakowski, The Fluorination of Copper, *J. Electrochem. Soc.* **111**(6), 633–636 (1964).
26. W. R. Myers and W. B. DeLong, Fluorine Corrosion. High-Temperature Attack on Metals by Fluorine and Hydrogen Fluoride. Behavior of Insulated Steel Parts in Fluorine Cells, *Chem. Eng. Progr.* **44**(5), 359–362 (1948).
27. A. K. Kuriakose and J. L. Margrave, Kinetics of Reaction of Elemental Fluorine. III. Fluorination of Silicon and Boron, *J. Phys. Chem.* **68**, 2671–2675 (1964).
28. E. A. Gulbransen, Surface Studies with the Vacuum Microbalance: High-Temperature Reactions, *Advan. Catalysis* **5**, 119 (1953).

29. W. Y. Shiu, D. J. Young, and M. J. Dignam, Kinetics of Chlorination of Metallic Sodium at Low Temperatures, *Oxid. Metals* **7**(2), 77–93 (1973).
30. G. L. Hung, I. M. Ritchie, R. J. Esdaile, and J. V. Sanders, Nickel–Fluorine Reactions in the Presence of Xenon, *J. Catalysis* **25**(3), 460–462 (1972).
31. M. J. Dignam and D. A. Huggins, A Kinetic Study of the Heterogeneous Reactions of Metallic Sodium with Chlorine and Bromine, *J. Electrochem. Soc.* **114**(2), 117–123 (1967).
32. D. E. Rosner and H. D. Allendorf, Kinetics of the Attack of Molybdenum by Dissociated Chlorine, *J. Phys. Chem.* **69**(12), 4290–4296 (1965).
33. D. E. Rosner and H. D. Allendorf, Kinetics of the Attack of Refractory Solids by Atomic and Molecular Fluorine, *J. Phys. Chem.* **75**(3), 308–317 (1971).
34. Y. Hasegawa, M. Shiojiri, and S. Matsumura, Quartz-Crystal Microbalance for Studying Chemical Reactions of Thin Metal Films, *Shinku* **13**(9), 296–302 (1970).
35. M. Shiojiri, Y. Hasegawa, and Y. Tsujikura, Thermal Effect of Ultrasonic Vibration of Quartz-Crystal Microbalance on Chemical Reactions, *Japan. J. Appl. Phys.* **10**(1), 143–148 (1971).
36. J. Gordon and F. L. Holloway, Handling Gaseous Fluorine and Chlorine Trifluoride in the Laboratory, *Ind. Eng. Chem.* **52**(5), 63A–66A, 69A (1960).
37. C. Slessor and S. R. Schram (eds.), *Preparation, Properties, and Technology of Fluorine and Organic Fluoro Compounds*, McGraw-Hill, New York (1951).
38. H. W. Schmidt, *Handling and Use of Fluorine and Fluorine–Oxygen Mixtures in Rocket Systems*, NASA SP-3037, National Aeronautics and Space Administration, Washington, D.C. (1967).
39. R. H. McBride, *Metering of Hydrofluoric Acid and Fluorine*, AECD-3690, E. I. duPont de Nemours and Co., Wilmington, Del. (1945).
40. J. F. Froning, M. K. Richards, T. W. Stricklin, and S. G. Turnbull, Purification and Compression of Fluorine, *Ind. Eng. Chem.* **39**, 275 (1947).
41. H. F. Priest and A. V. Grosse, Storage of Fluorine in Pressure Cylinders, *Ind. Eng. Chem.* **39**, 279 (1947).
42. S. H. Smiley and C. R. Schmitt, Continuous Disposal of Fluorine, *Ind. Eng. Chem.* **46**(2), 244–247 (1954).
43. C. J. Sterner and A. H. Singleton, *The Compatibility of Various Metals and Carbon with Liquid Fluorine*, WADD-TR-60-436, Wright Air Development Division, Wright-Patterson Air Force Base, Ohio (1960).
44. J. S. Sconce (ed.), *Chlorine: Its Manufacture, Properties and Uses*, Reinhold, New York (1967).
45. C. Wagner, Beitrag zur Theorie des Anlauf Vorgangs, *Z. Phys. Chem.* **B21**, 25–41 (1933).
46. C. Wagner, Beitrag zur Theorie des Anlauf Vorgangs II, *Z. Phys. Chem.* **B32**, 447–462 (1936).
47. C. Wagner, Diffusion and High Temperature Oxidation of Metals, in *Atom Movements*, pp. 153–173, American Society for Metals, Cleveland (1951).
48. R. A. Rapp and D. A. Shores, Solid Electrolyte Galvanic Cells, in *Techniques of Metals Research*, Vol. IV, Pt. 2 (R. A. Rapp, ed.), pp. 123–192, John Wiley, New York (1970).
49. C. Ilschner-Gench and C. Wagner, Local Cell Action During the Scaling of Metals, I, *J. Electrochem. Soc.* **105**, 198–200 (1958).
50. C. S. Tedmon, Jr., The Effect of Oxide Volatilization on the Oxidation Kinetics of Chromium and Iron–Chromium Alloys, *J. Electrochem. Soc.* **113**, 766–768 (1966).
51. J. P. Hirth and G. M. Pound, Condensation and Evaporation, Nucleation and Growth Kinetics, in *Progress in Materials Science*, Vol. 11, Macmillan, New York (1963).
52. C. Gelain, A. Cassuto, and P. LeGoff, Kinetics and Mechanism of Low-Pressure, High-Temperature Oxidation of Silicon—II, *Oxid. Metals* **3**, 139–151 (1971).

53. H. Graham and H. Davis, Oxidation/Vaporization Kinetics of Chromium(III) Oxide, *J. Amer. Ceram. Soc.* **54**, 89–93 (1971).
54. C. Wagner, Passivity During the Oxidation of Silicon at Elevated Temperatures, *J. Appl. Phys.* **29**, 1295–1297 (1958).
55. E. T. Turkdogan, P. Gieveson, and L. S. Darken, Enhancement of Diffusion-Limited Rates of Vaporization of Metals, *J. Phys. Chem.* **67**, 1647–1654 (1963).
56. F. P. Fehlner and N. F. Mott, Oxidation in the Thin-Film Range, in *Oxidation of Metals and Alloys* (D. L. Douglass, ed.), pp. 37–62, American Society for Metals, Metals Park, Ohio (1971).
57. C. Wagner, Formation of Thin Oxide Films on Metals, *Corrosion Sci.* **13**, 23–52, (1973).
58. R. Herchl, N. N. Khoi, T. Homma, and W. W. Smeltzer, Effect of Product Condensation on Reaction-Enhanced Vaporization Rates and on the Transition from Homogeneous to Heterogeneous Reaction in High-Temperature Metal Oxidation, *Oxid. Metals* **4**, 35–49 (1972).
59. L. Berry and J. Paidassi, Sur la cinétique et le mécanisme de réaction due nickel avec l'oxygène aux températures élevées, *C.R. Acad. Sci., Ser. C* **262**, 1353–1356 (1966).
60. J. J. Van den Broeck and J. L. Meijering, Kinetics of the Oxidation of Nickel and Some of Its Alloys, *Acta Met.* **16**, 375–379 (1968).
61. P. Kofstad, Effect of Impurities on the Defects in Oxides and Their Relationship to Oxidation of Metals, *Corrosion* **24**, 379–388 (1968).
62. W. E. Boggs, R. H. Kachik, and G. E. Pellissier, The Effects of Crystallographic Orientation and Oxygen Pressure on Oxidation of Iron, *J. Electrochem. Soc.* **114**, 32–39 (1967).
63. W. E. Boggs, The Role of Structural and Compositional Factors in the Oxidation of Iron and Iron-Based Alloys, in *High Temperature Gas-Metal Reactions in Mixed Environments* (S. A. Jansson and Z. A. Foroulis, eds.), Metallurgical Society of AIME, New York (1973).
64. A. G. Goursat and W. W. Smeltzer, Oxidation of Iron, in *Reviews of High-Temperature Materials*, Vol. I (J. Newkirk, ed.), pp. 351–396, Freund Publications, Tel-Aviv (1973).
65. A. Brückman, Mechanism of Transport of Matter Through the Scales During Oxidation of Metals and Alloys, *Corrosion Sci.* **7**, 51–59 (1967).
66. S. Mrowec, Mechanism of High-Temperature Oxidation of Metals and Alloys, *Corrosion Sci.* **7**, 563–578 (1967).
67. J. A. Roberson and R. A. Rapp, The Observation of Markers During the Oxidation of Columbium, *Trans. Met. Soc. AIME (Amer. Inst. Mining, Met., Petrol. Eng.)* **239**, 1327–1331 (1967).
68. J. S. Sheasby, The Oxidation of Niobium in the Temperature Range 450°–720°C., *J. Electrochem. Soc.* **115**, 695–700 (1968).
69. C. Wagner, Reaction Types in the Oxidation of Alloys, *Z. Elektrochem.* **63**, 772–782 (1959).
70. R. A. Rapp, Kinetics, Microstructures, and Mechanism of Internal Oxidation. Its Effect and Prevention in High-Temperature Alloy Oxidation, *Corrosion* **21**, 382–401 (1965).
71. J. Swisher, Internal Oxidation, in *Oxidation of Metals and Alloys* (D. L. Douglass, ed.), pp. 235–267, American Society for Metals, Metals Park, Ohio (1971).
72. G. C. Wood, Fundamental Factors Determining the Mode of Scaling of Heat-Resistant Alloys, *Werkst. Korros.* **22**, 491–503 (1971).
73. B. Chattopadhyay and G. C. Wood, The Transient Oxidation of Alloys, *Oxid. Metals* **2**, 373–400 (1970).
74. C. Wagner and K. E. Zimens, Die Oxydationsgeschwindigkeit von Nickel bei Kleinen Zusätzen von Chrom und Mangan, *Acta Chem. Scand.* **1**, 547–565 (1947).
75. F. A. Kroger, *The Chemistry of Imperfect Crystals*, North-Holland, New York (1964).

76. J. W. Stout and E. Catalano, Heat Capacity of Zinc Fluoride from 11 to 300°K. Thermodynamic Functions of Zinc Fluoride. Entropy and Heat Capacity Associated with the Antiferromagnetic Ordering of Manganous Fluoride, Ferrous Fluoride, Cobaltous Fluoride, and Nickelous Fluoride, *J. Chem. Phys.* **23**, 2013–2022 (1955).
77. T. C. Ehlert, R. A. Kent, and J. L. Margrave, Mass Spectrometric Studies at High Temperatures. VI. The Sublimation Pressure of Nickel(II) Fluoride, *J. Amer. Chem. Soc.* **86**, 5093–5095 (1964).
78. C. F. Hale, E. J. Barber, H. A. Bernhardt, and K. E. Rapp, *High-Temperature Corrosion of Some Metals and Ceramics in Fluorinating Atmospheres*, K-1459, Nuclear Division, Union Carbide Corporation, Oak Ridge, Tenn. (1960).
79. Y. A. Luk'yanychev, I. I. Astakhov, and N. S. Nikolaev, Mechanism of the Formation of Fluoride Films on Nickel and Their Properties, *Bulletin of the Academy of Science of the U.S.S.R., Division of Chemical Science 1965*, 577–581 (1965). [*Izv. Akad. Nauk SSSR, Ser. Khim.* **4**, 588–593 (1965).]
80. R. L. Jarry, W. H. Gunther, and J. Fischer, *The Mechanism and Kinetics of the Reaction Between Nickel and Fluorine*, ANL-6684, Argonne National Laboratory, Argonne, Ill. (1963).
81. R. L. Jarry, J. Fischer, and W. H. Gunther, The Mechanism of the Nickel–Fluorine Reaction, *J. Electrochem. Soc.* **110**, 346–349 (1963).
82. A. H. Singleton, J. F. Tompkins, Jr., S. Kleinberg, and C. J. Sterner, Corrosion of Metals by Liquid Fluorine, *Ind. Eng. Chem.* **57**(3), 47–53 (1965).
83. R. B. Jackson, *Corrosion of Metals and Alloys by Fluorine*, NP-8845, Allied Chemical Corporation, Morristown, N.J. (1960).
84. S. Kleinberg and J. F. Tompkins, *The Compatibility of Various Metals with Liquid Fluorine*, ASD-TDR-62-250, Air Force Systems Command, Wright-Patterson Air Force Base, Ohio (1962).
85. W. A. Cannon, S. K. Asunmaa, W. D. English, and N. A. Tiner, Passivation Reactions of Nickel and Copper Alloys with Fluorine, *Trans. Met. Soc. AIME (Amer. Inst. Mining, Met., Petrol. Eng.)* **242**(8), 1635–1643 (1968).
86. N. F. Mott, A Theory of the Formation of Protective Oxide Films on Metals, *Trans. Faraday Soc.* **35**, 1175–1177 (1939).
87. K. Hauffe and B. Ilschner, The Mechanism of the Oxidation of Nickel at Low Temperatures, *Z. Elektrochem.* **58**, 382–387 (1954).
88. S. Lawroski, W. A. Rodger, R. C. Vogel, and V. H. Munnecke, *Chemical Engineering Division Summary Report—Oct., Nov., Dec. 1959*, ANL-6101, Argonne National Laboratory, Argonne, Ill. (1960).
89. F. J. Kohl and C. A. Stearns, *Vaporization of Chromium Oxide from the Surface of TD-NiCr Under Oxidizing Conditions*, NASA TM X-52879, National Aeronautics and Space Administration, Washington, D.C. (1970).
90. J. D. McKinley, Mass-Spectrometric Investigation of the Nickel–Fluorine Surface Reaction, *J. Chem. Phys.* **45**(5), 1690–1693 (1966).
91. T. W. Godwin and C. L. Lorenzo, *Ignition of Several Metals in Fluorine*, Paper No. 740–58, presented at the American Rocket Society Meeting, New York (Nov. 17–21, 1958).
92. W. H. Gunther and M. J. Steindler, *Laboratory Investigations in Support of Fluid-Bed Fluoride Volatility Processes. Part XIV—The Corrosion of Nickel and Nickel Alloys by Fluorine, Uranium Hexafluoride, and Selected Volatile Fission Product Fluorides at 500°C*, ANL-7241, Argonne National Laboratory, Argonne, Ill. (1966).
93. M. J. Steindler and R. C. Vogel, *Corrosion of Materials in the Presence of Fluorine at Elevated Temperatures*, ANL-5662, Argonne National Laboratory, Argonne, Ill. (1957).
94. E. D. Weisert, Hastelloy Alloy C, *Chem. Eng.* **59**(6), 297–312 (1952).

95. C. Williams, *Reactor Science and Engineering Department Progress Report for January 1–March 31, 1952*, BNL-176, Brookhaven National Laboratory, Upton, N.Y. (1952).
96. A. A. Chilenskas and G. E. Gunderson, *Engineering Development of Fluid-Bed Fluoride Volatility Processes. Part VII—The Corrosion of Nickel in Process Environments*, ANL-6979, Argonne National Laboratory, Argonne, Ill. (1965).
97. L. E. Trevorrow and W. H. Gunther, *Fluorine Corrosion Test of Nickel–Thoria Material*, ANL-6687, Argonne National Laboratory, Argonne, Ill. (1963).
98. J. W. Johnson, D. Cubicciotti, and C. M. Kelly, Interactions of Metals with Their Molten Salts. I. The Nickel–Nickel Chloride System, *J. Phys. Chem.* **62**, 1107–1109 (1958).
99. W. Fisher and R. Gewher, The Thermal Properties of Halides. IX. Melting and Boiling Points and Polarization Effects of the Manganous (Type) Halides, *Z. Anorg. Allgem. Chem.* **222**, 303–311 (1935).
100. J. P. Coughlin, High-Temperature Heat Content of Nickel Chloride, *J. Amer. Chem. Soc.* **73**, 5314–5315 (1951).
101. H. Schafer, L. Bayer, G. Briel, K. Etzel, and K. Krehl, Sättigungsdrucke der Chloride $MnCl_2$, $FeCl_2$, $CoCl_2$ und $NiCl_2$, *Z. Anorg. Allgem. Chem.* **278**, 300–309 (1959).
102. K. L. Tseitlin and V. A. Strunkin, Effect of Water Vapor Concentration on the Corrosion of Metals by Chlorine, *J. Appl. Chem. USSR* **29**(11), 1793–1800 (1956). [*Zh. Prikl. Khim.* **29**(11), 1664–1672 (1956).]
103. K. L. Tseitlin, Effects of Water Vapor on the Corrosion of Metals by Chlorine, *Zh. Prikl. Khim.* **29**, 1182–1191 (1956).
104. A. A. Murashkina, Production of Fittings Corrosion-Resistant to Chlorine at the Zhdanov Heavy Machine Construction Plant, *Tekhnol. Organ. Proizvod.* **1971**(5), 57–58 (1971).
105. B. J. Downey, J. C. Bermel, and P. J. Zimmer, Kinetics of the Nickel–Chlorine Reaction at Temperatures Between 350 and 600°C, *Corrosion* **25**(12), 502–508 (1969).
106. P. J. Zimmer, Personal Communication, Department of Chemistry, Villanova University, Villanova, Pa. (Aug. 1973).
107. K. L. Tseitlin and V. A. Strunkin, Effect of Dilution of Chlorine with Nitrogen on the Corrosion of Metals at High Temperatures, *J. Appl. Chem. USSR* **31**, 1832–1838 (1958). [*Zh. Prikl. Khim.* **31**, 1843–1849 (1958).]
108. K. L. Tseitlin, Effect of Temperature in Corrosion of Metals by Chlorine, *J. Appl. Chem. USSR* **28**(5), 467–472 (1955). [*Zh. Prikl. Khim.* **28**(5), 490–496 (1955).]
109. K. Hauffe and J. Hinrichs, High-Temperature Corrosion of Nickel in Chlorine and Chlorine–Oxygen Mixtures, *Werkst. Korros.* **21**(11), 954–965 (1970).
110. J. D. McKinley, Mass-Spectrometric Investigation of the High-Temperature Reaction Between Nickel and Chlorine, *J. Chem. Phys.* **40**(1), 120–125 (1964).
111. J. D. McKinley, Jr., and K. E. Shuler, Kinetics of the High-Temperature Heterogeneous Reaction of Chlorine and Nickel Between 1200 and 1700°K, *J. Chem. Phys.* **28**, 1207–1212 (1958).
112. P. J. Gegner and W. L. Wilson, Corrosion Resistance of Titanium and Zirconium in Chemical Plant Exposures, *Corrosion* **15**, 341t–350t (1959).
113. R. S. Sheppard, D. R. Hise, P. J. Gegner, and W. L. Wilson, Performance of Titanium vs. Other Materials in Chemical Plant Exposures, *Corrosion* **18**, 211t–218t (1962).
114. M. H. Brown, W. B. DeLong, and J. R. Auld, Corrosion by Chlorine and by Hydrogen Chloride at High Temperatures, *Ind. Eng. Chem.* **39**, 839–844 (1947).
115. J. Halfdanarson and K. Hauffe, High-Temperature Chlorination of Nickel and Nickel–Chromium Alloys, *Werkst. Korros.* **24**(1), 8–15 (1973).
116. H. Schafer and H. Jacob, Sättigungsdrucke über Nickelbromid, *Z. Anorg. Allgem. Chem.* **286**, 56–57 (1956).
117. G. S. Haines, Materials for Bromine Containers, *Ind. Eng. Chem.* **41**, 2792–2797 (1949).

118. D. E. Lake and A. A. Gunkler, Moisture: Key to Bromine Corrosion, *Chem. Eng.* **67**, 137–138 (1960).
119. L. Gal-Or, Corrosion of Metals by Bromine, *Hamatekhet* **1971**(4), 1–3 (1971).
120. P. D. Miller, E. F. Stephan, W. E. Berry, and W. K. Boyd, Corrosion Resistance of Nickel and Two Nickel Alloys to Gaseous Bromine, BMI-X-489, Battelle Memorial Institute, Columbus, Ohio (1968).
121. J. D. McKinley, Mass-Spectrometric Investigation of the Nickel–Bromine Surface Reaction, *J. Chem. Phys.* **40**(2), 576–581 (1964).
122. R. F. Rolsten, *Iodide Metals and Metal Iodides*, John Wiley, New York (1961).
123. V. I. Ginzburg and O. I. Kabakova, Corrosion Stability of Metals in Iodine and Iodine-Containing Media, *Zashch. Metal.* **5**(6), 627–632 (1969).
124. N. S. Mott, Materials Selection Chart, *Chem. Eng.* **57**(8), 197–200 (1950).
125. L. Arbellot, Behavior of Nickel and Its Alloys in the Presence of Halogens, *Corros. et Anticorros.* **5**, 112–119 (1957).
126. H. von Wartenberg, Copper Fluoride, *Z. Anorg. Allgem. Chem.* **241**, 381–394 (1939).
127. H. M. Haendler, L. H. Towle, E. F. Bennett, and W. L. Patterson, Jr., The Reaction of Fluorine with Copper and Some of Its Compounds. Some Properties of Copper(II) Fluoride, *J. Amer. Chem. Soc.* **76**, 2178–2179 (1954).
128. R. A. Kent, J. D. McDonald, and J. L. Margrave, Mass-Spectrometric Studies at High Temperatures. IX. The Sublimation Pressure of Copper(II) Fluoride, *J. Phys. Chem.* **70**, 874–877 (1966).
129. J. Gillardeau, L. M. Vincent, and J. Oudar, Behavior of Copper in Gas Fluorinating Medium, *Metallurgie (Mons, Belg.)* **6**(3), 125–132 (1966).
130. S. M. Toy, W. D. English, and W. E. Crane, Studies of Galvanic Corrosion Couples in Liquid Fluorine, *Corrosion* **24**(12), 418–421 (1968).
131. J. D. Jackson, Corrosion in Cryogenic Liquids, *Chem. Eng. Progr.* **57**(4), 61–64 (1961).
132. J. M. Crabtree, C. S. Lees, and K. Little, The Copper Fluorides. Part I—X-Ray and Electron Microscope Examination, *J. Inorg. Nucl. Chem.* **1**, 213–217 (1955).
133. Y. A. Luk'yanychev, N. S. Nikolaev, I. I. Astakhov, and V. I. Luk'yanychev, A Study of the Mechanism of Copper Fluorination at High Temperatures, *Dokl. Akad. Nauk SSSR* **147**(5), 1130–1132 (1962).
134. U. R. Evans, Crack-Heal Mechanism of the Growth of Invisible Films on Metals, *Nature* **157**, 732 (1946).
135. N. F. Mott and N. Cabrera, Theory of the Oxidation of Metals, *Rept. Progr. Phys.* **12**, 163–184 (1949).
136. J. Gillardeau, Y. Macheteau, P. Plurien, and J. Oudar, Some Aspects of the Fluorination of Copper and Iron, *Oxid. Metals* **2**(3), 319–330 (1970).
137. J. Gillardeau, Thesis, Atomic Energy Commission, France, Report 3212, Faculté des Sciences, Paris (1967).
138. P. M. O'Donnell and A. E. Spakowski, *Reaction of Copper and Fluorine from 800° to 1200°F*, NASA-TN-D-768, National Aeronautics and Space Administration, Washington, D.C. (1961).
139. M. J. Steindler and R. C. Vogel, *Corrosion of Metals in Gaseous Fluorine at Elevated Temperatures*, ANL-5560, Argonne National Laboratory, Argonne, Ill. (1957).
140. J. Gillardeau, L. Vincent, and J. Oudar, The Existence of a Nucleation Phenomenon in the Reaction of Fluorine on Copper, *C.R. Acad. Sci., Ser. C* **263**(25), 1469–1472 (1966).
141. J. Gillardeau and P. Plurien, *Contribution à l'étude de la fluoruration du cuivre*, in Proceedings of the 6th International Symposium on the Reactivity of Solids, John Wiley, New York (1969).
142. R. Landau and R. Rosen, Industrial Handling of Fluorine, *Ind. Eng. Chem.* **39**(3), 281–286 (1947).

143. G. Brauer, *Handbook of Preparative Inorganic Chemistry*, Academic Press, New York (1963).
144. C. M. Fontana, E. Gorin, G. A. Kidder, and C. S. Meridith, Chlorination of Methane with Copper Chloride Melts, *Ind. Eng. Chem.* **44**, 363–368 (1952).
145. R. A. J. Shelton, Vapor Pressures of Solid Copper(I) Halides, *Trans. Faraday Soc.* **57**, 2113–2118 (1961).
146. American Brass Company, Corrosion Resistance of Copper and Copper Alloys, *Chem. Eng.* **58**(1), 108–112 (1951).
147. K. L. Tseitlin, Corrosion of Metals by Chlorine at High Temperatures, *J. Appl. Chem. USSR* **27**(9), 889–893 (1954). [*Zh. Prikl. Khim.* **27**(9), 953–958 (1954).]
148. K. L. Tseitlin, The Effect of Air on the Corrosion of Metals by Chlorine at High Temperatures, *J. Appl. Chem. USSR* **29**, 253–259 (1956). [*Zh. Prikl. Khim.* **29**, 229–235 (1956).]
149. L. G. Harrison and C. F. Ng, Reactivity and Catalytic Activity of Copper Chlorides. I. Kinetics of the Reaction of Copper(I) Chloride with Chlorine, *Trans. Faraday Soc.* **67**(6), 1787–1800 (1971).
150. Le-Van-My, G. Perinet, and P. Bianco, Thermal Modification of Copper Iodide and Copper Bromide, *Bull. Soc. Chim. France* **1965**, 3651–3654 (1965).
151. J. Krug and L. Sieg, Die Struktur der Hochtemperatur-Modifikationen des CuBr und CuI, *Z. Naturforsch. A* **7a**, 369–371 (1952).
152. Brussels University, *A Survey of Some Metal Oxidation Problems*, EURAEC-1619, Quarterly Report No. 13, Jan. 1–Mar. 31, 1966, U.S. Atomic Energy Commission, Washington, D.C. (1966).
153. Brussels University, *A Study of Some Metal Oxidation Problems. Solid Gas Reactions Study Section: Oxidation of Metals*, EURAEC-1897, Final Report No. 3, U.S. Atomic Energy Commission, Washington, D.C. (1967).
154. R. W. G. Wyckoff, *Crystal Structures*, Vol. I, Wiley-Interscience, New York (1963).
155. R. W. G. Wyckoff, *Crystal Structures*, Vol. II, Wiley-Interscience, New York (1964).
156. K. F. Zmbov and J. L. Margrave, Mass-Spectrometric Studies at High Temperatures. XV. Sublimation Pressures of Chromium, Manganese, and Iron Trifluorides and the Heat of Dissociation of $\text{Fe}_2\text{F}_6(\text{g})$, *J. Inorg. Nucl. Chem.* **29**, 673–680 (1967).
157. R. A. Kent and J. L. Margrave, Mass-Spectrometric Studies at High Temperatures. VIII. The Sublimation Pressure of Iron(II) Fluoride, *J. Amer. Chem. Soc.* **87**, 4754–4756 (1965).
158. Y. Macheteau, J. Gillardeau, P. Plurien, and J. Oudar, Fluorination Kinetics of Iron, *Oxid. Metals* **4**(3), 141–149 (1972).
159. P. M. O'Donnell, Kinetics of the Fluorination of Iron, NASA-TN-D-3575, National Aeronautics and Space Administration, Washington, D.C. (1966).
160. P. M. O'Donnell, Kinetics of the Fluorination of Iron, *J. Electrochem. Soc.* **114**(3), 218–221 (1967).
161. U. R. Evans, *The Corrosion and Oxidation of Metals: Scientific Principles and Practical Applications*, St. Martin's Press, New York (1960).
162. G. Heinemann, F. G. Garrison, and P. A. Haber, Corrosion of Steel by Gaseous Chlorine, *Ind. Eng. Chem.* **38**, 497–499 (1946).
163. S. F. Bohlken, A. Klinkenberg, and H. W. Nicolai, Reaction of Iron with Gaseous Chlorine, *Ind. Chim. Belge.* **20**, Special Number, 579–581 (1955).
164. S. F. Bohlken, A. Klinkenberg, and H. W. Nicolai, Reaction of Iron with Gaseous Chlorine, *C.R. Congr. Intern. Chim. Ind.* **27**^o, 2–4 (1954).
165. R. J. Fruehan, The Rate of Chlorination of Metals and Oxides. Part I. Fe, Ni, and Sn in Chlorine, *Met. Trans.* **3**(10), 2585–2592 (1972).
166. W. A. Luce and R. B. Seymour, Construction Materials in the Paper Industry. Part. II. Bleaching, *Chem. Eng.* **57**(10), 217–223 (1950).

167. S. D. Kirkpatrick and J. R. Callahan, Fourteenth Annual Report on Materials of Construction, *Chem. Eng.* **57**(11), 107–154 (1950).
168. M. R. Bloch, A. Bodenheimer, J. A. Epstein, and I. Schnerb, Prevention of Corrosion of Stainless Steel by Molecular Bromine, *Corrosion Sci.* **11**(1), 453–461 (1971).
169. L. Gal-Or, Corrosion of Metals by Bromine, *Hamatekhet* **1971**(4), 1–3 (1971).
170. E. I. Gurovich, Kinetics of the Formation of Corrosion Centers on Metals, *Bull. Acad. Sci. U.R.S.S., Cl. Sci. Math. Nat., Sér. Khim.* **1937**, 1453–1484 (1937).
171. F. W. Fink and E. L. White, Corrosion Effects of Liquid Fluorine and Liquid Oxygen on Materials of Construction, *Corrosion* **17**(2), 58t–60t (1961).
172. W. Davis, Jr., and F. D. Rosen, Constant Pressure Apparatus for Studying Reaction Rates, *Rev. Sci. Instrum.* **23**, 332–334 (1952).
173. M. G. Evans, The Attack of Aluminum by Chlorine. I. High-Pressure (100–600 torr) Investigation, *Mem. Proc. Manchester Lit. Phil. Soc.* **79**, 13–28 (1935).
174. H. P. Godard, W. B. Jepson, M. R. Bothwell, and R. L. Kane, The Surface Oxide Film on Aluminum, in *The Corrosion of Light Metals*, John Wiley, New York (1967).
175. E. Rabald, *Corrosion Guide*, American Elsevier, New York (1968).
176. E. R. Hodges, Further Notes on Aluminum, *Chem. News* **123**, 141 (1921).
177. L. R. Horst, Aluminum, *Chem. Eng. (New York)* **59**(5), 300–316 (1952).
178. P. M. O'Donnell, *Kinetics of the Fluorination of Beryllium*, NASA-TN-D-3992, National Aeronautics and Space Administration, Washington, D.C. (1967).
179. P. M. O'Donnell, Kinetics of the Fluorination of Beryllium, *J. Electrochem. Soc.* **114**, 1206–1209 (1967).
180. J. S. Lukesh, *Research on the Problem of Ductility in Beryllium*, NP-7706, Progress Report No. 2, Wright Air Development Center, Wright-Patterson Air Force Base, Ohio (1958).
181. M. Lemarchands and M. Jacob, Effect of Temperature on Phenomena of Chemical Inertia (Especially the Action of Chlorine on Metals), *Bull. Soc. Chim.* **53**, 1139–1144 (1933).
182. V. A. Fedoseev, Combustion of Magnesium and Aluminum Particles in Different Media, *Fiz. Aerodispersnykh Sist.* **1970**(3), 61–72 (1970).
183. L. McCulloch, Reactions of Magnesium and Aluminum with Iodine and with Concentrated Sulfuric Acid, *J. Chem. Educ.* **24**, 240 (1947).
184. J. H. Cabaniss and J. G. Williamson, *A Literature Survey of the Corrosion of Metal Alloys in Liquid and Gaseous Fluorine*, NASA-TM-X-54612, National Aeronautics and Space Administration, Washington, D.C. (1963).
185. D. A. Huggins, Kinetics of the Reactions of Metallic Sodium with Chlorine, Bromine, and Oxygen, *Diss. Abstr.* **26**(5), 2494–2495 (1965).
186. A. Tamisier, Chemical Inertness and Temperature, *Bull. Union Physicians* **61**(493), 261–263 (1967).
187. G. L. Ericson, W. K. Boyd, and P. D. Miller, *Corrosion of Titanium and Titanium-Base Alloys in Liquid and Gaseous Fluorine*, NP-6729, Battelle Memorial Institute, Columbus, Ohio (1958).
188. M. J. Steindler, D. V. Steidl, and R. K. Steunenberg, *The Fluorination of Metallic Titanium*, ANL-6002, Argonne National Laboratory, Argonne, Ill. (1959).
189. E. E. Millaway and M. H. Kleinman, Factors Affecting Water Content Needed to Passivate Titanium in Chlorine, *Corrosion* **23**(4), 88–97 (1967).
190. Imperial Chemical Industries, Ltd., Failure of Titanium in Dry Chlorine, *Tappi* **44**, 183A–184A (1961).
191. G. E. Hutchinson and P. H. Permar, Corrosion Resistance of Commercially Pure Titanium, *Corrosion* **5**(10), 319–325 (1949).
192. R. K. Swandby, Corrosion Charts: Guide to Materials Selection, *Chem. Eng.* **69**(11), 186–201 (1962).

193. K. Shimizu, Corrosion Resistance of Titanium to Chlorine and Chlorides, *Chitanium Jirukoniumu* **15**(2), 39–43 (1967).
194. I. Y. Klinov and V. V. Andreeva, Titanium and Its Alloys as a Material of Construction, *Khim. Mashinostroenie* **1960**(4), 5–8 (1960).
195. L. B. Golden, I. R. Lane, Jr., and W. L. Acherman, Corrosion Resistance of Titanium, Zirconium, and Stainless Steel in Mineral Acids, *Ind. Eng. Chem.* **44**, 1930–1935 (1952).
196. K. L. Tseitlin, L. L. Faingol'd, and V. A. Strunkin, Chemical Stability of Titanium in Halogen Acids and Halides, *Metalloved. Titana, Akad. Nauk SSSR, Gos. Kom. Sov. Min. SSSR po Chern. i Tsvetn. Met., Inst. Met., Tr. Pyatogo Soveshch., Moscow* **1963**, 150–159 (1964).
197. O. J. C. Runnalls and L. M. Pidgeon, Observations on the Preparation of Iodide Titanium, *J. Metals* **4**, 843–847 (1952).
198. O. Glemser, H. Roesky, and K. H. Hellberg, Preparation of Chromium(V) Fluoride and Chromium(VI) Fluoride, *Angew. Chem. Intern. Ed. Engl.* **2**, 266–267 (1963). [*Angew. Chem.* **75**, 346 (1963).]
199. A. J. Edwards, Chromium Pentafluoride and Chromium Oxide Tetrafluoride, *Proc. Chem. Soc.* **1963**, 205 (1963).
200. R. J. Sime and N. W. Gregory, Vaporization of Chromium(III) Bromide. Evidence for Chromium(IV) Bromide, *J. Amer. Chem. Soc.* **82**, 93–96 (1960).
201. R. L. Jarry, W. H. Gunther, and J. Fisher, *Metal-Fluorine Reactions*. Chemical Engineering Division Summary Report for Jan. Feb., Mar. 1960, ANL-6145, pp. 110–114, Argonne National Laboratory, Argonne, Ill.
202. L. Stein and R. C. Vogel, *The Behavior of Uranium, Thorium, and Other Selected Materials in Bromine Trifluoride, Bromine Pentafluoride, Chlorine Trifluoride, and Fluorine at Elevated Temperatures*, ANL-5441, Argonne National Laboratory, Argonne, Ill. (1955).
203. A. Garlick and P. D. Wolfenden, Fracture of Zirconium Alloys in Iodine Vapor, *J. Nucl. Mater.* **41**(3), 274–292 (1971).
204. A. Garlick, Stress-Corrosion Cracking of Zirconium Alloys in Iodine Vapor, *Eff. Environ. Mater. Prop. Nucl. Syst., Proc. Intern. Conf. Corrosion* **1971**, 21–35 (1971).
205. J. C. Wood, *Stress-Corrosion Cracking of Zirconium Alloy Fuel Sheaths in Iodine Vapor*, AECL-4353, Chalk River Nuclear Laboratory, Chalk River, Ontario, 13–15 (1972).
206. A. L. Percy, Tantalum, *Chem. Eng.* **59**(4), 259–264 (1952).
207. W. E. Pratt, L. R. Scribner, and C. G. Chisholm, Wet and Dry Chlorine vs. Materials of Chemical Plant Construction, *Chem. Eng.* **54**(2), 219 (1947).
208. G. Gottschalk and G. M. Neumann, Simulation of Heterogeneous Gas Equilibria. I. Metal-Halogen Systems with Examples for Tungsten-Halogen Systems, *Z. Metallk.* **62**(12), 910–915 (1971).
209. M. Iwasaki, T. Yahata, K. Suzuki, and K. Oshima, Reaction of Metallic Tungsten and Fluorine Gas, *Kogyo Kagaku Zasshi* **65**, 1165–1167 (1962). [UCRL-Trans-1044(L), University of California, Berkeley, Calif. (1962).]
210. P. C. Abbott and R. E. Stickney, Quasi-Equilibrium Analysis of the Reaction of Atomic and Molecular Fluorine with Tungsten, *J. Phys. Chem.* **76**(20), 2930 (1972).
211. J. D. McKinley, Jr., Mass-Spectrometric Investigation of the Surface Reaction of Tungsten with Chlorine-Oxygen Mixtures, in *Proceedings of the 6th International Symposium on the Reactivity of Solids*, John Wiley, New York (1969).
212. N. P. Galkin, M. F. Sviderskii, N. P. Petranin, and V. A. Bardin, Kinetics of the Fluorination of Tungsten-Rhenium Melts (at 200–600°C), *Russ. J. Inorg. Chem.* **16**(5), 711–713 (1971). [*Zh. Neorg. Khim.* **16**, 1345–1348 (1971).]
213. C. M. Nelson, G. E. Boyd, and W. T. Smith, Magnetochemistry of Technetium and Rhenium, *J. Amer. Chem. Soc.* **76**, 348 (1954).

214. A. Chow, Losses of Iridium During Heating in Various Atmospheres, *Talanta* **19**(7), 899–902 (1972).
215. Y. I. Ivashentsev and R. I. Timonova, Chlorination of Palladium and Behavior of Its Chloride on Heating, *Russ. J. Inorg. Chem.* **12**(3), 308–310 (1967). [*Zh. Neorg. Khim.* **12**(3), 592–595 (1967).]
216. Y. I. Ivashentsev and R. I. Timonova, Thermographic Study of Platinum Chlorination and Decomposition of Platinum Tetrachloride, *Zh. Vses. Khim. Obshchest.* **12**(1), 109–110 (1967).
217. J. S. Sconce, *Chlorine: Its Manufacture, Properties, and Uses*, Reinhold, New York (1962).
218. P. M. O'Donnell, A Kinetic Study of the Fluorination of Silver, *J. Electrochem. Soc.* **117**(10), 1273–1275 (1970).
219. G. Tammann, The Velocity of Action of Halogens, Oxygen and Nitrogen upon Metals as Judged on the Basis of Their Tempering Colors, *Rec. Trav. Chim.* **42**, 547–551 (1923).
220. V. G. Tammann and W. Koster, The Velocity of Reaction of Oxygen, Hydrogen Sulfide, and Halogens with Metals, *Z. Anorg. Allgem. Chem.* **123**, 196–221 (1922).
221. J. A. Lorenzen, Atmospheric Corrosion of Silver, *Inst. Environ. Sci., Tech. Meet., Proc.* **17**, 110–116 (1971).
222. C. Wagner, Beitrag zur Theorie des Anlaufvorganges. II, *Z. Phys. Chem.* **32B**, 447–462 (1936).
223. C. Wagner, Reactions of Metals and Alloys with Oxygen, Sulphur, and Halogens at High Temperatures, *Pittsburgh Intern. Cong. Surface React.* **1948**, 77–82 (1948).
224. H. B. Linford and M. J. Ford, Corrosion of Silver in a Water-Saturated Chlorine Atmosphere, *Trans. Electrochem. Soc.* **93**(1), 16–26 (1948).
225. J. L. Weininger, Room-Temperature Tarnishing of Silver in Bromine and Iodine, *J. Electrochem. Soc.* **105**, 577–581 (1958).
226. C. Gensch and K. Hauße, Speed of Bromination of Some Silver Alloys, *Z. Phys. Chem.* **195**, 386–393 (1950).
227. K. Hauße and C. Gensch, Über die Bromierungsgeschwindigkeit von Silber–Cadmium–Legierungen, *Z. Phys. Chem.* **195**, 116–128 (1950).
228. D. M. Smyth and M. Cutler, Tarnishing Reactions of Silver in Iodine Atmospheres, *J. Electrochem. Soc.* **106**, 107–113 (1959).
229. G. Tammann, Tarnishing of Metals, *Z. Anorg. Allgem. Chem.* **111**, 78–89 (1921).
230. R. Dubrisay, Periodic Phenomena in the Corrosion of Metals by Vapors, *C.R. Acad. Sci.* **229**, 829–831 (1949).
231. D. Balarew, Disperse Structure of Solid Systems and Its Thermodynamic Foundation, *Kolloid-Z.* **101**, 47–52 (1942).
232. A. Landsberg and C. L. Hoatson, Kinetics and Equilibriums of the Gold–Chlorine System, *J. Less-Common Metals* **22**(3), 327–339 (1970).
233. S. Lawroski, R. C. Vogel, M. Levenson, and V. H. Munnecke, *Chemical Engineering Division Quarterly Report—Jan., Feb., Mar. 1963*, ANL-6687, Argonne National Laboratory, Argonne, Ill. (1963).
234. H. M. Haendler, W. L. Patterson, Jr., and W. J. Bernard, The Reaction of Fluorine with Zinc, Nickel, and Some of Their Binary Compounds. Some Properties of Zinc and Nickel Fluorides, *J. Amer. Chem. Soc.* **74**, 3167–3168 (1952).
235. M. H. Zirin, The Formation of Cadmium Fluoride by Metal–Fluorine Reaction, *Oxid. Metals* **3**(4), 319–329 (1971).
236. M. H. Zirin, Observation on the Kinetic Behavior of a Parabolic Type Metal–Gas Reaction with Induced Cracks in the Scale: A Note, *Oxid. Metals* **3**(6), 539–544 (1971).
237. H. Sugier, Reaction of Cadmium Iodination and Isotopic Exchange in the $\text{CdI}_2(\text{s})\text{--I}_2(\text{g})$ System, *Nukleonika* **12**, 367–372 (1967).

238. E. Montignie, Action of Iodine on Copper and of Iodine on Mercury, *Bull. Soc. Chim.* **8**, 202–209 (1941).
239. V. A. P'yankov, Rate of Reaction of Several Gases with a Mercury Surface, *Ukr. Khim. Zh.* **28**, 585–589 (1962).
240. R. A. Ogg, Jr., H. C. Martin, and P. A. Leighton, Kinetics of the Vapor-Phase Reaction of Mercury and Halogens, *J. Emer. Chem. Soc.* **58**, 1922–1924 (1936).
241. H. Moissan, Sur la préparation à l'état de pureté du trifluorure de bore et du tétrafluorure de silicium et sur quelques constantes physiques de ces composés, *C.R. Acad. Sci.* **139**, 711–714 (1904).
242. H. Moissan, Nouvelles Recherches sur le Fluor, *Ann. Chim. Phys., Ser. 6* **24**, 224–282 (1891).
243. A. K. Kuriakose and J. L. Margrave, Kinetics of Reaction of Elemental Fluorine. III. Fluorination of Silicon and Boron, *J. Phys. Chem.* **68**, 2671–2675 (1964).
244. V. V. Tyapkina and N. S. Guseva, Interaction of a Silicon Surface with Fluorine and Hydrogen Fluoride, *Russ. J. Phys. Chem.* **40**(5), 573–576 (1966). [*Zh. Fiz. Khim.* **40**(5), 1064–1069 (1966).]
245. M. L. Bernard, A. Cointot, and J. P. Coulombier, Kinetics of the Fluorination of Powdered Silicon by Gaseous Fluorine, *C.R. Acad. Sci., Ser. C* **275**(3), 159–162 (1972).
246. P. S. Brallier, The Chlorination of Metals, *Trans. Amer. Electrochem. Soc.* **49**, 257–266 (1926).
247. J. P. Dismukes and R. Ulmer, Gas-Phase Etching of Silicon with Chlorine, *J. Electrochem. Soc.* **118**(4), 634–636 (1971).
248. S. E. Craig, Jr., Gas-Phase Etching of Silicon with Chlorine, *J. Electrochem. Soc.* **118**(12), 2034–2035 (1971).
249. G. N. Khodalevich, L. G. Sakovich, and V. V. Serebrennikov, Bromination of Silicon in the Presence of Copper and Its Bromides, *Zh. Prikl. Khim.* **45**(8), 1863–1864 (1972).
250. J. I. Carasso and I. Stelzer, The Surface Chemistry of Germanium. II. Erosion by Chlorine, *J. Chem. Soc.* **A1960**, 1797–1803 (1960).
251. D. R. Olander, Surface Chemical Kinetics and Gas-Phase Diffusion in the Germanium–Iodine Reaction, *Ind. Eng. Chem. Fundam.* **6**(2), 178–188 (1967).
252. W. J. Heinecke and S. Ing, Jr., Surface Kinetics and Physics Investigation of the Reaction Between Single-Crystal Germanium and Iodine, *J. Appl. Phys.* **32**, 1498–1504 (1961).
253. I. G. Khar'yuzov, G. A. Kurov, and E. A. Rakova, Local Growing of Epitaxial Films, *Protsessy Rosta Strukt. Monokrist. Sloev. Poluprov., Tr. Simp.* **1**, 296–304 (1966).
254. T. Arizumi and I. Akasaki, Etch Patterns and the Mechanism of Etching of Germanium by Iodine Vapor, *Japan. J. Appl. Phys.* **2**, 143–150 (1963).
255. J. J. Lander and J. Morrison, Low-Energy Electron-Diffraction Study of the Surface Reactions of Germanium with Oxygen and with Iodine, *J. Appl. Phys.* **34**, 1411–1415 (1963).
256. D. R. Olander, Variable Property, Interfacial Velocity, and the Multicomponent Diffusion Effects in the Transport-Limited Reaction of Iodine and Germanium, *Ind. Eng. Chem., Fundam.* **6**(2), 188–194 (1967).
257. N. F. Zakhariya and V. P. Grechanovskii, Iodination of Metallic Germanium, *Ukr. Khim. Zh.* **30**(11), 1141–1142 (1964).
258. H. M. Haendler, S. F. Bartram, W. J. Bernard, and D. Kippax, The Reaction of Fluorine with Tin, Its Oxides and Sulfides, *J. Amer. Chem. Soc.* **76**, 2179–2180 (1954).
259. Y. P. Kuznetsov, E. S. Petrov, and A. I. Vakhrusheva, Chemistry of the Reaction of Tin Oxides with Chlorine in the Presence of a Reducing Agent. III. Reaction of Tin with Chlorine, Phosgene and Tin Tetrachloride, *Izv. Sib. Otd. Akad. Nauk SSSR, Ser. Khim. Nauk* **1968**(5), 30–33 (1968).

- 260. V. Fomin, A. G. Zvezdin, and A. N. Ketov, High-Temperature Process of Tin Chlorination, *J. Appl. Chem. USSR* **44**(2), 409–411 (1971). [*Zh. Prikl. Khim.* **44**(2), 416–418 (1971).]
- 261. C. L. Mantell, Utilization of Chlorine in Recovery of Tin and Tin Salts from Tin Plate Scrap, *Trans. Amer. Electrochem. Soc.* **49**, 267–275 (1926).
- 262. G. Whitaker, Corrosion of Metals in Fluorine and Hydrofluoric Acid, *Corrosion* **6**, 283–285 (1950).
- 263. K. H. Roll, Lead and Lead Alloys, *Chem. Eng.* **60**(2), 264–280 (1953).
- 264. K. H. Roll, Discussion of Corrosion of Metals in Fluorine and Hydrofluoric Acid, *Corrosion* **9**, 74 (1953).
- 265. M. R. Bloch, D. Kaplan, and I. Schnerb, *Storage of Bromine*, Israeli Patent 8660 (Mar. 8, 1956).
- 266. H. Sugier, Isotopic Exchange in the $\text{PbI}_2(s)\text{--I}_2(g)$ System and the Mechanism of Lead Iodination, *Nukleonika* **12**, 357–365 (1967).

OXIDATION OF ZIRCONIUM AND ITS ALLOYS

B. Cox

*Chalk River Nuclear Laboratories
Atomic Energy of Canada Limited
Chalk River, Ontario, Canada*

INTRODUCTION

I have tried to summarize the oxidation behavior of zirconium and its alloys in both gaseous and aqueous environments, and to show how other environments, such as liquid metals, can be considered as special cases of one or other of the main classes. It will be appreciated from the extent of the literature on zirconium alloys (the over-600 references are by no means a complete bibliography) that it was impossible to discuss the details of many of the studies reported. To achieve a comprehensive survey in the space available it has been necessary to present a single coherent view of the field, without perhaps devoting sufficient space to opposing views and the evidence adduced in their favor. I have endeavored to make the references as comprehensive as possible, however, only omitting some early ones that are cited in later publications, which adequately summarized their contents. Readers who may be stimulated to pursue the details of any particular aspect of the field should have little difficulty tracing these other references from the bibliographies of the works that are cited. Finally, if the gaps in our knowledge, which I have attempted to illuminate, provide the inspiration for even one reader to devise experiments which can unambiguously resolve some of the many still unanswered questions, then I will consider this review to have been worthwhile.

Historical Development

Had it not been for the advent of nuclear reactors for propulsion and power production, it is probable that zirconium and its alloys would have remained

largely as laboratory curiosities, used for such minor purposes as photographers' flashbulbs and (until the advent of modern electronic devices) as getters for electronic tubes. Its use in the chemical industry remains of a relatively minor nature since, despite the enormous reductions in the cost of zirconium alloy components as a result of developments in the nuclear industry, it has yet to achieve any economic advantage over other corrosion-resistant alloys.

Our interest in this review, however, will be not in the behavior of zirconium alloys in chemical environments, where the corrosion process results primarily in the removal of metal, but in those environments where the primary physical process is the formation of a surface oxide film by thermally activated processes. By this qualification I have excluded studies of anodic oxide film growth, except for a few instances where anodic oxide films have been used as experimental surrogates for thermally formed films, and where it has been claimed that the results of such experiments are of direct applicability to the mechanism of thermal film growth or degradation.

I also intend, thereby, to exclude discussion of the stress corrosion cracking and liquid metal embrittlement of zirconium alloys, which have been the subject of several recent reviews.^{1,2} The area remaining has been very largely influenced by the development of the nuclear power industry.

Influence of the Nuclear Reactor Industry on Development

In the search for materials for fuel cladding and structural components in nuclear reactors the range of choice has been limited by the desire to achieve:

1. Low neutron capture cross section per unit volume.
2. Adequate strength, creep resistance, and ductility after prolonged irradiation in the reactor coolant.
3. Low oxidation rates such that metal loss and embrittlement from dissolved hydrogen (in water reactors) or oxygen are tolerable for the expected lifetime of the component in the reactor (~ 3 yr for fuel cladding, up to 30 yr for structural members).
4. Absence of interactions with the fuel material and fission products.

For gas-cooled reactors where temperatures are usually much higher than in water-cooled reactors, zirconium alloys have proved to be marginally useful at the low-temperature end of the spectrum. Thus they have found uses in CO_2 -cooled reactors, but strength and ductility after exposure to low

pressures of oxygen have proved to be inadequate for high-temperature reactors (HTRs) cooled by helium, and their oxidation resistance soon proved to be inadequate for reactors such as the aircraft reactor experiment (ARE).

In water-cooled reactors which operate in the temperature range $300 \pm 50^\circ\text{C}$, zirconium alloys have found extensive use. In systems where characteristic 1 above is of overriding importance for reasons of neutron physics, the choice is virtually restricted to zirconium or one of its alloys. For other water-cooled nuclear reactor systems, where this factor is not of overwhelming importance, the economics of nuclear electricity production provide a strong driving force toward the utilization of zirconium alloys wherever possible in the core of the reactor.

The early knowledge^{3,4} of the oxidation of unalloyed zirconium in oxygen suggested the possibility of the existence of almost ideal behavior for this metal. At low temperatures it apparently oxidized by a continuously decreasing rate law (near to parabolic, or cubic) with no evidence for any oxide breakdown within the duration of the then available information. Thus the oxidation at 500°C in oxygen has been continued for 22 days to a weight gain of 100 mg/dm^2 , and to twice this weight at 600°C without any evidence for oxide breakdown.⁵⁻⁷ Similar behavior at 350°C would result in 200 years oxidation without breakdown and a metal loss of less than 0.001 inch in this period (Fig. 1).

Unfortunately, the oxidation of unalloyed zirconium in water, rather than oxygen, at $250\text{--}360^\circ\text{C}$ soon produced evidence (Fig. 1) that its behavior was very much less than ideal.^{3,8} The subsequent history of zirconium alloy development for all reactor systems has been determined by the necessity to delay the breakdown of the protective oxide film for as long as possible, and at as high a temperature as possible, since it was subsequently learned that zirconium oxidizing in oxygen also underwent a transition. Although this transition occurred later in gaseous atmospheres than in water at equivalent temperatures, it nevertheless proved to occur too early for any reactor system to contemplate the use of unalloyed zirconium. In gas-cooled reactors this choice was further complicated by the necessity of producing alloys with better mechanical as well as oxidation properties at the operating temperature. In water-cooled reactors, while better mechanical properties have usually been desirable, it was the poor corrosion behavior of unalloyed zirconium which provided the main driving force for development.

As a result of these historical origins the courses taken by studies of zirconium oxidation show some interesting differences from locale to locale.

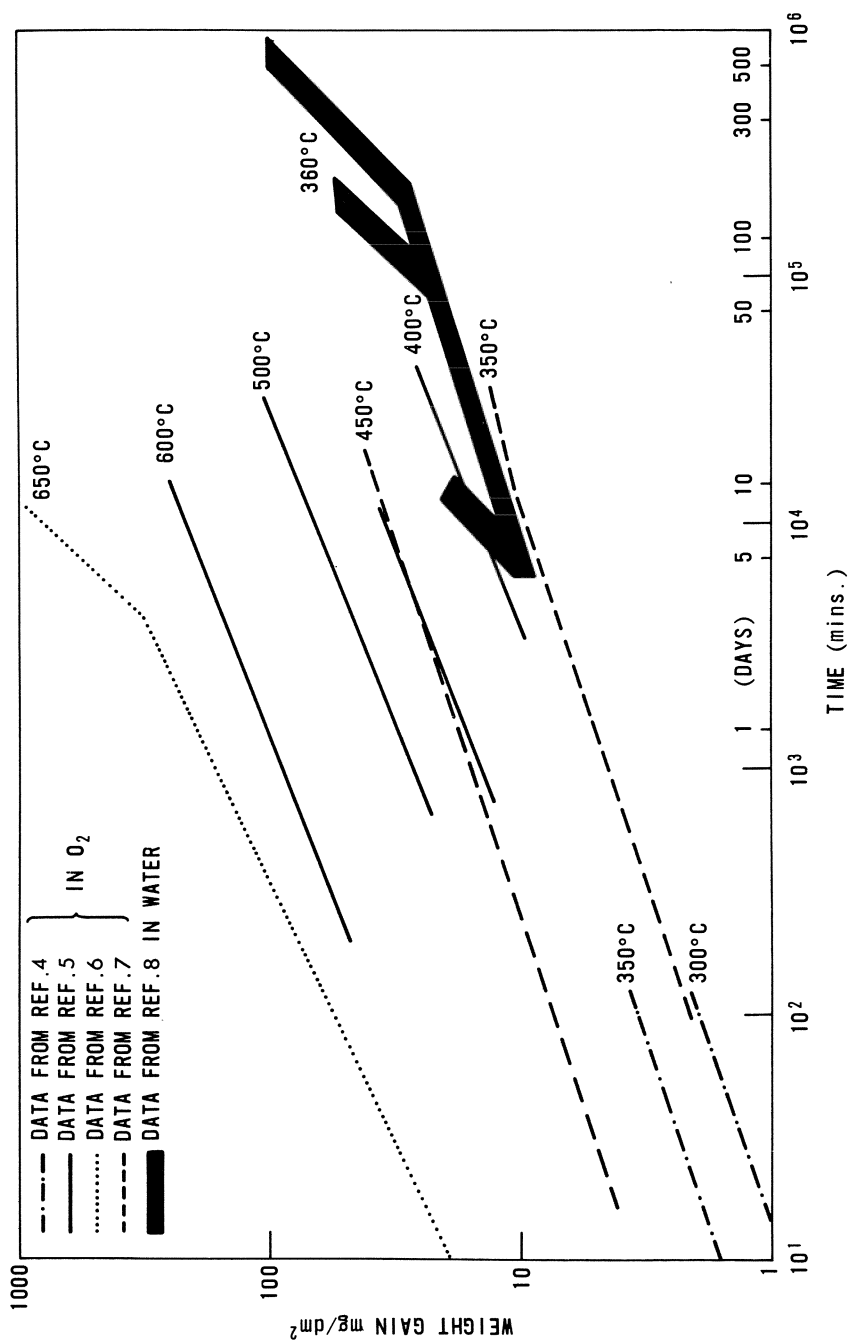


Fig. 1. Long-term oxidation of unalloyed zirconium in oxygen and water at 300–650°C. The three branches of the water curve correspond to the behavior of different grades of zirconium.

Thus, because of the general inadequacy of unalloyed zirconium for use in any reactor system, studies of this material have been largely restricted to university laboratories. Few such studies have emanated from government laboratories since the early days of the nuclear program. Studies of zirconium alloys have by contrast been almost exclusively restricted to government laboratories, particularly those studies in environments typical of nuclear reactors. As is to be expected, the zirconium alloy oxidation studies in any country are extensively colored by the route taken by the national nuclear program. Most continuing studies on corrosion in water reactors, for instance, have emanated from U.S. and Canadian laboratories, with some earlier contributions from the United Kingdom, whereas the studies of alloys in gaseous environments (especially CO_2) have been concentrated in the United Kingdom and latterly in France. The fact that no practical power reactor system uses air or oxygen as a coolant (or cover gas) has, after some small interest during the ARE programme,⁹ led to the almost exclusive restriction of studies in these gases to university laboratories.

Because of the strong segregation of the zirconium oxidation field, which has arisen in the above manner, it has been decided to subdivide the subject matter according to environment, at least as far as the phenomenological studies are concerned.

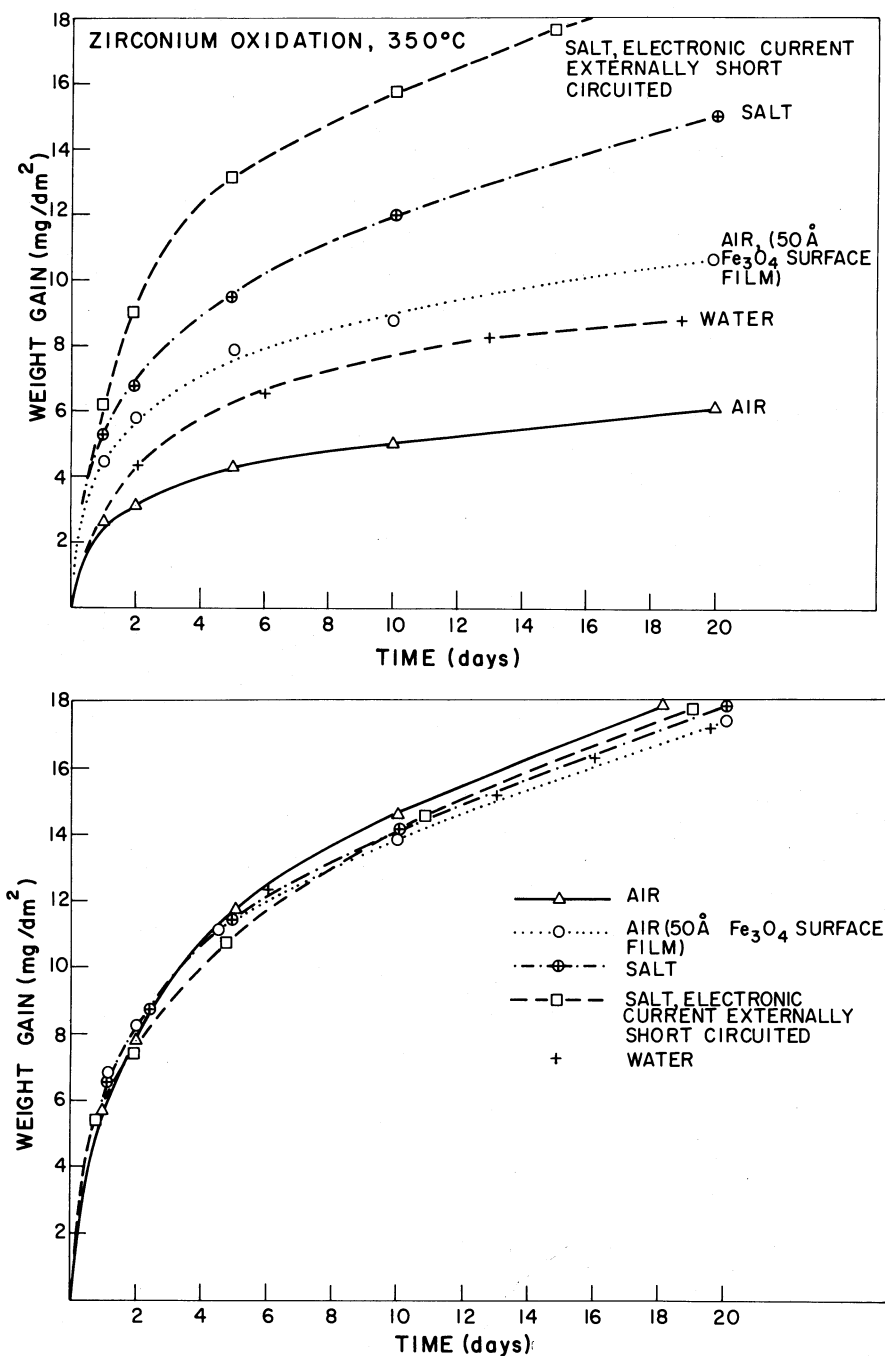
The strong similarities between behavior in all environments where oxide film formation is the primary rate-limiting process become more important when the mechanistic aspects of the field are discussed, and so we will attempt to provide a single coherent framework for contemplating these features.

Comparison of General Features of Gaseous Oxidation and Aqueous Corrosion

Before proceeding with the proposed segregation according to oxidation environment it may be worthwhile to draw some general comparisons between oxidation behavior in various environments. When we consider the behavior of an alloy such as one of the Zircalloys (Table 1) we find that at the same temperature the oxidation curves are identical in a number of environments. Figure 2 shows curves at 350°C in water, air, a fused salt mixture, and in air for specimens coated with a thin layer of iron oxide. The kinetic curves for Zircaloy-2 are effectively identical, whereas significant differences in rate are found for zirconium under these conditions. The similarity in the shape of the kinetic curves for zirconium and Zircaloy-2

Table 1. Compositions of the Zircaloy Series of Alloys⁸

Alloying addition (wt. %)	Zircaloy 1	Zircaloy 2	Zircaloy-3			Nickel-free Zircaloy-2	Zircaloy 4							
			a	b	c									
Sn	2.5	1.50 (1.20–1.70)	0.25	0.50	0.50	1.50 (1.20–1.70)	1.50 (1.20–1.70)							
Fe	—	0.12 (0.07–0.20)	0.25	0.40	0.20	0.15 (0.12–0.18)	0.20 (0.18–0.24)							
Cr	—	0.10 (0.05–0.15)	—	—	—	0.10 (0.05–0.15)	0.10 (0.70–0.13)							
Ni	—	0.05 (0.03–0.08)	—	—	0.20	<0.007	<0.007							
Total Fe, Cr, Ni	—	(0.18–0.38)	—	—	—	—	>0.28							
O (ppm)	—	1000–1400	—	—	—	1000–1400	1000–1400							
Maximum impurity levels:														
Element:	Al	B	Cd	C	Co	Cu	Hf	H	Mn	N	Si	Ti	W	U
ppm:	75	0.5	0.5	270	20	50	200	25	50	80	200	50	100	3.5

Fig. 2. Effect of environment conductivity on oxidation of (a) zirconium; (b) Zircaloy-2.¹⁰

extends to other environments, such as steam, wet organic liquids,¹¹ oxygen-containing sodium,¹² and carbon dioxide,¹³ when allowance is made for the differing effective oxygen pressures in each environment. Further discussion of these observations and conditions under which they do or do not hold will be discussed in the appropriate sections. However, mechanistically we are probably justified in considering all environments in one section and in studying the variations in behavior, which are more evident for unalloyed zirconium than Zircaloy-2, as a particular case.

We will deal with the experimental observations in different media separately, however, since in most instances this has been the way the observations have been carried out. There are many more studies in which the properties of the alloy are varied and the results compared in a single environment than there are studies in which the properties of the specimens are kept as nearly constant as possible and the results compared in a series of widely different environments.

Our aim throughout this review will be to attempt to provide a coherent picture of the phenomena that have been observed, and the best current evaluation of the mechanisms involved. For reasons of space this has necessitated some selectivity in the work discussed, and no attempt has been made to make this review completely comprehensive bibliographically. The reader should be encouraged therefore to examine other recent reviews^{14–17} when he is seeking bibliographic information for any specific aspect of the field.

OXIDATION IN DRY GASES

Oxygen and Air

Kinetics of Oxidation

The early studies of the oxidation of zirconium were generally of relatively short duration, and were often conducted on vacuum microbalances at gas pressures of a fraction of an atmosphere.^{4,5,7} The results (Fig. 3), at least initially, were fitted to a classical parabolic rate law. However, a dispute soon arose as to whether the results best fitted a parabolic or a cubic rate law. Although some longer experiments^{6,7} suggested that a better fit to a cubic rate law could be obtained (Fig. 4) when the initial stage of oxidation was reduced to a minor contributor to the total, this conclusion was not by any means generally accepted. Some investigators have related the closeness

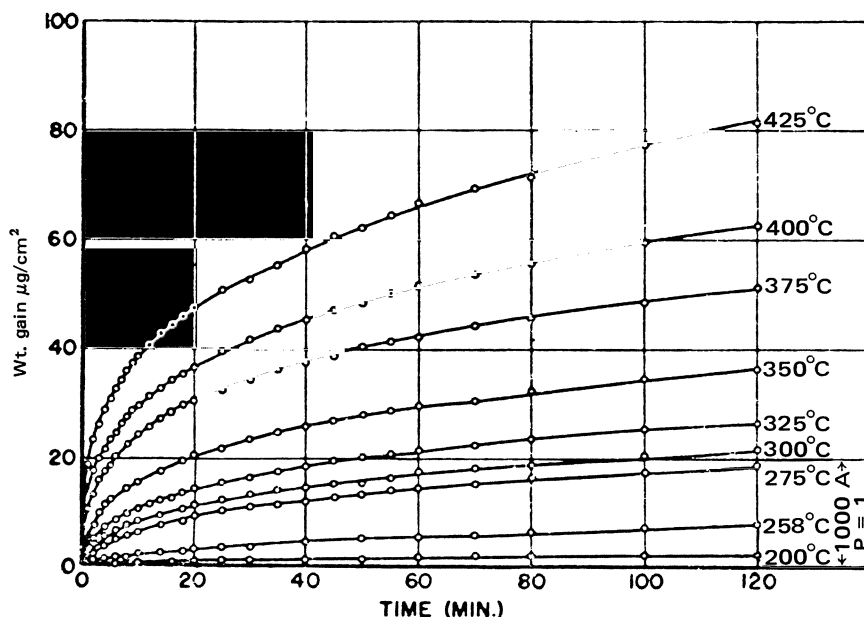


Fig. 3. Typical results for short-term oxidation of zirconium in oxygen.⁴ (By permission of the American Institute of Mining, Metallurgical, and Petroleum Engineers, Inc.)

of fit to either parabolic or cubic kinetics to an effect of surface preparation. A summary of these conclusions was tabulated by Douglass,¹⁴ but scrutiny shows that the correlation of kinetics and surface preparation is far from clear.

A detailed study of the kinetics by Dawson *et al.*^{20,21} showed that the confusion arose because of several changes in the kinetics, which occur during the early stages of oxide growth (Fig. 5) and are each associated with a minor inflection in the weight-gain curve. Thus, the first two periods (0–1 and 1–10 mg/dm²) appear to fit different parabolic laws, whereas a change to cubic kinetics occurs at ~ 10 mg/dm². Much the same argument has arisen about the kinetics during the aqueous oxidation of zirconium alloys and detailed studies (see later) have led to a similar conclusion about minor inflections in the early part of the kinetic curve. The first of these inflections is associated with a change in the electrical conductivity of the oxide,¹⁰ whereas the second marks the end of the period of interference color film growth and its replacement with black oxide.²² The departures from parabolic kinetics are related to the growth and recrystallization of the microcrystalline oxide and several factors, of which surface preparation is only one,²¹ may be important in determining the extent of these deviations.

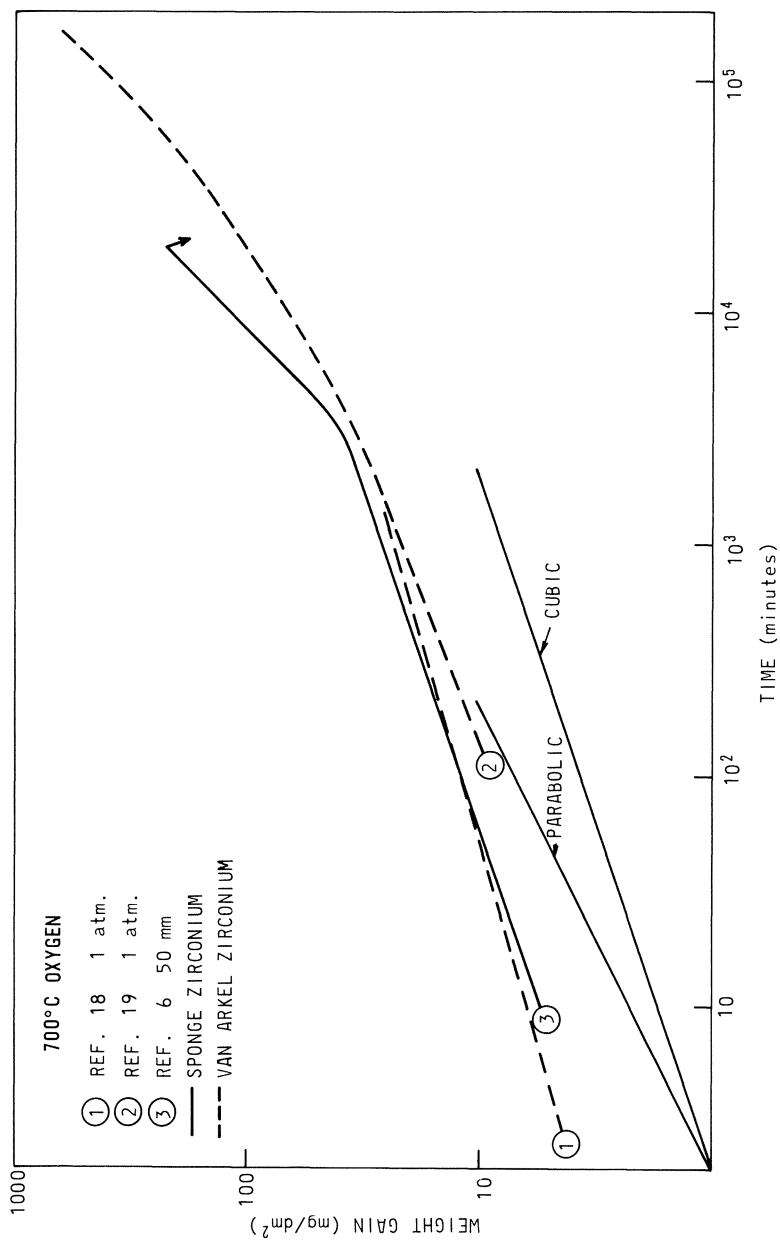


Fig. 4. Results of two long oxidation studies compared with short-term data.

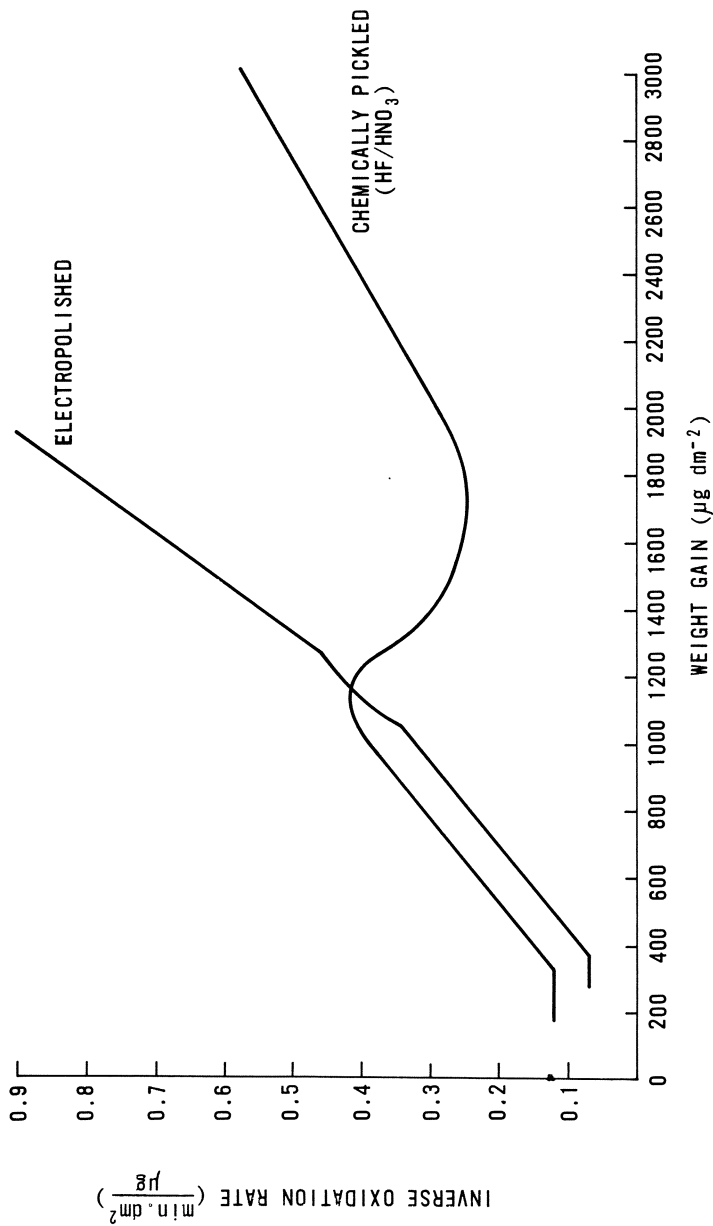


Fig. 5. Inflections in the oxidation rate curve of pickled and chemically polished Zircaloy-2 at $\sim 1 \text{ mg/dm}^2$ weight gain during oxidation in oxygen.²¹

In the light of the above it is probable that all investigators have been correct. Some specimens may behave with nearly parabolic kinetics, some near to cubic kinetics, whereas instances have been observed of specimens showing nearly quartic oxidation kinetics in high-temperature water. Thus while the detailed kinetics during the early part of the film growth curve are of mechanistic interest, we must concede that a range of behavior is possible, and the exact behavior of any specimen is probably only of qualitative value at present.

The short duration of much of the early oxidation work in oxygen did not reveal any breakdown of the oxide film on high-purity zirconium leading to increased oxidation and linear kinetics. Such a transition was evident

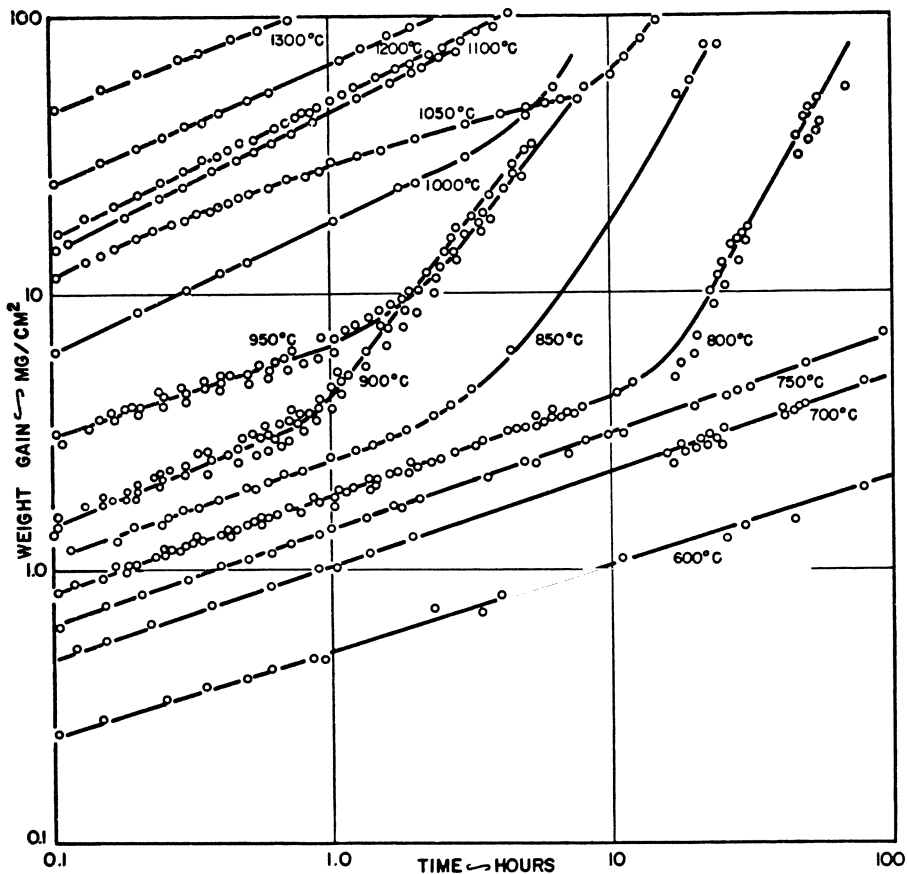


Fig. 6. Transition to linear oxidation kinetics observed in air.²³

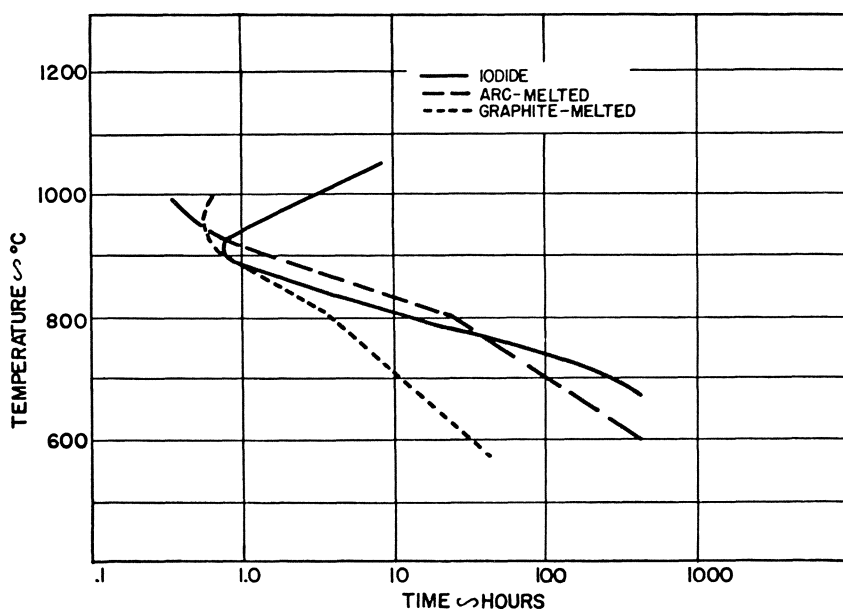


Fig. 7. Effect of temperature on time to transition in air.²³

(Fig. 6) in the high-temperature oxidation of zirconium in air²³⁻²⁵ from the earliest studies, and the dependence of this transition on temperature (Fig. 7), the purity of the zirconium and the composition of the gas phase (Fig. 8) was studied. The transition is accompanied by a visual change from a black oxide to a gray/white oxide, and ultimately at a later stage by oxide spalling.

Another feature of oxidation in air which was much more evident than in oxygen was specimen growth.^{23,24} Increases in specimen area of up to 100 % could be obtained in a few hours in air, whereas several hundred hours were required to achieve the same growth in oxygen (Fig. 8).

For a number of years, therefore, it was thought that the purest zirconium would not undergo oxide breakdown in pure oxygen at relatively low temperatures ($\leq 600^\circ\text{C}$) and that instances of breakdown resulted from impurities in either the metal or the gas.¹³ The long-term oxidation tests of Misch¹⁹ and Hillner⁶ finally demonstrated that this was not the case and that a transition ultimately occurred even for the best zirconium in the cleanest oxygen environments. The much longer times to transition in oxygen than in air for high-purity zirconium are shown by the results in Table 2.

Table 2. Breakaway Times and Growth Rates of Various Grades of Zirconium in Air and Oxygen²⁰

Temp. (°C)	Iodide		Arc-melted Sponge		Graphite melted		Zircaloy-2	
	O ₂	Air	O ₂	Air	O ₂	Air	O ₂	Air
Breakaway time (hr)								
600	>> 300	>> 300	—	300, 82 ^a	—	30, 20 ^b	8, 3 ^d	9 ^a
700	~ 400 ^e	270	100	95, 15 ^a	10	11, 5 ^b	3, 5 ^d	3 ^{a,f}
800	63 ^g	12	13	20	2	4, 2 ^b	3, 2 ^d	—
900	~ 120	0.8	2.5	1	0.5	0.7, 0.5 ^b	—	—
1000	—	3	0.5	0.5	2	0.4, 0.1 ^b	—	—
Growth rate (surface area) (°/hr)								
700	—	0.2	0	0.1	0	0.2 ^b	—	—
800	—	0.5	0.04	0.3	0.02	4, 1.5 ^b	—	—
900	0.2	11	0.8	8	3	30, 9 ^b	—	—
1000	—	9	0.8	8	11	40 ^b	—	—

^a Kendall.²⁴^b Phalnikar and Baldwin.²⁸^c Gulbransen and Andrew.²⁶^d Mallett and Albrecht.²⁷^e Misch.¹⁹^f Extrapolated.^g Hillner.⁶

Subsequent investigators have examined the transition phenomenon metallographically in both air^{28,29} and oxygen.^{30,31} The very localized nature of this process in oxygen, and its inception at cracks which develop in the oxide, is evident (Fig. 9a) from these studies.²⁸⁻³¹ There is also evidence for preferential oxidation at grain boundaries in the early stages of oxidation (Fig. 9b), which is revealed as differences between the oxidation of single crystal and polycrystalline specimens.³² Differences in oxidation rate with crystal orientation may also contribute to this effect.^{50,63}

Variations in the oxidation kinetics of zirconium reported by some workers have been quite considerable. Figures 10 and 11 show some collected data for two temperatures (600 and 850°C), restricted principally by congestion of the curves. While some of the observed variation can be ascribed to differences in zirconium quality, not all of the variation would appear to be explicable in this manner, and we conclude that calibration of specimen temperatures has not always been as good as it might be.

Although most of the studies in air and oxygen have been on zirconium, an alloy such as Zircaloy-2 has often been included for comparison. Results for commercial alloys such as Zircaloy-2 have shown the early transition to a

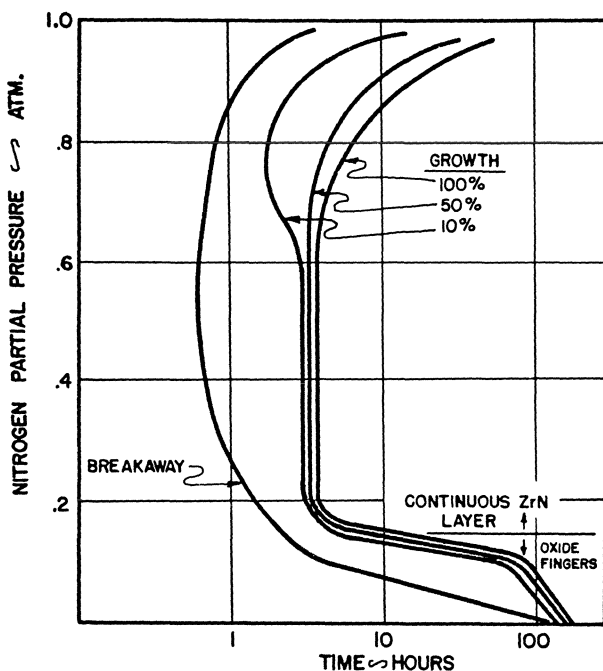


Fig. 8. Effect of gas composition (O_2/N_2 ratio) on transition and specimen growth for iodide zirconium at 900°C .²³

linear rate law (Fig. 12), which is typical of tin-containing alloys, in both oxygen and air, there being no discernible difference between results in the two gases. Prior to this transition the kinetics are similar to and the rates slightly higher than those of zirconium. Reproducibility from laboratory to laboratory also appears to be better for Zircaloy-2 than for zirconium.

Factors Affecting the Oxidation Kinetics

Temperature. Data obtained in oxygen at various oxidation temperatures have been plotted and used to derive an activation energy for the rate-controlling process during pre-transition oxidation (Fig. 13). The conclusions reached are conditioned somewhat by whether the kinetics are required to comply with a parabolic rate law, and the parabolic rate constant is plotted; or whether the often closer approximation to cubic kinetics is acknowledged and the cubic rate constant is plotted. Only the parabolic rate constant has any well-established theoretical significance, however, and the correlation of the results with either diffusion of oxygen in the oxide or metal has only a

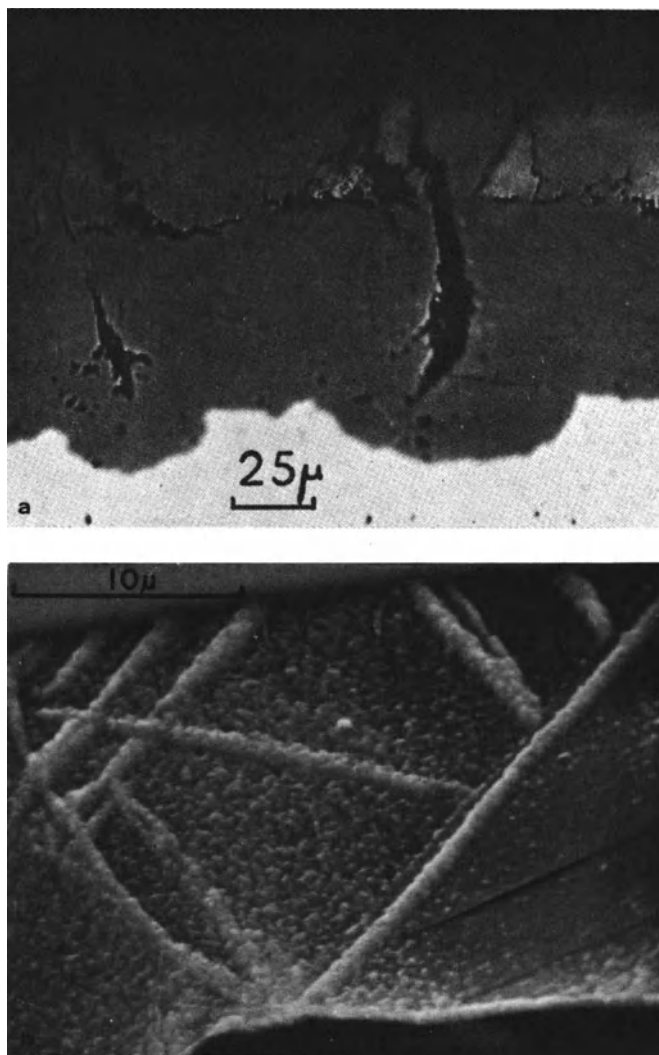
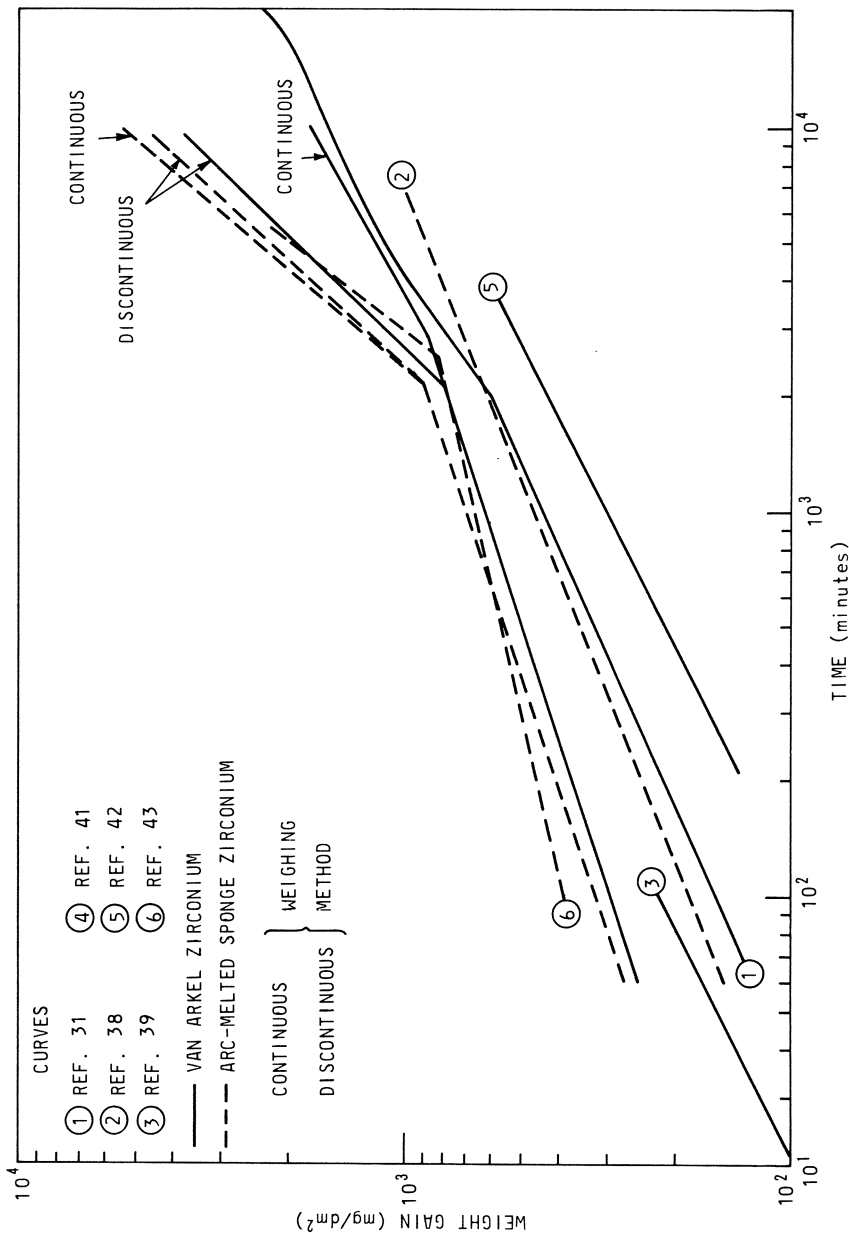


Fig. 9. Irregular development of the oxide/metal interface produced by (a) cracking of the oxide at high temperatures³⁰; (b) preferential oxidation along grain and twin boundaries at low temperatures.²² (By permission of Elsevier Sequoia, S.A.)

qualitative significance due to the absence of a quantitative theory which establishes the cubic kinetics.

The results obtained in air are very similar to those obtained in oxygen prior to the transition. The occurrence of transition shows an interesting



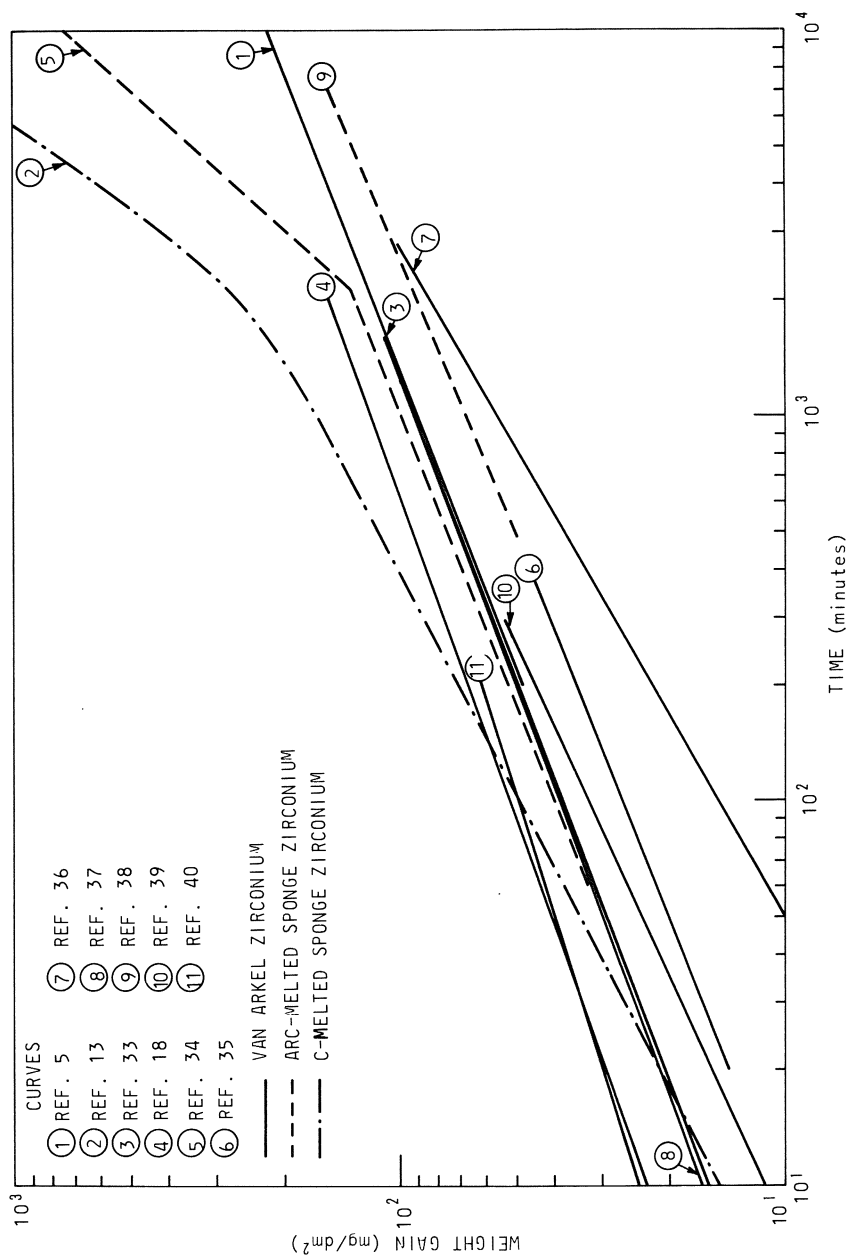


Fig. 11. Comparison of published oxidation curves from a number of laboratories for oxidation of zirconium at 850°C in oxygen.

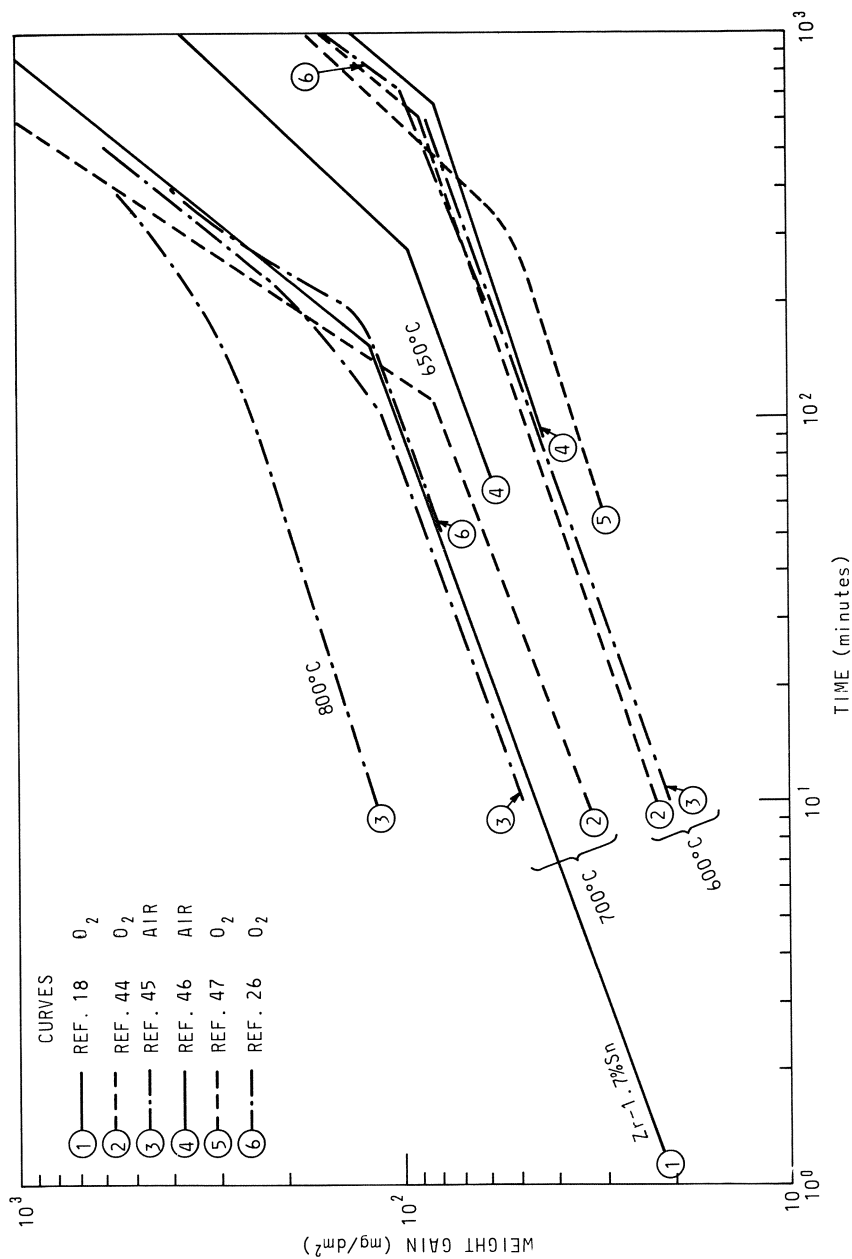


Fig. 12. Comparison of published oxidation curves from a number of laboratories for oxidation of Zircaloy-2 at 600–800°C in oxygen and air.

variation with temperature (Fig. 6), which is at least in part due to the increasing fraction of oxygen going into solution in the metal as the temperature is increased, and partly due to the changing proportion of nitride formed.

Pressure. Over the range of pressures from 1 atm to a few millimeters of mercury, the pre-transition oxidation rate in oxygen is virtually independent of pressure.^{5,18,32,33,48-51} Over much the same range of pressure the pre-transition behavior of Zircaloy-2 is equally independent of pressure in isobaric tests.⁵² However, beyond the transition to linear oxidation kinetics the oxidation rate becomes more sensitive to pressures below ~ 10 mm Hg,^{32,33,52} and particularly to a change in pressure. During oxidation of Zircaloy-2 on a microbalance, an instantaneous change in gas

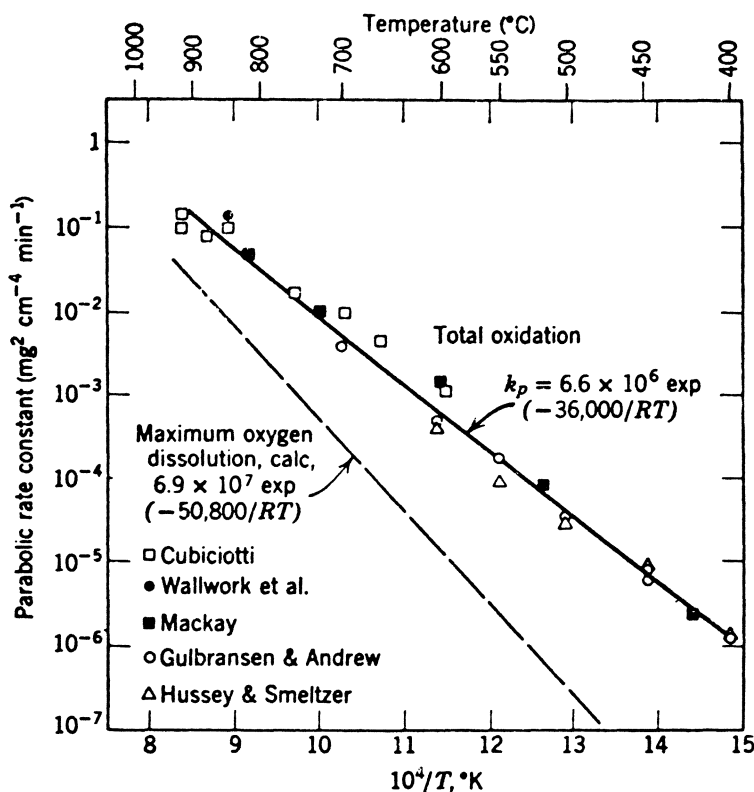
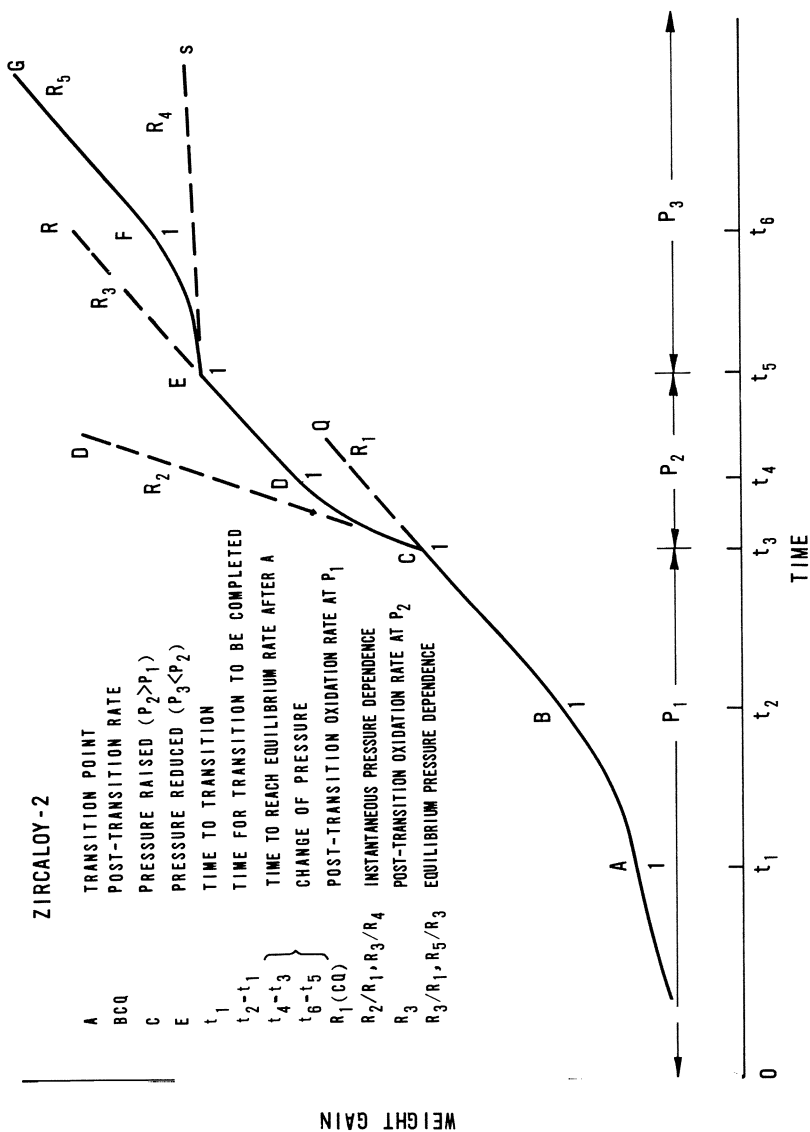


Fig. 13. Arrhenius plot of parabolic rate constants of oxidation data in oxygen. Points are from references 39, 48, 12, 4, and 5, respectively; figure is from reference 14.



pressure resulted in a proportionate increase or decrease in oxidation rate.⁵² Over a period of time roughly equal to the time to transition the oxidation rate slowly adjusted itself back to a value near to the rate prior to the change in pressure (Fig. 14). By studying the development of these transient pressure effects during the oxidation rate transition, and the effect of changing the pressure by additions of inert gas to the oxygen, it was deduced that the only satisfactory explanation of the phenomenon was in terms of porosity in the oxide. This porosity developed during the transition period and was adjusted dynamically during the growth of fresh oxide, following a change in pressure, in such a manner as to restore the oxidation rate to its previous value. A similar phenomenon was observed in water vapor⁵² and high-pressure steam⁵³ and appears to be a general aspect of the oxidation transition of alloys such as Zircaloy-2 in any environment. No transient pressure effects were found for Zircaloy-2 during pre-transition oxidation, or for zirconium oxidizing in oxygen prior to the rate transition.

At pressures below about 1 torr, the oxidation rate becomes pressure dependent; at very low pressures, because the rate of dissolution of oxygen in the metal is relatively unaffected by the environment pressure, and because oxygen in solution is thermodynamically more stable than ZrO_2 ⁵⁴ an oxide film does not form, and any preexisting oxide film dissolves.^{33,55} The differing

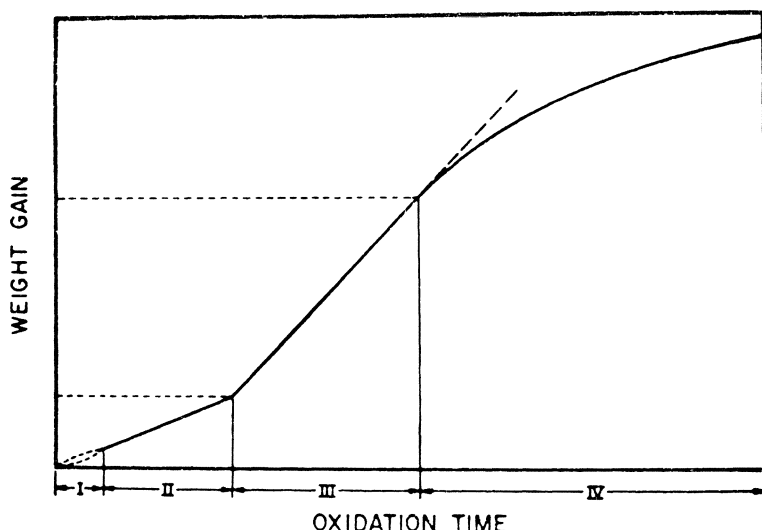


Fig. 15. Schematic representation of oxidation behavior of zirconium in low pressure of oxygen.⁶² (By permission of the Electrochemical Society, Inc.)

activation energies and kinetics for oxygen dissolution and oxide film formation result in different proportions of oxygen in solution at different temperatures. Thus the intermediate phenomena of oxide nucleation which have been studied by several investigators⁵⁶⁻⁵⁸ are strongly pressure and temperature sensitive. Even in a good vacuum, contamination of zirconium and thermal facetting occur at high temperatures.⁵⁹ Thermal facetting is associated with oxygen pressures above a critical value, and below that at which oxide nucleation occurs.

The oxidation kinetics at low pressures show major differences from those described above, particularly during the early stages of oxidation, when a linear period is often seen.^{60,61} They have generally been divided into four stages (Fig. 15) by investigators,^{57,62} although the processes occurring during each of these stages are differently ascribed. Since neither group checked the flow parameters of their apparatus, it cannot be determined whether some or any of the oxidation stages reported were determined by the apparatus rather than the specimen (i.e., the flow rate through the apparatus from a distant pressure measuring and/or controlling point to a specimen acting as a "getter").

Specimen Geometry and Preparation. The correlation between surface preparation and minor differences in the kinetics of oxidation of zirconium in oxygen and air has already been discussed. Over long periods of oxidation Probst *et al.*²³ found little difference between specimens given a range of specimen preparations (not including chemical polishing). Watson⁴⁶ also found relatively small differences in the long term oxidation in air of specimens given various polishing and shot blasting treatments. He did, however, find big differences in the uniformity with which the oxide passed through transition. Thus the smoother specimen preparations (e.g., chemical polishing) gave nucleation of post-transition oxide first around edges and at a few nucleation sites on specimen surfaces. Scratches were found to act as nucleation sites for post-transition oxide, and machined surfaces (as the equivalent of multiple scratches) gave uniform early nucleation of transition. Thus surface preparation differences can lead to large differences in weight gain at the transition point, the differences tend to diminish when oxidation is continued far beyond transition and the whole surface is covered with post-transition oxide. However, in oxidizing specimens in air at 1200–1300°C, Bentley and Mowat found that residual fluoride from an initial pickling treatment could give a factor of three increase in oxide thickness at equivalent times.⁶⁴ This effect was not seen in steam.

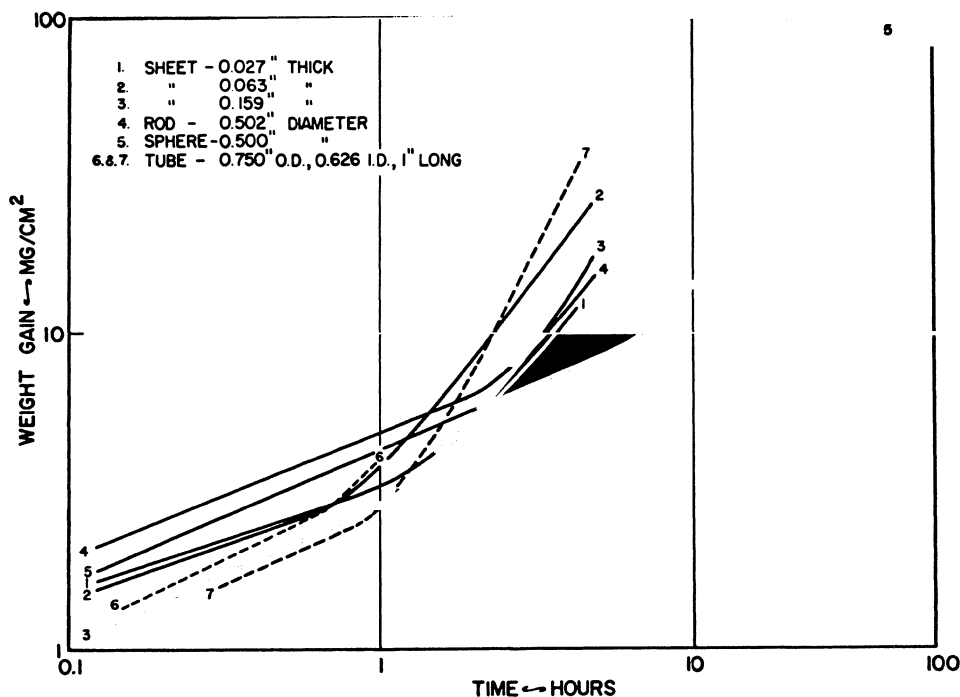


Fig. 16. Weight gain as a function of time for various specimen shapes of iodide-zirconium scaled in air at 900°C.²³

The effect of sharp edges as nuclei for transition is also reflected in the effect of specimen geometry reported by Probst *et al.*²³ Minimizing the proportion of edges and corners (e.g., with spherical specimens) leads to a considerable delay in the time to transition (Fig. 16) by minimizing the number of nucleation sites for post-transition oxide. It is probable that once all the specimen becomes covered with post-transition oxide, however, the oxidation rate would be much less dependent on the specimen geometry.

Effect of Impurities in the Metal. With increasing impurity content the pre-transition oxidation rate of zirconium in oxygen increases,^{23,65} the time to transition decreases, and the post-transition oxidation rate increases (Fig. 17; Table 2). The differences between iodide zirconium and arc-melted sponge zirconium may result from a number of impurities which are higher in the latter than in the former. Of these impurities, differences in iron, oxygen and nitrogen contents are usually among the most prominent.

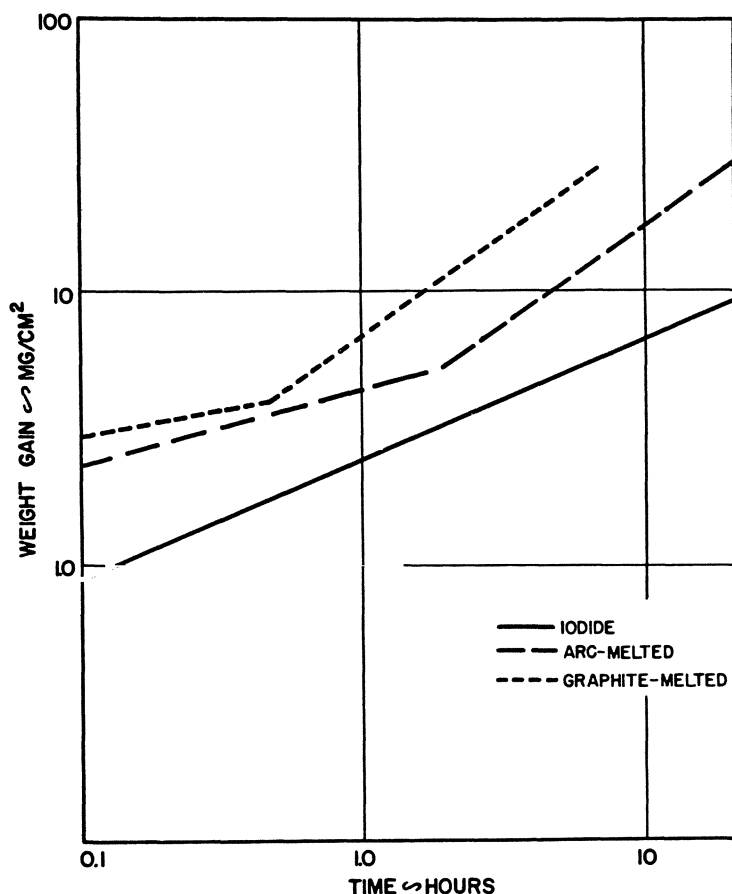


Fig. 17. Weight gain versus time for three grades of zirconium scaled in oxygen at 900°C.²³

In graphite-melted zirconium the presence of carbide particles is the primary cause of the increased oxidation^{66,67} and pustules of white oxide form at an early stage around the sites of the carbide particles. However, as was found for the similar phenomenon in aqueous corrosion,⁶⁸ it seems probable that the increased attack occurs on the metal adjacent to the carbide rather than on the carbide itself.

Both oxygen present uniformly in the metal and as a surface diffusion zone resulting from a pre-oxidation (or anneal in a poor vacuum) have been found to enhance the oxidation rate of zirconium.¹³ Östhagen and Kofstad⁶⁹ studied alloys with 2–17 at. % oxygen, and found a steady increase in oxidation rate with oxygen content up to ~ 15 at. % oxygen. The magnitude of the

enhancement in oxidation was observed to be a function of the degree of uniformity achieved in the oxygen distribution.⁷⁰ Increasingly homogeneous oxygen distributions gave smaller increases in oxidation rate at constant total oxygen content. This observation about the effect of oxygen homogeneity would be in general accord with the relatively large effects of oxygen diffusion zones observed by investigators^{23,71} who pre-oxidized and vacuum annealed specimens (or removed the oxide mechanically). Both Pemsler⁷² and Doerffler^{73,74} used wedge-shaped specimens and found increased oxide film formation in the thin part of the specimen where the metal became saturated with oxygen.

Although the effect of the nitrogen content of the metal on oxidation of zirconium in oxygen has not been studied as extensively as it has been in water, the effects of surface layers contaminated with nitrogen and the presence of a nitride layer results in large increases in the subsequent oxidation rate in air and catastrophic oxidation (burning) if subsequently exposed to oxygen.²³ Since these effects are intimately connected with the oxide breakdown process, they will be discussed in more detail in a later section.

Oxygen Partition between Oxide and Metal

The difference between the activation energies for oxygen diffusion in α -ZrO₂ and in α -zirconium results in the dissolution in the metal of a changing fraction of the total oxygen reacted at different temperatures. In the pre-transition region, if both oxide growth and oxygen dissolution are assumed to have parabolic kinetics, then the partition can be calculated as a simple moving boundary diffusion problem. For temperatures above the α/β transition of zirconium the problem is complicated by the intervention of a growing layer of oxygen stabilized α -Zr between the ZrO₂ and the β -Zr. This problem can still be treated relatively simply by treating the second moving boundary in the same way as the first. Treatments of this problem have been presented by Smith,⁷⁵ Wallwork *et al.*,⁴⁸ Rosa and Smeltzer,⁷⁶ and Rosa.⁷⁷⁻⁷⁹ Calculations of this type have reached their greatest refinement for loss of coolant accident (LOCA) conditions in steam.

These calculations only represent approximations to the actual situation since, as we have already seen, the kinetics of oxidation may be closer to cubic than parabolic, whereas the oxygen dissolution process at high temperatures closely approximates a true parabolic process, and irregularities in the phase boundaries are usually ignored. However, at low temperatures the Arrhenius plots of the diffusion coefficients for oxygen in the metal show

changes of slope (Fig. 18), which are best explained as preferential diffusion along the metal grain boundaries.^{80,81} Doerfler^{73,74} has demonstrated differences between the measured diffusion coefficients at and below 600°C on small- and large-grained specimens of zirconium, and by using an ¹⁸F autoradiographic technique has observed preferential diffusion of oxygen along the zirconium grain boundaries at 600°C.⁷³ Sainfort⁸⁸ had deduced that grain boundary diffusion is prominent up to 700°C from x-ray line-broadening studies.

The oxygen diffusion problem is always treated in terms of parallel sided slabs of oxide and metal, whereas (particularly for specimens under stress) the boundaries between oxide and metal and between oxygen stabilized α -Zr and β -Zr seem to become unstable at high temperatures, leading to tongues of penetrating oxide and oxygen saturated metal.^{13,89,90} Such features are of particular importance in the practical situation of the very high temperatures which may be reached by reactor fuel during a loss of coolant accident (LOCA) where the environment will be steam. Here it is the maximum depth of penetration by oxygen (leading to embrittlement) which is important.⁹⁰⁻⁹⁴ An additional factor to be considered where zirconium is present in a high-temperature gradient, as it would be in a LOCA, is the small positive (~ 20 kcal/g-atom) heat of transport of both oxygen and nitrogen.^{93,94} This results in a tendency for both oxygen and nitrogen to diffuse (as hydrogen does) toward the cold side of a zirconium specimen. Unlike hydrogen, however, these effects are only small until temperatures well above the α/β transition are reached, and even then the equilibrium times are long, of the order of hours at temperatures of 1600°C.^{93,94}

Under conditions where the specimen shows a transition to an enhanced rate of formation of surface oxide, the oxygen diffusion zone may actually contract with increasing oxidation time until a constant (possibly very small) thickness is reached.⁹⁰ Collected data for the measured fraction of the reacted oxygen in solution in the metal as a function of time and temperature are presented in Table 3. It can be seen that below about 600°C the fraction falls to a value $< 10\%$ of the total, but it can be $\geq 50\%$ of the total at high temperatures ($> 800^\circ\text{C}$).

Oxidation Rate Transitions and the Factors Affecting Them

It has often been assumed that the change in kinetics from cubic/parabolic to linear which occurs during the oxidation of zirconium and its alloys in oxygen, steam, or air is a single phenomenon. This has led to a

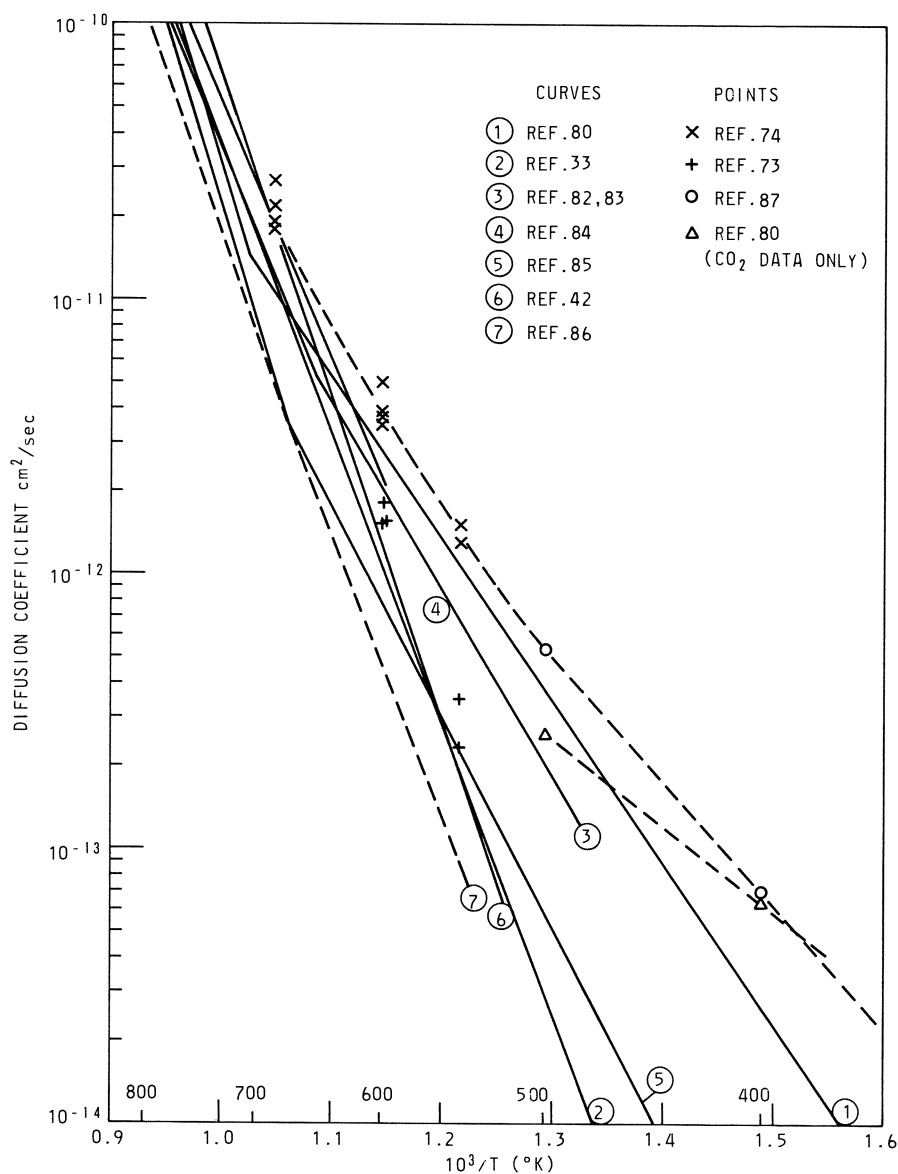


Fig. 18. Collected data for diffusion of oxygen in α -zirconium.

number of theories for the occurrence of this process which have been discussed by Douglass.¹⁴ A survey of the microscopic evidence, however, suggests that there may be (at least) two different oxide breakdown phenomena which have not been clearly distinguished during most previous summaries of the subject.

Thus, we have many clear metallographic examples where cracks in the oxide are associated with fingers of penetrating oxide and sometimes cracks in the oxygen-saturated zirconium substrate.^{13,30,31,90,97} This type of oxide breakdown occurs, typically, with unalloyed zirconium in oxygen at high temperatures,¹³ and some zirconium alloys⁹⁷ in oxygen at temperatures above 600°C. This process may be adequately explained by theories based on mechanical breakdown of the oxides resulting from cracks initiated either by stresses generated in the oxide during growth⁹⁷ or in the oxygen-saturated metal.^{30,31} Although it has proved possible to initiate transition in CO₂ by a single thermal cycle¹³ results for zirconium in oxygen^{13,41} or water vapor⁹⁸ are not as clear cut. Thermal cycling does appear to give higher post-transition oxidation rates for crystal bar but not for sponge zirconium in oxygen.⁴¹

At low temperatures (300–400°C) a variant on this process may operate (for unalloyed zirconium) as a result of the locally enhanced oxidation (Fig. 9b) which occurs along grain and twin boundaries (perhaps as a result of enhanced electrical conductivity of the oxide at these sites).^{22,99} The differential stresses resulting from the variation in oxide thickness lead to early cracking of the oxide along the ridges of thicker oxide,^{99,100} which enables the process to propagate over the surfaces. Prevention of the locally enhanced oxidation (e.g., at higher oxidation temperatures, or by distributing alloying elements as a second phase) can eliminate this early failure process,¹¹⁰ but subsequent failure by either of the two processes (described above and below) will still occur.

For alloys such as Zircaloy-2, for which a rate transition in oxygen has been observed at all test temperatures (down to at least 350°C), the transition process is often not associated with visible cracking, and hence an alternative mechanism must be in operation. The observation of instantaneous transients in the oxidation rate following a change in gas pressure⁵² demonstrates the presence of porosity in these films which appears to penetrate effectively to the oxide/metal interface. The ability of these specimens to reduce the degree of porosity in order to accommodate an increase in pressure⁵² suggests that a process based on the growth morphology of the oxide and preferential crystallization or recrystallization processes leads to the development of

Table 3. Fraction of Reacted Oxygen in Solution in Zirconium

Temp. (°C)	Time (hr)	Total O ₂ (mg/dm ²)	Fraction in metal	Ref.	Temp. (°C)	Time (hr)	Total O ₂ (mg/dm ²)	Fraction in metal	Ref.
400	6	2.26	0.084	95	800	0.1	~85 ^a	0.247	23
	644	~20	≥ 0.05	42		1.0	~190 ^a	0.342	23
450	6	5.91	0.085	95	840	6.41	235	0.306	96
	6	5.12	0.082	95		10	~430 ^a	0.465	23
500	6	11.2	0.071	95	840	20	~850 ^a	0.264	23
						22.9	415	0.39	96
	300	~77	0.10 ± 0.02	42	50	~4200 ^a	0.054	23	
	356	~78	0.11	42	78.75	700	0.407	96	
	409	~80	0.13 ± 0.02	42	840	7.0	460	0.35	50
	450	~95	0.07	42		40.0	860	0.49	50
	500	~97	0.12 ± 0.02	42		113.0	1300	0.555	50
	550	~105	0.10	42		234.0	11710	0.635	50
550	6	25.4	0.087	95		435.0	2190	0.635	50
						601.5	2450	0.65	50
550	316	~146	0.19	42	850	6	~306	0.51	42
	341	~152	0.14 ± 0.03	42				0.394	96
	371	~154	0.13	42		16	~543	0.42	42
	402	~145	0.16 ± 0.05	42		24	~800	0.57	42
	435	~166	0.23	42		24	671	0.556	96
	457	~165	0.19	42		48	~1050	0.56 ± 0.05	42
	486	~161	0.17 ± 0.03	42					

600	6	44.9	0.085	95	900	0.1	~150 ^a	0.40	23
	100	~160	0.22	42		1.0	~410 ^a	0.44	23
	125	~172	0.17 ± 0.03	42		5.0	~3300 ^a	0.066	23
	150	~194	0.22	42					
	186	~196	0.18 ± 0.05	42	910	0.75	200	0.58	50
	209	~226	0.21	42		4.0	550	0.45	50
	259	~232	0.18	42		17.0	900	0.58	50
668	40.66	173	0.139	96		63.7	1470	0.58	50
	92.55	263	0.175	96		146.0	2080	0.675	50
700	0.2	~60 ^a	0.185	23	975	4.0	840	0.47	50
	2.0	~130 ^a	0.246	23		16.7	1350	0.67	50
	2.75	66	0.091	96		63.7	2350	0.72	50
	16.41	150	0.167	96		237.5	4240	0.765	50
	20	~280 ^a	0.358	23					
	100	~500 ^a	0.46	23	1000	0.1	~630 ^a	0.27	23
	447	676	0.494	96		1.0	~1800 ^a	0.28	23
750	7.5	187	0.251	96		3.0	~3000 ^a	0.29	23
	23.1	315	0.315	96		7.0	~7000 ^a	0.14	23
	96	~590	0.37 ± 0.04	42	1100	0.1	~1500 ^a	0.20	23
						1.0	~4600 ^a	0.20	23
						4.0	~9500 ^a	0.18	23

^aSpecimens oxidized in air, all others in oxygen.

porosity. Porosity which is clearly visible in the optical microscope is observed at temperatures above $\sim 910^{\circ}\text{C}^{50,101}$ and has been associated by Pemsler with the occurrence of a phase transition in the oxide. The initial film is thought to be tetragonal ZrO_2 , stabilized by the compressive stress,^{101–103} which transforms to monoclinic as the stress relaxes in the outer layers of the oxide. It is possible that a similar process occurring on a finer scale can explain the transition process occurring without visible cracking. The various mechanisms suggested here are discussed more fully later.

The transition process for zirconium in air has many of the features of the second process described here at temperatures below about 600°C^{44} . However, at higher temperatures, penetrating fingers of oxide and gross cracking are observed.²⁹ The change to the more disruptive type of transition appears to be related to the onset of the formation of visible layers of ZrN between the oxide and the metal.^{23,25} Even at the lower temperatures the formation of ZrN on a smaller scale may be affecting the stresses in the oxide and hence its recrystallization and development of porosity. The effects of ZrN layers on the behavior of zirconium are discussed more fully in the following section.

Effect of Nitrogen on the Oxidation Kinetics, Specimen Growth, and Oxide Breakdown

The kinetics of the nitridation reaction will not be discussed here, although in the broadest sense it can be regarded as an oxidation process. However, the influence which nitrogen and ZrN layers can have on the oxidation behavior in O_2/N_2 mixtures is profound and warrants separate discussion.

The pre-transition oxidation rates of zirconium in oxygen and oxygen/nitrogen mixtures are very similar, as are the times to transition for arc-melted or graphite-melted zirconium, which show a transition in both oxygen and air. There is less than a factor of two difference in parabolic rate constant, which remains virtually constant from 10 to 95 % nitrogen (Fig. 19). The small magnitude of the pre-transition difference between air and oxygen is even more obvious when the instantaneous rate is plotted (Fig. 20), and in the case of iodide zirconium, the occurrence of the transition only in air shows very prominently, as does an instantaneous acceleration in oxidation rate on transferring a sample from air to oxygen. This acceleration is not explicable in terms of any difference in oxidation rate in oxygen since the rate soon falls to a value near to that for specimens oxidized continuously in

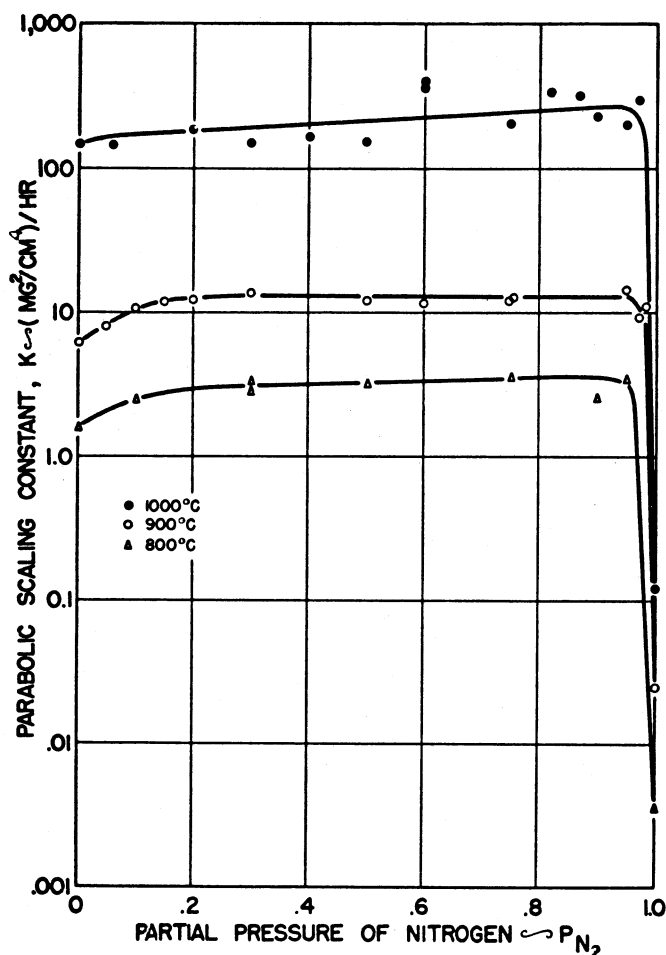


Fig. 19. Parabolic rate constant (k) plotted as a function of nitrogen partial pressure in several oxygen plus nitrogen compositions at the indicated temperatures for iodide zirconium.²³

oxygen (i.e., the transition process is reversible and fresh oxide grown in oxygen is protective). If the results after transferring to oxygen are plotted with the time of transfer as time zero, there is still an initial peak in oxidation, followed by a decrease to a rate near the normal one. This suggests that after the transient has passed, the new protective film formed at the metal/oxide interface is nearly as good as on a fresh specimen. The corresponding transfer from oxygen to air gives no transient and a transition in the kinetics similar to that of a specimen oxidized entirely in air, if the transfer is made at a time equal to, or greater than, the normal transition time in air. If made

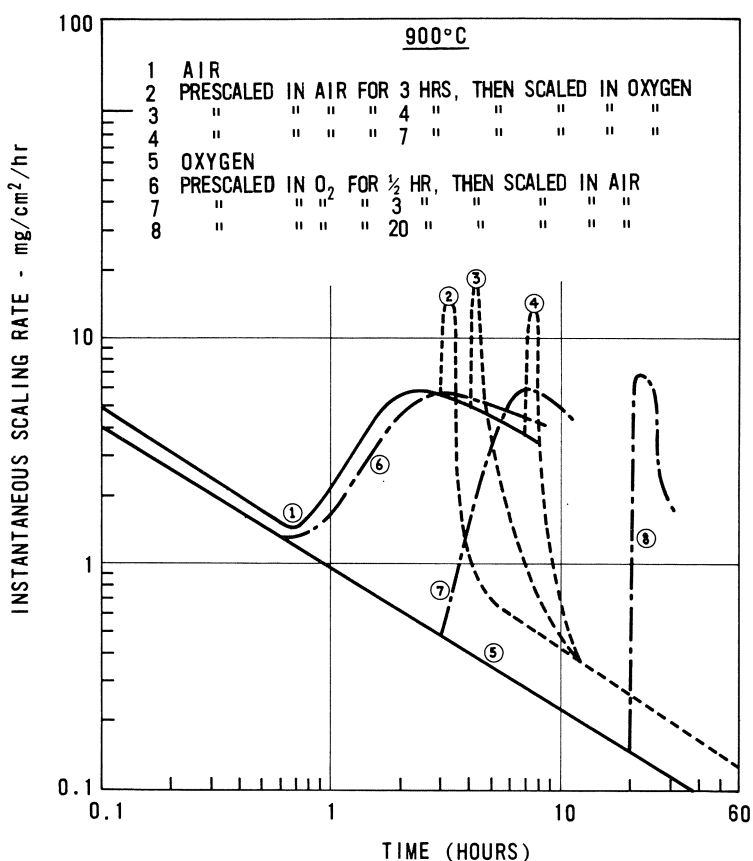


Fig. 20. Instantaneous scaling rates of iodide zirconium in oxygen and air after pre-scaling in either air or oxygen at 900°C.²³

before this time, then the oxidation continues according to pre-transition kinetics up to the expected transition time.²³

That the transient behavior on transferring from air to oxygen is related to the formation and subsequent decomposition of a ZrN layer at the oxide/metal interface has been shown metallographically,²³ and is emphasized by the much enhanced effects resulting from pre-scaling in nitrogen. Large transients are observed on transfer from nitrogen to air (Fig. 21), and specimens transferred from nitrogen to oxygen ignite and burn.²³ This phenomenon is further demonstrated at even higher temperatures by the explosion of molten zirconium drops oxidizing in air.¹⁰⁴

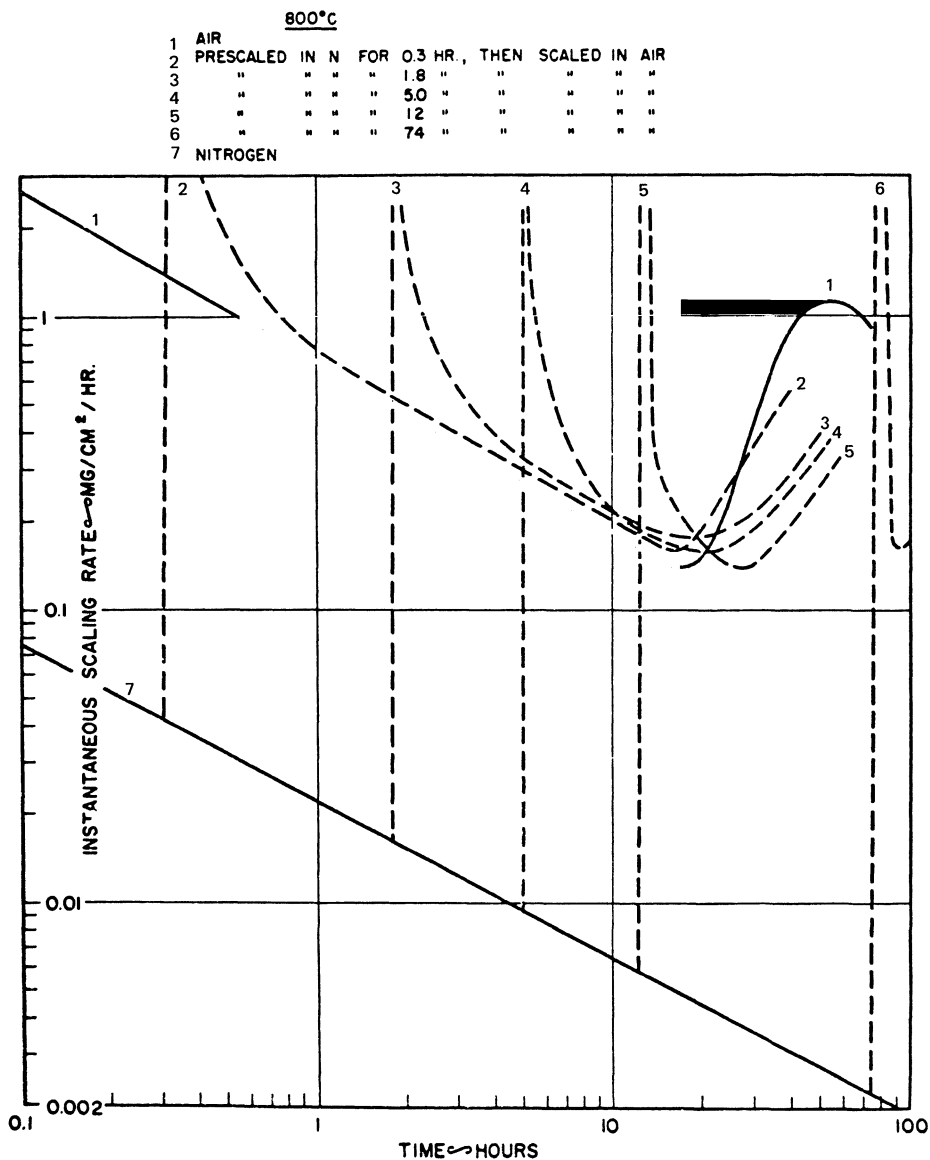


Fig. 21. Instantaneous scaling rate of iodide zirconium in air after prescaling in nitrogen at 800°C.²³

The effect of the ZrN layers appears to be related to its modification of the stresses developed during oxidation. These are clearly much greater for specimens oxidized under conditions where a continuous ZrN layer forms than under conditions where it does not (Fig. 8). The differences between the rates of growth of specimens oxidized in oxygen and in air are equally prominent (Fig. 22).^{23,105} Such a comparison as a function of time gives a valid indication of the different stresses involved because the growth process is essentially a creep phenomenon under the stress applied by the scale, and the majority of the stress is present in the 10% of the oxide nearest to the metal.¹⁰⁶ Thus for samples of equal thickness the creep rates will be proportional to the applied stress. Creep rates of specimens are about 10 times faster during oxidation in air than they are in oxygen.

Effect of Alloying Additions on Oxidation in Oxygen and Air

As a generalization it can be said that no alloying addition has been found which results in a major improvement over the pre-transition oxidation rate of iodide zirconium in oxygen or air.^{18,19,44,107-110} There were many alloying additions which increased the oxidation rate of zirconium, but only

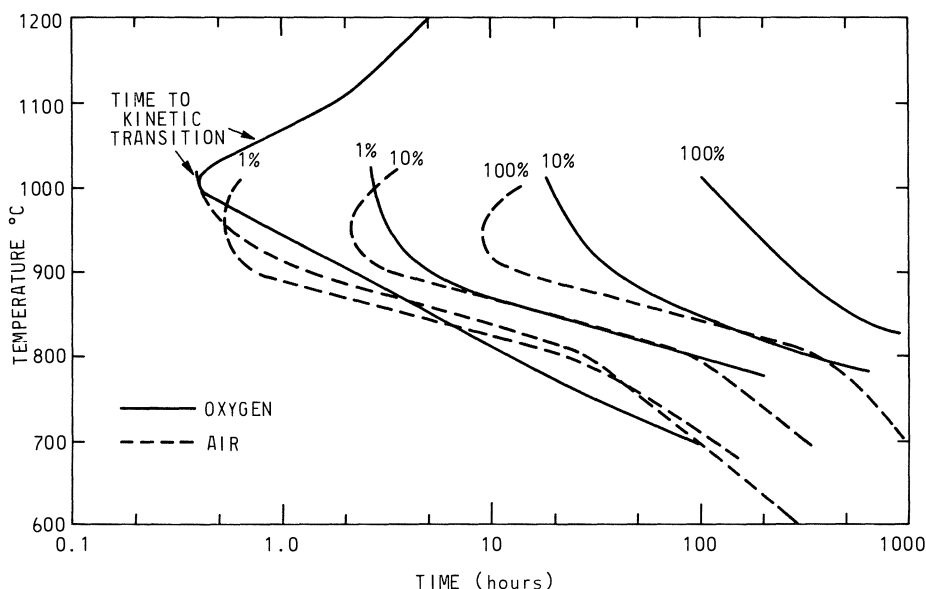


Fig. 22. Comparison of the times to transition and the rates of specimen growth for arc-melted sponge zirconium scaled in air and oxygen.²³

small additions of beryllium, copper, or nickel gave parabolic/cubic rate constants less than those of iodide zirconium.

Porte *et al.*¹⁸ divided the alloys they studied into four groups, depending upon whether the pre-transition oxidation kinetics were parabolic ($n = 0.42\text{--}0.66$) or cubic ($n = 0.29\text{--}0.40$) and whether the alloy showed a transition to linear kinetics. In the light of the earlier discussion of the significance of the exponent in the kinetic equation, it is possible that only the latter distinction is meaningful. On this basis alloys with Si, Sn, Ti, V, Nb, Ta, Pb, Al, Pt, Mo, and U all showed transitions to linear kinetics at some or all of the 1, 2, or 4 at. % addition levels. Only Cu, Ni, Be, Hf, Cr, Co, and Fe alloys did not show a transition at any level of addition (1, 2, or 4 at. %), and of these only Be, Cu, and the higher Ni alloys gave rate constants less than pure zirconium (or Zr with small amounts of Hf). This result has been confirmed by de G  las *et al.*,¹⁰⁸ who found the rate constants for Fe, Cr, and Mo alloys slightly higher than for the base metal; only Cu additions gave lower rate constants in their experiments. This effect was ascribed to the development of a copper rich layer at the metal oxide interface.¹¹¹ The observation of a layer of the alloying element at the oxide/metal interface was unique to copper alloys (among those studied by de G  las) but has also been reported for Ni alloys,^{44,107,109} but not for Nb,^{44,109} Sn,^{44,109} or Al¹⁰⁹ alloys. It is interesting that only Cu and Ni alloys showed prolonged oxidation resistance in oxygen better than that of base metal at 700  C.¹⁹ Neither Ni nor Fe additions were found to give any improvement over zirconium in air at 450  C.¹¹²

Misch and van Drunen¹⁹ showed that the distinction made by Porte *et al.*, on the basis of the occurrence of a rate transition, was only arbitrary, and resulted from the short duration of the oxidation experiments. By exposing specimens of those alloys of Porte *et al.* which had not shown a rate transition for much longer times than in the earlier study, Misch and van Drunen were able to show that all except three alloys ultimately underwent a transition to approximately linear kinetics. Of these three (1 and 4 at. % Cu, 4 at. % Ni), two were showing evidence of impending transition at the end of the experiment (3×10^5 min), and only the 4% Cu alloy showed no evidence for an increasing exponent (n) in the rate equation at the longest exposure times. These three alloys were also the only ones to show a significantly lower oxidation rate than zirconium, which underwent a transition in these experiments. Prior to the transition in the zirconium curve, these three alloys had been only marginally better. Oxidation of Zr-Cu alloys in oxygen has also been studied in France as part of the program for developing these alloys for CO₂-cooled nuclear reactors.

Tin was one of the alloying additions which was found to cause a transition at an early stage in the oxidation curve in oxygen.^{26,27,44,108,112} The time to transition decreased and the post-transition oxidation rate increased with tin content.^{18,44} Thus, of the alloying additions in the Zircaloy group of alloys, it appears that the tin content is the primary cause of the early transition observed in their oxidation kinetics.^{26,44,109} Further confirmation of this supposition comes from the relative rates of oxidation of Zircaloy-2 (1.45% Sn) and Zircaloy-3 (0.25% Sn)²⁶ and the comparable rates of oxidation of binary alloys with about the same tin concentrations.^{8,44}

Zirconium–niobium alloys have been studied extensively because of the improved strength of the low-niobium alloys when compared with the Zircaloys.¹⁴ Only Zmeskal and Brey³⁷ studied the whole composition range of Zr–Nb alloys at 525–1090°C. They found that with increasing niobium content the oxidation rate at 900°C increased to a maximum at ~16% Nb and then fell to a minimum in the range 25–50% Nb, followed by a further increase. At 600°C the first peak and minimum occurred at lower concentrations (8 and 15% Nb, respectively), to be followed by a second maximum at ~50% Nb, a second minimum at 90% Nb, and a final increase for pure niobium. The relative results for various alloys were influenced to a considerable extent by the method of starting the experiment. The occurrence of a peak in the oxidation rate at ~10–15% Nb agrees with a similar survey of the whole Zr–Nb composition range carried out in 1-atm steam.¹¹³

Most subsequent work has concentrated on niobium concentrations in the range 0.5–5.0%,^{44,108,109,114–121} this being the range of practical interest. A study of alloys in this composition range in 1-atm steam or air at 300–500°C¹¹⁵ showed that for binary alloys in air the oxidation rate increased steadily for the 1, 2, and 5% Nb alloys, whereas in steam a minimum occurred in the oxidation rate at about 2–2.5% Nb. The addition of 0.5% Sn caused a further increase in rate over that of the binary alloy.¹¹⁵ Both pre- and post-transition kinetics were affected similarly and times to transition decreased with increasing niobium content, in rough agreement with the results of Porte *et al.*¹⁸ Out of a range of ternary additions made at the 1 wt. % level to Zr–1 wt. % Nb, only Fe, Pd, and Cu additions decreased the oxidation rate, the magnitude of the effect being in that order.¹¹⁵ Mo, Pt, V, W, and Ge ternary additions caused increases in rate, depending upon the heat treatment.

The effect of heat treatment of the alloy was one of the major variables examined in later studies^{116,122,123} of the Zr–2.5 wt. % Nb alloy. Oxidation rates in air at 300–500°C were found to be much higher than in steam (at the same temperature and for the same heat treatment) for specimens

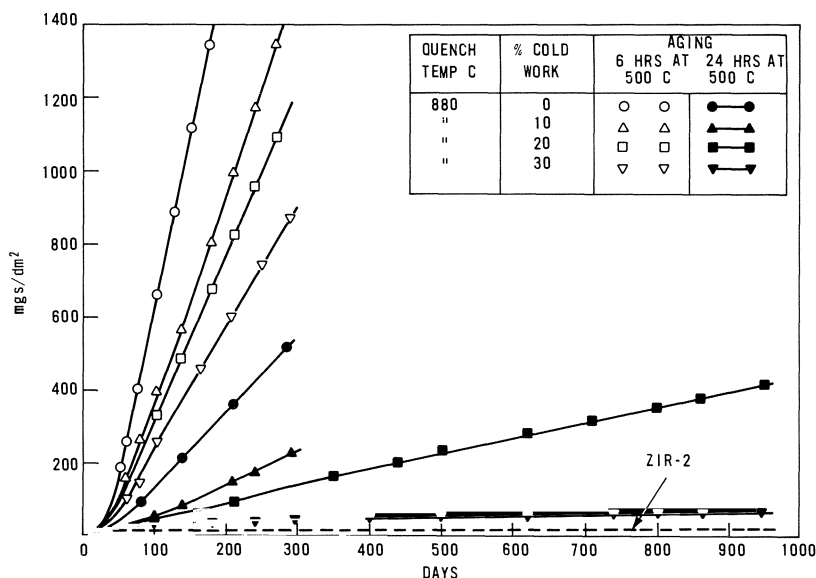


Fig. 23. Effect of heat treatment on the oxidation of a Zr-2.5 wt. % Nb alloy in a carbon dioxide-air mixture at 350°C. The oxidation behavior is dominated by the presence of air.¹²² (Reprinted by permission of ASTM from copyright material.)

quenched from the β or $\alpha + \beta$ phase and tempered at temperatures from 350 to 580°C (Fig. 23). The oxidation rate decreased with increasing tempering time as did the difference between oxidation rates in air and steam.¹¹⁶ The effect of tempering can be accelerated by an intermediate cold-working step, both in gaseous environments and in water.¹²² Alloys with only 1–1.5 wt. % Nb are insensitive to the effects of a quench from the β phase, while a ternary addition of 0.5% Sn to a Zr-2.5% Nb alloy reduces the high oxidation rate of β -quenched specimens.¹¹⁶ The effect of holding at different temperatures in the $\alpha + \beta$ region, and varying the quenching rate was studied for a Zr-2.7% Nb alloy in oxygen at 400°C.¹¹⁰ At higher oxidation temperatures the differences due to prior heat treatment diminish since tempering continues during oxidation, and differences resulting from prior tempering treatments soon become insignificant.^{116,117}

At short exposure times and temperatures of 400–500°C, alloys with 1 wt. % Nb show lower oxidation rates in air than in steam (Fig. 24).^{115,117,118} This difference disappears after transition,¹¹⁵ and at higher temperatures.¹¹⁷ At temperatures and times for which the oxidation rate is less in air than in steam, an interesting transient is obtained on transferring a specimen from steam to air¹¹⁹: the oxidation effectively stops until the exposure time reaches

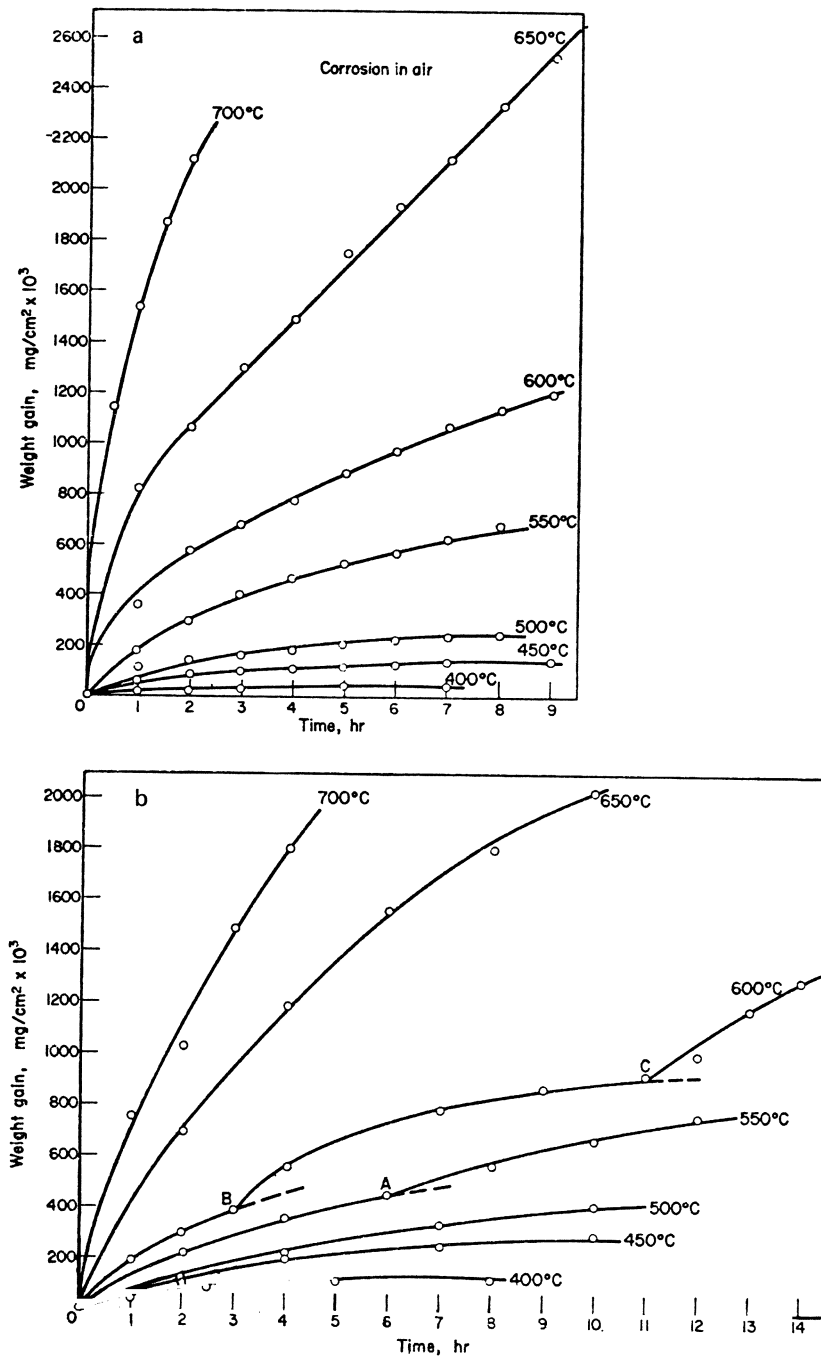


Fig. 24. Comparison of the oxidation of a Zr-1 wt. % Nb alloy: (a) in air; (b) in steam.¹¹⁸

the point on the oxidation curve in air equivalent to the weight gain attained in steam at the time of transfer. Even when the specimen again begins to gain weight, the oxidation rate was often below that for a specimen exposed only in air (Fig. 25). No significant transient was obtained on transferring from air to steam. A reduction in the oxidation rate of a Zr-1 wt. % Nb alloy with increasing cold working was observed in both air and steam at 450–550°C.¹²⁰ This effect is similar to the one observed in high-temperature water and steam for Zr-2.5 wt. % Nb alloys and may be due to a similar effect: cold-working accelerates the metallurgical processes [e.g., precipitation of β -Nb(Zr) phase] occurring during tempering, and these are known to occur during oxidation at temperatures $\geq 400^\circ\text{C}$.

Studies of high-valence (>4) additions to zirconium such as P, N, Ru, and Te have been made on the hypothesis that they should, according to the Wagner-Hauffe rules, produce a reduction in anion vacancy concentration in the oxide, and hence a reduction in oxidation rate. Phosphorus additions at relatively low concentrations ($\sim 0.15\%$) were claimed to reduce the

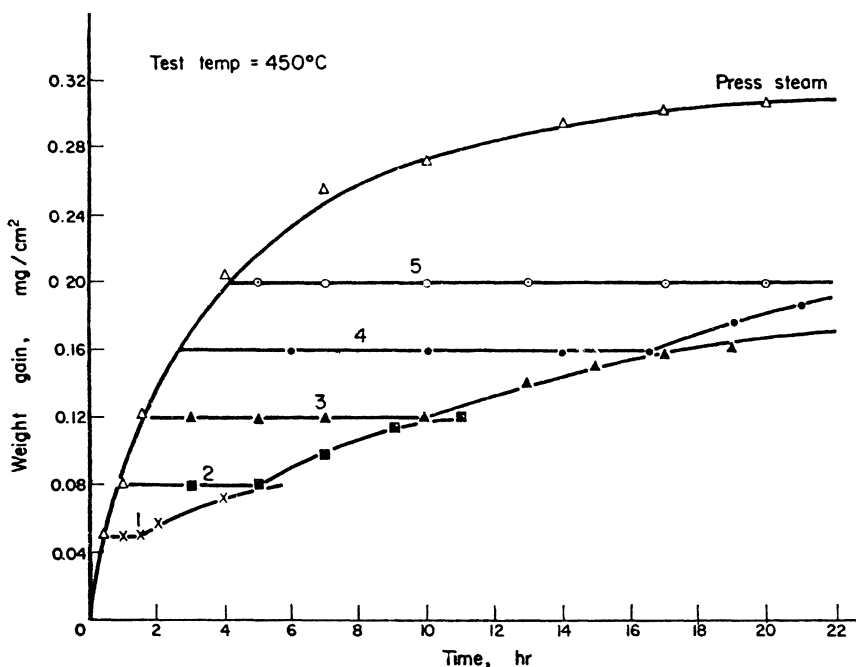


Fig. 25. Effect of transferring Zr-1% Nb alloy specimens from steam to air during oxidation. Numbered curves show the course of oxidation when specimens were transferred from steam to air at various points along the steam oxidation curve.¹¹⁹

oxidation of zirconium in air,¹²⁴ although the results as presented do not seem to support the claim. Nitrogen was again found to be a deleterious addition.¹²⁴ Small tellurium additions were observed to improve the oxidation resistance of zirconium in air at 750°C; a small increase in rate was observed in oxygen.⁴³ An 0.5% ruthenium alloy oxidized at a rate very similar to that of the base metal,¹⁰⁹ as did a 1.08 at. % Pt alloy.¹⁸ Higher platinum contents led to oxide breakdown.

The oxidation of zirconium–yttrium alloys in air at temperatures of 1200–1600°C was studied by Phalen *et al.*¹²⁵ The kinetics of oxidation were not reported, but the phases present at various depths in the oxide were determined by x-ray techniques. Extensive internal oxidation of the yttrium rich phase occurred to form Y_2O_3 . Attempts have been made to apply this phenomenon to the strengthening of zirconium by dispersions of Y_2O_3 particles.¹²⁶

The poor behavior of Zr–Al alloys in oxygen and air has been noted by several authors.^{18,108,109,114,127} Most of these studies were for relatively short times; long exposures in air (500 hr at 450°C) are reported to result in an interesting repeated exfoliation process, whereby the oxide flakes off in a series of thin complete layers.^{128,129} This suggests a cyclic post-transition oxidation process of repeated nucleation of oxide layers which do not adhere

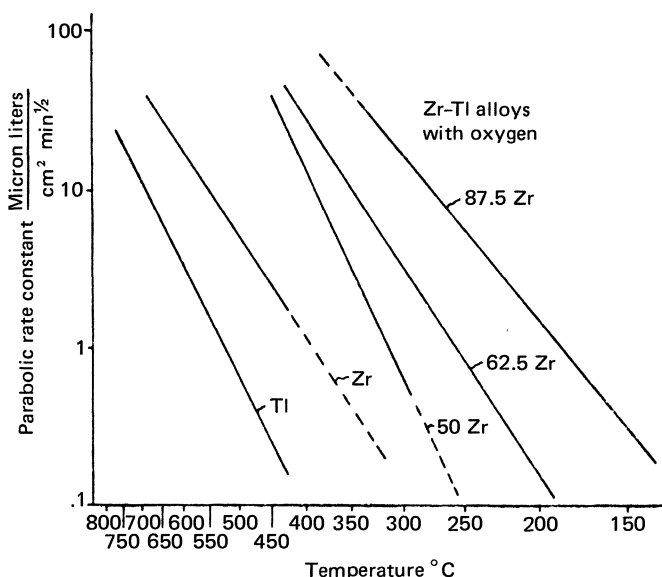


Fig. 26. Oxidation rates of Zr–Ti “gettering” alloys.¹³¹

well to each other. Ternary additions of Sn, Cr, V, or Mo to Zr–Al alloys did not effect any improvement.¹³⁰

Zirconium–titanium alloys have very poor oxidation resistance,^{18,114,131,132} and in addition the oxide becomes flaky and non-adherent with increasing titanium content. This has resulted in the development of these alloys for use as getters.¹³³ With continuous agitation the oxide flakes off continuously and does not offer any protection to the surface. The alloys can be used as getters at temperatures as low as 350–375°C (Fig. 26). Other binary and ternary alloys of zirconium containing Nb, Sn, Cr, Fe, Ni, Co, Cu, and Ta,^{130,132} have been studied without finding any alloys showing improved oxidation resistance.

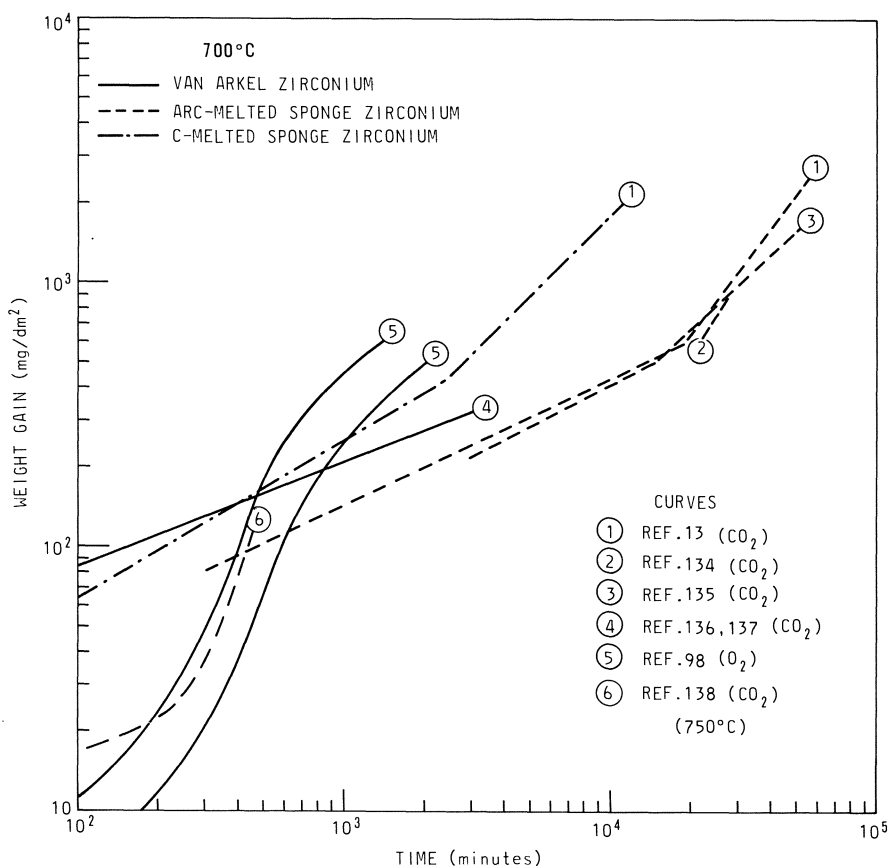


Fig. 27. Collected data for the oxidation of zirconium in carbon dioxide at 700°C compared with oxidation in oxygen.

Carbon Dioxide

Oxidation Kinetics

The oxidation kinetics of zirconium in carbon dioxide are formally similar to those in oxygen, although at any particular temperature and time the weight gains in carbon dioxide average about 70% of those in oxygen (Fig. 27). This is equivalent to oxidation at an oxygen pressure of 4×10^{-3} mm pressure,⁶² which is much higher than the equilibrium oxygen partial pressure in pure carbon dioxide. This result suggests that a major part of the reaction could be occurring with impurities in the gas stream.

Of the early studies of oxidation in carbon dioxide^{13,60,61,84,98,134-143} only Gregg *et al.*¹³⁸ and Shannon⁹⁸ reported weight gains in CO₂ very much less (a tenth under some conditions) than those in oxygen. This might be a result of the additional care taken by these authors to outgas both specimens and apparatus at the beginning of the experiment, and to “getter” the gas phase. Hussey and Smeltzer,¹³⁹ using essentially the same method of starting the experiment as Gregg *et al.*, did not confirm this difference, but did observe a short transient period of low oxidation at the start of the experiment. The shapes of the early stages of the oxidation curves reported by Gregg *et al.*,¹³⁸ Shannon,⁹⁸ and Hussey and Smeltzer¹³⁹ bear much similarity to low-pressure oxidation curves in oxygen (Fig. 28). In fact, no comprehensive study has been made of the effect of impurities in the carbon dioxide, using a rare isotope of oxygen to establish its origin, in the same way that ¹³C has been used to establish the presence and distribution of carbon deposits.¹³⁸

Factors Affecting the Kinetics

The effects of large impurity additions to the gas phase on the oxidation kinetics have been investigated^{13,134,145}; 0.1% H₂O additions to carbon dioxide, nominally containing 0.01% oxygen and the same amount of water, did not result in any significant increase in the oxidation rates of zirconium, Zircaloy-2, or a number of alloys at 500°C/150 psi,¹³ although Maxwell¹³⁴ reported a significant increase for Zircaloy-2 (but not other alloys) at 1150°F (620°C) and Darras *et al.*¹⁴⁵ also observed a small increase for Zr and Zr-Cu alloys at 600°C. Additions of nitrogen (at levels up to 275 ppm in the gas phase) did not affect the oxidation at 800°C/1 atm.¹³ The effect of surface preparation techniques on oxidation in carbon dioxide has received little attention;¹⁴⁶ techniques developed for oxidation in oxygen or water having generally been adopted without further investigation. Thermal cycling has a big influence on the occurrence of transition in unalloyed zirconium¹³ but

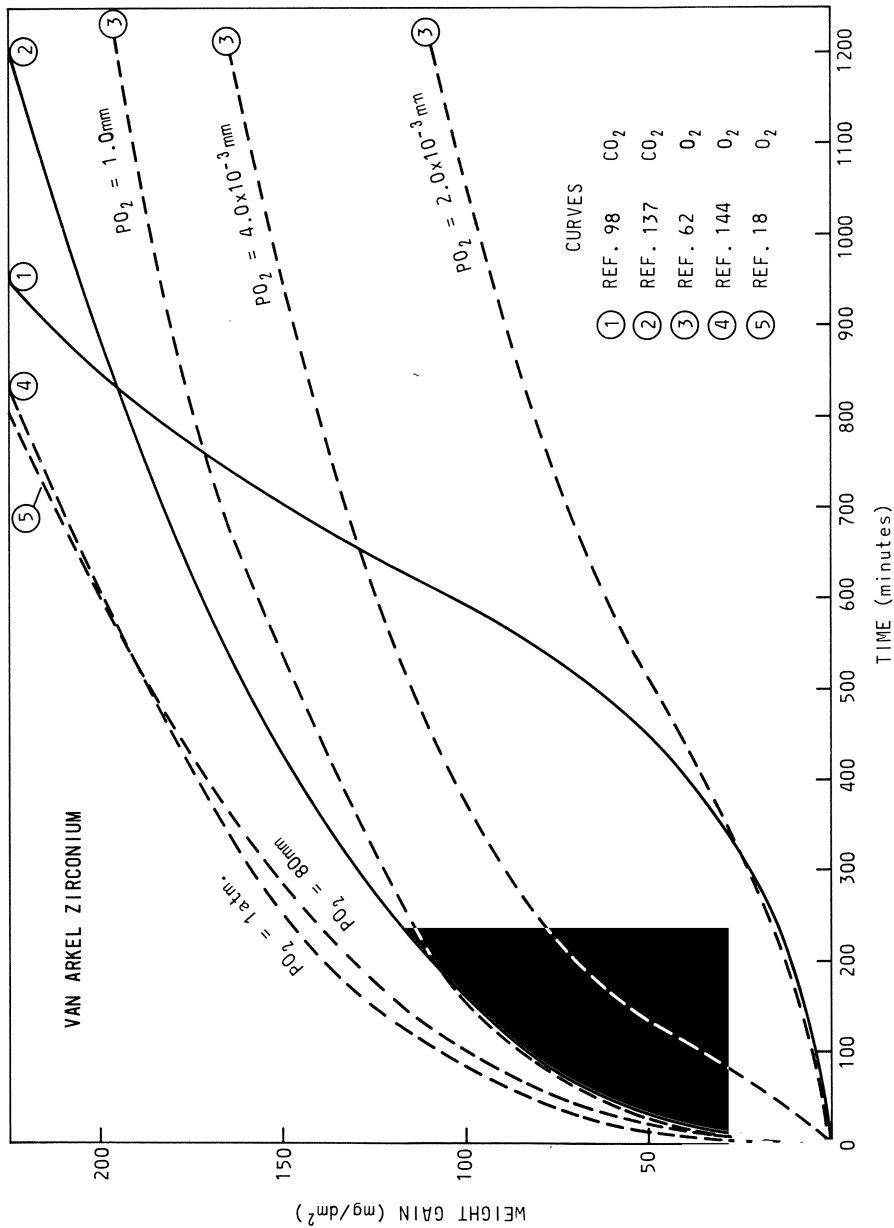


Fig. 28. Oxidation curves in low-pressure oxygen compared with results in clean carbon dioxide at 700°C.

not in alloys with good oxidation resistance.¹³⁴ Zirconium samples could be continued considerably beyond the normal time to transition if they were not thermally cycled. One thermal cycle was then enough to initiate the transition.¹³ This is a much more spectacular effect than that observed by Shannon¹⁴⁷ for Zircaloy-2 in water vapor, where thermal cycling had a small and variable effect on transition and post-transition oxidation rates. It supports a stress-induced cracking mechanism for the initiation of transition in unalloyed zirconium in carbon dioxide, but not for alloys such as Zr-0.5 Cu-0.5 Mo,¹³⁴ which, like Zircaloy-2, in water vapor showed little or no effect of thermal cycling.

In addition to the primary reaction with carbon dioxide to form carbon monoxide, further reactions are possible to give elemental carbon and for this to react with zirconium to form zirconium carbide. Carbon deposition has been observed and measured by several workers,^{138,139} but, since the early studies of Hayes *et al.*,¹⁴⁸ no one has produced evidence for the formation of zirconium carbide. Hussey and Smeltzer¹³⁹ observed the occurrence of a needle-like phase, which appeared first on those metal grains with the thickest oxide film. Morphologically they appeared very similar to the needles of oxide, which nucleate during oxidation at low pressures of oxygen⁵⁶; however, Hussey and Smeltzer considered them to be a suboxide phase stabilized by carbon. Guerlet and Lehr^{136,137,140-142} have observed the formation of an oxycarbide of zirconium under similar conditions, and this may be the unidentified phase of Hussey and Smeltzer.

Growth of zirconium and zirconium-copper alloys (under the influence of the compressive stresses in the oxide film) occurs during oxidation in carbon dioxide,^{13,149} as has been observed also in oxygen and air.^{23,46} No growth rates were measured for unalloyed zirconium which could be compared with the results in oxygen and air.¹³ Elongation of a Zr-1.6 wt. % Cu alloy was found to be dependent on heat treatment in CO₂ at 600°C.¹⁴⁹ Beta-heat-treated specimens grew at one-fourth the rate of α -annealed specimens.

Only small increases in oxidation (of a factor of at most 2-3) have been observed with increasing pressure from 1 atm to 500 psi (Fig. 29),^{13,134,135} the effects being generally more prominent for the less-oxidation-resistant alloys. At less than 1 atm, larger effects of pressure have been found for unalloyed zirconium. However, in view of the critical influence of oxygen and water vapor impurities⁹⁸ in determining the oxidation rate in carbon dioxide, one cannot say what fraction of these pressure effects are genuine and what fraction results from changing impurity levels.

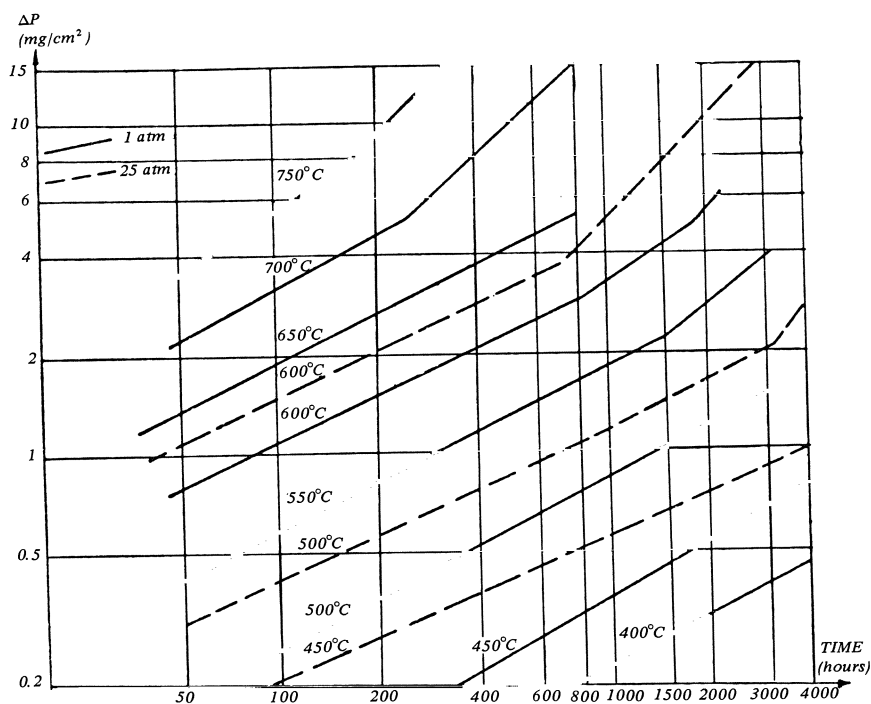


Fig. 29. Effect of temperature and pressure on the oxidation of zirconium in carbon dioxide.¹³⁵

Development of Alloys for Use in CO_2 -Cooled Reactors

The studies of zirconium alloys in the United Kingdom¹³ showed that the same alloying additions were effective in carbon dioxide as in oxygen.¹⁸ Thus copper proved to be the best addition, giving lower oxidation rates than unalloyed zirconium for all additions from 0.25 to 1.5 at. %. Iron, chromium, and nickel additions gave improved behavior only for small additions (0.25 at. % Fe; ≤ 0.5 at. % Cr; ≤ 1.0 at. % Ni).

Of the ternary additions tested, only molybdenum and chromium offered any advantages.¹³ Molybdenum appeared to be the most promising of these since the oxide film remained very adherent, and post-transition rate exponents (n) decreased with increasing total copper plus molybdenum concentration ($n = 1.05$ for 0.25 wt. % Cu–0.25 wt. % Mo; 0.89 for 0.5 wt. % Cu–0.5 wt. % Mo; 0.54 for 1.0 wt. % Cu–1.5 wt. % Mo).¹³ This work led to the adoption of ATR* (0.5 wt. % Cu–0.5 wt. % Mo) and TJR* (1.0 wt. % Cu–1.5 wt. % Mo) alloys for use as fuel element supports in the

*Names registered by Associated Electrical Industries Ltd., United Kingdom.

U.K. Magnox Reactors (CO₂-cooled, “Magnox” alloy fuel cladding), where they have performed satisfactorily.

Apart from further studies of Zr–Cu–Mo and related alloys by Maxwell,¹³⁴ Br  n and Vrt  lkov  ,¹⁵⁰ Mrkous *et al.*,¹⁵¹ Zaimovsky *et al.*,¹⁵² and Staab,¹⁵³ further development of zirconium alloys for use in carbon dioxide-cooled reactors has been almost exclusively in France,^{135,142,154–160} and has concentrated on the binary Zr–Cu alloys with some interest in a ternary Zr–Cu–Cr alloy. A study of Zr–Nb alloys (1–20% Nb) in carbon dioxide showed all alloys to be worse than unalloyed zirconium, with oxidation increasing with niobium content up to an approximately steady value for alloys with 10–20% Nb.¹⁶¹

The results on binary Zr–Cu alloys covered a wider range of compositions than those studied in the United Kingdom. While some studies^{155–157,159} showed a minimum in oxidation rate with copper content at ~2.5 wt. % Cu, other studies^{142,158} were not continued for long enough times to show these differences. Data for a variety of alloys in carbon dioxide are shown in Fig. 30. The improved oxidation resistance of the copper alloys, as in oxygen, was associated with the occurrence of a continuous layer of copper at the metal/oxide interface.¹⁵⁸ Heat treatment in the β -phase was found to give a small improvement over an α -annealed Zr–1.6 wt. % Cu alloy.^{158,159}

A considerable improvement in the oxidation rate could be achieved by chromium plating the binary alloy,¹⁶⁰ and at long times an even greater improvement resulted from using a ternary Zr–0.5 wt. % Cu–0.5 wt. Cr alloy as the base for the chromium plating. The chromium coating also prevented dissolution of oxygen (and embrittlement) of the surface layers of the alloy, and was much more effective in achieving this than an aluminum coating.

This development work has led to the adoption of a Zr–1.8% Cu alloy for use as fuel cladding in the French EL-4 reactor.¹⁶²

In-Reactor Experience with Zirconium Alloys in Carbon Dioxide

The effects of irradiation on Zircaloy-2 and Zr–2.5 wt. % Nb alloys in impure carbon dioxide (2 vol. % H₂O or D₂O; up to 1.5 vol. % air) have been studied by Asher *et al.*^{163,164} Zircaloy-2 experiences an oxidation rate which was increased by about a factor of 3 during irradiation in experimental rigs in the PLUTO reactor at Harwell (i.e., to approximately the same extent as was observed in steam at atmospheric pressure). The Zr–2.5 wt. % Nb alloys showed either a small decrease or a small increase in oxidation under irradiation; again similar to experience in steam. These tests were related to

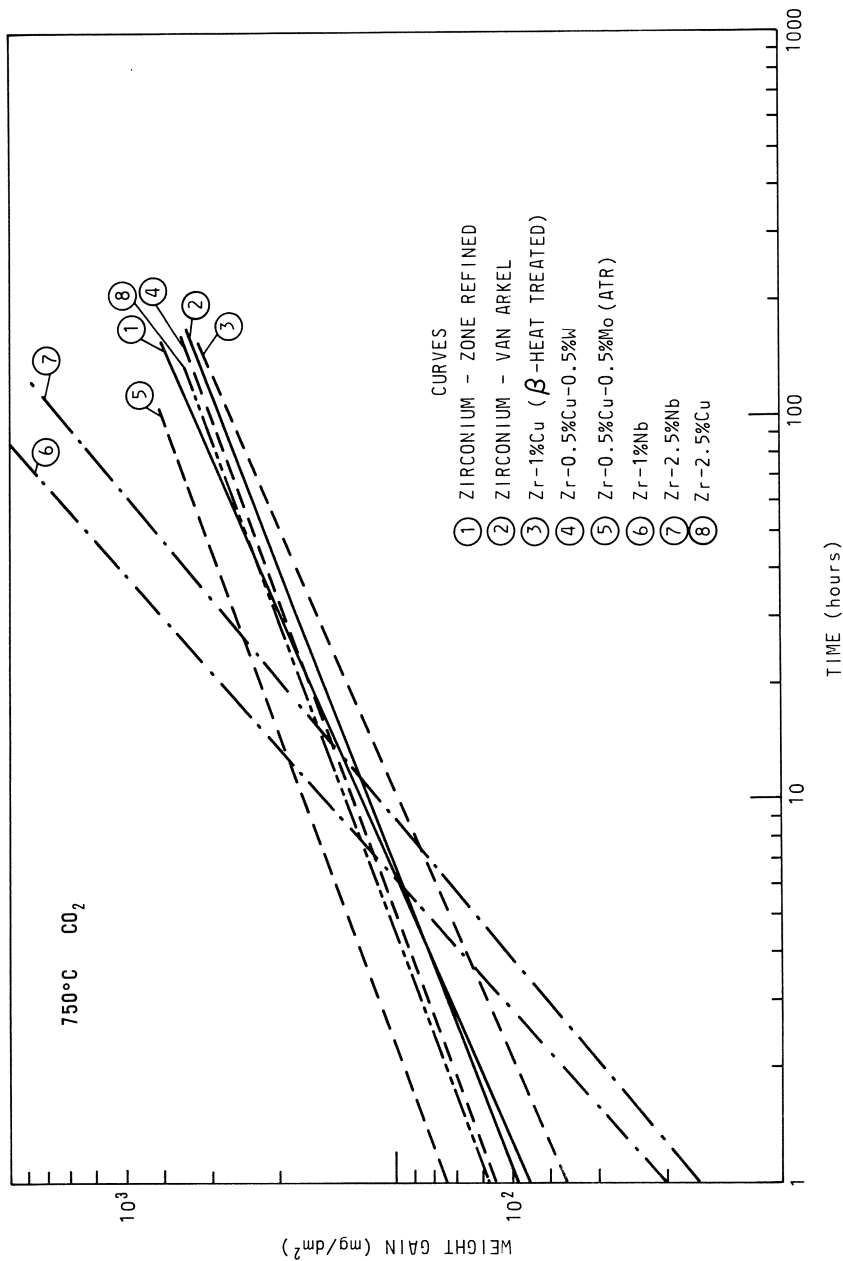


Fig. 30. Oxidation of Zr-Cu alloys, ATR, and zirconium in carbon dioxide.^{142,158}

the behavior of the outside of pressure tubes under the conditions of exposure to the gas annulus environment in an SGHW reactor, where this annulus is filled with carbon dioxide of relatively low purity. No confirmation of these results from examination of actual pressure tubes has been reported. Hurst and Tyzack,¹⁶⁵ however, reported that oxide film measurements on the outside of a Zircaloy-2 experimental pressure vessel agreed with similar measurements on corrosion coupons attached to the outside of the vessel. Both were exposed to an impure moist carbon dioxide atmosphere and showed increases in oxidation rate of between 2 and 6 times.

No results have been published on the behavior of ATR alloy ($\sim 0.5\%$ Cu– 0.5% Mo), which is used for fuel supports in the U.K. Magnox reactors, in dry carbon dioxide either in practice or in experimental irradiations. By default, therefore, one can assume that little effect of irradiation has been observed. Darras *et al.*¹⁴⁵ reported that they had observed small increases in the oxidation rate of unalloyed zirconium and alloys with only small additions of copper in dry (< 60 ppm of H_2O) carbon dioxide. Alloys containing higher copper contents (1.5 – 2.5%) showed no effect of irradiation.

Fuel cladding of Zr– 1.8% Cu alloy, with a corrugated surface, has performed well in the EL-4 reactor, where the outlet temperature of the carbon dioxide is 515°C and maximum cladding temperatures are in the range 610 – 670°C . By modification of the fuel design the limit on performance has been improved from $12,500$ MW day/ton uranium and a maximum surface temperature of 670°C for early fuel models, to $20,000$ MW day/ton uranium and a maximum surface temperature of 610°C for the latest model.¹⁶² End plates, grids, and jackets for this fuel are made of ATR alloy, which has also been considered for use as a hot-liner tube material in the composite pressure tube in EL-4.¹⁶⁶ The final design installed in the reactor consists of a cold (80°C) Zircaloy-2 pressure tube separated from an inner ATR liner (operating at 515°C maximum) by insulating material.¹⁶⁷ During the life of the fuel element in EL-4 ($10,000$ MW day/ton uranium $\equiv 21,000$ hr) the temperature of the fuel cladding passes through a maximum as the fuel is moved through the channel. The total exposure of $21,000$ hr at 275 – 600°C is equivalent to ~ 6200 hr at the maximum temperature.¹⁴⁹ Fissuring and penetrating oxidation have proved to be the limiting factors, since the fuel cladding must not fracture under refueling stresses.^{149,168}

Molten Sodium

Lyon has summarized the behavior of zirconium in a number of liquid metals;¹⁶⁹ however, only in the alkali metals is there a similarity to oxidation

in oxygen because molten sodium (or sodium/potassium alloy) always contains traces of oxygen and sodium oxide in solution. The concentration of oxygen is determined by the temperature of the “cold-trap” to freeze out sodium oxide or by the use of a getter to “hot-trap” the dissolved oxygen. Oxidation of zirconium in this environment has the same characteristics as oxidation in low-pressure oxygen,^{12,170–176} although no investigators report the occurrence of a transition for either zirconium or any of its alloys. This may be merely the result of limited exposure time, low effective oxygen pressure, and low temperature. Davis *et al.*¹⁶⁹ reported white oxide under conditions where the cold-trap temperature (i.e., oxygen content) was particularly high, and in a study of Champeix *et al.*¹⁷⁴ results at 700°C suggests that a transition had occurred, but that it had not yet proceeded to the point where white oxide was obvious.

The oxidation data published by the various investigators^{12,170–176} are in reasonably good agreement with each other and have been compared with data for oxygen in Fig. 31. Smith⁷⁵ has rationalized the difference between behavior in sodium and oxygen in terms of the different vacancy concentrations expected in the oxide and finds the agreement reasonable considering the expected activity of oxygen in sodium.

Less than a factor-of-3 variation in oxidation behavior has been found for a number of zirconium alloys by Champeix *et al.*,¹⁷⁴ although MacKay saw a much larger range ($\times 20$) for a similar range of alloys in his experiments.¹² This may be a variation from alloy to alloy or may represent differences in the oxygen content of the various experiments. Champeix *et al.* show that hot-trapping by gettering the sodium with zirconium at 650°C is much more effective than cold-trapping and reduced the weight gains of zirconium and two Zr–Al alloys to one-third of those found in cold-trapped sodium.^{12,170–176} As the oxidation rates diminish, so do the differences between the various alloys, Zr–Al alloys being no worse than zirconium under hot-trapped conditions.¹⁷⁴ This limiting value of the oxidation rate is probably that condition under which all the oxygen reacting goes into solution and no oxide film is formed. Certainly Champeix *et al.*'s micrographs of their specimens from hot-trapped sodium show no apparent oxide film.¹⁷⁴ One must be careful therefore in equating weight gains with “amount of oxidation” under these conditions, since in the absence of a protective oxide film appreciable dissolution of zirconium may have taken place. The apparently low rates of oxidation observed by Champeix in hot-trapped sodium should be treated, therefore, with considerable reserve.

Apart from its use as a getter for hot-trapping sodium,^{171,172,174} the use of zirconium or its alloys as a fuel cladding has not found favor in the

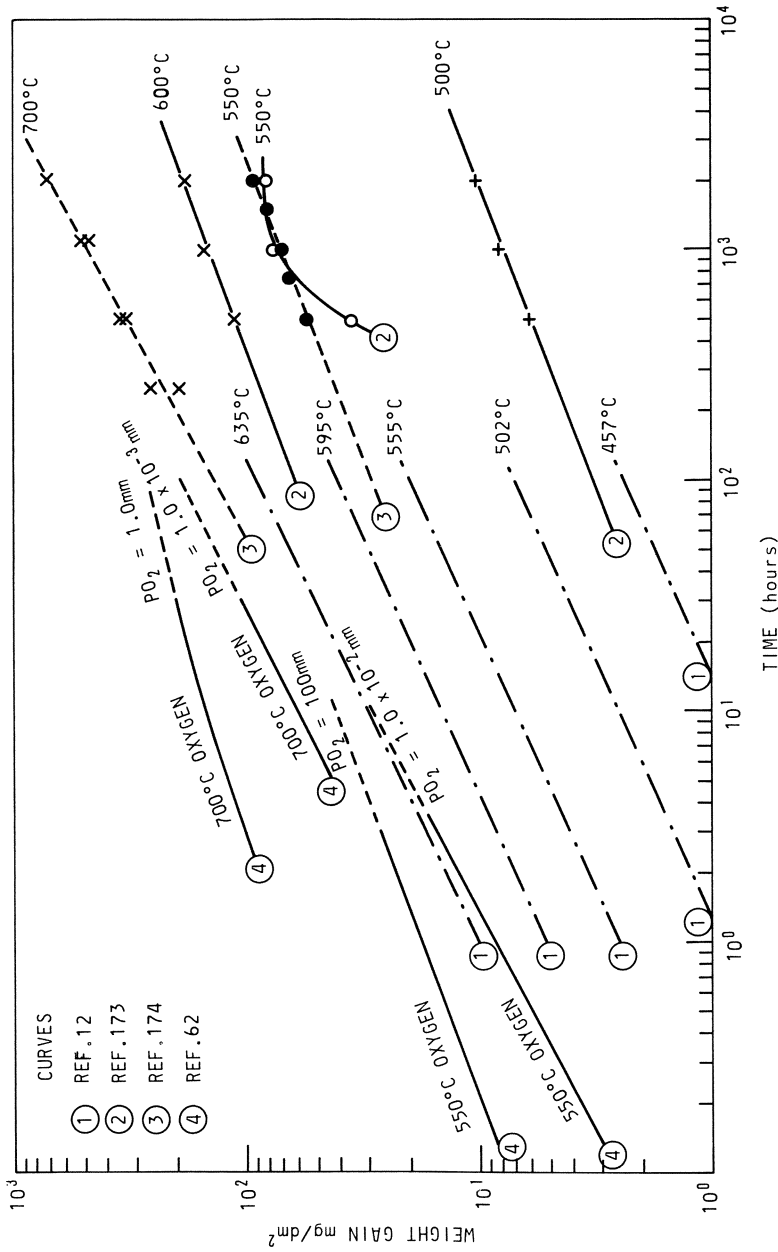


Fig. 31. Collected data for the oxidation of zirconium in liquid sodium compared with oxidation in low-pressure oxygen.

fast reactor field, despite their resistance to void growth and swelling.¹⁷⁷ Zirconium cladding was used for some fuel in the sodium/graphite reactor,¹⁷⁸ and performed satisfactorily, although the temperatures of operation were relatively low and variable. One possible explanation for this reluctance to use zirconium alloys may be the poor past experience with Zircaloy-2 control rod thimbles (in the sodium-graphite reactor) which hydrided catastrophically.¹⁷⁹ Although the hydrogen in this instance came from decomposition of a titanium hydride neutron shield, hydriding has been observed in other experiments where cold-trapping was inadequate. However, given good hot-trapping of the system, and the maintenance of a protective oxide, hydriding should not be a problem. A further restriction of the use of zirconium alloys in such reactors is the current desire to exceed the temperature at which zirconium alloys are known to have adequate strength and resistance to oxygen embrittlement by oxygen dissolution. However, the small differences in oxidation rate in sodium between some high-strength Zr–Al alloys and unalloyed zirconium,¹⁷⁴ the good behavior of the Zr–1.8% Cu alloy as fuel cladding at 610–670°C in EL-4,¹⁶² and the evidence that chromium or molybdenum coatings significantly reduce oxygen diffusion into zirconium alloys,^{145,166} may warrant a reconsideration of zirconium alloys, if alternative alloys resistant to swelling are not available.

Fused Salts

Oxidation of zirconium and Zircaloy-2 in a fused eutectic mixture of potassium nitrate, sodium nitrate, and nitrite was first studied by Anderson and Hill at 336–600°C.¹⁸⁰ They found the oxidation rates and kinetics to be essentially the same as those for oxygen over the temperature range studied, as did Hardy-Grena *et al.*¹⁸¹ in fused sodium nitrate. Later studies^{10,182–191} were mainly directed toward the use of the fused eutectic mixture as a conducting/oxidizing contact for studies of the electrical behavior of zirconium oxide films during growth. Again the oxidation rates and kinetics were essentially the same as those in oxygen (Fig. 32); an early indication that they might be significantly faster¹⁸² was subsequently¹⁸³ shown to be due to a thermocouple calibration error. With this error eliminated¹⁰ the curves for Zircaloy-2 were effectively identical to those in oxygen or air (Fig. 2); small differences observed for van Arkel zirconium could be explained by the different electrical conductivities of the oxidizing environments.¹⁰ Oxidation rates for zirconium alloys, other than Zircaloy-2, have not been extensively studied in fused salts, but Zr–Nb alloys^{181–183} and

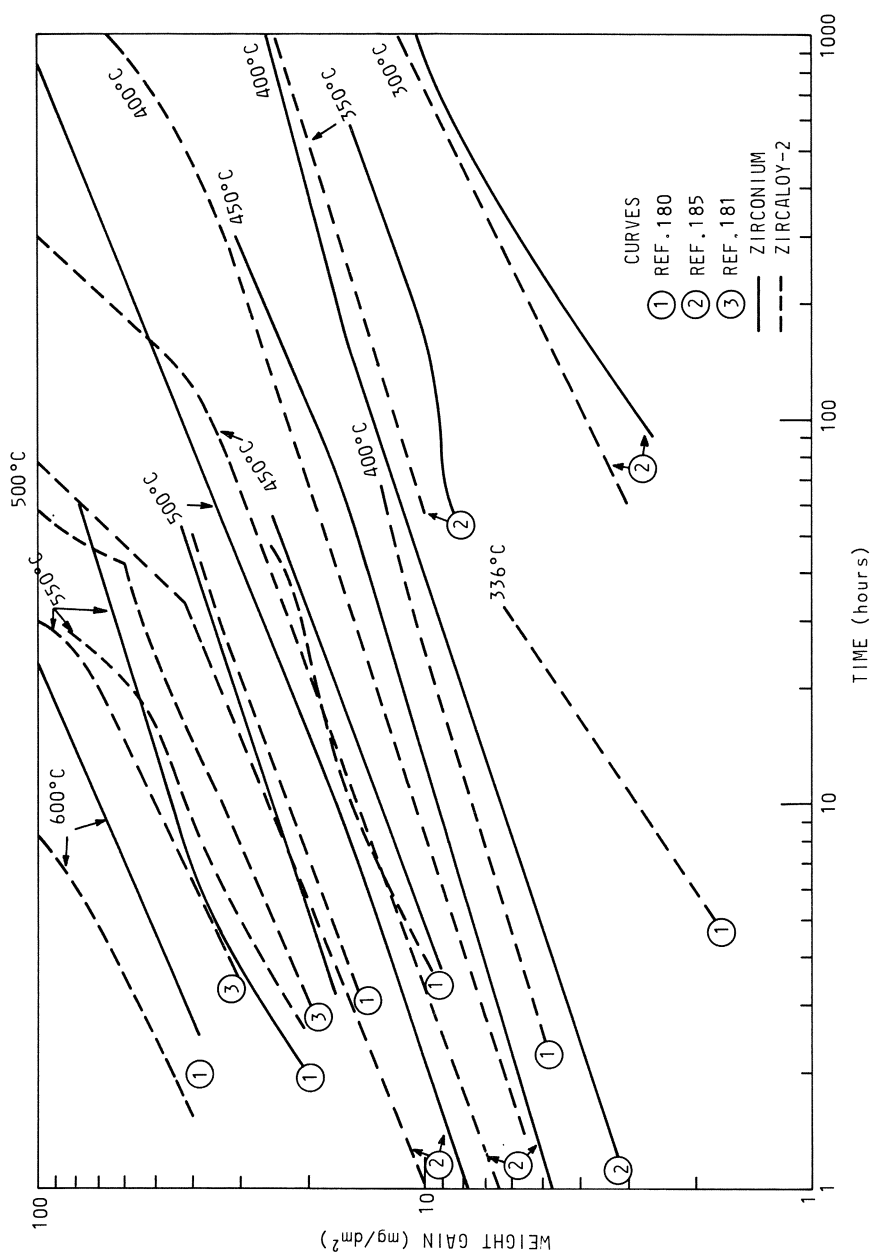


Fig. 32. Collected data for the oxidation of zirconium in fused salts.

binary alloys of the components of Zircaloy-2 (Sn, Fe, Cr, Ni)^{185,186} have been studied and also show rates comparable with those observed in oxygen.

The oxide film formed in fused salts is microcrystalline, and only minor differences have been observed from oxides formed in oxygen.^{180,181,192} The observation,¹⁸⁰ of significant effects of bubbling either oxygen or argon through the salt at 600°C suggests that the oxidation reaction is with dissolved oxygen¹⁸⁸ and not a reduction of the nitrate ion as suggested by Hardy-Grena *et al.*¹⁸¹ The information that the reversible potential for any redox reaction of the ionic species present in the salt¹⁹³ was much greater than the observed potentials of the surface of zirconium alloys also enhanced this supposition. However, recent work at lower temperatures¹⁸⁶ has failed to confirm Anderson and Hill's observation of an effect of gas bubbling, and since thermal decomposition of the salts is not expected to be adequate at 300°C (it may be at 600°C), a catalytic decomposition at the zirconia surface is now the preferred source of oxygen for oxide growth.¹⁸⁶

The potential of the zirconia/salt interface of a specimen oxidizing in a fused nitrate/mixture appears to be effectively the same as that of a smooth platinum electrode, and has been shown to be equal to the reversible oxygen electrode potential in the salt.¹⁸⁶ A smooth platinum electrode was found to be adequately stable for use as a practical reference electrode.¹⁸⁶

Oxidation in other fused nitrate mixtures containing halides has also been studied. In the case of iodide ion this more logically comes under the heading of stress corrosion cracking (SCC), since apart from the SCC aspects the surface oxidation rate appears to be normal, although small differences in oxide morphology are observed.¹ In the case of chloride and bromide additions, however, catastrophic oxidation penetrating along grain boundaries has been observed.¹⁹⁴ This phenomenon appears to be associated with major changes in the morphology and properties of the surface oxide film, and seems to be nonstifling even when considerable depths of penetration are achieved.¹⁹⁴

OXIDATION IN HIGH-TEMPERATURE AQUEOUS ENVIRONMENTS

Historical Background

The initial development of zirconium alloys in water-cooled nuclear reactors was carried out in secret under the auspices of the U.S. Naval Reactors Program. The first detailed evidence was presented to the world at the 1st Geneva Conference on the Peaceful Uses of Atomic Energy¹⁹⁵ and in an accompanying book sponsored by the USAEC.³

The results showed that the early promise of good oxidation behavior in water (i.e., the formation of a thin protective black oxide film) was not sustained by the purest zirconium then available in quantity (produced by the van Arkel process). White oxide spots and regions of white spalling oxide were formed with varying severity and number on different batches of zirconium, and much time was spent in determining and reducing the impurities thought to be related to this behavior. As the purity of the material is improved, however, the regions of localized white oxide formation, although they often become fewer, also often become individually more severe.¹⁹⁶ Thus there is little hope that the elimination of impurities would result in an ideal material.

The additional cost of achieving such purity would render the material uneconomical, and a means of utilizing the cheaper zirconium sponge produced by the Kroll process was sought. It was noticed with this material that the localized oxidation phenomenon was again very variable from batch to batch, but with Kroll material there were some batches which showed surprisingly little localized oxidation. A concerted development effort demonstrated that the elements N, C, O, Al, Ti, and Si, present as impurities, led to poor behavior. Some results for nitrogen and carbon are shown in Fig. 33. The presence of Fe, Cr, and Ni impurities could be correlated with good behavior. Further studies showed that the deleterious effects of the most difficult impurity to eliminate with the then current melting practices (nitrogen, and to some extent carbon and aluminum) could be counteracted by the addition of tin (Fig. 34). Another, but less effective, alternative was found to be niobium. It was by adding 2.5 wt. % tin to sponge-based zirconium that the first commercial alloy (Zircaloy-1) was produced. The tin level was set largely by the tensile properties which were desired. It was more than sufficient to counteract the nitrogen and resulted in unacceptably high post-transition oxidation rates.

This alloy had a relatively short commercial life, although it does occasionally appear in papers in the more recent literature, because it was soon superseded by Zircaloy-2 (Table 1). This alloy was produced by making deliberate additions of iron, chromium, and nickel (as well as tin) to the sponge zirconium so as to counterbalance the deficiencies of some batches of sponge in these elements (Fig. 35), and by reducing the tin content. By this means an alloy giving reproducible behavior in high-temperature water and steam was obtained. This alloy became the workhorse of the Western nuclear reactor industry, and still remains the standard against which all newer alloys are judged.

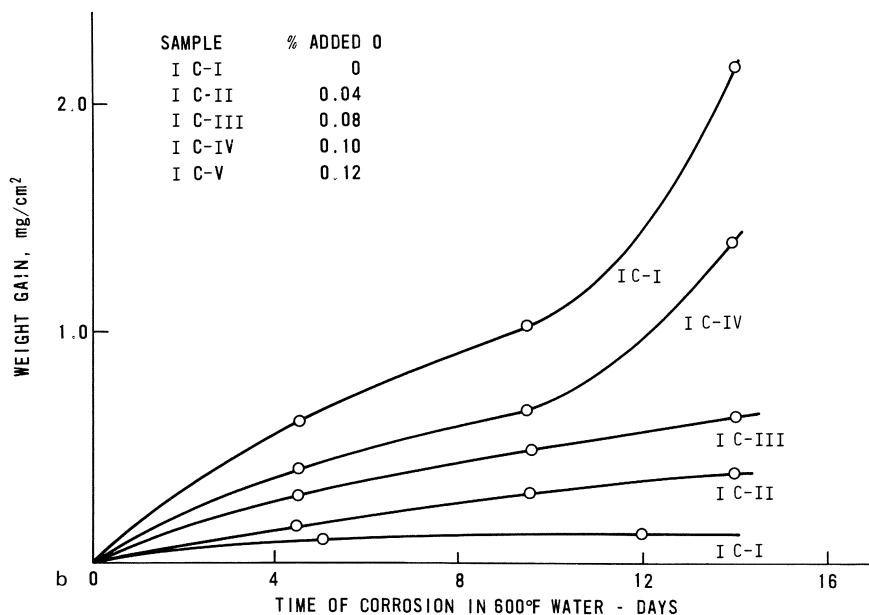
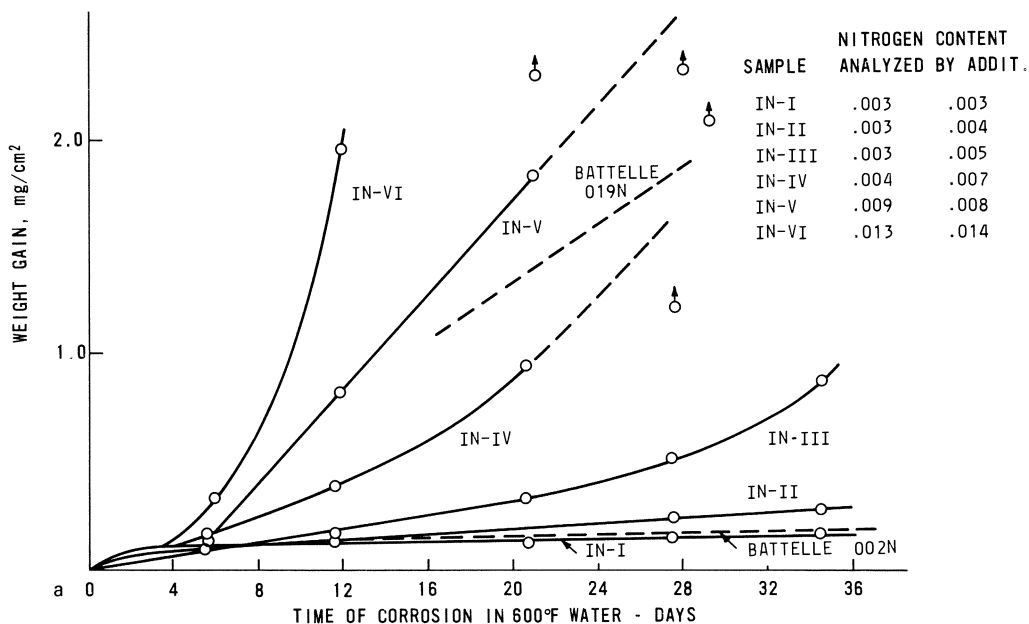


Fig. 33. Effect of (a) nitrogen and (b) carbon on the corrosion resistance of zirconium in 600°F water.⁸

Early studies of the effect of many variables (e.g., melting and fabrication practice, surface preparation, heat treatment, impurity levels, etc.) ensured specifications for this alloy (Table 1) which have permitted its extensive use at temperatures up to 360°C in water. (Details of the effects of these variables will be discussed later.) However, at temperatures above 400°C the behavior of Zircaloy-2 rapidly becomes relatively worse than that of alloys containing less tin. In an attempt to improve the corrosion resistance at 400°C and above, together with the long-term corrosion resistance at or near 300°C, Zircaloy-3

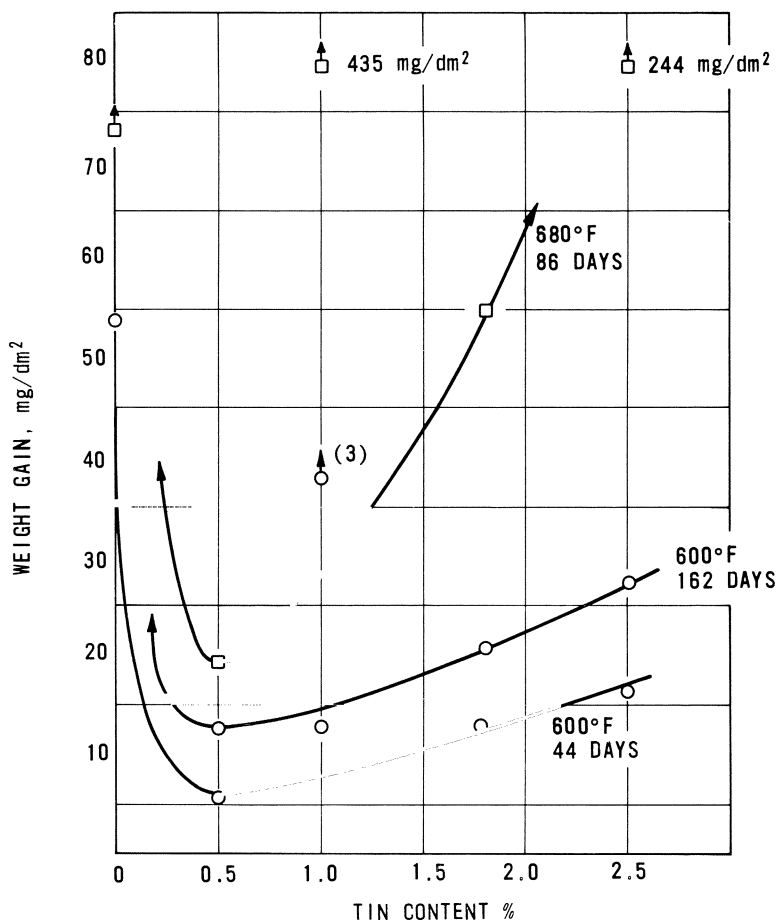


Fig. 34. Effect of tin content upon corrosion resistance of sponge zirconium in water at 600 and 800°F.⁸ (Reprinted by permission of ASTM from copyright material.)

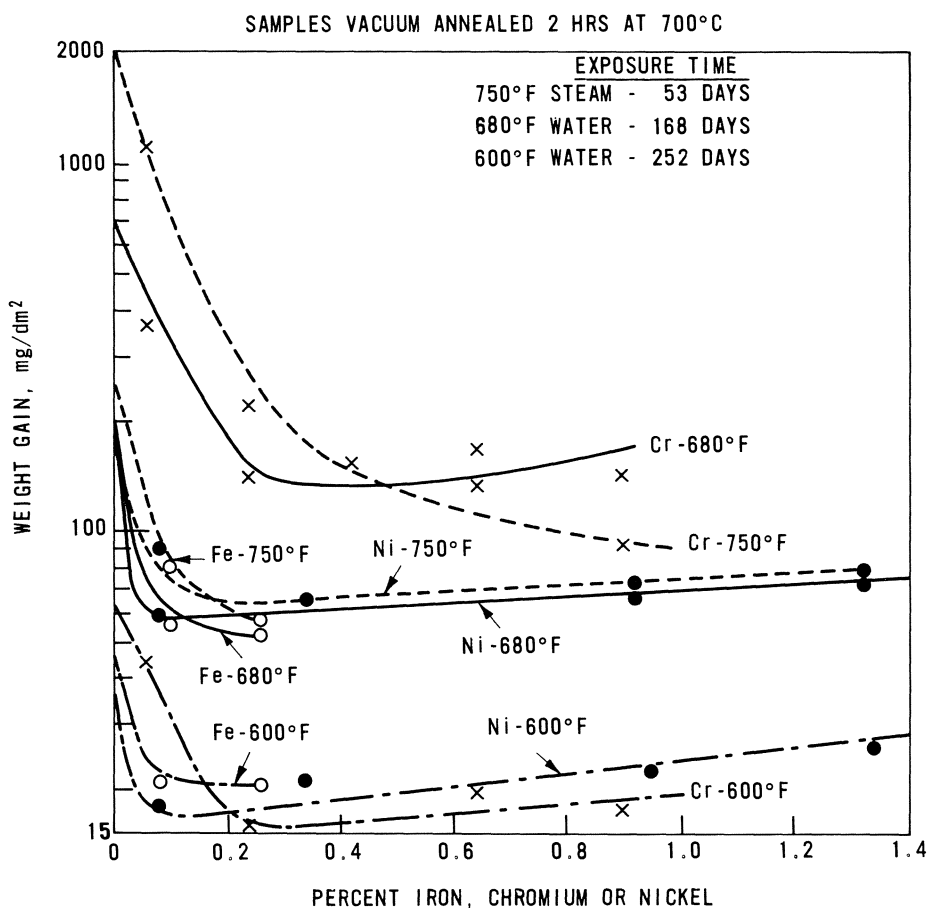


Fig. 35. Effect of Fe, Ni, and Cr additions on the corrosion resistance of an arc-melted sponge zirconium 2.5% Sn alloy.⁸ (Reprinted by permission from ASTM from copyright material.)

was developed. In this alloy the tin content was restricted to 0.5% or less.^{8,197} This alloy never achieved extensive commercial acceptance, as it offered too small an advantage over Zircaloy-2 (Fig. 36), and was found to suffer from the occurrence of white oxide stringers during corrosion. Subsequently, similar but less severe stringers were observed in Zircaloy-2 given certain fabrication treatments. An extensive program to eliminate this problem was necessary.^{8,198-200}

A further stage in this desire to improve the corrosion resistance at high

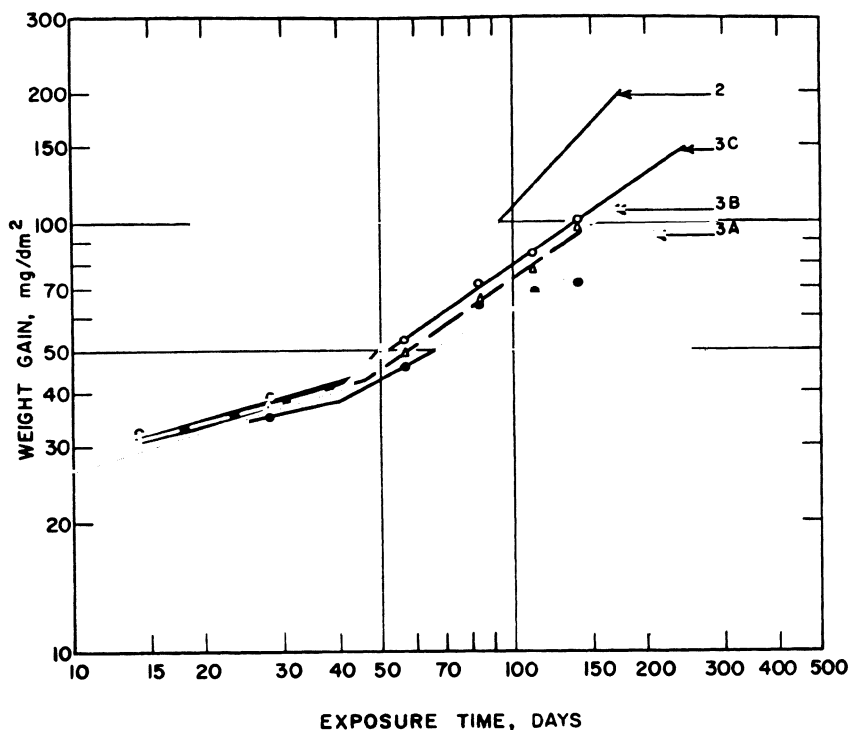


Fig. 36. Corrosion of Zircaloy-2 and Zircaloy-3 compared in 750°F steam (1500 psi). Specimens furnace-cooled from 775°C. Refer to Table 1 for compositions.⁸ (Reprinted by permission of ASTM from copyright material.)

temperature led at a later date to the Zr-1.2 wt. % Cr-0.08 wt. % Fe alloy (Valloy), containing no tin (Fig. 37), which again has not yet achieved wide commercial acceptance, owing to the variability of its behavior from batch to batch, especially at temperatures near 300°C.²⁰¹

In parallel with the desire to improve the high-temperature corrosion resistance in steam, there has been a necessity to minimize hydrogen absorption during corrosion. It was observed at an early stage in the development of zirconium alloys that the hydrogen content increased after exposure to high-temperature water or steam.^{3,8} The relation between the amount of hydrogen absorbed (during oxidation) and the amount of oxide formed has been studied extensively²⁰² and is apparently not a simple function (Fig.

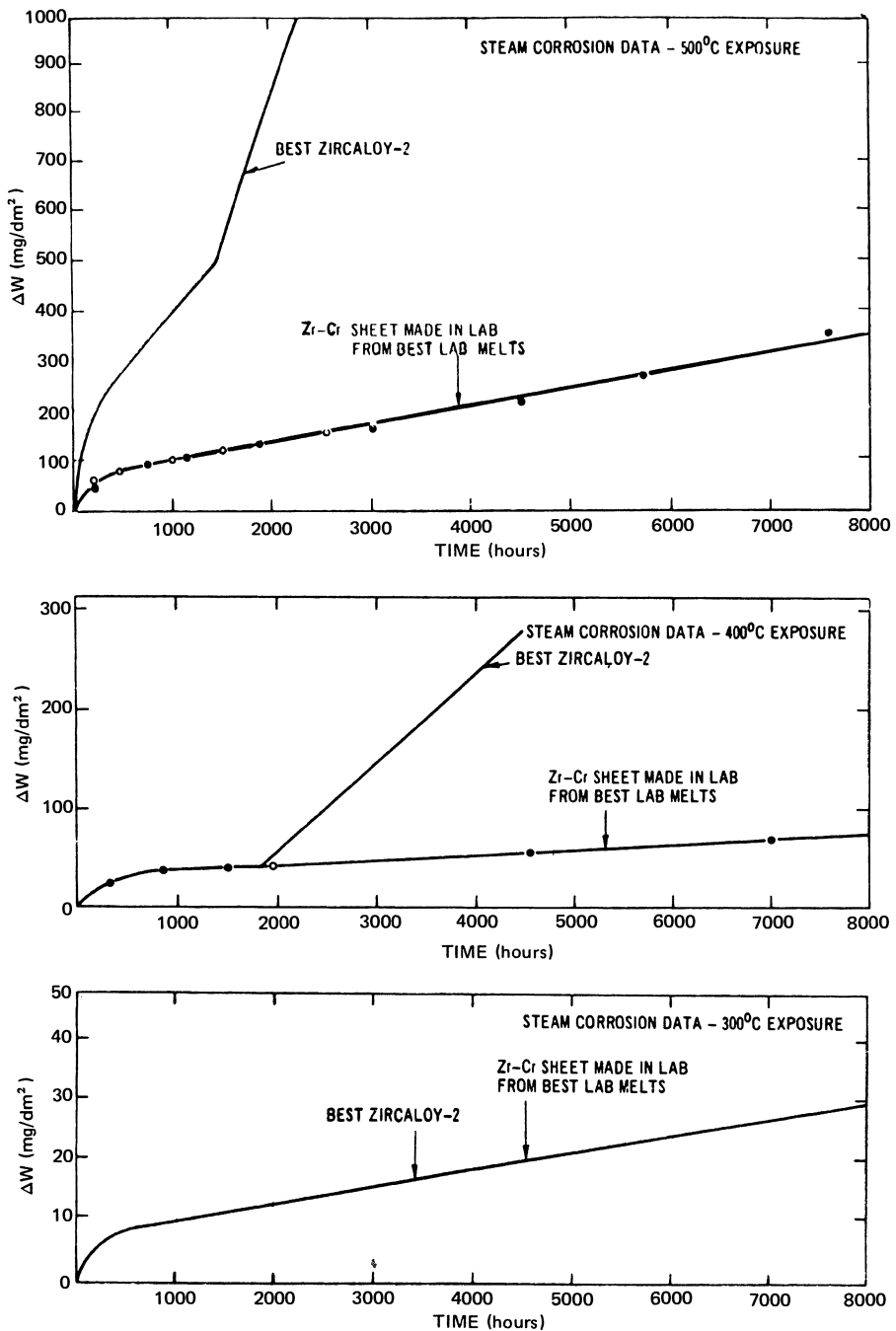


Fig. 37. Comparison of the oxidation of a Zr-Cr (Fe) alloy with Zircaloy-2 in 300, 400, and 500°C steam.²⁰¹

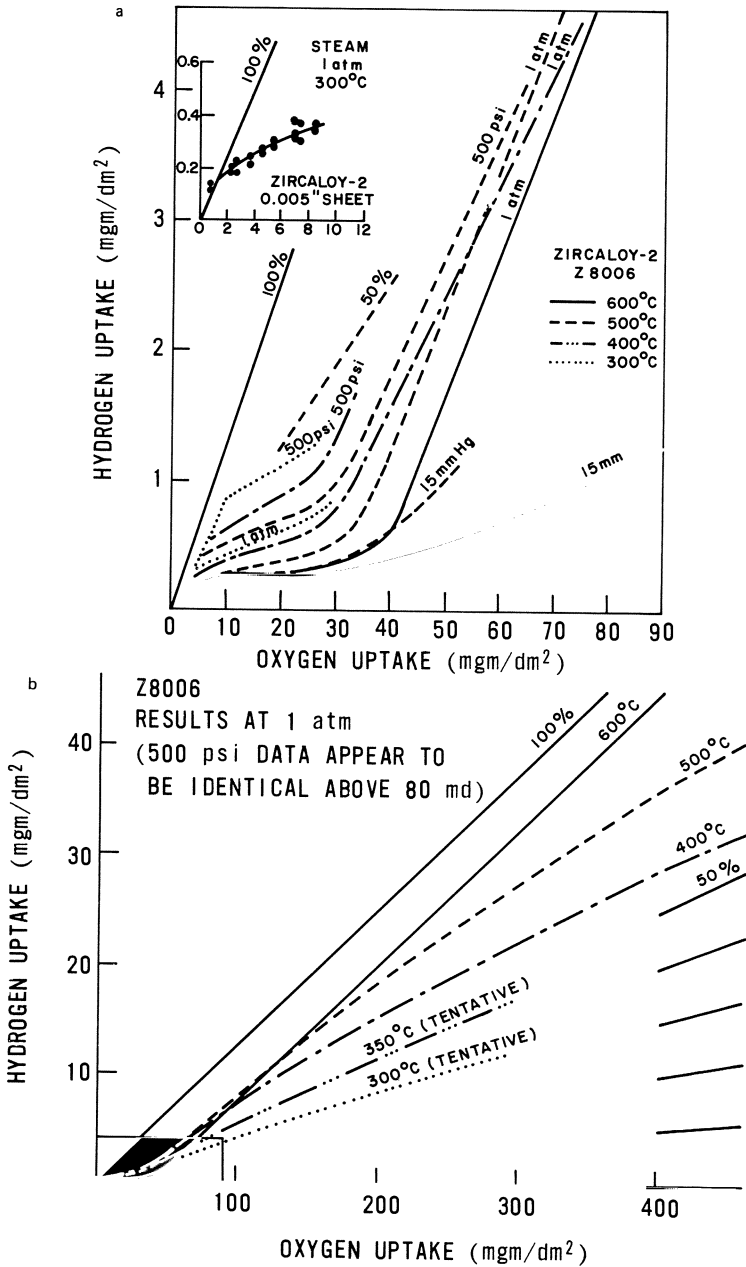


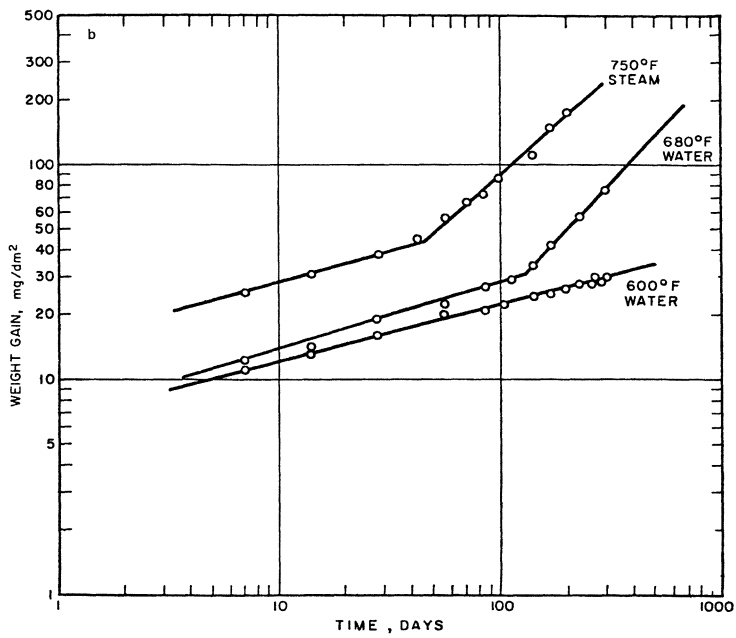
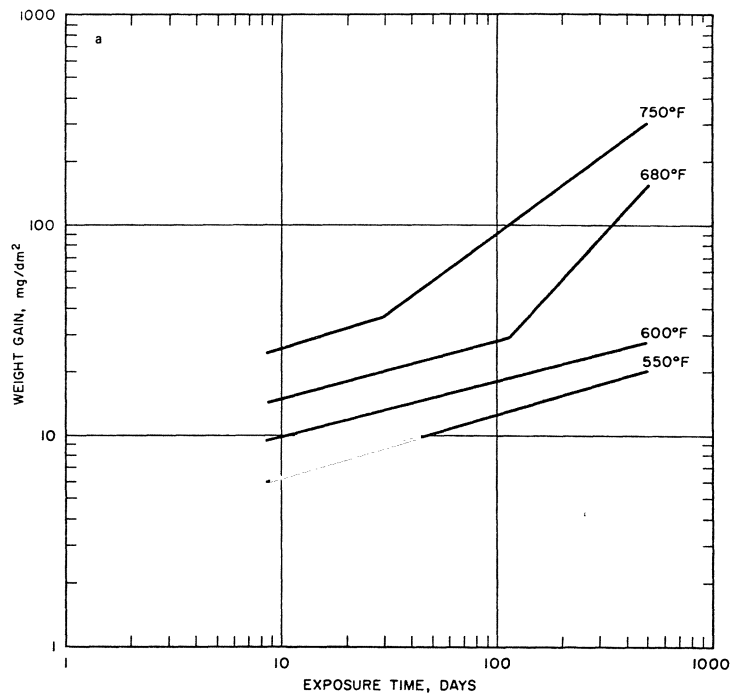
Fig. 38. Effect of temperature and pressure on hydrogen uptake by Zircaloy-2 in steam: (a) at low weight gains; (b) at high weight gains.⁴⁷

38).^{47,203–209} Progress on understanding the mechanism by which hydrogen enters the metal has been limited, but qualitative observations of the effect of various alloying additions on the magnitude of the hydrogen uptake have been a considerable spur to alloy development.

The observation of internal hydriding of the cladding on fuel which failed in early PWRs^{210,211} was the primary spur to the further development of the Zircalloys, since no hydriding problems had previously been encountered with Zircaloy-2. It was noted that alloys containing higher nickel contents than Zircaloy-2 picked up much more hydrogen during corrosion in water both in- and out-of-reactor.^{212–214} This observation led to the discovery that the small quantity of nickel normally added to Zircaloy-2 caused a significant increase in hydrogen uptake, and hence to the decision to eliminate nickel from Zircaloy-2. This gave the alloy known as nickel-free Zircaloy-2.^{8,215} Further studies showed that some alteration of the content of other transition metal additives in nickel-free Zircaloy-2 was necessary to improve the corrosion resistance in 400°C steam, and the alloy Zircaloy-4 resulted.^{8,215,216} The main difference from Zircaloy-2 besides the absence of nickel was an increase in the iron content, so that the total transition metal content remained the same (Table 1). The corrosion behavior of Zircaloy-2, nickel-free Zircaloy-2, and Zircaloy-4 is compared in Fig. 39. Subsequent development of alloys based on the Zircaloy range of compositions has not produced any commercially valuable products.^{217–220}

The development of zirconium alloys in the USSR^{36,221,222} followed a different course from that in the United States. Nevertheless, the Ozhennite alloys bear some resemblance to Zircaloy-2 in containing both transition metal additives (Fe, Cr, Ni), giving a second phase precipitate, and solid solution additives, capable of nullifying the effect of nitrogen (Sn, Nb). The standardization on iodide-process zirconium as a basis for alloying compared with the use of Kroll-process zirconium in the United States, probably accounts for the lower concentrations of tin and niobium found to be sufficient in the Russian alloys (Table 4), compared with the amounts of tin added to form the Zircalloys.

The Russians took the development of Zr–Nb alloys a step further using a Zr–1% Nb alloy for fuel cladding^{223,224,226} and utilizing the heat treatability of the alloys with 2–5% Nb to produce alloys with higher strength than the Zircalloys but still with adequate corrosion resistance.^{36,221–228} With suitable heat treatments corrosion rates comparable with those of Zircaloy-2 can be obtained with alloys containing 2% Nb and 3% Nb–1% Sn (Fig. 40). The further development of the Zr–Nb alloys has been taken up in several



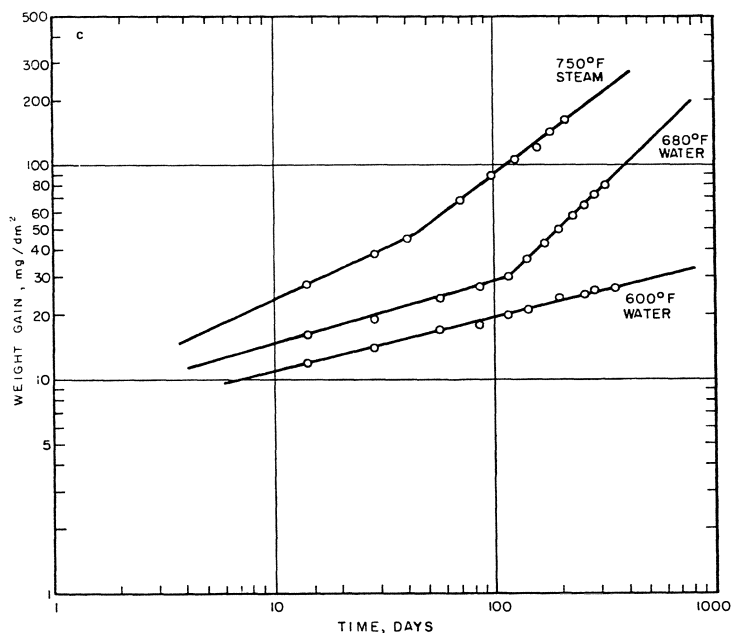


Fig. 39. Comparison of the corrosion resistance of the Zircaloys in the α -annealed condition: (a) Zircaloy-2; (b) Ni-free Zircaloy-2; (c) Zircaloy-4.⁸

laboratories.^{115,116,230-241} The Germans have concentrated on the Zr-3% Nb-1% Sn alloy, with some work on the 1% and 2.5% Nb alloys,^{242,243} and the Canadians on the Zr-2.5% Nb alloy. Only in Canada^{122,244-247} have these alloys seen extensive commercial use outside the USSR. The Russians have used the Zr-2.5% Nb alloy, and the Zr-2.5% Nb-0.1% B and Zr-1% Nb-0.2% B alloys (with boron added as a "burnable poison") in fuel bundle support structures and shroud tubes. The Canadians have used the Zr-2.5% Nb alloy, either in the heat-treated or cold-worked condition, as pressure tubes in their CANDU-type reactors, and the Zr-2.5% Nb-0.5% Cu alloy as "garter springs" to separate the pressure and calandria tubes in the same reactors.^{122,225,244-250}

Recent development of zirconium alloys has centered around the desire to obtain greater strength at high temperatures while still preserving adequate corrosion resistance. Most studies have been on a laboratory scale only, and no other alloys have yet reached the stage of commercial application. A large fraction of the elements in the periodic table have been studied on at least one occasion, and often in several investigations. There is not space here to

Table 4. Compositions of Zr-Nb Alloys Developed in the USSR^{36,223-225}

Alloying addition (wt. %)		Ozhennite 0.5	Ozhennite 1.0	Zr-1 Nb	Zr-2.5 Nb															
Sn		0.20 (0.18–0.22)	0.4	—	—															
Nb		0.10 (0.09–0.11)	0.2	1.0 (0.9–1.1)	2.50															
Fe		0.10 (0.09–0.11)	0.2	←	←															
Ni		0.10 (0.09–0.11)	0.2	<0.007	<0.007															
B ^a		—	—	(0.20) ^a	(0.10) ^a															
O		(0.09–0.12)	—	(0.09–0.12)	(0.09–0.12)															
Maximum impurity levels:																				
Element:	Al	B	Cd	C	Cr	Co	Cu	Hf	H	Ph	Mg	Mn	Mo	N	Si	Na	Ta	Ti	W	V
ppm:	75	0.5	0.5	270	200	20	50	150	24	130	20	50	50	60	120	10	200	50	200	50

^aAdded when burnable poison is included in fuel assembly.

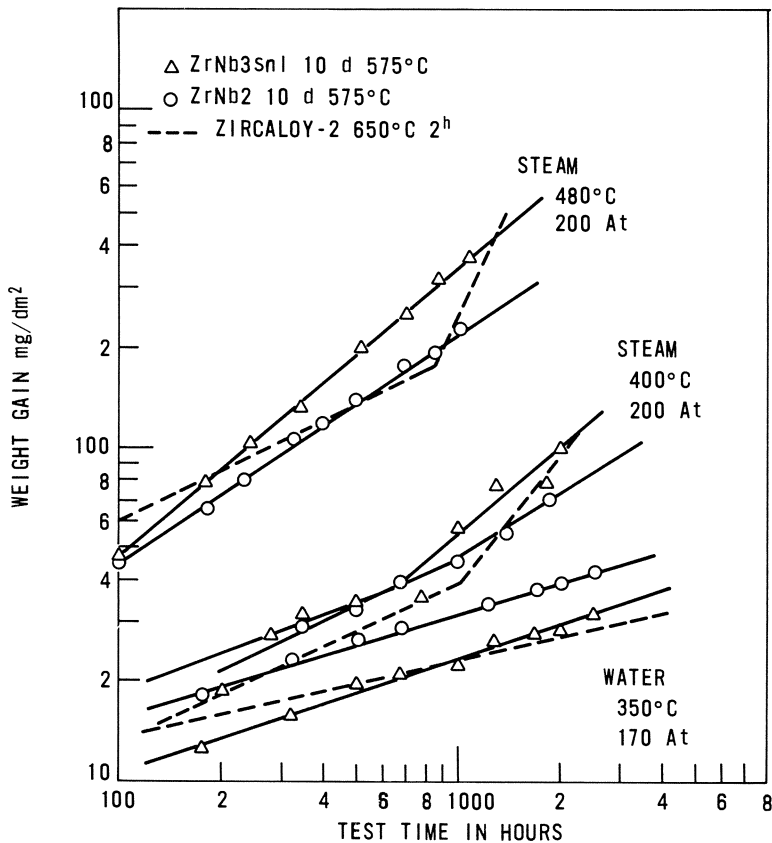


Fig. 40. Comparative corrosion curves for Zr-3% Nb-1% Sn, Zr-2% Nb and Zircaloy-2.²²⁹

discuss these studies in detail,²⁵¹⁻²⁷⁷ however, any investigator proposing a further survey of the periodic table in search of improved zirconium alloys would be well advised to study these references carefully.

The development of other alloys (e.g., ATR, TJR) for use in carbon dioxide-cooled reactors has already been discussed. Although the corrosion resistance of Zr-0.5% Cu-0.5% Mo (ATR), Zr-1.0% Cu-1.5% Mo (TJR) and Zr-Cu binary alloys has proved to be reasonable in high-temperature steam (500°C), they have behaved poorly in water and steam at 280-350°C, and are not, therefore, considered to be contenders for use in water-cooled reactors.^{241,262,272}

Corrosion in Water and Steam

In an attempt to simplify discussion of the behavior of zirconium alloys in high-temperature water and steam, the factors affecting corrosion will be considered separately for each of three main groups of alloys (Zircalloys; Zr–Nb alloys; Zr–Cr–Fe alloys). For the other miscellaneous alloys considered at the end of the last section,^{251–277} there is not usually enough information on any one alloy to warrant a detailed discussion. In the light of the major differences in behavior between the three main groups of alloys which have been revealed, it would be unwise to generalize by assuming that any particular one of these miscellaneous alloys will fit into one of the primary three groups. Thus the oxidation behavior of ATR (Zr–0.5 Cu–0.5 Mo) in steam is strongly heat-treatment-dependent,²⁷² and in this respect it resembles a Zr–Nb alloy; however, in its good high-temperature steam resistance²⁷² and poor 300°C water resistance²⁴¹ it is more like a Zr–Cr–Fe alloy. Thus the reader who is interested in an alloy which does not fall into one of the three main groups would be advised to assume that it will show a response to any condition which is unique, and not expect it to behave in general like any member of the three primary groups.

Since the early days of zirconium alloy development little work has been performed on unalloyed zirconium because of the variable nature of the “breakaway” process in water and steam, leading to white oxide spots and spalling oxide after (in some instances) very short exposures. For that reason zirconium will not be considered separately, but it will be used mainly in comparing effects on the Zircalloys.

The Zircalloys

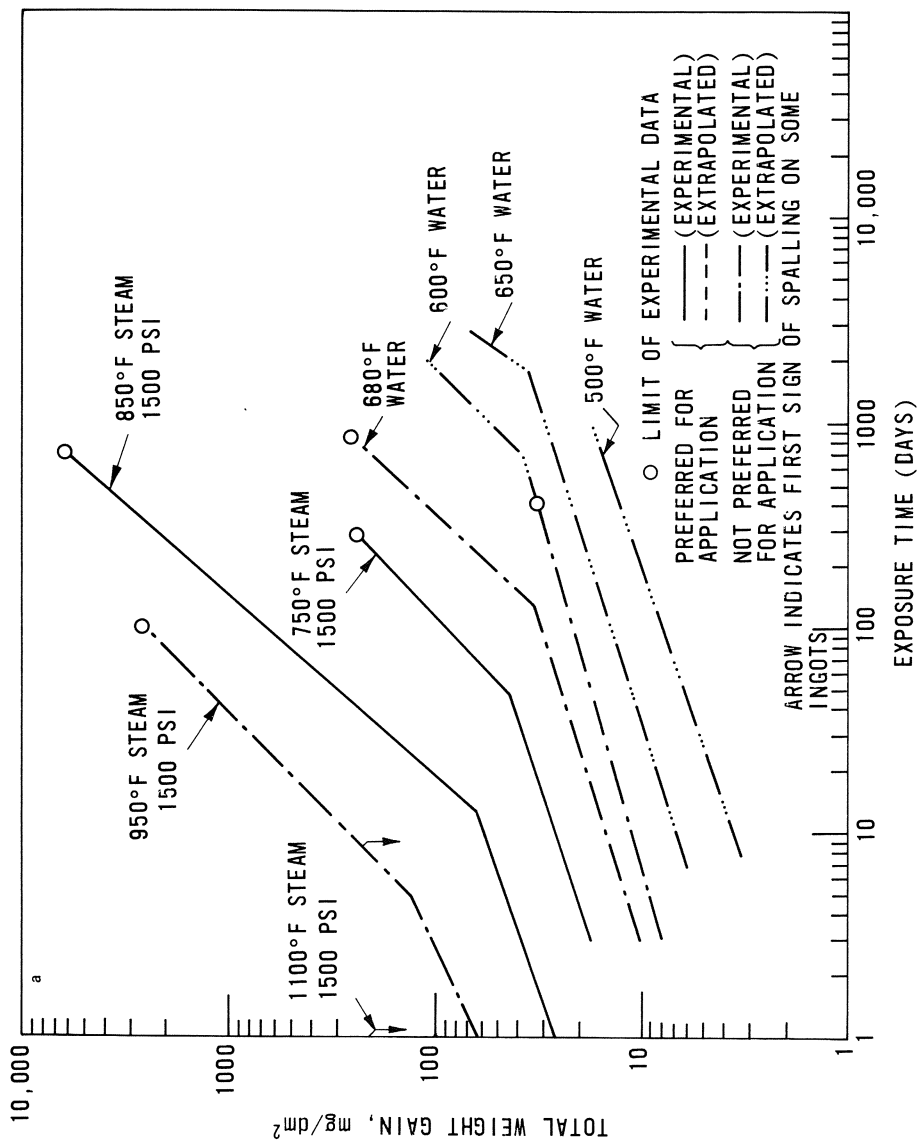
Oxidation Kinetics. The oxidation kinetics of all the Zircalloys in high-temperature water or steam can be divided into two main periods, colloquially referred to as pre- and post-transition. In this respect the behavior of these alloys is virtually identical with their behavior in oxygen. In the first of these periods a black coherent oxide film is formed (after the initial appearance of interference colors) and the oxidation rate diminishes with time according to a rate law approximating to the simplified form $\Delta w = kt^n$, with the exponent n lying in the range 0.25–0.6. A transition follows to a period where the rate law is nearer to linear on average ($n \sim 1$). This transition is followed by the replacement (or conversion) of the black oxide by a gray or white oxide (although this is seldom visible to the naked eye) for the Zircalloys, until some time after evidence for transition is available from a weight grain versus time plot. By using the above conventions for the

oxidation kinetics, it is possible to compare (Fig. 41) the long-term corrosion of Zircaloy-2 in the α -annealed and β -quenched conditions.^{278,279} The difference in response at high temperature and pressure should be noted.

As with the kinetics in oxygen,^{20,21} more detailed studies of the kinetics in steam and water^{21,280,281} have shown that this apparent simplicity is only superficial and that, when the kinetics of an individual specimen are followed, they are found to be very complex. At least one well-defined inflection has been found in the pre-transition kinetics by all investigators who have studied the oxidation in detail (Figs. 42 and 43). This inflection occurs at oxide film thicknesses, in the range 0.1–0.5 μm , in oxygen,²⁰ steam,²¹ and fused salts,^{10,186} depending upon the conditions of oxidation and the pre-treatment of the specimen (Fig. 5), and in one investigation has been shown to relate to an increase in the electrical conductivity of the oxide when its growth reaches a certain stage.^{10,282}

The significance of this inflection is of mainly mechanistic rather than practical importance at present, although changes in the oxide film which occur at this point in the oxidation curve have been found to trigger the localized internal oxidation of the Zircaloys in chloride and bromide containing fused salts,⁹⁴ and may also be involved in irradiation-induced changes in the oxidation rate²⁸³ which seem to appear at about this stage in the oxide growth. These points will be discussed in more detail later.

The transition point is apparently a “point” only when the results are plotted in log/log form; a method of plotting which has some qualitative advantages for comparing alloys, but which can often lead to misleading results if used to draw mechanistic conclusions.¹⁰⁰ Continuous recording of weight changes on a microbalance at subatmospheric pressure has shown that the transition process can take from an oxide thickness of ~ 2 to 5.7 μm (Fig. 44) before it is complete and a linear post-transition rate ensues.⁴⁷ This effect is paralleled (especially at high temperatures) by the observation of gray oxide nucleating along specimen edges and at spots on the specimen face and spreading slowly across the entire sample.³³ At low temperatures this effect is less prominent, and often little visual effect of transition is seen until well past the break in the kinetic curve, when an overall mottled gray appearance develops. Thus the transition process involves some nucleation phenomenon, resulting in a local change in the oxide properties, followed by spreading of this change. The rapidity with which this phenomenon spreads over the specimen surface is a function of specimen geometry,⁴⁷ temperature and pressure (Fig. 45).²¹ At low temperatures nucleation sites are apparently common, but spreading is slow; at high temperatures fewer nucleation sites are operative, but spreading is rapid. Transition is much faster at a given



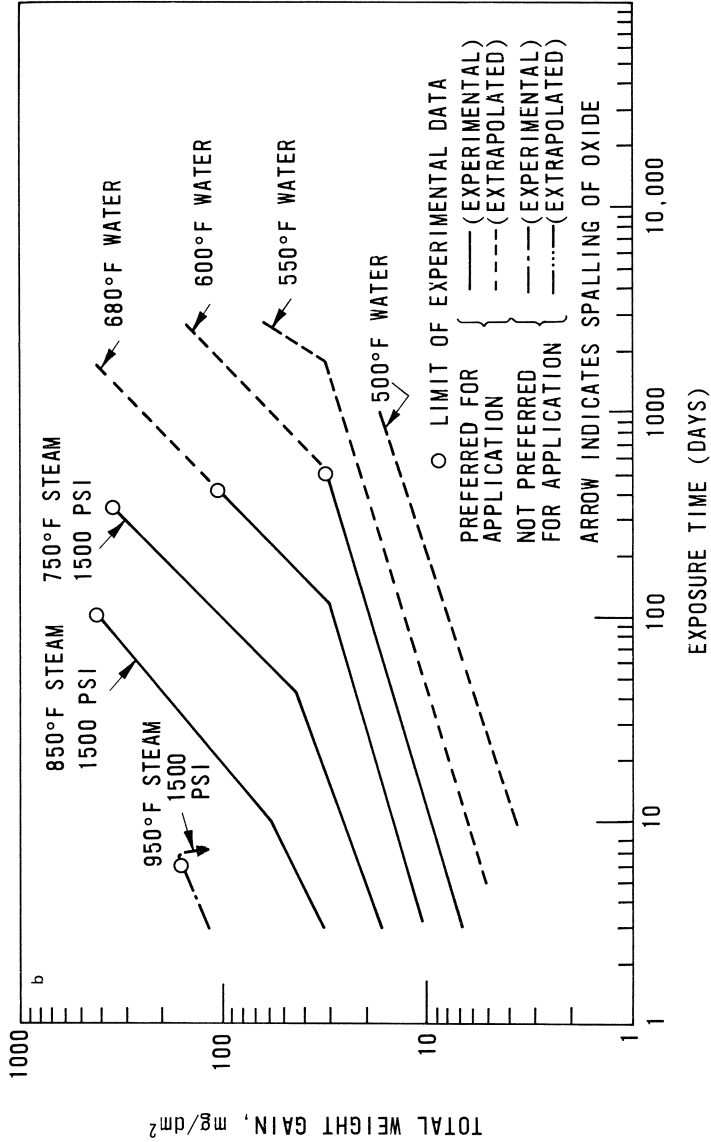


Fig. 41. Long-term oxidation curves for α -annealed (a) and β -quenched (b) Zircaloy-2.²⁷⁸

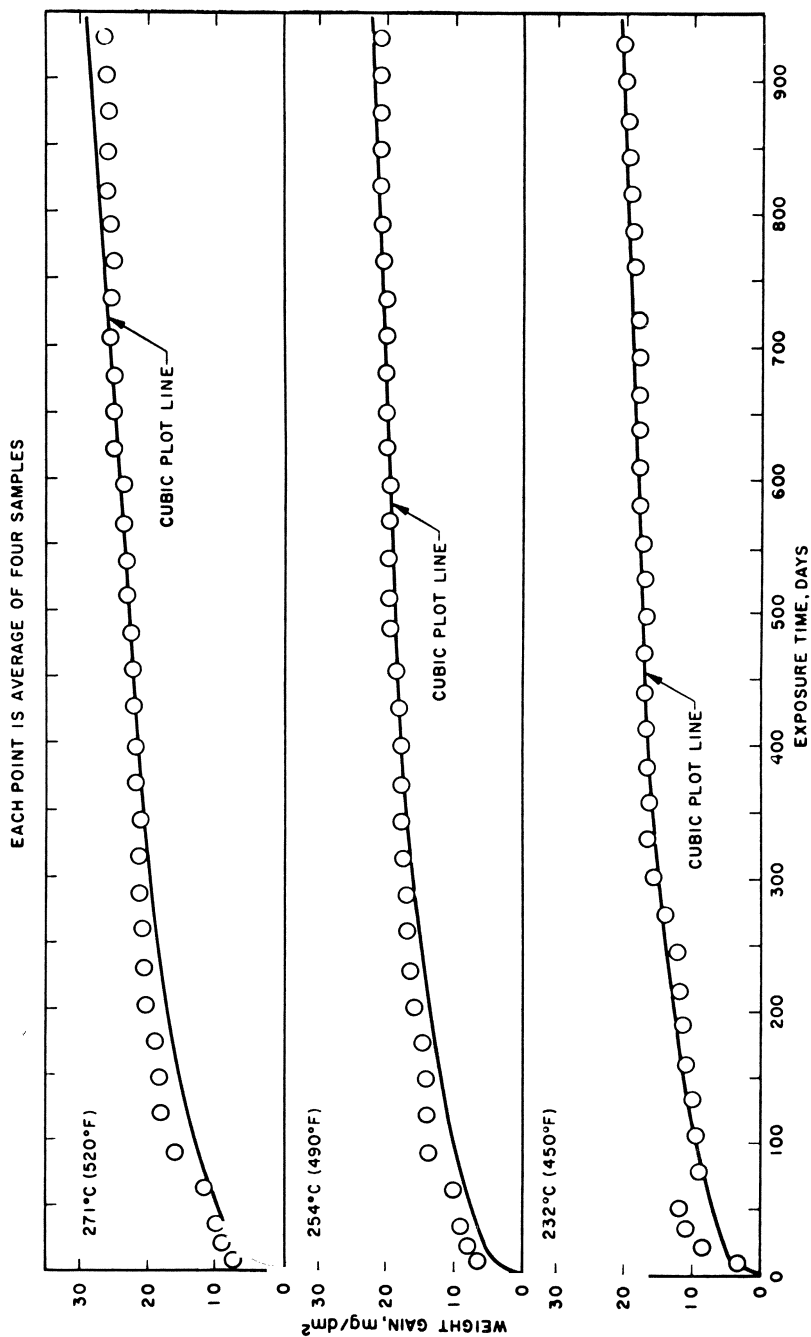


Fig. 42. Corrosion of Zircaloy-2 at low temperatures in pH-7, degassed water at saturation pressure showing departures from a smooth cubic kinetic curve.^{27/9}

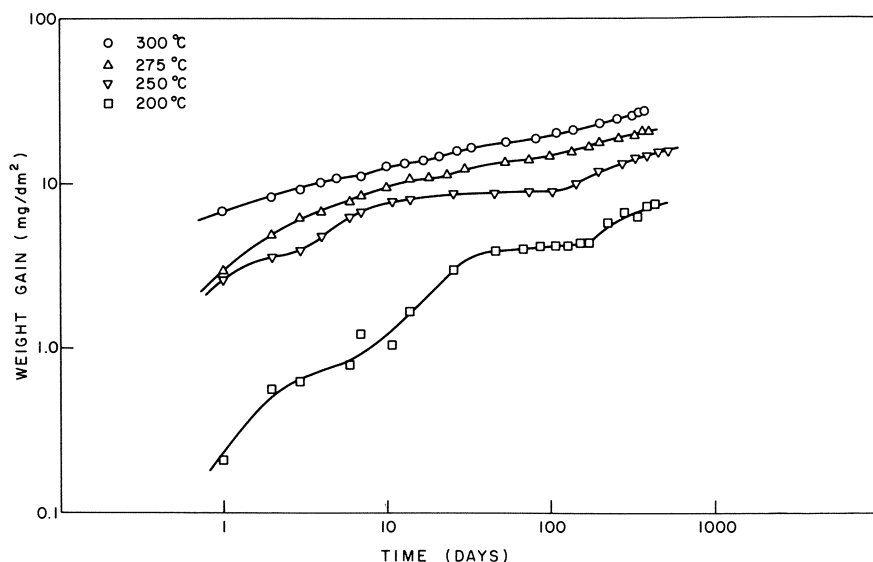


Fig. 43. Oxidation of Zircaloy-2 (batch Ac) in water at 200–300°C, showing inflections in the oxidation curve.²⁸⁰

temperature in high pressure than in low-pressure environments, despite the negligible effect of pressure on the pre-transition kinetics over a wide range of pressures. In all these respects the process is similar to the same phenomenon in oxygen or air for the Zircalloys. A direct involvement of hydrogen in the process does not seem probable except under special conditions²⁸⁴ for reasons to be stated later.

The nature of the post-transition kinetics is also influenced by the temperature and pressure of oxidation. These approximate to linear only at high temperature and/or low pressure.⁴⁷ When the behavior of individual specimens is followed at low temperature and high pressure the kinetics are found to be cyclic in nature.^{47,285–288} Some discussion has taken place of whether or not these cycles involve “starting again” at the beginning of oxidation. The answer is dependent upon a knowledge of the cause of the kinetic transition, a subject still in contention. The apparent linearity at high temperature may merely represent a condition where the transition process occurs on a small scale, and gets sufficiently out of phase on different parts of the specimen to average out; at long times this “averaging out” occurs under all conditions.

Oxidation at Very High Temperatures (LOCA). Loss of the coolant from a water-cooled nuclear reactor will lead to a severe transient overheating of

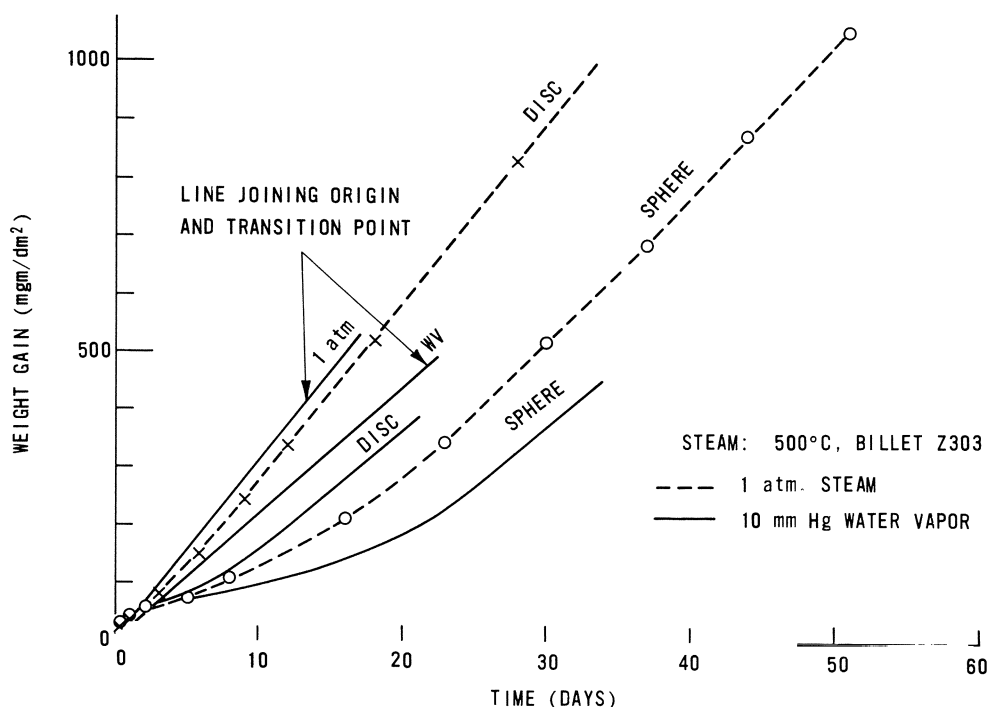


Fig. 44. Effect of specimen geometry on the propagation of the oxidation kinetic transition for Zircaloy-2 in steam.⁴⁷

the fuel and cladding. Concern about this situation arises from several possible consequences: (1) ballooning of the fuel cladding could block cooling channels and delay (or prevent) ingress of the emergency core cooling water; (2) embrittlement of the cladding by oxidation and the oxygen diffusion zone could lead to extensive cladding failure and fission product release when the cladding is quenched by the emergency cooling water; (3) hydrogen generated by the high-temperature oxidation reaction might lead to a chemical explosion; and (4) the exothermic heat of oxidation of zirconium might lead to a runaway ("burning") situation.

Experimental measurements of the oxidation behavior have used either unfueled specimens heated in water or steam,^{289,291} small fuel elements given power transients in an in-reactor loop,²⁹² discharge of capacitors through zirconium wires immersed in water,^{293,294} or the spraying of zirconium droplets into water.^{290,295,296} The most conservative of these data are those obtained from isothermal bulk specimens (Fig. 46), whereas the most pessimistic are those obtained by the capacitor discharge technique

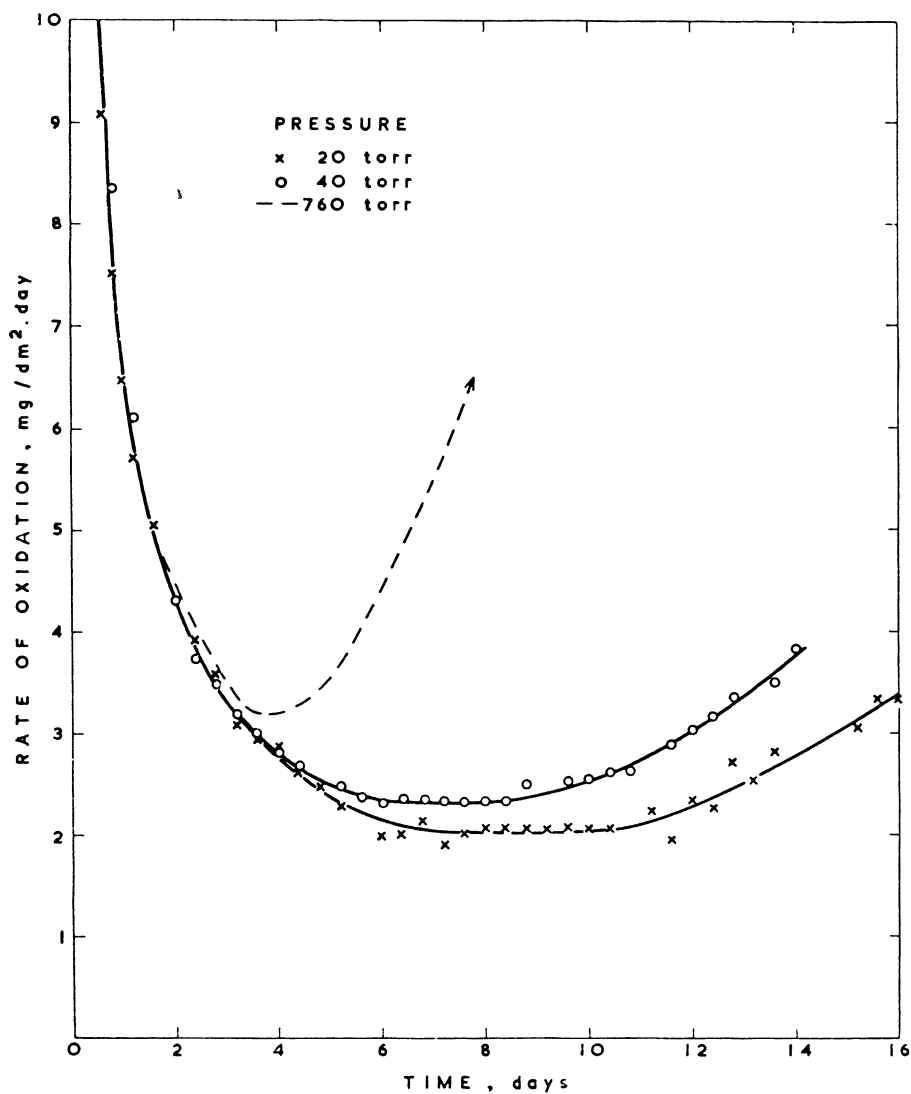


Fig. 45. Effect of pressure on the rate of propagation of the oxidation kinetic transition for Zircaloy-2 in steam.²¹

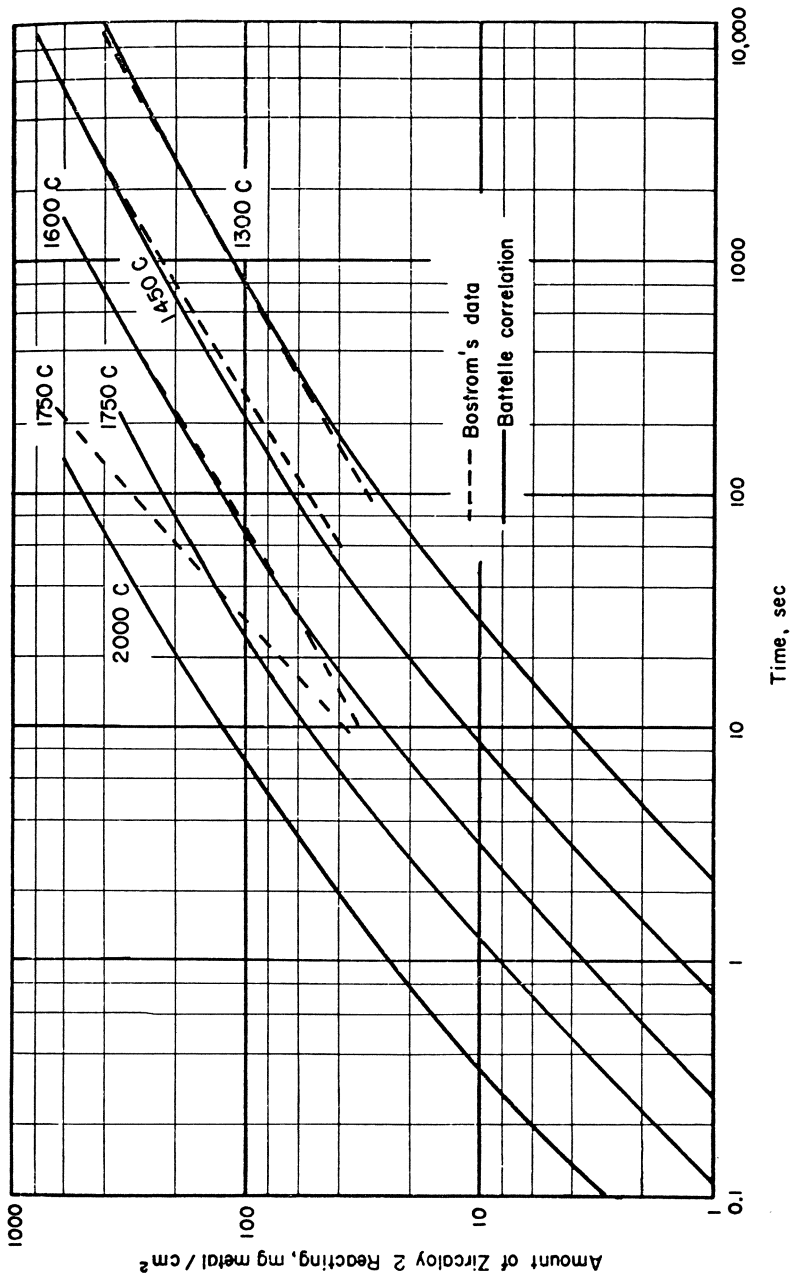


Fig. 46. Oxidation kinetics of Zircaloy-2 at very high temperatures.²⁹⁰

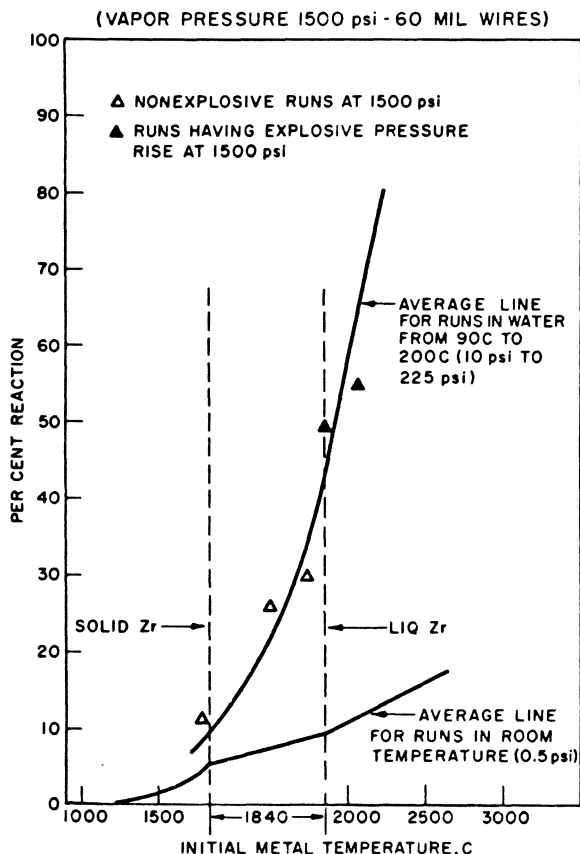


Fig. 47. Results for the fraction of zirconium reacting with 315°C water during capacitor discharge experiments.²⁹³

(Fig. 47). That these differences probably result from the degree of fragmentation of the specimens occurring in the tests is shown by Higgins' results (Fig. 48) for the extent of reaction as a function of particle size.

Assessments of the significance of these results²⁹⁷⁻³⁰¹ have varied according to the assumptions made about conditions during the transient. The extent of reaction observed with small fuel elements pulsed in the TREAT reactor has generally been less than would be predicted from capacitor-discharge tests²⁹² and fears about excessive reaction of the

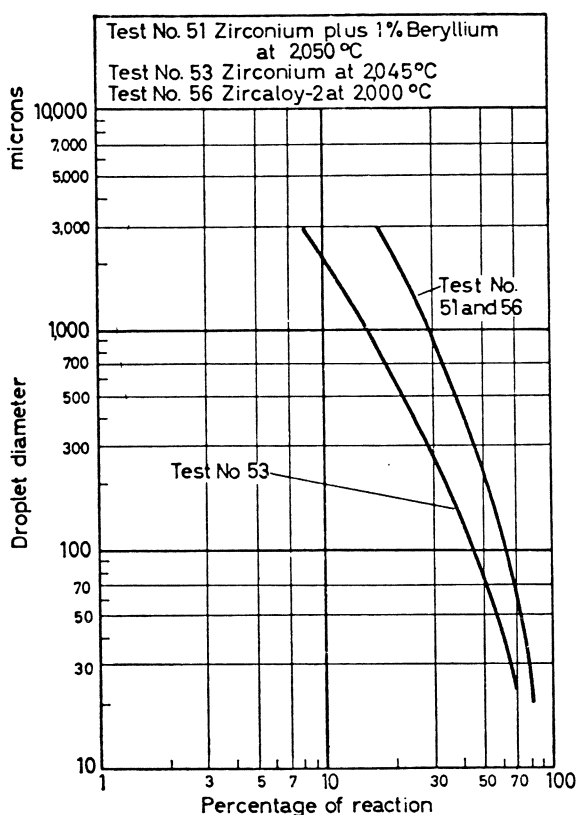


Fig. 48. Effect of zirconium particle size on the amount of reaction with water at very high temperatures.²⁹⁵

cladding and chemical explosions from the hydrogen produced are not now considered to be realistic; ballooning of the cladding³⁰²⁻³⁰⁵ and disruption as a result of embrittlement from oxygen diffusion are now the major concerns.³⁰⁶ Theoretical calculations of the depth of penetration of oxygen have been compared with experimental measurements, generally by treating the problem as a moving boundary diffusion process with two moving boundaries (oxide- α Zr; α Zr- β Zr). These have been treated in computer codes which fit the transient temperature experienced by the cladding.^{306,307}

All the above treatments deal with penetration of oxygen into unstressed zirconium alloys: Bradhurst and Heuer⁸⁹ have recently shown that, when Zircaloy-2 is stressed during exposure to steam at very high temperature, repeated cracking of the oxide can lead to penetrating fingers of both oxide

and dissolved oxygen which can embrittle the cladding to greater depths than would be calculated from a simple diffusion treatment, assuming plane-parallel interfaces for the several boundaries present (Fig. 49). The temperature, extent of pre-oxidation, and rate of deformation were important in determining the magnitude of the effect, which reached a maximum of about a factor of 2.⁸⁹

Effects of Surface Preparation and Contamination. In the early days of zirconium alloy development much work was done on the effect of surface preparation on the corrosion of unalloyed zirconium. Cold-working the surface (by abrasion) caused significant increases in oxidation and white oxide spots and spalling oxide occurred when the surface finish was rough. Finally, a standard pickling procedure was adopted which gave a reproducible, smooth surface finish, provided the specimen surface was not heavily oxidized to begin with,³⁰⁸ and this has remained the standard surface preparation for the Zircalloys for many years.³⁰⁹⁻³¹¹

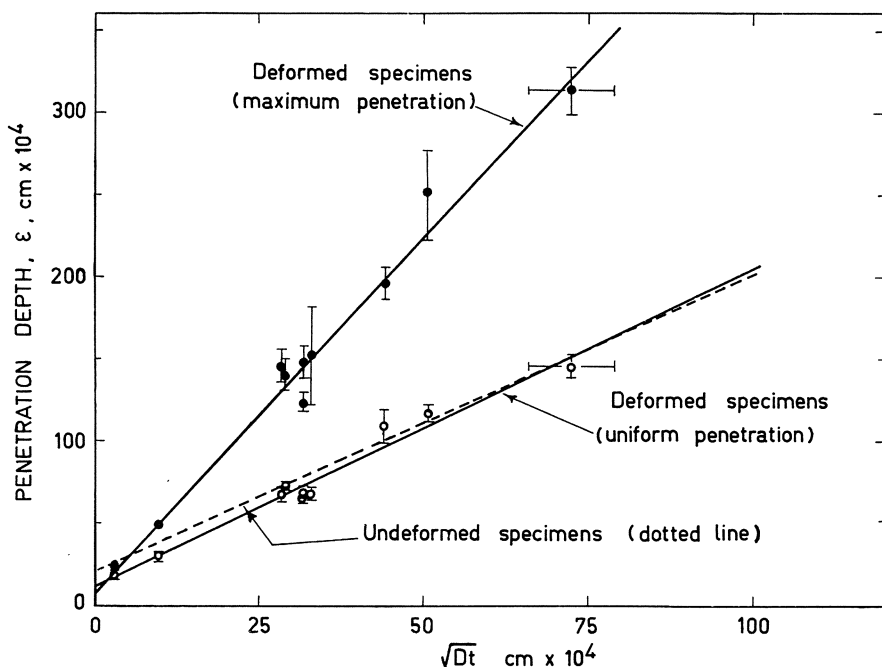


Fig. 49. Effect of deformation during oxidation in steam on the penetration of Zircaloy-2 specimens at very high temperatures (690–1140°C) expressed in terms of \sqrt{Dt} .⁸⁹

Concern for the effect of residual fluoride from the etching treatment on the subsequent corrosion resistance has been a primary concern of investigators from the beginning.^{312–317} Certainly, there is no doubt that gross contamination of either the specimen or the water³¹⁶ or steam³¹⁷ with fluoride either from the pickling treatment or from other sources such as gasketing materials,³¹⁸ or fluoride impurity in UO_2 fuel,^{317,319} can lead to severe pitting and gross corrosion of Zircaloy-2 samples. Claims have also been made that the amount of fluoride left on the specimen surface by even the most careful pickling and rinsing treatments^{314,320} was detrimental to the oxidation resistance, particularly in the early stages of oxidation.^{20,321–324} These studies showed that pickled specimens of zirconium and Zircaloy-2 oxidized somewhat faster than electropolished specimens (Fig. 5), and this was claimed to be an effect of fluoride adsorbed on the specimen surface.^{20,321–324}

Experiments in which electropolished specimens of Zircaloy-2 were immersed in neutral fluoride solutions showed that these specimens adsorbed fluoride on their surfaces to levels comparable with pickled specimens, but showed no increase in oxidation rate.¹⁰ Electron microscope studies showed that the behavior of the intermetallic particles in Zircaloy-2 was considerably different during pickling and electropolishing. Pickling dissolved only nickel-containing intermetallics and left chromium-containing intermetallics in the surface, whereas electropolishing removed both types of intermetallic.¹⁰ Since it is the presence of these particles which apparently controls the electronic component of the oxidation current, complete removal of intermetallic particles from the surface layers would lead to a more resistive oxide, and hence to an initially lower oxidation rate.¹⁸ Once the oxide became thick enough to intersect subsurface intermetallic particles, the effect should disappear, as is observed for the minor difference in oxidation between electropolished and well-pickled surfaces.²¹⁴ It seems likely that it is such a difference between pickled and electropolished specimens which influences the oxidation rate rather than the presence of minor amounts of fluoride ion.¹⁰

Grosser contamination with fluoride does not appear to give an oxidation rate which returns to normal by the time the kinetic transition is reached. This may be related to the difficulty of removing fluoride contamination, which is apparently volatile in 500°C steam, but may not be in high-temperature water.^{320,325} Hence, the supposition is that the fluoride ion diffuses into the oxide film and leads to oxide breakdown. Fluoride has been observed to diffuse to the oxide/metal interface in anodic tantalum

oxide films, where it disrupts the bond between oxide and metal,^{326–328} but evidence in zirconium is ambiguous. Möller and Starfelt's results³²⁵ could be interpreted as support for such a phenomenon in Zircaloy, but the experimental details given are inadequate; Mackintosh³²⁹ allowed fluoride to adsorb in pre-oxidized specimens but did not look at the distribution after subsequent oxidation.

Since it is apparently very difficult to obtain any zirconium surface which is fluoride-free after pickling the specimen,^{320,325} and since other methods of surface preparation (e.g., machining and grinding) seem to reduce the oxidation resistance of the Zircaloys far less than they do that of zirconium,^{324–330} there is no incentive to use a surface preparation technique which may give increased oxidation or hydrogen uptake for even a brief period. Hydrogen absorption during the actual pickling procedure is very difficult to prevent during the thinning of foils for electron microscopy, and presumably similar small amounts of hydrogen are absorbed by bulk specimens.^{331–333} The dangers of pickling are exemplified by the correlation between greatly enhanced oxidation in highly oxygenated high-temperature water and pickled specimens observed by Shirvington *et al.*^{187,334}

Because high-quality machined and ground Zircaloy-2 surfaces have been shown to oxidize no more rapidly than pickled surfaces over long periods of time,^{324,330,335} there is a current tendency to move away from the use of pickling for reactor components and to substitute a caustic and/or detergent wash. It is probable that pickling or electropolishing will remain standard for laboratory studies because of the advantages given by the smooth reproducible surface for mechanistic studies, particularly where visual examination of the surface is intended.

Few contaminants other than fluoride have been shown to have serious effects on the oxidation kinetics. However, very small quantities of mixed nitrate and chloride (or bromide) salts can lead to severe intergranular oxidation,¹⁹⁴ and the corresponding iodide mixture gives transgranular stress corrosion cracking³³⁶ in air, oxygen, or low-pressure steam. An instance of severe corrosion during in-reactor autoclave experiments as a result of inadvertent contamination of this type has been observed.³³⁷

Other studies have shown that contamination of the surface during annealing in silica capsules can lead to an increase in the initial oxidation rate.³²² This was ascribed by the authors to an effect of copper impurities in the silica; a further possibility, the deposition of silicon via the volatile silicon monoxide, does not seem to have been considered. Contamination of surfaces with iron, nickel, copper, and calcium ions from solution was

also shown to affect the initial oxidation rates. The largest effects were observed with copper and calcium contamination.³²² Most of these studies were performed on unalloyed zirconium, and the sensitivity of the Zircalloys to similar contamination is not known.

Effect of Impurities in the Metal. The corrosion resistance of unalloyed zirconium is very sensitive to the nitrogen content, and a number of other impurities have major but less disastrous effects.³ The Zircalloys are far less sensitive to variations in impurity levels—they were developed with this aim in view. Small effects of a number of impurities (e.g., C, N, Si, Al, O, Ti, Mn, and Cu) have been demonstrated in careful experiments, however.^{338–345} Results for the more important of these impurities (C, N, O, Si, and Al) are shown in Figs. 50–54.

Effect of Metallurgical Variables. During the development of the Zircalloys, localized corrosion of some batches of material (white-oxide spots)

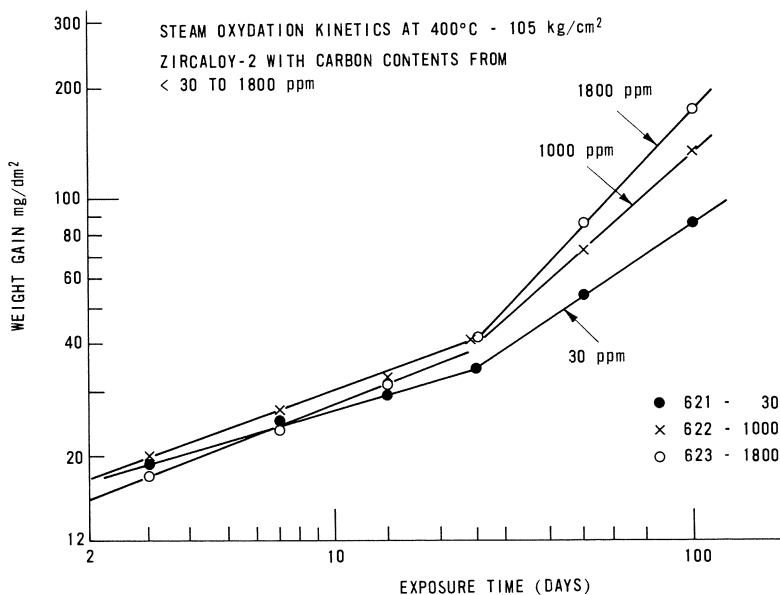


Fig. 50. Effect of carbon impurity on the oxidation of Zircaloy-2 in 400°C steam.³⁴⁴

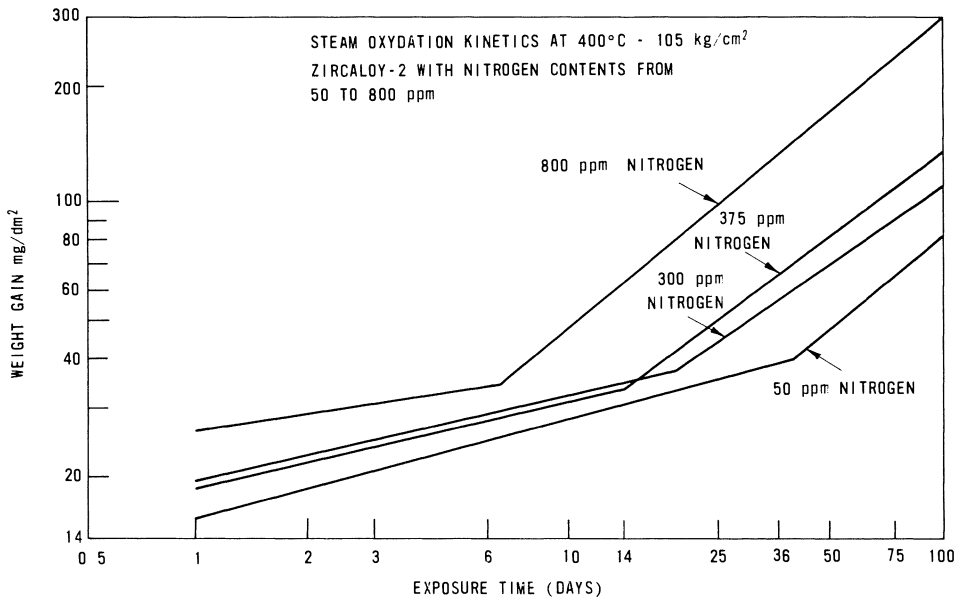


Fig. 51. Effect of nitrogen impurity on the oxidation of Zircaloy-2 in 400°C steam.³⁴⁴

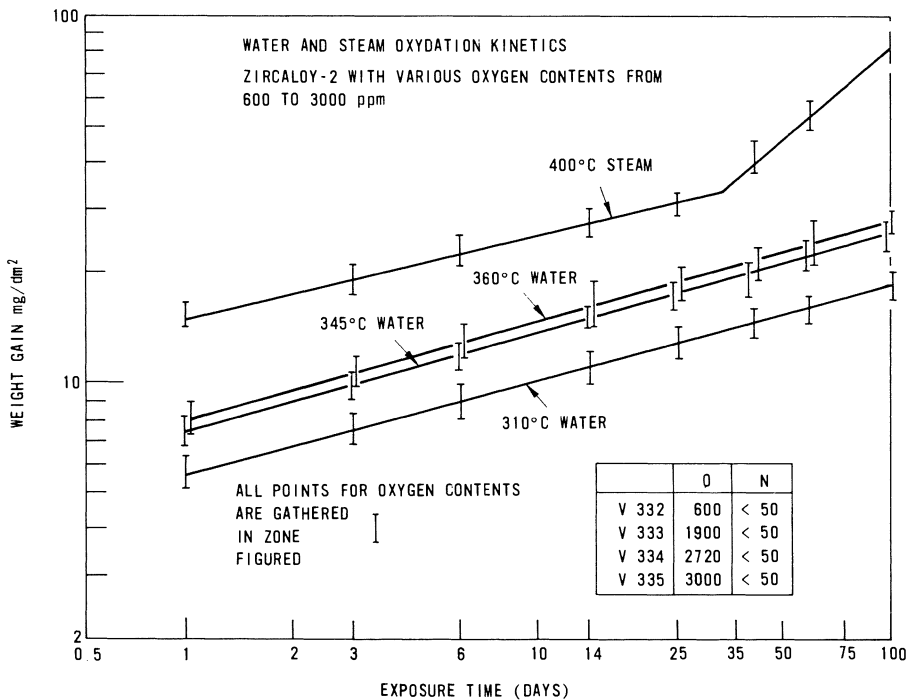


Fig. 52. Effect of oxygen impurity on the oxidation of Zircaloy-2 in 400°C steam.³⁴⁴

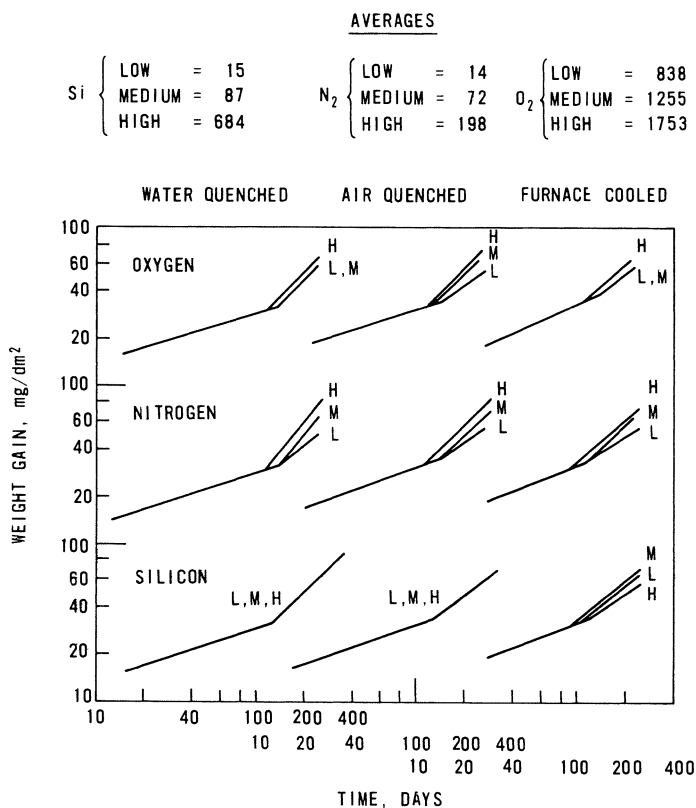


Fig. 53. Combined effect of Si, N, and O on the oxidation in 360°C water of Zircaloy-2 cooled at various rates through the ($\alpha + \beta$) phase region.³⁴⁰

was observed. This was associated with the occurrence of stringers of intermetallic particles in the material, and (in the case of inert atmosphere melted material) with gas-void stringers.^{8,198,346} The avoidance of these problems was found to depend on exceeding a critical cooling rate (Fig. 55) during cooling from the β -phase,^{8,347} or by giving a β -quench.^{348,349}

Provided the critical cooling rate was exceeded, only minor variations in the corrosion rate were observed with changes in heat treatment (Figs. 39 and 41). The phenomenon appears to be related to the size and separation of the intermetallic particles produced by the heat treatment. Other metallurgical factors, such as the degree of cold working and texture, do not affect the long-term corrosion rate significantly.

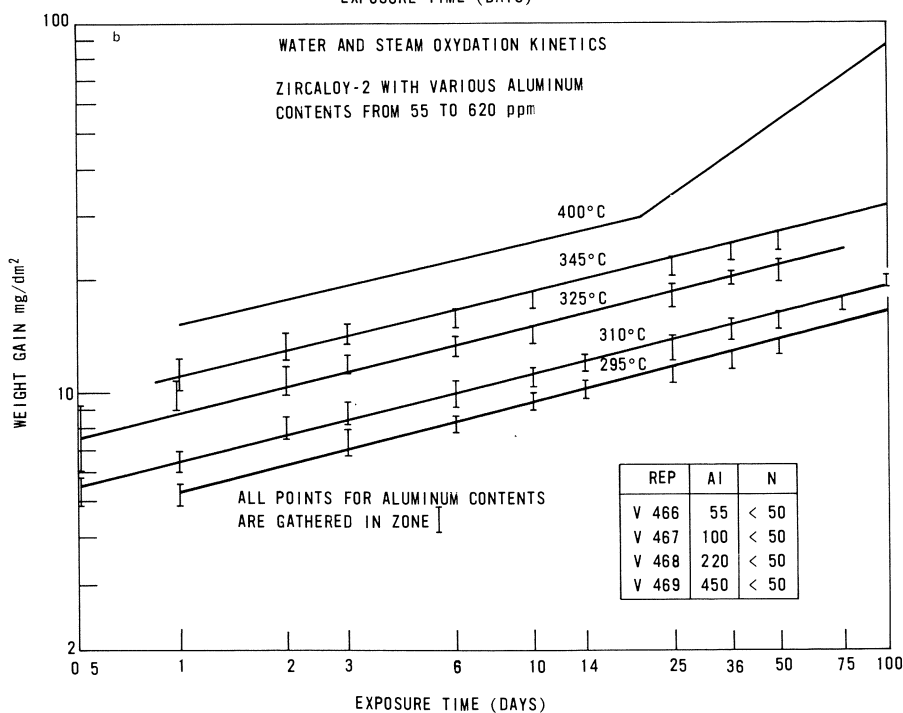
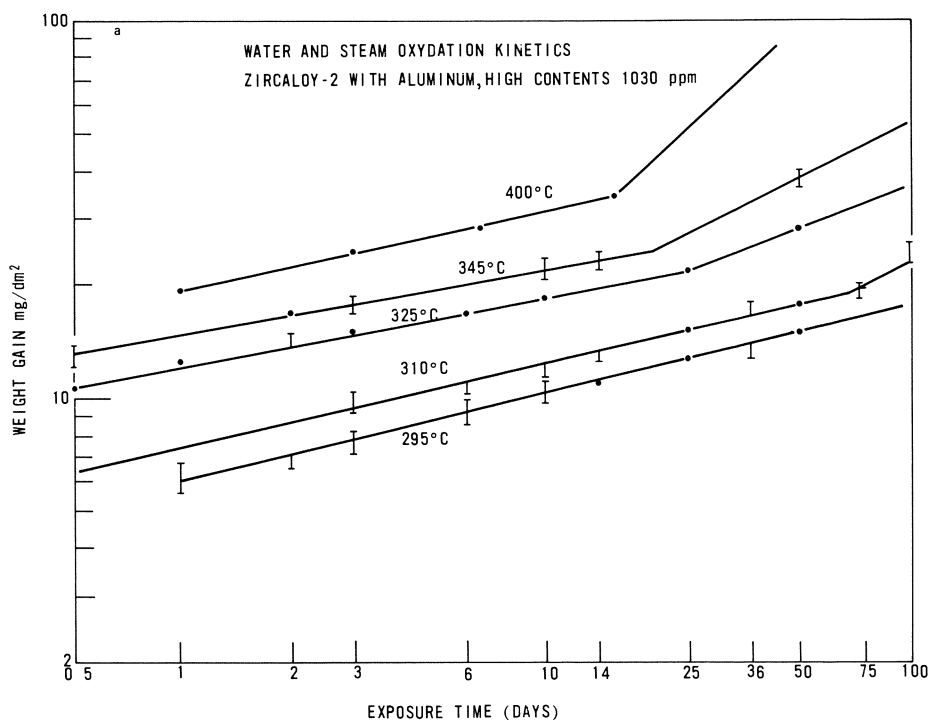


Fig. 54. Effect of (a) low and (b) high aluminum contents on the oxidation of Zircaloy-2 in water and steam.³⁴⁴

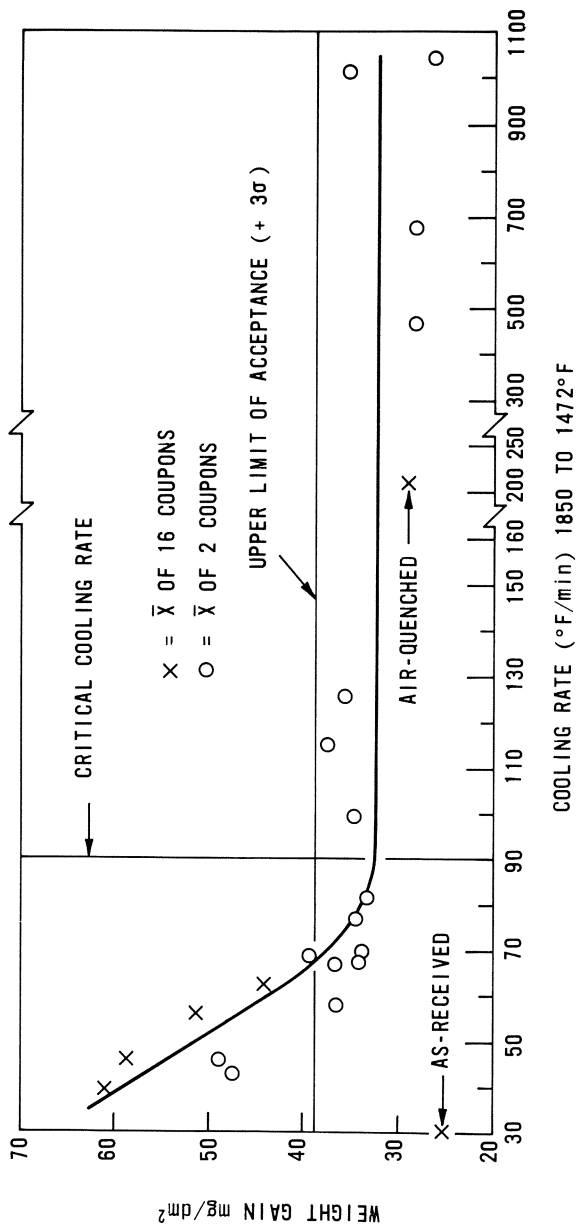


Fig. 55. Effect of cooling rate through the ($\alpha + \beta$) phase region on the corrosion resistance of Zircaloy-2 in 400 $^{\circ}\text{C}$ steam.⁸ (Reprinted by permission of ASTM from copyright material.)

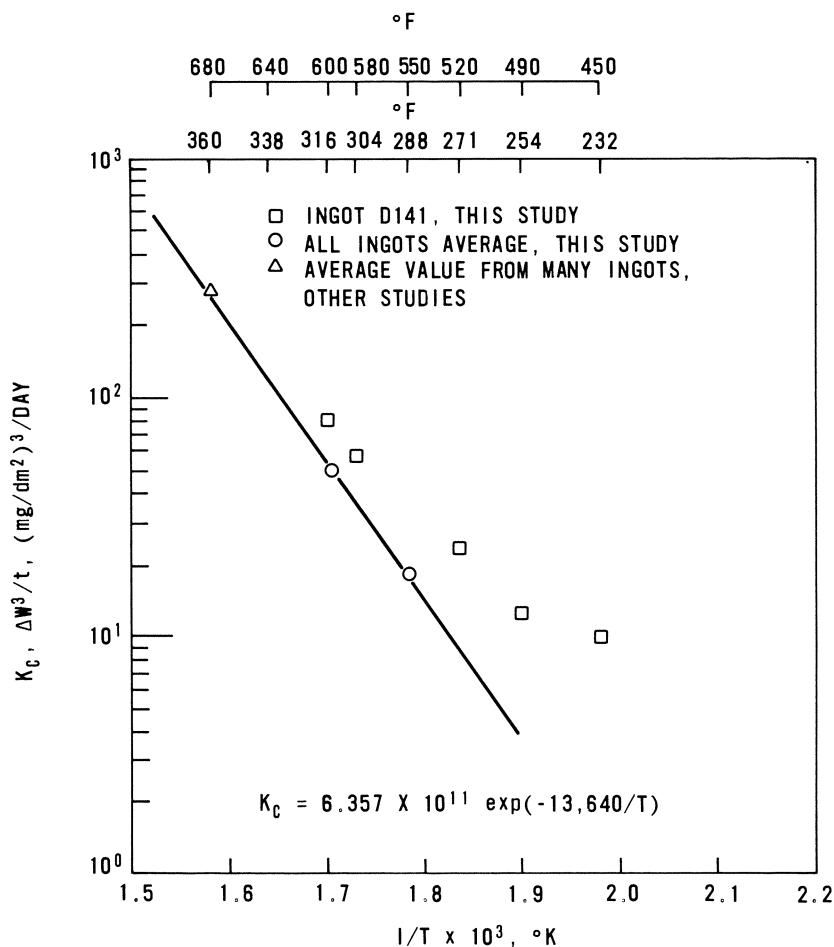


Fig. 56. Variations in the corrosion rates of batches of Zircaloy-2 in water at 450–680°F.²⁷⁹

Minor variations in corrosion resistance have been detected between batches of the same alloy in the pre-transition period²⁷⁹ (Fig. 56). These differences can be considerably larger for post-transition oxidation (Table 5).⁴⁷ Cold work has been found to have a small effect on zirconium,^{3,350} but no effect is detectable with Zircaloy-2, so it is unlikely that differences in residual cold work between batches can explain the above effect.

Effect of Environmental Impurities. In addition to the effect of fluoride, present in the water,³¹⁵ or steam,³¹⁷ there have been few reports of major

Table 5. Correlation of Pre- and Post-Transition Oxidation^{a,47}

Billet	Z431 ^b	Z8323 ^c	ZL9012	Z306	Z305	Z108	Z303	Z8006	Z105
350°C									
Wt. gain ^d at 14 days:	24.5	13.5	11.7	10.3	11.8	12.0	12.4	11.2	12.0
Post-transition rate:	<0.05	—	0.155	0.095	0.090	0.110	0.150	0.147	0.145
400°C									
Wt. gain at 3 days:	28.5	14.3	17.0	15.4	17.3	18.6	20.2	19.7	22.6
Post-transition rate:	<0.81	1.05	0.415	0.434	0.555	0.625	0.910	0.884	1.0
450°C									
Wt. gain at 1 day:	26.8	19.0	21.5	22.7	24.5	26.2	22.2	23.1	—
Post-transition rate:	2.22	2.08	1.87	7.41	4.37	5.62	9.8	8.01	—
500°C									
Wt. gain at 4 hours:	21.3	13.5	19.4	20.7	18.8	20.3	19.5	17.5	21.0
Post-transition rate:	12.1	14.0	20.4	23.1	27.5	27.9	30.3	32.2	35.5
Composition of Zircaloy-2 billets									
Sn (%)		1.46	1.70	1.46	1.42	1.45	1.54	1.55	1.58
Fe (%)		0.14	0.10	0.12	0.12	0.103	0.12	0.172	0.18
Cr (%)		0.08	0.082	0.11	0.12	0.088	0.10	0.138	0.104
Ni (%)		<40 ppm	0.0385	0.050	0.040	0.045	0.045	0.057	0.047
N (ppm)		50	100	160	80	160	210	120	150
O (ppm)		1000	1150	1200	1300	1150	1200	1050	—
H (ppm)		40	11	18	18	16	12	28	11
Total		1.69	1.920	1.74	1.70	1.686	1.805	1.918	1.911

^aResults are for atmospheric pressure steam.^bZ431, Zircaloy-3 (0.25 % Sn 0.25 Fe).^cZ8323, low-nickel Zircaloy-2.^dWeight gain in mgm/dm²; oxidation rates are mgm/dm²/day.

effects of impurities in the environment on the oxidation of the Zircalloys in high-temperature water or steam.

Thus, the inhibiting effect of boric acid on the oxidation of unalloyed zirconium in 500°C steam does not seem to extend to alloys which are already reasonably oxidation resistant, and Zircaloy-2 actually showed higher oxidation rates in steam plus boric acid than in steam alone.^{351,352} It is possible that boric acid may act as an inhibitor for the catastrophic oxidation of Zircaloy-2 at very high steam pressures,^{353,354} since it can be argued that the effect of boric acid on unalloyed zirconium is to eliminate the effect of steam pressure, which appears at relatively low pressures for zirconium.²⁶¹ No test of this possibility has been made.

Additions of chloride and iodide ions to the water do not appear to have any effect on the general corrosion rate.³¹⁶ However, the observation of stress corrosion cracking of Zircalloys in neutral aqueous chloride solutions at both room temperature³⁵⁵ and 300°C³⁵⁶ shows that some damage to the surface oxide films by chloride is possible. In both instances polarization of the specimen within a specific potential range is necessary for the initiation of SCC.

Dissolved gases (O₂, H₂, and N₂) in water, or added to the steam, have not been observed to have much effect on the long-term oxidation of the Zircalloys,^{3,202,204,357-359} despite the early claim that nitrogen in the water was as deleterious as nitrogen in the metal, where corrosion of unalloyed zirconium was concerned.³ Additions of oxygen to the water had not been thought, until recently, to have much effect on the oxidation rate in the absence of reactor irradiation, except possibly during the very thin oxide film region, such as during autoclave startup.³⁶⁰ Work by Shirvington *et al.* has suggested that this may not be the case, and that when large additions of oxygen are made to the water, a major increase in the oxidation of pickled specimens results.^{187,334} This effect has been compared with the effect of oxygen on the enhancement of corrosion under irradiation,²⁸³ and although the explanation does not seem to be the same in the two cases, nevertheless, they may be related through a similar type of oxide breakdown process in each instance.

A reduction in hydrogen absorption in the presence of oxygen dissolved in the water (or added to steam) has been established for a long time,^{204,205,357,358} although the mechanism is not understood. Hydrogen is commonly added to the water in PWR-type reactors at concentrations of 30 cm³/kg (or more). No effect of this on either the oxidation or hydrogen uptake has been established, although at higher concentrations (> 100 cm³/kg) an

increase in hydrogen absorption is observed.²⁰² A small effect of silica in the steam has been observed, which apparently renders the 400°C steam autoclave test insensitive to poorly heat treated Zircaloy.³⁶¹ This effect is probably partly responsible for the variability of the results of the “round-robin” tests.³⁶⁰

There appear to be no significant differences between oxidation rates in H₂O, D₂O, and T₂O at the same temperature and pressure.^{47,363,363} Although lower than expected weight gains were observed in T₂O,³⁶³ it is thought that these probably resulted from the low T₂O pressures used rather than any real difference between corrosion in the three forms of water.

A number of ionic species have been examined in nearly neutral water (acetate, nitrate, sulfate, carbonate) and no significant effect of any of them was observed.³⁶⁴

Effect of pH. The oxidation rates of the Zircaloys are apparently independent of pH over the range pH 1–12 in sulfuric or nitric acids, and ammonium, sodium, or potassium hydroxides. Lithium hydroxide has a disastrous effect on the oxidation resistance at a pH above 12. Sodium and potassium hydroxides show smaller effects, that for potassium being considerably less than that for sodium hydroxide.^{365–370} The effect is magnified if a crevice is present.³⁶⁵ The increased oxidation rates have been attributed to the incorporation of lithium into the oxide, although the precise manner in which this functions (i.e., by modifying the electron or ionic conductivities, or both) has not been established. Since control of the normal oxidation process is not simply related to the classical concept of lattice diffusion, controlled by point defect concentration, it seems doubtful that the simple explanation based on the increased vacancy content of the oxide, resulting from lithium incorporation, is the whole story.

Acidic solutions of sulfuric or nitric acids gave no significant difference in oxidation rate from water at concentrations up to 0.4 M.^{371,372} Hydrochloric acid solutions, however, cause oxide breakdown, leading to severe intergranular corrosion at temperatures of 200–250°C.³⁷³ Although stress corrosion cracking at elevated temperatures was reported only in neutral chloride solutions,^{1,356} it is possible that it would occur more readily in acid solutions at elevated temperatures if the relative effects of pH observed at room temperature persist to high temperature.³⁵⁵

Effect of Pressure. At temperatures close to 300°C, little or no effect of the pressure of the environment has been detectable prior to the oxidation

rate transition.⁴⁷ Effects on the transition and post-transition processes have already been discussed both for oxygen and steam, where they are formally similar. Thus, increasing pressure speeds up the rate at which transition propagates over the specimen surface (e.g., Fig. 45). Once one is well beyond transition, however, these effects become of relatively minor consequence, since the ultimate post-transition rates are little affected by pressure up to some critical value.^{20,21,52} At temperatures of 450°C and above, a major increase in the oxidation rate of Zircaloy-2 has been observed at pressures above this critical value.^{53,353,354} This effect takes the form of severe localized oxidation in the form of pustules, or (less commonly) patches of thick oxide. In this respect the phenomenon is similar to the formation of pustules and patches of thick oxide under irradiation in BWRs.

No satisfactory mechanism has been proposed for the phenomenon, although it is possible that it may be related to the similarly unexplained pressure dependence of the oxidation of unalloyed zirconium, which is observed at all temperatures.²⁶² It may also be related to the enhanced oxidation rate, which is observed in concentrated lithium hydroxide (and to a lesser extent sodium and potassium hydroxide) solutions (see above), although this usually leads to uniformly thick oxide films. However, a study of corrosion in fused lithium and sodium hydroxides at 600°C did not result in accelerated oxidation,¹⁴⁴ so this connection between the two phenomena cannot be related to (say) increasing hydrolysis of the oxide. Like other instances of pustular corrosion, it may result from the development of local high electronic conductivity in the oxide.

The effect of steam pressure on Zircaloy-2 is very variable from batch to batch of material,^{353–354} and the results at present are summarized in Figs. 57–59. The transient effect of changing pressure during the post-transition oxidation period has already been discussed in the section on oxidation in oxygen^{52,53}; it seems to be equally true of oxidation in steam at pressures below the critical pressure discussed above. An instantaneous change in oxidation rate proportional to the change in pressure was observed with a slow recovery to approximately the initial rate (Fig. 14). This effect was related to the porosity of the post-transition oxide film, and changes in gas flow through it resulted on changing the pressure. The oxide porosity in steam also changed in the appropriate direction during the recovery period, and these changes could be followed by studying the impedance of the oxide film.⁵³

At low pressures of steam (water vapor) the differences between good and bad alloys tend to diminish and oxidation curves are virtually

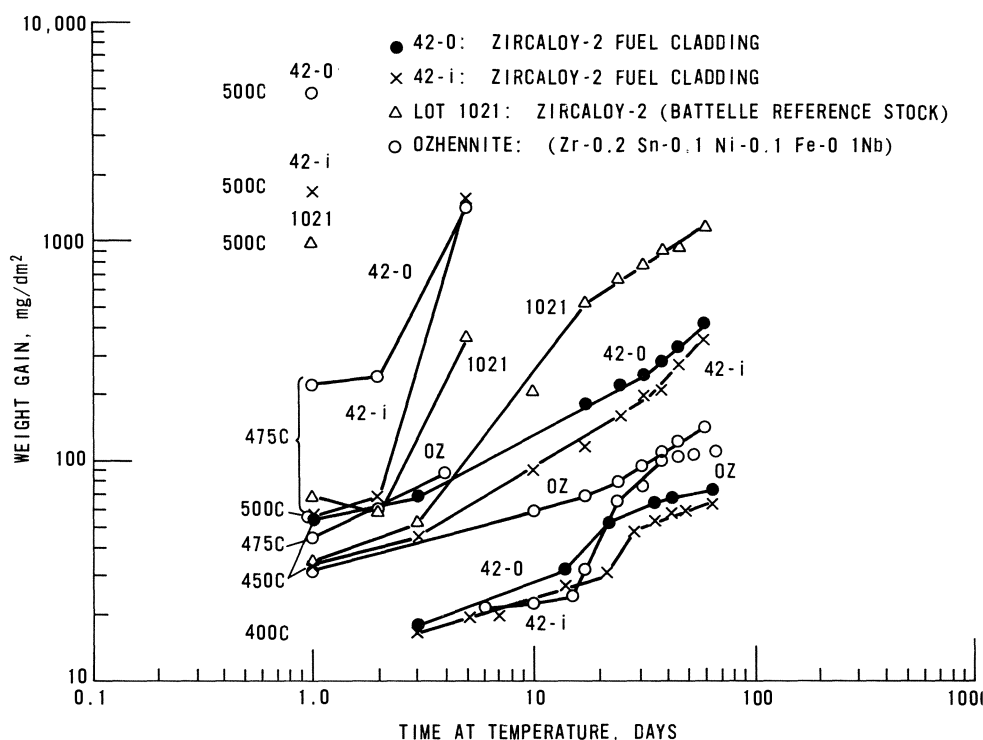


Fig. 57. High-temperature corrosion behavior of Zircaloy-2 and Ozhennite in steam at 1700 psig.³⁵³

independent of pressure and approach a lower limit which is similar to the oxidation rate in oxygen.^{51,261,374,375} At submillimeter pressures the oxygen diffusion into the metal becomes significant and a range of behavior is seen such as in low-pressure oxygen.

Effect of Prior Oxidation History. Experiments in which specimens were transferred from one oxidation temperature to another (or from oxygen to steam and vice versa) have been performed by several authors,^{47,53,287,376,317} because of the interest in whether any "memory effect" would result from the initial autoclave proof test, which is at a temperature higher than normal operation, or from a short temperature-excursion to high temperature. When specimens are transferred at temperatures well before the expected rate transition, they accommodate themselves to the new temperature with a minimum of transitional behavior. If they are transferred at a point near to the rate transition, then this may in itself trigger the breakdown of the

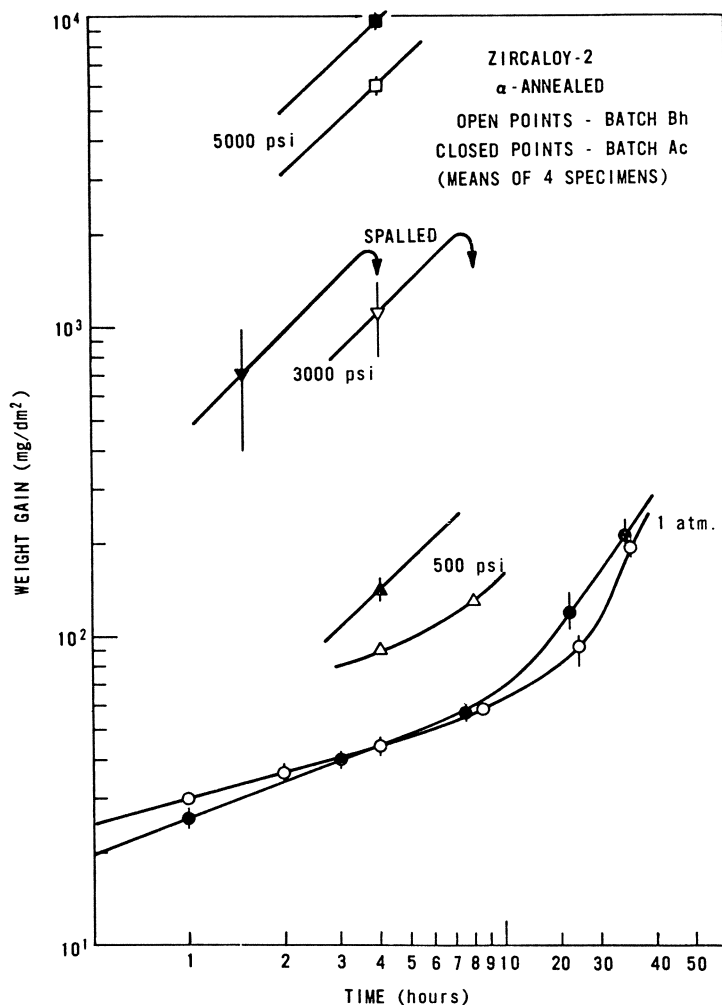


Fig. 58. Effect of pressure on the corrosion of Zircaloy-2 in steam at 600°C.³⁵⁴

oxide film, leading to a variety of transient effects.^{287,288,376,377} Some discussion has centered around whether this involves the equivalent of starting again at the beginning of the oxidation cycle or not. However, in view of the cyclic nature of the post-transition oxidation process at these temperatures, and the considerable scatter from specimen to specimen in the times at which successive cycles start, it is doubtful whether the evidence

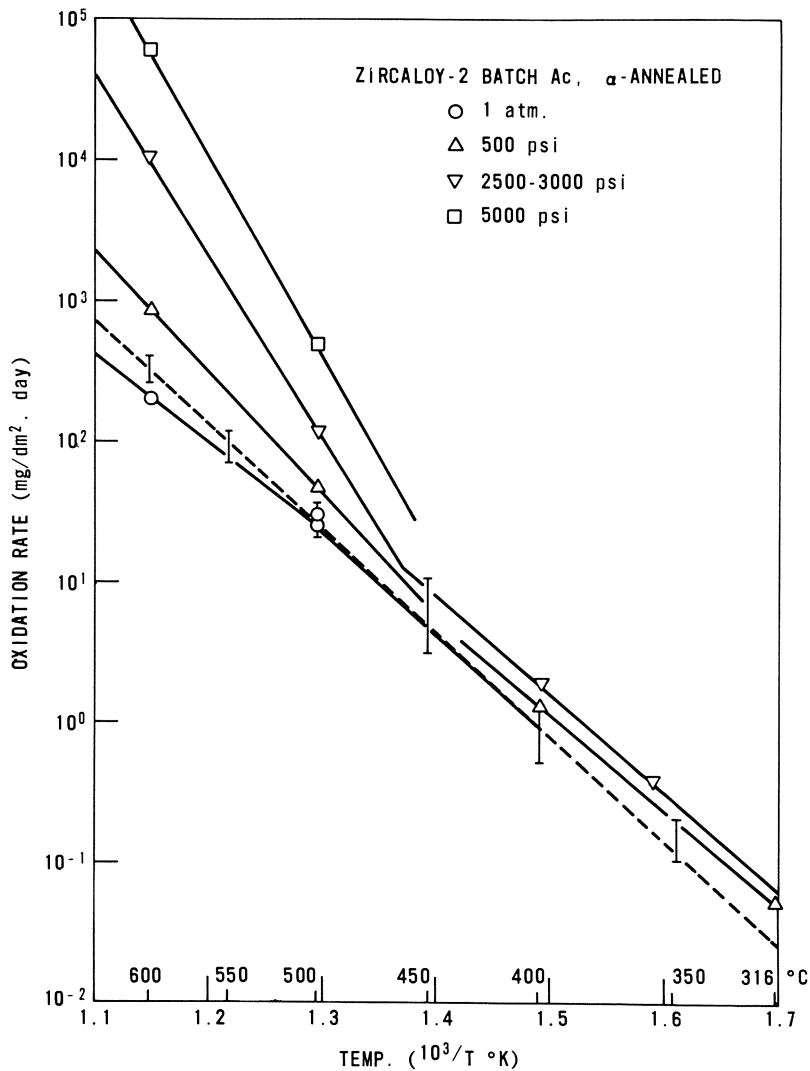


Fig. 59. Effect of pressure on the post-transition rate of oxidation of Zircaloy-2 as a function of temperature.³⁵⁴

is sufficient to reach any firm conclusion on this point. An understanding must certainly await a clearer idea of precisely what is occurring during transition at various temperatures and pressures. To some extent a vacuum anneal at high temperature, which dissolves part of the oxide, seems to act in a manner similar to a temperature transfer in stimulating the oxide

transition process.³⁷⁸ This is perhaps not surprising if, as is now suspected, oxide recrystallization processes are important contributors to the transition process.

If the transfer from one temperature to another is made well beyond transition, and between temperatures at which the cyclic nature of the post-transition is not evident, then a relatively long transient (memory effect) is observed; much like that observed on changing the pressure.^{52,53} During this transient the oxidation rate and the oxide properties (e.g., porosity) progressively revert to those typical of the new temperature. Thus the temperature coefficient of the post-transition linear oxidation rate can be divided into two components (Fig. 60); an instantaneous one resulting from the combined temperature coefficients of the ionic and electronic processes in an oxide of fixed morphology, and a transient change in rate as the properties of the oxide change with time and the formation of new layers of oxide at the oxide/metal interface.⁴⁷

Effect of Heat Flux. Concern has been expressed that, if the oxidation rate of zirconium alloys is controlled by the temperature of the metal/oxide interface, then under conditions of high heat flux, a runaway condition could be achieved in which catastrophic oxidation would occur.³⁷⁹ Although it seems unlikely, in view of the current mechanistic ideas, that the control of pre-transition oxidation should reside exclusively at this interface, nevertheless, during post-transition oxidation (where the outer layers of the oxide are porous, but thermally insulating) such a “snowball effect” might be observed, and a number of investigators have applied themselves either to the theoretical^{380,381} or experimental^{381–383} aspects of the phenomenon.

The experimental results in the Saxton reactor³⁸¹ do not extend to high-enough weight gains to determine whether a major post-transition effect would be evident. Since no allowance was made for any possible small irradiation effect, the small increase observed in the pre-transition period might result either from the heat flux, or the fast neutron flux or a combination of the two. In laboratory studies Coriou *et al.*³⁸⁴ observed no significant effect of heat flux on the oxidation of Zircaloy-2 during pre-transition oxidation, but in a longer test (1140 hr) the oxide thickness in the peak heat flux region was post-transition, suggesting that a major effect of heat flux might be expected during post-transition oxidation. Rubright and Koch³⁸³ observed only very minor differences in oxidation between heat transfer and isothermal specimens up to ~230 days at 360°C. Anderson and McGoff,³⁸⁵ by their failure to insulate the Zircaloy specimens from

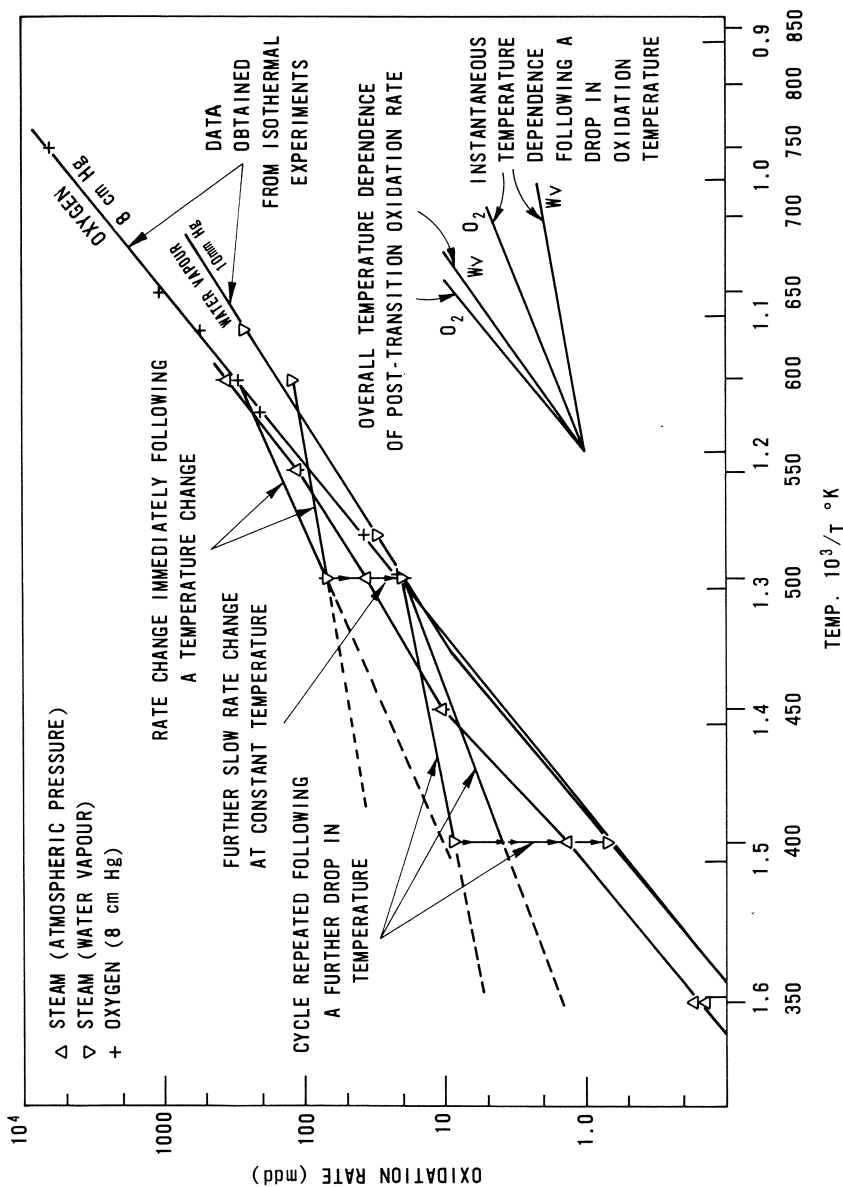


Fig. 60. Post-transition oxidation rates of Zircaloy-2 in oxygen and steam separating the instantaneous and slowly changing components of the temperature coefficient. Arrows indicate path taken during individual experiments.⁴⁷

any electrical current (ac or dc), succeeded only in causing excessive electrochemical corrosion as a result of the well-known rectifying properties of zirconium oxide films.³⁸⁶

Both Coriou *et al.*³⁸⁴ and Koch *et al.*^{382,383} observed increased hydrogen uptake under heat transfer conditions. In Coriou's case this could simply be related to the increased oxidation, since neither weight gain nor hydrogen content were accurately quantified, in Koch's case the film thicknesses under the heat flux were closer to the isothermal data than were the hydrogen absorption data (Fig. 61), so the evidence for an effect on hydrogen uptake, independent of the effect on oxide thickness, is more persuasive. In measurements of hydrogen uptake by fuel cladding, however, no enhancement of hydrogen absorption has been observed over that to be expected as a result of any enhanced oxidation which occurs.^{381,387} The heat flux of the Shippingport reactor "blanket" elements³⁸⁷ was not reported, however, and may have been relatively low; that of the elements from the Saxton reactor was high, however, so the prospect of enhanced hydrogen absorption does not seem to be realized in practice.

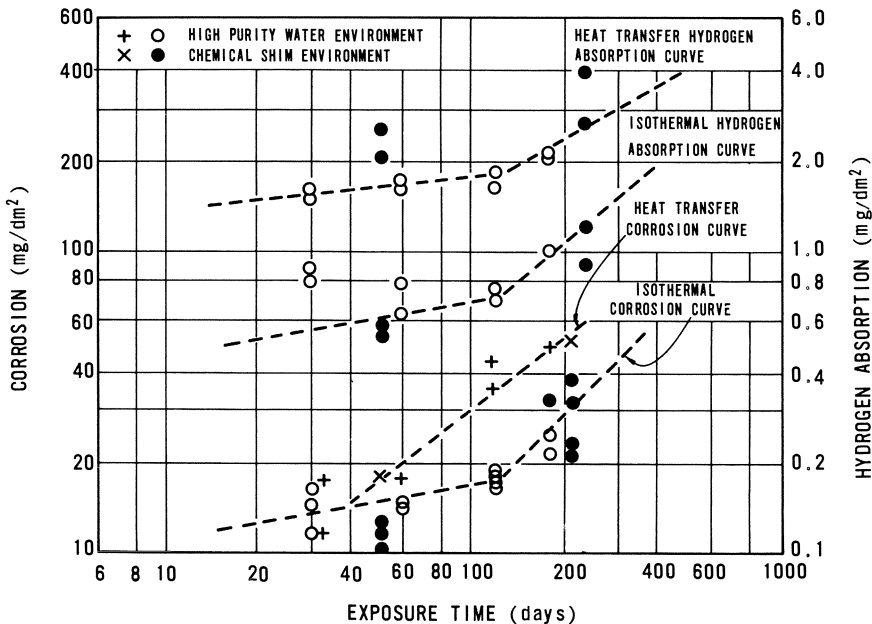


Fig. 61. Effect of 600,000 Btu/hr ft² surface heat flux on the oxidation of Zircaloy-2 in 640°F (340°C) water.³⁸³

Zr-2.5 wt. % Nb Alloy

The other principal alloy of zirconium which has seen extensive commercial use, and for which extensive data on its behavior in high-temperature water are available from several sources, is the Zr-2.5 wt. % Nb alloy. The composition of this alloy was selected to give good mechanical strength without losing too much corrosion resistance, since strength improves and corrosion resistance diminishes with increasing niobium content in the range 1-5% Nb.^{36,388} The oxidation kinetics of this alloy in water or steam²⁴⁴ follow the same formal rate laws as those of the Zircalloys (Figs. 62 and 63), although the first inflection in the oxidation curve is often more pronounced for the zirconium-niobium alloy than for the Zircalloys,³⁸⁹ and may have more mechanistic significance.

The oxidation rate in water (Fig. 64) is more sensitive to heat treatment than that of Zircaloy-2.^{122,246} The poorest corrosion resistance (unlike Zircaloy) results from a β -quench without any subsequent tempering; a progressive improvement in oxidation resistance occurs with tempering time at any temperature where tempering occurs.^{116,122,123} At 500°C, where tempering occurs quite rapidly, improvements in oxidation resistance are evident for tempering times up to at least 3 months. The introduction of cold work between the quench and the temper accelerates the metallurgical processes responsible for the improvement in oxidation resistance,^{122,123,246} thereby permitting approaches to the optimum corrosion resistance after relatively short tempering times (e.g., 24 hr at 500°C). Long tempering times could not be tolerated commercially, owing to the economic penalty involved.

The oxidation rate of Zr-2.5 Nb alloy in steam and water is sensitive to the presence of free oxygen in the environment.³⁶ Increased oxidation results immediately upon the addition of oxygen to the environment and returns to the previous rate if the oxygen is removed.¹¹⁶ Thus, in a manner similar to the behavior of unalloyed niobium,³⁹⁰ the Zr-2.5% Nb alloy will react preferentially with free oxygen in steam so that a step occurs in the oxidation curve whose height is equal to the weight of oxygen added to the system.¹¹⁶ This phenomenon is not related to any physical breakdown of the oxide film, since it is quickly reversible and repeatable; it is most probably related to changes in the electronic conductivity of the film, in the presence of free oxygen, which may cause a valence change in the niobium in the oxide.

A similar effect can be seen when even small concentrations of oxygen are added to a high-temperature water loop (Table 6). Under the same conditions, Zircaloy-2 was insensitive to the addition of oxygen.^{122,225} The sensitivity of Zr-2.5% Nb to free oxygen in the water is also a function

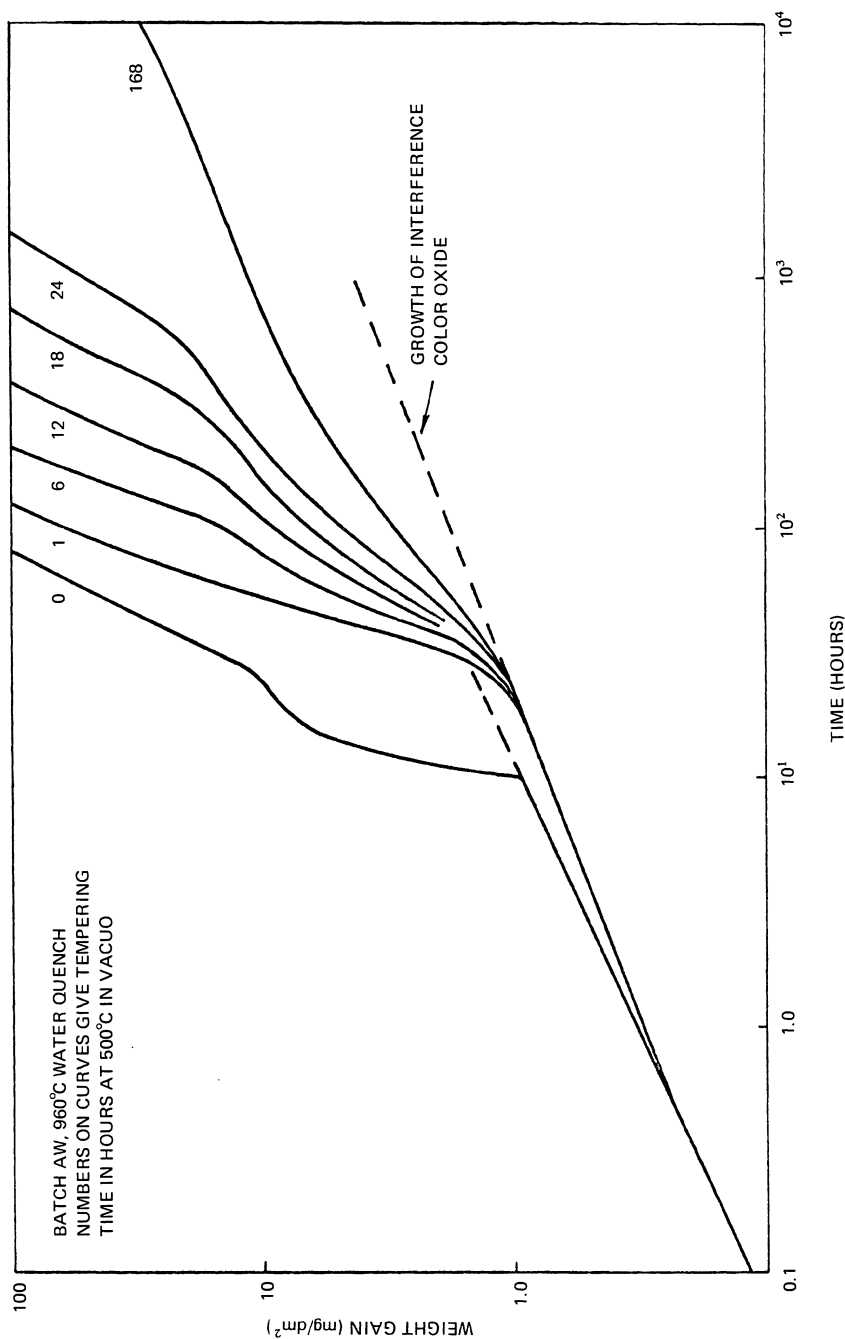
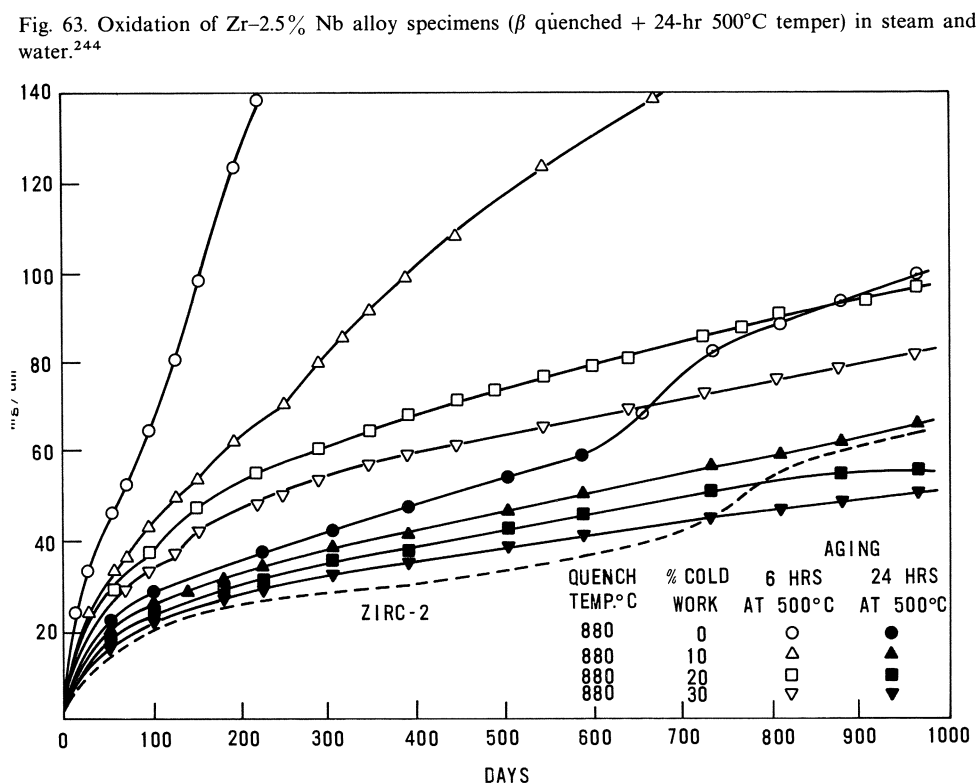
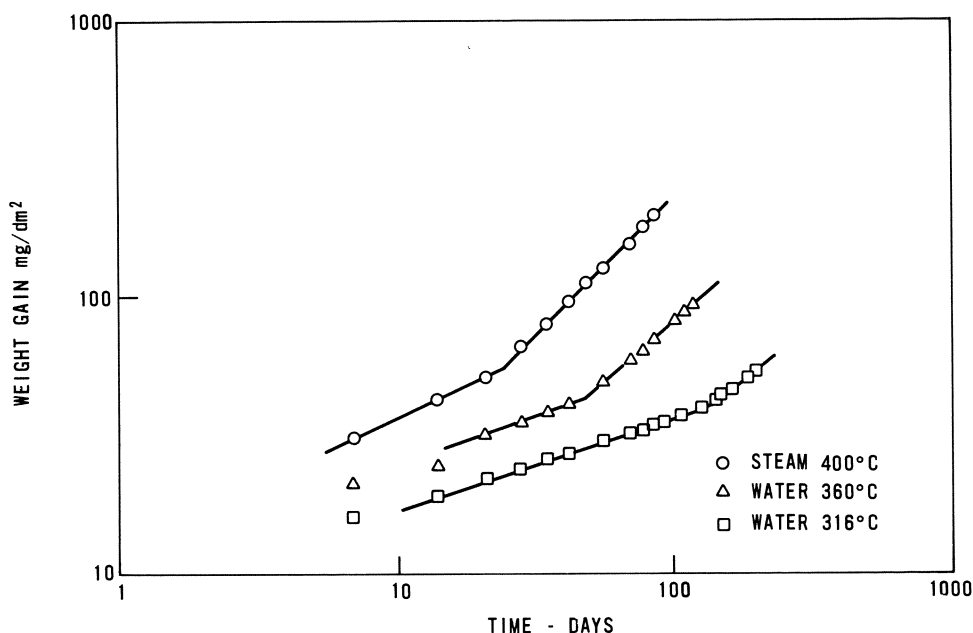


Fig. 62. Effect of tempering time on the oxidation of Zr-2.5% Nb alloy specimens in moist air at 300°C³⁸⁹

Table 6. Oxidation of Zircaloy-2 and Zr-2.5% Nb in an Out-Reactor Pressurized Water Loop^{a,391}

Duration (days)	28	84	154	217	259	284	368 84	459	551	639	728
	No oxygen added (O ₂ < 0.01 ppm)						O ₂ ~0.06 ppm			No oxygen added (O ₂ 0.02-0.03 ppm)	
Zircaloy-2 (annealed 800°C 1 hr)	11	14	17	19	21	20	27 17	23 23	24 21 14	25	27
Zr-2.5% Nb W.Q. from 880°C, 20% cold work, aged 500°C for 24 hr)	11	16	21	24	26	26	>200 spalled 56	260	spalled 48	12 15 12	16 18 16
										47 17	50 28

^aWeight gain, mg/dm²; temperature, 288°C; pH control, 10 ppm NH₃.



of heat treatment; long tempering times after quenching and cold working reduce the sensitivity to free oxygen in the steam or water.¹²² The highest corrosion rates and sensitivity to free oxygen occur with quenched material (i.e., with the maximum niobium in solution in the metal), and Shirvington,¹⁹¹ has recently shown that the presence of oxygen in the steam results in a large increase in the dc electronic conductivity of the oxide films on such specimens. Quenched, cold-worked, and aged material showed no effect on the electronic conductivity of its oxide from adding oxygen to steam at 295°C, but did show a significant increase in conductivity ($\times 4$) when oxygen was added to water at the same temperature. This effect was influenced by the surface preparation of the specimen and may, therefore, indicate a major contribution to the total oxide conductivity from surface conduction (which would be greater in water than in dry steam).

The conventional Zircaloy-2 pickling procedure is not satisfactory for Zr-2.5% Nb alloy and a solution containing sulfuric acid in addition to nitric and hydrofluoric acids has been recommended.²⁴⁴ The Zr-Nb alloy seems to be sensitive to increased corrosion from any residual etchant left on the specimen surface or to fluoride in the water to much the same extent at Zircaloy-2,²²² but the report that small quantities of carbonate in the water results in a large increase in corrosion rate²²² does not seem to have been confirmed elsewhere. If carbonate decomposition gave free oxygen in water, this might explain the original observations. The effect of irradiation on the Zr-Nb alloy behavior will be considered later. No extensive studies of the effects of trace impurities in the metal have been published. Specifications having been mainly based on those for the Zircaloys. The limits for nitrogen content have been studied experimentally³⁹² for the Zr-1% Nb alloy.

The Zr-3% Nb-1% Sn alloy shows similar effects of heat treatment to those reported for the Zr-2.5% Nb alloy.^{236,237} Its behavior under irradiation will be considered in detail later, but as might be expected from the presence of tin, it is somewhat intermediate between that of Zircaloy-2 and Zr-2.5% Nb.

Zr-Cr-Fe Alloys

The development of the Zr-Cr-Fe alloys, and, in particular, that with a nominal composition of Zr-1.15 wt. % Cr-0.1 wt. % Fe, to the point of near-commercial acceptance is primarily due to Klepfer and the group at Vallecitos Atomic Power Lab,²⁰¹ hence the colloquial name Valloy for this,

and similar, alloys. However, early indications of the good high-temperature corrosion resistance of binary and ternary alloys containing chromium, and no tin, were present in the early studies at Nuclear Metals, Inc.^{250,251}

The Vallecitos program showed that the Zr-Cr-Fe alloy had much better high-temperature ($\geq 400^\circ\text{C}$) corrosion resistance than Zircaloy-2, and could be heat-treated to give corrosion resistance at 300°C , which was not significantly worse than that of Zircaloy-2 (Fig. 37).²⁰¹ To achieve this, their results suggest that the chromium content in solution should not be allowed to fall below 0.7 at. % (0.4 wt. %) and that the second phase particles should be uniformly distributed and have an optimum size of about $1\ \mu\text{m}$ (Fig. 65).

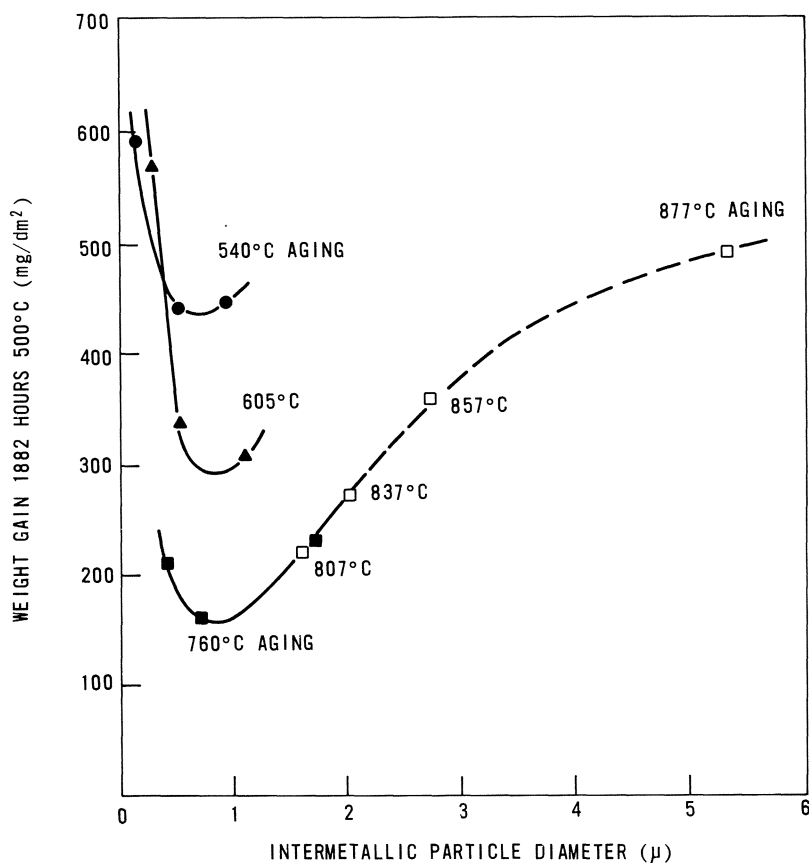


Fig. 65. Corrosion weight gain as a function of intermetallic particle size for a Zr-Cr-Fe alloy.²⁰¹

This is achieved by a quench-and-age treatment, in which the optimum treatment includes quenching from 955°C, hot rolling 50% at 605°C, cold working 40%, and finally stress relieving for 2 hr at 760°C.

Experience with a number of commercially fabricated billets of this alloy has shown that it is very susceptible to the formation of thick oxide pustules, especially during corrosion in water.³⁹³ These are due to the presence of large intermetallic particles, and it appears that the optimum size of 1 μm quoted by Klepfer is too large to ensure that oxide pustules do not form, and that a much smaller average size should be aimed for.³⁹³ However, heat treatments giving freedom from oxide pustule formation in 300°C water do not give optimum oxidation resistance in 400°C steam, and some compromise may be needed for commercial use if both high- and low-temperature exposure is expected. Without the presence of tin, the corrosion of the Zr–Cr–Fe alloy, as might be expected,³ is very sensitive to nitrogen content, and an upper limit of 60 ppm has been suggested for the specification.^{201,394}

The necessity for a uniform distribution of second phase particles if good corrosion resistance is to be achieved is a common observation with zirconium alloys, and recent work suggests that it is associated with the electronic component of the oxidation current. The significance of the amount of chromium in solid solution cannot be assessed positively. It may be related to the development of the crystallite morphology in the oxide, to the generation of stress at the oxide/metal interface, or to changes in the ionic conductivity of the film. Klepfer correlated the optimum chromium content in the metal with his observations of decreasing strain in the zirconium lattice with increasing aging of quenched specimens²⁰¹; however, in the absence of detailed studies of oxide morphology and growth stresses the relative importance of the various factors cannot be assessed. Shirvington found that the dc electronic conductivity of the oxide on the Zr–Cr–Fe alloy¹⁹⁰ was increased by oxygen in water, but not in steam, to about the same extent as the behavior of the Zr–Nb alloy¹⁹¹ or Zircaloy-2.¹⁸⁹ The effect was related to enhanced porosity of the oxide. Shirvington did not look at variations in the heat treatment of this alloy, however, and the metallurgical condition of the specimens used in the study was not quoted.

In addition to its considerable dependence on the fabrication schedule to achieve good corrosion resistance, the Zr–Cr–Fe alloy is very sensitive to surface preparation. This may arise from a sensitivity to contamination with fluoride ion during etching, or to differential removal of intermetallic particles from the surface with different qualities of etching treatment. Klepfer has suggested a special cleaning and etching technique for the Zr–Cr–Fe alloy

to avoid this problem.²⁰¹ However, since this involves rinsing and brushing simultaneously with a nylon brush, a technique that might be difficult to achieve satisfactorily under commercial conditions, there is an incentive to study the behavior of material after other surface preparations not involving fluoride-containing solutions.

Shirvington¹⁹⁰ compared the I - V characteristics of oxide films pre-formed on abraded and pickled specimens in oxygenated water, and found that both the ionic and electronic conductivities of the oxide on the pickled specimen were higher than on the abraded specimen. This correlated well with the relative oxidation rates. Hübner and Cox¹⁸⁵ similarly found the excessively high oxidation rates (at 300–350°C) of one batch of poorly pickled Zr–Cr–Fe alloy was associated with increases in both the ionic and electronic conductivities of the oxide film. No differences in the respective behavior of the intermetallic particles could be detected between the two batches of material, and it was concluded that the changes in oxide conductivity resulted from residual fluoride on the specimen surface. Higher surface fluoride analyses were obtained on the poorly pickled specimens than on the well-pickled ones. This conclusion seems to be borne out by the progressive disappearance of the phenomenon at higher oxidation temperatures: fluoride would be more volatile at these temperatures.¹⁸⁵ The electrical properties induced in the oxide by the presence of Zr/Cr second phase particles were different from those due to Zr/Fe particles. The electrical behavior of the oxide on Zircaloy-2 is closely similar to the behavior of a Zr–Fe binary, whereas, as might be expected, the Zr–Cr–Fe alloy more closely resembles the Zr–Cr binary, owing to the excess of chromium.¹⁸⁵ The difference in the oxide electrical behavior on Zr–Fe and Zr–Cr binary alloys has recently been confirmed by Ramasubramanian.¹⁸⁶

The effect of irradiation on the behavior of these alloys is included in the next section. Some other development programs^{219,266,394–397} have included the Zr–Cr–Fe alloy (or variations on this composition); however, no extensive publication of these studies has yet been made, and commercial application of these alloys, if it has occurred yet, remains veiled in secrecy.

Effects of Irradiation

The effects of irradiation on the corrosion of zirconium alloys were extensively reviewed in 1968,³⁹⁸ and a further review, bringing the field up to date, has recently been published.¹⁶ It is intended here, therefore, in the interests of saving space to summarize the phenomena briefly, and to concentrate on the new data and mechanistic studies which have appeared since

the last review by the present author. In the ensuing sections the discussion refers to the behavior of the Zircalloys unless otherwise specified; most work has been reported on these alloys since they are the ones which have seen the most in-reactor use.

Historical Background. The first observations of the acceleration of the oxidation rate of a zirconium alloy in an aqueous environment in-reactor go back to 1954 and the initial autoclave and loop tests carried out in uranyl sulfate solutions at Oak Ridge for the Homogeneous Reactor Project.³⁹⁹ At very much the same period of time, workers at the Knolls⁴⁰⁰ and Bettis²¹³ laboratories were reporting no effect of reactor irradiation on Zircaloy-2 after 2500 hr in pH-11 water at 580°F (305°C) containing 50 cm³ of hydrogen/liter. Thus, apparently contradictory experimental results were present from the earliest stages of the investigation.

There was no doubt about the presence of accelerated oxidation in the Oak Ridge tests, since the size of the effect was so large. In the absence of irradiation, the oxidation of zirconium alloys in uranyl sulfate solutions (Fig. 66) was virtually identical with that in high-temperature water.³⁷¹

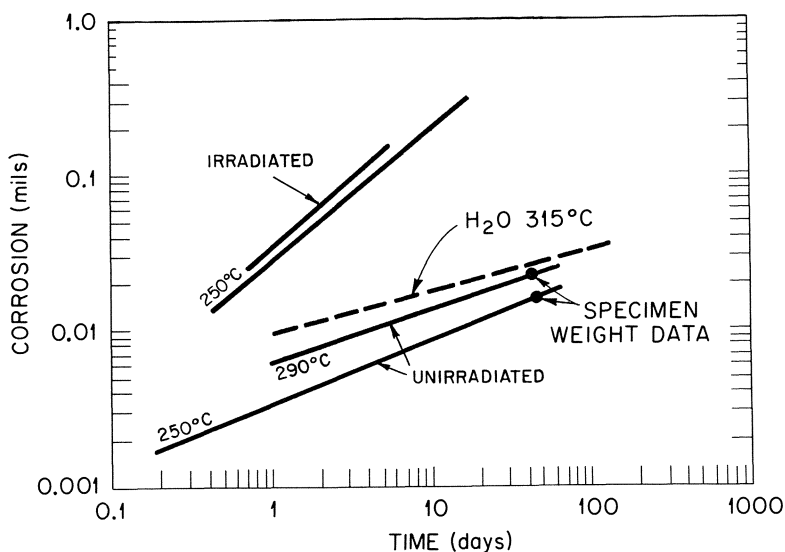


Fig. 66. Comparison of Zircaloy-2 corrosion calculated from the decrease in oxygen overpressure in uranyl sulfate solutions with and without irradiation at 250 and 290°C.⁴⁰¹

The effort at Oak Ridge was concentrated, therefore, on understanding the factors affecting the enhanced oxidation, and a search for alloys with improved corrosion resistance. Experiments were carried out either in autoclaves made of the alloy under test (with or without separate corrosion specimens supported within them)⁴⁰¹ or in circulating loops containing groups of test specimens.⁴⁰² Whereas in most experiments reported here oxidation was assessed from weight gain or oxide thickness, in these tests it was assessed from: (1) specimen weight loss, since the oxide film was often lost during the experiment (loop tests) or was friable and easily removed on drying; and (2) the rate of consumption of the oxygen overpressure added to ensure the stability of the uranyl sulfate solution.

During the same period workers at Harwell studied the low fission power density region and demonstrated the threshold for the observation of these effects.^{372,403} These results showed that fission fragment irradiation enhanced both the pre- and post-transition oxidation rates without materially changing the shapes of the curves. On the basis of these results, and an equivalence between the power density due to fission fragments in these tests and fast neutrons in a water reactor, a prediction was made of the magnitude of the effect to be expected in PWR and BWR systems. However, the significance of two autoclave tests carried out at Oak Ridge (one with an oxygen and one with a hydrogen overpressure) were not appreciated at this time (Fig. 67); they did, however, contain the clue to the apparent discrepancy between results obtained in water at different establishments.

Throughout the period 1956–1960, experiments in high-temperature water loops^{404,405} and examination of fuel cladding from pressurized water reactors^{406–408} had failed to reveal any measurable acceleration of zirconium alloy oxidation by reactor irradiation in pH-10 LiOH with $\sim 30 \text{ cm}^3/\text{kg}$ hydrogen overpressure at times up to 1157 full power days. The Oak Ridge experiments with an oxygen overpressure had indicated that at equivalent rates of energy deposition in the solution fast neutrons should be as effective as fission fragments at accelerating the oxidation of zirconium alloys.⁴⁰⁹ Experiments at Harwell in atmospheric-pressure steam in the DIDO and PLUTO reactors at 360–400°C showed about the amount of enhancement of the oxidation rate predicted from the energy deposition from fast neutrons and an assumed equivalence with fission fragments at equal energy deposition rates.^{410–414} Other experiments in relatively low neutron fluxes in the BEPO reactor at higher temperatures (500–600°C), which apparently showed an effect of irradiation,⁴¹² were subsequently shown to be due to errors in the location of the thermocouples during assembly of the in-reactor rigs. Further work confirmed the effects in the

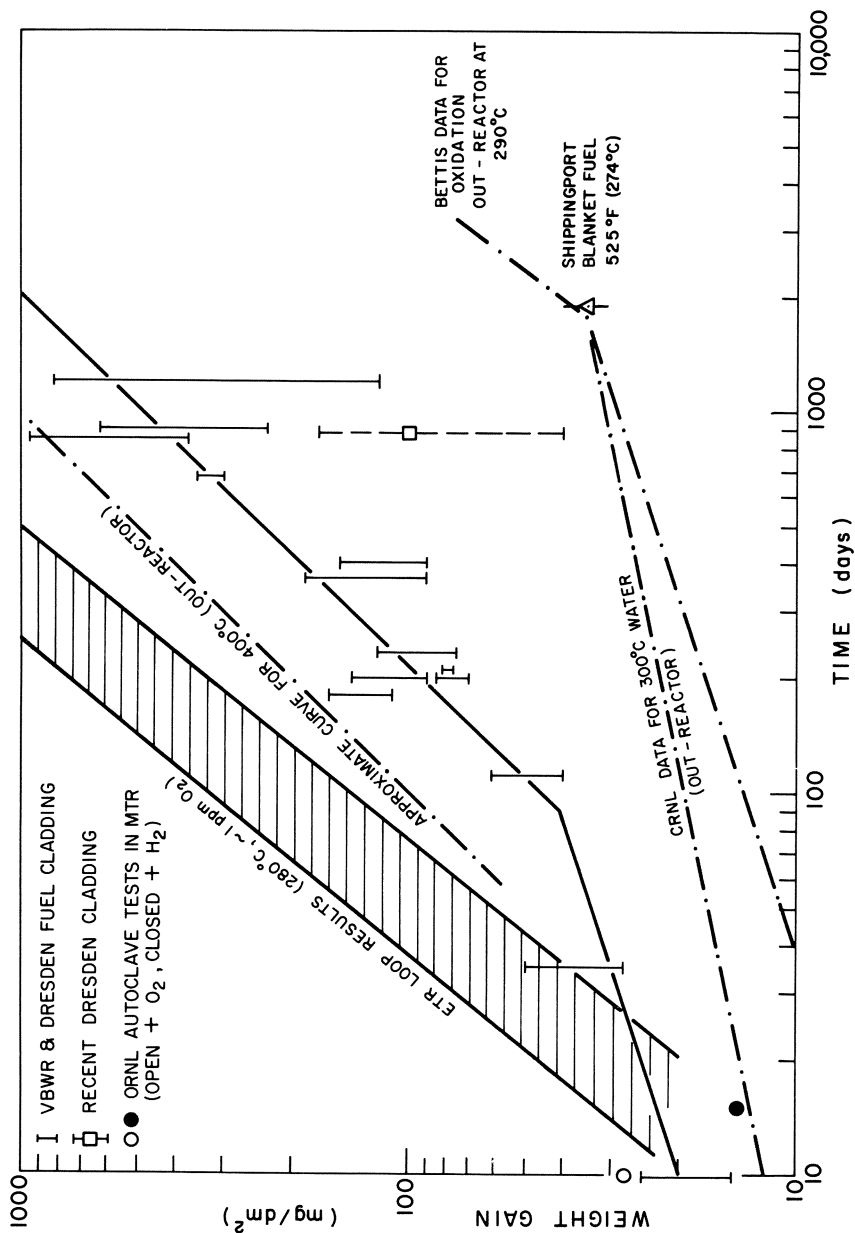


Fig. 67. Oxidation data in oxygenated water in-reactor compared with out-reactor data.³⁹⁸

high-flux reactors and showed that specimen overheating from the γ -flux could not account for the observed increase. The occurrence of a similar effect in high-temperature water was also shown.^{163,164,415-420} Nevertheless, because no equivalent enhancement had been observed in PWRs, these results were largely ignored.

Confirmation of an enhancement of corrosion in water came from the examination of BWR fuel from the Vallecitos and Dresden reactors (Fig. 67),⁴²¹⁻⁴²⁵ where large enhancements of oxidation were observed. The correlation between the water chemistry concerned (i.e., free oxygen from radiolysis in BWRs; added hydrogen in the PWRs), and the early Oak Ridge autoclave results with oxygen and hydrogen overpressures became evident (Fig. 67). The importance of oxygen in the water was ultimately demonstrated in a prolonged joint program between Hanford and Chalk River laboratories, conducted in the ETR and later the ATR water loops at Idaho Falls,⁴²⁶⁻⁴³⁵ in some in-reactor loops at Chalk River,^{391,436,437} and by the examination of zirconium alloy fuel cladding from reactors with different water chemistry.^{438,439} The ability of ammonia additions to suppress radiolysis (and hence lower the oxygen levels) in boiling water, and thereby to minimize corrosion, was demonstrated during these studies. Recent studies of fuel cladding from BWRs continue to support these observations,⁴⁴⁰ and have also confirmed the pustular nature of the oxide film reported in the U.S. studies,⁴²¹⁻⁴²⁵ and which seems to be peculiar to boiling conditions.

The conclusions from these studies were that, although oxygen in the coolant was a necessary condition for observing a major enhancement of the corrosion of the Zircalloys in-reactor, nevertheless, a small but definite enhancement of corrosion by fast neutrons was present in low-oxygen water^{441,442} and should be observed even with high hydrogen overpressures such as are used in PWRs. Results in small autoclaves^{398,442} were generally less reliable than those in loops in-reactor.⁴⁴¹ That this was the case was finally determined by Hillner³⁸⁷ from the examination of the Shippingport Blanket Fuel Cladding after additional exposure had brought the total to 1706 EFPD (effective full power days). At this point the irradiated cladding was obviously well beyond the oxidation rate transition (mean oxide thickness 8.2–10.9 μm), compared with the prediction that, in the absence of irradiation, the oxide should have been about 3.7–4.4 μm thick.

Kinetics of Oxidation Under Irradiation. The observed kinetics are a function of the amount of acceleration of the oxidation which takes place. Both pre-transition and post-transition oxidation rates are enhanced, and

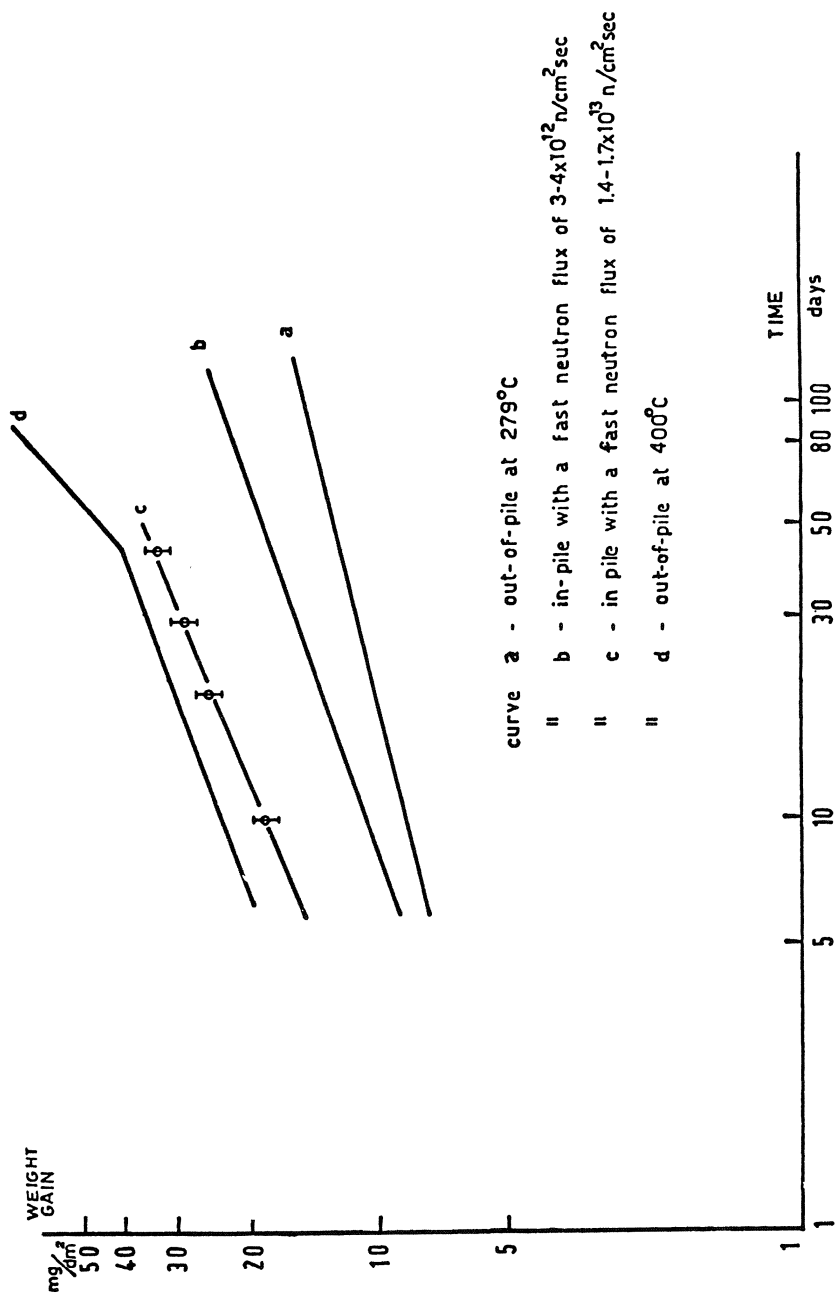


Fig. 68. CISE results for the oxidation of Zircaloy-2 in a water-steam fog, containing traces of oxygen, in-reactor at 280°C.⁴⁴⁵

there is some evidence that the weight gain at transition is reduced. Thus, under conditions where enhancements of the oxidation rate were relatively small, workers at CISE^{443–446} have shown that the enhanced pre-transition oxidation rate follows a kinetic law similar to those in the absence of irradiation (Fig. 68), but with an exponent in the kinetic equation that is higher than out of reactor. Under conditions where enhancement of the oxidation rate due to irradiation is higher, a transition to linear kinetics is observed, and evidence suggests that this may occur at a weight gain of about 15–20 mg/dm², compared with ~30 mg/dm² for normal out-reactor kinetics at 300–350°C.^{372,412} In fissile solutions at high power density, or with high fast neutron fluxes in highly oxygenated water, the kinetics are apparently linear from the start of oxidation.^{399,429,431} Allowing for the fact that a short pre-transition oxidation period occurred, but was not detected, at the start of these experiments an upper value for the weight gain at transition would be $\lesssim 10$ mg/dm² for fissile solutions and ≤ 15 mg/dm² for oxygenated water. Thus there seems to be a progressive decrease in the film thickness at which oxide breakdown occurs with increasing acceleration of the oxidation rate.

Factors Affecting the Oxidation Kinetics Under Irradiation. We have already seen that a combination of the oxygen content of the water and the energy deposition from radiation (either fission fragment or fast neutron) determines the actual oxidation rates of the Zircalloys in water at 300–350°C. In oxygenated uranyl sulfate solutions^{371,399} the oxidation rate (or weight gain at a given time for the linear kinetics) increases as the (power density)^{-0.4}. Although other relationships between oxidation rate and power density in the solution have been proposed,^{410,411,447,448} none of them have a theoretical basis and are merely successive attempts to fit the observed data which are all close to a parabolic dependence on energy deposition rate. In oxygenated water under fast neutron bombardment the oxidation rate again could be said to fit an approximately parabolic dependence on the rate of energy deposition (neutron flux > 1 MeV).⁴²⁸ However, at high fluxes the curve may be nearer to a shallow, almost linear dependence on flux, and the slope of this line is very similar to the almost linear dependence on flux observed for the much lower oxidation rates in low-oxygen water (Fig. 69). Only about 1 ppm of oxygen is needed in the water to give the increased oxidation in a fast neutron flux of $2\text{--}10 \times 10^{13} \text{ n}_f/\text{v}$; between this concentration and an overpressure of 27-atm O₂¹⁸⁹ only a small ($\times 2$) additional increase in oxidation results.

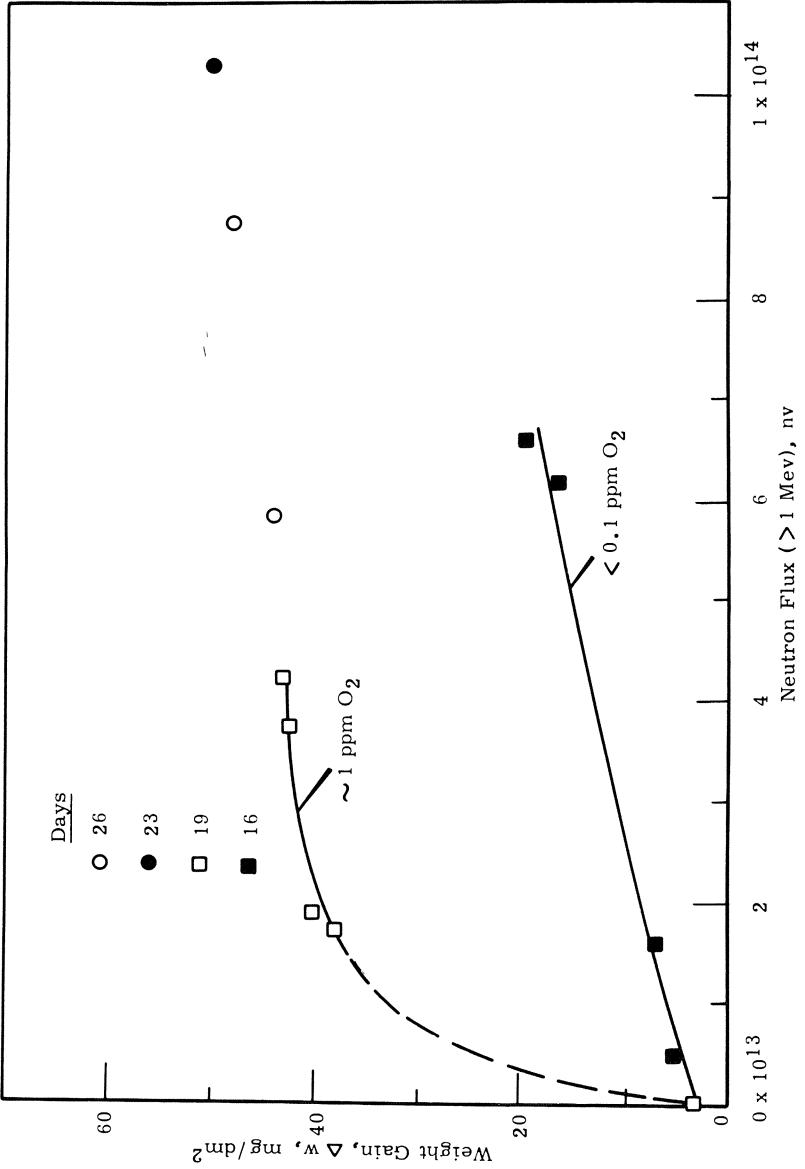


Fig. 69. Effect of neutron flux on the oxidation of Zircaloy-2 in high (~ 1 ppm) and low (< 0.1 ppm) oxygen water in the ETR G-7 loop.⁴²⁸

Thus the effect of oxygen apparently saturates at a fairly low concentration, and it is possible that we can separate the overall effects of irradiation into two parts: (1) a sharp increase in corrosion in the presence of low oxygen concentrations (< 1 ppm) at relatively low fluxes ($< 10^{13} n_f v$); plus an almost linear increase in oxidation rate with neutron flux which follows a constant slope irrespective of water conditions. The critical oxygen contents and fluxes could be temperature dependent. Such a scheme would be supported by the large enhancements observed by the Norwegians^{449,450} at very low fast neutron fluxes (10^{10} – $10^{12} n_f v$), low temperature (240°C), and low oxygen contents (0.03–0.04 ppm); and the fact that for constant water conditions a linear plot of weight gain versus dose is obtained, irrespective of exposure time.^{429,435} If some such saturation phenomenon were not evident, then extrapolation of the Norwegian results on a neutron flux dependence similar to the early ORNL proposals could imply oxidation rates at 240°C and high fluxes equal to or greater than those at 300°C . This seems unlikely on present evidence. A useful summary of experimental results in water has recently been made by Asher.⁴⁵¹

The largest enhancements have always been observed in the water phase. In steam, even with added oxygen,^{163,189,415,416,449,450} only small enhancements are observed, their magnitude being comparable to that observed under hydrogenated conditions in water. Where the oxygen content of the steam has been varied,¹⁸⁹ only small increases in oxidation rate in-reactor have been observed for quite large oxygen additions (1-atm O_2 in 2-atm steam). Results in steam are also similar to those in other gases such as carbon dioxide¹⁶⁴ and air,⁴⁵² where even fission fragment bombardment produces only small increases in oxidation rate.

In the light of the above evidence of significant differences between water and steam phases, we must be careful in comparing effects of oxidation temperature to restrict comparisons to one or other medium. Thus, the Harwell results,³⁹⁸ showing a decrease in the relative effect of irradiation (acceleration factor) with increasing temperature in steam, can be used to conclude that irradiation effects on both pre- and post-transition oxidation vanish at 400 – 450°C . Below 400°C the magnitude of the acceleration factor increases with decreasing temperature.³⁹⁸ This same effect appears to be present in the aqueous phase also, since the acceleration factors observed in HBWR^{449,450} are similar (acceleration factor ~ 100 , based on extrapolated post-transition rate at 240°C of $\sim 0.002 \text{ mg/dm}^2/\text{day}$) to those observed at 280 – 295°C ,⁴³⁵ despite the very low neutron fluxes in the Halden experiments. The supposition here is that at equivalent neutron fluxes the oxidation rates

in HBWR would have been even greater; this cannot be assumed with certainty, however, owing to the unknown contribution to the Halden results from fission fragment irradiation due to fissile material (from failed fuel) in the reactor coolant, and the possibility that the effects are already near saturation. Much effort was spent demonstrating that contamination by fissile material could not account for the results in ETR loop water.⁴³⁵

The unreliability of results from small autoclaves was discussed in the earlier review.³⁹⁸ Surface preparation techniques have only a relatively small effect on enhancement under irradiation in water⁴⁵⁰; even residual fluoride etchant stains do not result in any major increase in corrosion,⁴⁵³ and autoclave pretreatments in water tend to minimize the effect of irradiation. Weight gains of pre-autoclaved specimens (during radiation exposure) are usually less than those of etched specimens. However, autoclave treatments at high temperatures in steam (e.g., 3 days at 400°C) have given greater weight gains than etched specimens in long tests in low-oxygen water.^{398,430} Considerable scatter has also been observed between different billets of the same alloy under nominally identical conditions.³⁹⁸ This observation may be related to the variable behavior of fuel cladding (Fig. 67), which has led to the categorization of “good” and “bad” batches of cladding.^{421–425} This latter effect is related to the absence of local pustules of thick oxide from the “good” cladding; these pustules eventually coalesce on “bad” cladding to give an overall thicker oxide. As with other examples of oxide pustule formation in zirconium alloys, this may be related to the distribution of second phase particles, which may lead to locally high electronic conductivity in the oxide. Since Shirvington¹⁸⁹ observed predominantly increases in the ionic conductivity (and not the electronic conductivity) of oxides grown under irradiation, one would expect the initial intermetallic distribution (which primarily controls electronic conduction) to be more critical for good corrosion resistance in-reactor than it is out-reactor. However, the observation of pustular oxide films predominantly under boiling-water conditions, and on both fueled and unfueled specimens⁴⁵⁴ does not seem to be ascribable to material properties alone. It is possible that pustules develop at the sites of persistent steam bubble nucleation, where local high oxygen concentrations may develop. Only a few instances of this effect under non-boiling, but possibly oxygenated conditions have been reported.^{439,441} Shirvington reports only uniform oxide films, even at the highest oxygen overpressures. The mechanism of irradiation effects will be discussed in more detail later.

Although the equivalence of oxidation rates at equivalent energy deposition rates seems to work well for fission fragment and fast neutron

irradiation, experiments using other sources of bombardment have given mixed results.^{398,455,456} Accelerated oxidation in oxygen and water of specimens whose surface had previously been implanted with various high-energy ions have also been reported,^{457,458} although Spitznagel *et al.*⁴⁵⁸ only observed enhancements in instances where the range of the bombarding ion was sufficient to pass through the pre-existing oxide film. This observation, and the rapid disappearance of all the ion implantation effects, may imply that continuous bombardment of the oxide/metal interface is necessary before any enhancement of oxidation is seen. Further studies of this sort may be mechanistically valuable.

Behavior of Other Alloys under Irradiation. During the Homogeneous Reactor Project a large number of zirconium alloys were compared with Zircaloy-2 for their resistance to fissioning uranyl sulfate solution at high power densities. Alloys containing 15–30% niobium, with ternary additions of platinum, palladium, molybdenum, and copper (and various heat treatments), and binary alloys of platinum and palladium showed a spectrum of oxidation rates both higher and lower than Zircaloy-2.^{398,409,447} The greatest improvement (a factor of ~ 3 at 5 W/ml power density) was achieved by a Zr–15% Nb–5 Pt alloy and a Zr–15% Nb–1% Cu alloy both quenched from 900°C. However, all alloys showed oxidation rates considerably enhanced from normal out-reactor behavior.

In the light of this experience the observation that the Zr–2.5% Nb alloy could show lower oxidation rates in-reactor than out-reactor was treated with some scepticism when it was first observed.^{391,430} As we have seen, in laboratory tests this alloy is very sensitive to the presence of free oxygen in the water. In-reactor in oxygenated water, however, no increase in corrosion is observed and corrosion rates are the same as or less than those out-of-flux, depending upon heat treatment. In low-oxygen water or steam, weight gains in-flux are usually somewhat lower than out of flux (Figs. 70 and 71). These observations have been confirmed by all subsequent experiments, at least, for some heat treatments, or the early part of the oxidation curve.^{163,191,223,224,226,228,416,441} The conclusion is that in oxygenated water, provided a heat treatment is selected which does not give great sensitivity to the presence of free oxygen even in the absence of irradiation, then oxidation rates will be no higher, and in all probability will be lower than in the laboratory. In the case of Zr–2.5% Nb alloy cladding in German BWRs, which showed poor oxidation resistance,⁴⁴⁰ the heat treatment was not reported.

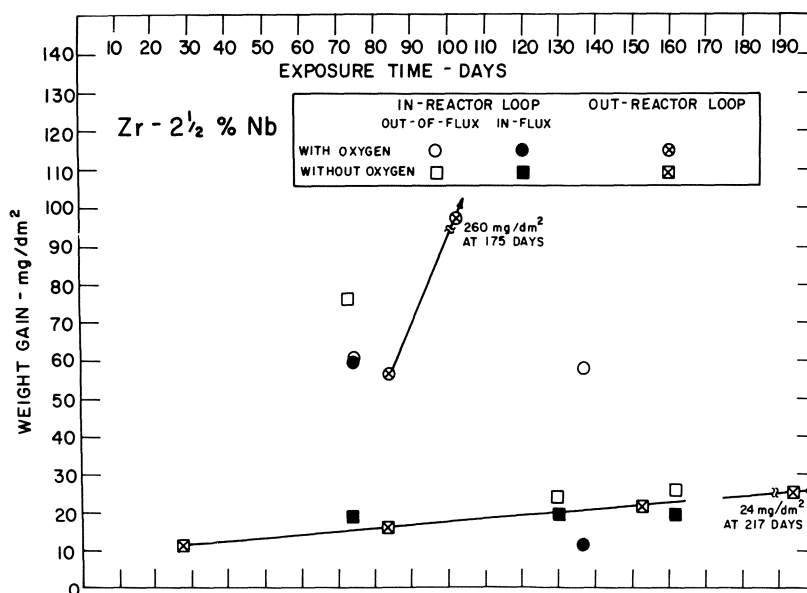
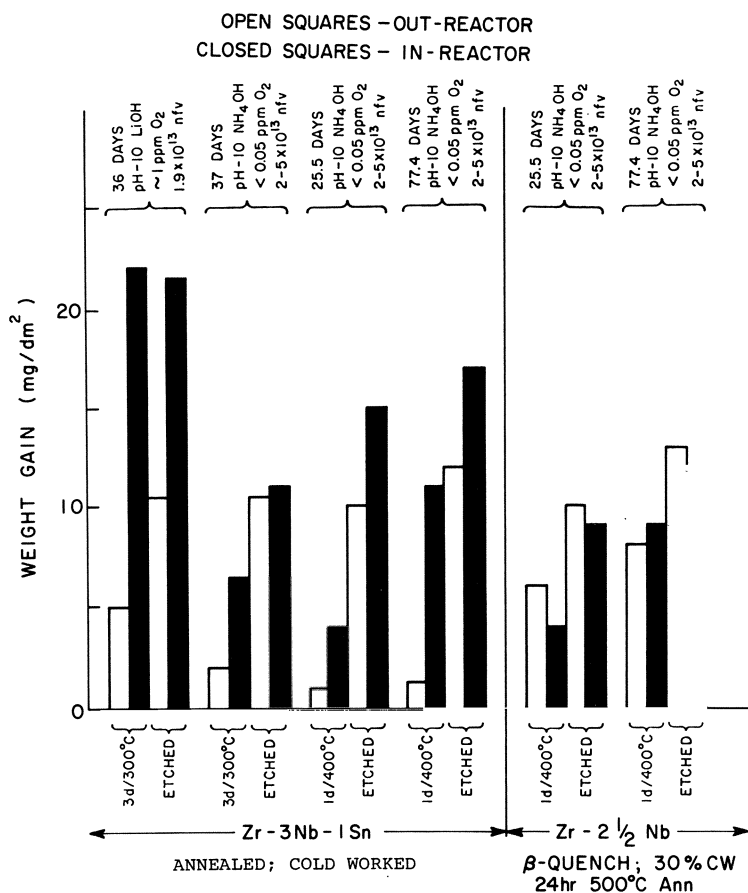


Fig. 70. Effect of oxygen content of the water on the oxidation of Zr-2.5% Nb alloy specimens in CRNL loop tests at $\sim 280^\circ\text{C}$.³⁹¹

The cause of the reduced oxidation under irradiation is ascribed to the same phenomenon which leads to improved resistance in the laboratory after prolonged annealing treatments. Irradiation is known to accelerate the tempering of Zr-2.5% Nb considerably at low temperatures,⁴⁵⁹ and experiments in which the oxide film was removed from irradiated samples and the specimens were re-exposed in the laboratory have confirmed this mechanism for the in-reactor reduction in oxidation.^{191,460}

The Zr-3% Nb-1% Sn alloy behaves more like Zircaloy-2 under irradiation than Zr-2.5% Nb, as far as its relative behavior in- and out-of-flux is concerned. It generally shows enhanced oxidation over that in the absence of irradiation; is less sensitive to oxygen in unirradiated water than Zr-2.5% Nb, and shows larger irradiation enhancements in oxygenated water than in low-oxygen water (Fig. 71).^{237,430,433,435} However, the actual weight gains are generally lower than for Zircaloy-2 and are only slightly higher than for Zr-2.5% Nb. Some of this work²³⁷ was carried out in small autoclaves with poor control on water purity, and the effects of the experimental technique are, therefore, difficult to separate from the effects of irradiation.



The Zr-1% Nb alloy, used by the Russians as fuel cladding,^{223,224-228} shows considerable sensitivity to the oxygen content of the water in the absence of irradiation, and only a small additional increment in oxidation in the presence of irradiation (Fig. 72).²²⁸ It does not show the reduction in oxidation which is shown by the Zr-2.5% Nb alloy, probably because the effect of tempering is much less for the 1% Nb alloy than for the 2.5% Nb alloy in the absence of irradiation. Corrosion rates for the 1% Nb alloy in-reactor in boiling water are generally higher than for the Zr-2.5% Nb alloy but are comparable with or less than those for Zircaloy-2. Long-term experience

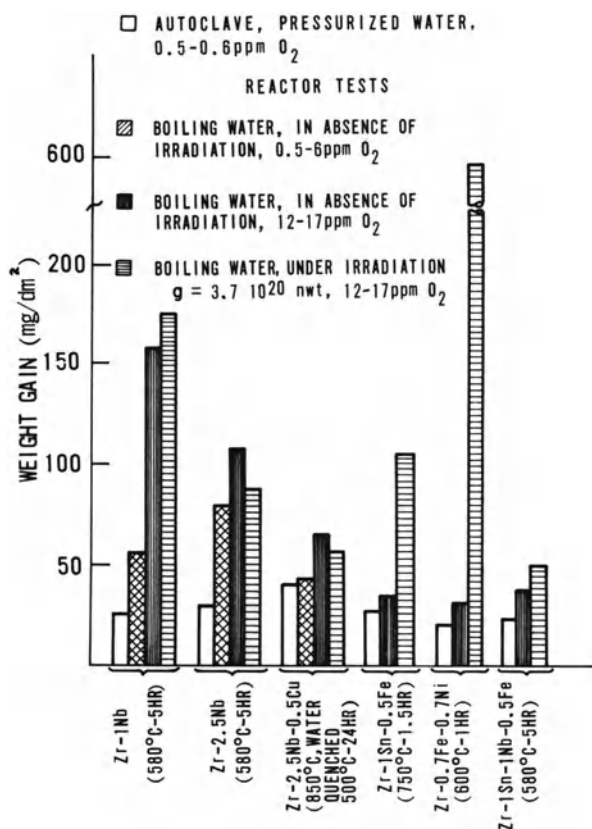


Fig. 72. In- and out-reactor corrosion of a number of zirconium alloys in water with various oxygen contents at 300°C for 3500 hr.²²⁸

with Zr-1% Nb alloy cladding at high heat ratings has been good,^{223,461} and despite its poorer general corrosion behavior, the 1% Nb alloy has advantages over the 2.5% Nb alloy (e.g., less severe corrosion of welds, better ductility after irradiation) for use as a fuel cladding. Ozhenite-0.5 (Table 4) has also shown only small enhancements of oxidation under irradiation, but tests were restricted to low-oxygen water.⁴³⁴

The Russians²²⁸ also have reported the results of in-reactor tests on Zr-2.5% Nb-0.5% Cu, Zr-1.5% Sn-0.5% Fe, Zr-0.7% Fe-0.7% Ni, and Zr-1% Sn-1% Nb-0.5% Fe alloys. Of these, the Zr-1% Sn-1% Nb-0.5% Fe alloys showed the best behavior. The Zr-Nb-Cu alloy showed a similar relative response to oxygen in the water and irradiation, as shown by the binary Zr-2.5% Nb alloy; the actual weight gains in the tests were less than

those of the binary alloy in all conditions except pressurized water in a laboratory autoclave.²²⁸ The Zr-Fe-Ni alloy gave very large in-reactor accelerations in the etched condition.²²⁸ This behavior is very similar to that observed for both pre-autoclaved Zr-1.2% Cu-0.28% Fe and Zr-1.2% Cr-0.08% Fe alloys in the G-7 loop tests⁴³³ (Table 7). Both these last two alloys showed weight gains of 700–900 mg/dm² when exposed for 174 days in the pre-autoclaved condition (Table 7) to water containing oxygen.⁴³³ In low-oxygen water⁴³⁰ this sensitivity to pre-autoclaving did not show up for the Zr-Cu-Fe alloy, but still remained Zr-Cr-Fe alloy (Fig. 73).

It would appear from these studies that erratic, grossly enhanced oxidation in reactor is a general feature of ternary alloys containing Cu, Cr, Fe, or Ni and no tin. Alloys containing 1% Sn in the Russian tests²²⁸ showed small enhancements under irradiation, but acceptably low absolute oxidation rates. The erratic behavior of the alloys without tin is also present in the absence of irradiation, as we have seen earlier.

Nevertheless, examination of Zr-Cr-Fe fuel clad tubing exposed in the Big Rock Point (U.S.) reactor to an average exposure of ~14,300 MW/day/ton uranium showed that they performed as well as (or better than, according to some criteria) Zircaloy-2 clad rods under similar irradiation conditions.²⁰¹ Oxide film thicknesses measured after irradiation were slightly less than those on Zircaloy-2 and no major effect of prefilming was seen (contrary to results in the ETR loop), although some thick oxide patches were found on tubing of both Zircaloy-2 and Zr-Cr-Fe prefilmed for 14 hr at 400°C (Table 8). Zr-Cr-Fe fuel cladding has also performed well in in-reactor loops at Chalk River, where it operated for 173 days in 500°C steam.⁴⁶²

Corrosion in Organic Coolants

Zirconium alloys have been used extensively in organic cooled reactors, where the coolant consists of a mixture of high-boiling aromatic hydrocarbons (e.g., terphenyls). These coolants are essentially noncorrosive to zirconium alloys when pure, and (as for liquid metals) it is the properties of the impurities which determine the behavior of the zirconium alloy.^{463,464}

Early experiments in organic coolants^{465–469} indicated that excessive hydriding could be a major problem in organic coolants. It was found that chlorine impurity in the organic was a major cause of the gross hydriding, and that by eliminating chlorine compounds and maintaining a surface oxide film in good repair by ensuring the presence of adequate water (>50 ppm) in the coolant, the behavior of zirconium alloys was satisfactory.^{11,181,464,470}

Table 7. In-Flux and Out-of-Flux Weight Gains on Zirconium Alloys after 174 Days in pH-10 NH₄OH^{4,3,3}

Alloy	Condition	Preautoclave ^a weight gain (mg/dm ²)	Out-of-reactor BNW ^b autoclave (mg/dm ²)	Out-of-flux (mg/dm ²)			Quadrant 234 1.7 × 10 ²¹ nvt (mg/dm ²)
				~ 1 min ^c	~ 1 sec ^c	Quadrant 233 1 × 10 ²⁰ nvt (mg/dm ²)	
Zircaloy-2	Annealed	E	13.7	—	14	16	121
	Annealed 80% Cold work	17.8–19.9 E	—	9 ^d	10	8	224
Zircaloy-4	Annealed	E	—	—	—	15	125
	Annealed	17.2–18.0 E	—	—	14	14	79
Zr-1.2 Cr-0.08 Fe	Annealed	—	16.3	12 ^d	4	9	81
Zr-1.2 Cu-0.28 Fe	Annealed	14.0–14.4 E	—	16 ^d	14	22	118
	Annealed	—	125.1	80	44	393	713
Zr-3 Nb-1 Sn	Annealed	19.2–20.5 E	—	92	94	106	380
	Quenched, aged	—	—	—	16	14	883
Zr-2.5 Nb	Quenched, aged	20.0–21.9 E	—	5	—	3	44
	Quenched 20% CW aged	—	29.0	—	22	11	28
Zr-2.5 Nb	Quenched 20% CW aged	13.4–14.6 E	—	13 ^d	23	3	52
	Quenched 30% CW aged	—	30.5	—	17	12	28
Zr-2.5 Nb	Quenched 30% CW aged	12.7–14.0 E	—	—	15	7	51
	Annealed 20% CW	—	18.9	16	15	13	35
Zr-2.5 Nb	Annealed 20% CW	11.9–12.8 E	—	—	12	9	52
	—	—	—	—	—	—	41

^aZr-2.5 Nb specimens prefilmed 400°C, 3 days, 100-psi steam; all other alloys prefilmed 400°C, 3 days, 1500-psi steam. E denotes specimens exposed as-etched.

^bWeight gain at 174 days: autoclaved, pH-10 NH₄OH, 280°C at Battelle Northwest.

^cCoolant transport time to out-of-flux specimens after leaving the flux zone.

^dFilm thicknesses determined metallographically on specimens where fretting was observed.

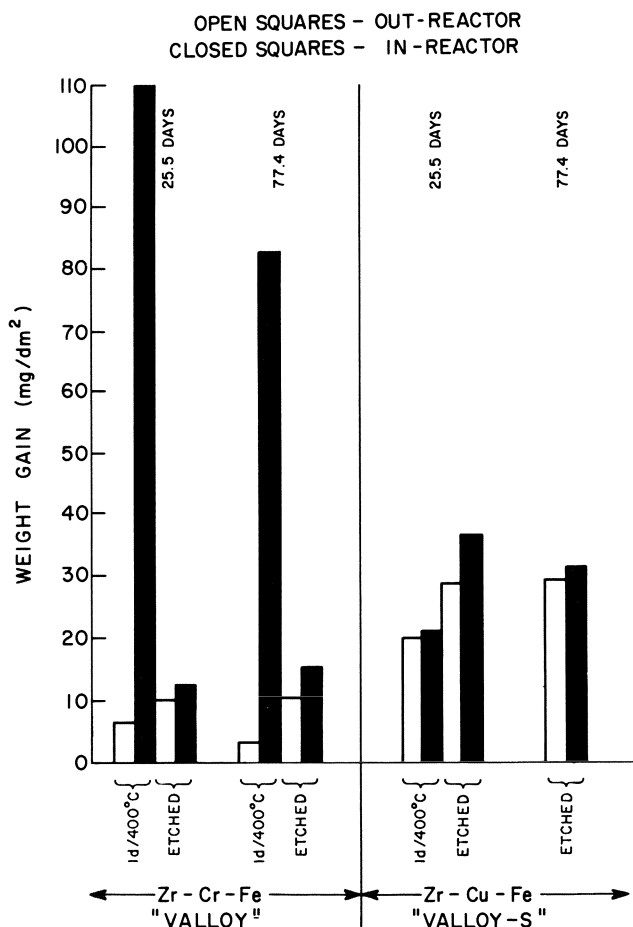


Fig. 73. In-reactor oxidation behavior of Zr-Cr-Fe and Zr-Cu-Fe alloys (Valloys) in pH 10 NH_4OH (<0.05 ppm O_2) at 280°C .⁴³⁰

Under these conditions oxidation rates were comparable with those in low-pressure steam (Fig. 74), and hydriding rates were acceptably low (Fig. 75). Of the alloys tested (low-Ni Zircaloy-2; Zircaloy-4; Zr-2.5% Nb; Zr-0.7% Cu-0.2% Fe, and Ozhennite 0.5), the Ozhennite 0.5 alloy proved to have both the lowest oxidation and hydriding rates.^{11,470-472}

Under irradiation the rates of hydriding are increased by a small factor, and presumably the oxidation is also accelerated, although no reports of

Table 8. Summary of Corrosion Results on In-Pile and Out-of-Pile Zircaloy-2 and Zr-Cr Test Specimens
(Weight Gains in mg/dm^2)

Surface pretreatment	Zircaloy-2			Zr-Cr			
	Isothermal out-of-pile ^a	Isothermal in-pile ^b	Fuel rods in-pile	Isothermal out-of-pile ^a	Isothermal in-pile	Heat transfer out-of-pile ^a	Fuel rods in-pile
As-etched	15.6	69	58	15.6	62	15.6	42
300° preoxidation for 60 hr	—	76	39	—	64	—	48
400° preoxidation for 14 hr	22.2 ^c	78	67 (126) ^d	18.2 ^c	56	20.3	53 (145) ^d

^aResults from CL-1 corrosion loop tests; preoxidation weight gain is included for the preoxidized specimens.

^bDummy rod cladding.

^cSecond set of specimens in CL-1 loop; data extrapolated to ~7900 hr.

^dTotal average weight gain, including thick oxide patches.

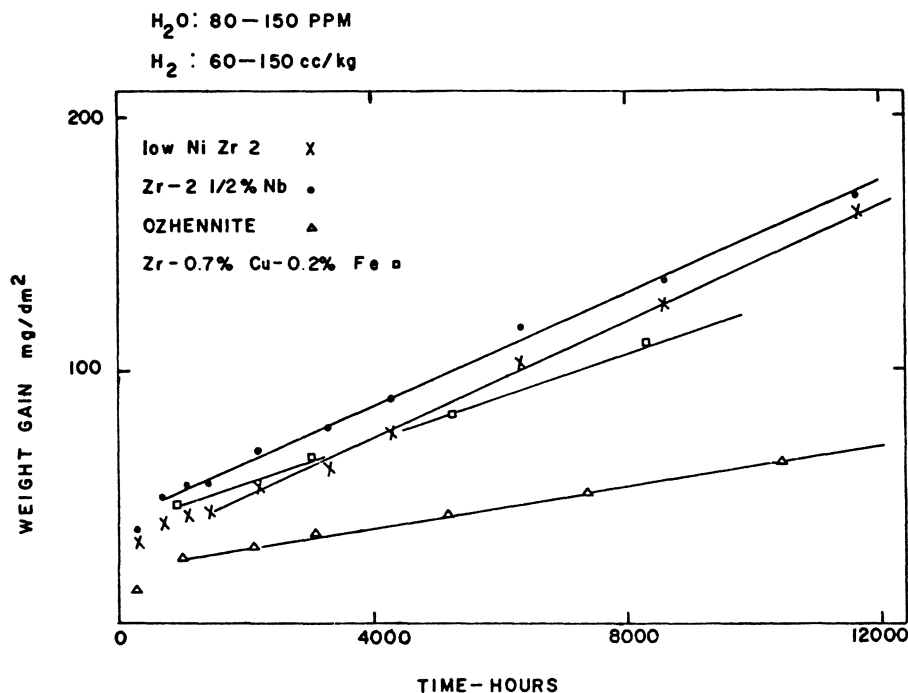


Fig. 74. Oxidation of Ni-free Zircaloy-2, Zr-2.5% Nb, Ozhennite 0.5 and Zr-0.7 Cu-0.2 Fe alloys in organic liquid (HB-40) at 400°C.¹¹

measurements of film thickness have appeared.^{464,472,473} The diffusion of hydrogen down the temperature gradient to the cold side of coolant tubes and fuel cladding, with resultant embrittlement of wire wrap spacers (which may become almost solid hydride) remains the primary long-term concern for the use of zirconium alloys in organic coolants.

OXIDATION MECHANISMS

It is evident from the data quoted that the behavior of Zircaloy-type alloys and the Zr-Nb alloys show many differences in their response to a number of variables. These differences extend to the oxidation mechanism, and, for that reason, it is useful to treat the two groups of alloys separately. Other alloys are often found to show intermediate behavior, or show some

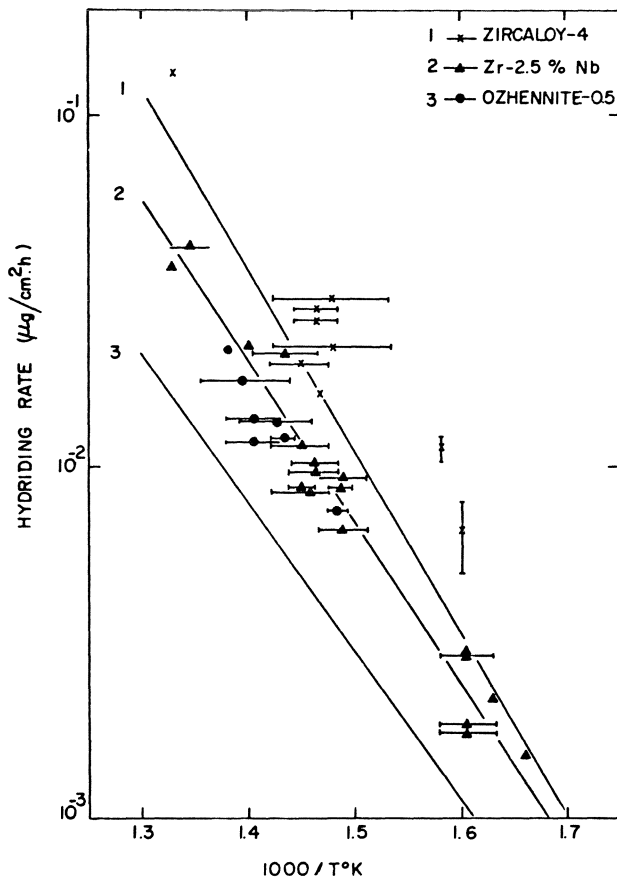


Fig. 75. Hydriding rates of Zircaloy-4, Zr-2.5% Nb and Ozhennite 0.5 in-reactor (points) in organic coolant (Santowax-om or HB-40) compared with out-reactor data (lines).^{4,7,2}

features typical of the Zircalloys and some typical of Zr-Nb alloys. Thus one cannot generalize from one alloy class to another, and each alloy should be studied separately to establish the oxidation mechanism.

The discussions here are treated in fairly general terms, and to delve into the finer points of the mechanistic arguments, the reader should consult the original references. In no instance has all the required information for the elucidation of the mechanism been obtained on one alloy under one set of oxidation conditions. Thus in many instances we have to draw data

together from high-temperature oxidation in oxygen, water, or steam and anodic oxidation. One must therefore make some attempt to assess whether information obtained under one set of conditions is relevant to another.

At the temperatures of primary importance to the practical use of zirconium alloys, the oxidation rate is effectively controlled by transport processes within the protective oxide. Zirconium alloys are used at temperatures where oxygen dissolution in the metal is only a small fraction of the total reacted; however, even at temperatures where this is not so, the processes occurring in the oxide film are probably unchanged, although the large effect of oxygen dissolution is superimposed upon these. This solid state diffusion process is relatively unaffected by metallurgical or environmental variables, and should be considered as an added factor at temperatures where it represents a major sink for oxygen transported through the oxide.

Zircaloy-Type Alloys

The early explanations of the oxidation mechanism of these alloys were framed in the classical context of an oxidation process controlled by the lattice diffusion of ions and ionic vacancies through a protective oxide film, which ultimately failed by a largely mechanical process, owing to some phenomenon such as a phase transformation, or the stress generated by the different specific volumes of oxide and metal.^{3,8,195,198} Thus the effect of nitrogen (for instance) on the corrosion rate in water or steam, and the counterbalancing effect of tin were seen in terms of the effect of these impurities in solid solution on the vacancy concentration in the oxide.³ The behavior of the oxygen vacancies was treated by the classical application of the law of mass action, and the necessity to transport electrons as well as ions through the protective oxide was neglected, or assumed to be unimportant in zirconium oxidation.⁴⁷⁴⁻⁴⁷⁸ Although more recent work has shown that the processes occurring are considerably more sophisticated than this simple theory, it still forms the basis of some mechanistic interpretations.⁴⁷⁹ Our current views require considerably more detailed analysis and experimentation before mechanistic conclusions are reached, and in many instances (such as the effect of nitrogen cited above) no recent mechanistic studies have been made. It is, therefore, often impossible to fit the observations of many of the factors affecting oxidation into the mechanistic framework outlined here because of lack of sufficient information. However, one can feel fairly confident that these early explanations are, at best, incomplete.

The observed variation in the rate law for oxidation between “cubic” and “parabolic” in various studies led some investigators at an early date to doubt the accuracy of the simple classical interpretation. Smeltzer *et al.*⁴⁸⁰ suggested that deviations from the parabolic rate law were due to short-circuit diffusion paths in the oxide. Nevertheless, despite the encouraging ability of such an hypothesis to fit an infinite range of intermediate rate laws between parabolic and cubic, this line of investigation was not immediately pursued. The observation that the alloying additions producing the improved performance of the Zircalloys were (with the exception of tin) of low solubility in α -zirconium, and occurred as second phase particles, whose distribution in the matrix had a critical effect on the corrosion resistance, warranted comment but little attempt to develop a theory which accounted for these facts. Where consideration was given to this dilemma, explanations were usually centered around the necessity for a satisfactory distribution of inter-metallic particles to ensure adequate alloying additions in solution throughout the metal and oxide.²⁶²

Application of Electrochemical Techniques

The relative magnitudes of the ionic and electronic resistance of the oxide on zirconium have interested only a few investigators in the past. Early studies employed either evaporated metal layers on the oxide surface or point contacts as a means of providing the external contact necessary for such studies.^{49,62,476,477,481–485} Point contacts, in particular, have given problems because they cause electrical breakdowns in thin oxides.^{482,485} Others have used standard electrochemical techniques in high-temperature aqueous solutions^{486–491} or high-conductivity oxidizing fused salts.^{183–191} A different technique which measures the mobility of implanted radioactive species directly in the oxide has also been employed.^{492,493}

Techniques using metallic contacts risk causing significant changes in the oxidation process occurring under the contact,⁴⁸⁴ and, because of a lack of knowledge of the contact area, they can be used only to measure the electric field across the oxide during oxidation. Inferences from these potential measurements have then been made based on the assumptions of the classical oxidation theory and the conclusion that both ionic and electronic resistances are ohmic.^{49,183} Electrochemical measurements in high-temperature aqueous electrolytes should ideally be able to overcome the problems associated with the use of metallic contacts. However, in studies which have been made by this technique,^{486–491} it has proved difficult to relate the electrochemical measurements to the relevant oxidation process. In Fig. 76 the corrosion

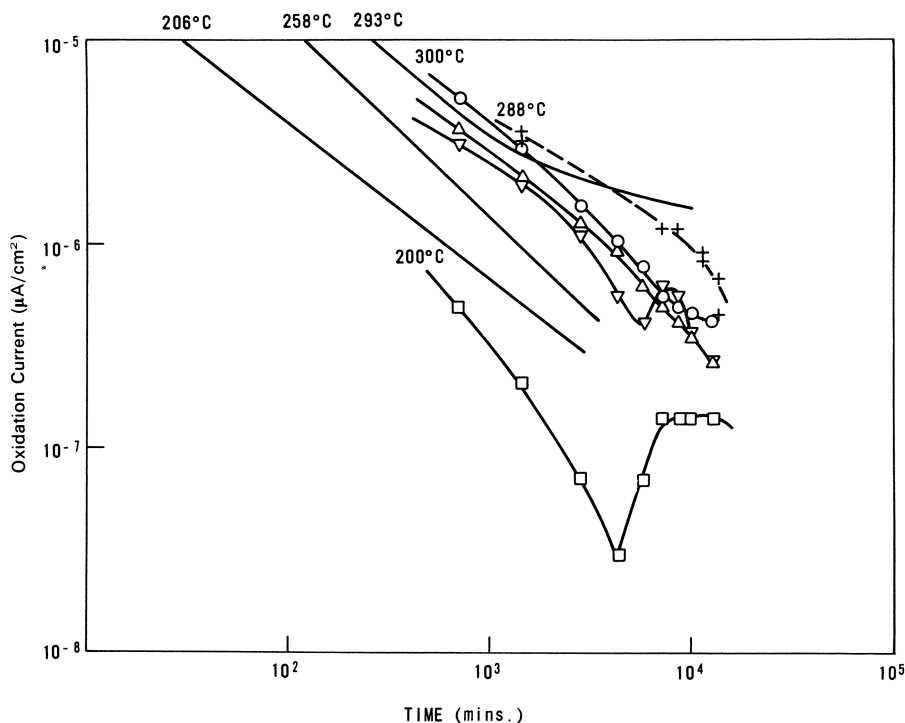


Fig. 76. Comparison of electrochemical (solid lines⁴⁸⁷ and crosses⁴⁹⁰) and weight gain (open points²⁸⁰) measurements on Zircaloy-2 in high-temperature aqueous solutions.

currents measured by the above authors are compared with values calculated from weight-gain curves obtained at similar temperatures and times.²⁸⁰ The agreement is good when allowance is made for the irregularity of the weight-gain curves and the possible differences between the material used by the various investigators.

Nevertheless, it is difficult to use results of such studies to determine the oxidation mechanism because of the difficulty in relating the various branches of the polarization curve to the partial processes occurring. For instance, are the rising branches of the polarization curves in Bacarella's studies^{486,487} limited by oxygen evolution and reduction, respectively (Fig. 77), or are they limited by the electronic conductivity of the oxide film on the metal? It is not possible to deduce this from the electrochemical measurements, and no data for the rates of the oxygen or hydrogen redox processes under the conditions of these experiments are presented. Thus,

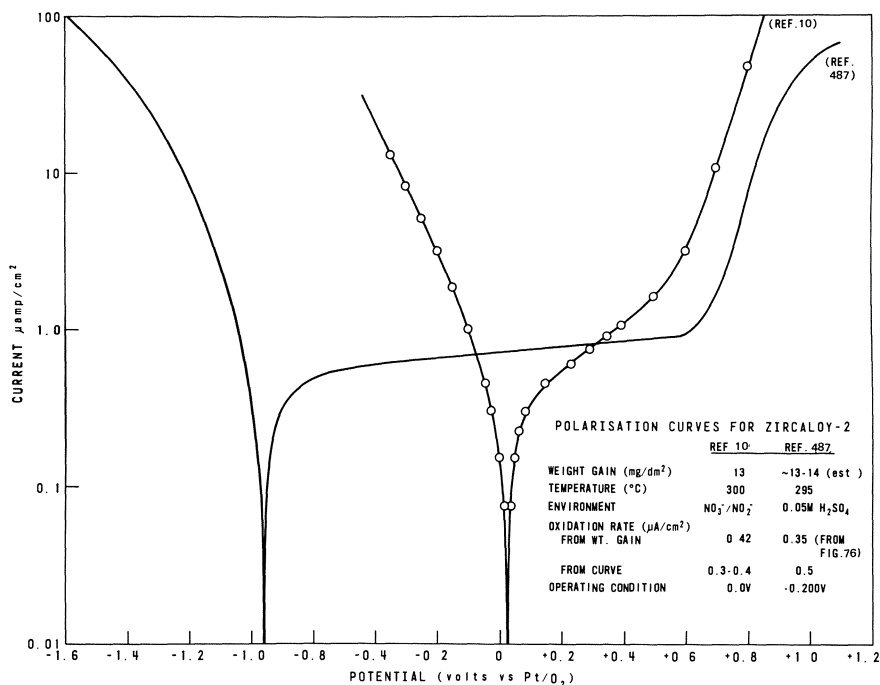


Fig. 77. Comparison of polarization curves for similar Zircaloy-2 specimens in aqueous solution and fused salt at $\sim 300^\circ\text{C}$.^{10,487}

the question of whether ionic or electronic transport in the oxide film is the most difficult cannot be determined from these measurements. There is no such ambiguity where metal electrodes are deposited on the surface. Provided these are ohmic contacts for all the processes occurring, the results must represent conductivity in the oxide film.

In an attempt to eliminate the problems associated with the use of such metal contacts, and at the same time avoid the possible intervention of electrochemical processes in series with the ionic and electronic resistivities of the oxide film, we have chosen to use a fused nitrate/nitrate bath in which to do electrochemical studies.^{10,183-191} The advantages of this have been argued elsewhere¹⁸⁸; however, it is interesting to compare the polarization curves for specimens in such a bath with those of Bacarella⁴⁸⁷ in Fig. 77. Considerable differences can be seen between the two curves, although the measured corrosion currents are in good agreement with those expected from weight gain curves. It is suggested that the high currents measured in

the fused salt are largely electronic currents in the oxide film, to which the fused salt apparently behaves in an almost ohmic fashion.^{186,188} The electronic current is apparently blocked in aqueous solution, presumably because the charge transfer processes at the oxide/electrolyte interface are slow.⁴⁸⁷ Thus such curves in aqueous solution may not give an accurate representation of the processes occurring during normal oxidation when no external current is required to flow.

Processes Occurring During Oxidation

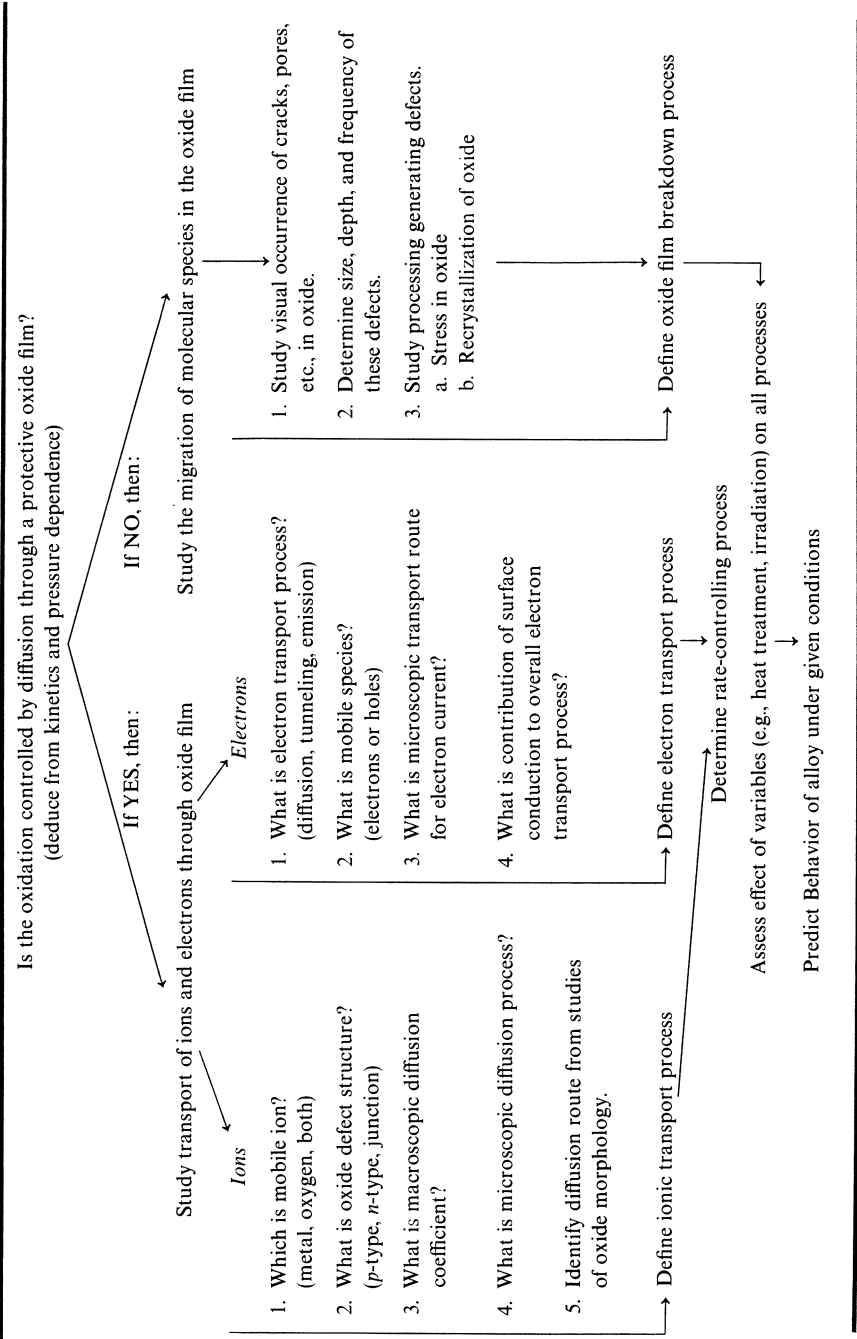
It is important in elucidating mechanisms first to list the questions which must be answered if the oxidation mechanism is to be understood (Table 9). We will then summarize the present status of the answers to these questions, without going into the experimental details and techniques, which can be found in the references cited. It will then be possible to determine where gaps in our knowledge could usefully be filled.

Ionic Transport in Oxide Films

Which is the mobile ion? Marker studies using injected rare gas atoms have shown that oxygen is the mobile species.⁴⁹² Other studies, on anodic films, have shown that the movement of zirconium ions represents less than 1% of the total.⁴⁹³ An earlier experiment to determine the mobile species using an electrochemical technique at room temperature reached the same conclusion, although the interpretation of this experiment is more open to question.⁴⁹⁴ An accurate value for the zirconium diffusion coefficient in growing thermal oxide films is still needed for the evaluation of the oxide recrystallization data.

What is the oxide defect structure? Studies of the conductivity of bulk zirconia versus P_{O_2} , at temperatures where electronic conduction makes a negligible contribution to the total, have shown that the oxide is *p*-type at pressures near to atmospheric and *n*-type below $\sim 10^{-16}$ atm.⁴⁹⁵⁻⁴⁹⁷ These measurements on bulk zirconia cannot necessarily be related to the properties of oxide films, and it has proved difficult to get equivalent data from measurements on thin films.^{485,498} The interpretations of these measurements in terms of defect types and concentrations in the bulk oxide or oxide films^{495-497,499,500} have been made on the basis of a purely ionic lattice containing only point defects. However, in the light of the distorted nature of the Zr-O coordination polyhedron indicated by the latest x-ray determination of the α -ZrO₂ structure⁵⁰¹ it appears impossible for such a structure to

Table 9. Understanding the Thermal Oxidation of Zirconium Alloys



arise by other than largely covalent bonding. The high-pressure orthorhombic form of ZrO_2 ^{502,503} has the $\alpha\text{-PbO}_2$ structure which is well known to accommodate nonstoichiometry by lattice shear rather than by point defects.⁵⁰⁴ Although the stresses generated during oxidation have not been shown to stabilize the orthorhombic phase, they do stabilize another phase in addition to $\alpha\text{-ZrO}_2$.¹⁰¹⁻¹⁰³ The identification of this second phase as tetragonal or cubic ZrO_2 has always been tentative and based on a minimum number of x-ray peaks. At oxidation temperatures below 600°C, the phase diagram of Bocquillon and Susse⁵⁰³ suggests that it ought to be the orthorhombic form that is stabilized by the growth stresses in the oxide. In such an event the relationship between nonstoichiometry and defect concentration via the law of mass action could easily be invalid.⁵⁰⁵

The observation that the lattice diffusion coefficient for oxygen in ZrO_2 is unaffected by the oxygen partial pressure,⁵⁰⁶ whereas the electrical conductivity is strongly dependent on P_{O_2} ,⁴⁹⁵⁻⁴⁹⁷ casts further doubt on the relationship between nonstoichiometry, conductivity, and point defect concentration in this material. A careful examination of the nature of the bonding and the types of lattice defect present is required by an independent method not requiring doubtful a priori assumptions.

What is the macroscopic diffusion coefficient for oxygen during oxidation? Using a nuclear reaction of oxygen⁸⁶ and by $^{16}\text{O}/^{18}\text{O}$ exchange⁵⁰⁷ it has been possible to determine the diffusion coefficient for oxygen in a growing oxide film by methods which do not require any assumptions about the oxidation mechanism for interpretation. Similar studies have been made on pure single-crystal and polycrystal spheres of zirconia.^{506,508} The diffusion coefficients for oxygen in growing oxide films^{86,507} agreed well with those for polycrystalline zirconia; the diffusion coefficient for single-crystal zirconia was several orders of magnitude lower (Fig. 78). Results for diffusion coefficients calculated from oxidation rates^{38,514,515} or from the interrupted oxidation technique of Rosenberg^{21,499} invariably correspond with the diffusion in polycrystalline and not single-crystal ZrO_2 .

What is the microscopic diffusion process? Using an ion bombardment mass spectrometer on the specimens from an earlier experiment,⁸⁶ Cox and Pemsler were able to distinguish between the bulk and short-circuit diffusion coefficients in growing oxide films.⁵¹³ Results for the lattice diffusion component were much less than for the line diffusion component and extrapolated close to the results obtained on single-crystal zirconia.⁵⁰⁸ Thus, oxygen diffusion through oxide films forming at 400–500°C is largely by a line diffusion rather than by a lattice diffusion process.⁵¹³ Similar conclusions

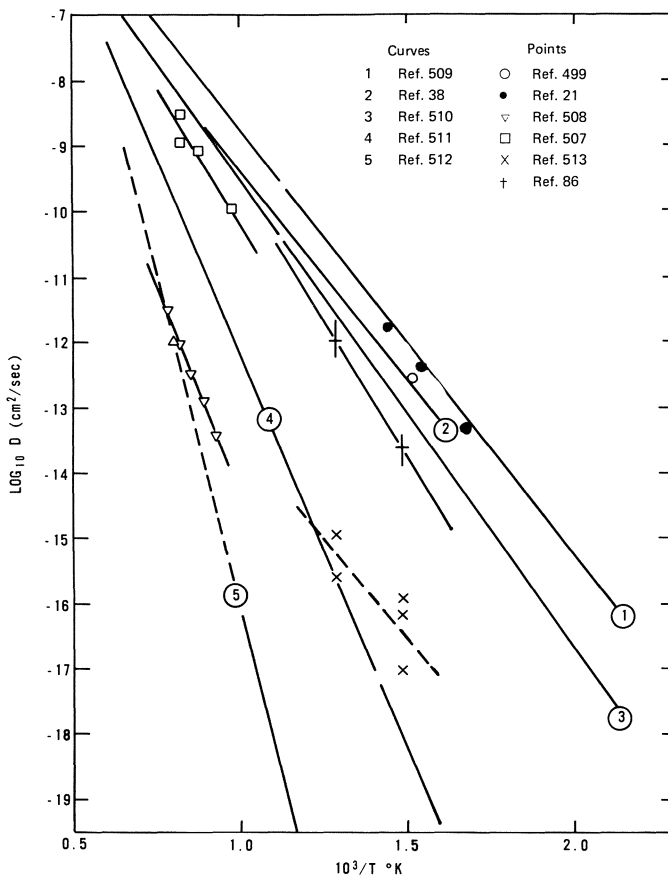


Fig. 78. Collected data for the diffusion of oxygen in α -ZrO₂.⁵¹³

have been reached for oxidation at 500–1000°C.^{516–517} The agreement between the rate of oxygen diffusion through the oxide film during oxidation and a line-diffusion rate in polycrystalline zirconia, with a much smaller lattice diffusion rate, also explains the bimodal oxygen distribution observed for zirconium anodized in solutions containing alternately ¹⁶O and ¹⁸O,⁵¹⁸ and explains the small fraction of implanted anionic species which migrated in Whitton's⁴⁹³ experiments (the majority of the implanted species would stop inside oxide crystallites and only a small fraction would end up on boundaries or dislocations).

Identification of the diffusion path. Transmission electron microscopy of stripped oxide films has shown that at a thickness of 100–200 Å, they consist of small epitaxially oriented ZrO_2 crystallites in a matrix which may be amorphous.¹⁵⁹ As the oxide thickens the crystallites become larger and occupy ~100% of the oxide volume by the time a thickness of 1000–2000 Å is reached (Fig. 79).^{321,519–527} The examples of amorphous patches in such films, reported by Douglass and van Landuyt⁵²⁸ have not been confirmed and were probably the result of poor specimen preparation. The question of whether the initial oxide film formed is cubic zirconia, which remains on the outside of the subsequently formed monoclinic zirconia film, or whether cubic zirconia is continuously formed under the high stresses at the interface and transforms to monoclinic as it moves away from the interface (and the

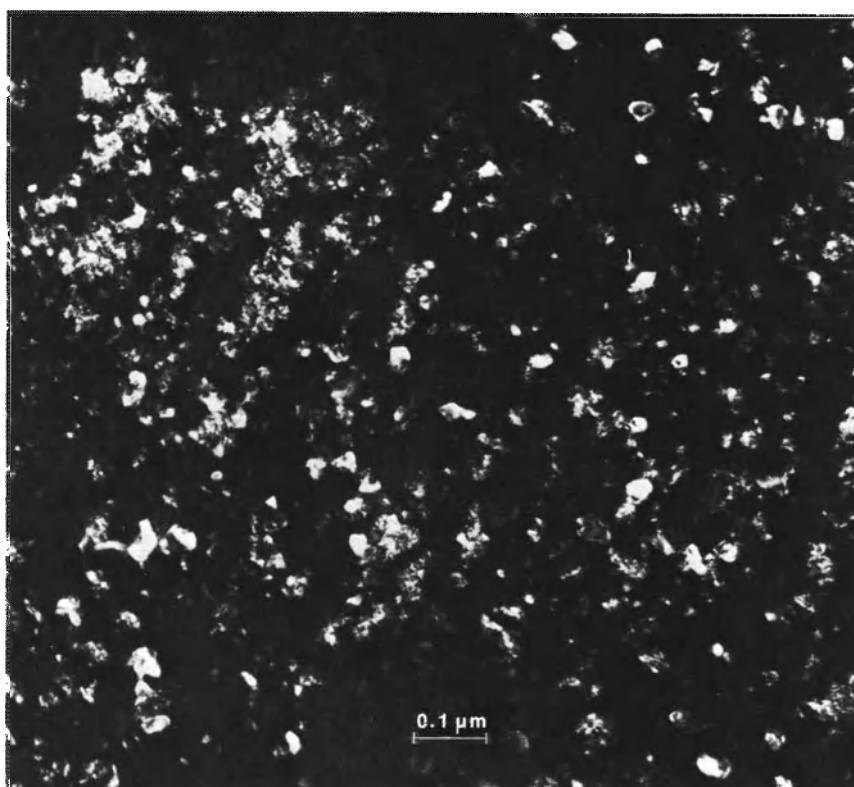


Fig. 79. Crystallite morphology in a thin zirconia film formed at 300°C in oxygen on zirconium.⁵¹⁹

stresses relax) has been considered several times, but is not yet finally resolved.^{102,103,198,526,527}

At greater thicknesses it is inferred from x-ray studies and oxide fractographs that some crystallite orientations grow preferentially at the expense of others.^{102,103,516,517,529,530} A cellular structure develops at the

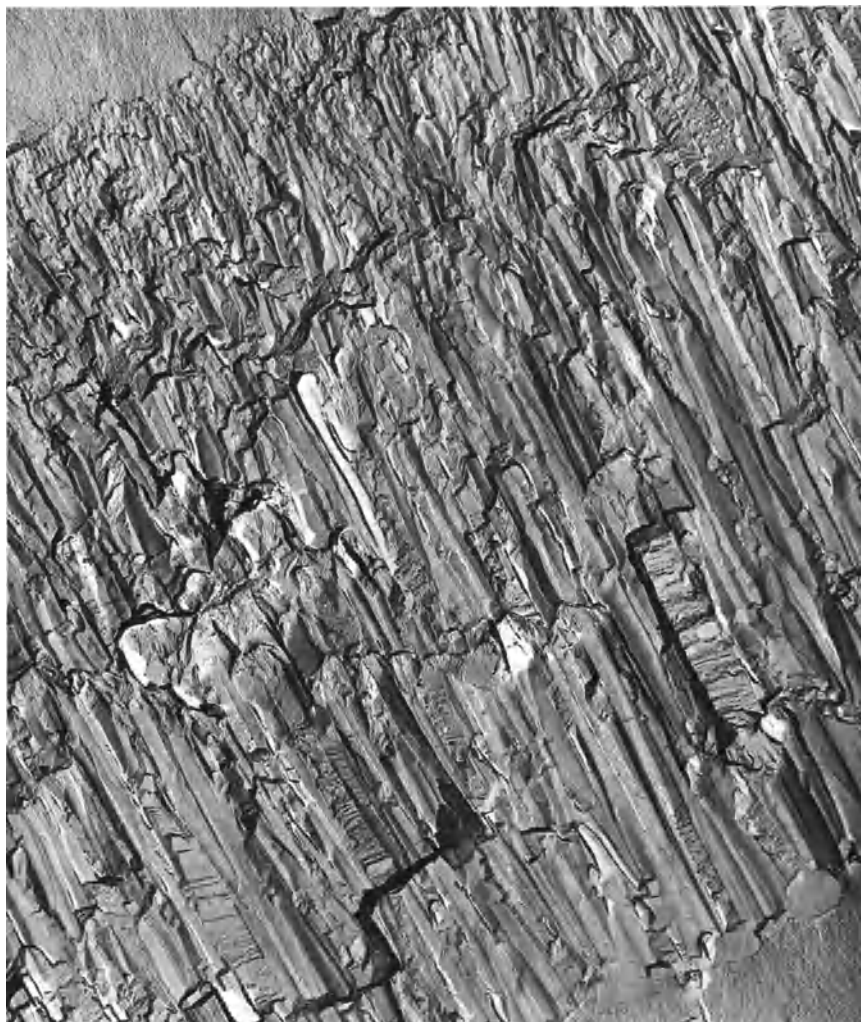


Fig. 80. Large columnar crystallites in an 11- μm -thick oxide on unalloyed zirconium (metal/oxide interface at bottom); $20,000\times$.⁵³¹

oxide/metal interface²² and a columnar growth morphology develops for zirconium at $\geq 500^\circ\text{C}$ (Fig. 80).^{48,50,96,531,532} In Zircaloy-2 this columnar growth fails to develop extensively and the result is successive layers of small and large oxide crystallites, with the renucleation of small crystallites probably representing the onset of repeated local oxidation rate transitions

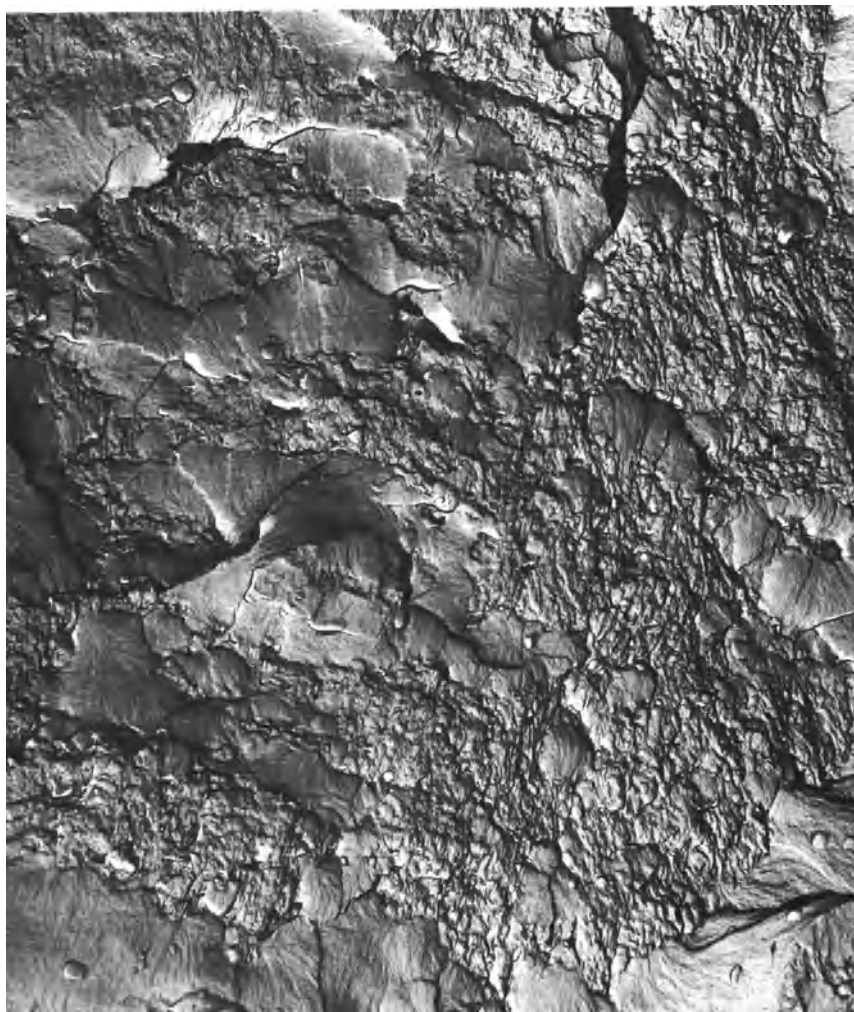


Fig. 81. Successive layers of large and small crystallites in a 100- μm -thick oxide film on Zircaloy-2; $10,000\times$.⁵³¹

(Fig. 81).⁵³¹ These structures are believed to result from the motion of oxygen primarily along the crystallite boundaries (Fig. 82); no evidence has been found for extensive dislocation networks within the oxide crystallites.

Recent studies in which thick oxide films have been stripped and thinned using an ion mill^{533–535} have largely confirmed these conclusions concerning oxide crystallite growth. Columnar crystallites were only found in limited regions of post-transition oxide films formed on the Zircaloys.⁵³⁵ However, the precise details of crystallite size and the distribution of small and large crystallites do differ from study to study,^{531–535} and it is probable that further work will be needed before a consensus on precisely how oxide films thicken can be reached. A combination of oxygen diffusion via crystallite boundaries and an increasing crystallite size with oxide thickness can readily explain departures from parabolic oxidation kinetics in the direction of cubic (or quartic) rate laws, and accounts for observations of exponents not accurately fitting any simple rate law. Attempts to make a comparison between crystallite size and kinetics have been published recently.⁶³²

During the oxidation of Zircaloy-2 in the β -phase, where all the alloying additions are in solution, no oxidation rate transition is observed (Fig. 46) and a columnar oxide is observed.⁴⁸ It may be that the presence of second phase particles is the factor which prevents the growth of large columnar crystallites on the Zircaloys during oxidation at lower temperatures.

Further work on this topic using an improved autoradiographic technique for oxygen and oxide films showing large columnar crystallites (Fig. 80) might confirm that the line-diffusion process is along crystallite boundaries.

Electron Transport in Oxide Films

What is the electron transport process? Many studies of MOS and MOM diodes have been made in other metal/oxide systems and a number of current/voltage (I - V) characteristics have been correlated with specific electron transport processes. By determining the I - V curves for oxidizing specimens of zirconium alloys, and separating the ionic and electronic components of these, it should be possible to fit the electronic current to one of the possible I - V relationships and thereby identify the electron transport mechanism. Results have shown that this can approximate to a Schottky emission process,¹⁸³ even when the bulk oxide film is much thicker than the possible barrier thickness for such an oxide. However, examination of a wider range of alloys and oxidation conditions has shown that this is not always the case and that often the electron current is intermediate between

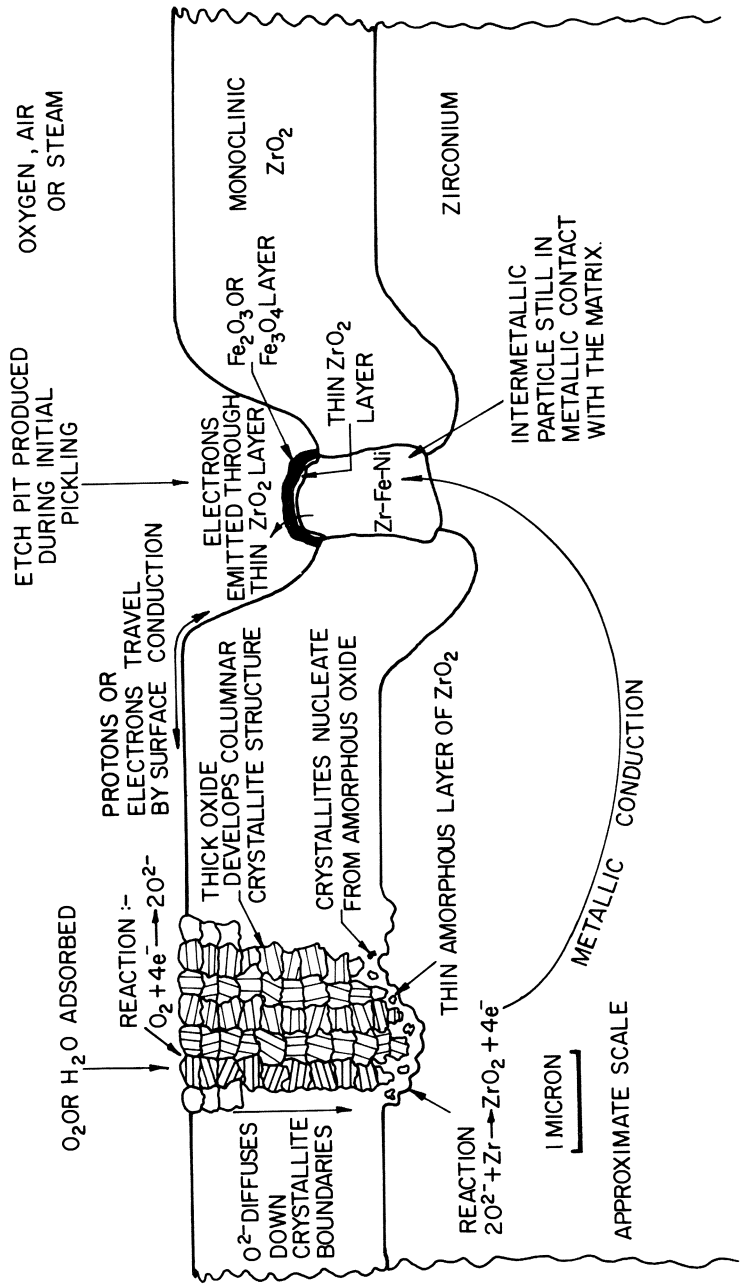


Fig. 82. Schematic diagram of oxide film on Zircaloy-2 and the processes occurring in it during oxidation in oxygen or water.²⁸²

a number of possible rate equations.^{10,184–186} The conclusion is that there are commonly several parallel electron conduction paths, obeying different rate equations, contributing simultaneously to the total electronic current. The only one of these to be positively identified is that associated with the iron-containing intermetallics in the Zircalloys, which arises from the thin ZrO_2 film formed on such intermetallics, through which iron diffuses outward to form a layer of an iron oxide on the surface. The electrical conduction properties of this complex barrier depend upon the relative thicknesses of ZrO_2 , Fe_3O_4 , and Fe_2O_3 formed on the intermetallics.^{10,184–186}

In other instances (e.g., Zr–Nb alloys) the electronic conduction appears to be largely a bulk process, while in unalloyed zirconium stray impurity particles and impurities segregated at grain boundaries may enhance the conductivity of the oxide at these sites, and cause the locally enhanced oxidation at grain boundaries, and the white oxide spots, which are prevalent in oxidation of zirconium at low temperature. Impurities, such as iron, in solution in zirconia, have been shown to cause large increases in electronic conductivity without a corresponding increase in ionic conductivity.⁵³⁶ This result supports the unique behavior of iron intermetallics observed in binary alloys containing Fe, Cr, Ni, or Sn.^{185,186}

What is the mobile species? Some preliminary studies of I – V curves have been made using semiconducting contacts with the intention of identifying the mobile species.⁵³⁷ The interpretation has been complicated by the localized nature of the electronic current,⁵³⁸ and results have shown both p -type and n -type behavior under different conditions. It is possible that the multi-layer nature of the thermionic emission barrier contains both p -type and n -type layers. Such a situation would explain the negative resistance phenomena observed in some I – V curves.^{183,186}

What is the microscopic transport route for electrons? Imaging techniques using evaporated CuI layers have shown that electron transport through oxide films on the Zircalloys (when measured at room temperature after oxidation) is localized at intermetallic particles.⁵³⁸ It is inferred from this and other circumstantial evidence that these are also the conduction sites at the oxidation temperature. The number of such sites and the surface conductivity of the oxide between them will have a major effect on the uniformity with which the oxide grows. Thus, with increasing purity of unalloyed zirconium the number of high-conductivity paths in the oxide will diminish and, if surface conductivity is inadequate, the oxygen transport process (and hence oxide thickening) will only be able to proceed rapidly in the vicinity of such high-conductivity sites. Hence pustular oxide will

develop, and the severity of this effect may increase with increasing purity of the metal.

What is the contribution of surface processes? Measurements of the rate of oxygen adsorption on zirconia surfaces show that these processes are sufficiently fast at normal temperatures and pressures that they should not limit the rate of oxidation.^{539,540} However, a number of observations, for instance, the increase in oxidation rate caused by some evaporated metal layers⁴⁸⁴ and iron oxide deposits,¹⁸⁴ suggest that the conductivity of the oxide surface may be a major fraction of the total electronic resistivity during oxidation. This factor will become more important as the separation between the sites of electron transport (i.e., intermetallic particles) and ionic transport (homogeneously distributed crystallite boundaries) increases. Thus the conductivity of the environment (which will influence surface conduction) should have a bigger effect on the oxidation of unalloyed zirconium (or poorly heat treated alloys) than on the Zircalloys. Observations (Fig. 2) have confirmed this supposition and have shown that (for unalloyed zirconium) surface conduction may represent up to 60% of the total electronic resistance.¹⁰ The surface conduction process has not been positively identified, but in water-containing environments it is probably protons migrating toward the intermetallic sites rather than electrons moving in the opposite direction. Measurements of the surface conduction of bulk zirconia⁵⁴¹ or zirconia films⁴⁹⁸ have shown it to be much greater in the presence of water vapor than in its absence.

Migration of Molecular Species Through Oxide Films

Visual occurrence of cracks and pores. Optical, electron, and scanning electron microscope studies of specimens oxidized under a variety of conditions have enabled us to characterize the visible flaws which occur in the surface of oxide films.⁵⁴² These fall into four main groups when specimens are studied at room temperature after oxidation (Fig. 83): (1) large cracks (~ 1000 Å wide), usually seen at specimen edges at almost any stage in the oxidation process; (2) fine cracks (~ 400 Å wide), which may be present as a network over the surface but are often absent even from post-transition oxides¹⁹⁸; (3) large pores (> 1000 Å dia.), which result from the etching out of intermetallic particles during the initial surface preparation; and (4) small pores (≤ 100 Å radius), which are occasionally seen in electron microscope replicas of post-transition oxide films, but are at the limit of the ability of the two-stage replica technique to reveal features penetrating the surface.

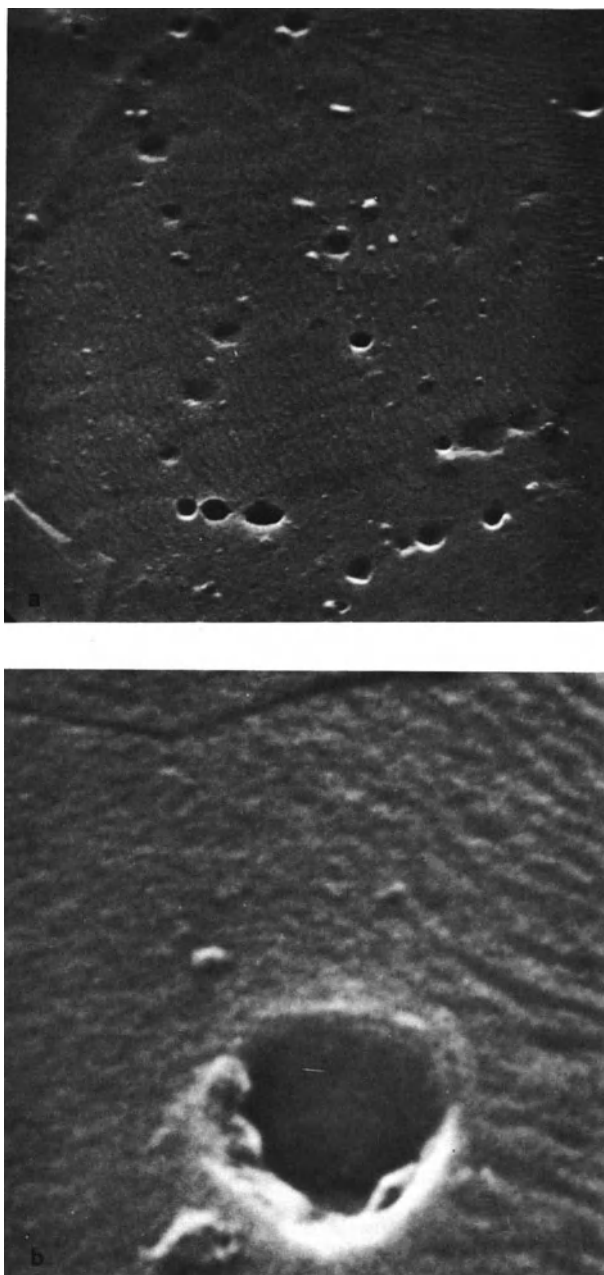


Fig. 83. Typical surface features of oxidized Zircaloy specimens:
(a) $3000\times$; (b) $20,000\times$.²⁸²

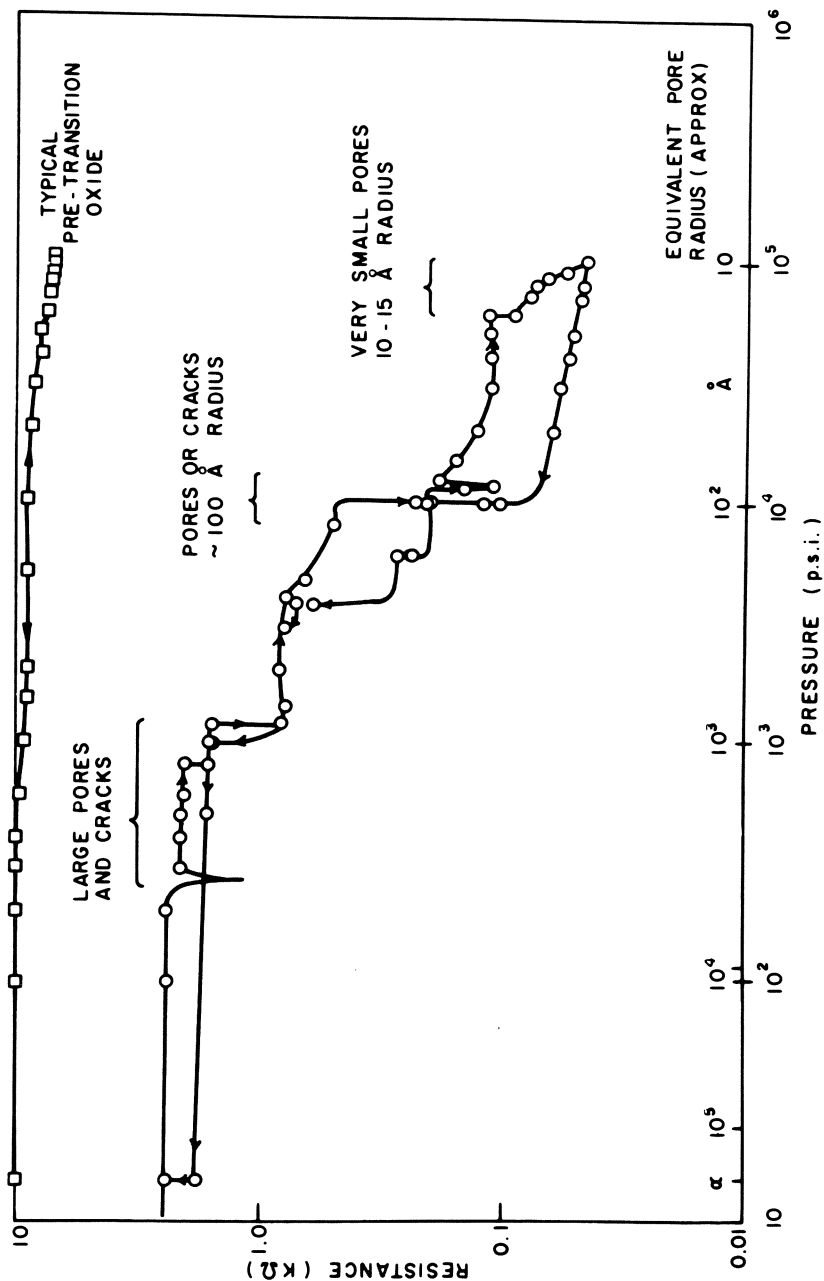


Fig. 84. Porosimeter traces for pre- and post-transition oxide films on Zircaloy-2.^{54,3}

Determination of pore size and depth. Mercury porosimeter⁵⁴³ and impedance measurements^{544–545} during immersion in an aqueous electrolyte have given results on the size of the important defects in post-transition oxide films. These have indicated that the small pores (Fig. 84) are the most important and universally present features of post-transition oxide films on the Zircalloys.^{542–545} Electron microscopy of ion thinned post-transition oxide films^{533–535} has confirmed the presence of these fine pores and the absence of gross cracks, and has shown that they occur at crystallite boundaries, and penetrate effectively up to the oxide/metal interface. Thus, the deductions made from results obtained with other techniques^{52,542} have been effectively confirmed.

Studies of Processes Generating Defects

Stresses in oxide films. Measurements of the extension or bending of thin foils of zirconium alloys^{97,106,546,547} and the plastic deformation of more massive specimens^{23,46,548,549} have shown that compressive stresses in the oxide approach the compressive yield point in thin oxide films (Fig. 85) and at the oxide/metal interface in thicker oxide films.^{97,106,546–549} Some relaxation of the stress occurs in the outer layers of thick films, and at the outer surface stresses may drop to zero or become tensile. The topography of the oxide/metal interface does not appear to be affected by the stresses generated at this interface (i.e., thin specimens which deform in creep during oxidation show the same topography as massive rigid specimens).²² Tensile stress applied to the specimen during oxidation causes an increase in oxidation only from a point near the normal transition.⁵⁵¹

One school holds that cracking (especially lateral cracks at the oxide/metal interface), caused by these stresses, is the primary cause of the oxidation rate transition.^{21,97,284,550,552,553} The effect of alloying elements on the ductility of oxide films is an important factor, if this hypothesis holds, and it has been studied by several investigators,^{510,520,554,555} who found significant differences in the ability of oxide films to resist impact-type tests (e.g., cracking by microhardness indenters). Experience in the ceramic field in producing zirconia forms resistant to destruction on cycling through the phase transformation may also be of relevance in considering plasticity effects in the oxide, particularly where high temperature oxidation is concerned.^{556–563} The improved plasticity of hypostoichiometric oxide, and the effect of porosity in nucleating cracking under stress and causing a reduction in compressive strength, would seem to be particularly relevant observations for the case of oxidation films.

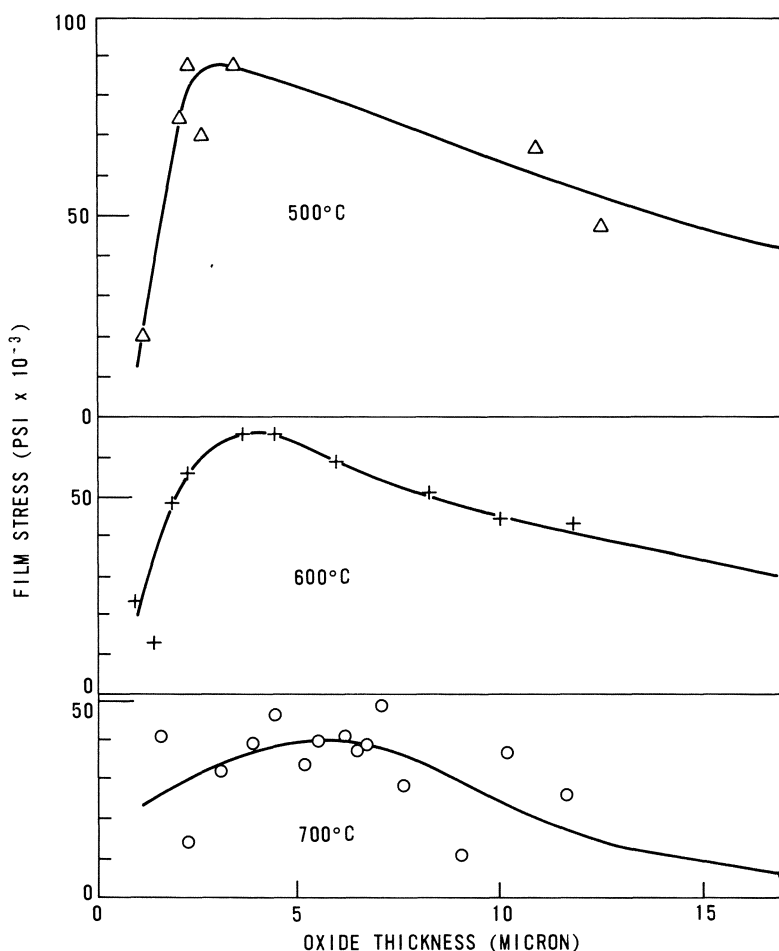


Fig. 85. Stresses measured in oxide films on Zircaloy-2.⁵⁵⁰

An alternative explanation holds that the stresses lead to recrystallization and pore generation in the oxide film, and that the cracks seen are either the result of the examination technique used^{542,552} or occur after the porosity has developed in the oxide, perhaps being nucleated by the pores.⁵⁶² That instances are observed where cracks have formed in the oxide film at the oxidation temperature is undeniable^{30,31,97,564}; however, when careful polishing and sectioning techniques are used^{533-535,552} examples are observed of post-transition oxides not showing any cracks but a continuous network of pores. The oxide cracking hypothesis cannot explain such instances, and therefore fails as a general mechanism for the rate transition, although it may be involved "post-hoc" as an added factor in the subsequent

degradation of the oxide film. Nevertheless, despite arguments to the contrary, and the evidence discussed below, the “oxide cracking” hypothesis still seems to have a subjective appeal as an overall mechanism for oxide breakdown.⁵⁶⁵

Recrystallization of the oxide films. Transmission electron microscopy of thin oxide films has shown steady increases in crystallite size between the thinnest ($\sim 100 \text{ \AA}$) and the thickest ($\sim 2000 \text{ \AA}$) oxide films which have been examined.⁵¹⁹ Beyond this thickness x-ray pole figure studies (Fig. 86) have shown continuing changes in the texture and epitaxy of the oxide film,^{102,103,529,530} and a corresponding increase in the crystallite size with film thickness has been observed.^{533–535} It is difficult to decide whether these effects result from the preferential growth of some orientations of crystallite, or whether some crystallites are recrystallizing. However, the disappearance of some reflections present in the diffraction patterns of thin oxide films⁵²⁵ indicates that both processes are occurring. It has been shown that these changes are related to the magnitude of the stress in the oxide, and represent one method for relaxing this stress.^{102–103} The stabilization of one of the high-temperature, high-pressure forms of zirconia near the oxide/metal interface and its subsequent recrystallization is a further manifestation of these changes.^{102,103,519}

The precise mechanism by which the recrystallization of the oxide leads to pores growing at crystallite boundaries is not known. The suggestion of vacancy condensation⁵⁴² is perhaps less likely than some mechanism (e.g., Nabarro–Herring) for creep of the crystallites leading to the generation of pores. Whatever the precise nature of their formation mechanism, there now seems to be no doubt about their presence (Fig. 87) or their being the primary cause of the rate transition for the Zircalloys under many conditions of temperature and environment.^{534,535} The cracking of the oxide may nevertheless be important under conditions of thermal cycling of unalloyed zirconium, where transition may be initiated by a single thermal cycle. The effect of alloying additions and impurities on the ionic component of the oxidation process is then probably through an effect on the growth and recrystallization of the oxide crystallites, and via their deformation properties in affecting the development of porosity. Impurities acquired from solution are known to have large effects on the sintering (i.e., crystallite growth) of precipitated zirconia.⁵⁶⁶

Deducing the Rate-Controlling Process. It is not immediately possible to deduce from the oxidation kinetics, particularly a simple weight gain or

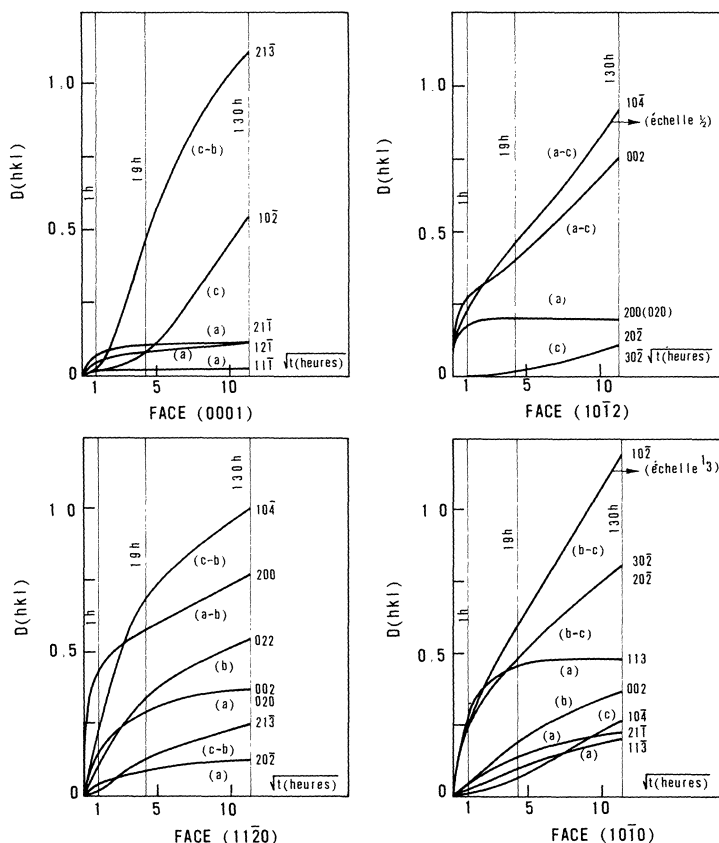


Fig. 86. Variation in the density of (hkl) poles observed on various faces of a zirconium monocrystal oxidized at 500°C .¹⁰³

oxide thickness versus time plot, whether or not diffusion through a protective oxide film is the rate-controlling process. Thus adherence to a parabolic rate law shows only that the oxidation rate is inversely proportional to the oxide thickness and can be obeyed equally for oxidation controlled by ionic diffusion through the bulk oxide or by diffusion of molecular oxygen through a porous compact. The distinction can only be made if the porosity of the oxide film is measured. An instance of the latter type of control is evident in the oxidation of niobium,³⁹⁰ where flow through a porous oxide film is limiting and the measured porosity of the oxide and the oxygen flow rate through it can be correlated with the oxidation rate. This situation still



Fig. 87. Transmission electron micrographs of a section of a post-transition oxide film on Zircaloy-2 ion-thinned to obtain transparency. Note the elongated shape of the small crystallites, the presence of fine pores at crystallite boundaries, and the absence of gross cracks.⁵³⁵

causes much confusion in the literature, for most investigators have not troubled to test the porosity of the oxide but have made their deductions solely from the formal kinetic equation which is followed.

Similarly, the observation of linear kinetics cannot be assumed to indicate control by diffusion through a constant thickness barrier oxide. It may, during oxidation at very low pressures, imply control by molecular diffusion through the oxidation apparatus from the point where the pressure is measured to the specimen. In fused salts or liquid metals it may indicate significant dissolution of the oxide or metal. In either case other tests, such as varying the geometry of the system or performing a complete mass balance on the system, will show which is the basic controlling factor.

For zirconium alloys it has been shown that dissolution of the oxide in high-temperature water is below the limits of detection, and pre-transition oxide films have been shown to be relatively impervious to molecular species.^{52,542-545} Hence, we can safely conclude that the pre-transition parabolic (or cubic) kinetics, at temperatures where oxygen dissolution in the metal is small (Table 3), are limited by diffusion of some species through the thickening oxide film. The ability to change the oxidation rate by modifying the electric field across the oxide^{10,182,183} suggests that the diffusing species is electrically charged; it does not prove this to be the case, however. The application of a field across the oxide could be superimposing an additional electrochemical process on what in the absence of the applied field could have been molecular diffusion through the film. The conclusion that the transport process is via charged species can only be reached if the charge carried across the oxide in unit time at zero applied field is determined and is shown to be equivalent to the mass of reactant (e.g., oxygen) transported in the same time, when reasonable values for the charge on the species are employed. To achieve this we need to know the complete current-voltage (I - V) characteristics of the system.

Current-voltage measurements in fused salt. Measurements of the potential across a growing oxide film are unlikely to help elucidate the rate-controlling process on their own. However, if coupled with a knowledge of the detailed I - V characteristics of the oxide during oxidation as a function of oxide thickness and the variable to be studied, they can be used to determine which aspect of the overall oxidation process is affected by the dependent variable, which process is then limiting the rate of oxidation, and whether the measured oxidation current is equivalent to the oxidation taking place. By such observations we have satisfactorily explained the early "inflection in the oxidation kinetics,"^{10,183,184} and have obtained good agreement between the oxidation current and the measured oxidation rate.^{185,186}

In practice, however, it is often desired to understand effects under conditions where the I - V curves cannot satisfactorily be measured during oxidation (e.g., enhancement of oxidation in oxygenated water in-reactor).

Here the closest approach to the ideal which is available is to compare the I - V curves of specimens which have undergone the effect under investigation with controls, by measuring both sets of specimens in fused salt after oxidation. We are then relying on the fact that the oxide properties do not change rapidly at low temperatures, and that large transient effects are not operating under irradiation. Neither of these conditions can be completely assured (particularly for the electronic currents); however, much progress has been made using this technique.¹⁸⁹⁻¹⁹¹

Use of polarization experiments. With evidence available from the I - V characteristics of the oxide, it should be possible to predict the effect of polarizing a specimen during oxidation, and thereby confirm the conclusions about rate-controlling processes. Only unalloyed zirconium was observed to behave in the simple manner predicted from theory in such experiments.¹⁸³ The Zircalloys behave in a like manner only prior to the "inflection" in the oxidation kinetics. Beyond this point, the shifts in the oxidation rate which result from polarization are small and in the opposite direction to those expected. This phenomenon is probably related to the complex nature of the barrier controlling electron transport after the early stages of oxide growth.^{183,184}

A hypothetical explanation can be made in terms of space charge in the oxide accumulating at a p - n junction near the surface of the oxide, perhaps where the oxide changes from hypo- to hyperstoichiometric.⁴⁹⁶ Such a hypothesis would be in agreement with the observation of negative resistance effects with Zircaloy-2 but not with zirconium,^{183,186} the disappearance of negative resistance when specimens are short-circuited during oxidation in fused salt, and the switching observed with diodes prepared from zirconia films with evaporated metal contacts.^{537,567} Despite the complicated nature of the electronic processes involved, it appears that they are the critical processes in controlling the oxidation of the Zircalloys as well as zirconium in the temperature range around 300°C. At higher temperatures this conclusion may be reversed.¹⁸⁵

Prediction of behavior. If the detailed I - V characteristics of new alloys as a function of oxide thickness, and the effect of a number of variables on these characteristics were known, then it should be possible to predict their behavior. However, the complications present in Zircaloy-2 compared with unalloyed zirconium make this a very difficult proposition in any instance. In most instances insufficient evidence is available to permit any new hypothesis to be proposed, or supported. Thus, the well-known major effect of the nitrogen content of the metal on the corrosion of zirconium in

water might be explicable if we knew its effect on the I - V characteristics of the oxide, and such other factors as oxide crystallite growth and the development of porosity. However, we do not have this information, and it is unlikely that the large effort which would be necessary to obtain it would be warranted by the practical advantages which would accrue. We already have an "ad hoc" solution (addition of tin) which has been explained by the classical oxidation models.³ It is unlikely that there would be sufficient incentive to do otherwise in this or other instances, and "ad hoc" solutions are likely to remain the preferred ones for improving the behavior of alloys in practice.

Mechanism of the Irradiation Enhancement of Oxidation. One situation where much effort has been expended on understanding the mechanism by which a particular variable affects the oxidation rate is the in-reactor enhancement of oxidation. Many mechanisms have been proposed in the past, a total of 24 having been considered by Asher.⁵⁶⁸ The most we can do here is to summarize these in the light of current knowledge of the oxidation mechanism in the absence of irradiation.

The first question to be answered is which is the important fraction of the radiation field. The possibilities (for various conditions) are fission fragments, fast neutrons, thermal neutrons, gammas, betas, or other heavy ions. We can probably dismiss thermal neutrons immediately because they have the energy neither to cause damage in the oxide nor to produce significant quantities of radiolytic species in solution.⁴¹⁶ Evidence on the effect of betas and other heavy ions is irreproducible,^{398,416,569,570} and while they may be shown to affect oxidation, they are not a primary component of the radiation field seen by fuel cladding or structural components in a reactor. The possible effect of gamma rays remains to be established; no effect of 6×10^6 R/hr was observed in atmospheric pressure steam,⁴¹⁶ whereas in high-pressure steam a small effect was observed in the first stage of oxidation (up to the plateau in the oxidation curve).^{398,412} Since there is a well-established difference in the magnitude of the overall irradiation enhancement between atmospheric pressure steam and water,⁴¹⁶ it is possible that the above difference in results for gamma radiation is real. Whether it is confirmed or not, the effect of a gamma flux appears likely to be only a minor one during the early stages of oxidation, and not the main source of the irradiation effect. Any effect of gamma flux will probably act only "in situ," most probably via an effect on the electronic component of the oxidation process, and hence would not be expected to cause any post-irradiation effect. The failure of Harrop *et al.*^{571,572} to observe any post-

irradiation effect of gamma rays on the ac conductivity of anodic or thermal oxide films at room temperature is hardly a sound basis for inferring the absence of an effect during simultaneous oxidation and irradiation.

We are thus left with fission fragments and fast neutrons as the prime contenders for the main source of the irradiation effect. Results at Oak Ridge showed that for equivalent energy deposition rates, these two species were equally effective.⁴⁰⁹ Nevertheless, for many years workers at Bettis denied any effect of fast neutrons, and claimed that all examples of increased oxidation in high-temperature water, whether obtained in Bettis experiments⁵⁷³ or in BWRs or loop experiments in ETR, were caused by fission fragments from uranium contamination of the system. The weight of evidence from environments other than high-temperature water under conditions where uranium contamination was absent militated strongly against this standpoint.^{410–417,443–446} The question was finally resolved when loop tests were conducted in a new and unsullied loop in ATR, and oxidation rates (at equal neutron fluxes) were found to be the same as in the earlier ETR tests, which were suspected of having uranium contamination.⁴³⁵ Finally, an effect on Shippingport blanket fuel was demonstrated, and again contamination with uranium was discounted and fast neutrons were acknowledged to be the primary cause.³⁸⁷

The next question to be settled is the site of the important damaging process. This might be in the environment, at the environment/oxide interface, in the oxide, or in the metal. In addition to fast neutron bombardment, the presence of oxygen, or radiolytic oxidizing species, is necessary to obtain the large enhancements observed in water. Small, roughly equal enhancements are obtained in steam and gaseous environments with the magnitude of the effect nearly independent of the amount of oxygen in the environment. We thus appear to have a small enhancement due to fast neutrons alone, with a large additive synergistic effect of oxygen in the water. The synergistic aspect of this effect of oxygen arises because oxygen has not previously been observed to have any major effect on oxidation in the absence of irradiation.³⁷⁰

The possibility of a direct chemical effect of either oxygen or oxidizing radiolytic species seemed to be effectively eliminated by the insensitivity of the Zircalloys to oxygen in the absence of irradiation and the absence of any downstream effect in in-reactor loops.^{416,423,443–446} However, recently Shirvington^{187,283,334} has shown that pickled, but not electropolished, specimens are very sensitive to high oxygen pressures in water, and that the properties of the oxide produced bear some resemblance to those of oxides formed under irradiation. Despite the similarity between the two effects it

was shown,²⁸³ that the irradiation effect required both oxygen in the water and fast-neutron irradiation and was not a direct chemical effect of oxygen alone.

The possibility that the metal is the effective site of the fast neutron damage has been eliminated by experiments in which pre-irradiated metal specimens (with only a thin air-formed oxide film) were corroded: no effect was observed.⁵⁶⁸ Enhanced creep of the metal in-reactor can be dismissed from consideration, because an effect of equal magnitude is seen with massive unstressed corrosion specimens as with thin fuel cladding.⁴⁵¹ Thus the primary site for fast neutron and fission fragment damage must be in the protective oxide film.

Of the many proposed mechanisms by which fast neutron or fission fragment damage in the oxide could affect the oxidation rate, the following are the best documented:

A radiation-induced phase change from monoclinic to cubic. This was one of the first mechanisms proposed, and arose because oxide films formed in fissile solutions were found to be largely cubic,⁵⁷⁴ and an early explanation of transition in the absence of irradiation also involved a phase change in the oxide.⁵⁷⁵ The irradiation-induced phase change was shown not to be fast enough to influence the in-reactor oxidation,^{576–583} and the phase change in unirradiated oxides is now thought to be a continuous effect of relaxing stress which is unrelated to transition,^{102,103} although it may play a greater part at very high temperatures.¹⁰¹ Kulcinski and Maynard showed that the presence of compressive stress, such as in oxide films, did not result in any significant change in the effect of irradiation on the transformation.⁵⁸⁴

Enhanced dissolution of ZrO_2 under bombardment. This was an early concern in the fissile solutions used for the Homogeneous Aqueous Reactor. No evidence for dissolution of zirconia has ever been obtained, although enhanced spalling of oxide, sometimes resulting in colloidal solutions, has been observed.³⁹⁸

Enhanced diffusion by production of point defects. A simple calculation will show that the rate of production of point defects cannot be sufficient to cause the enhanced oxidation. It is hardly surprising, therefore, that post-transition measurements of the conductivity of stabilized zirconia (which already has an enormous defect concentration) should fail to produce any observable effect.^{585,586}

Enhanced diffusion via increased numbers of "easy-paths." It was early realized that any enhanced diffusion which was occurring would have to be via permanent damage paths which could each transport large numbers of ions.³⁷² These were initially conceived to be fission fragment or primary

knock-on tracks. However, in the light of current theories of oxidation it seems more probable that the re-nucleation of small crystallites, or amorphous areas, would be the process by which additional paths are formed. Recent studies by Spitznagel *et al.*⁴⁵⁸ of Zircaloy-4 which was bombarded with oxygen or argon ions of sufficient energy to penetrate the surface oxide completely showed enhanced oxidation subsequently, although a reduction in oxidation usually occurred when the bombardment damage was restricted to the outer layers of the oxide. Such oxides did not show any observable change in the crystallite morphology, and other studies⁵⁸⁷ have shown that zirconia is very resistant to loss of crystallinity under irradiation. Thus there is no present evidence to support an hypothesis that irradiation-induced changes in the transport of oxygen through oxide films arise from any significant change in crystallite size or amorphicity of the oxide. These results⁴⁵⁸ are only for thin films, however, and there is still scope for irradiation to have a major effect on the subsequent growth of crystallites, on which there is no evidence. Shirvington's results¹⁸⁹⁻¹⁹¹ show that enhanced ionic transport results from increases in the oxide porosity under irradiation.

Embrittlement of the oxide leading to excessive cracking. Irradiation has been shown to cause embrittlement of anodic oxide films on zirconium alloys⁵⁸⁸ and excessive spalling of oxide films has been observed under irradiation.^{399,415} However, there is ample evidence of irradiation-enhanced pre-transition oxidation via a parabolic or cubic rate law^{412,443-446} which cannot be caused by embrittlement of the oxide. Cracking of the oxide is not regarded as being a primary cause of the oxidation rate transition for the Zircalloys, so that any enhanced cracking due to irradiation is more likely to have occurred after the primary mechanism of irradiation enhancement has operated than to be itself the primary mechanism.

Damage caused by neutron reactions with impurities. The most likely impurities to be effective are fissile elements (e.g., U, Th) or elements with high n, α cross sections (e.g., B). Analysis of typical samples, together with a simple calculation of the possible energy desposition from such sources, is sufficient to show that any such effects will be negligible.

Increased plasticity of the oxide. Just as the creep of zirconium is enhanced under irradiation, so one would expect creep of zirconium oxide to be enhanced. The mechanisms controlling in-reactor creep of the Zircalloys and densification of UO_2 under irradiation have recently been shown to be effectively identical.^{589,590} Such a process operating in the growing oxide might lead to more rapid relaxation of the compressive stress in the oxide, an earlier appearance of tensile stress at the outer surface of the oxide,⁹⁷ and

hence enhanced cracking or porosity in the oxide. If the enhanced ionic transport under irradiation is the result of the more rapid development of porosity under irradiation, then enhanced creep of the oxide could be one factor contributing to the development of the porosity.

Conversion of n -type to p -type oxide with enhanced diffusion. Campbell and Tyzack⁴⁷⁹ have proposed a mechanism by which different trapping efficiencies for oxygen interstitials and vacancies produced by irradiation result in a change in the oxide from n -type to p -type. This p -type oxide is considered to have a higher oxygen diffusion coefficient than n -type oxide. The main difficulty with this mechanism is that it treats the oxide as a uniform infinite matrix containing only point defects, and it fails to represent the true situation in the same way as the classical Wagner–Hauffe theory fails to represent the normal out-reactor oxidation process. Nevertheless, were this idea modified to consider the electron transport as well as the ionic transport process, it could be a relevant part of the total mechanism, particularly for alloys (e.g., Zr–2½% Nb), where the electron transport process is homogeneous and not predominantly at intermetallics.

Effect of heat flux. It has been suggested that the high oxidation rates in BWRs arise from an effect of heat flux across the oxide (or combined oxide and “crud” layer), raising the temperature of the oxide metal interface.³⁹⁸ We have already seen that the idea that oxidation rates are controlled at this interface, which is an implicit part of this hypothesis, may not be tenable for pre-transition oxidation, although it should be for post-transition oxidation. Any explanation of irradiation-enhanced oxidation must begin by explaining enhanced pre-transition kinetics. Even if it is considered only for the post-transition phase of oxidation, we find that oxidation rates of fuel cladding in BWRs are often lower than those observed on corrosion coupons in the ETR and ATR loops. Whatever increment of corrosion was added by the heat flux in a BWR must therefore be additional to an effect of irradiation which occurs independent of any heat flux.

We can see from the above that no single effect of irradiation on the oxide can be used by itself to explain the irradiation enhancement of oxidation. Both irradiation of the oxide and suitable environmental chemistry are needed, and it is of interest to try to distinguish the relative importance of these. Irradiation effects in the oxide should persist for a transient period after removal from reactor (whether they result from an acceleration of the normal pre-transition oxidation processes or from the acceleration of the transition phenomena). Irradiation effects on the environment, or on electronic conduction in the oxide, should revert rapidly to normal in the absence

of radiation. Experiments in which specimens oxidized under irradiation are continued in the same environment without irradiation may help to separate these factors.

Asher has performed post-irradiation experiments of this type on specimens corroded in reactor in moist carbon dioxide/air mixtures^{163,416} and in oxygenated water.⁴¹⁹ Specimens were pre-oxidized to a steady post-transition oxidation rate before the experiments. In the gaseous environment he found that (apart from a small immediate weight loss) the post-irradiation oxidation rate was the same as the in-reactor rate for about 2 weeks, and subsequently decreased slowly toward the normal out-reactor rate. In oxygenated water⁴¹⁹ the post-irradiation rate was intermediate between the in-reactor rate and the normal out-reactor rate. However, because the in-reactor enhanced oxidation rate was much higher in oxygenated water than in the gaseous environment, the post-irradiation rate in water (although only about one third the in-reactor rate) was still higher than the rate in the gaseous environment whether during or post-irradiation (Fig. 88). Thus in gaseous environments the whole irradiation enhancement apparently comes from relatively permanent changes in the oxide which require times equivalent to the growth of substantial fresh oxide layers to anneal out. This is similar to other transient types of behavior resulting from changing temperature or pressure which were discussed earlier. In water, however, only about one-third of the total enhancement arises from such semi-permanent effects; the other two-thirds comes from instantaneous effects either in the environment (interface) or in the electronic properties of the oxide.

We can now consider the hypothesis proposed in the earlier review³⁹⁸ and see how it measures up to subsequent results. In this instance we considered a hypothetical $I-V$ curve representing the normal ionic and electronic currents flowing during oxidation (Fig. 89), and showed that enhancing the ionic $I-V$ curve by an irradiation process could at most effect a small factorial increase in oxidation rate because the unmodified electronic current would then become the rate-limiting factor. This seems to explain satisfactorily the results obtained under PWR conditions and in gaseous environments (including steam), where only small enhancements are observed and the whole enhancement persists after irradiation for an extended period. Thus in these instances irradiation must be modifying the physical properties of the oxide in such a way as to enhance ionic transport, and one must wait for a new protective layer with normal properties to form before the oxidation rate returns to normal.

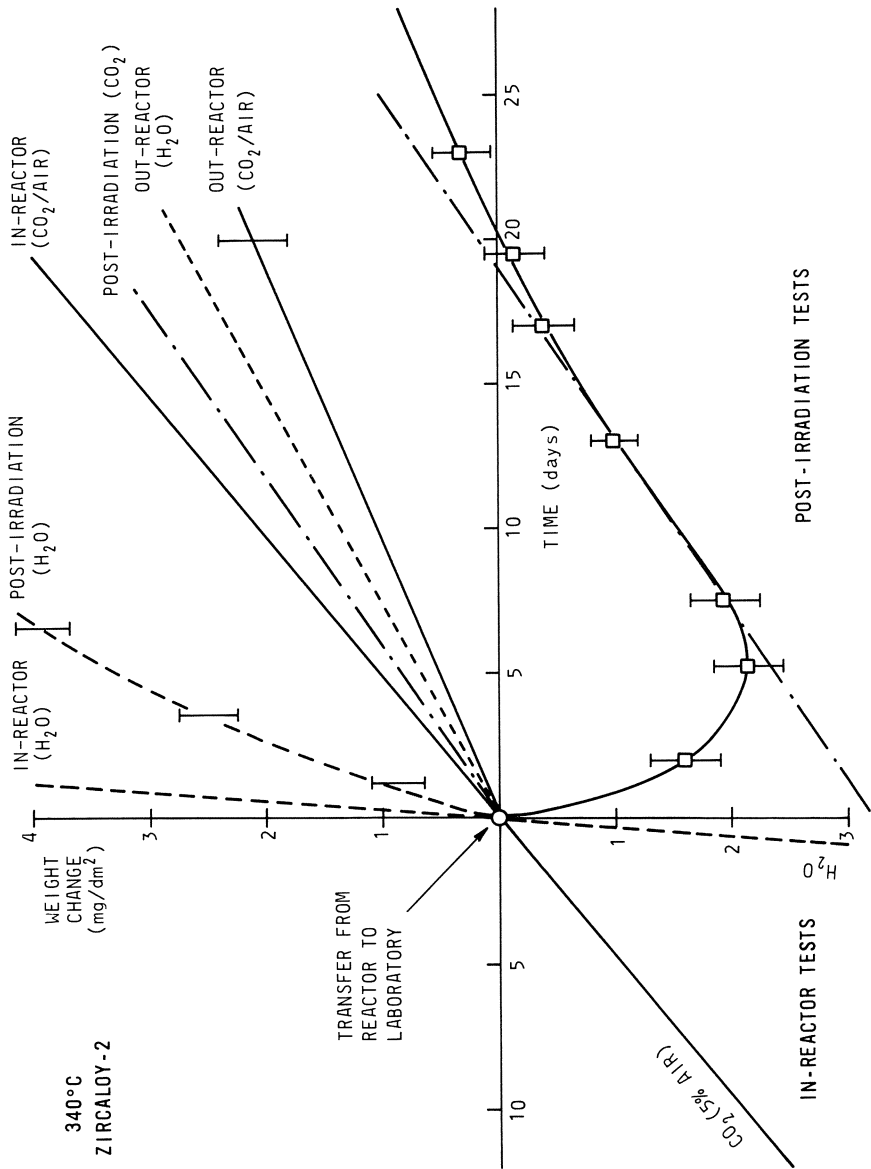


Fig. 88. Persistence of irradiation accelerated oxidation during post-irradiation exposure to the same environments.^{416,419}

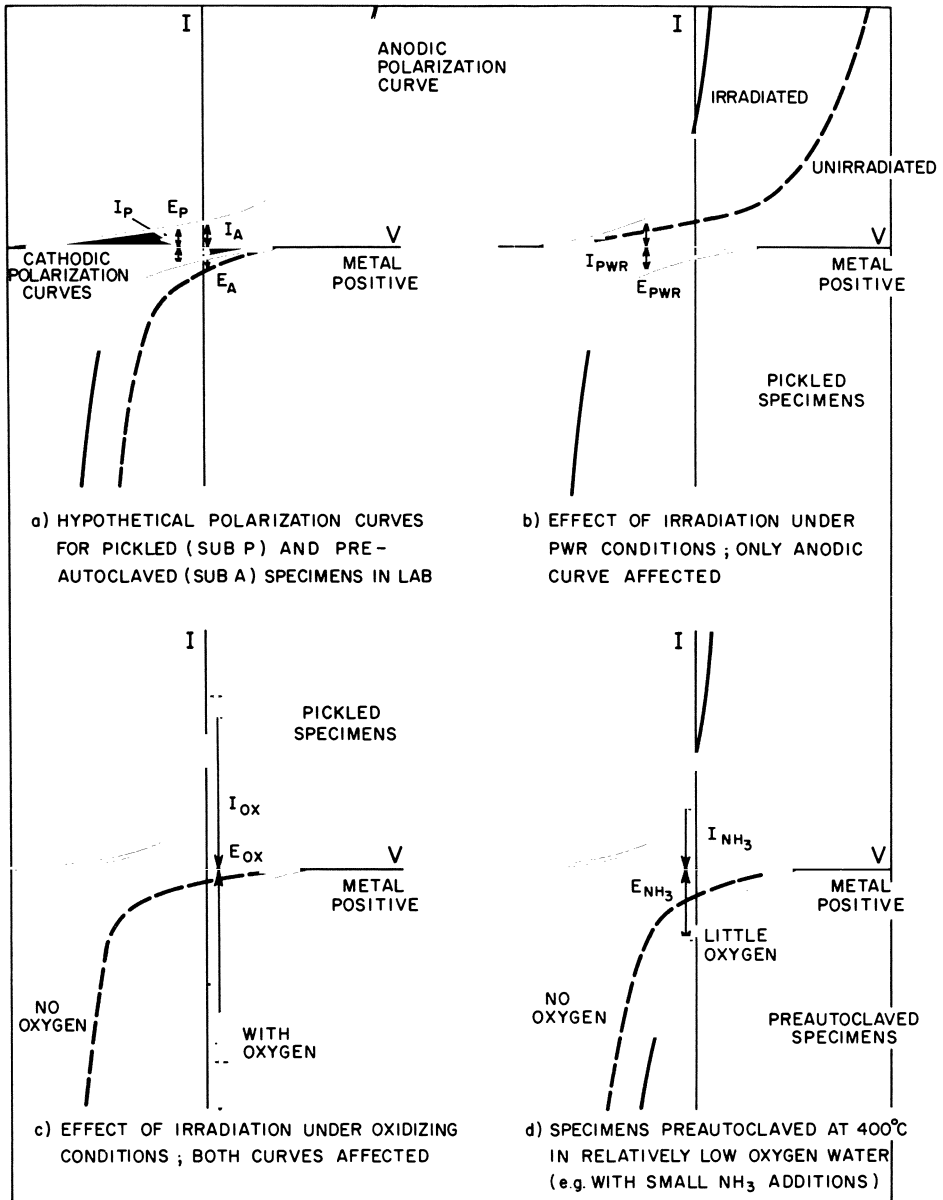


Fig. 89. Hypothetical effects of irradiation on electronic and ionic transport processes.³⁹⁸

In oxygenated high-temperature water it was hypothesized that a similar modification of ionic properties occurred, but in addition the oxygen (or oxidizing radicals) in the water interacted with the electronic conduction barrier at the surface to increase the electronic conductivity. This resulted in a much larger increase in oxidation rate than in PWR or gaseous environments because the electronic conductivity could not now become rate-limiting (at least not until much higher oxidation rates were reached). This added effect on the electronic process should vanish immediately (or very

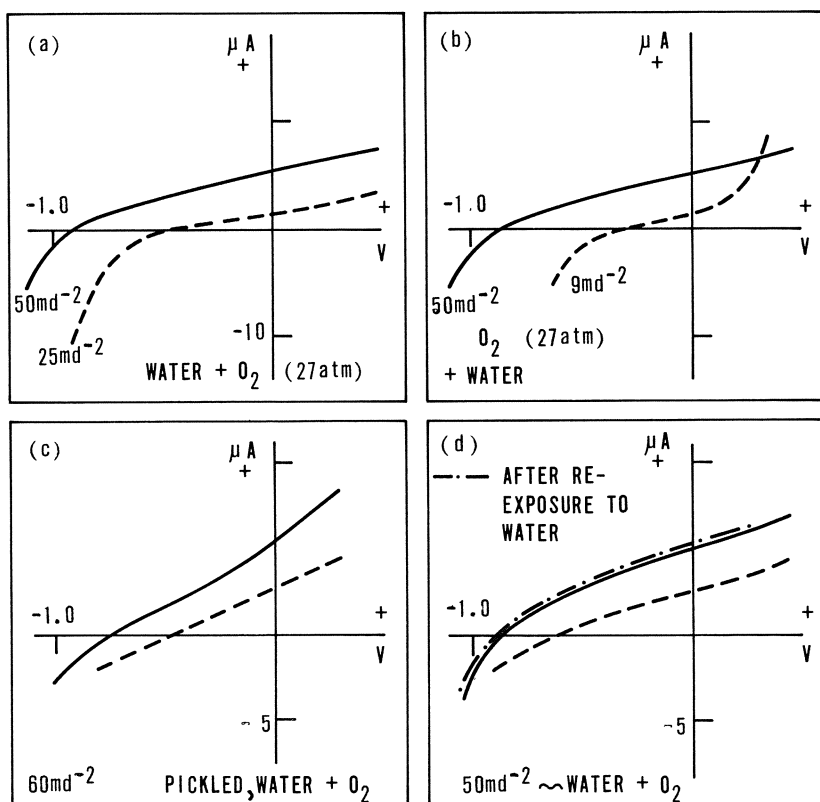


Fig. 90. Current-voltage characteristics of oxide films on Zircaloy-2 specimens which showed accelerated oxidation under irradiation. In-reactor (solid) and out-reactor (dashed) $I-V$ curves are compared for pickled (a) and abraded (b) specimens. In (c) the effect of baking (dashed) is compared with the original $I-V$ curve for a pickled specimen oxidized in high-oxygen water out-reactor, specimen in (d) was abraded and oxidized in-reactor.¹⁸⁹

quickly) after irradiation ceased, and the post-transition rate would then be enhanced by the modified ionic process alone, as has been observed.

Thus, this hypothesis continues to describe the situation in-reactor very well; however, it only describes and does not explain. To explain the phenomena we must demonstrate the precise mechanisms by which the ionic and electronic processes are modified. In oxygenated water, where enhanced oxidation was observed, Shirvington¹⁸⁹ has measured increased ionic conductivity of the oxide after irradiation (Fig. 90) and has found evidence that the oxide is much more porous than a normal oxide film. Asher *et al.*^{416,417} have also observed increased porosity in oxide films on specimens which showed enhanced oxidation in-reactor, but in this instance the roughness factor for specimens oxidized in gaseous environments was enhanced much more than for specimens oxidized in oxygenated water, despite the greater enhancement of the oxidation in water. There appears to be a discrepancy here which could bear further investigation. Could Asher's high roughness factors in gaseous environments have been caused by sputtering of silica from the in-reactor equipment onto the specimens? Clearances between the specimen and the silica wall were very small.

When the above observations are combined with Spitznagel's findings,⁴⁵⁸ that thin oxide films undergoing irradiation-induced changes in oxidation rate do not show any significant difference in crystallite morphology, we conclude that the enhanced ionic conduction in-reactor arises from an accelerated development of porosity by a mechanism comparable to that normally leading to the rate transition. Shirvington¹⁸⁹ did not observe any enhanced cracking of his oxides, but did see enhanced porosity; thus embrittlement leading to enhanced cracking is probably not the critical process. As yet we are uncertain how the recrystallization process in the oxide generates the small pores that have been observed, whether in or out of the reactor.

The prevalence of nodular oxide growth on Zircalloys in boiling water reactor conditions, but seldom in other in-reactor environments,^{421,422, 439,441} may be explained if enhanced localized electronic conductivity is stimulated, perhaps by locally high oxygen levels at sites of persistent bubble nucleation. This effect should not be obvious in PWR conditions, even in highly oxygenated water, such as that used by Shirvington *et al.*,^{189,283} electronic conductivity and oxide film thickness should be homogeneous on a macroscopic scale.

Shirvington¹⁸⁹ did not measure any enhanced electronic conduction in oxide films showing accelerated growth in-reactor, when the measurements were made after irradiation. However, the oxidation currents calculated from

his I - V curves are generally too low to explain the oxidation rates in oxygenated water if these were linear, and previous investigators have invariably found linear oxidation kinetics down to weight gains of 10–15 mg/dm². Thus, one would probably expect the kinetics in Shirvington's highly oxygenated conditions to be linear, and the apparent discrepancy in the measured currents may indicate that the electronic conductivity during the actual irradiation was much higher than that measured after irradiation. This deduction is an agreement with Asher's observation⁴¹⁹ of an immediate reduction to about one-third the in-reactor rate, in the oxidation rate of specimens irradiated in oxygenated water, when oxidation is continued in the laboratory. Shirvington's results could be explained by a similar decrease in rate on removal from the irradiation field caused by the return of the electronic conduction to its normal value.

Thus there would appear to be some evidence to justify the supposition that under irradiation the electronic conductivity of the oxide is increased significantly in oxygenated water, but not in gaseous environments, where the continued out-reactor rate is the same as the in-reactor one.⁴¹⁹ This enhanced electronic conduction would appear to be caused by some process at the interface, at present not well defined. We still need some measurements made during both irradiation and accelerated oxidation to demonstrate this increase in electronic conductivity. Previous attempts to measure this^{571,572} have departed too far from reality in both the methods used and the conditions of irradiation.

The hypothesis, proposed previously,³⁹⁸ that to observe the large enhancements in oxidation rate, such as those observed in oxygenated high-temperature water, both ionic and electronic conductivities of the oxide must be increased still seems to describe the observations well. Recent work^{163,189,416,417} has now succeeded in determining how the ionic process is affected; but it appears that an examination of the enhanced electronic conductivity will have to be made in situ in the reactor, because it reverts rapidly to normal on removal from the irradiation field.

Zr–Nb Alloys

A table of questions, similar to those listed for the Zircalloys in Table 9, can also be set up for the Zr–Nb alloys. Very little detailed study has been made of these alloys, however, so that most of the questions remain without positive answers. We will, therefore, summarize briefly the known answers using a format similar to that used for the Zircalloys.

Ionic Transport in Oxide Films. The oxide films formed on Zr-2.5% Nb alloy specimens are polycrystalline, and bear some similarities to oxide films on zirconium and the Zircalloys.^{110,591,592} Dark field micrographs show that crystallites of any one orientation are not uniformly distributed in oxides formed on Zr-2.5% Nb, as they usually are on zirconium and Zircaloy-2, and segregation of particular orientations along, or near, prior α/β boundaries has been observed.⁵⁹¹ However, the detailed morphology and epitaxy of oxide films on this alloy have not been worked out.

The crystallite size in oxide films on Zr-2.5% Nb alloy⁵⁹¹ appears to be comparable with that for other alloys in the same oxide thickness range; thus it is probable that the oxygen diffusion path is via oxide crystallite boundaries in this alloy as in other zirconium alloys.

Electron Transport in Oxide Films. Little is known about electron transport through oxide films on the Zr-2.5% Nb alloy. Imaging studies using CuI layers on pre-formed oxides at room temperature showed little evidence for a localized transport process until specimens had been given a sufficiently long temper to grow second phase particles.⁵⁹³

The effect of oxygen additions to the steam on the oxidation of unalloyed niobium has been related to the appearance of Nb(V) in the oxide film.³⁹⁰ It is tempting to relate the similar effect in Zr-Nb alloys to a similar change in the valence of niobium in the oxide.^{116,165} However, it is not clear whether this effect would appear predominantly in the electronic conductivity or the ionic conductivity. The rapidity with which increases in oxidation rate start (and stop) on adding (or removing) oxygen from the environment suggest that the effect should be primarily on the electronic conductivity. However, Shirvington's measurements¹⁹¹ of I - V curves of Zr-2.5% Nb specimens, after oxidation in water with or without oxygen, showed large increases in the ionic conductivity of films formed on β -quenched specimens in the oxygen-containing environment. Quenched, cold-worked, and aged specimens showed little sensitivity to oxygen in the water and no significant differences in either ionic or electronic conductivity of the oxides formed in either environment. I - V curves obtained after oxidation, and baking to remove water from the pores, suggested that the enhanced ionic conductivity resulted from increased oxide porosity, although the effect was not nearly as large as the effect of baking on pickled Zircaloy-2 after oxidation in highly oxygenated water.¹⁸⁹ These observations could be effects of the enhanced oxidation rather than causes, as changes in electronic conductivity could have been missed by virtue of not performing the measurements during the actual enhanced oxidation process.

It would appear, therefore, that the large effect of oxygen on the oxidation of Zr-2.5% Nb alloy in some heat-treated conditions arises primarily from an effect on the electronic conduction, because of its rapidity and reversibility. The increase in oxygen transport which accompanies this occurs by an apparently non-ionic process not involving any large increase in measurable porosity in the oxide. In view of the fact that Nb₂O₅-type oxides are largely covalently bonded,⁵⁰⁵ and that the ionicity of bonding in ZrO₂ is also in doubt, it appears that we should not expect any simple relation between niobium valence and vacancy concentration in these oxides, although an effect on electronic conductivity may occur. In Nb₂O₅ it appears to be possible for molecular oxygen to diffuse through the open channels between the NbO₆ coordination polyhedra.⁵⁹⁴ Such a phenomenon in the oxide on Zr-Nb alloys could explain the small changes in porosity which are observed, but needs some supporting evidence.

The potentials measured across oxide films on Zr-2.5% Nb alloy specimens in fused nitrate/nitrite melts have generally been greater than those measured for zirconium and the Zircalloys at equivalent times and weight gains,¹⁸³ again suggesting that electronic conduction is the rate-limiting process. However, detailed studies of the I - V characteristics of oxide films on the Zr-2.5% Nb alloy are rendered difficult by the excessive hysteresis in the curves obtained on this alloy.¹⁸³ This phenomenon is also found for oxide films on unalloyed niobium.¹⁸⁸ Prolonged tempering of the alloy minimizes this hysteresis and gives an alloy behaving somewhat like Zircaloy-2.¹⁸³ Shirvington¹⁸⁹ also had problems with hysteresis, and bypassed these merely by comparing similar segments of the I - V curve. To the extent that his curves do not represent an equilibrium I - V curve, therefore, there may be some doubts about the comparisons he made. However, little alternative is available if one is to attempt to work with this alloy.

Migration of Molecular Species in Oxide Films. Electron microscope and SEM studies of oxide films formed on Zr-2.5% Nb alloy specimens have shown fewer features of the crack and pore variety than for post-transition oxide films on other alloys. Apart from replicating the original metal surface, the oxide surface, on films formed in oxygen free steam, appears to be featureless even when well beyond the kinetic rate transition. The oxide/metal interface shows rough features similar to those observed with other zirconium alloys, and no layers of lateral "cracks" are seen in sections of oxide films.^{389,552} Very rough oxide/metal interfaces are observed as a result of preferential oxidation of the α' phase in specimens held in the $\alpha + \beta$ region during cooling.¹¹⁰

Mercury porosimeter and impedance measurements (during immersion in aqueous electrolytes) show evidence for many small pores in the post-transition oxide even when no such features are detectable by electron microscope techniques.^{389,543} These pores are conceived to be the main route for molecular oxygen passing through thick post-transition films.

Stresses generated in thin oxide films on the Zr-2.5% Nb alloy were similar to those generated on the Zircalloys at similar times and temperatures.⁵⁹⁵ The development of crystallite textures in these oxides⁵⁹⁵ was also similar to that observed for the Zircalloys. Despite the importance of the development of these textures to the recrystallization of the oxide, which may be the process generating the porosity in the oxide, we lack any firm evidence for the precise mechanism by which these pores arise.

Mechanism of Irradiation Effect on Oxidation. As we have seen earlier, the effect of irradiation is to produce either no change or a slight reduction in the oxidation rate of Zr-2.5% Nb alloy in oxygenated water in-reactor. The reason for this has been shown to be enhanced tempering of the alloy in a fast neutron flux, a process which leads to steadily improving corrosion resistance in the laboratory.^{191,460} Shirvington¹⁹¹ has shown that the reduction in oxidation rate in-reactor is associated with a reduction in the ionic conductivity of the oxide film with no effective change in the electronic properties, as measured after irradiation (Fig. 91). This change in ionic conductivity is not apparently related to changing porosity in-reactor, as the effect of baking is about the same for both in-reactor and out-reactor oxides (i.e., conductivity reduced about a factor of 2). A significant reduction in the hysteresis was shown by films grown under irradiation.¹⁹¹ This change in ionic conductivity may, therefore, be related to the enhanced tempering and the resultant change in the distribution of the niobium. There is not enough evidence on the effect of tempering in the absence of irradiation to assess this possibility, however.

Other Alloys

Even less evidence is available on other zirconium alloys. Only one detailed study of the morphology of the oxide on a range of alloys has been reported.⁵⁹⁶ The authors found that all oxide films were microcrystalline and predominantly monoclinic ZrO_2 . The amount of cubic ZrO_2 detected varied from alloy to alloy being small for Cu, Fe, Cr, and Mo alloys, and larger (i.e., more readily detectable) for Al, Sn, and Nb alloys. In examining the oxide formed over the intermetallic particles (all the first group of

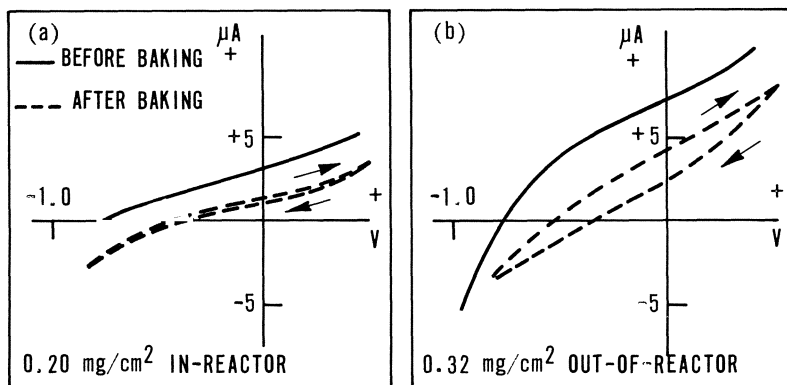


Fig. 91. Current-voltage characteristics of oxide films on Zr-2.5% Nb alloy specimens (Q + CW + A) grown both in- and out-reactor in water + 27 kg/cm² of O₂.¹⁹⁰

additions above have very low solubilities in zirconium) de Gélès *et al.* found Cr₃O₃ on the ZrCr₂ precipitates.⁵⁹⁶ However, these were by far the largest precipitates in their alloys and the failure to detect oxides of the addition element in other alloys does not mean that it does not form. Fe₂O₃ and Fe₃O₄ have been detected by other methods on ZrFe₂ intermetallics.¹⁸⁴ Copper oxide was observed on the surface of polished ATR (Zr-0.5% Cu-0.5% Mo), but soon “disappeared” following oxidation.^{597,598}

Studies of the partition of alloying additions between the oxide and the metal have shown several different types of behavior. Generally the alloying additions which have high solubilities in zirconium, or can be maintained in solution by a suitable heat treatment (e.g., Sn, Nb), remain in solution in the oxide at concentrations close to those in the metal.^{44,108,109,599} Despite indications from the phase diagram,³ it is very difficult to obtain tin-containing precipitates in alloys containing less than ~5 wt. % tin. The appearance of tin-containing precipitates at the metal oxide interface in a 1.7% Sn alloy after prolonged oxidation at 600°C¹⁰⁹ suggests that some tin may be rejected by the oxide and precipitate at the oxide/metal interface.

Alloying additions which are present as precipitates in the metal commonly persist as concentrations of the alloying addition in the oxide film (e.g., Fe, Cr, Ni, Al).^{44,108,109,600,601} The extent of the solution and oxidation of these precipitates in the oxide is probably a function of temperature and time of oxidation.⁶⁰⁰ In addition to persisting in the oxide as

precipitates, both Fe and Ni alloying additions appear to accumulate as a layer at the metal/oxide interface^{44,108}; again the proportion rejected by the oxide probably depends on time and temperature. Cu seems to be almost totally rejected by the oxide and builds up a continuous layer at the oxide/metal interface.^{44,108}

The electrical properties of the oxides formed on binary zirconium alloys containing Sn, Fe, Cr, and Ni show large differences.^{185,186} The films on Zr–Sn alloys, which did not contain any second phase, were very similar to those on unalloyed zirconium. Conduction through the other oxides occurred at the intermetallic particles. ZrFe₂ intermetallics gave highly conducting oxide films^{185,186} consisting of layers of Fe₂O₃ and Fe₃O₄ overlying a thin film.¹⁸⁴ The films formed on Cr and Ni intermetallics at 300°C were highly conducting, but were much more resistive if formed at 400°C or above (or became so if equilibrated at these temperatures).¹⁸⁶ At the higher temperatures these alloys showed *I–V* characteristics similar to unalloyed zirconium.¹⁸⁵ Thus the behavior of Zircaloy-2 is largely controlled by its ZrFe₂ intermetallics (containing Cr in solution), whereas the Zr–Cr–Fe alloy behaves similarly to a Zr–Cr binary, because the small amount of Fe present (0.08 wt. %) is insufficient to modify the behavior of the ZrCr₂ intermetallics. The second intermetallic phase^{601,602} in Zircaloy-2, Zr₂Ni(Fe), seems to be ineffective in the oxidation process, although it plays a significant part in the hydrogen absorption process. Presumably this is why the nickel can be removed to form Zircaloy-4 without any significant effect on the oxidation behavior.

Shirvington¹⁹¹ has compared the *I–V* curves of a Zr–Cr–Fe alloy and crystal-bar zirconium before and after irradiation. He finds that for both materials enhanced in-reactor oxidation is associated with increased ionic conductivity and no change in the electronic conductivity, when measured after irradiation (Fig. 92). The enhanced ionic conductivity was associated with increased oxide porosity for both materials, except for the thinnest oxide films. Thus, as for Zircaloy-2,¹⁸⁹ the increased in-reactor oxidation appears to be related to an enhancement of the oxide recrystallization processes which lead to the generation of porosity in the oxide. No obvious increase in cracking of the oxides was evident. For the Zr–Cr–Fe alloy in steam, the measured ionic currents after irradiation were too low to explain the in-reactor oxidation rate on the basis of linear kinetics, and may imply an additional increase in electronic conduction during irradiation. The same was true for crystal-bar zirconium in highly oxygenated water in-reactor. The Zr–Cr–Fe alloy under the same conditions gave ionic currents after irradiation.

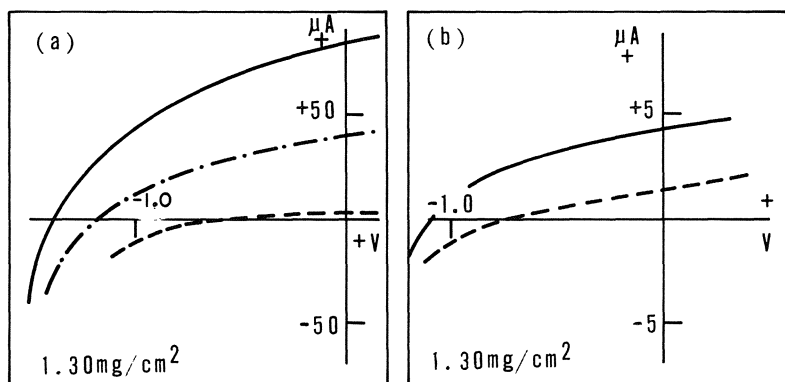


Fig. 92. Current-voltage characteristics of oxide film on Zr-Cr-Fe alloy specimens which showed accelerated oxidation under irradiation. The effect of baking on the I - V curve is shown (dashed) in (a) for a specimen oxidized in-reactor and in (b) for a specimen of equivalent oxide thickness formed out-reactor in steam (20 days/475°C) and water (13 days/295°C).¹⁹¹

tion, agreeing well with a linear in-reactor oxidation rate. This alloy under these conditions also showed the most porosity of any material tested, and in this instance therefore the enhanced porosity may overwhelm any contribution from increased electronic conduction during irradiation.

HYDROGEN ABSORPTION

Initially it was hydrogen absorption, and the embrittlement which it might cause, which was the primary concern behind studies of enhanced oxidation of zirconium alloys under irradiation (for example, reference 603). However, the knowledge that hydride precipitates underwent a ductile/brittle transition⁶⁰⁴ (and hence could be tolerated in far larger quantities at the reactor operating temperature than had earlier been expected) and the observation that in-reactor oxidation conditions leading to enhanced oxidation rates were almost universally accompanied by normal or reduced hydrogen uptake rates³⁹⁸ largely removed the pressure to understand the hydrogen absorption process. As a result of this, no review of hydrogen uptake, and little fresh work, has been published between Hillner's review in 1964²⁰² and the recent review by Douglass.¹⁴ Nevertheless, there should

still be concern because hydrogen absorbed while the component is hot may migrate to local areas of high stress and cause problems when the components are at a temperature below the ductile/brittle transition temperature. New alloys must still be carefully scrutinized for sensitivity to hydrogen embrittlement, therefore, and the critical amounts of hydrogen compared with the amount likely to be acquired from corrosion during the component's lifetime. Since hydride distribution, precipitation, and effects on mechanical properties will be considered in detail in another review, only the absorption mechanisms which may operate during corrosion are considered here.

In surveying the results on hydrogen absorption we will distinguish between two possible routes; first, direct reaction with molecular hydrogen (gaseous hydriding), and second, absorption of hydrogen liberated by the decomposition of water or steam during the oxidation process and absorbed as part of the oxidation mechanism. The source of the hydrogen entering the metal has been the occasion of much argument as it is difficult to demonstrate whether hydrogen absorbed from high-temperature water has or has not passed through a stage where it was recombined into molecular hydrogen. Cox and Roy³⁶³ were able to show from studies in mixtures of T_2 and H_2O (steam), where exchange between the two components is slow, that during the pre-transition oxidation of Zircaloy-2, no gaseous tritium was absorbed. Thus there is a clear distinction between the mechanisms of uptake from the two sources (H_2 or H_2O) and they should be studied separately.

Hydrogen Absorption from Gaseous Hydrogen

The reaction of clean zirconium surfaces with gaseous hydrogen has been known to occur for many years.³ Gulbransen and Andrew⁶⁰⁵ and Aronson⁶⁰⁶ showed that oxide films present on the zirconium surface represented barriers to this gaseous hydriding, that incubation periods of variable duration occurred (Fig. 93), and that these probably represented the time required for the oxide to break down and admit hydrogen via small flaws. The often localized nature of the hydriding reaction (e.g., at specimen edges), once this had started⁶⁰⁷ suggested that only one or two points of breakdown were necessary to initiate hydriding, and electron microscope replicas have shown that a few cracks in the oxide are often prevalent at specimen edges.⁵⁴³ These could be points of weakness where the first breakdown of the oxide would occur in hydrogen gas. Boyle and Kisiel⁶⁰⁸ showed that provided the H_2/O_2 ratio in the gas phase did not exceed 10^4 , there was sufficient oxygen present to maintain these sites in the oxide in

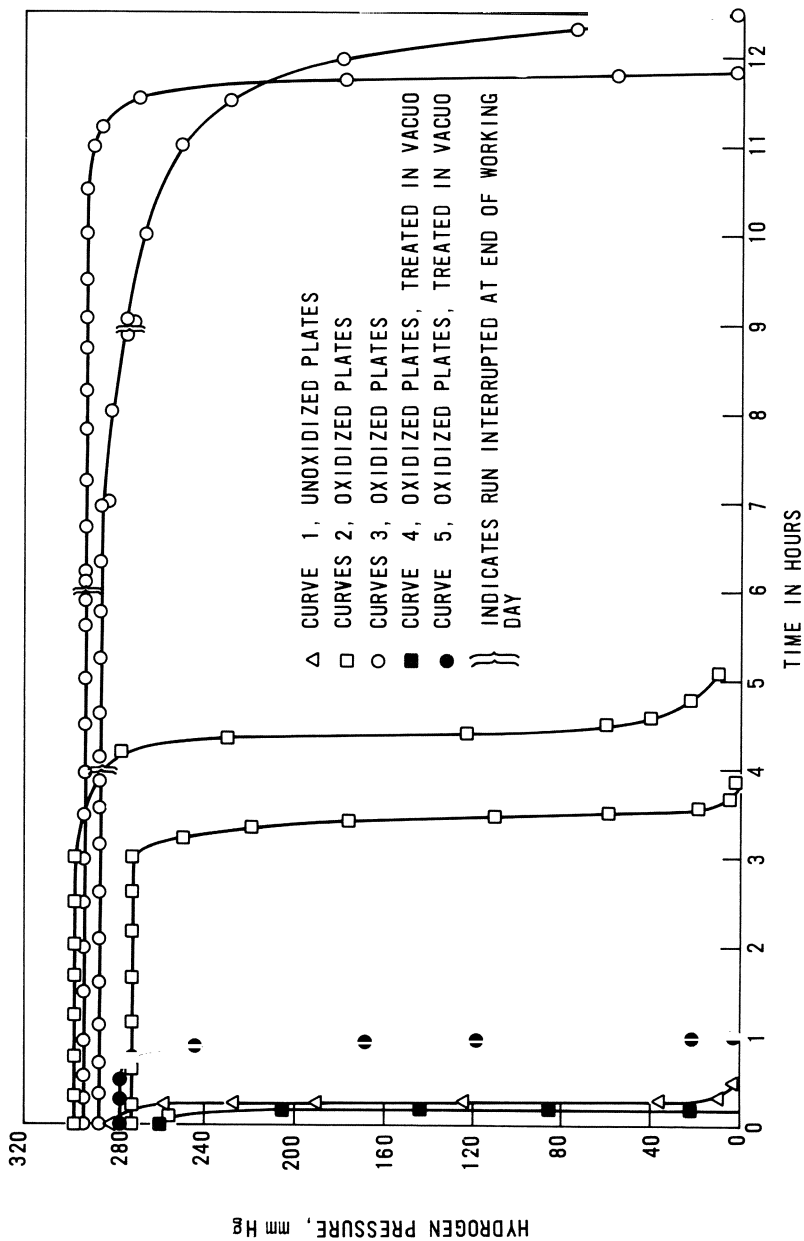


Fig. 93. Incubation periods during the absorption at 400°C of gaseous hydrogen by preoxidized zirconium plates.⁶⁰⁶

good repair and to prevent direct access of molecular hydrogen. The magnitude of this critical ratio would be expected to vary with temperature, pressure, and other factors.

Shannon⁶⁰⁹ studied the variations in the resistivity of the oxide film during the gaseous hydriding process and showed that the reaction started when the resistivity of the oxide fell to a low level as a result of the removal of oxidant (Fig. 94). He was able to show that, provided there was suffi-

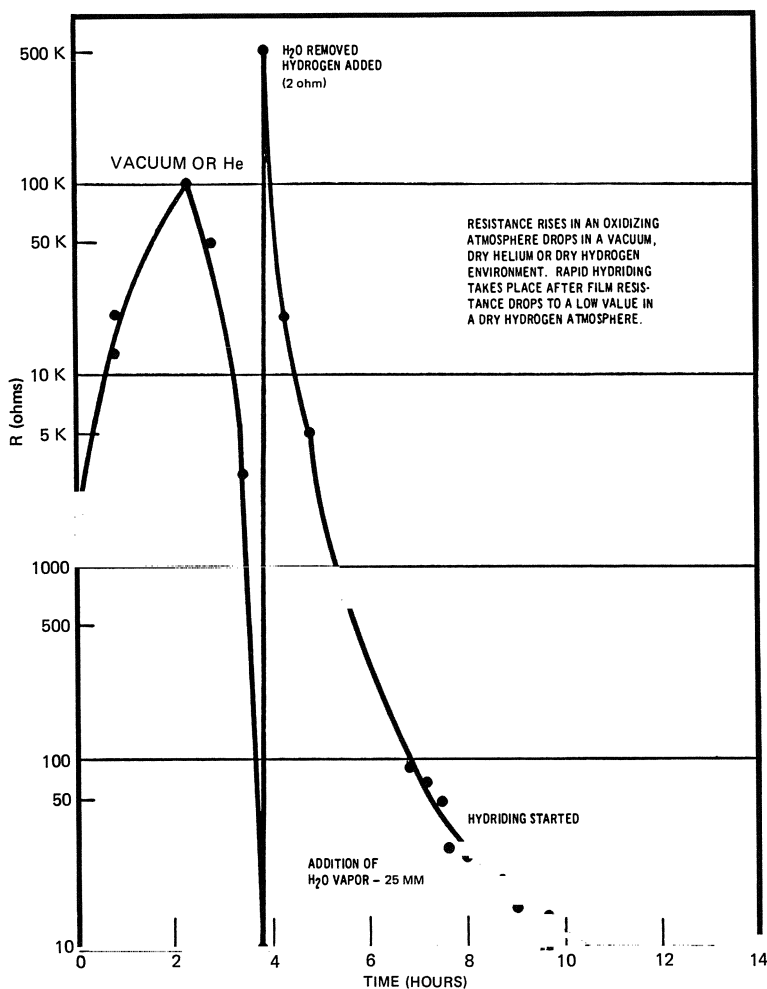


Fig. 94. Plot of the electrical resistance of the oxide on Zircaloy-2 during exposure to gaseous hydrogen environments at 450°C.⁶⁰⁹

cient oxidant to maintain the normal oxidation rate, gaseous hydriding would be prevented.⁶¹⁰ The hydriding failures in leaking reactor fuel elements²¹⁰ and the “sunburst” hydrides (Fig. 95) which form in fuel contaminated with hydrogenous material^{611–614} are a practical reflection of the local oxide breakdown phenomenon and the ensuing rapid gaseous hydrogenation which occurs when there is insufficient oxidant present to maintain the oxide film in good repair. The significance of the state of the oxide film on the metal surface in determining whether localized or uniform hydriding occurs has been shown by Lunde.⁶¹⁵ She found that, whether the specimens were pickled or sandblasted, fluoride contamination led to sunburst formation at the edge of the dried acid fluoride deposit (highest fluoride contamination?). It seems unlikely that all the above effects can be explained by cracking of the oxide leading to absorption of hydrogen. Annealing in vacuum is known to result in a rapid drop in the stresses in oxide films,¹⁰⁶ and Shannon has shown a relation with a sharp rise in oxide conductivity. This and the effect of fluoride may indicate that porosity is being generated in the oxide by a recrystallization process. Other impurities also seem to stimulate gaseous hydrogen absorption, and conditions which

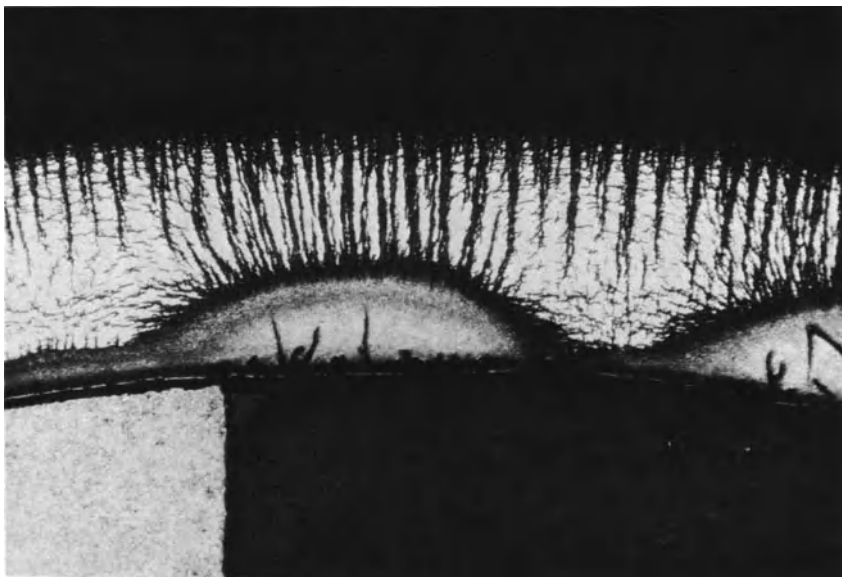


Fig. 95. Typical hydride “sunbursts” formed by gaseous hydriding of Zircaloy fuel cladding: 50 \times .⁴³⁸

could lead to hydriding of fuel cladding have recently been well summarized by Proebstle *et al.*⁶¹⁶

Smith studied the permeation of zirconium oxide films of various thicknesses by gaseous hydrogen and found that the rate was inversely proportional to oxide thickness.⁶¹⁷ He was not able to show, however, that during these experiments the hydrogen passed through the oxide lattice rather than through a few cracks or pores in the oxide. Since tritium autoradiography⁶¹⁸ has shown the presence of hydrogen in oxide films grown in steam and water, but not in those heated in tritium gas (even when tritium had entered the metal), it seems unlikely that Smith was studying a lattice diffusion process. In general, the evidence on gaseous hydriding is in agreement with a mechanism whereby oxide breakdown (to give local cracks or pores) leads to direct access of hydrogen to the metal/oxide interface, in the absence of sufficient oxidant to maintain a protective oxide at the base of the cracks or pores. Insufficient work has been done to establish whether or not a slow absorption of hydrogen during the incubation period contributes to this breakdown process; however, the absence of tritium fixed in such oxides argues strongly against it.

Unambiguous instances where gaseous hydrogen has been absorbed in the presence of water or steam adequate to maintain the oxide in good repair are few, and comprise two instances of Zircaloy-2 exposure to either water with very high hydrogen overpressures (Fig. 96)²⁰² or 50:50 steam/hydrogen mixtures (Fig. 97).^{204,205} In the latter instance the excess absorption of hydrogen occurred only after the specimen reached the oxidation rate transition. This is further evidence that the process leading to oxide breakdown on Zircaloy-2 generated pores which penetrate to the oxide/metal interface and permit direct access of hydrogen to the metal.^{52,542} In water with a high hydrogen overpressure,²⁰² a similar incubation period is evident; however, this extends only to a weight gain of 10 mg/dm², which is well before there is any evidence for a transition in the oxidation kinetics, but where there is still evidence for cracks in the oxide along specimen edges.⁵⁴³

It is not certain, therefore, whether or not these two examples both arise from oxide breakdown processes, or whether the effect in water arises from the special properties of the Zr₂Ni(Fe) intermetallics in Zircaloy-2. The same effect was not observed with Zircaloy-4 (Fig. 98), where oxide cracking at edges would be just as prevalent as in Zircaloy-2, and supports a connection with the nickel-containing intermetallics in Zircaloy-2. We will see in the next section that nickel-containing alloys are able to absorb gaseous hydrogen directly even in the presence of adequate oxidant.

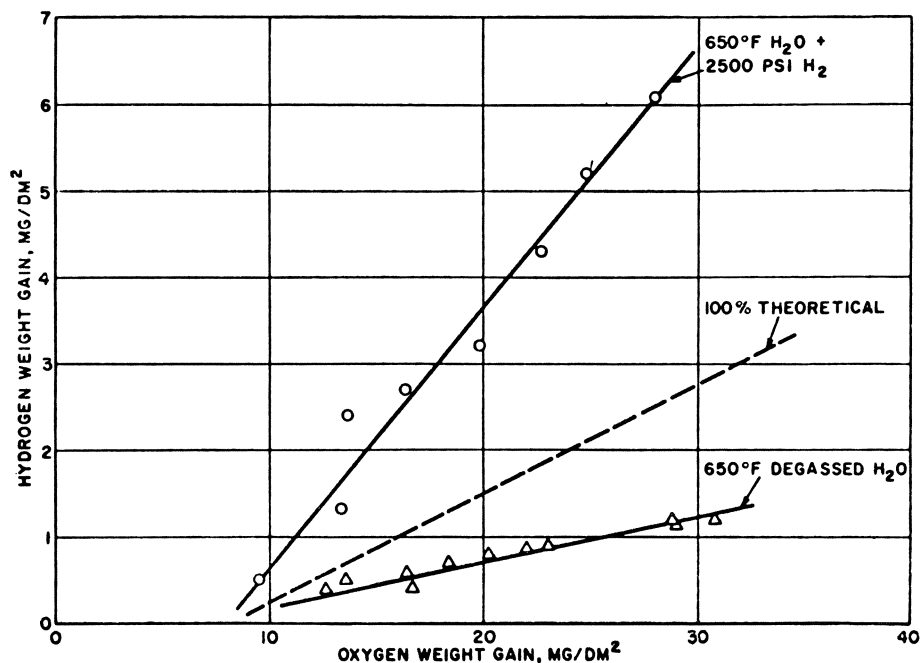


Fig. 96. Hydrogen pickup by Zircaloy-2 in 650°F water + 2500 psi hydrogen.²⁰²

Hydrogen Absorption via the Decomposition of H₂O

In addition to the rapid gaseous hydriding reaction on clean surfaces, Goldman and Thomas⁶¹⁹ showed that, in parallel with the oxide film formation process in water or steam, a fraction of the hydrogen generated by decomposition of the water entered the metal. In contrast to the localized nature of the gaseous hydriding, this hydrogen is usually fairly uniformly distributed throughout the metal. That this difference in distribution reflects merely the relative magnitudes of the rate of ingress to the metal and the rate of diffusion away from the point of entry in the two circumstances is shown by the work of Attermo and Sietnieks⁶²⁰ on cathodic hydrogenation in fused hydroxides. At their lowest temperatures (220°C) a hydride layer built up because hydrogen was unable to diffuse away from the surface fast enough, whereas at 400°C a uniform distribution was obtained. Tritium autoradiography has shown⁶¹⁸ that under normal oxidation conditions the hydrogen is largely excluded from the oxygen diffusion zone immediately

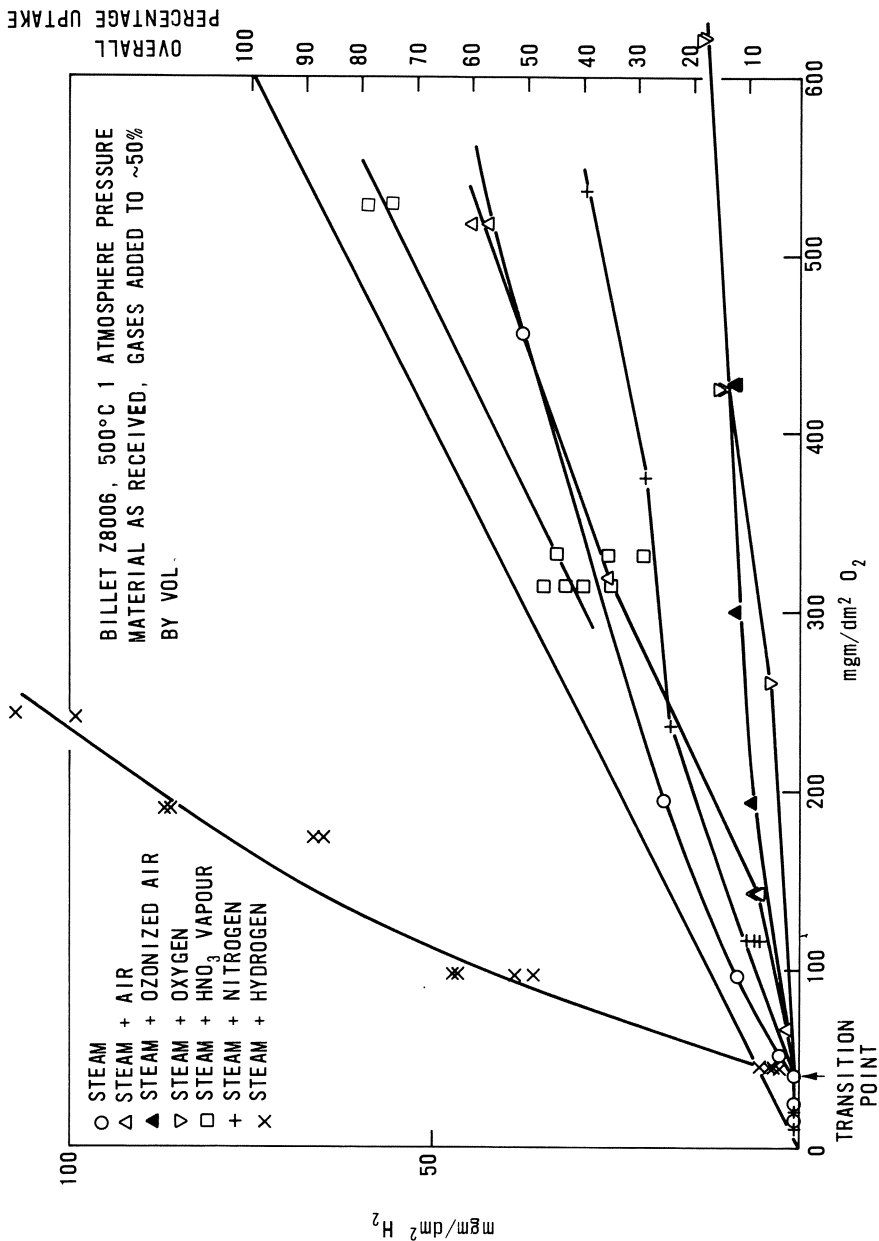


Fig. 97. Hydrogen uptake by Zircaloy-2 in steam plus added gases at 500°C.²⁰⁵

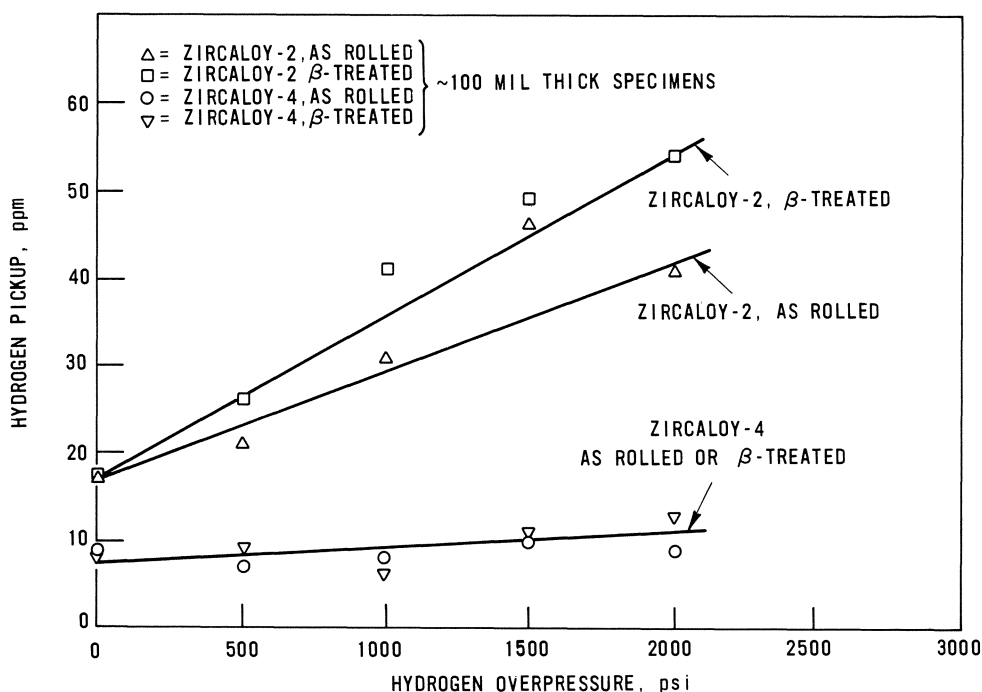


Fig. 98. Hydrogen uptake by Zircaloy-2 and Zircaloy-4 as a function of hydrogen overpressure in 650°F water for 14 days.²⁰²

beneath the oxide. Hydride does not, therefore, precipitate adjacent to the oxide except under special conditions, such as when a very high oxidation rate at a low temperature effectively eliminates the oxygen diffusion zone.^{620,284} It seems unlikely, therefore, that hydrides could play any significant part in causing the oxidation rate transition under normal conditions.

Factors Affecting Hydrogen Uptake by Zircaloy-2. The relationship between the amount of oxidation occurring and the amount of hydrogen absorbed is not a simple function (Fig. 38), although it follows a characteristic pattern which seems to be general for all alloys, provided the analytical technique is sensitive enough to distinguish changes in the "uptake fraction" (that fraction of the hydrogen liberated by the corrosion process during any time period and which is absorbed by the metal).^{47,202-208,219} Zircaloy-2 apparently absorbs $\geq 50\%$ of the hydrogen produced during the initial

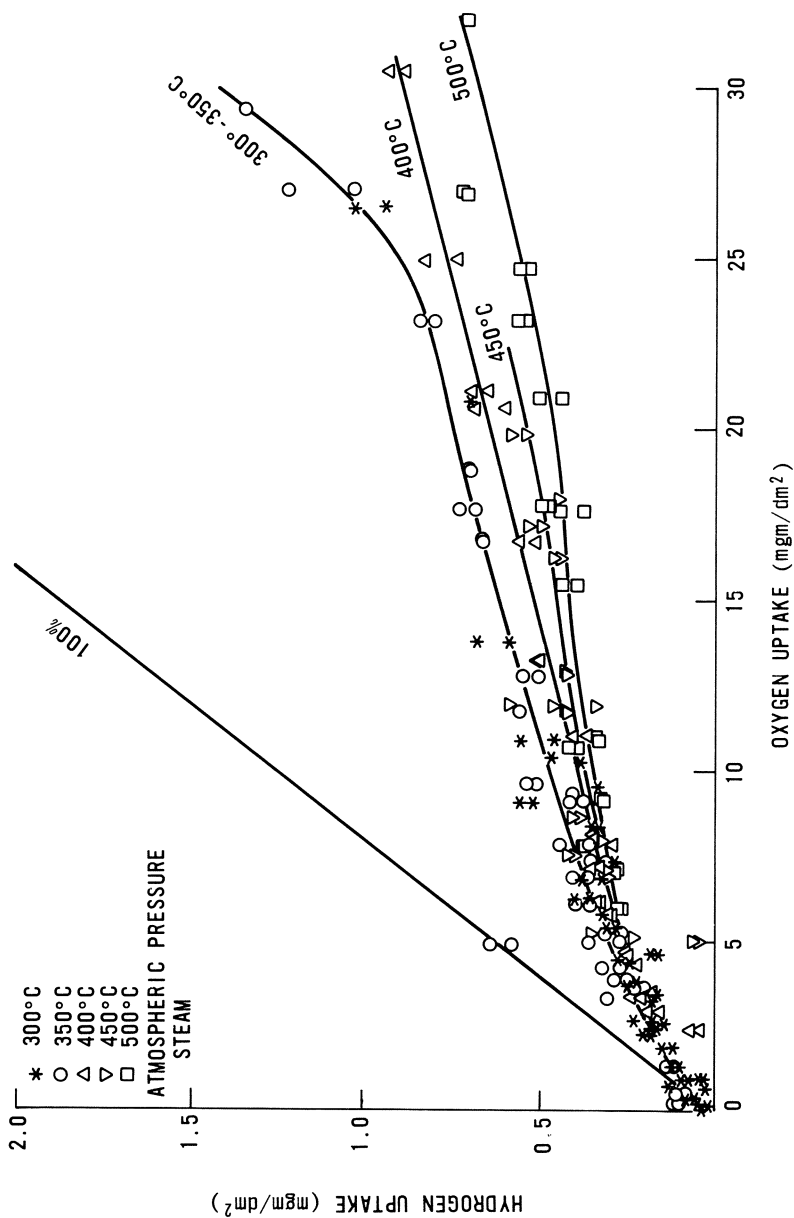


Fig. 99. Hydrogen uptake as a function of weight gain for Zircaloy-2 during pre-transition oxidation at 300–500°C.^{4,7}

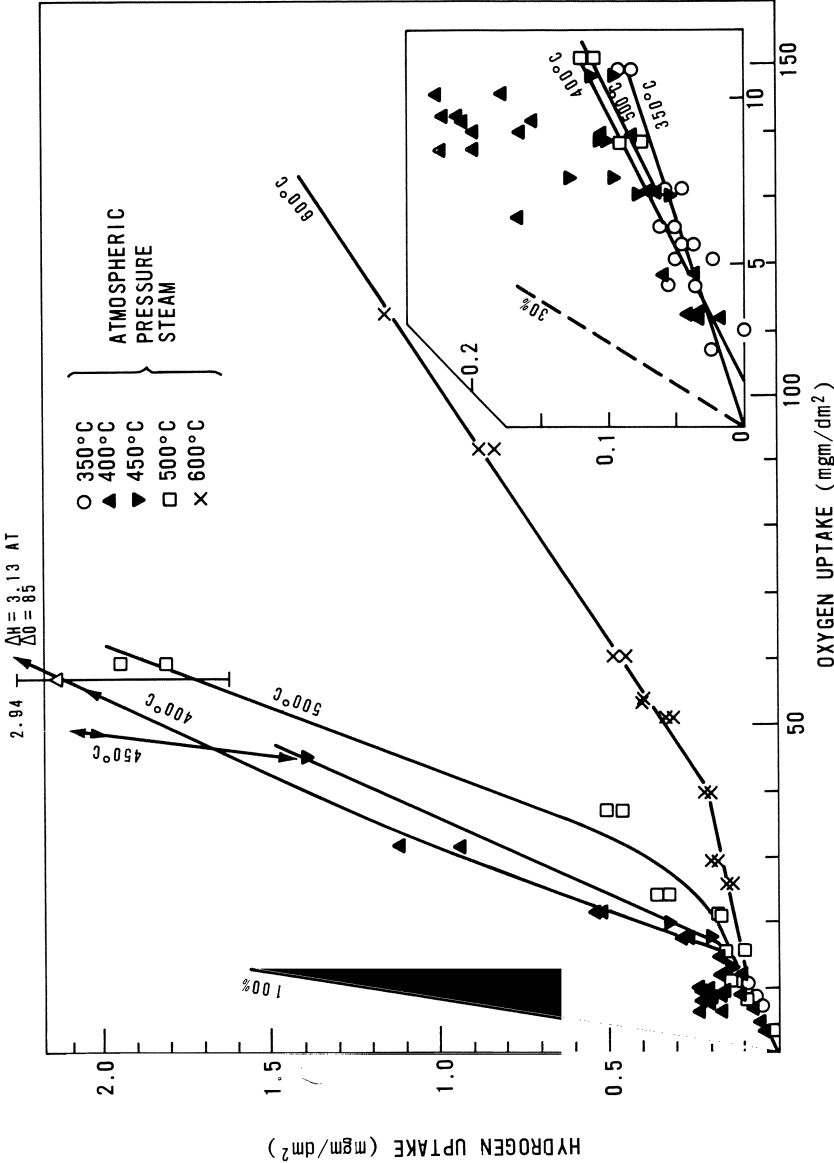


Fig. 100. Hydrogen uptake by unalloyed zirconium in steam at 300–500°C as a function of weight gain.⁴⁷

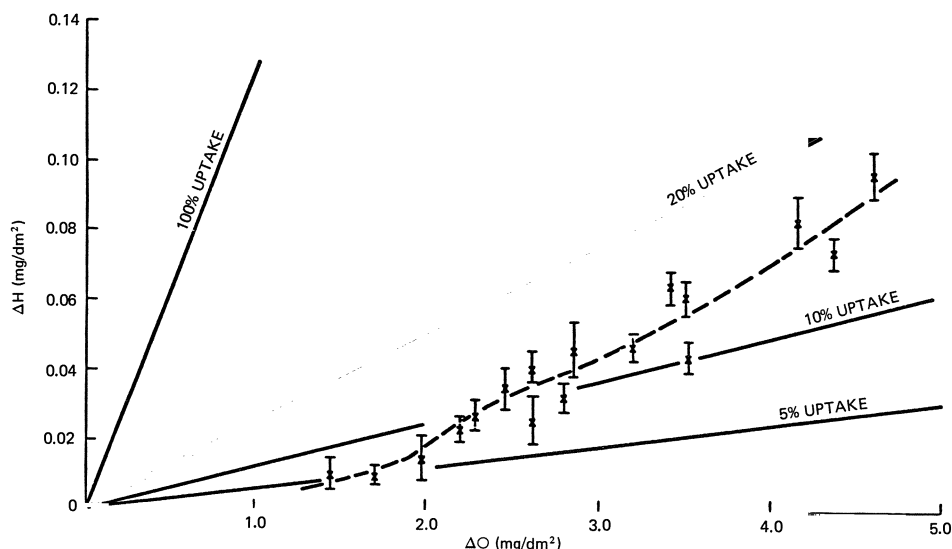


Fig. 101. Hydrogen uptake by Zr-1% Fe in steam at 500°C, 1 atm at weight gains less than 5 mg/dm².²⁰⁷

period of oxidation.^{47,204,205} This percentage decreases monotonically as the oxide thickness increases until transition is reached (Fig. 99). For unalloyed zirconium^{207,262} and alloys which absorb lower overall fractions of hydrogen than Zircaloy-2, the initial rate of uptake is harder to determine and the results are compatible with a constant uptake fraction independent of oxide thickness during the pretransition period (Figs. 100 and 101).²⁰⁷

After the transition in the oxidation kinetics (i.e., after the oxide has become porous), all alloys show an increase in the fraction of hydrogen absorbed, even when the uptake fractions during both oxidation periods are small. However, for Zircaloy-2 the fraction absorbed after transition is often close to 100% (Fig. 38), particularly at temperatures above 400°C, but at lower temperatures than this it decreases with increasing post-transition oxide thickness, to an extent that has not been firmly established.⁴⁷ In-reactor, where thick oxides can be grown at low temperatures in oxygenated water, the decreasing rate of absorption is more obvious, but is lowered anyway by the presence of oxygen.^{398,439,454,621} In both the pre- and post-transition periods the uptake fraction is a function of temperature and pressure.^{47,202,204,205}

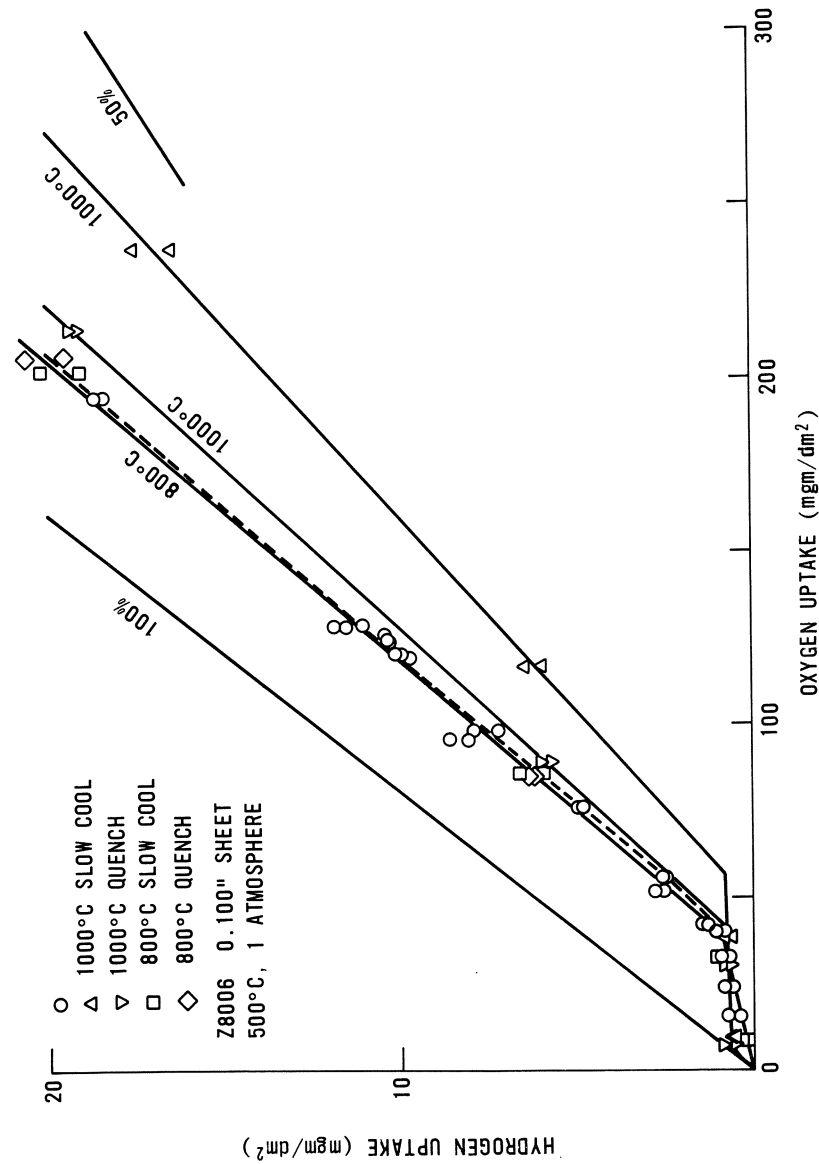


Fig. 102. Effect of heat treatment on the hydrogen absorption by Zircaloy-2 in 500°C steam.^{4,7}

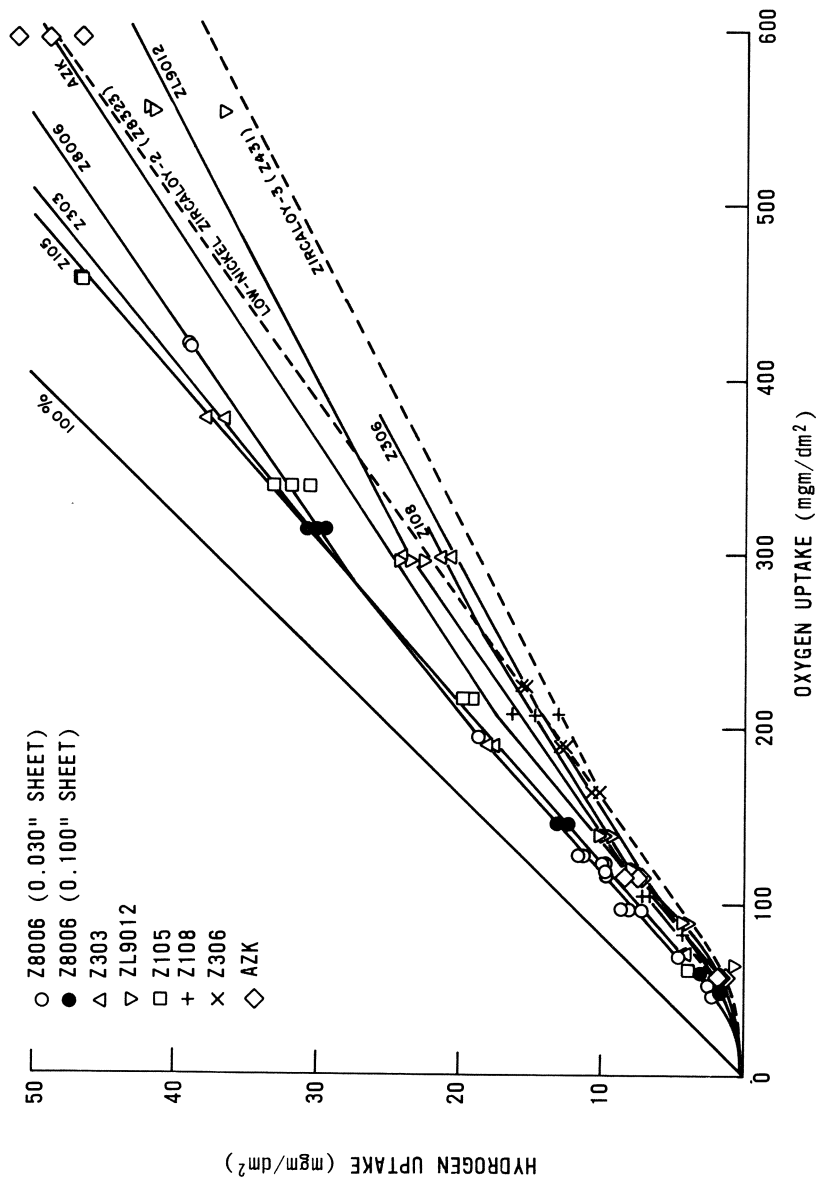


Fig. 103. Variation in hydrogen uptake from batch to batch for Zircaloy-2 in 500°C steam at 1 atm. (See Table 5 for analyses of batches.⁴⁷)

The uptake fraction for the Zircalloys is also affected by the prior heat treatment of the alloy (Fig. 102)^{202,205,622}; minor variations in composition, such as those from batch to batch (Fig. 103)^{47,205} and variations in the levels of impurities such as Si, N, and C.³⁴⁰⁻³⁴² Silicon levels of several hundred parts per million give a significant reduction of hydrogen uptake³⁴² for Zircaloy-2, but not for Zircaloy-4 (Fig. 104). The thickness of the specimens employed (Fig. 105),^{47,205} the pre-oxidation treatment of the specimens,^{364,623} and the presence of impurities in the water (Table 10), especially oxygen (Fig. 106),^{47,203-205,358,362,624,625} also affect hydrogen absorption. Of these effects, that of oxygen in the environment is probably the largest and

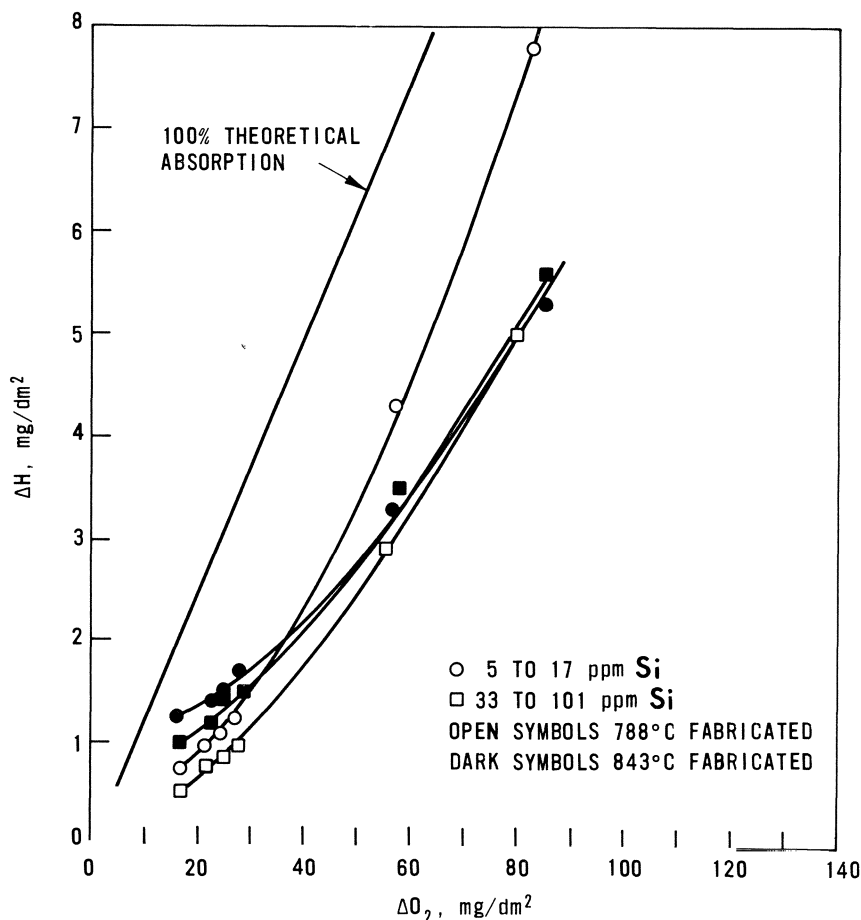


Fig. 104. Effect of small variations in silicon content of Zircaloy-2 on the hydrogen absorption in 360°C water.³⁴⁰

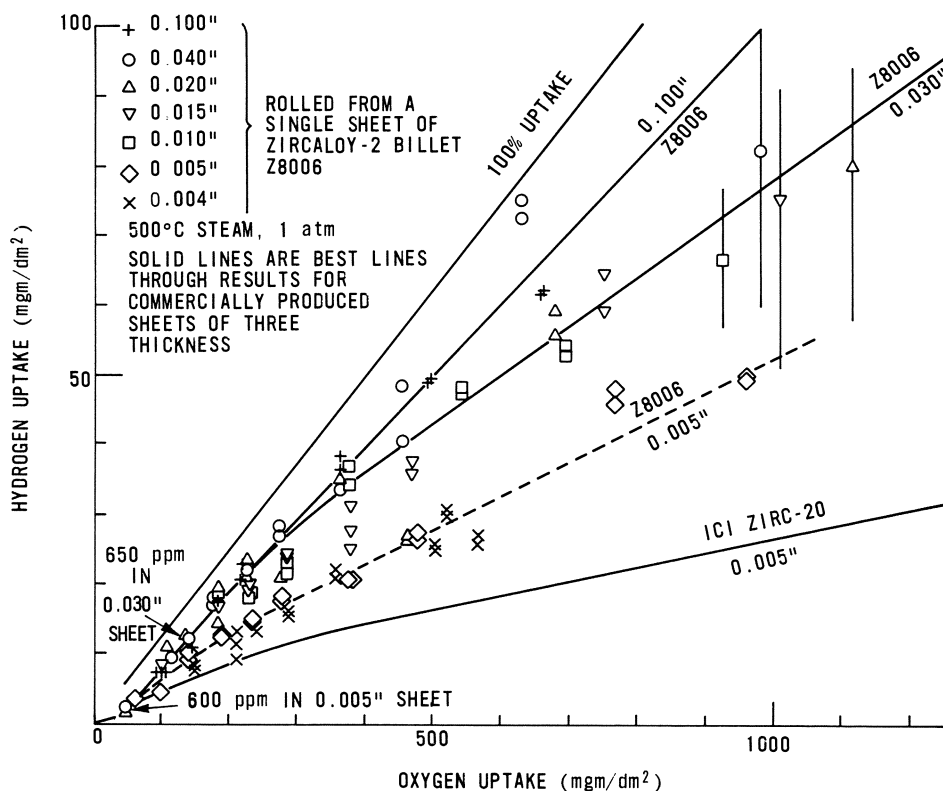


Fig. 105. Effect of specimen thickness on hydrogen absorption by Zircaloy-2 in 500°C steam.⁴⁷

best documented, and increasing the oxygen content invariably acts to reduce the hydrogen uptake fraction. Even the effect of autoclave startup procedure affects the hydrogen uptake. This may operate through its effect on the residual oxygen content of the autoclave.^{35,626} Although LiOH at pH above 12 increases the oxidation rate enormously, the hydrogen uptake fraction remains relatively unaffected³⁶⁵⁻³⁶⁹; the total hydrogen therefore increases in proportion to the increased oxide thickness.

Effect of Alloying. Increasing purity of unalloyed zirconium, which results in increasing oxidation in 400°C steam, also results in increased hydrogen uptake and an interesting change in hydride morphology from isolated platelets to gross islands of hydride.⁶²⁷ This also seems to be an example of only a small number of instances during oxidation where hydrogen ingress is so rapid that a layer of hydride develops at the oxide/metal interface. Whether this hydride layer is, in part, responsible for the excessive oxidation has not been explored.

During the development of Zircaloy-2 the effect of varying the alloying additions (Sn, Fe, Cr, Ni) on hydrogen absorption was studied²⁵⁶ and only nickel additions were found to have a deleterious effect (Fig. 107). Studies of nickel-enriched Zircaloy-2 showed that more hydrogen than that produced by the corrosion process was absorbed by some alloys when molecular hydrogen was present in the water or steam.^{212,213} Thus in this instance molecular hydrogen is absorbed from the environment despite the presence of adequate oxidant.

A wide range of other alloys (Fig. 108) has been examined in several laboratories, and none of these have consistently given uptakes greater than 100%^{47,202-209,261} although in most instances molecular hydrogen contents of the environment were probably low (probably only hydrogen accumulated from corrosion of other specimens in most instances). Some alloys, such as those containing Pd, Pt, and ternaries of these with copper, give close to 100% uptake over a wide range of conditions of temperature

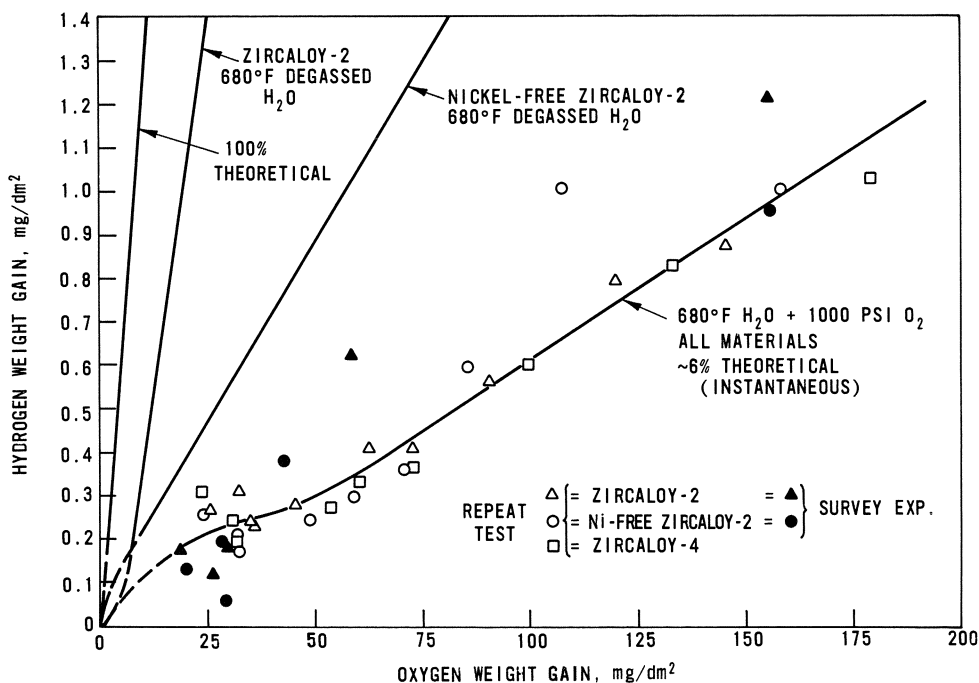


Fig. 106. Effect of oxygen additions to 680°F water on the hydrogen absorption rates of the Zircalloys.²⁰²

Table 10. Effects of Additives^a to 680°F Water on Oxidation and Hydrogen Pickup of Zircaloy-2²⁰²

Solution	Additives	pH	Effect on oxidation ^b	Effect on Hydrogen pickup ^b
1	NaOH, NH ₃	9.5–10	No systematic effect	No systematic effect
2	NH ₃ + NiSO ₄	7.5	2-fold increase	2- to 3-fold decrease
3	NaNO ₂	4	Slight increase	No effect
4	H ₂ SO ₄	7	No systematic effect	Slight increase with CO
	He, N ₂			
	CO, CO ₂			Slight decrease with CO ₂
5	H ₂	7	Slight decrease	Probably no increase
6	D ₂ (over D ₂ O)	7	Slight decrease	2-fold increase
7	O ₂	7	2-fold increase	4- to 5-fold decrease

^aSolids in concentrations of 10⁻³–10⁻⁴ M (refreshed autoclaves); gases in concentrations of 3–4 × 10³ cm³/kg (static autoclave).
^bRelative to that in pure degassed H₂O at 680°F.

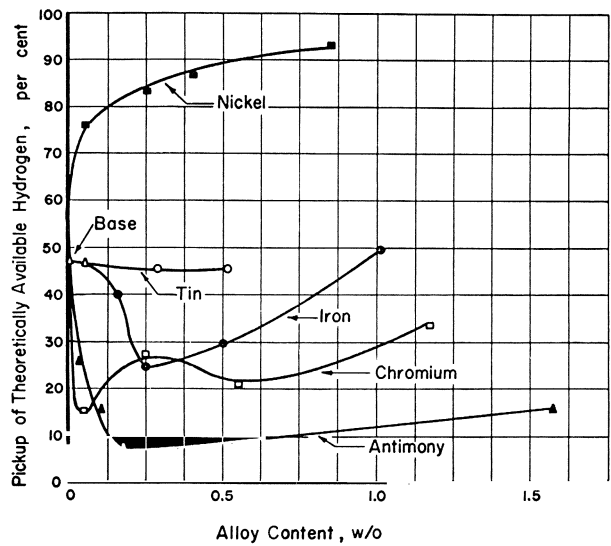


Fig. 107. Effect of tin, iron, chromium, nickel, and antimony on hydrogen uptake by sponge-base zirconium alloys exposed to 680°F water.²⁵⁶

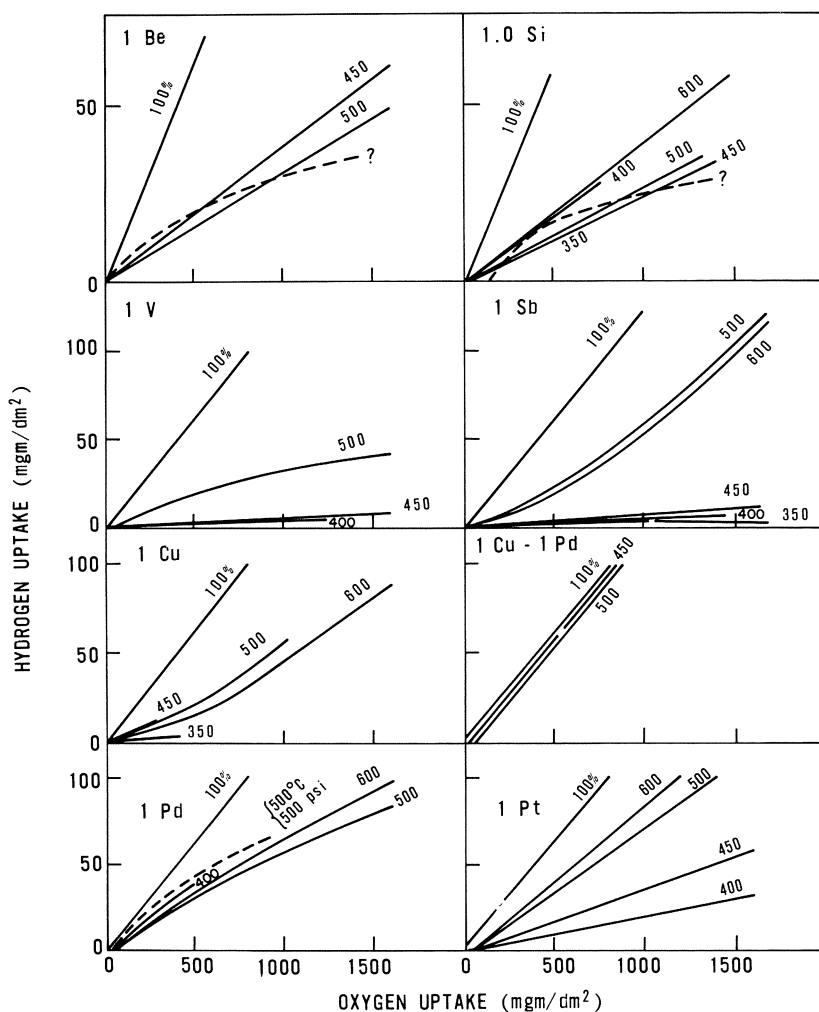


Fig. 108. Hydrogen absorption by 1% alloys of zirconium with Be, Si, V, Sb, Cu, Cu/Pd, Pd, and Pt in steam at 350–600°C. (Dashed lines indicate possible curves on which results at all temperatures may lie.²⁶¹)

and pressure²⁶¹ and would be expected to absorb molecular hydrogen if large quantities of this were present in the environment. Klepfer²⁰⁸ reports occasional values of hydrogen uptake > 100% for Zr–Fe alloys in steam and water (Fig. 109). These are the exception, however, and might be explained by combined errors in weight gain and/or hydrogen analysis. A study of the transition metal additives from titanium to germanium gives the inter-

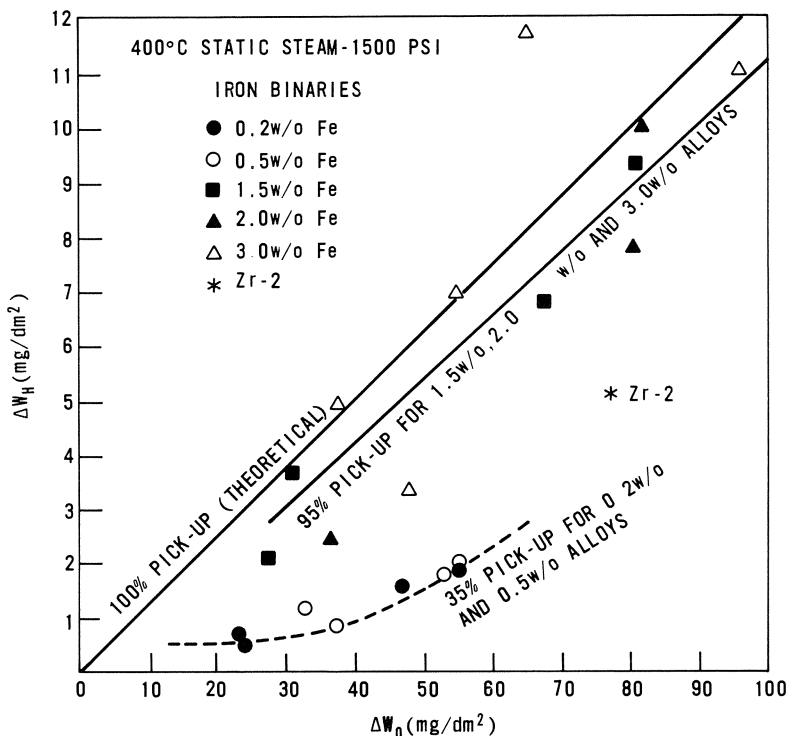


Fig. 109. Hydrogen uptake as a function of oxidation for Zr-Fe binary alloys tested in 400°C static steam at 1500 psi.²⁰⁸

esting observation (Fig. 110) of a regular trend in hydrogen absorption, with nickel falling on the peak of the curve. Since all these additions (other than titanium) will be present as second phase particles in zirconium alloys, we conclude that the hydrogen uptake properties of these alloys result more from the properties of the second phase particles present than from any modification of the properties of the bulk oxide by the small amount of alloying addition in solution in it.

Elimination of the nickel from the Zircalloys has resulted in alloys showing considerably lower hydrogen uptake fractions than for Zircaloy-2, and in particular a low sensitivity to large hydrogen overpressures (Fig. 98) such as might be experienced in PWRs. This results in a low sensitivity of these alloys to the gaseous hydriding type of fuel failure.^{202,210}

Hydrogen uptake by Zr-Nb alloys (Fig. 111) appears to follow the same sort of complicated relationship to the amount of oxidation occurring as

was observed for alloys of the Zircaloy type.^{115,116,239,240} However, the overall uptake fraction is generally much lower, and changes in uptake fraction as a function of oxide thickness are more difficult to detect. Hence, some investigators have not observed any increase in the fraction of hydrogen absorbed by Zr-Nb alloys in the post-transition region.^{231,233,241,244} Since hydrogen absorption by these alloys is also sensitive to the amount of oxygen in the steam or water, these differences in results may be the result of small variations in experimental technique.^{204,205} An effect of heat treatment on the hydrogen absorption curve has also been found in some instances and not in others. Again an effect of different experimental techniques, coupled with the low hydrogen contents often being analyzed, may account for these discrepancies.

Hydrogen Absorption Mechanism Hydrogen absorption by zirconium alloys has usually been considered to proceed in three steps.²⁰² First, reaction of an adsorbed water molecule with an anion vacancy to leave two protons on the surface and an oxygen anion (or one proton and hydroxyl on an anion site). Second, discharge of the protons on the surface by electrons

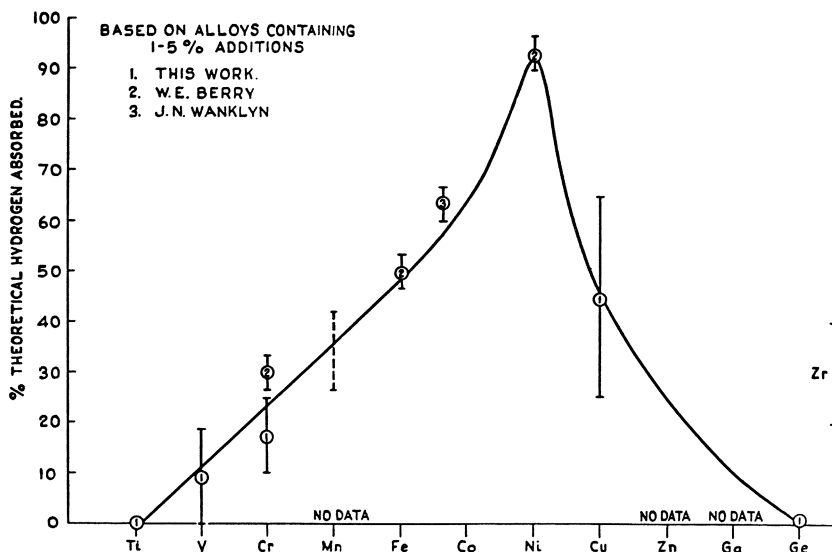


Fig. 110. Effect of transition metal alloying additions, from the first long period of the periodic table, on hydrogen absorption by zirconium.²⁰⁴

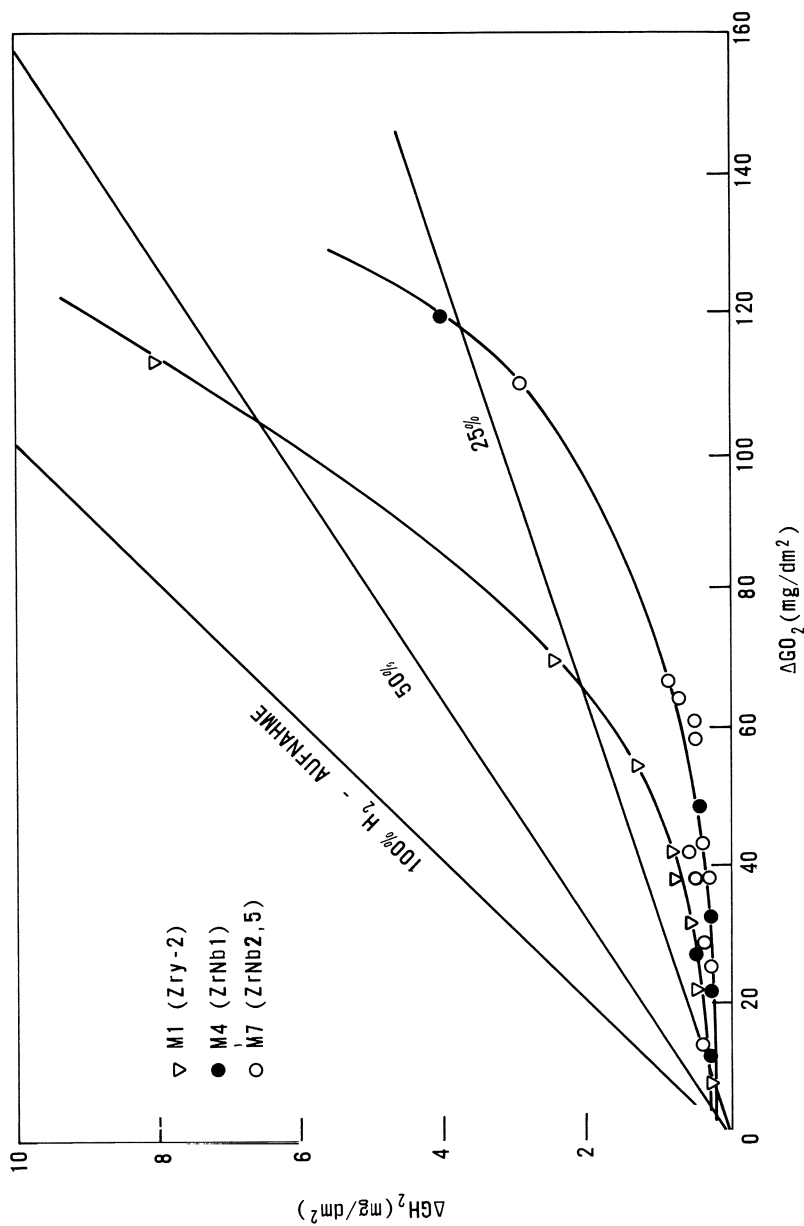


Fig. 111. Comparison of hydrogen uptake by Zr-1% Nb, Zr-2.5% Nb, and Zircaloy-2 in 500°C steam at 1 atm.²⁴⁰

migrating from the oxide/metal interface, and third, migration of the hydrogen through the bulk of the oxide film. It is the third of these processes which is difficult to establish, and the migration of hydroxyl ions, atomic hydrogen, or even H^- on an anionic site have been proposed from time to time.

Infrared studies have failed to demonstrate the presence of OH^- in zirconia films²⁰⁶; however, a nuclear analysis technique using deuterium⁶²⁸ and tritium autoradiography⁶¹⁸ have both demonstrated the presence of hydrogen in oxide films $\leq 0.5 \mu m$ thick, formed in water or steam. Apparently, uniform tritium distributions have been seen in oxide films near but probably still preceding the rate transition. Tritium has also been identified in post-transition oxide films formed in water, but not when films formed in oxygen were heated in gaseous tritium until tritium absorption by the metal occurred.⁶¹⁸ Thus, although it appears that pre-transition oxide films formed in water-containing environments contain a uniform concentration of hydrogen, we cannot be sure that the resolving power of the techniques would reveal any fine scale inhomogeneities.

Autoradiography cannot demonstrate that the observed tritium is mobile, however, although it might be possible to demonstrate this by a suitable sequence of experiments in which specimens were corroded in H_2O , D_2O , and T_2O . All three species can be analyzed separately by mass spectrometry, deuterium could be determined by a nuclear technique,⁶²⁸ and the tritium can of course be located by autoradiography. Combined with analysis of the environment it could be established by these techniques whether hydrogen in the oxide (observed by autoradiography) subsequently entered the metal or exchanged with hydrogen species in the environment. The observation that some autoradiographs of thick oxide films show a fine scale ($1-2 \mu m$) nonuniform distribution of tritium may be evidence that in post-transition oxides, at least, the observed tritium is present on pore walls, probably as T_2O .

Tritium effusion experiments^{363,629-631} have shown that migration out of a tritided zirconium specimen is possible when the oxide film is less than 500 \AA thick, but that the rate of effusion falls rapidly to a negligible rate as the oxide thickens. Whether the effusion took place into an oxygen or a steam environment, the amount of tritium gas appearing in the environment was the same. However, approximately 100 times this amount of tritium appeared as T_2O in a steam environment. It was concluded from this that there are two operating mechanisms by which tritium escapes from a tritided metal specimen. The first is escape of hydrogen gas via cracks or pores in the oxide which penetrate to the metal/oxide interface; the second

involves exchange of tritium (in the metal) with hydrogen (in the oxide film) and thence into the steam phase.³⁶³ However, since both these processes decrease rapidly with increasing oxide thickness, and the quantity escaping was only about 1 part in 10^4 of the hydrogen entering the metal during the same period of time, we cannot infer from this experiment that the small concentration of hydrogen observed in pre-transition oxide films is sufficiently mobile to be the primary route for hydrogen uptake.

Whether or not these hypotheses remain acceptable in retrospect, when recent evidence on the oxidation mechanism is considered, the results show that hydrogen can move to and fro through thin ($< 2000 \text{ \AA}$) oxide films with relative ease, compared with thicker oxides. We have seen that the electron current in the Zircaloys (and some other alloys) flows predominantly at intermetallic sites. Thus the electrons available to discharge the protons released on incorporation of oxygen at the surface appear at these sites, and the big increase in surface conductivity of the oxide in the presence of water⁵⁴¹ suggests that protons may be migrating to the intermetallic particles under these conditions. Iron and chromium oxides have been positively identified on the surface of the appropriate intermetallic particles,^{184,596} and the presence of nickel oxide has been suspected but not proved, in alloys containing small quantities ($\leq 2\%$) of these elements. It is suspected that these oxides form on the surface of the intermetallic particle, after the formation of a thin layer of zirconia, by outward migration of the alloying addition (e.g., Fe) from the continuous layer of iron which will form at the zirconia/intermetallic interface as a result of the initial formation of a ZrO_2 film. This Fe layer will limit the further growth of a ZrO_2 film by acting as a diffusion barrier to zirconium from within the intermetallic.¹⁸⁴ Because of this outward diffusion of the alloying addition the thin zirconia film on the intermetallic probably becomes doped with the alloying element.

Whether the hydrogen atoms discharged at the surface of the oxide on the intermetallic particle recombine to form hydrogen molecules, or whether they migrate through the complex thin oxide layer on the intermetallic, will probably be dictated by the properties of the oxide layer they first contact (i.e., the oxide of the alloying addition; Fe, Cr, or Ni for Zircaloy-2) and the probability of their recombination and desorption compared with absorption. It is presumably at this point in the process that environmental conditions affect the uptake (e.g., oxygen in the water could react with hydrogen at this stage and enhance desorption at the expense of absorption).

Whether the hydrogen is released at a relatively smooth oxide surface or deep within a porous oxide, there is general agreement between the trend in hydrogen uptake fraction and the chemical nature of the alloying additions present (Figs. 38 and 110). A film of NiO on the surface of a Zr_2Ni intermetallic particle may be able to dissociate molecular hydrogen, as well as preventing the hydrogen discharged in the oxidation reaction from recombining, and hence allow the hydrogen to migrate into the metal. One might then expect a ternary addition to a Zr–Ni alloy which was known to poison NiO catalysts (e.g., arsenic) to reduce hydrogen uptake by the alloy. To do this, however, the ternary addition would have to be incorporated into the same intermetallic particle as the nickel, it would have to diffuse out through the thin initial zirconia film along with the nickel, and it would then have to be incorporated into the NiO layer. We have already seen that for Zircaloy-2 the three insoluble additives (Fe, Cr, and Ni) do not all appear in the same intermetallic phase, but that at least two different intermetallic phases are formed.^{282,601,602} Such an effect could account for the observation that nickel additions appear to increase the hydrogen absorption rate whatever other alloying additions are present, for nickel may prefer to form a separate Zr_2Ni phase rather than dissolve in an intermetallic phase formed from the other alloying additions.

The conclusions from this hypothesis are that to obtain low hydrogen uptakes one should study alloys where the alloying additions are in solid solution. In such alloys the hydrogen discharged at the oxide surface would have to pass through the bulk oxide, a longer and more difficult route than through the thin oxide over an intermetallic particle. Any insoluble alloying additions should be selected from elements whose oxides are good recombiners of atomic hydrogen. The low hydrogen uptake by the Zr–Nb alloys and by Zr–Ti alloys would seem to support the case for solid solution alloys^{115,204,205}; the low hydrogen absorption by alloys containing vanadium, antimony, and germanium may reflect the properties of the alloying metal oxides, since all these elements have low solubilities in α -zirconium and will be present as a second phase.

ACKNOWLEDGMENTS

The author is grateful to the various people, known and unknown, who have read the manuscript and commented upon it; also to the organizations who have given permission for the use of the figures used in this review.

REFERENCES

1. B. Cox, Environmentally Induced Cracking of Zirconium Alloys, *Rev. Coat. Corr.* Vol. 1, No. 4, p. 366 (1974) (Freund, Tel Aviv).
2. B. Cox and J. C. Wood, Proc. Symp. Corrosion Problems, in *Energy Conversion and Generation*, Electrochemical Society (1974), p. 275.
3. B. Lustman and F. Kerze; *Metallurgy of Zirconium*, McGraw-Hill, New York (1955).
4. E. A. Gulbransen and K. F. Andrew, Kinetics of the Reactions of Zirconium with O_2 , N_2 and H_2 , *Trans. AIME* **185**, 515 (1949).
5. R. J. Hussey and W. W. Smeltzer, The Oxidation Kinetics of Zirconium in the Temperature Range 400°–600°C, *J. Electrochem. Soc.* **111**, 564 (1954).
6. E. Hillner, The High Temperature Oxidation Kinetics of Zirconium in Dry Oxygen, *Electrochem. Tech.* **4**, 132 (1966).
7. R. G. Charles, S. Barnartt, and E. A. Gulbransen, Prolonged Oxidation of Zirconium at 350° and 450°C, *Trans. Met. Soc., AIME* **212**, 101 (1958).
8. S. Kass, The Development of the Zircaloys, *Proc. USAEC Symp. Zirconium Alloy Development*, Castlewood, Calif., 1962, GEAP-4089; *Proc. ASTM Symp. Corrosion of Zirconium Alloys*, New York, 1963, ASTM-STP-368, p. 3; and WAPD-T-1549 (1962).
9. S. M. Shelton, *Zirconium Alloys for High Temperature Service*, U.S. Air Force Report AF-TR-5932 (1949).
10. P. J. Shirvington and B. Cox, A Study of Charge Transport Processes During the Oxidation of Zirconium Alloys, *J. Nucl. Mat.* **35**, 211 (1970).
11. J. Boulton, *The Use of Zirconium Alloys in Organic Coolants*, Atomic Energy of Canada Ltd. Report AECL-2619 (1966).
12. T. L. MacKay, Oxidation of Zirconium and Zirconium Alloys in Liquid Sodium, *J. Electrochem. Soc.* **110**, 960 (1963).
13. W. G. O'Driscoll, C. Tyzack, and T. Raine, The Oxidation of Groups IVA, VA and VIA Elements in Carbon Dioxide and the Development of Oxidation Resistant Zirconium Alloys, *Proc. 2nd Intern. Conf. Peaceful Uses Atomic Energy, Geneva*, Vol. 5 (1958), p. 75 (Paper 1450).
14. D. L. Douglass, The Metallurgy of Zirconium, *IAEA Rev.* (Suppl., 1971).
15. B. G. Parfenov, V. V. Gerasimov, and G. I. Venediktova, *Corrosion of Zirconium and Zirconium Alloys*, Atomizdat, Moscow, AEC-TR-6978 (1967).
16. A. B. Johnson, Jr., A Review of Corrosion Phenomena on Zirconium Alloys, Niobium, Titanium, Inconel, Stainless Steel and Nickel Plate Under Irradiation, *Rev. Coat. Corr.* Vol. 1, No. 4, p. 299 (1974) (Freund, Tel Aviv).
17. W. E. Berry, *Corrosion in Nuclear Applications* (ECS Corrosion Monograph Series), John Wiley, New York (1971).
18. H. A. Porte, J. G. Schnizlein, R. C. Vogel, and D. F. Fischer, Oxidation of Zirconium and Zirconium Alloys, *J. Electrochem. Soc.* **107**, 506 (1960); and USAEC Report ANL-6046 (1959).
19. R. D. Misch and C. J. van Drunen, The Oxidation of Zirconium Binary Alloys in 700°C Oxygen for Times up to 200 Days, *Proc. USAEC Symp. Zirconium Alloy Development*, Castlewood, Calif., 1962, GEAP-4089, Paper 15.
20. J. K. Dawson, U. C. Baugh, and J. F. White, Observations on the Early Stages of Oxidation of Zirconium and Zircaloy-2, *Electrochem. Tech.* **4**, 137 (1966).
21. J. K. Dawson, G. Long, W. E. Seddon, and J. F. White, The Kinetics and Mechanism of the Oxidation of Zircaloy-2 at 350–500°C, *J. Nucl. Mat.* **25**, 179 (1968); and UKAEA Report AERE-R4820 (1964).
22. B. Cox, The Zirconium–Zirconia Interface, *J. Aust. Inst. Met.* **14**, 123 (1969).

23. H. B. Probst, E. B. Evans, and W. M. Baldwin, Jr., *Scaling of Zirconium at Elevated Temperatures*, USAEC Report AECU-4113 (1959).
24. L. F. Kendall, *Reaction Kinetics of Zirconium and Zircaloy-2 in Dry Air at Elevated Temperatures*, USAEC Report HW-39190 (1955); see also *Nucl. Sci. Eng.* **3**, 171 (1958).
25. T. Maekawa, T. Mata, and Y. Tachihara, Studies on the Oxidation of Zirconium in Air, *Nippon Kinzoku Gakkalshi* **22**(3), 150 (1958).
26. E. A. Gulbransen and K. F. Andrew, Breakaway Oxidation of Zirconium-Tin Alloys, *Corrosion* **14**, 32t (1958); *Trans. AIME* **212**, 281 (1958).
27. M. W. Mallett and W. M. Albrecht, High Temperature Oxidation of Two Zirconium-Tin Alloys, *J. Electrochem. Soc.* **102**, 407 (1955).
28. C. A. Phalnikar and W. M. Baldwin, Jr., Scaling of Zirconium in Air, *ASTM Proc.* **31**, 1035 (1951).
29. D. Whitwham, J. Boghen, and J. Hérenghuel, Surface Flow Phenomena During High Temperature Oxidation, The Ease of Zirconium and Its Alloys, *Rev. de l'Aluminium* **43** (244), 611 (1957).
30. W. H. Keys, G. Béranger, B. de Gélas, and P. Lacombe, Metallographic Study of Breakaway During the Oxidation of Zirconium, *J. Less-Common Metals* **14**, 181 (1968); and USAEC Report WAPD-trans-0092.
31. G. Wallwork, C. J. Rosa, and W. W. Smeltzer, Breakaway Phenomena in the Oxidation of Zirconium at 850° and 950°C, *Corrosion Sci.* **5**, 113 (1965).
32. T. L. MacKay, Oxidation of Single-Crystal and Polycrystalline Zirconium, *Trans. Met. Soc. AIME* **227**, 1184 (1963).
33. R. E. Westerman, High-Temperature Oxidation of Zirconium and Zircaloy-2 in Oxygen and Water Vapour, *J. Electrochem. Soc.* **111**, 140; (1964); and USAEC Report HW-73511 (1963).
34. S. Harper and J. C. Greenbank, *The Mechanism of Oxidation of Zirconium*, UKAEA Report TRG 392 (R) PT.
35. E. A. Gulbransen and K. F. Andrew, Oxidation of Zirconium Between 400° and 800°C, *Trans. AIME (J. Metals)* **209**, 394 (1957).
36. R. S. Ambartsumyan, A. A. Kiselev, R. V. Grebennikov, V. A. Myshkin, L. J. Tsuprun, and A. V. Nikulina, Mechanical Properties and Corrosion Resistance of Zirconium and Its Alloys in Water, Steam and Gases at Elevated Temperatures, *Proc. 2nd Intern. Conf. Peaceful Uses Atomic Energy, Geneva*, Vol. 5 (1958), p. 12 (p. 2044).
37. O. Zmeskal and M. L. Brey, Oxidation of Zirconium-Columbian Alloys in Oxygen at 525° to 1090°C, *Trans. ASM* **53**, 415 (1961).
38. J. Debuigne and P. Lehr, Corrosion sèche du zirconium non allié, *Proc. IAEA Symp. Corrosion Reactor Mat. Salzburg*, 1962, p. 105.
39. D. Cubicciotti, The Oxidation of Zirconium at High Temperatures, *J. Amer. Chem. Soc.* **72**, 4138 (1950).
40. J. Belle and M. W. Mallett, Kinetics of High Temperature Oxidation of Zirconium, *J. Electrochem. Soc.* **101**, 339 (1954).
41. E. Hillner, Further Observations on the Oxidation of Zirconium in Dry Oxygen, *J. Electrochem. Soc.* **114**, 237 (1967).
42. R. J. Hussey and W. W. Smeltzer, The Mechanism of Oxidation of Zirconium in the Temperature Range of 400° to 850°C, *J. Electrochem. Soc.* **111**, 1221 (1964).
43. T. Sano, S. Imoto, and M. Kan, The Effect of Tellurium on the Oxidation Resistance of Zirconium, *Tech. Repts. Faculty Eng., Osaka U.* **10**, 377 (1960).
44. S. Nomura and C. Akutsu, Oxidation Kinetics and Oxide Film Breakaway of Zirconium and Its Alloys at High Temperatures, *Electrochem. Tech.* **4**, 93 (1966); and JAERI-1161.

45. E. Fukushima, Oxidation of Zircaloy-2 at 600°–800°C, *Nippon Kinzoku Gakkaishi* **30**, 910 (1966).
46. R. D. Watson, *Forming Uniform Thick Oxide Layers on Zircaloy-2 for Friction and Wear Applications in High Temperature Water*, Report AECL-2542 (1966).
47. B. Cox, *Some Factors Which Affect the Rate of Oxidation and Hydrogen Uptake of Zircaloy-2 in Steam*, UKAEA Report AERE-R4348 (1963).
48. G. R. Wallwork, W. W. Smeltzer, and C. J. Rosa, The Parabolic Oxidation Kinetics of Alpha-Zirconium at 850°C, *Acta Met.* **12**, 409 (1964).
49. D. H. Bradhurst, J. E. Draley, and C. J. van Drunen, An Electrochemical Model for the Oxidation of Zirconium, *J. Electrochem. Soc.* **112**, 1171 (1965).
50. J. P. Pemsler, Diffusion of Oxygen in Zirconium and Its Relation to Oxidation and Corrosion, *J. Electrochem. Soc.* **105**, 315 (1958); and **111**, 381 (1964); Studies on the Oxygen Gradients in Oxidizing Metals, III. Kinetics of the Oxidation of Zirconium at High Temperatures *J. Electrochem. Soc.* **112**, 477 (1965).
51. K. Leclercq, *Contribution to the Study of the Mechanism of Oxidation of Pure or Alloyed Zirconium by Oxygen and Steam*, Euratom Report EUR-4507f (1970).
52. B. Cox, Some Effects of Pressure on the Oxidation of Zircaloy-2 in Steam and Oxygen, *J. Less-Common Metals* **5**, 325 (1963); and *Proc. USAEC Symp. Zirconium Alloy Development, Castlewood, Calif.*, 1962, GEAP-4089, Paper 16.
53. J. N. Wanklyn, C. F. Britton, D. R. Silvester, and N. J. M. Wilkins, Influence of Environment on the Corrosion of Zirconium and Its Alloys in High-Temperature Steam, *J. Electrochem. Soc.* **110**, 856 (1963); and AERE-R4130 (1962).
54. K. L. Komarek and M. Silver, Thermodynamic Properties of Zirconium–Oxygen, Titanium–Oxygen and Hafnium–Oxygen Alloys, *Proc. IAEA Symp. Thermodynamics Nuclear Metals, Vienna*, 1962, p. 749.
55. R. M. Treco, Solution and Diffusion of Corrosion Oxide Film in Zircaloy *J. Electrochem. Soc.* **109**, 208 (1962).
56. G. Béranger and P. Lacombe, Study of Corrosion and Protection of Zirconium and Its Alloys. Nucleation and Growth Phenomena During the Surface Oxidation of Zirconium, *Proc. IX^{me} Colloque de Métallurgie, Saclay*, 1966, p. 181; and USAEC Report WAPD-Trans-111.
57. J. Pädassi and J. Nierlich, Sur les phénomènes de germination et de croissance de la zircone, ainsi que de striation du zirconium, au cours de la réaction de ce métal avec l'oxygène sous basses pressions, aux températures élevées, *Compt. Rend* **267**, 1085 (1968); and Sur la cinétique de la réaction du zirconium avec l'oxygène sous basses pressions aux températures élevées, *Compt. Rend.* **267**, 1429 (1968).
58. M. Perdureau and J. Bardolle, Etude micrographique de l'oxydation ménagée du zirconium, *Compt. Rend.* **257**, 2477 (1963).
59. L. Renucci and J. P. Langeron, Oxydation du zirconium en phase β sous très basses pressions, aspect superficiel présenté par les alliages zirconium–oxygène, *J. Nucl. Mat.* **23**, 79 (1967).
60. C. M. Quinn and M. W. Roberts, High Temperature Oxidation of Zirconium Ribbons, *Trans. Faraday Soc.* **59**, 985 (1963).
61. W. G. Guldner and L. A. Wooten, Reactions of Zirconium with Gases at Low Pressures, *J. Electrochem. Soc.* **93**, 223 (1948).
62. J. Levitan, J. E. Draley, and C. J. van Drunen, Low Pressure Oxidation of Zirconium, *J. Electrochem. Soc.* **114**, 1086 (1967); and USAEC Report ANL-7252 (1966).
63. J. C. Wilson, *ORNL Metallurgy Division Annual Progress Report, 1965*, USAEC Report ORNL-3870, p. 182.

64. M. J. Bentley and J. A. S. Mowat, Oxidation of Zircaloy-2 Under Simulated Loss of Coolant Accident Conditions and Its Effect on Room-Temperature Ductility of SGHWR Cladding, *Proc. British Nuclear Energy Soc. Conf. Nuclear Fuel Performance*, London, 1973, Paper 82.
65. M. Perdereau and J. Bardolle, Étude cinétique de l'oxydation de zirconium aux températures élevées, *Compt. Rend.* **256**, 4665 (1963).
66. G. Chauvin, E. Boudouresques, H. Coriou, and J. Huré, Influence du carbone sur l'oxygénation du zirconium à haute température, *Rev. Met.* **55**, 939 (1958); and CEA-R1191 (1959).
67. H. Coriou, J. Gauduchau, L. Grall, and J. Huré, Influence du carbone et de sa répartition sur la corrosion du zirconium par l'eau à 315°C, *Rev. Met.* **56**, 693 (1959).
68. B. Cox, The Effect of Carbide Inclusions on Oxide Film Failure, *Corrosion* **16**, 188t (1960); and UKAEA Report AERE-R2873 (1959).
69. K. Östhagen and P. Kofstad, Oxidation of Zirconium and Zirconium-Oxygen Alloys at 800°C, *J. Electrochem. Soc.* **109**, 204 (1962).
70. B. Cox and B. R. Harder, The Effect of Dissolved Oxygen on the Oxidation of Zircaloy-2 by Steam, *J. Electrochem. Soc.* **110**, 1110 (1963).
71. K. H. Akram and W. W. Smeltzer, The High-Temperature Oxidation Kinetics of Zirconium, *Can. Met. Quart.* **1**, 41 (1962).
72. J. P. Pemsler, Studies on the Oxygen Gradients in Oxidizing Metals, V. The Oxidation-Saturated Zirconium, *J. Electrochem. Soc.* **113**, 1241 (1966).
73. W. W. Doerffler, A Contribution to the Mechanism of Dissolution and Diffusion of Oxygen in Zirconium, *Proc. IAEA Conf. Thermodynamics with Emphasis on Nuclear Material and Atomic Transport in Solids*, Vienna, 1965 (SM66/18); and EIR Report 82 (1965).
74. W. W. Doerffler, *The Dissolution and Diffusion of Oxygen in Zirconium*, Atomic Energy of Canada Ltd. Report AECL-2268 (1965).
75. T. Smith, Mechanism of the Oxidation of Zirconium in Oxygen and Liquid Sodium, *J. Electrochem. Soc.* **112**, 39 (1965).
76. C. J. Rosa and W. W. Smeltzer, The Parabolic Oxidation Kinetics of Beta-Zirconium, *Acta Met.* **13**, 55 (1965).
77. C. J. Rosa, Evaluation of Oxidation Rates for Alpha Zirconium, *J. Less-Common Metals* **15**, 35 (1968).
78. C. J. Rosa, Evaluation of Oxygen Partition in a Three-Phase Beta-Zirconium-Oxygen Alloy, *J. Less-Common Metals* **15**, 183 (1968).
79. C. J. Rosa, Oxidation of Zirconium—A Critical Review of Literature *J. Less Common Metals* **16**, 173 (1968).
80. M. Davis, K. R. Montgomery, and J. Standring, The Diffusion Coefficient for Oxygen in Alpha-Zirconium, *J. Inst. Met.* **89**, 112 (1960); and UKAEA Report IGN-TN C-588.
81. G. Shinoda and Y. Amano, On the Dissolution of Oxygen in Zirconium, *Nippon Kinzoku Gakkaishi* **28**, 639 (1964).
82. G. Béranger and P. Lacombe, Contribution à l'étude de la cinétique de l'oxydation du zirconium α et la diffusion de l'oxygène dans le métal sous-jacent à l'oxyde, *J. Nucl. Mat.* **16**, 190 (1955).
83. G. Béranger, Comparaison des courbes de variation de microdureté et de concentration en oxygène dissous dans le zirconium α après oxydation prolongée à 850°C, *Compt. Rend.* **259**, 4663 (1964).
84. J. J. Kearns and J. Chirigos, *The Use of Microhardness in the Determination of the Diffusivity of Oxygen in Alpha Zirconium*, USAEC Report WAPD-TM-306 (1962).
85. J. Debuigne and P. Lehr, Étude de l'oxydation du zirconium non allié et de la diffusion de l'oxygène dans la couche d'oxyde et dans le métal, *Rev. Met.* **60**, 911 (1963); *Metaux (Corrosion Ind.)*, **42**, 235 (1967); and USAEC Report WAPD-trans-0091.

86. D. Quataert and F. Coen-Porisini, Utilization of the Ion Analyzer for the Study of Oxygen Diffusion in Solids and Its Application to Zirconium, *J. Nucl. Mat.* **36**, 20 (1970).
87. B. Cox and C. Roy, Transport of Oxygen in Oxide Films on Zirconium Determined by the Nuclear Reaction $O^{17} (He^3, \alpha) O^{16}$, *Electrochem. Tech.* **4**, 121 (1966).
88. G. Sainfort, R. Jacquesson, and P. Laurent, Diffusion de l'oxygène dans le zirconium, *2^{me} Colloque de Métallurgie on Diffusion in the Solid State, Saclay*, 1958, p. 79; and Les Mécanismes et les lois d'oxydation du zirconium à haute température, *Rev. Met.* **56**, 704 (1959).
89. D. H. Bradhurst and P. M. Heuer, The Effects of Deformation on the High Temperature Steam Oxidation of Zircaloy-2, *J. Nucl. Mat.* **55**, 311 (1975).
90. J. P. Pemsler, Studies on the Oxygen Gradients in Corroding Zirconium Alloys, *J. Nucl. Mat.* **7**, 16 (1962); and USAEC Report NMI-1251.
91. R. E. Pawel, Oxygen Diffusion in Beta-Zircaloy During Steam Oxidation, *J. Nucl. Mat.* **50**, 247 (1974).
92. D. O. Hobson and P. L. Rittenhouse, *Ductile-Brittle Behavior of Zircaloy Fuel Cladding*, ORNL-4758 (1972); and *Proc. Topical Meeting on Water Reactor Safety, Salt Lake City*, 1973, AEC-Conf. 73-0304.
93. G. D. Rieck and D. L. Vogel, Thermotransport of Oxygen in β -Zirconium. *Acta Met.* **14**, 1703 (1966).
94. G. D. Rieck and D. L. Vogel, *Thermal Diffusion of Oxygen in Refractory Metals*, Plansee Proc., 1964, Vth Seminar, p. 636.
95. E. A. Gulbransen and K. F. Andrew; calculated by Debuigne and Lehr (34, 86) from results of (31). Basis for this is doubtful.
96. J. Debuigne, J. P. Guerlet, and P. Lehr, Fundamental Aspects of Zirconium Oxidation Phenomena with Pure Oxygen, *Proc. IX^{me} Colloque de Métallurgie, Saclay*, 1966, p. 9.
97. J. C. Greenbank and S. Harper, The Mechanism of Breakaway Oxidation in Zirconium Alloys, *Electrochem. Tech.* **4**, 88 (1966).
98. D. W. Shannon, *Hanford Metallurgy Research Operation, Progress Reports*, USAEC Reports HW-76228, HW-77052, HW-78962, and HW-81269 (1964).
99. B. Cox, Oxide Film Breakdown in Arc-Melted Sponge Zirconium, *Corrosion* **16**, 380t (1960); and UKAEA Report AERE-R2874 (1959).
100. B. Cox, Mechanism of Film Growth and Breakdown on Zirconium and Zircaloy-2, *J. Electrochem. Soc.* **108**, 24 (1961); and UKAEA Report AERE-R2931 (1960).
101. J. P. Pemsler, The Kinetics and Mechanism of Oxide Film Growth of Zirconium, *Electrochem. Tech.* **4**, 128 (1966).
102. C. Roy and G. David, X-Ray Diffraction Analyses of Zirconia Films on Zirconium and Zircaloy-2, *J. Nucl. Mat.* **37**, 71 (1970).
103. G. David, R. Geschier, and C. Roy, Étude de la croissance de l'oxyde sur le zirconium et le zircaloy-2, *J. Nucl. Mat.* **38**, 329 (1971); discussion pp. 343, 344.
104. L. S. Nelson, Explosion of Burning Zirconium Droplets Caused by Nitrogen, *Science* **148**, 1594 (1965); and Sandia Corp. Report SC-RR-65-569.
105. G. Saur, H. J. Laue, and H. Borchers, Deformation of Zirconium Sheets During Oxidation, *Metall* **18**, 704 (1964).
106. C. Roy and R. Burgess, A Study of the Stresses Generated in Zirconia Films During the Oxidation of Zirconium Alloys, *Oxid. Metals* **2**, 235 (1970).
107. T. Kondo and T. Kimura, Oxidation and the Associated Morphological Changes in Zr-Ni Binary Alloys, *J. Nucl. Mat.* **41**, 121 (1971).
108. B. de Gélas, G. Béranger, and P. Labombe, L'Oxydation à haute température du zirconium et de ses alliages binaires à faible teneur en élément d'addition, *J. Nucl. Mat.* **29**, 1 (1969); and USAEC Report WAPD-Trans-120.

109. J. C. Greenbank and S. Harper, Solute Distribution in Oxidised Zirconium Alloys, *Electrochem. Tech.* **4**, 142 (1965).
110. M. G. Cowgill and W. W. Smeltzer, The Oxidation Properties of a Zirconium–2.7 w/o Niobium Alloy in the Temperature Range 300°–500°C, *J. Electrochem. Soc.* **114**, 1089 (1967).
111. B. de Gélès, G. Béranger, C. Marion, and P. Lacombe, Influence de la teneur croissante en cuivre sur la formation d'une couche intermédiaire à 750°C des alliages zirconium-cuivre, *J. Nucl. Mat.* **20**, 337 (1966).
112. I. I. Korobkov and A. I. Yevstyukhin, Effect of Alloying on Protective Properties and Critical Thickness of Oxide Film on Zirconium, *Metallurgiya i Metallovedenie Chistykh Metallov* **2**, 91 (1961).
113. B. Cox, M. J. Davies, and T. Johnston, *The Oxidation Kinetics of Zirconium–Niobium Binary Alloys in Steam at 300–500°C*, UKAEA Report AERE-R3256 (1960).
114. I. I. Korobkov, D. V. Ignatov, A. I. Yevstyukhin, and V. S. Yemelyanov, Electron Diffraction and Kinetic Investigations of the Reactions of Oxidation of Zirconium and Some of Its Alloys, *Proc. 2nd Intern. Conf. Peaceful Uses Atomic Energy, Geneva*, Vol. 5 (1958), p. 60 (p. 2054); and *Metallurgiya i Metallovedenie Chistykh Metallov* **1**, 144 (1959).
115. B. Cox, P. G. Chadd, and J. F. Shiort, *Further Studies of Zirconium–Niobium Alloys*, UKAEA Report AERE-R4134 (1962).
116. B. Cox and J. A. Read, *Oxidation of a Zr–2½% Nb Alloy in Steam and Air*, UKAEA Report AERE-R4459 (1963).
117. M. G. Cowgill, S. H. Wong, and W. W. Smeltzer, Breakaway Oxidation Transition for a Zirconium–2.7 w/o Niobium Alloy, *J. Electrochem. Soc.* **115**, 927 (1968).
118. I. A. El-Shanshoury, V. A. Rudenko, M. E. El-Dahshan, and F. H. Hammad, Kinetics of Oxidation of Zr–1% Nb Alloy in Pressurized Steam and Air at 400°–700°C, *Corr. Sci.* **9**, 217 (1969).
119. I. A. El-Shanshoury, V. A. Rudenko, M. E. El-Dahshan, and F. H. Hammad, The Effect of Changing the Corrosive Medium on the Oxidation of Zr–1% Nb Alloy in Pressurized Steam and Air, *Corrosion Sci.* **9**, 315 (1969).
120. I. A. El-Shanshoury, V. A. Rudenko, and M. E. El-Dahshan, The Effect of Cold Work on the Oxidation of Zr–1% Nb Alloy in Air and Pressurized Steam at 450°–550°C, *Corrosion Sci.* **9**, 479 (1969); and Egyptian Report UAREE-72 (1969).
121. F. Bychov, A. N. Rozanov, and D. M. Skorov, Some Properties of Zirconium Niobium Alloys, *Atomnaya En.* **2**, 146 (1957); and USAEC Report AEC-tr-3133.
122. J. E. Le Surf, The Corrosion Behaviour of 2.5% Nb Zirconium Alloy, *Proc. ASTM Symp. Applications Related Phenomena in Zirconium and Its Alloys, Philadelphia*, 1968, ASTM-STP 458, p. 286.
123. D. G. Lees, The Effect of Production Route, Ageing Time and Oxygen Content on the Properties of Zr–2.5 wt. % Nb, *Corrosion Sci.* **5**, 565 (1965).
124. J. Takamura and Y. Sasaki, Study on the Oxidation Resistance of Zirconium, *Tech. Repts. Eng. Res. Inst., Kyoto Univ.* **9**(6), R-58 (1959).
125. D. I. Phalen, D. A. Vaughan, and N. A. Richard, Oxidation of Zirconium–Yttrium Alloys, *Advan. X-Ray Anal.* **8**, 143 (1965).
126. B. J. S. Wilkins, J. Chater, and A. R. Reich, *The Internal Oxidation of Zirconium–Yttrium Alloys*, Atomic Energy of Canada Ltd. Report AECL-2717 (1968).
127. S. Aoki, High Temperature Oxidation of Zr–Al–X and Zr–Mo–X Ternary Alloys, *Nippon Kinzoku Gakkaishi* **27**, 212 (1963).
128. C. Judge, *U. K. Admiralty Materials Lab. Report A/71(5)* (1957).
129. D. R. Harries, The Technology of Zirconium and Its Alloys, II. Corrosion Behaviour in Contact with Various Media, *Chem. Proc. Eng.* **40**, 363 (1959).

130. Papers on Oxidation of Zirconium Alloys, in *Stroenie Svoistva Splavov Urana, Toriya; Tzirkoniya*, Gosatomizdat, Moscow (1963) pp. 303–377 (NSA, **17**, 39652–59).
131. T. Nakayami, F. Shoji, and E. Yagi, On Catastrophic Oxidation of Ti–Zr, *Nippon Kinzoku Gakkaishi* **27**, 289 (1963).
132. I. N. Frantsevich and R. F. Voitovich, Oxidation of Binary Alloys, in *Surface Interactions Between Metals and Gases*, Arkharov and Gorbunova (eds.), Atomizdat, Moscow (1964), p. 135; Trans. JPRS-82341.
133. Brochure *Zr-Ti Gettering Alloys*, Oregon Metallurgical Corp., Albany, Ore.
134. W. A. Maxwell, An Investigation of Zirconium Alloys for Resistance to Carbon Dioxide Corrosion, *Proc. USAEC Symp. Zirconium Alloy Development*, Castlewood, 1962, GEAP 4089; and USAEC Reports GNEC 218 and 235 (1962).
135. P. Baqué, R. Dominget, and J. Bossard, Recherche d'alliages de zirconium compatibles avec le gaz carbonique sous pression jusqu'à 500° ou 600°C, *En Nucl.* **6**, 89 (1965); and French Report CEA-R-2392 (1963).
136. J. P. Guerlet and P. Lehr, On the Oxidation of Zirconium by Carbon Dioxide, *Compt. Rend.* **258**, 930; **260**, 899 (1964).
137. J. P. Guerlet and P. Lehr, Oxidation of Zirconium in a Carbon Dioxide Atmosphere, *Rev. Met.* **62**, 151 (1965); and USAEC Report WAPD-trans-112.
138. S. J. Gregg, R. J. Hussey, and W. B. Jepson, Reaction of Zirconium with Carbon Dioxide at 550°–750°C, *Corrosion* **17**, 575t (1961).
139. R. J. Hussey and W. W. Smeltzer, The Reaction of Zirconium with Carbon Dioxide and Carbon Monoxide at 850°C, *J. Electrochem. Soc.* **112**, 554 (1965).
140. J. P. Guerlet and P. Lehr, Aspects fondamentaux de l'oxydation du zirconium sous gaz carbonique, *Métallurgie* **6**(2), 69 (1966).
141. J. P. Guerlet and P. Lehr, Comportement du zirconium sous oxyde de carbone, *Rev. Met.* **64**, 745 (1967).
142. J. P. Guerlet, J. Debuigne, and P. Lehr, Study of the Oxidation of Zirconium and Certain of Its Alloys in Carbon Dioxide, *Proc. IX^{me} Colloque de Métallurgie*, Saclay, 1965.
143. T. Maekawa, High Temperature Oxidation of Zirconium and Its Alloys in Carbon Dioxide, *Nippon Kinzoku Gakkaishi* **24**, 608 (1960).
144. B. Cox, unpublished results.
145. R. Darras, H. Loriers, P. Baqué, and J. L. Berry, Alliages de zirconium utilisables dans le gaz carbonique aux températures élevées, *Proc. 2nd Intern. Conf. Use of Zirconium Alloys in Nuclear Reactors*, Mariánské Lázně, 1968, p. 285 (Skoda Pilsen).
146. R. Syre, J. Bonmarin, and A. Saulnier, Observations on the Preparation of Sheet Alloys of Zirconium for Corrosion Tests in CO₂, *Corr. et Anti-Corr.* **12**, 43 (1964).
147. D. W. Shannon, *Hanford Metallurgy Research Operation, Progress Reports*, USAEC Reports HW-82651 and HW-84281 (1964).
148. E. T. Hayes, A. H. Roberson, and R. H. Robertson, Heat Resistance of Zirconium in Several Media, *J. Electrochem. Soc.* **97**, 316 (1950).
149. J. M. Frenkel and M. Weisz, Étude des phénomènes de déformation et fissuration de gaines d'alliage zirconium-cuivre dans le gaz carbonique, *Proc. 2nd Intern. Conf. Use of Zirconium in Nuclear Reactors*, Mariánské Lázně, 1968, p. 311 (Skoda, Pilsen).
150. J. Brén and V. Vrtliková, Vliv Zavlhčení Kyslíčniku Uhlíčitého na Rychlost Koreze Slitiny Zr/Cu/Mo v Provozních Podmínkách ČS. Jaderných Elektráren, *Proc. 1st Intern. Conf. Use of Zirconium Alloys in Nuclear Reactors*, Mariánské Lázně, 1966, p. 251 (Skoda, Pilsen).
151. P. Mrkous, N. Staif, and K. Benda, Oxidation of Zr–0.8 Cu–0.8 Mo Alloy in Carbon Dioxide, *Proc. 2nd Intern. Conf. Use of Zirconium in Nuclear Reactors*, Mariánské Lázně, 1968, p. 151 (Skoda, Pilsen).

152. A. S. Zaimovsky, L. J. Tsuprun, and A. A. Tchaikovsky, Corrosion and Mechanical Properties of Zirconium Alloys in Helium and Carbon Dioxide Gases, *Proc. 2nd Intern. Conf. Use of Zirconium Alloys in Nuclear Reactors, Mariánské Lázně*, 1968 (Skoda, Pilsen).
153. J. Staab, Über die Hochtemperaturoxydation einiger Zirkoniumlegierungen, *Z. Phys. Chem. N.F.* **43**, 371 (1964).
154. R. Darras, La Corrosion du zirconium et de ses alliages par les gaz aux températures élevées, *Ind. At. Nos.* 1/2, 2 (1963).
155. R. Darras, H. Lories, and P. Baqué, Alliages zirconium-cuivre résistants à l'oxydation par le gaz carbonique aux températures élevées, *J. Nucl. Mat.* **17**, 79 (1965).
156. R. Darras, *Study of Oxidation Resistant Zirconium Alloys in Carbon Dioxide at High Temperatures*, French Report CEA-R-4103 (1971).
157. H. Lories, R. Darras, and P. Baqué, Amélioration de la résistance à l'oxydation du zirconium par des faibles additions de cuivre, *Proc. IAEA Conf. Thermodynamics of Nuclear Materials, Vienna*, 1966, p. 391 (SM-66/49).
158. J. P. Guerlet and P. Lehr, Contribution à l'étude de la corrosion par le gaz carbonique des alliages de zirconium, I. Oxydation des alliages zirconium-cuivre, *J. Nucl. Mat.* **28**, 152 (1968).
159. J. Decours, J. M. Frenkel, H. Lories, P. Baqué, and M. Weisz, Oxydation et fissuration des alliages ZrCu dans le CO₂, *J. Nucl. Mat.* **30**, 196 (1969).
160. P. Baqué, R. Darras, A. Lafon, and H. Lories, Protection du zirconium contre l'oxydation au moyen de revêtements métalliques, *J. Nucl. Mat.* **25**, 166 (1968); and USAEC Report WAPD-trans-0094.
161. J. P. Guerlet and P. Lehr, Contribution à l'étude de la corrosion par le gaz carbonique des alliages de zirconium, II. Oxydation des alliages zirconium-niobium, *J. Nucl. Mat.* **28**, 165 (1968).
162. F. Decool, Y. Gouchen, G. Orsier, and C. Ringot, Les Combustibles d'EL4: Évolution, technique et expérience du renouvellement en marche, *Proc. IAEA Conf. Experience from Operating and Fuelling Nuclear Power Plants, Vienna*, 1973, p. 477 (SM-178/9).
163. R. C. Asher, D. Davies, T. B. A. Kerstein, P. A. J. McCullen, and J. F. White, The Effects of Radiation on the Corrosion of Some Zirconium Alloys. *Proc. 4th Intern. Cong. Met. Corr., Amsterdam*, 1969, p. 178.
164. R. C. Asher, D. Davies, and T. B. A. Kerstein, The Corrosion of Some Zirconium Alloys Under Radiation in Moist Carbon Dioxide-Air Mixtures, *J. Nucl. Mat.* **49**, 189 (1973/74).
165. P. Hurst and C. Tyzack, The Effect of Environment on the In-Pile Corrosion and Hydrogen Pick-up of Some Zirconium Alloys, *Proc. British Nuclear Energy Soc., Conf. Effects of Environments on Materials Properties in Nuclear Systems, London*, 1971, Paper 4.
166. J. L. Bernard, H. Foulquier, and P. Thomie, Structures du coeur du réacteur eau lourde-gaz EL4, *Proc. 3rd Intern. Conf. Peaceful Uses Atomic Energy, Geneva*, Vol. 9 (1964), p. 3 (Paper 69).
167. H. Foulquier, Structures en alliages de zirconium des réacteurs à eau lourde. Expérience EL4 et perspectives d'avenir, *Proc. 2nd Intern. Conf. Use of Zirconium Alloys in Nuclear Reactors, Mariánské Lázně*, 1968, p. 465 (Skoda, Pilsen).
168. H. Bailey, C. Ringot, and H. Vidal, Les Alliages de zirconium-cuivre utilisés dans le gainage des éléments combustibles des réacteurs eau lourde/gaz, *Proc. 2nd Intern. Conf. Use of Zirconium in Nuclear Reactors, Mariánské Lázně*, 1968, p. 329 (Skoda, Pilsen).
169. R. N. Lyon, Liquid Metals, Chapter 49 in *Reactor Handbook*, Vol. 1, Materials, C. R. Tipton, Jr. (ed.), 2nd ed., Wiley-Interscience, New York (1960).
170. M. Davies and A. Draycott, Compatibility of Reactor Materials in Flowing Sodium, *Proc. 2nd Intern. Conf. Peaceful Uses Atomic Energy, Geneva*, Vol. 7 (1958), p. 94 (Paper 25).

171. R. F. Koenig, *Corrosion of Zirconium and Its Alloys in Liquid Metals*, USAEC Report KAPL-982 (1953).
172. R. L. Carter, R. L. Eichelberger, and S. Siegal, Recent Developments in the Technology of Sodium-Graphite Reactor Materials, *Proc. 2nd Intern. Conf. Peaceful Uses Atomic Energy, Geneva*, Vol. 7 (1958), p. 72 (Paper 705).
173. H. U. Borgstedt, G. Frees, and G. Drechsler, Korrosionsreaktionen sauerstoffempfindlicher Metalle in flüssigem Natrium mit Oxidgehalten, I. Reaktionen von Zirkonium und Zircaloy-2, *Werk. Korr.* **21**, 568 (1970).
174. L. Champeix, W. Graff, and J. Sannier, Effect of Various Additives on the Compatibility of Zirconium with Liquid Sodium, *Proc. IX^{me} Colloque de Métallurgie, Saclay*, 1966, p. 63; and CEA Report 2371 (1963).
175. A. B. McIntosh and K. Q. Bagley, Selection of Canning Materials for Reactors Cooled by Sodium/Potassium and Carbon Dioxide, *J. Inst. Met.* **84**, 251 (1956).
176. D. de L. Slatter, *Oxidation of Zirconium Alloy in Liquid Sodium at Different Oxygen Levels*, South African Report PEL-201 (1970).
177. G. J. C. Carpenter, Void Formation in Zirconium under Irradiation in the High-Voltage Electron Microscope, *Radiation Eff.* **19**, 189 (1973).
178. H. E. Johnson, *Corrosion and Activity Transfer in the SRE Primary Sodium System*, USAEC Report NAA-SR-5363 (1961).
179. C. Starr and S. Siegel, Sodium-Cooled Thermal Reactors, *Proc. 3rd Intern. Conf. Peaceful Uses Atomic Energy, Geneva*, Vol. 6 (1964), p. 294 (Paper 206).
180. L. L. Anderson and G. R. Hill, Corrosion of Zirconium and Zircaloy-2 in Fused KNO_3 - NaNO_2 - NaNO_3 , *Electrochem. Tech.* **4**, 157 (1966).
181. C. Hardy-Grena, A. Avogadro, and J. G. Wurm, Traitement superficiel d'alliages de zirconium par le nitrate de sodium fondu, *J. Nucl. Mat.* **25**, 296 (1968); and Euratom Report EUR-3476 (1968).
182. B. Cox, *Rate Controlling Processes During the Oxidation of Zirconium Alloys*, Atomic Energy of Canada Ltd. Report AECL-2777 (1967).
183. B. Cox, Rate Controlling Processes During the Pre-transition Oxidation of Zirconium Alloys, *J. Nucl. Mat.* **31**, 48 (1969).
184. P. J. Shirvington, Electron Conduction Through Oxide Films on Zircaloy-2, *J. Nucl. Mat.* **37**, 177 (1970).
185. W. Hübner and B. Cox, *Electrochemical Properties and Oxidation of Some Zirconium Alloys in Molten Salt at 300°–500°C*, Atomic Energy of Canada Ltd. Report AECL-4431 (1973).
186. N. Ramasubramanian, Localised Electron Transport in Corroding Zirconium Alloys, *J. Nucl. Mat.* **55**, 134 (1975); and *Proc. 1975 NACE Annual Meeting, Toronto*, 1975, Preprint 160.
187. P. J. Shirvington, The Mechanism of Radiation Enhancement of Zirconium Alloy Oxidation—Implications of New Data, *J. Nucl. Mat.* **42**, 108 (1972).
188. B. Cox, A. Technique for Studying the Rate Controlling Processes During Metal Oxidation, *Proc. 5th Intern. Conf. Met. Corrosion, Tokyo*, 1972, p. 682, NACE, Houston (1974).
189. P. J. Shirvington, A Mechanism for In-Reactor Oxidation of Zirconium Alloys from Oxide Electrical Characteristics, (I). Zircaloy-2, *J. Nucl. Mat.* **50**, 183 (1974).
190. P. J. Shirvington, A Mechanism for In-Reactor Oxidation of Zirconium Alloys from Oxide Electrical Characteristics, (II). Crystal-Bar Zirconium and Zr-1.2 wt. % Cr-0.8 wt. % Fe, *J. Nucl. Mat.* **52**, 1 (1974).
191. P. J. Shirvington, A Mechanism for In-Reactor Oxidation of Zirconium Alloys from Oxide Electrical Characteristics, (III). Zr-2.5 wt. % Nb, *J. Nucl. Mat.* **52**, 13 (1974).
192. R. A. Ploc, *Chemistry and Materials Div., Progress Reports*, Atomic Energy of Canada Ltd. Reports AECL-4204, 4259, and 4351 (1972).

193. H. E. Bartlett and K. E. Johnson, Cathodic Processes in Molten Nitrates and Nitrites, *J. Electrochem. Soc.* **114**, 64 (1967).
194. B. Cox, Catastrophic Oxidation of Zircalloys in Fused Salts at 300°C, *Oxid. Metals* **3**, 399 (1971).
195. D. E. Thomas, Corrosion of Zirconium Alloys, *Proc. 1st Intern. Conf. Peaceful Uses Atomic Energy, Geneva*, Vol. 9 (1955), p. 407.
196. E. A. Gulbransen and K. F. Andrew, Oxidation Studies on Zirconium Alloys in High Pressure Liquid Water at 360°C, *J. Electrochem. Soc.* **116**, 659 (1969).
197. F. Forscher, S. Kass, and K. Goldman, Mechanical Properties and Corrosion Behavior of Zircaloy-3, *Proc. Metallurgy Information Meeting, Ames, Iowa, 1956*, TID-7526, p. 69; and U.S. AEC Report WAPD-T-336 (1956).
198. B. Cox, *Recent Developments in Zirconium Alloy Corrosion Technology*, Progress in Nuclear Energy Ser. IV, Vol. 4, p. 166, Pergamon Press, Oxford (1961).
199. J. D. Grozier, L. S. Rubenstein, and J. G. Goodwin, Metallographic Study of Stringers in Inert Atmosphere Melted Zircaloy-2, *Trans. ASM* **52**, 812 (1960).
200. J. R. Moon, A Metallographic Examination of General White Spotting in Oxide Films on Zircaloy-2, *Corrosion Sci.* **8**, 109 (1968).
201. H. H. Klepfer *et al.*, *Specific Zirconium Alloy Design Programme*, Joint U.S. Euratom Programme, Reports appear under General Electric and EURAEC numbers: GEAP-3979 (EURAEC-422), 4076 (488), 4139 (529), 4211 (604), 4284 (754), 4368 (834), 4484 (943), 4821 (1375), 4840 (1460), 4960 (1538), 5065 (1574), 5134 (1654), 5188 (1740),—(1738), 5424 (1851), 5516 (1901), 5603, 5649, 5743; Summary Reports GEAP-4504 (EURAEC-1193) and GEAP-10044 (EURAEC-2130); U.S. Patent 3287111 (1965).
202. E. Hillner, *Hydrogen Absorption in Zircaloy-2 During Aqueous Corrosion; Effect of Environment*, USAEC Report WAPD-TM-411 (1964) and references therein.
203. N. J. M. Wilkins and J. N. Wanklyn, *The Kinetics of the Uptake of Corrosion Hydrogen by Zirconium Alloys*, UKAEA Report AERE-M787 (1960).
204. B. Cox, M. J. Davies, and A. D. Dent, *Hydrogen Absorption During Oxidation in Steam and Aqueous Solutions*, UKAEA Report AERE-M621 (1960).
205. B. Cox, Hydrogen Absorption by Zircaloy-2 and Some Other Alloys During Corrosion in Steam, *J. Electrochem. Soc.* **109**, 1 (1962); disc. p. 1213; and UKAEA Report AERE-3556 (1961).
206. J. N. Wanklyn, D. R. Silvester, J. Dalton, and N. J. M. Wilkins, *The Corrosion of Zirconium and Its Alloys in High Temperature Steam, Pt. II, The Uptake of Hydrogen During Corrosion*, UKAEA Report AERE-R3768 (1961).
207. D. W. Freer, D. R. Silvester, and J. N. Wanklyn, Hydrogen Uptake of Zirconium and Its Alloys During the Early Stages of Corrosion in Steam, *Corrosion* **24**, 137 (1965); and UKAEA Report AERE-R4531 (1964).
208. H. H. Klepfer, Hydrogen Uptake of Zirconium Alloys During Water and Steam Corrosion, *Corrosion* **19**, 285t (1963).
209. S. Kass, Hydrogen Pickup in Various Zirconium Alloys During Corrosion Exposure in High Temperature Water and Steam, *J. Electrochem. Soc.* **107**, 594 (1960).
210. B. Lustman, M. L. Bleiberg, E. S. Byron, J. N. Chirigos, J. G. Goodwin, and G. J. Salvaggio, Zircaloy Cladding Performs Well in PWR, *Nucleonics* **19**, 58 (1961).
211. J. M. Markowitz, *Internal Zirconium Hydride Formation in Zircaloy Fuel Element Cladding Under Irradiation*, US AEC Report WAPD-TM-351 (1963).
212. W. Yeniscavich, R. A. Wolfe, and R. M. Lieberman, Hydrogen Absorption by Nickel Enriched Zircaloy-2, *J. Nucl. Mat.* **3**, 271 (1959).
213. W. Yeniscavich, R. A. Wolfe, and R. M. Lieberman, Irradiation-Induced Hydrogen

- Absorption by Nickel-Enriched Zircaloy-2, *Proc. Nuclear Eng. Sci. Conf. (A.I.M.M. and P.E.)*, Cleveland 1959; and USAEC Report WAPD-T-912.
214. J. N. Wanklyn, L'Influence de l'hydrogène sur la corrosion du zirconium dans l'eau à haute température, *Proc. 3^{me} Colloque de Métallurgie, Saclay*, 1959, p. 137.
 215. S. Kass and W. W. Kirk, Corrosion and Hydrogen Absorption Properties of Nickel-Free Zircaloy-2 and Zircaloy-4, *Trans. ASM* **55**, 77 (1962).
 216. J. N. Chirigos, S. Kass, W. W. Kirk, and G. J. Salvaggio, Development of Zircaloy-4, *Proc. IAEA Conf. Fuel Element Fabrication, Vienna*, 1960, p. 19; and USAEC Report WAPD-T-1188 (1960).
 217. W. F. Bourgeois and J. N. Chirigos, *Development of Zirconium-Base Alloys*, USAEC Report WAPD-TM-546 (1965).
 218. S. Kass, *The Corrosion and Hydrogen Absorption Properties of Zircaloy-4 Alloys Containing Additions of Niobium*, USAEC Report WAPD-TM-647 (1967).
 219. S. Kass, *The Corrosion and Hydrogen Absorption Characteristics of Zirconium Alloys Containing Iron and Chromium in High Temperature Water*, USAEC Report WAPD-TM-517 (1968).
 220. S. Kass, *The Corrosion and Hydrogen Absorption Characteristics of Zirconium Alloys Containing 2.5% Tin and Additions of Iron, Chromium and Niobium*, USAEC Report WAPD-TM-619.
 221. A. A. Kiselev, V. A. Myshkin, A. V. Kozhevnikov, S. I. Korolev, and E. G. Shorina, Research on the Corrosion of Zirconium Alloys in Water and Steam at High Temperature Pressure, *Proc. IAEA Conf. Corrosion of Reactor Materials, Salzburg*, 1962, Vol. II, p. 67, and Atomic Energy of Canada Ltd., Translation, AECL-1724 (1963).
 222. I. K. Rosenfel'd, O. P. Olxovnikov, and A. A. Cydarikova, The Effect of the Water Composition on the Corrosion of Zirconium Alloys at High Temperatures and Pressures, *Proc. IAEA Conf. Corrosion of Reactor Materials, Salzburg*, 1962, Vol. II, p. 257; and AEC-TR-5374.
 223. A. D. Amaev, R. S. Ambartsumyan, V. V. Goncharov, *et al.*, Investigation of an Assembly of Rod Type Fuel Elements with Sintered UO_2 , with Zirconium Alloy Cladding and with Maximum Burnup of 68,000 MWd/TU, *Proc. 1st Intern. Conf. Use of Zirconium in Nuclear Reactors, Mariánské Lázně*, 1966, p. 143, Paper 7; Kurchatov Institute Report IAE-1181 (1966); and AEC-TR-6847.
 224. A. D. Amaev, R. S. Ambartsumyan, V. V. Goncharov, J. G. Ivanov, L. M. Lebedev, and E. P. Rysantsev, Investigation of the Behavior of Zirconium Alloys in Water and Steam-Water Mixture in the Reactor Loops, *Proceedings of the 2nd Int. Conf. on The Use of Zirconium Alloys in Nuclear Reactors, Mariánské Lázně*, 1968, p. 37, Paper 3 (Skoda, Pilsen); and Kurchatov Institute Reports IAE-1717 and IAE-1926 (1969).
 225. W. Evans, J. E. LeSurr, and W. R. Thomas, Heat Treated Zr-2.5 % Nb Pressure Tubes for Water-Cooled Power Reactors, presented at *CNA Ann. Conf.*, 1967, Atomic Energy of Canada Ltd. Report AECL-2890 (1967).
 226. A. D. Amaev, R. S. Ambartsumyan, A. A. Kiselev, *et al.*, Influence of Some Factors upon Hydriding and Variation of Properties of Zirconium Alloy with 1% Nb used for Fuel Element Cladding in Water-Moderated Water-Cooled Power Reactors, *Proc. 3rd Intern. Conf. Peaceful Uses of Atomic Energy, Geneva*, Vol. 9 (1964), p. 492 (Paper 342).
 227. I. S. Lupakov, B. S. Rodchenkov, and A. I. Gromova, Effect of Cold Deformation on the Corrosion Resistance of Zr-2.5 wt. % Nb Alloy, *Atomnaya Energiya* **24**, 91 (1968).
 228. A. D. Amaev, J. A. Anisimova, A. V. Nikulina, G. P. Saenko, A. V. Sedova, and M. B. Fiveisky, Corrosion Behaviour of Zirconium Alloys in Boiling Water Under Irradiation, *Proc. 4th Intern. Conf. Peaceful Uses Atomic Energy, Geneva*, Vol. 10, (1971), p. 537 (Paper 428).

229. U. Rösler, Corrosion Resistance of Improved Zirconium Alloys in High Temperature Steam, *Proc. USAEC Symp. Zirconium Alloy Development*, Castletwood, Calif., 1962, GEAP-4089, Paper 7.
230. D. L. Douglass and B. E. Dearing, *Effect of Heat Treatment on the Corrosion of Zr-2 at % Sn-2 at. % Nb*, USAEC Report KAPL-2071 (1960).
231. H. A. Fisch, *Hydrogen Absorption by Zr-2 at. % Sn-2 at. % Nb Alloy During Corrosion*, USAEC Report KAPL-2149 (1961).
232. D. L. Douglass, Creep and Corrosion Behaviour of Some High Strength Zirconium Alloys, *Nucl. Met.* **7**, 19 (1960).
233. D. L. Douglass and H. A. Fisch, The Effect of Heat Treatment on the Corrosion and Hydrogen Pickup Behaviour of a Zr-Sn-Nb Alloy in High Temperature Water and Steam, *J. Electrochem. Soc.* **111**, 787 (1964).
234. H. H. Klepfer, Zr-Nb Alloys for Boiling Water Reactor Service; Pt. I, Corrosion Resistance; Pt. II, Corrosion Hydrogen Embrittlement, *J. Nucl. Mat.* **9**, 65, 77 (1963); USAEC Report GEAP-3729 (1961).
235. W. C. Rous and C. J. Baroch, *Evaluation of Zirconium 1.5% Nb Cladding for Use in Boiling Water Environments*, USAEC Report GEAP-4098 (1962).
236. J. C. Tverberg and H. Richter, Development of Zr-Nb-Sn Alloys for Reactor Applications, *Proc. USAEC Conf. Zirconium Alloy Development*, Castletwood, Calif., 1962, GEAP-4089, Paper 4.
237. H. Richter, W. Rückdeschel, W. Spalthoff, and E. Starke, Influence of Neutron Irradiation on the Corrosion Behaviour and Mechanical Properties of Zr-Nb3-Sn1 and Zircaloy-2, *Proc. 1st Intern. Conf. Use of Zirconium Alloys in Nuclear Reactors*, Mariánské Lázně, 1966, p. 111; and *Atomkernenergie* **11**, 47 (1966).
238. U. Rösler, Studies on the Corrosion of Zirconium Alloys in Superheated Steam, *Proc. Symp. Corrosion in the Nuclear Industry*, Paris, 1961.
239. H. Rubel, W. Debray, and U. Rösler, Hydrogen Pickup and Embrittlement of Zircaloy-2, Zr-Nb1 and Zr-Nb2.5, *Nucleonik*, **4**, 159 (1964).
240. U. Rösler, *Research on Zirconium Hydride in Zircaloy-2 and Zr-Nb Alloys*, EURATOM Report EUR-2013d (1965).
241. J. Boulton, The Corrosion of Zirconium Alloys, *Proc. IAEA Conf. Corrosion of Reactor Materials*, Salzburg, 1962, Vol. II, p. 133.
242. W. Rückdeschel and P. Wincierz, Development of Corrosion Resistant Zr-Nb Alloys with High Strength for Water-Cooled Nuclear Reactors, *Proc. Conf. Eigenschaften und Anwendung Hochschmelzender und Reaktiver Metalle*, 1968, pp. 126-158.
243. B. Beyer, R. Juknat, and R. Rauschenbach, Corrosion of Zr-1 % Nb and Zr-2.5% Nb in Pressurised Water and Pressurised Steam. *Proc. Conf. Eigenschaften und Anwendung Hochschmelzender und Reaktiver Metalle*, 1968, pp. 102-116.
244. S. B. Dalggaard, Corrosion and Hydriding Behaviour of Some Zr-2.5% Nb Alloys in Water, Steam and Various Gases at High Temperature, *Proc. IAEA Conf. Corrosion of Reactor Materials*, Salzburg, 1962, Vol. II, p. 159; and Atomic Energy of Canada Ltd. Reports CR Met-911, AECL-1308, and AECL-1513.
245. W. R. Thomas, The Development of Zirconium Alloys for Pressure Tubes in Water-Cooled Power Reactors, *Proc. USAEC Symp. Zirconium Alloy Development*, Castletwood, Calif., 1962, GEAP-4089, Paper 2.
246. C. E. Ells, S. B. Dalggaard, W. Evans, and W. R. Thomas, Development of Zirconium-Niobium Alloys, *Proc. 3rd Intern. Conf. Peaceful Uses of Atomic Energy*, Geneva, Vol. 9, (1964), p. 91; and Atomic Energy of Canada Ltd. Report AECL-2022 (1964).
247. J. Boulton and M. G. Wright, Ozhennite 0.5—Its Potential and Development, *Proc. ASTM Symp. Applications Related Phenomena in Zirconium and Its Alloys*, Philadelphia, 1968, ASTM-STP 458, p. 325.

248. P. A. Ross-Ross, Fuel Channel Development for Canada's Power Reactors, presented at 82nd Ann. Meeting Eng. Inst. Canada, 1968, Atomic Energy of Canada Ltd. Report AECL-3126 (1968).
249. P. A. Ross-Ross, W. Evans, and W. J. Langford, Experience with Zirconium-Alloy Pressure Tubes, *Proc. IIIrd Intern. Amer. Conf. Materials Technology, Rio de Janeiro*, 1962; Atomic Energy of Canada Ltd. Report AECL-4262 (1972).
250. S. Kass, The Effects of Heat Treatment on the Corrosion and Hydrogen Absorption Characteristics of a Zirconium-Niobium-Copper (Zr + 2.5% Nb + 0.5% Cu) Alloy, USAEC Report WAPD-TM-500 (1966); WAPD-TM-754 (1970); and *Corrosion* **27**, 443 (1971).
251. D. S. Kneppel, *Effect of Temperature and Pressure on Steam Testing of Zirconium Alloys*, USAEC Report NMI-119 (1954).
252. J. P. Pemsler, The Corrosion of Zirconium Alloys in 900°F and 1000°F Steam, *Proc. AEC-EURATOM Conf. Aqueous Corrosion of Reactor Materials, Brussels*, 1959, TID-7587, p. 96; and USAEC Report NMI-1208 (1958).
253. R. D. Misch and C. J. van Drunen, *Corrosion Studies of Ternary Zirconium Alloys in High-Temperature Water and Steam*, USAEC Report ANL-6370 (1961).
254. J. P. Pemsler, *Corrosion of Zirconium Alloys in 900°F and 1000°F Steam*, USAEC Report NMI-1235 (1960).
255. S. Greenberg and C. A. Youngdahl, Corrosion of Zirconium Alloys Containing Minor Additions of Iron and Copper or Nickel in Superheated Steam at 540° and 650°C and 600 psig, *Corrosion* **21**, 113 (1965); and USAEC Report ANL-6714 (1964).
256. W. E. Berry, D. A. Vaughan, and E. L. White, Hydrogen Pickup During Corrosion of Zirconium Alloys, *Corrosion* **17**, 109t (1961); and USAEC Report BMI-1380 (1959).
257. W. E. Berry, E. L. White, and F. W. Fink, *Effect of Additions to Zircaloy on Hydrogen Pickup During Aqueous Corrosion*, USAEC Report BMI-1402 (1959).
258. J. A. DeMastry, F. R. Shober, and R. F. Dickerson, *Development of High-Strength Corrosion Resistant Zirconium Alloys*, USAEC Report BMI-1418 (1960).
259. W. K. Boyd, D. J. Maykuth, R. S. Peoples, and R. I. Jaffee, *Compositional Factors Affecting Corrosion Resistance of Zirconium in High-Temperature Water and Steam*, USAEC Report, BMI-1-56 (1955).
260. A. E. Bibb, A. P. Beard, and D. L. Douglass, *Investigations of Binary Zirconium Alloys*, USAEC Report KAPL-2162 (1960).
261. B. Cox, *The Effect of Some Alloying Additions on the Oxidation of Zirconium in Steam*, UKAEA Report (AERE-R-4458 (1963).
262. J. N. Wanklyn, J. T. Demant, and D. Jones, *The Corrosion of Zirconium and Its Alloys by High Temperature Steam, Pt. I, Effect of Alloy Composition*, UKAEA Report AERE-R3655 (1961).
263. J. N. Wanklyn, The Corrosion of Zirconium and Its Alloys in High Temperature Steam, *Proc. Symp. Corrosion dans L'Industrie Nucléaire, Paris* (1961).
264. L. Bangert and K. Henneman, Zirconium and Zirconium Alloys for Water-Cooled Reactors, *Proc. IAEA Symp. Fuel Element Fabrication with Special Emphasis on Cladding Materials, Vienna*, 1960; and *Metall* **14**, 704 (1960).
265. R. Syre, J. Orsay, A. Guildhandis, M. Croutzeilles, R. Bourbon, and J. Bonmarin, *Recherches d'Alliages de zirconium*, EURATOM Report EUR-2074f (1965).
266. G. Jangg, E. F. Baroch, R. Kieffer, and B. Lindinger, Studies on the Corrosion Behaviour of Zirconium Alloys, *Werk. Korr.* **22**, 989 (1971).
267. A. S. Zaimovskii and A. V. Nikulina, Effect of Impurities and Alloy Elements on Zirconium Corrosion in High-Temperature Water, *Proc. 1st Intern. Conf. Use of Zirconium Alloys in Nuclear Reactors, Mariánské Lázně*, 1966, p. 183 (Skoda, Pilsen).

268. J. Blanchet, H. Coriou, L. Grall, P. Olivier, and M. Pelras, Influence des éléments d'addition et de la structure sur la corrosion d'alliages de zirconium dans l'eau et la vapeur à haute température, *Proc. of 2nd Int. Conf. on The Use of Zirconium Alloys in Nuclear Reactors, Mariánské Lázně*, 1968, p. 173 (Skoda, Pilsen), *Én. Nucl.* **11**, 345 (1969); and USAEC Report AEC-tr-7235.
269. C. D. Williams, C. E. Ells, and P. R. Dixon, Development of High-Strength Zirconium Alloys, *Can. Met. Quart.* **11**, 257 (1972).
270. E. M. Schulson, *Order Strengthening of Zirconium Alloys* (Materials Res. in AECL) (1974), p. 13; Atomic Energy of Canada Ltd. Report AECL-4842.
271. D. J. Cameron and A. E. Unger, *The Corrosion of Zr₃Al Based Alloys by Carbon Dioxide and a Carbon Dioxide-Water Vapour Mixture*, Atomic Energy of Canada Ltd. Reports: Pt. I, AECL-4662; Pt. II, AECL-4665 (1974).
272. J. R. Moon and E. W. Evans, Some Observations on the Oxidation of Zr-Cu-Mo and Zr-Cu-W Alloys in Steam at 400°, 1500 psi, *Corrosion Sci.* **9**, 323 (1969).
273. A. Grutter, *Corrosion of Zirconium Alloys in Superheated Steam: Results of Long-Term Tests*, Swiss Report EIR-184 (1970) and USAEC-Report AEC-tr-7287.
274. G. P. Walters, *Preliminary Corrosion Tests of Some Steam Treated Zirconium Alloys*, UKAEA Report AERE-M1854 (1967).
275. T. E. Clare, *Corrosion Resistance of Some Alpha-Dispersoid Zirconium Alloys in Water Vapour at 400°C and 500°C*, Australian Report AAEC/TM-601 (1971).
276. E. Tolksdorf, Corrosion Behaviour of New Zr Alloys, *J. Nucl. Mat.* **51**, 330 (1974).
277. E. Tolksdorf, Die Oxydation von Intermetallischen Zirkoniumlegierungen in Sauerstoff und Wasserdampf bei 400°C, *Werk. Korr.* **25**, 430 (1974).
278. J. Hino, *Long-Term Corrosion Behaviour of Zircaloy*, USAEC Reports WADP-MRP-107 and 108.
279. S. Kass, Aqueous Corrosion of the Zircalloys at Low Temperatures, *J. Nucl. Mat.* **28**, 315 (1969).
280. B. Cox, Low Temperature (<300°C) Oxidation of Zircaloy-2 in Water, *J. Nucl. Mat.* **25**, 310 (1968).
281. B. Cox, Comments on Aqueous Corrosion of the Zircalloys at Low Temperatures, *J. Nucl. Mat.* **30**, 351 (1969).
282. B. Cox, *The Morphology of Zirconia Films and Its Relation to the Oxidation Kinetics*, Atomic Energy of Canada Ltd. Report AECL-3285 (1969).
283. D. H. Bradhurst, P. J. Shirvington, and P. M. Heuer, The Effects of Radiation and Oxygen on the Aqueous Oxidation of Zirconium and Its Alloys at 290°C, *J. Nucl. Mat.* **46**, 53 (1973).
284. E. Tolksdorf, The Transition Phenomenon, a Hypothesis Concerning the Behaviour of Zirconium and Its Alloys During Oxidation in Oxygen, *Corrosion Sci.* **14**, 565 (1974).
285. B. Griggs, H. P. Maffei, and D. W. Shannon, Multiple Rate Transitions in the Aqueous Corrosion of Zircaloy, *J. Electrochem. Soc.* **109** (1962); and USAEC Report HW-6781 (1960).
286. W. E. Berry, paper presented at *10th USAEC Corrosion Symp.* (1961).
287. S. Kass, Corrosion of Prefilmed Zircaloy, *Corrosion* **23**, 374 (1967).
288. S. Kass, The Aqueous Corrosion of Zircaloy Containing Prior Corrosion Films, presented at *24th NACE Annual Meeting, Cleveland*, 1968, Preprint No. 1.
289. W. A. Bostrom, *The High Temperature Oxidation of Zircaloy in Water*, USAEC Report WADP-104 (1954).
290. A. W. Lemmon Jr., *Studies Relating to the Reaction Between Zirconium and Water at High Temperatures*, USAEC Report BMI-1154 (1957).
291. R. H. Leyse, *Zircaloy-2 and Type-304 Stainless Steel at 2000°F in Water-Steam for Brief Times*, USAEC Report APED-4413 (1964).

292. R. C. Liimatainen, R. O. Ivins, M. F. Deerwester, and F. J. Testa, *Studies of Metal–Water Reactions at High Temperatures, Pt. II*, USAEC Report ANL-6250 (1962).
293. L. Baker, Jr., R. L. Warchal, R. C. Vogel, and M. Kilpatrick, *Studies of Metal–Water Reactions at High Temperatures, Pt. I*, USAEC Report ANL-6257 (1961).
294. L. Baker, Jr., and L. C. Just, *Studies of Metal–Water Reactions at High Temperatures, Pt. III*, USAEC Report ANL-6548 (1962).
295. H. M. Higgins and R. D. Shultz, *The Reaction of Metals with Water and Oxidising Gases at High Temperatures*, USAEC Report IDO-28000 (1957).
296. H. M. Higgins, *The Reaction of Zircaloy-2 with Water and with Uranyl Sulphate Solution: Final Report*, USAEC Report AGC-AE-40.
297. B. Lustman, *Zirconium–Water Reaction Data and Application to PWR Loss of Coolant Accident*, USAEC Reports WAPD-137 (1955) and WAPD-SC-543 (1957).
298. L. Baker, Jr., and R. O. Ivins, Analysing the Effects of a Zirconium–Water Reaction, *Nucleonics* **23**(7), 70 (1963).
299. P. L. Rittenhouse, Fuel-Rod Failure and Its Effects in Light-Water Reactor Accidents, *Nuclear Safety* **12**, 487 (1971); and *Power Eng.* **78**(3), 53 (1974).
300. M. J. Bentley and F. W. Trowse, *The Embrittlement of Zircaloy Fuel Cladding by Corrosion in LOCA Conditions*, UKAEA Report TRG-R 2498(S), 1974.
301. G. J. Scatena, Behaviour of BWR/6 Fuel During Loss of Coolant Conditions, *Proc. British Nuclear Energy Soc. Conf. Nuclear Fuel Performance*, London, 1973, Paper 85.
302. J. C. Hesson, R. O. Ivins, R. E. Wilson, K. Nishio, and C. Barnes Jr., *Laboratory Simulations of Cladding-Steam Reactions Following LOCA in Water-Cooled Power Reactors*, USAEC Report ANL-7609 (1970).
303. P. L. Rittenhouse, *Progress in Zircaloy Cladding Failure Modes Research*, USAEC Report ORNL-TM-3188 (1970).
304. D. O. Hobson, R. D. Waddell, P. L. Rittenhouse, and C. G. Lawson, *Nuclear Safety Program Annual Progress Report to December 31, 1970*, USAEC Report ORNL-4647 (1970), pp. 2–47.
305. K. M. Rose and E. D. Hindle, The Deformation of Zircaloy-2 Fuel Cladding Under Loss of Coolant Accident Transients, paper presented at *British Nuclear Energy Soc. Conf. Nuclear Fuel Performance*, London, 1973, Paper 83.
306. D. O. Hobson and P. L. Rittenhouse, *Embrittlement of Zircaloy-Clad Fuel Rods by Steam During LOCA Transients*, USAEC Report ORNL-4758 (1972).
307. R. E. Pawel, Oxygen Diffusion in β -Zircaloy During Steam Oxidation, *J. Nucl. Mat.* **50**, 247 (1974); also *J. Nucl. Mat.* **49**, 281 (1973/74).
308. C. V. Taylor and J. G. Goodwin, *Effect of Temperature and Time on Zircaloy Oxide Formation and Its Removal by Pickling*, USAEC Report WAPD-TM-786 (1968).
309. S. Kass, Corrosion Testing of Two Zirconium Alloys, *Corrosion* **16**, 93t (1960).
310. S. Kass, D. J. Fontanese, A. E. Oaks, and D. C. Scott, *Pickling of the Zircaloys Prior to Corrosion Exposure*, USAEC Report WAPD-TM-141 (1958).
311. D. W. Shannon and B. Griggs, *Preparing Zircaloy-2 for Autoclave Testing*, USAEC Report HW-60433 (1959).
312. S. Kass, Effect of Residual Etchant on the Corrosion Behaviour of Zircaloy-2, *Corrosion* **7**, 566t (1961).
313. F. H. Krenz, *A Preliminary Study of the Effect of Added Fluoride on the Corrosion of Zircaloy-2 in Water at 300°C*, Atomic Energy of Canada Ltd. Report AECL-1507 (1962).
314. E. Hillner and H. D. Cook, *Fluorine Content of Zircaloy Corrosion Films*, USAEC Report WAPD-T-1639 (1963).
315. W. E. Berry, Effect of Fluoride Ions on the Aqueous Corrosion of Zirconium Alloys, *Proc. ASTM Symp. Corrosion of Zirconium Alloys*, New York, 1963, ASTM-STP 368, p. 28.

316. W. E. Berry, E. L. White, and F. W. Fink, *Zircaloy-4 Corrosion in Halide Solutions and at Crevices in High Temperature Water*, USAEC Report BMI-1571 (1962).
317. R. S. Young, *Corrosion of Zircaloy-2 in Steam Containing Fluoride-Ion Additions*, USAEC Report APED 4145 (1963).
318. R. E. Moore and E. Ram, *Evaluation of Viton and Other Non-metallic Gasketing Materials in Contact with Structural Materials*, USAEC Report WAPD-BT-22 (1961), p. 71.
319. M. J. Notley, R. D. MacDonald, G. W. Parry, and G. M. Allison, *The Irradiation of Defected Zircaloy-2 Clad UO_2 Containing Fluoride Impurities*, Atomic Energy of Canada Ltd. Report CRFD-1067 (1961); and *Nucleonics* **19**, 77 (1961).
320. K. Beg and F. Brown, *Preliminary Study of Pick-up and Release of Fluorine by Zircaloy*, Atomic Energy of Canada Ltd. Report AECL-1903 (1964).
321. J. N. Wanklyn, Recent Studies of the Growth and Breakdowns of Oxide Films on Zirconium and Its Alloys, *Proc. ASTM Symp. on the Corrosion of Zirconium Alloys*, New York, 1963, ASTM-STP 368, p. 58.
322. J. T. Demant and J. N. Wanklyn, *The Effects of Contamination on the Oxidation of Zirconium in Steam*, UKAEA Report AERE-R4788 (1965).
323. A. Sietniks and G. Östberg, Influence of Surface Preparation and Fluorine Contamination on the Corrosion of Zircaloy-2 in Water and Steam, *British Corrosion J.* **3**, 7 (1968).
324. M. Warzee, C. Sonnen, and Ph. Berge, Influence du traitement de surface sur la corrosion de deux alliages de zirconium dans l'eau sous pression et dans la vapeur surchauffée à haute température, *Proc. 2nd Intern. Conf. Use of Zirconium Alloys in Nuclear Reactors, Mariánské Lázně*, 1968, p. 485; and EURATOM Report EUR-3386f (1967).
325. E. Möller and N. Starfelt, Microanalysis of Fluorine in Zircaloy by the Use of the ^{19}F (p. $\alpha\gamma$) ^{16}O Reaction, *Nucl. Instr. Meth* **50**, 225 (1967).
326. D. A. Vermilyea, The Crystallisation of Anodic Tantalum Oxide Films in the Presence of a Strong Electric Field, *J. Electrochem. Soc.* **102**, 207 (1955).
327. L. Young, Anodic Oxide films; Influence of the Film Present Before Anodisation, *Trans. Faraday Soc.* **53**, 841 (1957).
328. R. E. Pawel, Procedure for Stripping Anodic Oxide Films from Tantalum and Niobium, *Rev. Sci. Instr.* **35**, 1066 (1964).
329. W. D. MacKintosh, Investigation of Fluorine Deposits on Zircaloy Surfaces by Proton Activation, *Nucl. Tech.* **13**, 65 (1972).
330. B. Cox, *The Effect of Surface Preparation and Neutron Irradiation on the Corrosion of Zircaloy-2 in High Temperature Aqueous Solutions*, UKAEA Report AERE-C/M353 (1958).
331. J. E. Bailey, Electron Microscope Observations on the Precipitation of Zirconium Hydride in Zirconium, *Acta Met.* **11**, 267 (1963).
332. D. O. Northwood and R. W. Gilbert, Comments on the Preparation of Thin Foils of Zirconium and Zirconium Alloys for Electron Microscopy, *J. Aust. Inst. Met.* **18**, 158 (1973).
333. A. J. Bedford and D. R. Miller, Zirconium Hydride Precipitates in Zirconium, *J. Aust. Inst. Met.* **17**, 120 (1972).
334. P. J. Shirvington, D. H. Bradhurst, and P. M. Heuer, Accelerated Oxidation of Zirconium Alloys—Significance of Surface Preparation, *J. Nucl. Mat.* **44**, 79 (1972).
335. J. Cotton, paper presented at *Symp. sur la corrosion dans l'industrie nucléaire*, Paris, 1961.
336. B. Cox, Environmentally Induced Cracking of Zirconium Alloys, *Corrosion* **28**, 207 (1972).
337. B. Cox, *Destructive Internal Oxidation of Zircaloy-2 in Steam Under Irradiation at 300°C*, UKAEA Report AERE-C/R 2826 (1959).
338. L. G. Rubenstein, J. G. Goodwin, and F. L. Shubert, Effect of Five Impurities on the High Temperature Water and Steam Corrosion Resistance of Zircaloy-2, *Corrosion* **18**, 45t (1962).

339. S. Kass and J. D. Grozier, Effect of Carbon Content on Corrosion and Tensile Properties of Zircaloy-2, *Corrosion* **20**, 158t (1964).
340. S. Kass, J. D. Grozier, and F. L. Shubert, Effects of Silicon, Nitrogen and Oxygen on the Corrosion and Hydrogen Absorption of Zircaloy-2, *Corrosion* **20**, 350t (1964); and USAEC Report WAPD-283 (1963).
341. F. L. Shubert, H. C. Twiehaus, E. J. Enrico, and R. W. Staehle, *Evaluation of Columbia National Sponge*, USAEC Report WAPD-TM-246 (1960).
342. S. Kass, *The Effect of Silicon on the Corrosion and Hydrogen Absorption Characteristics of Zircaloy-4 and Nickel-Free Zircaloy-2*, USAEC Report WAPD-TM-544 (1966).
343. L. S. Rubenstein, J. G. Goodwin, and F. L. Shubert, Effect of Oxygen on the Properties of Zircaloy-2, *Trans. ASM* **54**, 20 (1961).
344. J. Delafosse and P. Poeydomenge, A Study of Zircaloy Type Alloys: Influence of Impurities on Zircaloy-2 Water Corrosion and Mechanical Properties, *Proc. 1st Intern. Conf. Use of Zirconium Alloys in Nuclear Reactors, Mariánské Lázně*, 1966, p. 271 (Skoda, Pilsen).
345. J. Delafosse and P. Poeydomenge, Étude de l'influence du silicium sur les alliages du type zircaloy-2 et zircaloy-4, *Proc. 2nd Intern. Conf. Use of Zirconium Alloys in Nuclear Reactors, Mariánské Lázně*, 1968, p. 121 (Skoda, Pilsen).
346. J. R. Moon, A Metallographic Examination of General White Spotting in Oxide Films on Zircaloy-2, *Corrosion Sci.* **8**, 109 (1968).
347. H. S. Kalish and H. M. Cobb, Investigation of the Effects of Fabrication Variables on the Corrosion Resistance of Zircaloy-2, *Trans. ASTM* **54**, 247 (1961).
348. J. H. Schemel, Effect of Heat Treatment on the Structure, Mechanical Properties, and Corrosion Resistance of Heavy Forged Sections of Zircaloy-2, *Trans. AIME* **221**, 1129 (1961).
349. H. Demars, J. P. Givord, and M. Armand, Influence de la structure du zircaloy-2 sur la résistance à la corrosion par la vapeur d'eau, *Mem. Sci., Rev. Met.* **62**, 269 (1965).
350. R. F. Mocharnyuk, High Temperature Oxidation of Zirconium in Cold-Hardened and Recrystallised States, *Zh. Fiz. Khim.* **35**, 112 (1961).
351. C. F. Britton and J. N. Wanklyn, Inhibition by Boric Acid of the Oxidation of Zirconium High Pressure Steam, *J. Nucl. Mat.* **5**, 326 (1962).
352. C. F. Britton, J. V. Arthurs, and J. N. Wanklyn, Further Studies on the Inhibition by Boric Acid of the Oxidation of Zirconium in High Pressure Steam, *J. Nucl. Mat.* **15**, 263 (1965); and UKAEA Report AERE-R4702 (1964).
353. A. B. Johnson, Jr., Corrosion and Failure Characteristics of Zirconium Alloys in High Pressure Steam in the Temperature Range 400 to 500°C, *Proc. Symp. Applications Related Phenomena in Zirconium and Its Alloys, Philadelphia*, 1968, ASTM-STP 458, p. 271; and USAEC Report, BNWL-SA-1929 (Pt. 2), 1968.
354. B. Cox, *Accelerated Oxidation of Zircaloy-2 in Supercritical Steam*, Atomic Energy of Canada Ltd. Report AECL-4448 (1973).
355. B. Cox, Stress Corrosion Cracking of Zircaloy-2 in Neutral Aqueous Chloride Solutions at 25°C, *Corrosion* **29**, 157 (1973); and Atomic Energy of Canada Ltd. Report AECL-4353 (1972).
356. R. L. Cowan, Discussion of paper presented at *Intern. Conf. High Temperature High Pressure Electrochemistry in Aqueous Solutions, Guildford, Surrey*, 1973 (NACE).
357. H. P. Maffei, *Effect of Oxygen on Hydrogen Pickup of Zircaloys During Autoclaving*, USAEC Report HW-72266 (1962).
358. F. H. Krenz, *Can Hydrogen Pick-up in Zircaloy Be Prevented*, Atomic Energy of Canada Ltd. Report AECL-1626 (1962).
359. R. J. Davies, T. H. Mauney, and J. R. Hart, Corrosion of Zircaloy-2 by Hydrogen Peroxide at Elevated Temperatures, *J. Electrochem. Soc.* **113**, 1222 (1966).

360. P. E. C. Bryant, Round-Robin Tests to Develop a Standard Autoclave Testing Procedure for Zirconium Alloys, *Proc. Symp. Applications-Related Phenomena in Zirconium and Its Alloys*, Philadelphia, 1968, ASTM-STP 458, p. 306.
361. E. J. Callahan and J. F. Kabat, *The Effects of Silica in Autoclave Test Water on the Steam Corrosion of Zircaloy*, USAEC Report KAPL-M-6748 (1968).
362. F. H. Krenz, The Steam and Water Corrosion of Zirconium Alloys, *Proc. 1st Intern. Cong. Metallic Corrosion*, London, 1961, p. 462 (Butterworth).
363. B. Cox and C. Roy, *The Use of Tritium as a Tracer in Studies of Hydrogen Uptake by Zirconium Alloys*, Atomic Energy of Canada Ltd. Report AECL-2519 (1965).
364. S. Kass, *Influence of Prior Corrosion History upon the Hydrogen Pick-up by Zircaloy During Subsequent Exposure in Hot Water*, USAEC Report WAPD-TM-906 (1970).
365. H. Coriou, L. Grall, J. Meunier, M. Pelras, and H. Willermoz, Corrosion du zircaloy dans divers milieux alcalins à haute température, *J. Nucl. Mat.* **7**, 320 (1963); and *Proc. IAEA Conf. Corrosion of Reactor Materials*, Salzburg, 1962, Vol. 2, p. 193.
366. H. P. Maffei, *Effect of Lithium Hydroxide Leakage on the High Temperature Corrosion of Zircaloy-2*, USAEC Report HW-78819 (1963).
367. A. M. Andrako, *The Effect of Media on the Corrosion Resistance of Zircaloy-2*, USAEC Report KAPL-M-6102 (1963).
368. R. A. Murgatroyd and J. Winton, Hydriding of Zircaloy-2 in Lithium Hydroxide Solutions, *J. Nucl. Mat.* **23**, 249 (1967).
369. S. Kass, Corrosion and Hydrogen Pickup of Zircaloy in Concentrated Lithium Hydroxide Solutions, *Corrosion* **25**, 30 (1969); and USAEC Report WAPD-TM-656 (1967).
370. E. Hillner and J. Chirigos, *The Effect of Lithium Hydroxide and Related Solutions on the Corrosion Rate of Zircaloy in 680°F Water*, USAEC Report WAPD-TM-307 (1962).
371. G. H. Jenks, Radiation-Induced Corrosion of Zircaloy-2 and Zirconium, in *Fluid Fuel Reactors*, A. D. Lane, H. G. MacPherson, and F. Maslan (eds.), Addison-Wesley, Reading, Mass. (1958), p. 732.
372. B. Cox, K. Alcock, and F. W. Derrick, The Mechanism of the Fission Fragment Induced Corrosion of Zircaloy-2, *J. Electrochem. Soc.* **108**, 29 (1961); and UKAEA Report AERE-R2932 (1959).
373. W. E. Kuhn, High Temperature and High Pressure Corrosion of Zirconium in Hydrochloric Acid, *Corrosion* **16**, 136t (1960); **18**, 103t (1962); **19**, 169t (1963).
374. M. W. Mallett, W. M. Albrecht, and R. E. Bennett, Reaction of Zirconium with Water Vapor at Subatmospheric Pressures, *J. Electrochem. Soc.* **104**, 349 (1957).
375. T. Maekawa and J. Kai, High Temperature Oxidation of Zirconium and Its Alloys in Water Vapour, *Nippon Kinzoku Gakkaishi* **24**, 581 (1960).
376. D. E. Thomas and S. Kass, Effect of Prior Corrosion History on the Corrosion of Zircaloy-2 in High Temperature Water, *J. Electrochem. Soc.* **103**, 478 (1956).
377. D. E. Thomas and S. Kass, Effect of Pre-oxidation in Oxygen on the Steam Corrosion Behaviour of Zircaloy-2, *J. Electrochem. Soc.* **104**, 261 (1957).
378. S. Kass and D. B. Scott, Effect of Partial Dissolution of the Oxide Film on the Aqueous Corrosion Resistance of Zircaloy-2, *J. Electrochem. Soc.* **109**, 92 (1962).
379. H. H. Klepfer and D. L. Douglass, Factors Limiting the Use of Zirconium Alloys in Superheated Steam, *Proc. ASTM Symp. Corrosion of Zirconium Alloys*, New York, 1963, ASTM-STP 368, p. 118.
380. I. H. Dyce, Corrosion of Zircaloy Fuel Cladding. The Influence of High Heat Fluxes, *Nucl. Eng.* **9**, 253 (1964).
381. K. C. Thomas and R. J. Allio, Prediction by Computer of Corrosion and Hydriding of Zircaloy-4 Under Heat Transfer Conditions, *Trans. ASM* **58**, 658 (1965).
382. C. R. Johnson, D. W. Koch, and T. M. Campbell, Corrosion and Hydriding of Zircaloy Under Heat Transfer Conditions in Pressurised Water, *Trans. ANS* **9**, 30 (1966).

383. M. M. Rubright and D. W. Koch, Corrosion and Hydriding of Zircalloys Under Heat Transfer Conditions, paper presented at *25th Ann. NACE Meeting, Houston*, 1969, Preprint 78.
384. H. Coriou, L. Grall, J. Huré, M. Pelras, and H. Willermoz, Étude de l'influence de divers facteurs sur la corrosion du zircaloy par l'eau ou la vapeur à haute température et sur l'absorption de l'hydrogène par le métal, *Én. Nucl.* **4**, 109 (1962); and C.E.A. Report DM-1114 (1961).
385. W. K. Anderson and M. J. McGoff, *Corrosion of Zircaloy in Crevices Under Nucleate Boiling Conditions*, USAEC Report KAPL-2203 (1962).
386. J. N. Wanklyn and R. Aldred, Rectification by Zircaloy-2 in High-Temperature Water, *J. Electrochem. Soc.* **106**, 529 (1959).
387. E. Hillner, Corrosion and Hydriding Performance of Zircaloy Tubing After Extended Exposure in the Shippingport PWR, *Proc. Conf. Zirconium in Nuclear Applications, Portland, Oregon*, 1973, ASTM-STP-551, p. 449.
388. O. S. Ivanov and V. K. Grigorovich, Structure and Properties of Zirconium Alloys, *Proc. 2nd Intern. Conf. Peaceful Uses Atomic Energy, Geneva*, Vol. 5 (1958), p. 34 (Paper 2046).
389. B. Cox, *Long Term Corrosion Behaviour of Zr-2.5 wt. % Nb Alloy*, Atomic Energy of Canada Ltd. Report (to be published).
390. B. Cox and T. Johnston, The Oxidation and Corrosion of Niobium, *Trans. AIME* **227**, 36 (1963).
391. J. E. LeSurr and P. E. C. Bryant, The Effect of Water Chemistry on the Oxidation of Zirconium Alloys Under Reactor Radiation, *Proc. 23rd Ann. NACE Conf. Symp. High Purity Water Corrosion of Metals*, 1967, p. 42; and Atomic Energy of Canada Ltd. Report AECL-2797 (1968).
392. W. Huetig, Influence of Nitrogen Content on the Corrosion Behaviour of Zr-1 % Nb in High Temperature Water and Steam. *Proc. Conf. Eigenschaften und Anwendung Hochschmelzender und Reaktiver Metalle*, 1968, pp. 102-116.
393. D. O. Northwood and L. E. Bahen, *Correlation of Microstructure and Corrosion Performance of Zr-1.15 wt. % Cr-0.1 wt. % Fe in Water and Steam*, Atomic Energy of Canada Ltd. Report AECL-5019 (1975).
394. J. Delafosse and P. Poeydomenge, Étude de l'influence de l'azote sur les alliages du type Zr-Cr-Fe, *Proc. 2nd Intern. Conf. Use of Zirconium Alloys in Nuclear Reactors, Mariánské Lázně*, 1968, p. 93 (Skoda, Pilsen).
395. *Annual Progress Reports of Metallurgy Department*, Danish Atomic Energy Commission, Risø, Reports 225 (1970) and 244 (1971).
396. W. J. Bentley and F. W. Trowse, *The Corrosion Behaviour of Zr/Cr/Fe Alloy Fuel Tube*, UKAEA Report TRG Memo 4904(s) (1969).
397. G. Ullrich and K. W. Wiedemann, Das Korrosionsverhalten von Zirkonium und Zr-Cr legierungen in Dampf bei Temperaturen Zwischen 235° und 700°C, *Z. für Metallkunde* **62**, 899 (1971); and Atomic Energy of Canada Ltd., Translation, AECL-4502 (1973).
398. B. Cox, Effects of Irradiation on the Oxidation of Zirconium Alloys in High Temperature Aqueous Environments, *J. Nucl. Mat.* **28**, 1 (1968).
399. G. H. Jenks *et al.*, *Homogeneous Reactor Project, Quarterly Progress Reports*, USAEC Report ORNL-1813, 1943, 2004, 2057, 2096, 2148, 2222, 2272, 2331, 2379, and 2432 (1954-1957).
400. G. E. Galonian, R. E. Callahan, and W. Koenig, *Effects of Radiation on the Corrosion of Metallic Materials in 580°F Water*, USAEC Report KAPL-M-GEG 4 (1955); and paper presented at *15th NACE Ann. Meeting* (1958).
401. K. S. Warren and R. J. Davies, *In-Reactor Autoclave Corrosion Studies—LITR, I. Outline of Methods and Procedures*, USAEC Report ORNL-CF-57-5-110 (1957).

402. H. C. Savage, G. H. Jenks, and W. D. Reel, *In-Pile Corrosion Test Loops for Aqueous Homogeneous Reactor Solutions*, USAEC Report ORNL-2977 (1960).
403. B. Cox, The Effect of Fission Fragment and Neutron Irradiation on the Kinetics of Zirconium Oxidation, *Proc. 4th Intern. Symp. Reactivity of Solids*, Amsterdam, 1960, p. 425 (Elsevier).
404. J. D. Eichenberg, R. M. Lieberman, and F. P. Mrazik, *Irradiation of UO₂ Fuel Rods—The X-I-1 Experiment*, USAEC Report WAPD-208 (1960).
405. R. G. Wheeler, *The Effect of Reactor Atmosphere on Zirconium and Zirconium Alloys*, USAEC Report HW-55958 (1958).
406. B. Rubin and L. Lynam, *Behaviour of Blanket UO₂ Fuel Rods in PWR Core 1*, USAEC Reports WAPD-TM 308 (1961), WAPD-TM 326 (1963), and WAPD-TM 433 (1964); *Trans. ANS* **8**, 359 (1965); and *Nucl. Appl.* **2**, 499 (1966).
407. D. R. McClintock, In-Pile Experience with Zircaloy-Clad Fuel Rods in a Borated PWR Environment, *Trans. ANS* **9**, 32 (1966).
408. H. M. Ferrari and R. J. Allio, Fuel-Element Experience in Pressurized Water Reactors, *Nucl. App.* **2**, 492 (1966).
409. G. H. Jenks, *Homogeneous Reactor Project, Quarterly Progress Reports*, USAEC Report ORNL-2561 (1958), 2654 (1958), and 3004 (1960).
410. R. C. Asher, B. Cox, and J. K. Dawson, Investigations Relating to the Use of Zirconium Alloys in Steam-Cooled Reactors, *Proc. IAEA Symp. Power Reactor Experiments*, Vienna, 1961, Paper SM-21/1, p. 135.
411. R. C. Asher, A. Hall, C. Howard, and T. B. A. Kerstein, Irradiation Effects on Zirconium-Steam Reactions, *Nucl. Eng.* **9**, 171 (1964).
412. R. C. Asher and B. Cox, The Effects of Irradiation on the Oxidation of Zirconium Alloys, *Proc. IAEA Symp. Corrosion of Reactor Materials*, Salzburg, 1962, p. 209.
413. J. K. Dawson, R. C. Asher, J. Boulton, B. Wilkins, and J. N. Wanklyn, The Properties of Zirconium Alloys for Use in Water-Cooled Reactors, *Proc. 3rd Intern. Conf. Peaceful Uses of Atomic Energy*, Geneva, Vol. 9 (1964), (Paper 158).
414. R. C. Asher, D. Davies, A. Hall, T. B. A. Kerstein, J. W. Marriott, and P. J. Wright, Effects of Radiation on the Oxidation and Hydrogen Absorption of Zirconium Alloys in Steam, *Electrochem. Tech.* **4**, 231 (1966).
415. R. C. Asher, D. Davies, A. Hall, T. B. A. Kerstein, and P. J. White, The Corrosion of Zircaloy-2 Under Radiation in High Pressure Water, *Proc. 1st Intern. Conf. Use of Zirconium Alloys in Nuclear Reactors*, Mariánské Lázně, 1966, p. 233 (Skoda, Pilsen).
416. R. C. Asher, D. Davies, T. B. A. Kerstein, P. A. J. McCullen, and J. F. White, The Effects of Radiation on the Corrosion of Some Zirconium Alloys, *Corrosion Sci.* **10**, 695 (1970).
417. R. C. Asher and J. F. White, Effect of Reactor Irradiation on the Internal Surface Area of Corrosion Films on Zirconium Alloys, *Nature* **223**, 497.
418. R. W. Nichols, R. C. Asher, R. Hesketh, B. W. Pickles, M. F. Sheppard, and D. S. Wood, Irradiation Effects in Zirconium Alloy Pressure Tubes, *Proc. 4th Intern. Conf. Peaceful Uses of Atomic Energy*, Geneva, Vol. 10 (1971), p. 549 (Paper 502).
419. R. C. Asher and T. B. A. Kerstein, Mechanism of the In-Reactor Corrosion of Zircaloy, *J. Nucl. Mat.* **49**, 105 (1973/74).
420. H. P. Maffei, *Irradiation Effects on the Corrosion of PRTR Zircaloy-2 Process Tubes*, Metallurgy Research Operation, Quarterly Progress Reports, USAEC Reports HW-82651, 84281, and 84573 (1964).
421. R. C. Nelson, The Corrosion of Zircaloy-2 Fuel Element Cladding in a Boiling Water Reactor Environment, *Proc. USAEC Symp. Zirconium Alloy Development*, Castlewood, Calif., 1962, GEAP-4089, Paper 17.

422. H. E. Williamson, C. J. Baroch, J. P. Hoffman, and D. T. Ikeuye, *AEC Fuel Cycle Program Examination of Zircaloy Clad UO_2 Fuel Rods Operated in the VBWR to 10,000 MWD/TU*, USAEC Reports GEAP-4597 (1965) and 4849 (1966).
423. T. J. Pashos, H. E. Williamson, and R. N. Duncan, Fuel Performance in Boiling-Water Reactors, *Nuclear App.* **2**, 510 (1966).
424. S. Naymark and C. N. Spalaris, Oxide Fuel Fabrication and Performance, *Proc. 3rd Intern. Conf. Peaceful Uses of Atomic Energy, Geneva*, Vol. 11 (1964), 425 (Paper 233).
425. R. N. Duncan, F. H. Megerth, and T. J. Pashos, Corrosion of Zircaloy-2 Fuel Rod Cladding in Boiling Water Reactors, presented at *23rd Ann. NACE Conf., Los Angeles, Symp. High Purity Water Corrosion of Metals*, 1967.
426. W. A. Burns, H. P. Maffei, and R. A. Thiede, *Hanford Metallurgy Research Operation, Quarterly Progress Reports*, USAEC Reports HW-76228, 77052, 77954, 78962, and 79766 (1962 onward).
427. W. A. Burns and H. P. Maffei, Neutron Irradiation and Cold Work Effects on Zircaloy-2 Corrosion and Hydrogen Pickup, *Proc. ASTM Symp. Corrosion of Zirconium Alloys, New York*, 1963, ASTM-STP 368, p. 101; and USAEC Reports HW-SA-3168 (1963) and HW-76636 (1962).
428. W. A. Burns, *Effects of Fast Neutron Irradiation, Fabrication History, and Water Oxygen on the Environmental Behaviour of Zirconium Alloys*, USAEC Report BNWL-88 (1965).
429. J. E. Irvin, Effects of Irradiation and Environment on the Mechanical Properties and Hydrogen Pickup of Zircaloy, *Electrochem. Tech.* **4**, 240 (1966).
430. A. B. Johnson, Jr., In-Reactor Oxidation of Zirconium Alloys in pH-10 LiOH and NH_4OH , *Proc. 23rd Ann. NACE Conf., Los Angeles, Symp. High Purity Water Corrosion of Metals*, 1967, p. 49; and USAEC Report BNWL-SA-822 (1967).
431. A. B. Johnson, Jr., and J. E. Irvin, *Radiation-Enhanced Oxidation of Zircaloy-2 in pH-10 LiOH and pH-10 NH_4OH* , USAEC Reports BNWL-463 (1967) and BNWL-SA-1234 (1967).
432. A. B. Johnson, Jr., *In-Reactor Oxidation and Hydriding of Titanium Niobium and Zircaloy-2*, USAEC Report BNWL-SA-1210 (1967).
433. A. B. Johnson, Jr., Effects of Nuclear Radiation on the Corrosion Hydriding, and Oxide Properties of Six Zirconium Alloys, *Proc. ASTM Symp. Applications-Related Phenomena in Zirconium and Its Alloys, Philadelphia*, 1968, ASTM-STP 458, p. 301; and USAEC Report BNWL-SA-1719 (1968).
434. A. B. Johnson, Jr., Aqueous Corrosion and Hydriding of Zirconium Alloys in Nuclear Reactor Environments, *Proc. 4th Intern. Conf. Metallic Corrosion, Amsterdam*, 1969, p. 165.
435. A. B. Johnson, Jr., J. E. LeSurr, and R. A. Proebstle, Study of Zirconium Alloy Corrosion Parameters in the Advanced Test Reactor, *Proc. ASTM/AIME Symp. Zirconium in Nuclear Appl. Portland, Oregon*, 1973, ASTM-STP 551, p. 495; and Atomic Energy of Canada Ltd. Report AECL-4651 (1964).
436. J. E. LeSurr, P. E. C. Bryant, and M. C. Tanner, *Use of Ammonia to Suppress Oxygen Production and Corrosion in Boiling-Water Reactors*, Atomic Energy of Canada Ltd. Report AECL-2562 (1967); and *Corrosion* **23**, 57 (1967).
437. B. Cox, *AECL Experiments on the Corrosion of Zirconium Alloys Under Irradiation*, Atomic Energy of Canada Ltd. Report AECL-2257 (1965).
438. R. D. Page and A. D. Lane, *The Performance of Zirconium Alloy Clad UO_2 Fuel for Canadian Pressurised and Boiling Water Power Reactors*, presented at Joint ANS-CNA Conf., Toronto (1968); and Atomic Energy of Canada Ltd. Report AECL-3068.
439. A. S. Bain and J. E. LeSurr, *Oxidation and Hydriding of Zircaloy in NPD Reactor*, Atomic Energy of Canada Ltd. Report AECL-3065 (1969).

440. F. Garzarolli, W. Diez, K. P. Francke, and W. Fricke, Corrosion and Hydriding of Zircaloy-2 and Other Zirconium Alloys in BWR's, *Proceedings of British Nuclear Energy Society Conf. on Effect of Environment on Material Properties in Reactor Systems*, London, 1971, Paper 2.
441. A. van der Linde, Some Observations on In-Flux Corrosion of Zirconium Alloys Exposed in a Pressurized Water Loop, *Can. Met. Quart.* **11**, 7 (1972).
442. J. Blanchet, *Effect of Irradiation on the Oxidation and Hydrogenation of Alloys of Zirconium in High Temperature Water*, French Report CEA-Conf. 1293 (1968).
443. Centro Informazione Studi Esperienze, *Development Program on the Application of Steam-Water Spray to Reactor Cooling*, Italian Report CISE-R-136 (1964).
444. E. Cerrai, F. Gadda, and A. Scaroni, *In-Pile Corrosion of Zircaloy-2 in Steam-Water Mixtures*, Italian Report CISE-R-140 (1966).
445. E. Cerrai, F. Gadda, and A. Scaroni, *Further Experiments on the Corrosion Rate of Zircaloy-2 in Steam-Water Mixture Under Reactor Radiations*, Italian Report CISE-R-290 (1969).
446. E. Cerrai, F. Gadda, and A. Scaroni, Zircaloy-2 Corrosion in Steam-Water Mixture under Reactor Radiations, *Can. Met. Quart.* **11**, 21 (1972).
447. G. H. Jenks, *Review and Correlation of In-Pile Zircaloy-2 Corrosion Data and a Model for the Effect of Irradiation*, USAEC Reports ORNL-3039 (1961) and 3099 (1963).
448. G. H. Jenks, Zircaloy-2 In-Pile in Aqueous Homogeneous Reactor Solutions, *Proc. ASTM Symp. Corrosion of Zirconium Alloys*, New York, 1963, ASTM-STP 368, p. 41.
449. L. Lunde and K. Videm, The Influence of Neutron Irradiation on the Corrosion of Zircaloy-2 at 240°C, *Proc. 6th Scandinavian Corrosion Congr.*, Gøteborg, 1971, Paper 4; and USAEC Report AEC-Conf 7105020-4.
450. L. Lunde and K. Videm, The Effect of Surface Treatment on the Irradiation Enhancement of Corrosion of Zircaloy-2 in HBWR, *Proc. ASTM/AIME Symp. Zirconium in Nuclear Applications*, Portland, Oregon, 1973, ASTM-STP 5511, p. 514.
451. R. C. Asher, *The Effect of Radiation on the Aqueous Corrosion of Zircaloy. A Survey of World Experience*, UKAEA Report AERE-R7454 (1973).
452. W. C. Yee, G. H. Jenks, and E. E. Stansbury, Fission Fragment Recoil Effects on Zirconium Oxidation, *J. Electrochem. Soc.* **109**, 198 (1962).
453. E. R. Marx, *In-Reactor Corrosion Behaviour of Etchant Stained Zircaloy-2* USAEC Report DUN-7745 (1971).
454. F. W. Trowse, *The Significance of Corrosion and Hydrogen Uptake for Zircaloy Fuel Cladding in Normal Operation of Boiling Water Reactors*, UKAEA Report TRG-R2499(s), 1974.
455. B. O. Heston and M. D. Silverman, USAEC Report ORNL-CF-56-2-2; and *Homogeneous Reactor Project, Quarterly Progress Reports*, ORNL-2222 (1956) and 2432 (1958).
456. H. Glick, work referred to in USAEC Report ORNL-2222 and by T. Rockwell and P. Cohen in *Proc. 1st Intern. Conf. Peaceful Uses Atomic Energy*, Geneva, Vol. 9 (1955), p. 423.
457. G. Dearnaley, The Use of Ion Beams in Corrosion Science, *Proc. Intern. Conf. Applications of Ion Beams in Metals*, Albuquerque, N.M., 1973, p. 63; and UKAEA Report AERE-R 7579.
458. J. A. Spitznagel, L. R. Fleischer, and W. J. Choyke, The Effects of Ion Bombardment on the Thin Film Oxidation Behaviour of Zircaloy-4 and Zr-1.0 Nb, *Proc. Intern. Conf. Applications of Ion Beams to Metals*, Albuquerque, N.M., 1973, p. 87.
459. C. D. Williams and C. E. Ells, The Influence of Niobium in Irradiation Strengthening of Dilute Zr-Nb Alloys, *Phil. Mag.* **18**(154) 763 (1968).

460. V. F. Urbanic, J. E. LeSurr, and A. B. Johnson, Jr., *Effect of Aging and Irradiation on the Corrosion of Zr-2.5 wt. % Nb*, Atomic Energy of Canada Ltd. Report AECL-4842 (1974); and *Corrosion* **31**, 15 (1975).
461. K. Videm, Properties of Zirconium Base Cladding Materials—Corrosion and Hydrogen Pickup, *Nucl. Eng. Design* **21**, 200 (1972) (summarizes results of Russian tests).
462. *Atomic Energy of Canada Ltd. Annual Report 1970/71*, AECL-3913 (1971).
463. D. G. Boxall, W. M. Brown, D. B. Nazzar, J. T. Rogers, R. G. Hart, and K. L. Smith, Development of Fuel and Coolant Tubes for a Reactor Cooled by Organic Liquid, *Proc. 3rd Intern. Conf. Peaceful Uses of Atomic Energy, Geneva*, Vol. 9 (1964), p. 102 (Paper 23).
464. A. Sawatzky, *The Behaviour of Zirconium Alloys in Santowax OM Organic Coolant at High Temperatures*, Atomic Energy of Canada Ltd. Report AECL-2118 (1964).
465. W. K. Boyd *et al.*, *Corrosion Studies in Organic Heat-Exchange Media*, USAEC Report BMI-1160 (1957).
466. H. E. Kline *et al.*, *Dynamic Corrosion in Polyphenyls Under Irradiation*, USAEC Report NAA-SR-2046 (1958).
467. H. E. Davies, *The Compatibility of Some Metals with Santowax*, UKAEA Report AERE-M/M153 (1957).
468. V. H. Troutner, Hydrogen Corrosion in Organic Reactor Coolants, *Corrosion* **16**, 281t (1960).
469. R. S. Naymark, *Corrosion of Structural Materials in Impure Santowax*, USAEC Report NAA-SR-7755 (1963).
470. J. Boulton, *Current Knowledge of Zirconium Alloys for Reactor Usage*, Atomic Energy of Canada Ltd. Report AECL-3365 (1969).
471. J. Boulton and M. G. Wright, Ozhennite 0.5—Its Potential and Development, *Proc. ASTM Symp. Applications Related Phenomena in Zirconium and Its Alloys, Philadelphia*, 1968, ASTM-STP 458, p. 325.
472. J. Boulton, Behaviour of Zirconium Alloys in Organic Coolants, *Can. Met. Quart.* **11**, 1 (1972).
473. J. F. Walker, *The Behaviour of Zircaloy-2 and Zr-2.5% Nb Clad Uranium Dioxide Fuel in an Organic Coolant*, Atomic Energy of Canada Ltd. Report AECL-2661 (1966).
474. O. Kubaschewski and B. E. Hopkins, *Oxidation of Metals and Alloys*, Butterworth, London (1962).
475. K. Hauffe, *Oxidation of Metals*, Plenum Press, New York (1965), p. 288.
476. K. Hauffe, Corrosion of Metals in Gases and Aqueous Solutions, *Proc. 6th Intern. Conf. Reactivity of Solids, Schenectady*, 1968, p. 311.
477. J. H. Eriksen and K. Hauffe, The Influence on the Oxidation Rate of Metals with Ionically Conducting Surface Layers of an Electrochemical Cell, II, Oxidation of Zirconium, *Z. Phys. Chem. N.F.* **59**, 332 (1968).
478. P. Kofstad, *High Temperature Oxidation of Metals*, John Wiley, New York (1966).
479. C. S. Campbell and C. Tyzack, Effects of Alloying and Irradiation on the Oxidation Behaviour of Zirconium Alloys, *British Corrosion J.* **5**, 172 (1970); and *Proc. 2nd Intern. Conf. Use of Zirconium Alloys in Nuclear Reactors, Mariánské Lázně*, p. 7 (Skoda, Pilsen).
480. W. W. Smeltzer, R. R. Haering, and J. S. Kirkaldy, Oxidation of Metals by Short-Circuit and Lattice Diffusion of Oxygen, *Acta Met.* **9**, 880 (1961).
481. L. D. Kirkbride and D. E. Thomas, *Ionic Transport in Zirconium Oxide*, USAEC Report WAPD-T-308 (1956).
482. S. B. Dalgaard, *Transference Numbers and the Relation to In-Reacto Oxidation of Zirconium*, Atomic Energy of Canada Ltd. Report AECL-2066 (1964).
483. S. B. Dalgaard and K. Hauffe, reported in *Oxidation of Metals*, K. Hauffe (ed.), Plenum Press, New York (1965) p. 235.

484. A. Fiegna and P. Weisgerber, Influence of Thin Noble Metal Films on Zirconium Oxidation, *J. Electrochem. Soc.* **115**, 369, 1259 (1968).
485. R. D. Misch and F. H. Gunzel, Jr., The Electrical Resistance of Oxide Films on Zirconium in Relation to Corrosion, *J. Electrochem. Soc.* **106**, 15 (1959).
486. A. L. Bacarella, Electrochemical Measurements of Corrosion Rates on Zirconium and Zircaloy-2 at Elevated Temperatures, *J. Electrochem. Soc.* **108**, 331 (1961).
487. A. L. Bacarella and A. L. Sutton, Electrochemical Measurements on Zirconium and Zircaloy-2 at Elevated Temperatures II, 200–300°C, *J. Electrochem. Soc.* **112**, 546 (1965).
488. H. S. Gadiyar, *Electrochemical Measurements on Crystal-Bar Zirconium in Oxygenated 0.05 M K₂SO₄ Solutions Between 200° and 240°C*, USAEC Report ORNL-TM-1834 (1967).
489. A. L. Bacarella and A. L. Sutton, Anodic Film Growth on Zirconium at Temperatures from 200° to 300°C, *Electrochem. Tech.* **4**, 117 (1966); and USAEC Report ORNL-4076 (1967), p. 58.
490. M. E. Indig and C. Groot, Electrochemical Measurement of Corrosion, *Corrosion* **26**, 171 (1970).
491. J. Beran, J. Svec, and V. Zajic, Measuring the Speed of Corrosion in Zirconium Alloys Using the Method of Polarising Resistance in Water Pressure Loops of the Reactor, *2nd Intern. Conf. Use of Zirconium Alloys in Nuclear Reactors, Mariánské Lázně*, 1968, p. 25, Paper 2 (Skoda, Pilsen).
492. J. A. Davies, B. Domeij, J. P. S. Pringle, and F. Brown, The Migration of Metal and Oxygen During Anodic Film Formation, *J. Electrochem. Soc.* **112**, 675 (1965); and unpublished results on thermal oxide films.
493. J. L. Whitton, The Measurement of Ionic Mobilities in the Anodic Oxides of Tantalum and Zirconium by a Precision Sectioning Technique, *J. Electrochem. Soc.* **115**, 58 (1968).
494. O. Flint and J. H. O. Varley, An Experiment to Determine the Type of Ion Migration in a Metal/Metal Oxide System, *J. Phys. Chem. Sol.* **6**, 213 (1958); and UKAEA Report AERE-M/M 133 (1956).
495. P. Kofstad and D. J. Ruzicka, On the Defect Structure of ZrO₂ and HfO₂, *J. Electrochem. Soc.* **110**, 181 (1963); and *Proc. USAEC Symp. Zirconium Alloy Development, Castlewood, Calif.*, 1962, GEAP-4089, Paper 21.
496. R. M. Vest, N. M. Tallan, and W. C. Tripp, Electrical Properties and Defect Structure of Zirconia, I. Monoclinic Phase, *J. Amer. Ceram. Soc.* **47**, 635 (1964).
497. A. Kumar, D. Rajdev, and D. L. Douglass, Effect of Oxide Defect Structure on the Electrical Properties of ZrO₂, *J. Amer. Ceram. Soc.* **55**, 439 (1972).
498. D. K. Dawson and R. H. Creamer, The Electrical Conductivity of Zirconium Dioxide Films at Intermediate Temperatures, *British J. Appl. Phys.* **16**, 1643 (1965).
499. T. Smith, Diffusion Coefficients and Anion Vacancy Concentrations for the Zirconium–Zirconium Dioxide System, *J. Electrochem. Soc.* **112**, 560 (1965).
500. D. L. Douglass and C. Wagner, The Oxidation of Oxygen-Deficient Zirconia and Its Relationship to the Oxidation of Zirconium, *J. Electrochem. Soc.* **113**, 671 (1966).
501. D. K. Smith and H. W. Newkirk, The Crystal Structure of Baddeleyite (Monoclinic ZrO₂) and Its Relation to the Polymorphism of ZrO₂, *Acta Cryst.* **18**, 983 (1965).
502. N. A. Bendeliani, S. V. Popova, and L. F. Vereshchagin, A New Modification of ZrO₂ and HfO₂, *Geokhimiya* **6**, 677 (1967).
503. G. Bocquillon and C. Susse, Diagramme de phase de la zircone sans pression, *Rev. Int. Hautes Temper. Refract.* **6**, 263 (1969).
504. *Proc. Symp. Solid State Chemistry*, R. S. Roth and S. J. Schneider, Jr. (eds.), NBS Spec. Publ. 364 (1972).

505. B. G. Hyde, A. N. Bagshaw, S. Andersson, and M. A. O'Keefe, Some Defect Structures in Crystalline Solids, Chapter 3 in *Ann. Rev. Mat. Sci.* **4**, 43 (1974) (Annual Reviews, Palo Alto, Calif.).
506. D. J. Poulton and W. W. Smeltzer, Oxygen Diffusion in Monoclinic Zirconia, *J. Electrochem. Soc.* **117**, 378 (1970).
507. A. Madeyski, D. J. Poulton, and W. W. Smeltzer, Parabolic Oxidation Kinetics of α -Zirconium, *Acta Met.* **17**, 579 (1969).
508. A. Madeyski and W. W. Smeltzer, Oxygen Diffusion in Monoclinic Zirconia, *Mat. Res. Bull.* **3**, 369 (1968).
509. W. D. Kingery, J. Pappis, M. E. Doty, and D. C. Hill, Oxygen Ion Mobility in Cubic $Zr_{0.85}Ca_{0.15}O_{1.85}$, *J. Amer. Ceram. Soc.* **42**, 393 (1959).
510. D. L. Douglass, Corrosion Mechanism of Columbium, Zirconium and Their Alloys—I. Diffusion of Oxygen in Columbium Pentoxide and Zirconium Dioxide, paper presented at *IAEA Symp. Corrosion of Reactor Materials*, Salzburg, 1962, p. 224.
511. S. Aronson, Oxidation and Equilibrium in Non-stoichiometric Zirconium Dioxide Powder, *J. Electrochem. Soc.* **108**, 312 (1961).
512. L. A. McClaine, *Electrical and Ionic Conductivity of Zirconia*, USAEC Report ASD-TDR-62-204, Pt. II, p. 54 (1963).
513. B. Cox and J. P. Pemsler, Diffusion of Oxygen in Growing Zirconia Films, *J. Nucl. Mat.* **28**, 73 (1968).
514. C. J. Rosa and W. C. Hagel, Oxygen Diffusion in Hypostoichiometric Zirconium Oxide in the Temperature Range of 875° to 1050°C, *Trans. AIME* **242**, 1293 (1968).
515. C. J. Rosa and W. C. Hagel, Oxygen Ion Diffusivity in Hypostoichiometric Zirconium Dioxide, *J. Nucl. Mat.* **27**, 12 (1968).
516. J. B. Lightstone and J. P. Pemsler, Considerations on the Atomistics of Oxidation, *Proc. Intern. Symp. Kinetics of Reactions in Ionic Systems*, Alfred, N.Y., 1969, p. 461 (Plenum Press, New York).
517. J. B. Lightstone and J. P. Pemsler, The Effect of Structure on the Mechanism of Zirconium Oxidation, *Proc. 6th Intern. Conf. Reactivity of Solids*, Schenectady, N.Y., 1968, p. 615.
518. G. Amsel, C. Cherki, J. P. Nadai, and J. Siejka, Applications of the Microanalysis of O^{16} and O^{18} by Nuclear Reactions to the Study of Anodic Oxide Films, papers presented at *135th Meeting of the Electrochemical Society*, New York, 1969, *Ext. Abs.*, Vol. 6, No. 1, p. 20; and at *147th Meeting*, Toronto, 1975, *Ext. Abs.*, Vol. 75-1, p. 217.
519. R. A. Ploc, Transmission Electron Microscopy of Thin ($<2000 \text{ \AA}$) Thermally Formed ZrO_2 Films, *J. Nucl. Mat.* **28**, 48 (1968); and Atomic Energy of Canada Ltd. Report AECL-2794.
520. J. N. Wanklyn, The Properties of Oxide Films on Zirconium Alloys and Their Relevance to Corrosion and Hydrogen Uptake, *Electrochem. Tech.* **4**, 81 (1966).
521. F. Barbesino, R. di Pietro, G. Perona, and R. Sesini, Structure of Zirconium Oxide Films, *En. Nucl.* **11**, 567 (1964).
522. G. Béranger, F. Duffaut, B. de Gélas, and P. Lacombe, Observations en microscopie électronique de films minces de zircone obtenus par oxydation du zirconium, *J. Nucl. Mat.* **19**, 290 (1966); and USAEC Report WAPD-Trans-109.
523. P. Gondi and G. F. Missiroli, Electron Microscope Observations on the Oxidation of Zirconium, *Nuovo Cim.* **48**, 223 (1967).
524. F. W. Vahldiek, Epitaxial Oxidation of Zirconium at Various Temperatures, *J. Less-Common Metals* **12**, 19 (1967).
525. R. A. Ploc, Physical Changes in Thin ZrO_2 Films with Thickening, *Proc. 7th Intern. Conf. Electron Microscopy*, Grenoble, 1970, p. 373.
526. R. A. Ploc, Existence of Cubic ZrO_2 at 300°C on Bulk Zirconium, *Proc. 27th Ann. EMSA Meeting*, St. Paul, Minn., 1969, p. 166.

527. E. S. Sarsikov, N. T. Chebotarev, A. A. Nevzorova, and A. I. Zverkov, The Oxidation of Zirconium at High Temperatures and the Structure of the Primary Oxide Layers, *Atomnaya En.* **5**, 550 (1958).
528. D. L. Douglass and J. van Landuyt, The Oxidation of Zirconium, an Electron Microscopy Study of Zirconia Formed in the Thin-Film Region, *Acta Met.* **13**, 1069 (1965); and *Proc. IX^{me} Colloque de Métallurgie, Saclay*, 1965, p. 155.
529. R. Pennelle, P. Boisot, G. Béranger, and P. Lacombe, Influence de l'orientation de monocristaux de zirconium sur les textures de croissance de la zircone monoclinique, *J. Nucl. Mat.* **38**, 340 (1971).
530. P. Boisot, G. Béranger, and R. Penelle, Étude quantitative des textures développées dans la zircone formée par oxydation à 850°C du Zirconium Polycrystallin, *Compt. Rend.* **271**, 257 (1970).
531. B. Cox and A. Donner, The Morphology of Thick Oxide Films on Zircaloy-2, *J. Nucl. Mat.* **47**, 72 (1973).
532. J. Debuigne and P. Lehr, Micrographic Structure of Oxide Layers Formed During the Oxidation of Massive Zirconium, *Compt. Rend.* **266c**, 903 (1968); and USAEC Report WAPD-trans-118.
533. G. P. Airey and G. P. Sabol, Transmission Electron Microscopy of Ion-Thinned Oxides Formed During Corrosion of Zircaloy-4, *J. Nucl. Mat.* **45**, 60 (1972/73).
534. G. P. Sabol, S. G. McDonald, and G. P. Airey, Microstructure of the Oxide Films Formed on Zirconium-Based Alloys, *Proc. ASTM/AIME Symp. Zirconium in Nuclear Applications, Portland, Oregon*, 1973, ASTM-STP 551.
535. A. W. Urquhart and D. Vermilyea, Characterisation of Zircaloy Oxidation Films, *Proc. ASTM/AIME Symp. Zirconia in Nuclear Applications, Portland, Oregon*, 1973, ASTM-ARP 551, p. 463.
536. A. D. Neumin, A. G. Kotlyar, S. F. Pal'guyev, V. N. Strekalovskii, and N. A. Batrakov, The Structure and Conductivity of the ZrO_2 - Y_2O_3 Systems Containing Iron, Manganese, Cobalt and Nickel Oxides, Trudy No. 12, Akad. Nauk SSSR, Uralskii Fil., Sverdlovsk Inst. Elektrokhimii., in *Electrochemistry of Molten and Solid Electrolytes*, Vol. 9, p. 73; translated by Consultants Bureau (1972).
537. N. Ramasubramanian and T. P. Trottier, Rectification by Anodic Oxide Films on Zircaloy-2, *J. Electrochem. Soc.* **119**, 1375 (1972); and Atomic Energy of Canada Ltd. Reports AECL-3909, p. 61 (1971); AECL-4065, p. 71 (1971); and AECL-4204, p. 68 (1972).
538. N. Ramasubramanian, An Imaging Technique for Studying Localised Electronic Conduction in Valve Metal-Oxide Systems, *J. Electrochem. Soc.* **116**, 1237 (1969); and **118**, 1797 (1971).
539. T. Smith, Zirconium Dioxide-Oxygen Reactions, I. Molecular Oxygen Adsorption with Electron Transfer, *J. Electrochem. Soc.* **111**, 1020 (1964).
540. T. Smith, Zirconium Dioxide-Oxygen Reactions, II. Chemisorption of Atomic Oxygen, *J. Electrochem. Soc.* **111**, 1027 (1964).
541. A. J. Stirling, *Conductivity of Bulk Zirconia*, Atomic Energy of Canada Ltd. Report AECL-3909, p. 63 (1971).
542. B. Cox, Processes Occurring During the Breakdown of Oxide Films on Zirconium Alloys, *J. Nucl. Mat.* **29**, 50 (1969).
543. B. Cox, A Porosimeter for Determining the Sizes of Flaws in Zirconia or Other Insulating Films, in situ, *J. Nucl. Mat.* **27**, 1 (1968).
544. B. Cox, *The Use of Electrical Methods for Investigating the Growth and Breakdown of Oxide Films on Zirconium Alloys*, Atomic Energy of Canada Ltd. Report AECL-2668 (1967).
545. B. Cox, Porosity in Oxide Films on Zirconium Alloys, *Proc. 3rd Intern. Cong. Met. Corrosion, Moscow*, Vol. 4 (1966), p. 341.

546. J. E. Draley, D. H. Bradhurst, and C. J. van Drunen, *Stress in Growing Oxide Films*, Metallurgy Division, Argonne National Lab., Annual Reports, USAEC Reports ANL-6868 (1963) and 7000 (1965).
547. D. H. Bradhurst and P. M. Heuer, paper presented at *Electrochemical Soc., Fall Meeting 1967, Chicago*, and Australian Report AAEC-MAT/TN8 (1967).
548. F. Bollenrath and F. E. Buresch, La Déformation plastique du zirconium au cours de l'oxydation, *Métaux* **295**, 402 (1966); and *J. Nucl. Mat.* **24**, 270 (1967).
549. R. D. Watson, *On the Oxidation of Zirconium Alloys in Air and the Dimensional Changes Associated with Oxidation*, Atomic Energy of Canada Ltd. Report AECL-3375 (1969).
550. D. H. Bradhurst and P. M. Heuer, The Influence of Oxide Stress on the Breakaway Oxidation of Zircaloy-2, *J. Nucl. Mat.* **37**, 35 (1970).
551. C. F. Knights and R. Perkins, The Effect of Applied Tensile Stress on the Corrosion Behaviour of Zircaloy-2 in Steam and Water, *J. Nucl. Mat.* **36**, 180 (1970).
552. B. Cox, Comments on paper by Bradhurst and Heuer, *J. Nucl. Mat.* **41**, 96 (1971).
553. G. Ullrich, Breakaway Mechanism During the Corrosion of Zirconium, *Z. Metallk.* **59**, 292 (1968); and USAEC Report WAPD-trans-122.
554. D. L. Douglass, Oxide Plasticity in the Oxidation Mechanism of Zirconium and Its Alloys, *Corrosion Sci.* **5**, 255 (1965).
555. D. L. Douglass, Corrosion Mechanism of Zirconium and Its Alloys, III. Solute Distribution Between Corrosion Films and Zirconium Alloys Substrates, *Corrosion Sci.* **5**, 347 (1965).
556. B. C. Weber, H. J. Garratt, F. A. Mauer, and M. A. Schwartz, Observations on the Stabilisation of Zirconia, *J. Amer. Ceram. Soc.* **39**, 197 (1956).
557. C. E. Curtis, Development of Zirconia Resistant to Thermal Shock, *J. Amer. Ceram. Soc.* **30**, 180 (1947).
558. A. Arias, Thermal Shock Resistance of Zirconia with 15 mole % Titanium, *J. Amer. Ceram. Soc.* **49**, 334 (1966).
559. A. Arias, Mechanism by Which Metal Additions Improve the Thermal Shock Resistance of Zirconia, *J. Amer. Ceram. Soc.* **49**, 339 (1966).
560. E. Ryshkewitch, Compression Strength of Porous Sintered Alumina and Zirconia, *J. Amer. Ceram. Soc.* **36**, 65 (1953).
561. J. L. Hart and A. C. D. Chaklader, Superplasticity in Pure ZrO_2 , *Mat. Res. Bull.* **2**, 521 (1967).
562. A. G. King, Interaction Between Stress and Porosity in Zirconia Ceramics, *J. Amer. Ceram. Soc.* **53**, 424 (1970).
563. P. E. Evans, Creep in Yttria- and Scandia-Stabilized Zirconia, *J. Amer. Ceram. Soc.* **53**, 365 (1970).
564. J. R. Moon and D. G. Lees, Cracking in Oxides on Zr Alloys, *Corrosion Sci.* **10**, 85 (1970).
565. T. H. Ahmad and L. H. Keys, The Breakaway Oxidation of Zirconium and Its Alloys—A Review, *J. Less-Common Metals.* **39**, 99 (1975).
566. R. Cypres, R. Wollast, and J. Raucq, Contribution on the Polymorphic Conversion of Pure Zirconia, *Ber. Deut. Keram. Ges.* **40**, 527 (1963).
567. N. Ramasubramanian, Electrical Switching in Anodic Oxide Films on Zircaloy-2, *J. Electrochem. Soc.* **119**, 649 (1972).
568. R. C. Asher, *A Summary of Mechanisms for the Enhancement of Corrosion of Zircaloy-2 by Radiation*, UKAEA, internal report (1969).
569. P. J. Harrop, N. J. M. Wilkins, and J. N. Wanklyn, The Effect of Neon Bombardment on the Corrosion of Zr, *Corrosion Sci.* **7**, 289 (1967); and UKAEA Report AERE-R5279 (1966).
570. P. J. Harrop, N. J. M. Wilkins, and J. N. Wanklyn, Radiation Damage in Zirconia, *Proc. British Ceram. Soc.*, 1967, No. 9, 279.

571. P. J. Harrop and J. N. Wanklyn, Influence of Gamma Flux on the Electrical Conductivity of ZrO_2 Films and Its Relevance to Corrosion in Nuclear Reactors, *British J. Appl. Phys.* **16**, 155 (1965); and UKAEA Report AERE-R4703 (1964).
572. P. J. Harrop, N. J. M. Wilkins, and J. N. Wanklyn, *Effect of Gamma Dose on Oxide on Zirconium and Zircaloy-2—Relevance to Corrosion*, UKAEA Report AERE-R4779.
573. R. C. Daniel, M. L. Bleiberg, H. B. Meieran, and W. Yeniscavitch, *Effects of High Burnup on Zircaloy Clad, Bulk UO_2 , Plate Fuel Element Samples*, USAEC Report WAPD-263 (1962).
574. J. R. Johnson, Development of a Cubic Oxide Protective Film on Zirconium, *Trans. AIME* **212**, 13 (1958); and USAEC Report ORNL-2029 (1956).
575. C. M. Schwartz, D. A. Vaughan, and G. G. Cocks, *Identification and Growth of Oxide Films on Zirconium in High Temperature Water*, USAEC Report BMI-793 (1952).
576. J. H. Crawford and M. C. Wittels, Radiation Stability of Nonmetals and Ceramics, *Proc. 2nd Intern. Conf. Peaceful Uses of Atomic Energy, Geneva, 1958*, Vol. 5, p. 300 (Paper 679).
577. M. C. Wittels and F. A. Sherrill, Irradiation-Induced Phase Transformation in Zirconia, *J. Appl. Phys.* **27**, 463 (1956).
578. J. Adam and B. Cox, The Irradiation-Induced Phase Transformation in Zirconia Solid Solutions, *J. Nucl. Eng.* **A11**, 31 (1959).
579. M. C. Wittels and F. A. Sherrill, Fission-Fragment Damage in Zirconia, *Phys. Rev. Lett.* **3**, 176 (1959).
580. M. C. Wittels, J. O. Stiegler, and F. A. Sherrill, Radiation Effects in Uranium-Doped Zirconia, *J. Nucl. Eng.* **A16**, 237 (1962).
581. J. Adam and B. Cox, Neutron and Fission Fragment Damage in Zirconia, *Phys. Lett.* **3**, 543 (1959).
582. J. Adam and B. Cox, The Irradiation-Induced Phase Transformation in Zirconia, *J. Nucl. Eng.* **A17**, 435 (1963).
583. J. Adam and M. D. Rogers, Radiation-Induced Phase Change and Recovery in ZrO_2 , *J. Nucl. Mat.* **9**, 211 (1963).
584. G. L. Kulcinski and C. W. Maynard, Combined Effect of Ultrahigh Pressure and Nuclear Irradiation on Solid-Solid Phase Transformations, *J. Appl. Phys.* **37**, 3519 (1966).
585. P. J. Harrop and J. N. Wanklyn, The Influence of Neutron Irradiation on Ionic Mobility in Cubic Zirconia, *J. Nucl. Mat.* **22**, 350 (1967).
586. P. J. Harrop and J. N. Wanklyn, Studies of the Mechanism by Which Nuclear Radiation Increases the Corrosion of Zirconium Alloys, *Proc. 3rd Intern. Congr. Met. Corrosion, Moscow*, Vol. 4 (1966), p. 332.
587. R. Kelly and N. P. Lam, The Sputtering of Oxides, I: A Survey of Experimental Results, *Rad. Eff.* **19**, 39 (1973).
588. P. J. Harrop and J. N. Wanklyn, The Embrittlement of Oxide Films on Zirconium by Neutron Irradiation, *J. Nucl. Mat.* **21**, 310 (1967); and UKAEA Report AERE-R5294 (1966).
589. S. R. MacEwen and I. Hastings, Densification of Uranium Dioxide, *Phil. Mag.*, **31**, 135 (1975).
590. S. R. MacEwen, The Effect of Neutron Flux on Dislocation Climb, *J. Nucl. Mat.*, **54**, 85 (1974).
591. M. G. Cowgill and W. W. Smeltzer, The Properties of Oxide Films Formed on a Zirconium-2.7 w/o Niobium Alloy in the Temperature Range 300°–500°C, *J. Electrochem. Soc.* **115**, 471 (1968).
592. R. A. Ploc, Atomic Energy of Canada Ltd., unpublished results.
593. N. Ramasubramanian, Atomic Energy of Canada Ltd., unpublished results.

594. J. S. Sheasby and B. Cox, Oxygen Diffusion in Alpha-Niobium Pentoxide, *J. Less-Common Metals* **15**, 129 (1968).
595. C. Roy and J. P. Wu, *Stress Generation in Zr-2.5 wt. % Nb During Oxidation at 500°C*, Faculty of Engineering Science, University of Western Ontario, Research Report, 1970.
596. B. de Gêlas, G. Béranger, and P. Lacombe, Étude par microscopie électronique en transmission de films minces d'oxyde obtenus par oxydation d'alliages de zirconium à teneur en élément d'addition inférieure à 4% en poids, *J. Nucl. Mat.* **28**, 185 (1968).
597. R. H. Alderson, Surface Films on Zirconium and Zirconium—ATR Alloy, *Proc. Eur. Reg. Conf. Electron Microscopy, Delft*, Vol. 1 (1960), p. 297.
598. D. Fisher, Electron Diffraction Studies in the Oxidation of Zirconium in Carbon Dioxide, *Proc. Eur. Reg. Conf. Electron Microscopy, Delft*, Vol. 1 (1960), p. 293.
599. D. L. Douglass, Solute Distribution Between Corrosion Films and Zirconium Alloy Substrates, *Proc. USAEC Symp. Zirconium Alloy Development, Castlewood, Calif.*, 1962, USAEC Report GEAP-4089, paper 19.
600. B. Cox, *Oxidation of Zirconium-Aluminum Alloys*, Atomic Energy of Canada Ltd. Report AECL-2776 (1967).
601. K. F. J. Heinrich, *Microprobe Studies of Zircaloy Corrosion Films*, USAEC Report DP-906 (1964).
602. G. Östberg, Determination of the Composition of the Second Phase in Zircaloy, *J. Nucl. Mat.* **7**, 103 (1962).
603. E. Bodmer, Influence of Steam Corrosion and the Properties of Reactor Grade Zircaloy-2, *Schweiz. Arch. Angew. Wiss. Tech.* **27**, 114 (1961).
604. W. Evans and G. W. Parry, The Deformation Behaviour of Zircaloy-2 Containing Directionally Oriented Zirconium Hydride Precipitates, *Electrochem. Tech.* **4**, 225 (1966); and *Nucleonics* **22**, 65 (1964).
605. E. A. Gulbransen and K. F. Andrew, Mechanism of the Reaction of Zirconium with Hydrogen, I. Role of Oxide Films, Pretreatments and Occluded Gases, *J. Electrochem. Soc.* **101**, 348 (1954).
606. S. Aronson, *Some Experiments on the Permeation of Hydrogen Through Oxide Films on Zirconium* (Bettis Tech. Rev.), USAEC Report WAPD-BT-19 (1960).
607. E. A. Gulbransen and K. F. Andrew, Reaction of Hydrogen with Pre-Oxidised Zircaloy-2 at 300 to 400°C, *J. Electrochem. Soc.* **104**, 709 (1957).
608. R. F. Boyle and T. J. Kisiel, Hydrogen Permeation of Zircaloy-2 Corrosion Films (Bettis Tech. Rev.), USAEC Report WAPD-BT-10 (1958).
609. D. W. Shannon, Electrical Properties of ZrO₂ Corrosion Films, I. Electrical Resistance Measurements, *Proc. USAEC Symp. Zirconium Alloy Development, Castlewood, Calif.*, 1962, USAEC Report GEAP-4089, Paper 18.
610. D. W. Shannon, Effect of Oxidation Rate on Hydriding of Zirconium Alloys in Gas Mixtures Containing Hydrogen, *Corrosion* **19**, 414t (1963).
611. G. R. Caskey, Jr., G. R. Cole, and W. G. Holmes, Failures of UO₂ Fuel Tubes by Internal Hydriding of Zircaloy-2 Sheaths, *Proc. Symp. Powder-Packed UO₂ Fuel Elements*, 1961, CEND-153, Vol. II, p. 77.
612. R. Billingham, Fifteen Years in Nuclear Power, *Proc. IAEA Symp. Experience from Operating and Fuelling Nuclear Power Reactors, Vienna*, 1974, p. 169.
613. H. J. Schenk, Experience from Fuel Performance at the Obrigheim Nuclear Power Plant (KWO), *Proc. IAEA Symp. Experience from Operating and Fuelling Nuclear Power Reactors, Vienna*, 1974, p. 435.
614. N. Eichelpasch, Six Years Experience with Core Performance at KRB Power Station Gundremmingen, *Proc. IAEA Symp. Experience from Operating and Fuelling Nuclear Power Reactors, Vienna*, 1974, p. 449.

615. L. Lunde, Localized or Uniform Hydriding of Zircaloy: Some Observations on the Effect of Surface Conditions, *J. Nucl. Mat.* **44**, 241 (1972).
616. R. A. Proebstle, J. H. Davies, T. C. Rowland, D. R. Rutkin, and J. S. Armijo, The Mechanism of Defection of Zircaloy-Clad Fuel Rods by Internal Hydriding, *Proc. ANS/CNA Topical Meeting on Commercial Nuclear Fuel Technology Today*, Toronto, April 1975, pp. 2–15.
617. T. Smith, Kinetics and Mechanism of Hydrogen Permeation of Oxide Films on Zirconium, *J. Nucl. Mat.* **18**, 323 (1966); and USAEC Report NAA-5R-6267 (1962).
618. C. Roy, *Hydrogen Distribution in Oxidised Zirconium Alloys by Autoradiography*, Atomic Energy of Canada Ltd. Report AECL-2085 (1964).
619. K. M. Goldman and D. E. Thomas, *Hydrogen Pickup During Corrosion Testing of Zirconium and Zirconium-Tin Alloys*, USAEC Report WAPD-MM-153 (1953).
620. R. Attermo and A. Sietnieks, Electrolytic Hydriding of Zirconium, *Electrochim. Acta* **14**, 121 (1969).
621. F. H. Megerth, R. N. Duncan, and T. J. Pashos, *Zircaloy-Clad UO_2 Fuel Rod Evaluation Programme*, USAEC Report GEAP-10371 (1971).
622. J. R. Findlay, C. F. Knights, and R. Perkins, *Post-Transition Corrosion of Zircaloy-2, Low-Nickel Zircaloy-2 and Zircaloy-4 by Steam at 300°C and 340°C: Deuterium Absorption and the Influence of Heat Treatment*, UKAEA Report AERE-R5903 (1968).
623. W. Debray, L. Stieding, and U. Rösler, Influence of Initial Oxide-Layer Formation on the Hydrogen Pickup of Zircaloy-2, *Electrochem. Tech.* **4**, 113 (1966).
624. G. J. Biefer and F. H. Krenz, *A Preliminary Survey of Factors Affecting Hydrogen Pickup and Oxidation of Zircaloy-2 in High Temperature Aqueous Solutions*, Atomic Energy of Canada Ltd. Report CR-Met-945 (1960).
625. H. P. Maffei, *Effect of Oxygen on Hydrogen Pickup of Zircaloys During Autoclaving*, USAEC Reports HW-72266 (1962) and HW-SA-2408 (1962).
626. P. L. Allen, D. A. Moore, and F. W. Trowse, *The Relation of Proof Testing to Long-Term Corrosion Behaviour of Zirconium Alloys*, UKAEA Report TRG R-1134(s) (1966).
627. H. Coriou, L. Grall, M. Pelras and M. Salesse, Comportement du zirconium tres pur dans l'eau déminéralisée et la vapeur à haute température, *Compt. Rend.* **259**, 1862 (1964).
628. J. P. Butler, The Determination of Deuterium in the Surface Layers of D_2O Oxidised Zircaloy-2 by the $D(\alpha, n) He^3$ Reaction, *Proc. IAEA Symp. Radiochemical Methods of Analysis, Salzburg*, Vol. I (1964), p. 391; and Atomic Energy of Canada Ltd. Report AECL-2302 (1964).
629. J. H. Austin, T. S. Elleman, and K. Verghese, Surface Effects on the Diffusion of Tritium in 304-Stainless Steel and Zircaloy-2, *J. Nucl. Mat.* **48**, 307 (1973).
630. J. H. Austin, T. S. Elleman, and K. Verghese, Tritium Diffusion in Zircaloy-2 in the Temperature Range – 78 to 204°C, *J. Nucl. Mat.* **51**, 321 (1974).
631. T. S. Elleman and K. Verghese, Surface Effects on Tritium Diffusion in Niobium, Zirconium and Stainless Steel, *J. Nucl. Mat.* **53**, 299 (1974).
632. G. Sabol and S. B. Dalgaard, The Origin of the Cubic Rate Law in Zirconium Alloy Oxidation, *J. Electrochem. Soc.* **122**, 316 (1975).

INDEX

A

Acid, hydrofluoric vs. glass, 16, 21
Acid, hydrochloric
vs. Cu, temp. infl, 123
vs. glass, 21
vs. silver, 153
Acid, phosphoric vs. glass, 16, 22
Acids, inorganic vs. glass, 21
Air, Zr alloys kinetics vs., 184, 204
Al and alloys
Br vs., ignition, 140
Cl vs., kinetics (table), 139
F vs., 135, 138
salts as inhibitor for glass, 16
Zr, as alloy vs. high temperature water
and steam, 228, 257
Alkaline metals halides melting points, 66
Alkalis, glass type infl. on attack by, 23, 26, 28
Ammonia adsorption on porous glass, 46
Ammonium hydroxide vs. Zr alloys with
and without heat flux, 292
Anion mobility in scaling, 85, 86
Atomic effects
ammonia chemisorption on glass, 45
bonding in glass, 3
hydrogen absorption by Zr, 357
sodium, molten vs. glass, 34
Zr alloying infl. on ion diffusion, lattices,
213, 297
Zr lattice, infl. Cr, particle size in high
temperature water, 276
Zr oxides, defects due to stress, 314
Zr oxides electron transport data, 308,
326, 332
Atomistic theory of glass structure, 2

B

Beryllium vs. F, 141
Beryllium salts as inhibitor for glass, 16

Boron, halogens vs., 156
Boron acids as inhibitor for Zr vs. 500C
steam, 261
Boron halides' melting points, 67
Boron reactions at leached glass surface, 45
Bromides, metal, standard free energies of
formation, 64, 65

Bromine

Al vs. scale properties, 140
chromium vs., 146
Cu and alloys vs., infl. water, 124
Cu bromide vapor pressure, 124
gold vs., 154
iron reactions, 133
Mn vs., 147
monel vs., 113
Ni and alloys vs., 111
Pt vs., 151
silver vs., kinetics, rates, infl. water, 153
Ti vs., 145
vanadium vs., 146
Zr vs., 148

C

Cadmium vs. halogens, 155
Carbide particles in Zr, 195
Carbon, Zr reactions with, 218, 228
Carbon dioxide vs. Zr, 215, 219
Carbon halides' melting points, 68
Cation screening of exchange sites on glass, 13
Ceramics' corrosion resistance, 49
Chlorides, metal, standard free energies of
formation, 62, 63
Chlorides vs. Zr in high temperature water
and steam, 261
Chlorimet-3 vs. Cl, 109
Chlorine
Al scale properties in, 138
Be vs., temperature infl., 141
Cr vs., temperature infl., 146

Chlorine (*Cont'd*)

- copper alloys vs., 122, 123
- gold vs., 154
- magnesium vs., 143
- manganese vs., 147
- Ni vs., infl. water, 105, 109, 110
- organic coolant containing vs. Zr in nuclear reactor, 291
- Pt vs., infl. temperature water, 151
- pressure infl. on Ni attack, 108
- silver scale properties, kinetics in, 153
- Ta vs. liquid, wet or dry, 148
- Ti ignition temperature, 144
- vanadium vs., 145
- Zr vs., 147

Chromel-A vs. Cl, 109

Chromium

- Br vs., 146
- F vs., temperature infl., 146
- I vs., 146
- Ni alloyed with vs. Cl, 109
- plating on ZrCu, ZrCuCr vs. carbon dioxide, 220
- Zr lattice effects in ZrCrFe, 276

Cobalt, halogens vs., 147

Cold work of ZrNb infl. on oxidation, 213, 270

Copper and alloys

- Br vs., infl. water, 124
- Cl vs., infl. water, 122
- F vs., 115, 121
- I vs., 114, 124
- Zr alloyed with vs. carbon dioxide, 220, 222

D

Dehydration–hydration of porous glass, 42

Dessicant, leached glass as, 50

Deuterium + deuterium oxide in Zr vs. water, 262

Diffusion, halides, halogens, temperature infl., 59

Dopants, activity during scaling by halogens, 88, 98, 154

Duranickel vs. Br, 113

Duranickel vs. F, 103

E

Electron deficiency sites on glass, chemical attack at, 17

Evaporation of Ni bromide scales, rate vs. temperature, 111

Everdur vs. F, 122

F

Fluoride deposits in Zr oxides as sites for hydriding, 341

Fluorides, standard free energies of formation, 60, 61

Fluorine

- Al vs., 135
- Be vs., 141
- Cu vs., 116, 121
- Cr vs., 146
- gold vs., 154
- Hf vs., 147
- Inconel vs., 103
- iron and alloys vs., 124
- manganese vs., temperature infl. on scaling, 146
- Mg vs., scale properties, rates, 142
- monel ignition, 102
- Ni alloys vs., 93, 101
- Pd vs., 151
- silver vs., scale properties, kinetics, 152
- Ti vs., 144
- vanadium vs., 145
- Zr vs., 147, 252, 277

G

Gallium, halogens vs., 156

Germanium, halogens vs., 156

Glass

- acids vs., 18
- alkali silicate properties, 5
- aluminosilicate properties, 6
- boron reactions at leached surface, 45
- borosilicate properties, 6
- chelating agents vs., 28
- chemical attack, 15, 31
- composition, infl. of oxides, 4
- etching by HF + sulfuric acid, 50
- high temperature attack, 49
- ion selectivity, infl. on surface reactions, 11
- lead, properties, 6
- Lewis acid sites on aluminosilicate, 45
- molecular activity at surface, 40
- molten salts increasing strength, 34
- nonpolar materials on surface, 48
- phase reactions, 35
- polishing by acids, 50
- silica properties, 5
- soda-lime properties, 5
- structure theories, 2
- sulfur oxides vs., 33
- surface reaction layer protective vs. acids, 18
- water resistance, 17
- weathering, 49

Gold, halogens vs., 154, 155

Grain effects, Zr oxides' preferential attack, 187, 199

H

Hafnium vs. F, 147

Halides

binary metal properties, 57, 66-68

diffusion properties, 59

scale formation mechanisms, 75

temperature effects, 59

Zr vs., 227, 253, 261

Halogens

alkaline earth metals vs., 143

Be vs., 141

Bo vs., 156

Cd vs., 155

Co vs., 147

Fe and alloys vs., 124

Ga, In, Th vs., 156

germanium vs., 156

iridium vs., 151

lead vs., 157

magnesium vs., 143

mercury vs., 155

Mo vs., 149

niobium vs., 148

osmium vs., 151

rhodium vs., 151

ruthenium vs., 150

silicon vs., 155

tantalum vs., 148

technetium and rhenium vs., 150

testing methods, 70

tin vs., 157

tungsten vs., 149

zinc vs., 155

Hastelloys vs. halogens, 103, 109, 113, 114

Heat treatment, Zr and alloys, 235, 256,

270, 349

Hydrogen

bromide vs. stainless steels, 134

fluoride vs. Al, 135

copper vs., 114

nickel vs., 93

Zr reactions with, 232, 246, 253, 261,

269, 293, 337, 342, 349, 357

Hydrolysis of glass atomic bonds, 15

I

Illium vs. F, 103

Inconel vs. Cl, 109

Incol vs. F, 103

Indium, halogens vs., 156

Inhibitors, Al, B, Zn salts vs. salt solution

attack on glass, 16

Inhibitors, boric acid for Zr in 500 C steam, 261

Iodides vs. Zr in high temperature water and steam, 261

Iodine

Al vs., rates, infl. vapor, water, 140

copper vs., 114, 124

Cr vs., 146

gold vs., 155

iron vs., 135

Ni alloys vs., 113

Pt vs., 152

scale formation of metal binaries with, 75

silver vs., kinetics, dopant infl., 154

tantalum vs., 149

Ti vs., 145

tungsten vs., 150

vapor effects, 135, 143, 152

Zr stress corrosion cracking in, 148

Ionic effects

Ca, Cu, Fe and Si vs. Zr, 254

chelating agents vs. glass, 29

F anions in Ni-fluorine scale, 97

glass surface, infl. on solubility, 12

scale mechanisms, 74, 84, 85

Iridium, halogens vs., 151

Iron and alloys

Br vs., scale properties, 134

Cl vs., 13, 129, 131, 133

F reactions with, 125, 127, 129

iodine vs., 135

L

Lead, halogens vs., 157

Lithium hydroxide + radiation vs. Zr, 279

M

Magnesium vs. F, 142

Mn vs. Br, 147

Mn vs. Cl, 147

Mercury, halogens vs., 155

Mo, F vs., ignition, 149

Monel vs. Cl, 109

N

Nickel and alloys

18-8 recession rate, temperature vs.

time in Cl, 134

Br vs., 111

-chloride evap. vs. temperature, 121

chlorine vs., 105, 106, 110

fluorides of Ge, Mo, S, Se and U vs., 93

fluorine vs., 101-104

halides vs., 92

I vs., 113

ignition in F, 100

monel vs. Br, 113

Nickel and alloys (*Cont'd*)

monel vs. F, 100

Th as alloy vs. F attack on, 104

Zr alloyed with, 228, 353

Niobium, halogens vs., 148

Niobium, Zr alloys containing, 210, 228

Nitrogen effects in Zr, 196, 204, 261

O

Osmium vs. halogens, 151

Oxidation, Zr alloys

alloying with high valency metals, effects, 213

catastrophic in fused salts with Cl, Br, 227

diffusion data, 303

mechanisms, 295

N infl. on kinetics, 204

prediction of rates, 320

radiation infl., 278, 287, 281, 321

stress infl., 250

surface preparation vs, 251

temperature effects, 248, 302

transition phenomena, 260, 263

steam and water, 228, 240, 264

Oxidation of binary alloys, 86

Oxides, Zr alloys

absorption after transition, 348

cracking mechanism, 201

diffusion, dissolution, 319

hydrogen attack, 338, 342

ionic and electronic transport in, 332

molecular migrations, 311, 333

morphology, 306, 334

pore sizes, cracks, topography, 314

radiation vs, 323, 326, 334

recrystallization phenomena, 267, 316

Oxygen

Cu vs. Cl in, 123

embrittlement of Zr in LOCA, 249

+ F vs. Cu, 116, 119

+ F vs. iron, 125

iron + Cl vs., 129

pressure infl. on Zr kinetics, 192, 218

quantity and pressure infl. on Zircalloys, 322

sodium in solution vs. Zr alloys, 223

Zr vs., carbon dioxide infl. on kinetics, 216

Zr, infl. in water vs., 216, 270

Zr, infl. of N on kinetics in, 216

Zr, temperature effects in, 200, 202, 311

Zr diffusion, 196, 199

Zr hydrogen absorption influence, 353

Zr kinetics, mechanism in, 174, 181

Zr pressure infl., 218

Zr vs. steam, infl. of, 216, 261

ZrAl vs., scaling mode, 214

P

Palladium vs. F, 151

Passivation of metals by halides, 56

pH < 7 vs. glass, 15

pH of water, infl. vs. Zr, 262

Pitting, NiCr in I, 113

Platinum

Br vs., 151

F vs., 151

hydrochloric acid vs., 151

iodine vs., 152

Polymeric-type theory of glass structure, 2

Pore diameters in leached glass, 36

Potassium nitrate + Na nitrate–nitrite

molten vs. Zr₂, 225

Pressure

F infl. on Cu scales, 119

F vapor vs. silver, infl. on rates, 152

oxygen vs. Zr, 218

Zr hydrogen uptake in steam vs., 234

Zr oxide transition, infl. of, 241

R

Radiation

Zr alloys vs. ammonium hydroxide, hydriding from, 293

ZrFeNi, ZrCuFe vs. high temperature

water, infl. of, 291

ZrNb vs. impure carbon dioxide, infl. of, 220

Zr oxidation influenced by, 277, 283, 321, 323, 326, 334

Rhenium vs. halogens, 150

Rhodium vs. halogens, 151

Ruthenium vs. halogens, 150

S

Scales

chlorine vs. Al, water infl., 139

chlorine vs. Cr steel, 18–9+Ti, 18–8+

Mo, 18–8, recession rates, temperature vs. time, 134

Cl–Ni, mechanism and properties, 108

Cl–Ta properties, 149

Cl–Ti, infl. of water, 144

conductivity of Zr oxide, 274

Cu–Cl properties, kinetics, 122

Cu fluoride evap. vs. temperature, 121

Cu–F, properties, mechanism, 116

Cu–I, kinetics and mechanism, 114

Cu-oxide interface on Zr, 209

dopants, infl. in, 88

Scales (*Cont'd*)

- evaporation mechanism, 78
 - F–Al properties, 137
 - F–Cu, infl. of oxygen, 119
 - F–Ti, properties and rates, 144
 - Hf–F properties, 148
 - iron–Br properties, 134
 - iron–Cl, 129, 132
 - iron–F, 125, 127
 - monel–F, 100, 102
 - morphological factors, 84
 - Ni bromide evaporation rate vs. temperature, 111
 - Ni–F, 93, 95, 98
 - temperature effects, 81, 83
- Scales, Zr and alloys
- breakdown mechanism, 198, 201, 214
 - cracking at high temperature, 187
 - fused salts, causing, 227
 - + Hf vs. fluorine, 147
 - oxide, deuterium and tritium content, 359
 - oxide defect structure, 301
 - oxide, intermetallic particles' properties, 360
 - oxide, ionic transport in, 301
 - oxide rectification of electrical currents, 269
 - oxide transition phenomena, 185, 241
- Silica solubility vs. pH, 10
- Silicon, halogens vs., 156
- Silicon in Zr, infl. on hydrogen absorption, 351
- Silver, halogens vs., 152
- Sodium
- Br, Cl < 50°C vs., 143
 - glass, reactions on surface of, 34
 - graphite reactor vs. Zr fuel cladding, 225
 - Zr attack in Na compared to that in oxygen, 223
- Steam
- boric acid inhibitor for Zr vs. 500°C, 261
 - Zircaloy oxidation kinetics in high temperature, 240
 - Zr alloying infl. vs., 210, 239
 - Zr, heat treatment vs. hydrogen absorption in, 349, 355
 - Zr radiation effects in, 279, 283
 - Zr temperature effects in, 233, 235, 245, 258
- Steels, stainless, Br and I vs., infl. of water, 134
- Stress vs. Zr oxides, 250, 314
- Sulfur dioxide vs. glasses, 33
- Sulfur trioxide vs. glasses, 33
- Surface prep. Zr alloys, 274, 276

T

- Ta vs. halogens, 148
- Technetium vs. halogens, 150

Temperature

- > 450°C vs. Zr₂, pressure infl., 263
 - alkaline earths vs. halogens, infl., 143
 - Bo and Si ignition in F at room, 156
 - Br–Al, ignition, 140
 - Br vs. Cr, infl., 146
 - Br vs. Ni and alloys, 111
 - Cl vs. Be, infl., 141
 - Cl vs. Cr, infl., 146
 - Cl–Ni reaction kinetics vs., 107
 - Cl vs. Ti ignition, 144
 - Cu + Cl ignition, 290–310°C, 122
 - Cu–F scales, infl. on, 121
 - F at -196°C vs. Cu, 196
 - F at -196°C vs. CuNi, CuZn, 121
 - F at -196°C vs. Ni, 95
 - F vs. Al, infl., 138
 - F vs. Cr + pressure, infl., 146
 - F vs. Cu, 117, 119
 - F vs. Mg, infl., 143
 - F vs. Mn, infl., 147
 - F vs. Ni, 93
 - F vs. Pd, Pt, infl., 151
 - flux effect on Zr alloy oxidation, 267
 - glass resistance to materials at high, 49
 - halides' melting, 59
 - HCl anhydrous vs. Cu, infl., 123
 - I vs. Cr, infl., 146
 - I vs. silver, infl. on scaling, 154
 - iron–Cl reactions, infl., 129, 132
 - iron–F reactions, infl., 125
 - Ni–F scale growth infl., 99
 - Pt vs. Cl infl., 151
 - scales, general infl., 74, 81, 83
 - Ti ignition in Br and I, 145
 - Zr hydrogen absorption in steam influenced by, 234
 - Zr oxidation, infl. on, 191, 200, 201, 218, 248, 304
 - Zr oxidation vs. radiation, infl. of, 285
 - Zr oxide heat flux effects in BWR, 325
 - Zr oxide transition, 241
- Testing
- deuterium and tritium analyses indicative of hydrogen absorption, 359
 - electrochemical of Zr oxidation parameters, 298
 - glass, 7, 9
 - halogen attack rate ambiguity, 91
 - metal–halogen reactions, 70
 - polarization of Zr₂ in fused salts, 300
 - tracers in Zr oxides, 298
 - Zr oxides, current–voltage in fused salt, 319
 - Zr oxides, polarization, 320
 - Zr specimen geometry, preparation, 195

Thorium, halogens vs., 156
 Ti as Zr alloy vs. oxygen, 215
 Tin, halogens vs., 157
 Tin infl. on Zr oxidation, 210, 228, 289
 Titanium vs. halogens, 144, 145
 Transition metal halides' melting points, 66, 67
 Transition metals, halogens vs., 158
 Tritium infl. on Zr in water, 262
 Tungsten, halogens, vs, 149

V

Vanadium vs. Br, F, 145, 146
 Vapor pressures of halide binaries, 66, 67, 68
 Vapors of alkali and lead oxides vs. glass at high temperature, 49

W

> 250°C vs. glass, 17
 300–650°C long term vs. Zr, 176
 alkali extraction from glass by, 16
 Br vs. Cu in, 124
 Br vs. iron in, 134
 Br vs. Ni alloys in, 111
 Br–silver, infl. on reactions, 153
 + carbon dioxide, radiation vs. ZrNb, 220
 Cl vs. Al, infl., 139
 Cl vs. Cu, infl., 122
 Cl vs. iron, infl., 129
 Cl vs. Ni alloys, infl., 109
 Cl +, vs. NiCr steels, 133
 Cl vs. Pt, infl., 151
 Cl vs. Ta, infl., 148
 Cl vs. Ti, infl., 144
 Cl vs. Zr, infl., 147
 F vs. Al, infl., 135
 glass resistance to, 18
 I vs. Al, infl., 140
 I vs. iron, infl., 135
 I vs. Ni alloys, infl., 114
 Zr alloys vs. high temperature, 227, 230, 279
 Zr and alloys' oxidation in, 240, 262, 276, 329
 Zr hydrogen attack in, 232, 342, 351
 Zr vs., infl. pH, 262
 Weathering of glass, 49

Z

Zinc, halogens vs., 155

Zinc halides' melting points, 67
 Zinc salts as inhibitors for glass, 16
 Zirconium and alloys
 air vs., 179, 184, 214
 alloying infl., 208, 214, 223, 228, 257, 334
 ammonium hydroxide vs., infl., heat flux, 292
 Br vs., 148
 carbon dioxide cooled nuclear reactors, used in, 219
 carbon dioxide vs. ZrNb, heat treatment infl., 210, 220
 carbon reactions, 218
 Cl, recession rates in, 147
 Cr plating vs. embrittlement, 220
 F vs., 147
 halogens vs., 148
 heat flux infl., 267
 heat treatment, 210, 235
 hydrogen reactions, 232, 253, 337, 345, 352, 357, 361
 impurities infl. on oxidation, 195
 I vs., 148
 ionic and electron activities in oxides, 308
 metallurgical variables' infl., 256
 molecular migration in oxides, 311
 N content infl., 196
 Nb alloys, 220, 228, 332
 nuclear application research abroad, 237
 organic coolants vs, 291
 oxidation phenomena, 182, 191, 240, 264, 295, 298, 317, 320, 332
 oxide films' rectification of electrical currents, 269
 oxygen absorption, infl. surface state, temperature, 311
 oxygen reactions, 174, 193, 196, 200
 potassium + Na nitrates vs., 225
 radiation vs., 277, 287, 290, 291
 scale breakdown mechanisms, 201
 sodium, NaK vs., 222, 223
 steam vs., 228, 231, 235, 245, 254, 256, 262, 274
 stress infl., 250, 314
 surface preparation vs. oxidation, 251
 Ti infl. on oxidation, 215
 tin as getter vs. Al, C, N, 228
 transition metals' infl. on hydrogen absorption by, 357
 transition phenomena, 208, 262
 water vs., 176, 179, 227, 231, 254, 256, 262, 274, 276, 290